ARCHIVES OF MECHANICS **Appears since 1949**

Aims and Scope

ARCHIVES OF MECHANICS provides a forum for original research on mechanics of solids, fluids and discrete systems, including the development of mathematical methods for solving mechanical problems. The journal encompasses all aspects of the field, with the emphasis placed on:

- mechanics of materials: elasticity, plasticity, time-dependent phenomena, phase transformation, damage, fracture; physical and experimental foundations, micromechanics, thermodynamics, instabilities
- methods and problems in continuum mechanics: general theory and novel applications, thermomechanics, structural analysis, porous media, contact problems
- dynamics of material systems
- fluid flows and interactions with solids

Address of the Editorial Office:
Institute of Fundamental Technological Research
Świętokrzyska 21
PL 00-049 Warsaw, Poland

Tel.(48-22) 826 60 22, Fax (48-22) 826 98 15, E-mail: publikac@ippt.gov.pl

Abstracted/indexed in:

Applied Mechanics Reviews, Current Mathematical Publications, Mathematical Reviews, MathSci, Zentralblatt für Mathematik, UnCover.

http://am.ippt.gov.pl/

Polish Academy of Sciences
Institute of Fundamental Technological Research

Archives of Mechanics

Archiwum Mechaniki Stosowanej

volume 53 issue 4-5

SUBSCRIPTIONS

Address of the Editorial Office: Archives of Mechanics
Institute of Fundamental Technological Research, Świętokrzyska 21
PL 00-049 Warsaw, Poland
Tel. (48 - 22) 826 60 22, Fax (48 - 22) 826 98 15,
e-mail:publikac@ippt.gov.pl

Subscription orders for all journals edited by IFTR may be sent directly to the Editorial Office of the Institute of Fundamental Technological Research

Subscription rates

Annual subscription rate (2001) including postage is US $ 210.
Please transfer the subscription fee to our bank account: Payee: IPPT PAN,
Bank: PKO SA. IV O/Warszawa,
Account number 12401053-40054492-3000-401112-001.

All journals edited by IFTR are available also through:

- Foreign Trade Enterprise ARS POLONA Krakowskie Przedmieście 7, 00-068 Warszawa, Poland fax (48 - 22) 826 86 73
- RUCH S.A. ul. Towarowa 28, 00-958 Warszawa, Poland fax (48 - 22) 620 17 62
- Agencja Reklamowo-Wydawnicza A. Grzegorczyk, Bitwy Warszawskiej 1920r. 3, 00-973 Warszawa, Poland tel./fax (48 - 22) 822 49 36

Warunki prenumeraty

Redakcja przyjmuje prenumeratę na wszystkie czasopisma wydawane przez IPPT PAN. Bieżące numery można nabyć, a także zaprenumerować roczne wydanie Archiwum Mechaniki Stosowanej bezpośrednio w Dziale Wydawnictw IPPT PAN, Świętokrzyska 21, 00-049 Warszawa, Tel. (48 - 22) 826 60 22; Fax (48 - 22) 826 98 15.
Cena rocznej prenumeraty z bonifikatą (na rok 2001) dla krajowego odbiorcy wynosi 180 PLN

Również można je nabyć, a także zamówić (przesyłka za zaliczeniem pocztowym) we Wzorcowni Ośrodka Rozpowszechniania Wydawnictw Naukowych PAN,
00-818 Warszawa, ul. Twarda 51/55, tel. (48 - 22) 697 88 35.
Wpłaty na prenumeratę przyjmują także jednostki kolportażowe RUCH S.A. Oddział Krajowej Dystrybucji Prasy, 00-958 Warszawa, ul. Towarowa 28. Konto: PBK. S.A. XIII Oddział Warszawa nr 11101053-16551-2700-1-67. Dostawa odbywa się pocztą lotniczą, której koszt w pełni pokrywa zleceniodawca. Tel. (48 - 22) 620 10 39, Fax (48 - 22) 620 17 62

Arkuszy wydawniczych 25. Arkuszy drukarskich 20.5.
Papier offset. kl III 70g. B1.
Oddano do składania w październiku 2001r. Druk ukończono w październiku 2001r.
Skład i łamanie: E. Jaczyńska.
Druk i oprawa: Drukarnia Braci Grodzickich, Piaseczno ul. Geodetów 47A.

Arch. Mech., **53**, 4-5, pp. 287-288, Warszawa 2001

Preface

This special issue of the Archives of Mechanics contains selection of some papers presented at the 33rd Solid Mechanics Conference, Zakopane, 5-9 September, 2000.

Let me recall that the series of Polish Solid Mechanics Conferences have been organised by the Institute of Fundamental Technological Research of the Polish Academy of Sciences since 1953, when the first conference was held in Karpacz, south of Poland. Initially, these conferences had a more national character and concentrated mostly on problems of elasticity, plasticity and structural mechanics. Later on, they became international conferences with considerable participation of scientists from Poland as well as from foreign countries, and with much wider scope covering actual active research areas in solid mechanics.

This beautiful idea of the organisation of such conferences was due to two leading scientists from the Institute of Fundamental Technological Research, namely Wacław Olszak and Witold Nowacki.

These conferences have maintained high scientific standard and served as a real forum for exchange of new ideas and research information in the field of mechanics of solids.

Our aim was to keep this beautiful tradition and to bring together researchers engaged in all major areas of contemporary mechanics of solids and structures. The program of the Conference included 13 general lectures, 21 key-note sectional lectures and 180 contributed presentations. Besides general sessions, the Conference included special sessions dealing with the following specific topics:

- Biomechanics
- Damage and Fracture Mechanics
- Sensitivity Analysis and Optimization
- Homogenization and Composites
- Nonlinear Structures
- Computational Methods
- Porous Media and Geomechanics
- Strain Localization and Localized Fracture
- Experimental Mechanics
- Elasticity and Thermoelasticity
- Thermomechanics of Phase Transformation

- Nonlinear Waves
- Vehicle – Infrastructure Interactions and Structural Dynamics
- Inelastic Structure
- Plasticity and Thermoplasticity
- Plastic Forming Processes
- Contact Problems

The Editorial Board of the Archives of Mechanics kindly offered to publish a special conference issue of the journal, in order to assemble some papers presented at the 33rd Solid Mechanics Conference and not yet available in scientific journals. The interest of the Editorial Board in the Conference papers and the assistance in publishing this volume are gratefully acknowledged.

Finally, I would like to thank the authors who have contributed to this special Conference issue.

Warsaw, September 28, 2001

Piotr Perzyna
Chairman of the 33rd Solid Mechanics Conference

Arch. Mech., **53**, 4-5, pp. 289–306, Warszawa 2001

Dependence of adsorption/diffusion processes in porous media on bulk and surface permeabilities

B. ALBERS

Weierstrass Institute,
for Applied Analysis and Stochastics,
Mohrenstrasse 39,D-10117 Berlin,
e-mail : albers@wias-berlin.de

THE PAPER CONTAINS a macroscopic continuum model for adsorption in porous materials (B. ALBERS [1, 2]) which is an extension of the model for porous bodies by K. WILMAŃSKI [7] on mass exchange processes. We consider the flow of a fluid/adsorbate mixture through channels of a solid component. The fluid serves as carrier for an adsorbate whose mass balance equation contains a source term. Due to low adsorbate concentration we deal with a physical adsorption process which means that particles of the adsorbate stick to the skeleton due to weak van der Waals forces. The model contains two different permeability parameters whose nature is completely different: The first one, the usual bulk permeability coefficient, describes the resistance of the skeleton to the flow of the fluid/adsorbate mixture. The second one describes the surface resistance to the outflow of the mixture from the solid. This work shows within a simple example the range of these parameters and the dependence of adsorption/diffusion on them.

1. Introduction

IN THIS PAPER we present a parameter analysis within a continuum mechanical approach on adsorption/diffusion processes in three component porous media. The considered model and possible practical applications have extensively been shown in ALBERS [2, 1]. We consider the flow of a fluid through channels of the skeleton. The latter serves as a carrier for an adsorbate whose mass balance contains a source term. This term consists of two parts: one of them extends Langmuirs theory about possible places for the adsorbate to settle down on the internal surface to non-equilibrium processes. The other one takes into account changes of the internal surface and couples them with the source of porosity which is a part of a balance equation for the scalar field of porosity (see: WILMAŃSKI [8]).

1.1. Type of adsorption process considered

We consider physical adsorption processes. This means that particles of the adsorbate stick to the skeleton due to weak van der Waals forces. The type of mass exchange between fluid and skeleton (adsorption, chemisorption, capillary effects) mainly depends on two factors namely the particle size of the solid and the concentration of the adsorbate in the fluid.

For our model we consider very low adsorbate concentration. This entitles us to use the LANGMUIR theory of adsorption (see: [7]). It is based on the concept of the number of bare and occupied sites on the surface of a solid. Langmuir assumed that the adsorbate particles settle down on the solid in one single layer, and that there is – depending on the energy landscape of the surface – a certain number of places where they are able to settle down.[1)]

Obviously this is only possible if the adsorbate concentration is small. Otherwise the Langmuir isotherm of occupied sites reaches saturation. In the past many modifications of this theory appeared. One of them is the BET-model (see: [4]) which is based on the Langmuir theory but allows multilayer adsorption. This means that particles are also able to stick to already adsorbed particles and therefore there can appear several layers of adsorbate particles. For our purpose there is no need to use this more complicated version of the Langmuir model because we assume low concentrations. In addition it should be mentioned that there are some doubts concerning the description of multilayer adsorption (e.g. interaction of adsorbate particles of different layers).

One of the important factors for the shape of the adsorption isotherm is the size of solid particles in relation to the pore size between them. According to GREGG/SING [5] there occur six types of adsorption isotherms. The three most important of them are shown in the figure below.

The first one a) is the graph of the common monolayer Langmuir isotherm. In principle it describes the adsorption of particles on plane surfaces. But it also holds in our case considering the porous material to be a soil. The pore size of

[1)]The assumption of a monolayer adsorption is related to the way in which particles of the adsorbate interact with the internal surface. In the case of crystalline solids the energy landscape of the internal surface is periodic, i.e. energetic isolines form a 2D family of closed lines which define spots of the highest interactions. This yields the concept of occupied and bare sites introduced by Langmuir. As a consequence we obtain a formula for the mass source which is used in this work. The assumption on the monolayer structure of adsorption yields the necessity of the assumption on small concentration of the adsorbate. In contrast to the above described mechanism a multilayer adsorption occurs when particles of the adsorbate in the fluid phase interact with particles of the adsorbate which have already settled down on the internal surface. Such an interaction is isotropic, i.e. one cannot introduce the notion of bare sides and, even if applicable, the formula for mass sources used in this paper would have to admit a discontinuous change of material parameters which is not the case. A detailed description of such adsorption processes can be found in GREGG/SING [5].

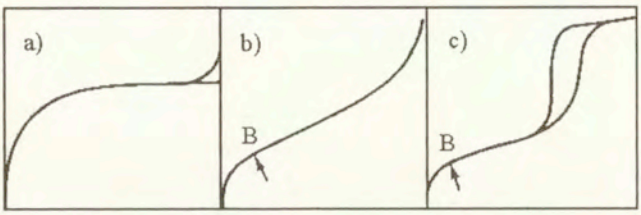

FIG. 1. Three most important types of adsorption isotherms (adsorbed amount vs. relative partial pressure)

this soil is big enough for the curvature of the pores not to play any important role. This is different in the case of isotherm c). This form of isotherm arises in case of the so-called mesopores (20-500 Å in diameter). Both b) and c) describe multilayer adsorption processes which is indicated by the existence of the inflection point B. Before reaching this point the monolayer process runs according the Langmuir isotherm i.e. adsorption is restricted to a thin layer on the walls. After that b) and c) show different behaviour. Although in both cases the slope increases, in b) the rise first is approximately linear and then rather rapid for higher relative pressures while in c) the amount adsorbed possesses another inflection point before the saturation vapour pressure is reached. A characteristic feature of c) is its hysteresis loop. This is due to the capillary condensation in the finest pores.

Summing up the investigated model is intended to describe physical adsorption with low concentrated adsorbate on a porous medium with relatively large pores. Then the Langmuir isotherm looks as shown in a) which is restricted to monolayer adsorption.

1.2. Intention of the work

The intention of this work is to show the dependence of the fields and the adsorption rate on model parameters. The two most important of them are the permeability coefficient π and the surface permeability α. These two permeability parameters possess a completely different nature. The first one is an element of the field equations and reflects properties of the material. It has been shown in [1] that the two component continuum model can be simplified to the so-called reaction-diffusion models widespread among mathematicians (for example KNABNER [6]) if one entirely neglects the motion of the skeleton, and the acceleration of the fluid. From two momentum balance equations there remains solely the Darcy law. If we do so we see that the permeability parameter π of the two component model is related to a coefficient of the Darcy law which contains

the true viscosity of the fluid. This implies the importance of the permeability parameter: it describes the resistance of the skeleton to the flow of the fluid as well as the true viscosity of the fluid.

In this work we study the parameters within a one-dimensional example. In this case the permeability parameter is a constant scalar. But for multidimensional investigations it is conceivable that it could be tensorial.

The other permeability coefficient, the surface resistance α, enters the model due to the boundary conditions of third type and, consequently, accounts for properties of the surface. Boundary conditions for porous media are strongly related to flow conditions in the vicinity of the boundary. Generally there arises a boundary layer: a thin layer where friction forces play an important role because the fluid sticks to the body. But especially for dull bodies this boundary layer can come off the body if the pressure in flow direction increases rapidly which means that there arise whirls if the fluid arives at the end of the body. That is what happens if the body enters the surface of the porous media and flows through and against the channels of the skeleton. The parameter α is the leading quantity for the fluid velocity. Therefore we show at the end a very important feature, namely a maximum in the dependence of the adsorption rate on diffusion.

2. Adsorption/diffusion model

We consider a process in a three component porous medium. A fluid-adsorbate mixture flows through channels of a porous medium. Particles of adsorbate settle down on the internal surface of the skeleton.

2.1. Mass balances (in terms of mass densities)

Then the mass balance equations have the form

$$
\begin{aligned}
&\frac{\partial \rho^S}{\partial t} + \operatorname{div}\left(\rho^{\mathrm{S}}\mathbf{v}^{\mathrm{S}}\right) = -\hat{\rho}^{\mathrm{A}},\\
&\frac{\partial \rho^F}{\partial t} + \operatorname{div}\left(\rho^{\mathrm{F}}\mathbf{v}^{\mathrm{F}}\right) = 0,\\
&\frac{\partial \rho^A}{\partial t} + \operatorname{div}\left(\rho^{\mathrm{A}}\mathbf{v}^{\mathrm{F}}\right) = \hat{\rho}^{\mathrm{A}},
\end{aligned}
\tag{2.1}
$$

where ρ^S, ρ^F and ρ^A are the mass densities of the components, $\mathbf{v}^F$ is the common velocity of fluid and adsorbate before the adsorbate settles down and its velocity changes to that of the skeleton $\mathbf{v}^S$. $\hat{\rho}^A$ denotes the intensity of the mass source. Of course, it appears with opposite signs in the balances for skeleton and adsorbate, as the total conservation of mass must be fulfilled.

2.2. Mass source

This mass transfer rate from the liquid to the solid phase per unit time is given by the relation

$$\hat{\rho}^A = -\frac{m^A}{V}\frac{d(\xi f_{\text{int}})}{dt} = -\frac{m^A}{V}\left(f_{\text{int}}\frac{d\xi}{dt} + \xi\frac{d f_{\text{int}}}{dt}\right), \tag{2.2}$$

whose derivation is based on the classical LANGMUIR adsorption theory about *occupied* (ξ) and *bare* ($1-\xi$) *sites* (see [7]) where the existence of possible places for adsorption on a surface is mainly explained by the landscape of the interaction energy with their quasiperiodic distribution of maxima for crystalline skeletons). Another important factor for the extent of adsorption is the *internal surface area* of the solid f_{int}. V is the representative elementary volume REV which is small in comparison with the volume of the whole flow regime but big against volumes of single pores of the skeleton. The mass of adsorbate per unit of the internal surface area is denoted by m_A.

The first contribution on the right-hand side of (2.2) describes the change of the fraction of occupied sites. It is specified by the Langmuir evolution equation

$$\frac{d\xi}{dt} = a(1-\xi)p^A - b\xi e^{-\frac{E_b}{kT}}, \tag{2.3}$$

where p^A is the partial pressure of the adsorbate in the fluid phase and a and b are material parameters. The energy barrier E_b for particles adsorbed on the skeleton is assumed to be constant. Furthermore k denotes the Boltzmann constant and T is the absolute temperature. The right hand side of (2.3) again consists of two terms: the adsorption rate (first term) and the desorption rate (second term). In full phase equilibrium they are equal so that the time change of occupied sites is equal to zero. In this case we get from (2.3) the well-known *Langmuir isotherm* of occupied sites

$$\xi_L = \frac{\frac{p^A}{p_0}}{1+\frac{p^A}{p_0}}, \quad \text{with} \quad p_0 := \frac{b}{a}e^{-\frac{E_b}{kT}}. \tag{2.4}$$

The other part of (2.2) describes the change of the internal surface. We assume that this change is coupled with relaxation of the porosity n, which is described by the balance equation of porosity. Motivated by elementary considerations about changes of the internal surface and of the porosity in a porous medium yielding film adsorption we assume [2)]

[2)] As an example let us consider a porous body with spherical holes connected with each other by negligibly small channels (one of the holes is shown in the picture). A film adsorption process

$$\frac{1}{f_{\text{int}}}\frac{d f_{\text{int}}}{dt} \propto \frac{\hat{n}}{n}. \tag{2.5}$$

Finally we arrive at

$$\hat{\rho}^A = -\rho^A_{ad}\left\{\left[(1-\xi)\frac{cp^L}{p_0} - \xi\right]\frac{1}{\tau_{ad}} - \xi\frac{\nu}{\tau}\Delta\right\}, \tag{2.6}$$

where τ_{ad} denotes the characteristic time of adsorption, p_0 is a reference pressure of adsorption defined in (2.4), ν is a proportionality factor and $\rho^A_{ad} := \frac{m^A f_{\text{int}}}{V}$.

2.3. Mass balances (in terms of concentration)

It is common to use a form of mass balances containing quantities related to the concentration c:

$$\begin{aligned}
&\frac{\partial \rho^S}{\partial t} + \operatorname{div}\left(\rho^{\mathrm{S}}\mathbf{v}^{\mathrm{S}}\right) = -\rho^{\mathrm{L}}\hat{\mathrm{c}},\\
&\frac{\partial \rho^L}{\partial t} + \operatorname{div}\left(\rho^{\mathrm{L}}\mathbf{v}^{\mathrm{F}}\right) = \rho^{\mathrm{L}}\hat{\mathrm{c}},\\
&\frac{\partial c}{\partial t} + \mathbf{v}^F \cdot \operatorname{grad}\mathrm{c} = (1-\mathrm{c})\,\hat{\mathrm{c}}.
\end{aligned} \tag{2.7}$$

For the transformation we have used the following definitions

$$\rho^L := \rho^F + \rho^A, \qquad c := \frac{\rho^A}{\rho^L}, \qquad \hat{c} := \frac{\hat{\rho}^A}{\rho^L}, \tag{2.8}$$

where ρ^L denotes the mass density of liquid phases, c is the concentration and $\hat{c}$ is the concentration source.

---

takes place if the adsorbate settles down on the internal surface in an almost homogeneous manner. This yields small changes of the radius R of the pores, say δR. If N is the number of holes in REV then the total volume of holes V^F and the internal surface f_{int} in REV are satisfying the relations

$V^F = N \cdot \frac{4}{3}\pi$
$R^3, \quad \delta V^F = N \cdot 4\pi R^2 \delta R \Rightarrow \frac{\delta n}{n} = 3\frac{\delta R}{R}$
$f_{\text{int}} = N \cdot 4\pi R^2, \quad \delta f_{\text{int}} = N \cdot 8\pi R \delta R \Rightarrow \frac{\delta f_{\text{int}}}{f_{\text{int}}} = 2\frac{\delta R}{R}$
$\Rightarrow \frac{\delta n}{n} \propto \frac{\delta f_{\text{int}}}{f_{\text{int}}}.$

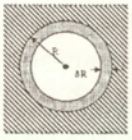

2.4. Momentum balances

We want to account for the deformations of the skeleton which means that we also need momentum balance equations to describe the problem. Due to the common velocity of fluid and adsorbate we are left with two of them

$$\frac{\partial \rho^S \mathbf{v}^S}{\partial t} + \operatorname{div}\left(\rho^{\mathrm{S}} \mathbf{v}^{\mathrm{S}} \otimes \mathbf{v}^{\mathrm{S}} - \mathbf{T}^{\mathrm{S}}\right) = \hat{\mathbf{p}}^{\mathrm{S}}, \tag{2.9}$$

$$\frac{\partial \rho^L \mathbf{v}^F}{\partial t} + \operatorname{div}\left(\rho^{\mathrm{L}} \mathbf{v}^{\mathrm{F}} \otimes \mathbf{v}^{\mathrm{F}} + \mathrm{p}^{\mathrm{L}} \mathbf{1}\right) = \hat{\mathbf{p}}^{\mathrm{F}},$$

where the partial pressure in the liquid phase p^L (i.e. in the fluid and adsorbate phases together) is the sum of the partial pressures in the fluid p^F, and in the adsorbate p^A. For small adsorbate concentration as assumed in our case we expect according to Dalton's law that $p^A \cong cp^L$. Furthermore $\mathbf{T}^S$ denotes the partial Cauchy stress tensor in the skeleton, and $\hat{\mathbf{p}}^F = -\pi\left(\mathbf{v}^F - \mathbf{v}^S\right) + \rho^L \hat{c} \mathbf{v}^F$ is the momentum source in the liquid and $\hat{\mathbf{p}}^S = \pi\left(\mathbf{v}^F - \mathbf{v}^S\right) - \rho^L \hat{c} \mathbf{v}^S$ is the momentum source in the skeleton where π denotes the permeability coefficient of the whole system. [3)]

2.5. Porosity balance

According to the works of K. WILMAŃSKI (see e.g. [7]) we have an additional balance equation for the scalar field of porosity

$$\frac{\partial n}{\partial t} + \mathbf{v}^S \cdot \operatorname{grad} n + \mathrm{n_E} \operatorname{div}\left(\mathbf{v}^{\mathrm{F}} - \mathbf{v}^{\mathrm{S}}\right) = \hat{\mathrm{n}} = -\frac{\Delta}{\tau}. \tag{2.10}$$

Here $\Delta = n - n_E$ is the deviation of the porosity n from its equilibrium value n_E and τ is the *relaxation time of porosity*. The above shape of the source of porosity $\hat{n}$ is based on assumptions on small deviations from thermodynamic equilibrium. In this work we consider a linear model in which $n_E = \text{const}$.

3. One-dimensional example

We are interested in the influence of the two permeability coefficients π and α on the flow of a fluid-adsorbate mixture through soils. Therefore we solve the following one-dimensional example:

[3)] This form of the momentum sources follows in a thermodynamically linear approach from the principle of material objectivity together with the bulk conservation laws which yield

$$\hat{\mathbf{p}}^S + \hat{\mathbf{p}}^L = 0 \text{ and } \hat{\rho}^L + \hat{\rho}^S = 0.$$

In the typical situation which we consider in this paper the form of the momentum sources can be simplified if we compare the order of magnitude of terms: $\pi \approx 10^9 \frac{\mathrm{kg}}{\mathrm{m^3 s}}$ and $\hat{\rho}^L = \rho^L \hat{c} \approx 230 \frac{\mathrm{kg}}{\mathrm{m^3}} \cdot 10^{-5} \frac{1}{\mathrm{s}} = 2.3 \cdot 10^{-3} \frac{\mathrm{kg}}{\mathrm{m^3 s}}$, i.e. we can neglect the influence of mass sources.

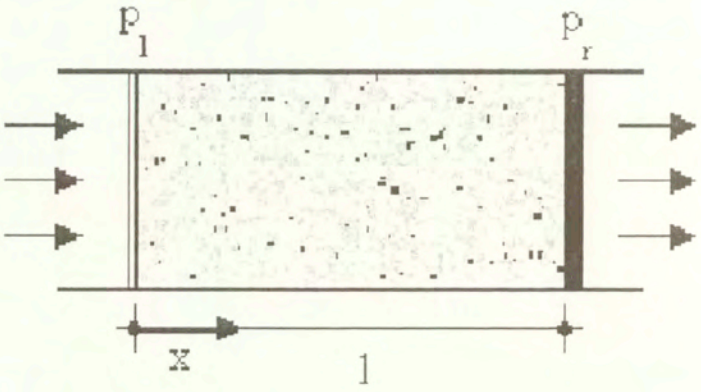

FIG. 2. Flow through porous body

Due to a difference of the external pressure, with p_l at $x = 0$ being larger than p_r at $x = l$ (see: Fig. 2), the mixture flows along the direction x through the porous body. The low concentrated adsorbate is carried by the fluid and has therefore the same velocity v^F. Then the isothermal process is described by the fields

$$\{\rho^S, \rho^L, c, v^F, v^S, e^S, \Delta, \xi, f_{\text{int}}\}, \tag{3.1}$$

where the last three unknowns are the above introduced additional microstructural fields describing changes of porosity and mass exchange processes.

For simplification we make the following assumptions:

- the skeleton does not move, i.e. $v^S \equiv 0$,
- the inertia forces are small i.e. the acceleration terms in the momentum balances can be neglected,
- small changes in time of the velocity gradient, i.e. the porosity balance reduces to the algebraic relation $\Delta \simeq -n_E \tau \frac{\partial v^F}{\partial x}$.

The third assumption follows from the fact that the relaxation time of porosity τ is very small. In the formal solution of the balance equation of porosity

$$\frac{\partial \Delta}{\partial t} + \frac{\Delta}{\tau} = -n_E \frac{\partial v^F}{\partial x} \Rightarrow \Delta$$

$$= -n_E \int_0^t \frac{\partial v^F}{\partial x}(\eta)\, \mathrm{e}^{-\frac{t-\eta}{\tau}}\, d\eta \simeq -n_E \frac{\partial v^F}{\partial x}(t) \int_0^t \mathrm{e}^{-\frac{t-\eta}{\tau}}\, d\eta = -n_E \tau \frac{\partial v^F}{\partial x}, \tag{3.2}$$

we have assumed that the characteristic macroscopic time t is much larger than τ.

3.1. Governing set of equations and constitutive relations

Under these assumptions the balance equations for the example have the following form

$$\frac{\partial \rho^L}{\partial t} + \frac{\partial \rho^L v^F}{\partial x} = -\rho_{ad}^A \left\{ \left[\frac{cp^L}{p_0} - \left(1 + \frac{cp^L}{p_0}\right) \xi \right] \frac{1}{\tau_{ad}} - \xi \frac{\nu}{\tau} \Delta \right\},$$

$$\frac{\partial c}{\partial t} + v^F \frac{\partial c}{\partial x} = -(1-c) \frac{\rho_{ad}^A}{\rho^L} \left\{ \left[\frac{cp^L}{p_0} - \left(1 + \frac{cp^L}{p_0}\right) \xi \right] \frac{1}{\tau_{ad}} - \xi \frac{\nu}{\tau} \Delta \right\}, \tag{3.3}$$

$$\frac{\partial p^L}{\partial x} + \pi v^F = 0, \qquad n_E \frac{\partial v^F}{\partial x} = -\frac{\Delta}{\tau}, \qquad \frac{\partial \xi}{\partial t} = \left[(1-\xi) \frac{cp^L}{p_0} - \xi \right] \frac{1}{\tau_{ad}}.$$

The constitutive relation for the pressure in the liquid phase p^L is assumed to be linear

$$p^L = p_0^L + \kappa \left(\rho^L - \rho_0^L \right) + \beta \Delta, \tag{3.4}$$

where p_0^L and ρ_0^L are initial values of the pressure and the mass density for the liquid phase. κ denotes the constant compressibility coefficient and β is a constant material coupling parameter.

3.2. Boundary conditions

The boundary conditions are assumed to be of third type. They express the flow through the boundary of the body in dependence on the difference of the partial pressure in the liquid and the part of the external pressure which acts on the fluid, as well as on the permeability α of the surface. The latter is one of the permeability coefficients whose influence we want to determine furtheron. Hence

$$\begin{aligned} x &= 0: \quad -\rho^L v^F = \alpha \left(p^L - n p_l \right), \\ x &= l: \quad \rho^L v^F = \alpha \left(p^L - n p_r \right). \end{aligned} \tag{3.5}$$

3.3. Solution method

We use a regular perturbation method to find an approximate solution of the problem. We make the following linear ansatz

$$\begin{gathered} \rho^L = \rho_0^L + \varepsilon \rho_1^L, \qquad v^F = \varepsilon v_1^F, \qquad \Delta = \varepsilon \Delta_1, \\ c = c_0 + \varepsilon c_1, \qquad \xi = \xi_L + \varepsilon \xi_1, \qquad \varepsilon = \frac{p_l - p_r}{p_r}, \end{gathered} \tag{3.6}$$

where ρ_0^L, c_0 and ξ_L are the initial values of the corresponding fields. Initial values of fluid/adsorbate velocity and the change of porosity are zero. The expansions which depend on a small parameter ε are truncated after first order contributions. The definition of ε is based on the assumption that the pressure difference between the left and the right boundary is small.
We use Laplace transforms to find an analytical solution of the linear problem and to get numerical solutions for the inverse Laplace transform we use a FORTRAN-solver. For a detailed illustration of the solution and a discussion of the results for the fields see [1], [2].

3.4. Parameters

To illustrate the above presented example and to study the permeability parameters we choose the following values

Length of the body l	1m	Coupling constant β	1GPa
Initial mass density ρ_0^L	$2.3 \cdot 10^2 \frac{\text{kg}}{\text{m}^3}$	Equilibrium porosity n_E	0.23
Initial concentration c_0	10^{-3}	Initial pressure p_0^L	23 kPa
Langmuir pressure p_0	10 kPa	Pressure on right h.s. p_r	100 kPa
Proportionality factor ν	10	Compressibility κ	$2.25 \cdot 10^6 \frac{\text{m}^2}{\text{s}^2}$
Permeability of solid π	$10^9 \frac{\text{kg}}{\text{m}^3\text{s}}$	Permeability of surface α	$4 \cdot 10^{-8} \frac{\text{s}}{\text{m}}$
Relaxation time τ	10^{-3} s	Charact. time of adsorp. τ_{ad}	1 s
Fraction of occupied sites in equilibrium ξ_L	$2.3 \cdot 10^{-2}$	mass density of adsorbate on internal surface ρ_{ad}^A	$40 \frac{\text{kg}}{\text{m}^3}$

Mass density and porosity have been chosen to have typical values for rocks and soils. The values for material parameters $\beta$and τ have been chosen on the basis of estimates of the attenuation of acoustic waves. The influence of permeability is expressed by two constants π and α. The first one describes the resistance of the skeleton to the flow of the fluid/adsorbate mixture. The second one describes the surface resistance to the outflow of the mixture from the solid. Its appearance is connected with a boundary layer between the porous body and the external world.

4. Parameter analysis

In this section we investigate the influence of several model parameters on the behavior of the fields and the adsorption rate (negative value of the source of concentration).

Special attention is paid to permeability coefficients π and α. Physically they describe the resistance of the skeleton to the flow of fluid but they arise from different microstructural properties of the system. While π represents the resis-

tance of the skeleton against theflow of the liquid in the inner part of the porous body, α describes the surface resistance against in- and outflow of the liquid into and out of the body. The latter parameter is coupled with the appearance of a boundary layer in the transition zone between the porous body and the external world (see [2]).

First we consider the influence of the bulk permeability parameter π. Some results connected to variations of this parameter are already shown in earlier works without mass exchange [3], [2]. There we have studied the radial flow through a cylinder under small and large deformations.

The role played by this coefficient in the present case is illustrated in the figures bellow (Fig. 3) where the fields (11) of our example are shown in dependence on π for three different times (at the beginning, $\frac{t}{\tau_{ad}} = 1$, curve 1 in the Figures, at an intermediate instance, $\frac{t}{\tau_{ad}} = 5$, curve 2, and for the large time lapse of the process, $\frac{t}{\tau_{ad}} = 10$, curve 3). For π we have chosen values between 10^8 and 10^{10} $\frac{\mathrm{kg}}{\mathrm{m^3 s}}$. The value $\pi = 10^9$ $\frac{\mathrm{kg}}{\mathrm{m^3 s}}$ used in former works lies in the middle of this region. A further reduction of π beneath $10^8 \frac{\mathrm{kg}}{\mathrm{m^3 s}}$, i.e. for a more permeable material, the relative velocity becomes so big that the mass exchange cannot appear, and, consequently, all fields become independent of the bulk permeability. On the other hand, for values bigger than 10^{10} $\frac{\mathrm{kg}}{\mathrm{m^3 s}}$ the numerical inverse Laplace transformation cannot be performed by the code used in this work (huge exponents). In this part of the analysis we use, as in the earlier works, the value of the surface permeabiltity parameter $\alpha = 4 \cdot 10^{-8}$ $\frac{\mathrm{s}}{\mathrm{m}}$.

As we see in Fig. 3 (the upper left diagram) the change of the mass density of the liquid increases with decreasing permeability parameter π (i.e. with increasing permeability of the material) at any instant of time. However for advanced times this change is much better pronounced. The velocity of the liquid increases with decreasing permeability coefficient (the upper right diagram). Essential changes of the velocity appear solely in the middle region of the permeability coefficient. These changes are nonmonotonous in time (there exists a local minimum!). This is different in the case of changes of porosity (the middle left diagram). Changes of porosity have a similar time dependence for different permeabilities with a rapid growth in an initial time interval, and a subsequent decay for large times. The value of the maximum change of porosity appearing between these two regions is decaying with growing permeability coefficient with a simultaneous shift to larger times. In the Figure we can see solely a projection of this behavior for a chosen interval of time. Obviously for small permeabilities we observe already a large time behavior (a monotonous decay from curve 1 to curve 3) while for large permeabilities we see still the behavior in the initial interval of time (a monotonous growth from curve 1 to curve 3). The absolute values of changes of the adsorbate concentration in the fluid (the middle right

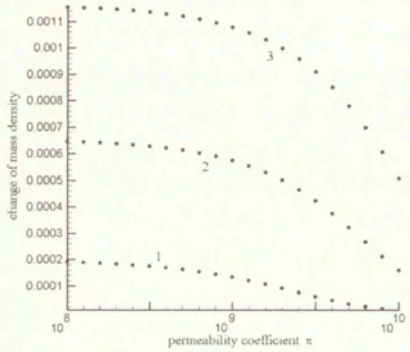

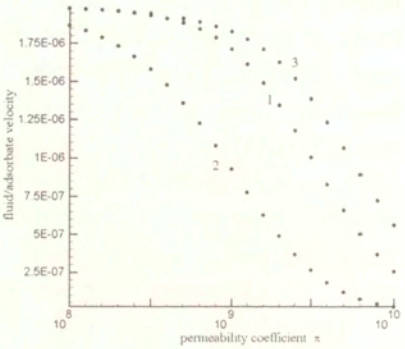

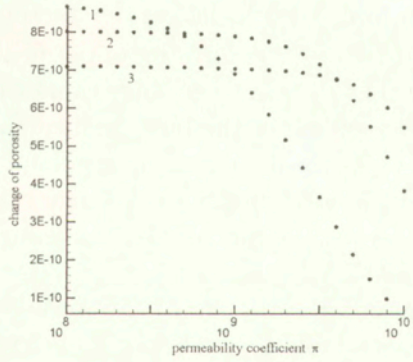

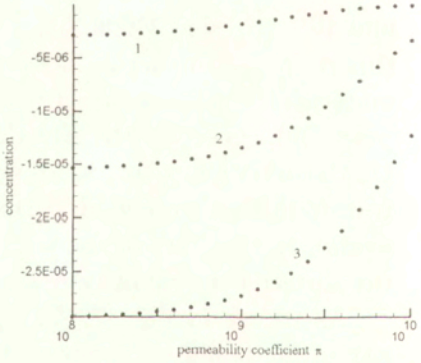

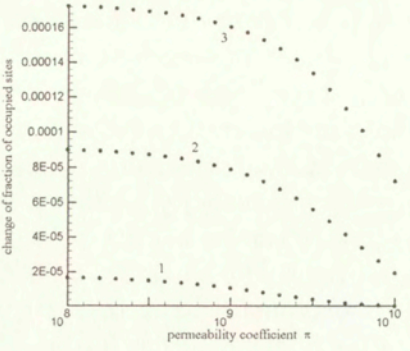

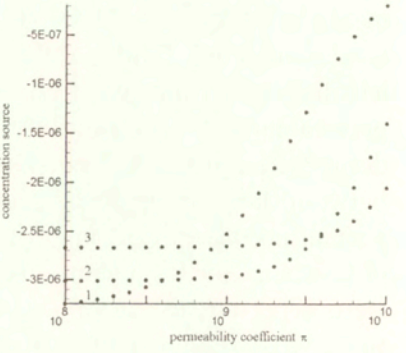

FIG. 3. Influence of the permeability parameter π on several fields and the concentration source.

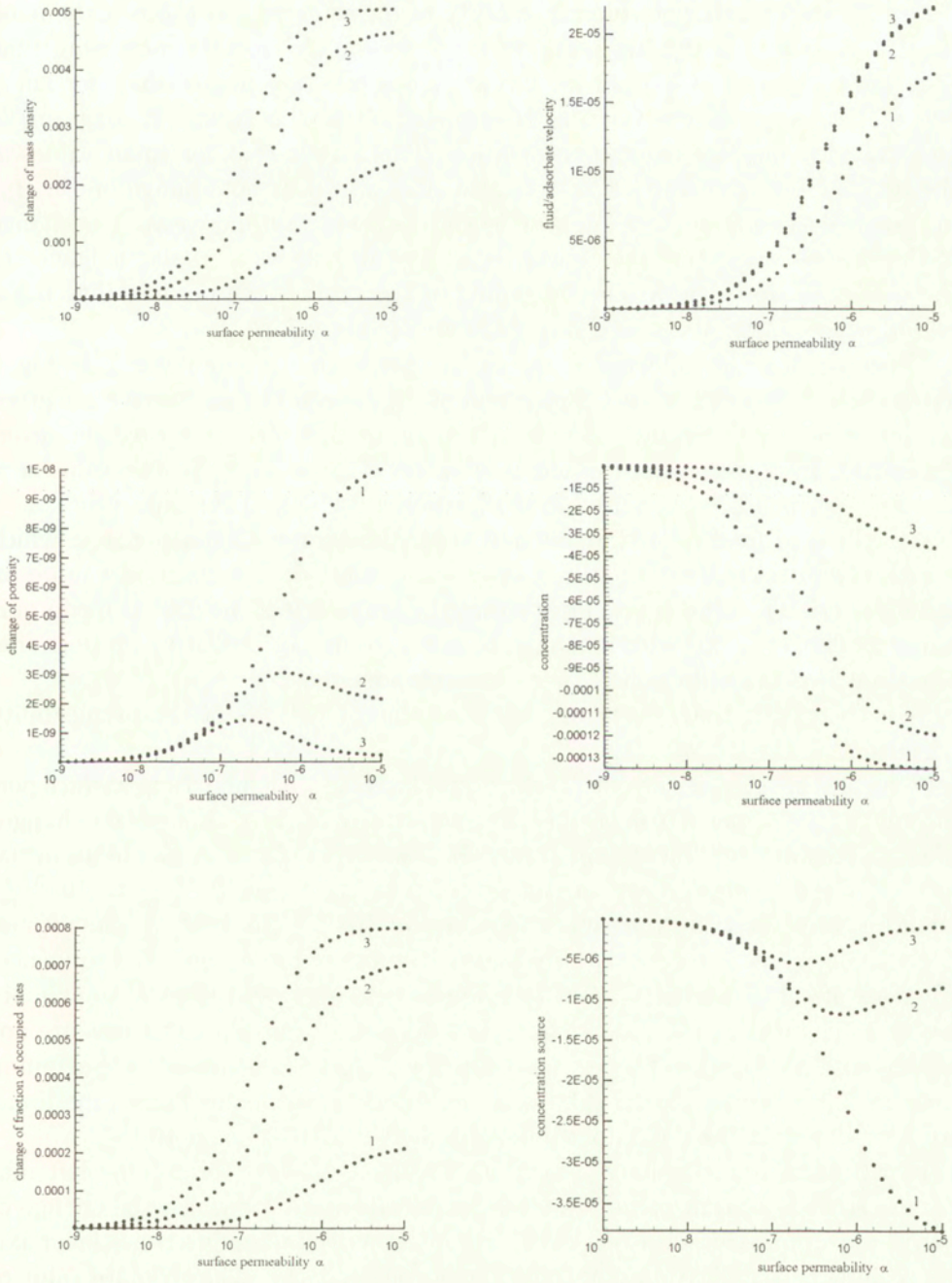

FIG. 4. Influence of the permeability parameter α on several fields and the concentration source.

diagram) react on changes in permeability in the same way as these of the mass density of liquid: at the beginning changes are small but with increasing time they become larger. Changes for larger values of π are higher than for small ones. The change of the fraction of occupied sites (the lower left diagram) is coupled with the change of concentration. This means that for small values of the permeability the fraction of occupied sites also does not change much. But in time it decreases in the same way as the concentration increases. The change of the rate of adsorption (the lower right diagram) shows a similar behavior to the change of porosity. At the beginning of the process the permeability has a big influence. Later the rate changes mainly for big values of π.

Now we show the influence of the surface permeability parameter α. In Fig. 4 again changes of fields $\rho^L, v^F, \Delta, c, \xi$ and of the concentration source $\hat{c}$ are given for the same three instants of time which we used before, this time, however, depending on α with values in the interval $10^{-9}\ \frac{\mathrm{s}}{\mathrm{m}}$ to $10^{-5}\ \frac{\mathrm{s}}{\mathrm{m}}$. The value $\alpha = 4 \cdot 10^{-8}\ \frac{\mathrm{s}}{\mathrm{m}}$ which has been used in earlier works lies within this interval.

It follows from Fig. 4 that outside of the above mentioned region – which means towards the limiting values of α – the fields do not react any more on changes of α. The limit $\alpha = 0$ means that the boundary of the porous medium is impermeable. $\alpha \to \infty$ yields a behavior similar to composites with a proportional (constant) load distribution between the components.

For the calculations we have used the value of $10^9\ \frac{\mathrm{kg}}{\mathrm{m^3 s}}$ of the permeability coefficient π.

Changes of the mass density of the liquid increase with increasing surface permeability (the upper left diagram). The sensitivity of these changes on changes of α is different in different time intervals. Namely, in our example, in an initial interval these changes react on changes of α in the range $10^{-8}\ \frac{\mathrm{s}}{\mathrm{m}}$ to $10^{-5}\ \frac{\mathrm{s}}{\mathrm{m}}$, while in later intervals it reduces to a region $10^{-8}\ \frac{\mathrm{s}}{\mathrm{m}}$ to $10^{-6}\ \frac{\mathrm{s}}{\mathrm{m}}$. Simultaneously changes become considerably bigger in these reduced regions of influence. Changes of velocity of the liquid (the upper right diagram) show a similar behavior to changes of the mass density but differences for different times are not so strongly developed as for the mass density. They are smaller at the beginning than for later times, and they become nearly identical in this large time limit. Also for this field the region of influence is between $10^{-8}\frac{\mathrm{s}}{\mathrm{m}}$ and $10^{-5}\frac{\mathrm{s}}{\mathrm{m}}$.

Changes of porosity have a very interesting behavior (the middle left diagram). For any instant of time there exists a value of α for which the change of porosity as a function of α reaches a maximum. With increasing time this maximum shifts to smaller values of α, and its value decreases. The absolute value of changes of concentration (the middle right diagram) behaves in similar manner to changes of the mass density. At the beginning of the process the surface permeability has much bigger influence on changes of concentration than for larger times. Simultaneously for each time the change of concentration as a function

of α decreases. The change of fraction of occupied sites (the lower left diagram) also changes similar to the mass density. It increases with increasing surface permeability. In a small region of influence changes are very rapid. The behavior of the source of concentration (the lower right diagram) is similar to changes of porosity. Also for this quantity there arises an extremum. At the beginning of the process changes are much bigger than for larger times.

Another important parameter of the model is the equilibrium value of porosity n_E. Its role in the model is still not fully understood. For instance, in [3] we had mentioned that for the nonlinear example without mass exchange arose problems with values of $n_E \gtrsim 0.6$. For higher values of porosity the deformations exceeded 100%, and most likely the mechanical behavior of the model should be unstable. We know as well that in many processes of practical bearing the equilibrium porosity cannot be assumed to be constant but it should rather fulfil a constitutive relation of its own. It is easy to check that such models must be nonlinear.

These questions do not arise in the present model with adsorption. The reason is that we consider linear deviations from an initial state, and, consequently, small deformations, and a linear dependence on n_E in constitutive quantities. The initial porosity itself is a constant material parameter rather than a constitutive quantity. Therefore we can admit a bigger range of n_E ($0.1 \leq n_E \leq 0.9$). Certainly solutions for fields may depend parametrically on the initial porosity in a nonlinear manner. In our model all fields but one are linear with respect to n_E. This is the field of velocity v^F. Also the source of concentration depends in a nonlinear way on n_E. We have:

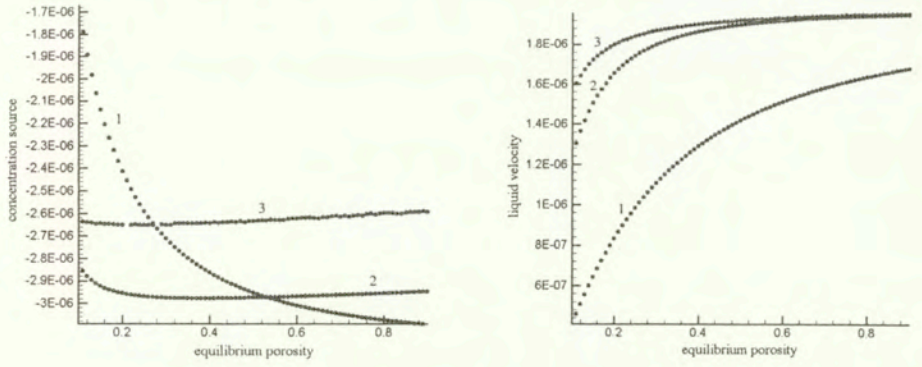

FIG. 5. Influence of the equilibrium porosity n_E on several fields and the concentration source.

The liquid velocity is, of course, zero for $n_E = 0$. For porosities in the range $0 \lesssim n_E \lesssim 0.5$ it increases rapidly with increasing porosity. The source of concen-

tration as a function of time jumps at the initial interval of time to high values for small initial porosities, and subsequently relaxes towards a constant value. A similar behavior with a smaller initial jump is visible also for bigger equilibrium porosities, but the behavior is not monotonous. For high porosities the jump does not appear at all.

The model contains another new parameter, namely the coupling parameter β. In problems of wave propagation it has high influence (see e.g. K. WILMAŃSKI [9]). Therefore it was very interesting to see that this coefficient did not have any influence in these adsorption problems.

5. Coupling of adsorption and diffusion

The most important result of the adsorption model is the form of coupling of adsorption and diffusion. It is shown how the amount adsorbed (absolute value of the concentration source) depends on the relative velocity of the components. In Fig. 6 the source of concentration over the fluid/adsorbate velocity is shown. Due to the assumption that the skeleton does not move the fluid/adsorbat velocity in our case stands for the relative velocity of the components. As follows from the boundary conditions this quantity is mainly driven by the surface permeability parameter α. According to (3.5) holds at the boundary

$$v^F = \mp \frac{\alpha \left(p^L - n p_{l/r}\right)}{\rho^L}. \tag{5.1}$$

This yields solutions for the fluid/adsorbate velocity dependent parametrically on α [1]. Therefore for calculation of the source of concentration in dependence on the velocity we choose the permeability coefficient α as a control parameter. This is done for $x = 0.5$ m, i.e. in the middle of the region.

According to the initial conditions the source starts with thevalue zero for both $(v^F - v^S,\ t = 0)$, and $\left(v^F - v^S = 0, t\right)$. Of course, the source of concentration is a negative value because the adsorbate sticks to the skeleton and the concentration in the liquid becomes lower than the initial value. The results shown in Fig. 6 are twofold: firstly one can see the characteristic time behavior of the intensity of adsorption. The concentration source decreases after a jump at the beginning of the process until it reaches a value of approximately $-3.5 \cdot 10^{-5}$. The duration of the initial jump is not clearly visible in this Figure but probably it is of the order of the relaxation time of porosity τ of 10^{-3} s (see: Sec. 3, Table with material parameters). We recall that the source of concentration consists of two contributions: the Langmuir part, and the change of the internal surface due to changes of porosity. After the initial jump (the influence of the second contribution) values increase – first rapidly and then more and more slowly (the first contribution) – until they reach an asymptotic value of nearly $-1.5 \cdot 10^{-6}$.

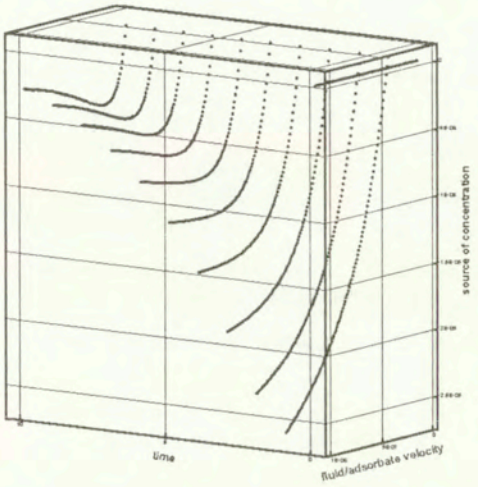

FIG. 6. Influence of diffusion

The other important feature is the dependence on the relative velocity. This also depends on the progress of the process. At the beginning the source of concentration decreases for every velocity and approaches an asymptotic value. However after a certain time lapse the curves possess a minimum with respect to the velocity dependence, and it lies in the range of relatively small velocities. With increasing time this minimum becomes stronger pronounced.

This behavior though expected can be used in practical applications to control rates of adsorption processes by changing diffusion velocities. For instance processes running along maxima would be most effective in procedures of settling the pollutants on solid filters.

6. Final Remarks

The present work on adsorption/diffusion is restricted to isothermal processes. However, it is obvious that, at least in some practically relevant mass exchange processes, it is necessary to extend the model by accounting also for chemical reactions. This requires the presence of thermal effects, and it shall be the subject of the forthcoming work. Another restriction is, that only small adsorbate concentration is allowed because we use the Langmuir theory which accounts for monolayer adsorption. If we want to describe transport processes with any concentration we have to consider multilayer adsorption which should be a further possible extension of the model.

References

1. B. ALBERS, *Coupling of adsorption and diffusion in porous and granular materials. A 1-D example of the boundary value problem,* Arch. Appl. Mech. **70**, 7, 519-531, 2000.

2. B. ALBERS, *Makroskopische Beschreibung von Adsorptions-Diffusions-Vorgängen in porösen Körpern,* PhD-Thesis, Logos-Verlag, Berlin 2000.

3. B. ALBERS, K. WILMAŃSKI, *An axisymmetric steady-state flow through a poroelastic medium under large deformations,* Arch. Appl. Mech. **69,** 2, 121 - 132, 1999.

4. S. BRUNAUER, P.H. EMMETT, E. TELLER, *Adsorption of gases in multimolecular layers,* J. Amer. Chem. Soc., **60**, 309-319, 1938.

5. S. J. GREGG, K. S. W. SING, *Adsorption, surface area and porosity,* Academic Press, London 1982.

6. P. KNABNER, *Mathematische Modelle für Transport und Sorption gelöster Stoffe in porösen Medien,* Peter Lang Verlag, Frankfurt 1991.

7. I. LANGMUIR, *The constitution and fundamental properties of solids and liquids,* Part 1, J. Am. Chem. Soc., **38**, 2221-2295, 1916. I. LANGMUIR, *The constitution and fundamental properties of solids and liquids,* Part 2, J. Am. Chem. Soc., **39**, 1848, 1917. I. LANGMUIR, *The adsorption of gases on plane surfaces of glass, mica and platinum,* J. Am. Chem. Soc., **40,** 1361-1403, 1918.

8. K. WILMAŃSKI, *A thermodynamic model of compressible porous materials with the balance equation of porosity,* Transport in Porous Media, **32**, 21-47, 1998.

9. K. WILMAŃSKI, *On weak discontinuity waves in porous materials,* [in:] M. MARQUES, J. RODRIGUES (Hrsg.), Trends in Applications of Mathematics to Mechanics, 71-83, Longman, Harlow, Essex 1995.

Received December 18, 2000; revised version August 24, 2001.

Arch. Mech., **53**, 4-5, pp. 307–317, Warszawa 2001

Possible constitutive equations of micropolar solids

GY. BÉDA

Department of Applied Mechanics
Technical University of Budapest
H-1521 Budapest, Hungary

RECENTLY THE MICROPOLAR continuum is used for investigation of some problems of solids. There exist several theories of micropolar continuum; We will study two types of them. The simplest one is Cosserat's continuum while the Eringen's model is more complicated. If the solid is not elastic then the constitutive equations are not generally known. In the paper, a method will be shown for the determination of possible constitutive equation in case of inelastic solids.

1. Introduction

THE MICROPOLAR SOLID MODEL is now frequently used in mechanics, for example for investigation of localization, material instability, plastic bodies, granular materials etc. The first micropolar model was the Cosserat continuum being the simplest model, which extends classical elasticity to a generalised form, supplementing the displacement vector field with the rotation vector field and the stress with the couple-stress tensor. Then the equations of geometry and motion contain more unknown functions than in the classical model. The rotation vector is not an independent vector; consequently, the antisymmetric part of the stress and the symmetric part of the couple-stress remain undetermined [1,2].

Eringen introduced a general theory of a nonlinear microelastic continuum. This theory in a special case contains the Cosserat continuum. Presently, there exist several approaches to the formulation of a micropolar continuum. Moreover, we should also deal with the constitutive equation of micropolar continuum because it exhibits not only the elastic behaviour [1,2].

We would like to investigate the constitutive relations or equations assuming that the second order wave exists in the micropolar solid. Function $\varphi(x_1, x_2, x_3, x_4)$, which describes the wave surface, satisfies a system of nonlinear partial differential equations. This system of partial differential equations results from the constitutive compatibility conditions. The system of partial differential equations has a solution if the Poisson-bracket is zero. It is the necessary condition of

existence of the second order waves. The sufficient condition is that the speed of propagation of wave c cannot be infinite. The necessary and sufficient conditions yield the general restriction concerning to the constitutive equations [3,4].

The second order waves are the acceleration and spin wave. When the solid is isotropic, both longitudinal and transversal waves are possible. There are four direct and reverse waves. First of all we will investigate the constitutive equations in case of the simplest theory. We use rectangular Cartesian coordinates in the following equations.

2. Possible constitutive equations of a Cosserat continuum

2.1. General equations

The fundamental equations of Cosserat continuum are equations of motion, kinematic and constitutive equations, that is, [1]

$$t_{ji,j} + q_i = \rho \dot{\nu}_i, \tag{2.1}$$

$$m_{\ell k,\ell} + \in_{kmn} t_{mn} + \ell_k = \tilde{I} \dot{w}_k, \tag{2.2}$$

$$\dot{\gamma}_{ij} = \nu_{j,i} + \varepsilon_{jik} w_k, \tag{2.3}$$

$$\dot{\kappa}_{k\ell} = w_{\ell,k}, \tag{2.4}$$

$$f_\alpha \left(\gamma_{rs,\hat{i}} , t_{rs,\hat{i}} , \kappa_{pq,\hat{j}} , m_{pq,\hat{j}} , \gamma_{rs} , t_{rs} , \kappa_{pq} , m_{pq} \right) = 0, \tag{2.5}$$

$$\alpha = 1, 2, ...18 ; \quad r, s, p, q... = 1, 2, 3, \ \hat{i}, \hat{j} = 1, 2, 3, 4,$$

where t_{ji}, $m_{\ell k}$ and q_i, ℓ_k are stress, couple-stress and body forces, couple body forces and ρ, $\tilde{I}$ are mass and inertia moment densities, γ_{ij} and $\kappa_{k\ell}$ the asymmetric strain and the torsion tensor and w_i is the rotation vector, ε_{kmn} is Levi-Civita's symbol, $\dot{v}_i$ is the acceleration vector. In all expressions of the paper we use index notation for the partial derivative of tensors like stress $t_{ji,j} \equiv \frac{\partial t_{ji}}{\partial x^j}$ etc. Indices with hat $\hat{i}$ are equal to 1,2,3,4, while if there are no hats, $q = 1, 2, 3$. Space coordinates are denoted by x_1, x_2, x_3 and $x_4 \equiv t$ is the time. Constitutive equations (2.5) are not generally well known, and for this reason we will look for their possible form.

2.2. Conditions of jumps on the acceleration wave surface

In case of acceleration waves, functions $t_{ji}, m_{\ell k}, \gamma_{ij}, \kappa_{k\ell}, v_i$ and w_k are continuous, however their derivatives have jumps on the wave surface.

Let the acceleration wave surface be $\varphi\,(x_1, x_2, x_3, x_4) = \text{const}$ or with $x_{\hat{i}}$ it is $\varphi\,(x_{\hat{i}}) = \text{const} \quad \left(\hat{i} = 1, 2, ...4\right)$. When, for example, acceleration $\dot{v}_i$ in front and behind the wave surface is denoted by $\dot{v}_i^-$ and $\dot{v}_i^+$, then the jump is $\dot{v}_i^+ - \dot{v}_i^- \equiv [\dot{v}_i]$. The jumps can be written as

$$[t_{ji,j}] \equiv \mu_{ji}\varphi_j\,,\ [\dot{\nu}_i] \equiv \beta_i\varphi_4\,,\ [\dot{\gamma}_{ij}] \equiv \Gamma_{ij}\varphi_4\,,\ \ \varphi_{\hat{i}} \equiv \frac{\partial\,\varphi}{\partial\,x^{\hat{i}}}\,,$$

$$[m_{\ell k,\ell}] \equiv \lambda_{\ell k}\varphi_\ell,\ [\dot{w}_k] \equiv \eta_k\varphi_4,\ [\dot{\kappa}_{k\ell}] \equiv \Omega_{k\ell}\varphi_4.$$

The coefficients of derivatives φ denote the appropriate amplitudes of the waves. Function φ and the amplitudes should satisfy three kinds of compatibility conditions. These are the dynamic compatibility conditions

$$\mu_{ji}\varphi_j = \rho\,\beta_i\,\varphi_4, \tag{2.6}$$

$$\lambda_{\ell k}\varphi_\ell = \tilde{I}\eta_k\varphi_4, \tag{2.7}$$

the kinematic compatibility conditions

$$\Gamma_{ij}\varphi_4 = \beta_j\varphi_i, \tag{2.8}$$

$$\Omega_{k\ell}\varphi_4 = \eta_\ell\varphi_k \tag{2.9}$$

and

$$f_\alpha\left(\gamma^\circ_{r,s,\hat{i}} + \Gamma_{rs}\varphi_{\hat{i}}\,,\ t^\circ_{rs,\hat{i}} + \mu_{rs}\varphi_{\hat{i}}\,,\,.....\right) - f^\circ_\alpha = 0 \tag{2.10}$$

$(\alpha = 1, 2, 3..., 18)$ are the constitutive compatibility conditions [3].

2.3. Constitutive equations

2.3.1. Possible constitutive equation when the stresses and couple stresses depend on the strain and torsion. Now the constitutive equations are

$$t_{ji} = f_{ji}\,(\gamma_{rs}\,,\ \kappa_{pq})\,,$$

$$m_{\ell k} = g_{\ell k}\,(\gamma_{rs}\,,\ \kappa_{pq})\,.$$

Let us form the time-derivatives of these equations. We obtain

$$\dot{t}_{ji} = \frac{\partial f_{ji}}{\partial \gamma_{rs}}\dot{\gamma}_{rs} + \frac{\partial f_{ji}}{\partial \kappa_{pq}}\dot{\kappa}_{pq} \equiv A_{jirs}\dot{\gamma}_{rs} + B_{jk\ell}\dot{\kappa}_{k\ell}, \tag{2.11}$$

$$\dot{m}_{\ell k} = \frac{\partial g_{\ell k}}{\partial \gamma_{rs}}\dot{\gamma}_{rs} + \frac{\partial g_{k\ell}}{\partial \kappa_{pq}}\dot{\kappa}_{pq} \equiv D_{\ell krs}\dot{\gamma}_{rs} + E_{\ell kpq}\dot{\kappa}_{pq}. \tag{2.12}$$

The constitutive compatibility conditions are obtained from equations (2.11) and (2.12), have the form

$$\mu_{ji} = A_{jirs}\Gamma_{rs} + B_{jik\ell}\Omega_{k\ell}, \tag{2.13}$$

$$\lambda_{\ell k} = D_{\ell krs}\Gamma_{rs} + E_{\ell kpq}\Omega_{pq}. \tag{2.14}$$

Using the unit normal vector n_i of the wave front and the wave speed c, that is,

$$n_i \equiv \frac{\varphi_i}{\sqrt{\varphi_j\varphi_j}}, \qquad c \equiv -\frac{\varphi_4}{\sqrt{\varphi_j\varphi_j}},$$

we obtain the wave propagation equation from the dynamic, kinematic and constitutive equations [3,4]:

$$\left(A_{jirs}n_jn_r - \rho c^2\delta_{si}\right)\beta_s + B_{jik\ell}n_jn_\ell\eta_k = 0, \tag{2.15}$$

$$D_{qprs}n_qn_r\beta_s + \left(E_{qpk\ell}n_qn_\ell - \tilde{I}c^2\delta_{pk}\right)\eta_k = 0, \tag{2.16}$$

or in invariant (or matrix) form:

$$\left(\underline{\underline{A}} - pc^2\underline{\underline{I}}\right)\cdot\underline{\beta} + \underline{\underline{B}}\cdot\underline{\eta} = \underline{0}, \tag{2.17}$$

$$\underline{\underline{D}}\cdot\underline{\beta} + \left(\underline{\underline{E}} - \tilde{I}c^2\underline{\underline{I}}\right)\cdot\underline{\eta} = \underline{0}. \tag{2.18}$$

The acceleration and spin waves exist, therefore the amplitudes $\underline{\beta}$ and $\underline{\eta}$ cannot be zero. Thus the corresponding determinant should be equal to zero, namely

$$\det\left[\underline{\underline{D}} - \left(\underline{\underline{E}} - \tilde{I}c^2\underline{\underline{I}}\right)\cdot\underline{\underline{B}}^{-1}\left(\underline{\underline{A}} - \rho c^2\underline{\underline{I}}\right)\right] = 0, \tag{2.19}$$

if $\det\left(\underline{\underline{B}}\right) \neq 0$. Equation (2.19) is wave speed equation, which has at least four positive roots c. These roots are the propagation speeds of the wave.

Additional special cases are the following:

CASE (A1). The couple-stress tensor does not depend on strain γ_{rs}, that is $\frac{\partial g_{\ell k}}{\partial \gamma_{rs}} \equiv 0$ if $\underline{\underline{D}} \equiv 0$. Now we obtain two equations for the wave speed: one for the acceleration wave the other for the spin wave. They are

$$\det\left(\underline{\underline{A}} - \rho c^2 \underline{\underline{I}}\right) = 0, \tag{2.20}$$

and

$$\det\left(\underline{\underline{E}} - \tilde{I} c^2 \underline{\underline{I}}\right) = 0. \tag{2.21}$$

The acceleration and the spin waves are independent of each other.

CASE (A2). The couple-stress is independent of the strain and the stress is independent of the torsion tensor, that is

$$\frac{\partial g_{\ell k}}{\partial \gamma_{rs}} \equiv 0 \quad \text{or} \quad \underline{\underline{D}} \equiv 0 \quad \text{and} \quad \frac{\partial f_{ji}}{\partial \kappa_{k\ell}} \equiv 0 \quad \text{or} \quad \underline{\underline{B}} = \underline{\underline{0}} .$$

The wave speed equations are (2.20) and (2.21) again. These equations can be obtained from (2.17) and (2.18).

CASE (A3). Assume that the inertia moment $\tilde{I}$ is very small. We obtain from Eqs. (2.17) and (2.18)

$$\underline{\eta} = -\underline{\underline{E}}^{-1} \cdot \underline{\underline{D}} \cdot \underline{\beta} \quad \text{therefore} \quad \tilde{I} \equiv 0$$

and the wave speed equation

$$\det\left[\underline{\underline{A}} - \underline{\underline{B}} \cdot \underline{\underline{E}}^{-1} \cdot \underline{\underline{D}} - \rho c^2 \underline{\underline{I}}\right] = 0. \tag{2.22}$$

The spin wave propagates together with the acceleration wave.

2.3.2. The stress and couple-stress depend on strain and torsion and also on their rates. The possible constitutive equations are

$$\dot{t}_{ji} = F_{ji}\left(\dot{\gamma}_{rs}\,,\ \dot{\kappa}_{pq}\,,\ \gamma_{rs}\,,\ \kappa_{pq}\right), \tag{2.23}$$

$$\dot{m}_{\ell k} = G_{\ell k}\left(\dot{\gamma}_{rs}\,,\ \dot{\kappa}_{pq}\,,\ \gamma_{rs}\,,\ \kappa_{pq}\right). \tag{2.24}$$

Now the constitutive compatibility conditions are

$$\mu_{ji}\varphi_4 = F_{ji}\left(\dot{\gamma}^{\circ}_{rs} + \Gamma_{rs}\varphi_4\,,\ \dot{\kappa}^{\circ}_{pq} + \Omega_{pq}\varphi_4\,,\ \gamma_{rs}\,,\ \kappa_{pq}\right) - F^{\circ}_{ji}, \tag{2.25}$$

$$\lambda_{\ell k}\varphi_4 = G_{\ell k}\left(\dot{\gamma}^{\circ}_{rs} + \Gamma_{rs}\varphi_4\,,\ \dot{\kappa}^{\circ}_{pq} + \Omega_{pq}\varphi_4\,,\ \gamma_{rs}\,,\ \kappa_{pq}\right) - G^{\circ}_{\ell k}, \tag{2.26}$$

where γ°_{rs} and κ°_{pq} are the strain and torsion rate in front of the wave surface. The constitutive compatibility equations have the form of a system of first order nonlinear partial differential equations. Considering its characteristic equations and using the dynamic and kinematic compatibility conditions, we obtain the wave propagation equations [3,4]

$$\mu_{ji}\varphi_4 = F_{ji}\left(\dot{\gamma}^{\circ}_{rs} + \Gamma_{rs}\varphi_4\,,\ \dot{\kappa}^{\circ}_{pq} + \Omega_{pq}\varphi_4\,,\ \gamma_{rs}\,,\ \kappa_{pq}\right) - F^{\circ}_{ji}, \tag{2.27}$$

$$\lambda_{\ell k}\varphi_4 = G_{\ell k}\left(\dot{\gamma}^{\circ}_{rs} + \Gamma_{rs}\varphi_4\,,\ \dot{\kappa}^{\circ}_{pq} + \Omega_{pq}\varphi_4\,,\ \gamma_{rs}\,,\ \kappa_{pq}\right) - G^{\circ}_{\ell k}, \tag{2.28}$$

or in invariant form

$$\left(\underline{\underline{A}}^{*} - \rho\, c^2 \underline{\underline{I}}\right)\cdot\underline{\beta} + \underline{\underline{B}}^{*}\cdot\underline{\eta} = \underline{0}, \tag{2.29}$$

$$\underline{\underline{D}}^{*}\cdot\underline{\beta} + \left(\underline{\underline{E}}^{*} - \tilde{I}c^2\underline{\underline{I}}\right)\cdot\underline{\eta} = \underline{0}. \tag{2.30}$$

Equations (2.29) and (2.30) are similar as (2.17) and (2.18).

We can speak about cases A1, A2 and A3 similarly as it was done in Sec. 2.3.1. in cases B1, B2 and B3, and the conclusions are similar, too.

2.3.3. An important conclusion of the general constitutive equations [3,4]. We return to the general constitutive equations, (2.5) and the compatibility conditions (2.10). Constitutive compatibility conditions (2.10) form a system of first order nonlinear partial differential equations with respect to $\varphi\left(x_{\hat{i}}\right)$. This system has a solution if the Poisson bracket is equal to zero, that is if

$$\left(\frac{\partial f_\alpha}{\partial \varphi_{\hat{i}}}\frac{\partial f_\beta}{\partial x_{\hat{i}}} - \frac{\partial f_\alpha}{\partial x_{\hat{i}}}\frac{\partial f_\beta}{\partial \varphi_{\hat{i}}}\right) = 0. \tag{2.31}$$

It is satisfied if the constitutive equations are written in form

$$f_\alpha\left(\tau_{rs\hat{i}}\,,\ \vartheta_{pq\hat{j}}\,,\ \gamma_{rs}....m_{pq}\right) = 0,$$

where $\tau_{rs,\hat{i}}$ and $\vartheta_{pq,\hat{j}}$ mean connections among $t_{rs,\hat{i}}$, $\gamma_{k\ell,\hat{j}}$, $m_{pq,\hat{j}}$, $\kappa_{k\ell,\hat{j}}$

$$\tau_{rs\hat{i}} \equiv t_{rs,\hat{i}} + H_{rsk\ell\hat{i}\hat{j}}\,\gamma_{k\ell,\hat{j}},$$
$$\vartheta_{pq\hat{j}} \equiv m_{pq,\hat{j}} + L_{pqk\ell\hat{j}\hat{i}}\,\kappa_{k\ell,\hat{j}}$$

if the next equations satisfy

$$\delta_{\hat{j}\hat{p}}\mu_{rs,\hat{i}} + H_{k\ell rs\hat{j}\hat{p}}\,\Gamma_{k\ell,\hat{i}} = 0,$$
$$\delta_{\hat{j}\hat{p}}\lambda_{rs,\hat{i}} + L_{k\ell rs\hat{j}\hat{p}}\,\Omega_{k\ell,\hat{i}} = 0$$

thus we may reduce the number of tensorial variables in equations (2.5) from 8 to 6.

3. Basic variables and connections of Eringen's continuum

The Eringen continuum consists of macroelements. A macroelement is divided into microelements. The microelements form a nonpolar continuum. Let $\bar{x}_k$ be the particle of a microelement and x_k – the mass centre of the macroelement in the spatial configuration. Similarly, $\overline{X}_K$ and X_K are the particle and the centre of mass in the reference configuration. The followings define vectors $\overline{p}_k$ and $\overline{P}_K$ in the spatial and reference configurations:

$$\overline{x}_k = x_k + \eta_{kK}\overline{P}_K$$

and

$$\overline{X}_K = X_K + \zeta_{Kk}\overline{P}_k\,.$$

The geometrical relations between the two configurations are written in the form:

$$d\overline{x}_k = \left(x_{k,K} + \eta_{kL,K}\overline{P}_L\right) dX_K + \eta_{kK}d\overline{P}_K,$$

$$d\overline{X}_K = \left(X_{K,k} + \zeta_{K\ell}d\overline{p}_\ell\right) dx_k + \zeta_{Kk}d\overline{p}_k,$$

the deformation gradient and microdeformation gradient are

$$x_{k,K} = (\delta_{LK} + U_{L,K})\ \delta_{kL}$$

and

$$\eta_{kK} = (\delta_{LK} + \psi_{LK})\ \delta_{kL}\,,$$

or their inverse tensors

$$X_{K,k} = (\delta_{\ell k} - u_{\ell,k})\ \delta_{K\ell}$$

and

$$\zeta_{Kk} = (\delta_{\ell k} - \psi_{\ell k})\ \delta_{K\ell},$$

where u_ℓ, U_L and $\psi_{\ell k}$, Ψ_{LK} are the displacement vector and the microdisplacement gradient in the spatial and reference configurations. Let us denote the Euler's strain by $\gamma_{k\ell}$ and the first and second microdeformation tensors by $\kappa_{k\ell}$ and $\gamma_{k\ell m}$. According to [2], they can be expressed by the following formulae:

$$2\gamma_{k\ell} = u_{k,\ell} + u_{\ell,k} - u_{m,k}u_{m,\ell},$$

$$\kappa_{k\ell} = \psi_{k\ell} + u_{\ell,k} - u_{m,k}\psi_{m\ell},$$

$$\gamma_{k\ell m} = -\psi_{k\ell,m} + u_{n,k}\psi_{n\ell,m}.$$

From these formulae we obtain the kinematic equations by differentiating with respect to time, that is,

$$\dot{\gamma}_{k\ell} = \nu_{k\ell} - \left(\gamma_{km}\nu_{m,\ell} + \gamma_{m\ell}\nu_{m,k}\right), \tag{3.1}$$

$$\dot{\kappa}_{k\ell} = \alpha_{k\ell} + \nu_{\ell,k} - (\kappa_{km}\alpha_{m\ell} + \kappa_{m\ell}\nu_{m,k}), \tag{3.2}$$

$$\dot{\gamma}_{k\ell m} = -\alpha_{k\ell,m} + \kappa_{kr}\alpha_{r\ell,m} - (\gamma_{k\ell r}\nu_{r,m} + \gamma_{krm}\alpha_{r\ell} + \gamma_{r\ell m}\nu_{r,k}), \tag{3.3}$$

where $v_{k,\ell}$ is the velocity gradient and $\alpha_{k\ell} = \dot{\eta}_{kK}\zeta_{K\ell}$ is microrotation tensor.

Let us interpret the densities of internal force system in both macro- and microstructures. Denote by dV and $d\overline{V}$ the volumes of macro- and microelements. These volumes are bounded by closed surfaces dA and $d\overline{A}$. If $\bar{t}_{k\ell}$ is the microstress on $d\overline{A}_k$ then $t_{k\ell}$ is the macrostress on dA_k, that is, $\int\limits_{dA} \bar{t}_{k\ell} d\overline{A}_k = t_{k\ell} dA_k$. Similarly we can introduce

$$\int\limits_{dV} \overline{q}_k d\overline{V} = q_k dV,$$

$$\int\limits_{dA} \bar{t}_{k\ell}\overline{p}_m d\overline{A_k} = \lambda_{k\ell m} dA_k\,, \quad \int\limits_{dV} \overline{q}_k \overline{p}_m d\overline{V} = \ell_{km} dV,$$

$$\int\limits_{dV} \overline{s}_{m\ell} d\overline{V} = s_{m\ell} dV\,, \quad s_{m\ell} = s_{\ell m},$$

for body force q_k, couple-stress $\lambda_{k\ell m}$, couple body force ℓ_{km} and microstress $s_{m\ell}$ on dV.

Equations of motion are [2]

$$t_{k\ell,k} + q_\ell = \rho \dot{v}_\ell, \tag{3.4}$$

$$t_{k\ell} - s_{k\ell} + \lambda_{p\ell m,p} + \ell_{\ell k} = \rho \dot{\pi}_{\ell k}, \tag{3.5}$$

where $\dot{v}_k$ is the acceleration, $\rho\, i_{nm}$ is Euler's inertia tensor and $\dot{\pi}_{kn}$ – the spin tensor. Following [2], they are expressed by the formulae

$$\int\limits_{dV} \overline{\rho}\,\overline{p}_m \overline{p}_n d\overline{V} = \rho\, i_{mn} dV,$$

$$\dot{\pi}_{kn} \equiv i_{mn}\,(\dot{\alpha}_{km} + \alpha_{k\ell}\alpha_{\ell m})\,.$$

We look for the constitutive equations in the following form

$$t_{k\ell} = f_{k\ell}\,(\gamma_{pq}\,,\, \kappa_{pq}\,,\, \gamma_{pqr})\,, \tag{3.6}$$

$$\lambda_{k\ell m} = g_{k\ell m}\,(\gamma_{pq}\,,\, \kappa_{pq}\,,\, \gamma_{pqr})\,, \tag{3.7}$$

$$s_{k\ell} = k_{k\ell}\left(\gamma_{pq}, \kappa_{pq}, \gamma_{pqr}\right). \tag{3.8}$$

We use the material time derivative of the system of equations (3.6)–(3.7), that is,

$$\dot{t}_{k\ell} = \frac{\partial f_{k\ell}}{\partial \gamma_{pq}}\dot{\gamma}_{pq} + \frac{\partial f_{k\ell}}{\partial \kappa_{pq}}\dot{\kappa}_{pq} + \frac{\partial f_{k\ell}}{\partial \gamma_{pqr}}\dot{\gamma}_{pqr} \equiv F_{k\ell pq}\dot{\gamma}_{rq} + A_{k\ell pq}\dot{\kappa}_{pq} + B_{k\ell pqr}\dot{\gamma}_{pqr}$$

$$\dot{\lambda}_{k\ell m} = \frac{\partial g_{k\ell m}}{\partial \gamma_{pq}}\dot{\gamma}_{pq} + \frac{\partial g_{k\ell m}}{\partial \kappa_{pq}}\dot{\kappa}_{pq} + \frac{\partial g_{k\ell m}}{\partial \gamma_{pqr}}\dot{\gamma}_{pqr}$$

$$\equiv H_{k\ell mpq}\dot{\gamma}_{rq} + D_{k\ell mpq}\dot{\kappa}_{pq} + E_{k\ell mpqr}\dot{\gamma}_{pqr}.$$

We determine the microstress $s_{m\ell}$ from (3.5) by taking its symmetric part.

The jumps of the deformations and internal force system and their derivatives on wave surface φ can be written as

$$[\gamma_{k\ell}] = 0, \quad [\kappa_{k\ell}] = 0, \quad [\gamma_{k\ell m}] = 0, \quad [\alpha_{k\ell}] = 0, \quad [\psi_{m\ell}] = 0,$$

$$[\psi_{k\ell,m}] = 0, \quad [t_{k\ell}] = 0, \quad [s_{k\ell}] = 0, \quad [\lambda_{k\ell m}] = 0,$$

$$[\dot{\gamma}_{k\ell}] = \Gamma_{k\ell}\varphi_4, \quad [\dot{\kappa}_{k\ell}] = \Omega_{k\ell}\varphi_4, \quad [\dot{\gamma}_{k\ell m}] = \vartheta_{k\ell m}\varphi_4,$$

$$[\dot{\alpha}_{k\ell}] = \sigma_{k\ell}\varphi_4, \quad [t_{k\ell,k}] = \mu_{k\ell}\varphi_k, \quad [\lambda_{p\ell m,p}] = \Lambda_{p\ell m}\varphi_p.$$

The dynamic, kinematic and constitutive compatibility equations are

$$\mu_{k\ell}\varphi_k = \rho\beta_\ell\varphi_4,$$

$$\Lambda_{k\ell m}\varphi_k = \rho\, i_{nm}\sigma_{\ell n}\varphi_4,$$

$$2\Gamma_{k\ell}\varphi_4 = aL_{k\ell m}\beta_m,$$

$$\Omega_{k\ell m}\varphi_4 = aM_{k\ell m}\beta_m,$$

$$\vartheta_{k\ell m}\varphi_4 = -a\left(M_{mkp}\sigma_{p\ell} + N_{mk\ell r}\beta_r\right),$$

$$\mu_{pq} = A_{pqk\ell}\Omega_{k\ell} + B_{pqk\ell}\vartheta_{k\ell m} + F_{pqk\ell}\Gamma_{k\ell},$$

$$\Lambda_{pqr} = D_{pqrk\ell}\Omega_{k\ell} + E_{pqrk\ell m}\vartheta_{k\ell m} + H_{pqrk\ell}\Gamma_{k\ell},$$

where

$$L_{k\ell m} \equiv (\delta_{km} - 2\gamma_{km})\, n_\ell + (\delta_{\ell m} - 2\gamma_{\ell m})\, n_k,$$

$$M_{k\ell m} \equiv n_k\left(\delta_{m\ell} - \kappa_{m\ell}\right), \quad N_{mk\ell r} \equiv n_m\gamma_{k\ell r} + n_k\gamma_{r\ell m},$$

$$a \equiv (\varphi_j\varphi_j)^{\frac{1}{2}}.$$

We use equations of motion (3.4), (3.5), kinematic equations (3.1) – (3.3) and the constitutive equations in the form (3.9), (3.10). The wave propagation equations are

$$\left\{n_p\left(A_{pqk\ell}M_{k\ell r}-B_{pqk\ell m}N_{mk\ell r}+\frac{1}{2}F_{pqk\ell}L_{k\ell r}\right)-\rho c^2\delta_{qr}\right\}\beta_r - n_pB_{pqk\ell m}N_{mkr}\sigma_{r\ell}=0,$$

$$n_p\left(D_{pqrk\ell}M_{k\ell s}-E_{pqrk\ell m}N_{mk\ell s}+\frac{1}{2}H_{pqrk\ell}L_{k\ell s}\right)\beta_s - \left(n_pB_{pqrk\ell m}N_{mks}+\rho i_{\ell r}\delta_{sq}\right)\sigma_{\ell s}=0.$$

The wave propagation equations in invariant form are

$$\left(\underline{\underline{A}}^{**}-\rho c^2\underline{\underline{I}}\right)\cdot\underline{\beta}-\underline{\underline{\underline{B}}}^{**}..\underline{\underline{\sigma}}=\underline{0},$$

$$\underline{\underline{\underline{D}}}^{**}\cdot\underline{\beta}-\left(\underline{\underline{\underline{E}}}^{**}+\rho c^2\underline{\underline{\underline{J}}}\right)..\underline{\underline{\sigma}}=\underline{0}.$$

These equations are similar to (2.17) and (2.18) if $\underline{\underline{\underline{G}}}^{**}=0$ or $\underline{\underline{\underline{E}}}^{**}+\rho c^2\underline{\underline{\underline{J}}}\approx\underline{\underline{\underline{E}}}^{**}$. These can be investigated as it was already shown.

The wave propagation equations are a system of linear homogeneous algebraic equations for $\underline{\beta}$ and $\underline{\sigma}$. The determinant of the system is equal to zero. This equation is called the wave speed equation, which has at least eight real roots c with different signs [3]. The existence of the roots results from the constitutive equations.

4. Conclusions

These investigations show the general behaviour of the possible constitutive equations. It follows that the investigations are similar for the Cosserat continuum and the special Eringen continuum. However, in case of the Eringen continuum, the determination of a more general internal force system is possible. In both cases the investigation is based on the existence and regular (nonzero wave-speed) propagation of acceleration and speed waves. Such waves may be coupled or independent for various constitutive equations.

The results may also be useful for experimental works: they show what kind of data of wave propagation should be measured to obtain numerical values for the constitutive equations.

Acknowledgements

This work was partly supported by the National Scientific Research Fund of Hungary under contracts OTKA T022163 and T034535.

References

1. W. NOWACKI, *Theory of micropolar elasticity*, Springer, Wien–New York 1970.
2. A. C. ERINGEN, *Theory of Micropolar Elasticity* [in:] *Fracture on advanced treatise*, Vol. II, 621-729, H. LIEBOWITZ [Ed.], Academic Press, New York 1968.
3. GY. BÉDA, *Constitutive equations and nonlinear waves*, Nonlin. Anal. Theory, Methods and Appl. **30**, 1, 397-407, 1997.
4. GY. BÉDA, P. B. BÉDA, *A study on constitutive relations of copper using the acceleration waves and the theory of dynamic systems*, Proc. Estonian Acad. Scis. Eng. **5**, 2, 101-111, 1999.

Received February 19, 2001; revised version September 10, 2001.

Arch. Mech., **53**, 4-5, pp. 319–331, Warszawa 2001

Constitutive relations for dynamic material instability at finite deformation

P. B. BÉDA

Technical University Budapest,
Department of Mechanics,
Budapest, Hungary

THIS PAPER AIMS to present a mathematically consistent formulation of the second gradient dependence in the constitutive equations for material instability phenomena in case of finite deformations. Thus the set of fundamental equations of the solid continuum (the kinematic equations, the Cauchy equations of motion and the constitutive equations) should also be written for finite deformations. Two basic properties are required: the existence and regular propagation of waves and the generic behavior at the loss of stability. Firstly, the wave dynamics is studied. To encounter the second gradient effects, we should use the third order waves here. Secondly, the system of fundamental equations completed with initial and boundary value conditions forms a dynamical system. Then, identifying material stability with Lapunov stability of a state of the continuus body, the loss of stability should be one of the two basic types of instabilities of dynamical systems: a static or a dynamic bifurcation. These instability modes should be strictly different for a generic dynamical system.

1. Introduction

IN THE RECENT YEARS, the study of material instability problems received an increasing interest [8, 13]. However, most of the investigations published dealt with small deformations and static or quasi-static loading conditions. To perform works encounter also dynamic effects with high rate loadings we need appropriate constitutive equations. Such materials were studied by postulating the existence of a (second order) acceleration wave with finite wave speed [2].

Unfortunately, the constitutive theory based on the second order waves cannot include such cases of non-locality as the so-called second gradient materials [16] being widely used for numerical investigations of post-localization. The effect of inclusion of second gradient terms and the difficulties in dynamic studies can be described by applying the theory of dynamical systems [5, 6]. Dynamical systems are widely used for (Lapunov) stability investigations of various cases. Quite recently we obtained results for the forms of possible constitutive relations

by combining the acceleration wave dynamics and the theory of dynamical systems [4].

The aim of the paper is to find constitutive formulation for non-local material instability problems. The definition of material stability/instability is based on the Lapunov stability concept of the theory of dynamical systems (see [5] for the details) for this reason we call it "dynamic material instability". We assume for the solid body that a generalized wave exists in the derivative of the acceleration field [7] and this singular surface propagates forwards and backwards with finite velocities. From that assumption, the conditions are obtained for the second order derivatives of the variables of the constitutive equations. Additionally we assume that the loss of stability should be a generic [1] one in terms of the theory of dynamical systems [15], which is essential in dealing with instability problems. There are two main points at this topic. The one is quite practical: a numerical solution of the material instability problems in non-generic case may suffer serious technical difficulties (loss of convergence, mesh sensitivity [8] etc.). The other is of theoretical significance. By modeling physical phenomena we should obtain a set of equations which is typical (or generic), that is, differs only a little from the "exact unknown mathematical model". This modeling concept is treated in details by FARKAS [10].

All the studies are performed for finite deformations. The resulting constitutive equations are suitable for solving material stability/instability problems with large deformations.

The second section presents the set of fundamental equations of the solid continuum at large deformation. It consists of the Cauchy equtions of motion, the kinematic equation (for large displacements) and the constitutive equations. Constitutive formulation should satisfy the so-called Axiom of Objectivity, that is, should be form-invariant under arbitrary rigid motions of the spatial frame of reference and a constant shift of the origin in time. As a special case, this requirement includes the invariance under Galilean transformation (see for example [9] or [12]). Such physically objective quantities are the Lie derivative of the stress gradient tensor, the Lie derivative of the (Euler) strain gradient tensor and the second covariant derivative of the stress and strain tensors.

In the next section, a dynamical wave study of constitutive equations is applied based on the existence of a third order generalized wave with regular propagation properties. Here the wave speed equation [2] derived from the fundamental equations implies conditions (Wave Dynamical Condition, WDC) for the existence of the required waves.

In the fourth section, as an application of wave dynamical theory, we perform a material instability investigation for finite displacements with an appropriate constitutive equation in uniaxial case. In this section, the wave speed equation is a scalar third order algebraic equation and should have real nonzero solutions

[2]. By using dynamical systems theory we should be able to study a generic behavior (as it is defined in the theory of dynamical systems [5]) at the loss of stability because of the aforementioned general modeling concept of physical phenomena. Thus we obtain additional conditions. There are two different ways for the loss of stability of a dynamical system [15]. These are the so-called static and dynamic bifurcations and should be strictly different phenomena (Dynamical Systems Condition, DSC). Thus the system of fundamental equations (especially the constitutive equation) should meet both the WDC and DSC requirements.

2. The basic equations for large deformation

If we would like to have constitutive equations containing the second (physically objective) derivatives of the stress and strain tensors, we should need besides the conventional equations of motion

$$t^{kp}_{;p} + q^k = \rho \dot{v}^k, \quad t^{kp} = t^{pk}, \tag{2.1}$$

also the equation of motion for the Lie derivative of the stress tensor [3, 7]

$$\left(L_v t^{kp}\right)_{;p} + \left(t^{qp} v^k_{;q} + t^{kp} v^s_{;s}\right)_{;p} + \dot{q}^k - q^s v^k_{;s} = \rho \left(\ddot{v}^k - \dot{v}^s v^k_{;s} - \dot{v}^k v^s_{;s}\right), \tag{2.2}$$

where

$$L_v t^{kp} \equiv \dot{t}^{kp} - t^{ks} v^p_{;s} - t^{ps} v^k_{;s}$$

denotes the Lie derivative of the stress tensor. Here, in (2.1), (2.2) and in all further equations and expressions, Roman indices run from 1 to 3.

For finite deformation

$$v_{ij} = L_v\left(a_{ij}\right), \tag{2.3}$$

where

$$L_v a_{ij} \equiv \dot{a}_{ij} + a_{ip} v^p_{;j} + a_{pj} v^p_{;i}.$$

Then the kinematic equation is written for the Lie derivative of the deformation rate tensor

$$\begin{aligned} L_v\left(v_{ij}\right) = {} & \ddot{a}_{ij} + a_{ik}\dot{v}^k_{;j} + a_{kj}\dot{v}^k_{;i} + 2\dot{a}_{ik} v^k_{;j} \\ & + 2\dot{a}_{kj} v^k_{;i} + a_{ik} v^k_{;\ell} v^\ell_{;j} + a_{kj} v^k_{;\ell} v^\ell_{;i} + 2 a_{\ell k} v^k_{;j} v^\ell_{;i} \end{aligned} \tag{2.4}$$

The notations are: q^k denotes the body force, ρ is the mass density, $X^K_{,p}$ is the deformation gradient, g_{pq}, G_{KL} are metric tensors in the current and the initial

configurations, v^i and $v^i_{;j}$ are velocity and velocity gradient, v_{ij} is the deformation rate tensor. Cauchy stress tensor is denoted by t^{pk}, and

$$a_{ik} = \frac{1}{2}\left(g_{ik} - X^K_{,i} X^L_{,k} G_{KL}\right)$$

denotes the Euler strain tensor, respectively. Semicolon means covariant derivative and an overdot indicates material time derivative:

$$\dot{v}^i = \frac{\partial v^i}{\partial \tau} + v^k v^i_{;k},$$

where τ denotes time. Remark that brackets used at the Lie derivative preserve upper and lower indices as in (2.3); we use them to show clearly for which variable it is applied. (For example $L_v\left(t^{kp}_{\ ;\ell}\right)$ is the Lie derivative of the covariant derivative of the stress tensor t^{kp} and not the covariant derivative of the Lie derivative.) Assume that the constitutive equation has the form

$$f_\alpha\left(L_v\left(t^{kp}_{\ ;\ell}\right), L_v\left(a_{ij;\ell}\right), t^{kp}_{\ ;\ell m}, a_{ij;\ell m}\right) = 0, \tag{2.5}$$

where $\alpha = 1, 2, \ldots, 6$. We use physically objective quantities such as

- the Lie derivative of the stress gradient tensor

$$L_v\left(t^{kp}_{\ ;\ell}\right) = \left(t^{kp}_{\ ;\ell}\right)^{\cdot} - t^{qp}_{\ ;\ell} v^k_{;q} - t^{kq}_{\ ;\ell} v^p_{;q} + t^{kp}_{\ ;q} v^q_{;\ell},$$

- the Lie derivative of the (Euler) strain gradient tensor,

$$L_v\left(a_{ij;k}\right) = \left(a_{ij;k}\right)^{\cdot} + a_{qj;k} v^q_{;i} + a_{iq;k} v^q_{;j} + a_{ij;q} v^q_{;k},$$

- the second covariant derivative of the stress tensor $t^{kp}_{\ ;\ell m}$,
- the second covariant derivative of the strain $a_{ij;\ell m}$.

In the set of equations (2.2), (2.4) and (2.5), the number of scalar variables and equations are the same thus it can be considered the set of fundamental equations. Remark that the continuity equation for ρ can also be introduced, but it is not necessary for the following calculations. Moreover,the dissipation inequality should also be satisfied

$$\dot{s} = {}_D t^{ij} L_v\left(a_{ij}\right) > 0, \tag{2.6}$$

where s denotes entropy and ${}_D t^{ij}$ is the dissipative part of the stress tensor. Introducing also the reversible part ${}_E t^{ij}$ we have

$$t^{ij} = {}_E t^{ij} + {}_D t^{ij},$$

and by introducing the elasticity tensor $C^{ijk\ell}$

$$ {}_D t^{ij} = t^{ij} - C^{ijk\ell} a_{k\ell} \, . $$

Thus (2.6) implies

$$ t^{ij} L_v (a_{ij}) - C^{ijk\ell} a_{k\ell} L_v (a_{ij}) > 0. \tag{2.7} $$

3. A wave dynamical theory of constitutive equations

As promised in the Introduction, assume that there are jumps in the second derivatives of stress and strain and in the third derivative of acceleration fields along surface $\varphi (x^i, \tau) = 0$, that is,

$$ \begin{aligned} \left[\left(t^{kp}{}_{;\ell}\right)^{\cdot}\right] &= \gamma^{kp} (\varphi_4 + \nu^n \varphi_n) \varphi_\ell, \\ [(a_{ij;k})^{\cdot}] &= \alpha_{ij} (\varphi_4 + \nu^n \varphi_n) \varphi_k, \\ \left[\left(v^k{}_{;q}\right)^{\cdot}\right] &= -\nu^k (\varphi_4 + \nu^n \varphi_n) \varphi_q, \\ \left[\ddot{v}^k\right] &= \nu^k (\varphi_4 + \nu^n \varphi_n)^2 , \end{aligned} \tag{3.1} $$

where jumps are denoted by [ ] and $\varphi_k = \frac{\partial \varphi}{\partial x^k}$ and $\varphi_4 = \frac{\partial \varphi}{\partial \tau}$. There are no jumps in other derivatives. The dynamic, kinematic and constitutive compatibility conditions can be obained by using (3.1).

The wave speed can be expressed as

$$ c = -\frac{\varphi_4 + \nu^n \varphi_n}{\sqrt{g^{k\ell} \varphi_k \varphi_\ell}}, $$

and the unit normal vector of the wave front reads $n_p = \frac{\varphi_p}{\sqrt{g^{k\ell} \varphi_k \varphi_\ell}}$.
The set of the dynamical compatibility conditions are

$$ \left[\left(L_v t^{kp}\right)_{;p}\right] + \left[\left(t^{qp} v^k_{;q} + t^{kp} v^s_{;s}\right)_{;p}\right] + \left[\dot{q}^k + q^k v^s_{;s} - q^s v^k_{;s}\right] = \left[\rho \left(\ddot{v}^k - \dot{v}^s v^k_{;s}\right)\right], \tag{3.2} $$

that is

$$ \left[\left(L_v t^{kp}\right)_{;p}\right] + t^{qp} \left[v^k_{;qp}\right] + t^{kp} \left[v^s_{;sp}\right] = \rho \left[\ddot{v}^k\right] \tag{3.3} $$

the kinematic compatibility conditions are (for large displacements)

$$(3.4)\quad [L_v(v_{ij})] = [\ddot{a}_{ij}] + \left[a_{ik}\dot{v}^k_{;j}\right] + \left[a_{kj}\dot{v}^k_{;i}\right] + \left[2\dot{a}_{ik}v^k_{;j} + 2\dot{a}_{kj}v^k_{;i} + a_{ik}v^k_{;\ell}v^\ell_{;j} + a_{kj}v^k_{;\ell}v^\ell_{;i} + a_{\ell k}v^k_{;j}v^\ell_{;i}\right],$$

that is

$$(3.5)\quad [\dot{v}_{ij}] = [\ddot{a}_{ij}] + a_{ik}\left[\dot{v}^k_{;j}\right] + a_{kj}\left[\dot{v}^k_{;i}\right].$$

The constitutive compatibility conditions are

$$(3.6)\quad f_\alpha\left(\mathring{L}_v\left(t^{kp}_{\ ;\ell}\right) + \left[L_v\left(t^{kp}_{\ ;\ell}\right)\right], \mathring{L}_v(a_{ij;\ell}) + [L_v(a_{ij;\ell})], \dot{t}^{kp}_{\ ;\ell m} + \left[t^{kp}_{\ ;\ell m}\right], \mathring{a}_{ij;\ell m} + [a_{ij;\ell m}]\right) - \mathring{f}_\alpha = 0,$$

where circle over a symbol denotes its value in front of the surface $\varphi(x^i,\tau) = 0$. For example, $\mathring{f}_\alpha$ is the value of function f in front of the surface $\varphi(x^i,\tau) = 0$.

By using the set of equations (3.1), (3.2), (3.4) and (3.6), we can introduce kinematic, dynamic and constitutive compatibility conditions for such generalized waves [2]. These conditions lead to the wave propagation equation

$$(3.7)\quad \frac{\partial f_\alpha}{\partial \varphi_4}\varphi_4 + \frac{\partial f_\alpha}{\partial \varphi_r}\varphi_r = 0.$$

Introducing notations

$$T_{\alpha kp}{}^{\ell} \equiv \frac{\partial f_\alpha}{\partial L_v\left(t^{kp}_{\ ;\ell}\right)}, \quad A^{ijk}_\alpha \equiv \frac{\partial f_\alpha}{\partial L_v(a_{ij;k})},$$

$$S_{\alpha kp}{}^{ms} \equiv \frac{\partial f_\alpha}{\partial \dot{t}^{kp}_{\ ;ms}}, \quad E^{ijhz}_\alpha \equiv \frac{\partial f_\alpha}{\partial a_{ij;hz}},$$

equation (3.7) takes the form

$$(3.8)\quad \Big\{2\rho T_{\alpha kp}{}^{\ell} n_\ell c^3 - 2\rho S_{\alpha kp}{}^{ms} n_m n_s c^2 - A^{ijr}_\alpha n_r n_p \left((2a_{ik} - g_{ik})n_j + (2a_{kj} - g_{kj})n_i\right)c + E^{ijhz}_\alpha n_h n_z n_p \left((2a_{ik} - g_{ik})n_j + (2a_{kj} - g_{kj})n_i\right)\Big\}\gamma^{kp} = 0.$$

For $\gamma^{kp} \neq 0$, Eq. (3.8) should have a solution, thus the polynomial of matrices in brackets $\{...\}$ should have a zero determinant

$$\det\{\ldots\} = 0. \tag{3.9}$$

Equation (3.9) is called the wave speed equation which implies Wave Dynamical Conditions (WDC) for the existence of the required waves (for details see [2]). These conditions should be added to (2.7).

By using the dynamical systems theory and assuming a generic behavior (as it is defined in the theory of dynamical systems [5]), at the loss of stability we obtain additional Dynamical Systems Condition (DSC). Thus in studying the system of fundamental equations, we should consider (2.7) and both the WDC and DSC. The next part shows how DSC can be formulated in a uniaxial case.

4. Material instability and dynamical systems

Now we perform a material instability investigation of state S^0 of the solid body by considering finite displacements in uniaxial case with an appropriate constitutive equation

$$L_v(t_{,x}) + K_1 L_v(a_{,x}) + K_2 t_{,xx} + K_3 a_{,xx} = 0, \tag{4.1}$$

where partial derivatives of a function g are denoted by $g_{,x} = \frac{\partial g}{\partial x}$, or $g_{,\tau} = \frac{\partial g}{\partial \tau}$ and coefficients K_1, K_2, K_3 are considered to be piecewise constant. Now at S^0, Eq. (2.7) has the form

$$(t_0 - Ea_0)\frac{\partial a_0}{\partial \tau} > 0, \tag{4.2}$$

where E denotes the Young modulus, as usual. Then WDC means that the scalar third-order algebraic equation

$$\rho c^3 - \rho K_2 c^2 - K_1(2a-1)c + K_3(2a-1) = 0 \tag{4.3}$$

should have real nonzero solutions ([2]). Assume that S^0 is described by values a_0, t_0, v_0 of the field variables. Then such values should satisfy the system of fundamental equations formed by (4.1) and the uniaxial forms of (3.2) and (3.4)

$$\dot{v} = \frac{1}{\rho} t_{,x}, \quad \dot{a} = v_{,x} - 2a v_{,x}. \tag{4.4}$$

Lapunov stability investigates the response of a mechanical system for sufficiently small perturbations, thus the perturbed quantities $a_0 + \Delta a, t_0 + \Delta t, v_0 + \Delta v$ should

be substituted into (4.1) and (4.4). Having done the necessary calculations and by linearizing the set of equations at S^0, a system of differential equations is obtained for the perturbations

$$
\begin{aligned}
v_{,\tau\tau} &= C_1 v + C_2 a_{,x} + C_3 a + C_4 v_{,x} + C_5 v_{,xx} + C_6 a_{,xx} + C_7 v_{,x\tau}, \\
a_{,\tau} &= D_1 v + D_2 a_{,x} + D_3 a + D_4 v_{,x},
\end{aligned} \tag{4.5}
$$

where Δ is omitted for the sake of simplicity, and the following notations are used:

$$
C_1 = -2v_{0,x\tau} - 2v_{0,xx}v_0, C_2 = \frac{2K_1}{\rho} v_{0,x},
$$

$$
C_3 = \frac{2K_1}{\rho} v_{0,xx}, C_4 = \frac{2K_1}{\rho} a_{0,x} - K_2,
$$

$$
C_5 = v_0^2 - \frac{K_1}{\rho} + \frac{2K_1}{\rho} a_0, C_6 = -\frac{K_3}{\rho}, C_7 = 2v_0,
$$

$$
D_1 = -a_{0,x}, D_2 = -v_0, D_3 = -2v_{0,x}, D_4 = -2a_0 + 1.
$$

Introducing new variables $y_1 = a, y_2 = v, y_3 = v_{,\tau}$ and vector $y = [y_1, y_2, y_3]$, a dynamical system can be added to (4.5) [5]

$$
\frac{\partial}{\partial \tau} y = \begin{bmatrix} H_1 & H_2 & 0 \\ 0 & 0 & 1 \\ H_3 & H_4 & H_5 \end{bmatrix} y, \tag{4.6}
$$

where operators $H_1 = D_2 \frac{\partial}{\partial x} + D_3, H_2 = D_4 \frac{\partial}{\partial x} + D_1, H_3 = C_6 \frac{\partial^2}{\partial x^2} + C_2 \frac{\partial}{\partial x} + C_3, H_4 = C_5 \frac{\partial^2}{\partial x^2} + C_4 \frac{\partial}{\partial x} + C_1, H_5 = C_7 \frac{\partial}{\partial x}$.

The characteristic equation of (4.6) reads

$$
\lambda y = \begin{bmatrix} H_1 & H_2 & 0 \\ 0 & 0 & 1 \\ H_3 & H_4 & H_5 \end{bmatrix} y. \tag{4.7}
$$

and the linear Lapunov stability condition of state S^0 is: $\operatorname{Re} \lambda \leq 0$ for all eigenvalues of (4.7). Stability boundary is at $\operatorname{Re} \lambda = 0$. The loss of stability can be classified as a static bifurcation (or divergence) type instability ($\operatorname{Re} \lambda = 0$, $\operatorname{Im} \lambda = 0$), or a dynamic one ($\operatorname{Re} \lambda = 0$, $\operatorname{Im} \lambda \neq 0$) [5]. Determination of the eigenvalues of (4.7) requires the solution of a boundary value problem, which may cause serious difficulties and needs numerical computations.

To remain at analytic methods, we should perform simplifications: the use of small periodic perturbations. While stability is considered here as a local

property of state, the small perturbation technique is quite obvious, but not the periodicity of perturbations. It is really a restriction, but used widely in engineering literature of the linear case [16]. (A detailed study on that restriction is presented in [5].) While perturbations are small, $a_\tau = v_x$ and then Eq. (4.5) can be transformed into the velocity field,

$$\begin{aligned} v_{\tau\tau\tau} &= C_1 v_\tau + C_2 v_{xx} + C_3 v_x + C_4 v_{x\tau} + C_5 v_{xx\tau} + C_6 v_{xxx} + C_7 v_{x\tau\tau} \\ v_{x\tau} &= D_1 v_\tau + D_2 v_{xx} + D_3 v_x + D_4 v_{x\tau}. \end{aligned} \tag{4.8}$$

By assuming periodic perturbations

$$v = \exp(i\omega x) \tag{4.9}$$

in a similar way as it was done in the general case with (4.7), the characteristic equation yields a set of algebraic equations

$$\begin{aligned} \lambda^3 &= C_1\lambda - C_2\omega^2 - C_5\omega^2\lambda^2, \\ 0 &= C_3 + C_4\lambda - C_6\omega^2 + C_7\lambda^2 \\ 0 &= D_1\lambda - D_2\omega^2, \\ \lambda &= D_3 + D_4\lambda, \end{aligned} \tag{4.10}$$

and the static bifurcation condition is the existence of a $\lambda = 0$ solution of (4.10). Then we obtain the following relations:

$$D_3 = 0, \iff \frac{\partial v_0}{\partial x} = 0, \tag{4.11}$$

$$D_2 = 0, \iff v_0 = 0, \tag{4.12}$$

$$C_2 = 0, \iff K_2 \frac{\partial v_0}{\partial x} = 0, \tag{4.13}$$

and finally, the equations

$$C_3 = 0, \iff K_1 \frac{\partial^2 v_0}{\partial x^2} = 0, \tag{4.14}$$

and

$$C_6 = 0, \iff K_3 = 0, \tag{4.15}$$

or

$$C_3 - C_6\omega^2 = 0, \iff 2K_1 \frac{\partial^2 v_0}{\partial x^2} + K_3\omega^2 = 0, \tag{4.16}$$

should be satisfied. Obviously (4.11) implies (4.13) thus there is a static bifurcation if

A : (4.11), (4.12), (4.14) and (4.15), or

B : (4.11), (4.12) and (4.16) are valid.

Now let us return to wave dynamics. Case **A** does not meet the WDC: there is a zero wave speed solution c of (4.3) because of (4.15). In the classical material instability concept [13] it means localization. On the other hand, if (4.15) holds the constitutive equation (4.1) has no second strain gradient-dependent term, which corresponds to the fact that there is a stationary singular surface (a localization zone of zero width). Thus we have exactly the classical result of Rice [13]. However, in case **B**, from (4.16) we obtain

$$\omega^2 = -\frac{2K_1}{K_3}\frac{\partial^2 v_0}{\partial x^2},$$

if $\frac{2K_1}{K_3}\frac{\partial^2 v_0}{\partial x^2} < 0$. This means that there is a critical eigenfunction to the zero eigenvalue, that is, we have a critical periodic perturbation (4.9)

$$v_{cr} = \exp\left(ix\sqrt{-\frac{2K_1}{K_3}\frac{\partial^2 v_0}{\partial x^2}}\right),$$

at which state S^0 unergoes a static bifurcation.

Let us now study the dynamic bifurcation case. Then we need for $\lambda^2 < 0$, a solution of (4.10). The corresponding conditions are (4.11), (4.12) and

$$C_5 = 0 \iff v_0^2 - \frac{K_1}{\rho} + \frac{2K_1}{\rho}a_0 = 0, \tag{4.17}$$

$$C_4 = 0 \iff \frac{2K_1}{\rho}a_{0,x} - K_2 = 0, \tag{4.18}$$

$$D_1 = 0 \iff a_{0,x} = 0, \tag{4.19}$$

$$D_4 = 1 \iff a_0 = 0. \tag{4.20}$$

Then from (4.17), (4.12) and (4.20)

$$K_1 = 0, \tag{4.21}$$

and from (4.18) and (4.19)

$$K_2 = 0. \tag{4.22}$$

Moreover from the second equation of (4.10) and (4.18) with (4.12) we obtain (4.15)

$$K_3 = 0.$$

Finally, from the first equation of (4.10) substituting (4.12), (4.11) and (4.17), we have

$$\lambda^2 = -2\frac{\partial^2 v_0}{\partial x \partial \tau}, \tag{4.23}$$

thus there is a dynamic bifurcation if conditions (4.11), (4.12), (4.15), (4.19), (4.20), (4.21), (4.22) are satisfied and

$$\frac{\partial^2 v_0}{\partial x \partial \tau} > 0. \tag{4.24}$$

Additionally, if (4.20) is substituted into the dissipation inequality, the condition

$$t_0 \frac{\partial a_0}{\partial \tau} > 0$$

is obtained. Unfortunately this is not a generic dynamic bifurcation. We can easily see that (4.21) implies (4.14); consequently, dynamic bifurcation is coexistent with a static bifurcation of case **A**. Moreover, if (4.15), (4.21) and (4.22) are valid, Eq. (4.3) has a zero solution $c = 0$, thus neither WDC nor DSC are satisfied.

As a summary of this section we find that costitutive equation (4.1) can only be used for the description of the static bifurcation-type loss of stability. In case **B** both WDC and DSC are valid. When we disregard WDC, even case **A** can be accepted, if at least one of the conditions (4.19), (4.20), (4.22), or (4.24) fails, because then no coexistent dynamic bifurcation is present and we may speak about a stationary discontinuity as the instability phenomenon.

5. Summary

In the nonlinear case of finite deformations, by using a second order constitutive equation of form (4.1), both **A** and **B** types of static bifurcation instability are generic in the sense of dynamical systems theory because there is no coexistent dynamic bifurcation. Moreover, we could preserve the nice property of the linear study of second strain gradient-dependent material: the dimension of the critical eigenspace at the static bifurcation type loss of stability remains finite (case **B**). This result shows that in a post-localization study even now we should use constitutive equations including second strain gradient dependence. When we neglect this term (case **A**) we cannot find a unique critical eigenfunction

but a "stationary discontinuity": the jump (discontinuity surface in the higher derivatives of the field variables) stops at the conditions of instability. Now the material instability condition and the critical eigenfunctions (if they exist) are explicitly dependent on the values of the field variables at the state under consideration. Of course they do depend implicitly on the material properties (K_1, K_2, K_3) because the values of the field variables at state S^0 are determined by solving the whole set of fundamental equations. Unfortunately such constitutive equation cause a seriously ungeneric behavior at the dynamic bifurcation instability. It does not exist as a distinct type of instability, because the necessary conditions of a dynamic bifurcation are sufficient for a static one.

References

1. V. I. ARNOLD, *Geometrical methods in the theory of ordinary differential equations*, Springer, New York, 1983.
2. GY. BÉDA, *Constitutive equations and nonlinear waves*, Nonlinear Analysis, Theory, Methods and Appl., **30**, 397-407, 1997.
3. GY. BÉDA, *Generalization of Clapeyron's theorem of solids*, Periodica Polytechnica, Ser. Mech. Eng., **44**, 5-7, 2000.
4. GY. BÉDA and P. B. BÉDA, *A study on constitutive relations of copper using the existence of acceleration waves and dynamical systems*, Proc. of Estonian Academy of Sci. Engin., **5**, 101-111, 1999.
5. P. B. BÉDA, *Material instability in dynamical systems*, European Journal of Mechanics, A/Solids, **16**, 501-513, 1997.
6. P. B. BÉDA, *On rate and gradient dependence of solids as dynamical systems*, Arch. Mech., **51**, 229-241, 1999.
7. P. B. BÉDA, and GY. BÉDA, *Acceleration waves and dynamic material instability in constitutive relations for finite deformation*, Structural Failure and Plasticity, IMPLAST 2000, X.L. ZHAO and R. H. GRZEBIETA,[Eds.] Elsevier, pp. 585-590. Oxford 2000.
8. R. DE BORST, L.J. SLUYS, H-B. MÜHLHAUS and J. PAMIN, *Fundamental issues in finite element analyses of localization of deformation*, Engineering Computations, **10**, 99-121, 1993.
9. A.C. ERINGEN and G.A. MAUGIN, *Electrodynamics of Continua, I*, Springer, pp. 136 New York 1990.
10. M. FARKAS, *Periodic Motions*, Springer, pp. 400, New York 1994.
11. R. HILL, *Some basic principles in the mechanics of solids without a natural time*, Journal of the Mech. and Phys. of Solids, **7**, 209-225, 1959.
12. G.A. HOLZAPFEL, *Nonlinear solid mechanics*, Wiley, Chichester, 2000, pp. 184.
13. J.R. RICE, *The Localization of Plastic Deformation*, Theoretical and Applied Mechanics, W.T. KOITER, [Ed.] North-Holland Publ. pp. 207-220. Amsterdam 1976.

14. E.G. THOMPSON AND Y. SZU-WEI, *A flow formulation for rate equilibrium equations,* Int. J. for Numerical Methods in Engineering, **30**, 1619-1632, 1990.

15. S. WIGGINS, *Introduction to applied nonlinear dynamical systems and chaos,* Springer, New York, 1990.

16. H.M. ZBIB AND E.C. AIFANTIS, *On the localization and post-localization behavior of plastic deformation,* I, Res Mechanica, **23**, 261-277, 1988.

Received January 30, 2001 revised version June 11, 2001.

Arch. Mech., **53**, 4-5, pp. 333–366, Warszawa 2001

Nonstationary two-phase flow through elastic porous medium

W. BIELSKI[1], J. J. TELEGA[2] and R. WOJNAR[2]

[1] *Institute of Geophysics, Warsaw, Poland,*
e-mail:wbielski@igf.edu.pl

[2] *Institute of Fundamental Technological Research, Warsaw, Poland*
e-mail:jtelega@ippt.gov.pl, rwojnar@ippt.gov.pl

THE AIM OF THIS CONTRIBUTION is to derive macroscopic equations governing the dynamic flow of two immiscible viscous fluids through an elastic microperiodic porous medium. To this end homogenization methods were employed. The procedure used can be justified by the method of two-scale convergence. Passage to the stationary case and illustrative example were also provided.

1. Introduction

IN THE PAPERS [14, 15] we studied one-phase nonstationary flow of incompressible viscous Stokes fluid through a linear elastic microporous medium. The present paper is aimed at examining a similar problem in the case of two different immiscible Stokesian fluids. The new phenomenon which has to be taken into account is the surface tension on interfaces between the two fluids. The model of surface tension we use is the one proposed by LEVICH and KRYLOV [61], cf. also [41, 58]. The fluids are described by the Stokes equations with different viscosities. The solid phase is made of a linear anisotropic elastic material.

The macroscopic equations and Darcy's law, the last being nonlocal in time (see also [3]), are obtained by using the homogenization methods. Similar problem was studied by Auriault *et al.* [6] in the case of *harmonic* unsaturated flow and different from our scaling on interfaces between the fluids.

In our case, the passage to the stationary two-phase flow through a porous medium yields the equations similar to those previously derived by SAINT JEAN PAULIN and TAOUS [74] provided that the skeleton is rigid, see also [8].

The time-dependent permeabilities involve an implicit dependence on the matrix structure, saturation, interfacial tension and fluid densities. This dependence is inherently present in the local problems which allow to determine the formula for the extended Darcy law. Consequently, at the expense of simplifica-

tions it seems possible to recover the approach exploiting the notion of relative permeabilities, cf. [20, 41, 58]. We observe that if we can predict the permeability for single-phase flow through a porous material from digitized information obtained from cross-sections of the rocks, then we may also be able to obtain estimates of traditional relative permeability as well when two fluids phases are present, cf. BLAIR and BERRYMAN [17].

We observe that problems of fluid transport through porous media, including multi-phase flows are important in many branches of chemical technology, biomechanics and geological research. For instance, soft tissues are porous materials, cf. [57].

The plan of the paper is as follows. In Sec. 2 a rather intensive, though not exhaustive, overview of previous results on two-phase flows through porous media is compiled. Formulation of the flow problem to be studied is given in Secs. 3 and 4. Homogenization is performed in Sec. 5. Among the results obtained in the present paper the most important are the macroscopic equations of Biot-type involving the nonlocal in time extended Darcy's law. The formal homogenization procedure is justified in Sec. 6 by the method of two-scale convergence. Passage to the stationary case is performed in Sec. 7. An illustrative example of stationary flow through bundles of tubes is performed in Sec. 8. In Appendix A main points of the asymptotic analysis are derived.

2. Overview of previous results on two-phase flow through porous media

In essence, there are four approaches to modelling the behaviour of porous media filled with fluids. The first approach is in fact macroscopic from the very beginning, though microscopic information is somewhat hidden, see COUSSY [35].

The second approach is typical for mixture theories, see DE BOER [18], KUBIK *et al.* [60], SIMON [77] and the references therein. It seems that MORLAND [68] was the first who used the volume fraction concept in connection with the mixture theory. According to ZIENKIEWICZ *et al.* [85], the mixture theory introduces some arbitrariness in the selection of various parameters. GANESAN and BRENNER [47] critically reviewed the convential mixture theory, and other theories where spatial averaging is used. According to these authors, we cite ([47], p.736): "Our identification of appropriate macrofields is based upon their rigorous *physical, scale-invariant* definitions rather than upon simple *ad hoc* volume averaging of the corresponding microfields". Consequently the paper contains quite a lot of definitions. The generalized Darcy's law has the form similar to the one given on p. 419 of [58] and is a particular case of the law rigorously derived by SAINT-JEAN PAULIN and TAOUS [74], cf. also Sec. 5 of our paper.

The third approach, often used in the mechanics of porous media, relies on volume and surface averaging, see BEAR and BACHMAT [10], BRENNER and EDWARDS [28], FRAS and BENET [46], GRAY and HASSANIZADEH [49, 50, 51, 52] DU PLESSIS [72], WHITAKER [81]. Similarly to micromechanics, one introduces the concept of representative elementary volume (REV). With every microscopic field $\varphi(x,t)$, a macroscopic field defined at every point x of a domain $\Omega \subset \mathbb{R}^3$ by the average of φ in the translation V of REV is centered at $x \in \Omega$. For a density φ, the macroscopic field is defined by

$$\langle\varphi\rangle(x,t) = \frac{1}{|V|}\int_V \varphi(y,t)\,dy(x). \tag{2.1}$$

For a quantity φ_s on a surface S, the average is written as follows:

$$\langle\varphi_s\rangle(x,t) = \frac{1}{|V|}\int_{V\cap S} \varphi_s(y,t)\,dS(x). \tag{2.2}$$

Such averaging is used to derive macroscopic balance equations. The system of balance equations requires a sufficient number of equations such that all unknowns can be determined. It is accomplished by providing equations of state and constitutive relations [66, 81]. It is worth noticing that in a comprehensive paper by MILLER *et al.* [66], the following topics related to multiphase flow and transport modelling were discussed: balance equations, constitutive relationships for both pressure-saturation-conductivity and interphase mass transfer, and stochastic and computional issues. Experimental observations were also reported. As an evolving approach, a Lattice Boltzmann (LB) method to simulate multiphase flow at the pore scale was discussed, see also ADLER and THOVERT [2], KRAFCZYK *et al.* [59] and the references therein. We observe that Lattice Gas (LG) and LB models were originally developed for single-phase flows. One major interest of these techniques is their potential ability to cope with interfaces [2].

For more information on multi-phase, and particularly two-phase flows, where various physical approaches were used, the reader is referred to the books by CUSHMAN [37], DULLIEN [41], KAVIANY [58] and SAHIMI [76], and the papers by ALLAIRE and KOKH [5], DARTLEY and RUTH [40], BENNETHUM and GIORGI [11], BLAIR and BERRYMAN [17], CHAVENT *et al.* [30], CONSTANTINIDES and PAYATAKES [32, 33, 34] CHRISTAKOS *et al.* [31], DALE [38, 39], EKRANN and DALE [42], EKRANN *et al.* [43], GRAY and HASSANIZADEH [49, 50], HASSANIZADEH and GRAY [54], HARTER and YEH [53], MONTEMAGNO and GRAY [67], RUDMAN [73], THIGPEN and BERRYMAN , TZIMAS *et al.* [79], VALAVANIDES *et al.* [80], YARIN and HESTRONI [82], ZANOTTI and CARBONELL [83], ZHANG and PROSPETTI [84]. The approach used by CUSHMAN [37] to modelling flow

and swelling in hierarchical porous media is extremely complicated, similar in spirit of the modelling used by GRAY [48], GRAY and HASSANIZADEH [49], HASSANIZADEH and GRAY [54].

The books by LEWIS and SCHREFLER [62] and ZIENKIEWICZ *et al.* [85] present the basis of modern computational approaches to various practical problems of geomechanics. In each of these books an important role is attributed to the derivation of macroscopic equations by using averaging techniques.

Less familiar in the mechanics of porous media seems to be the ganglion dynamics, cf. [32, 33, 34, 80]. Experimental observations of steady-state flow of water and oil through planar and nonplanar chamber-and-throat pore networks etched in glass have shown that over broad ranges of values of the main dimensionless parameters (capillary number, viscosity ratio, water saturation) the oil is disconnected in the form of ganglia. In [32, 33, 34, 80] a new approach for the study of two-phase flow processes in porous media on mesoscopic scale, when ganglion dynamics is the main flow regime, has been developed.

We observe that in the study of flows through porous media, mainly the transport problems are investigated. The solid component is then obviously undeformable.

We proceed to the fourth important approach used in modelling flows through porous media, both deformable and undeformable, cf. BIELSKI and TELEGA [13], the books by BOURGEAT *et al.* [19], CROLLET and EL HATRI [36], HORNUNG [56], ENE and POLIŚEVSKI [44], PANFILOV [71], SANCHEZ-PALENCIA [75]. For instance, it is now clear that Darcy's law and its extensions can be derived by using homogenization methods, see also Sec.5 of the present paper. A characteristic feature of various homogenization approaches is that a small parameter $\varepsilon > 0$ is introduced. The homogenization procedure consists in a formal (the method of multiple scales) or rigorous passage with ε to zero (G- and H-convergence, Γ-convergence, two-scale convergence), see the Appendix A by ALLAIRE to the book [56].

Surprisingly, the author of a comprehensive paper [18] who pursued the developments of the porous media theory from the middle of the 18th century until 1996, mentioned no contribution to this theory by rapidly developing field of homogenization.

From the physical viewpoint one can distinguish two classes of homogenization problem related to two-phase flows, similarly to one-phase flows.

The first class comprises problems where micro-macro approach is used. Then one arrives at Darcy's law and its generalizations, cf. AURIAULT - SANCHEZ-PALENCIA [7, 8], BERNABÉ [12], ENE and POLIŚEVSKI [44], FIRDAOUSS *et al.* [45], HORNUNG [56], MARUSIĆ - PALOKA [63] and MIKELIĆ [64]. In the case of elastic porous media one additionally obtains Biot-type equations, cf. AURIAULT *et al.* [6], BIELSKI *et al.* [14, 15, 16], BURRIDGE and KELLER [29], and the

references therein. The second class comprises a meso-macro approach, where the quantities like porosity, permeability and dispersion are assumed to be microperiodic, cf. BOURGEAT [20,21], BOURGEAT and HIDAMI [23], BOURGEAT and MIKELIĆ [27], BOURGEAT and PANFILOV [22], BOURGEAT *et al.* [25,26], MIKELIĆ [64]. MIKELIĆ and PAOLI [65] derived the Buckley-Leverett system for a two-phase immiscible incompressible flow through a thin slab, starting from the incompressible Navier-Stokes system governing a flow of two fluids separated by a free boundary and disregarding surface tension.

In what concerns homogenization of two-phase flow through randomly heterogeneous media, only two papers are known to us [9,25], cf. also [24,31]. In these papers the authors considered incompressible two-phase flow in heterogeneous reservoirs with randomly distributed inhomogeneities, that is in media with permeability and porosity being stationary random fields.

3. Notations and basic relations

We assume that the porous skeleton reveals a micro-periodic structure. The basic cell Y has a form of a cube and consists of three parts (three disjoint open sets): Y_S, Y_A and Y_B, where the subscript S denotes the solid part, and A and B stand for the fluid parts. We also set $Y_L = Y_A \cup Y_B \cup \Gamma_{AB}$, where Γ_{AB} stands for the interface between Y_A and Y_B.

The interface between the sets Y_L and Y_S is denoted by Γ. We observe that the surface of liquid-liquid contact Γ_{AB}, is in general unknown, and $\Gamma_{AB} = \Gamma_{AB}(t)$.

The porous medium is identified with a bounded set $\overline{\Omega} \subset \mathbb{R}^3$, where Ω is a sufficiently regular domain. The domain Ω is assumed to possess an εY - periodic structure: $\Omega = \Omega_S^\varepsilon \cup \Omega_L^\varepsilon$ where Ω_L^ε denotes the part occupied by the liquid, and $\Omega_S^\varepsilon = \Omega \backslash \overline{\Omega}_L^\varepsilon$. We have $\overline{\Omega} = \overline{\Omega}_S^\varepsilon \cup \overline{\Omega}_A^\varepsilon \cup \overline{\Omega}_B^\varepsilon$.

A small parameter ε $(0 < \varepsilon < 1)$ characterizes the microstructure of the porous medium considered. Namely $\varepsilon = l/\mathcal{L}$, and $l, \mathcal{L}$ are typical length scales associated with the dimension of micropores and with length of waves contributing to the considered transient phenomenon. To obtain the macroscopic relationships (homogenization) we pass with ε to zero.

The subsets Ω_S^ε, Ω_A^ε and Ω_B^ε correspond to the parts of Ω occupied by the solid and two immiscible fluids. We have $\overline{\Omega} = \overline{\Omega}_S^\varepsilon \cup \overline{\Omega}_A^\varepsilon \cup \overline{\Omega}_B^\varepsilon$, $\Gamma_{AB}^\varepsilon = \partial\Omega_A^\varepsilon \cap \partial\Omega_B^\varepsilon$. We set

$$\langle(\cdot)\rangle = \frac{1}{|Y|}\int_Y (\cdot)\,dy, \qquad \langle(\cdot)\rangle_\alpha = \frac{1}{|Y|}\int_{Y_\alpha} (\cdot)\,dy, \qquad \alpha = S, L, A, B. \tag{3.1}$$

Note that the surfaces of the solid phase and the A-liquid and B-liquid phases

are given by

$$\partial Y_S = \Gamma \cup P_S, \quad \partial Y_A = \Gamma \cup \Gamma_{AB} \cup P_A, \quad \partial Y_B = \Gamma \cup \Gamma_{AB} \cup P_B \text{ and } \partial Y_L = \Gamma \cup P_L.$$

Here P_S, P_A, P_B and P_L denote the cross-sections of the Y_S, Y_A, Y_B and Y_L with the faces of the basic cell Y. Obviously we have $\Gamma = \Gamma_A \cup \Gamma_B$.

The porosity f is defined as the volume fraction of the liquid in the considered solid-liquid medium. We have

$$f_\alpha = \frac{|Y_\alpha|}{|Y|}, \qquad f = f_A + f_B = \frac{|Y_L|}{|Y|}, \quad 1 = f_S + f_A + f_B = f_S + f. \tag{3.2}$$

We note that f_A and f_B depend on time. By $\mathbf{n}^\alpha$ we denote the exterior unit normal to $\Omega_\alpha^\varepsilon$. The summation convention is used, unless otherwise stated.

4. Basic equations for the motion of porous medium with biphasic fluid

Let $\mathbf{u} = \mathbf{u}(\mathbf{x}, t)$ denote the displacement field in the solid, $\mathbf{v}^A = \mathbf{v}^A(\mathbf{x}, t)$ and $\mathbf{v}^B = \mathbf{v}^B(\mathbf{x}, t)$ denote the velocity in the liquids A and B, $p^A = p^A(\mathbf{x}, t)$ and $p^B = p^B(\mathbf{x}, t)$ being the respective pressures in both fluid phases.

Further, let ρ^S, ρ^A and ρ^B denote the densities of phases S, A and B. We assume that these quantities do not exhibit the microstructure. The viscosities of both fluids A and B are denoted by η^A_{ijmn} and η^B_{ijmn}, respectively.

For a fixed $\varepsilon > 0$ all the relevant quantities that exhibit the microstructure are denoted with the superscript ε. The fields $\mathbf{u}^\varepsilon$, $\mathbf{v}^{A\varepsilon}$, $\mathbf{v}^{B\varepsilon}$ $p^{A\varepsilon}$ and $p^{B\varepsilon}$ satisfy the following equations:

$$\begin{aligned}
\rho^S \ddot{u}_i^\varepsilon &= \partial_{x_j}\left(a^\varepsilon_{ijmn}\partial_{x_n} u^\varepsilon_m\right) + F_i^S && \text{in} \quad \Omega_S,\\
\rho^A \dot{v}_i^{A\varepsilon} &= \partial_{x_j}\left(-p^{A\varepsilon}\delta_{ij} + \varepsilon^2 \eta^{A\varepsilon}_{ijmn}\partial_{x_n} v^{A\varepsilon}_m\right) + F_i^A && \text{in} \quad \Omega_A,\\
\partial_{x_i} v_i^{A\varepsilon} &= 0 && \text{in} \quad \Omega_A,\\
\rho^B \dot{v}_i^{B\varepsilon} &= \partial_{x_j}\left(-p^{B\varepsilon}\delta_{ij} + \varepsilon^2 \eta^{B\varepsilon}_{ijmn}\partial_{x_n} v^{B\varepsilon}_m\right) + F_i^B && \text{in} \quad \Omega_B,\\
\partial_{x_i} v_i^{B\varepsilon} &= 0 && \text{in} \quad \Omega_B.
\end{aligned} \tag{4.1}$$

On the known solid-liquid interface Γ^ε and on the unknown liquid-liquid interface Γ^ε_{AB} the jump conditions are

$$\begin{aligned}
&[\![S^\varepsilon_{ij}]\!]\, n_j = 0 \qquad v_i^{A\varepsilon}|_A = \dot{u}_i^\varepsilon|_S \qquad v_i^{B\varepsilon}|_B = \dot{u}_i^\varepsilon|_S \quad \text{on} \quad \Gamma^\varepsilon,\\
&\left[\!\!\left[\left(-p^\varepsilon\delta_{ij} + \varepsilon^2 \eta^\varepsilon_{ijmn}\partial_{x_n} v^\varepsilon_m\right)\right]\!\!\right]_{AB} n_j = \varepsilon\sigma H^\varepsilon_{ij} n_j \qquad [\![v_i^\varepsilon]\!] = 0 \quad \text{on} \quad \Gamma^\varepsilon_{AB},
\end{aligned} \tag{4.2}$$

where

$$S_{ij}^{\varepsilon} = \begin{cases} a_{ijmn}^{\varepsilon} \partial_{x_n} u_m^{\varepsilon} & \text{in } \Omega_S^{\varepsilon}, \\ -p^{A\varepsilon}\delta_{ij} + \varepsilon^2 \eta_{ijmn}^{A\varepsilon} \partial_{x_n} v_m^{A\varepsilon} & \text{in } \Omega_A^{\varepsilon}, \\ -p^{B\varepsilon}\delta_{ij} + \varepsilon^2 \eta_{ijmn}^{B\varepsilon} \partial_{x_n} v_m^{B\varepsilon} & \text{in } \Omega_B^{\varepsilon}. \end{cases} \tag{4.3}$$

Here, σ denotes the coefficient of surface tension and H_{ij}^{ε} is the curvature tensor of the surface $\Gamma_{AB}^{\varepsilon}$. In Eqs. $(4.1)_{2,4}$ and $(4.2)_4$ the following rescaling is introduced, cf. Appendix B,

$$\eta_{ijmn}^{\varepsilon} \rightsquigarrow \varepsilon^2 \, \eta_{ijmn}^{\varepsilon} \quad \text{and} \quad \sigma \rightsquigarrow \varepsilon \, \sigma.$$

The following interpretation can be ascribed to the quantity $\mathbf{H} = (H_{ij})$. We perform the decomposition in normal and tangential parts as follows:

$$\sigma \mathbf{H}\mathbf{n} = \sigma H_{\mathbf{n}} \mathbf{n} + \sigma \mathbf{H}_{\tau},$$

where

$$H_{\mathbf{n}} \equiv H_{ij} n_i n_j \equiv H,$$

and

$$\mathbf{H}_{\tau} \equiv \mathbf{H}\mathbf{n} - H_{\mathbf{n}} \mathbf{n}.$$

We assume that

$$\sigma \mathbf{H}_{\tau} = \sigma \frac{1}{\sigma} \frac{\partial \sigma}{\partial \boldsymbol{\tau}} \boldsymbol{\tau} = \frac{\partial \sigma}{\partial \boldsymbol{\tau}} \boldsymbol{\tau}.$$

According to the method of two-scale asymptotic expansions, we assume the following expansions for the scalar field p^{ε} and vector field $\mathbf{u}^{\varepsilon}$, cf. [56, 57],

$$p^{\alpha\varepsilon} = p^{\alpha(0)}(\mathbf{x}, \mathbf{y}, t) + \varepsilon p^{\alpha(1)}(\mathbf{x}, \mathbf{y}, t) + \varepsilon^2 p^{\alpha(2)}(\mathbf{x}, \mathbf{y}, t) + \ldots$$

$$\mathbf{y} = \mathbf{x}/\varepsilon, \ (\alpha = A, B) \tag{4.4}$$

$$u_i^{\varepsilon} = u_i^{(0)}(\mathbf{x}, \mathbf{y}, t) + \varepsilon u_i^{(1)}(\mathbf{x}, \mathbf{y}, t) + \varepsilon^2 u_i^{(2)}(\mathbf{x}, \mathbf{y}, t) + \ldots \qquad \mathbf{y} = \mathbf{x}/\varepsilon,$$

as well as similar expansions for $\mathbf{v}^{\mathbf{A}\varepsilon}$ and $\mathbf{v}^{\mathbf{B}\varepsilon}$.

The initial conditions are specified by

$$\mathbf{v}^{\alpha\varepsilon}(x, 0) = \mathbf{0} \ \text{ in } \ \Omega_{\alpha}^{\varepsilon}, \quad \alpha = A, B; \ \mathbf{u}^{\varepsilon}(x, 0) = \mathbf{0}, \quad \dot{\mathbf{u}}^{\varepsilon}(x, 0) = \mathbf{0} \ \text{ in } \ \Omega_S^{\varepsilon}. \tag{4.5}$$

5. Results of homogenization

More detailed analysis related to the homogenization procedure is performed in Appendix A. In the present section we are going to present the final results.

The analysis of terms of the order ε^{-2} carried out in Appendix A yields, cf. (A.16),

$$u_i^{(0)} = u_i^{(0)}(\mathbf{x}, t), \tag{5.1}$$

and from (A.19) we get

$$p^{A(0)} = p^{B(0)} \equiv p^{(0)} = p^{(0)}(\mathbf{x}, t) \qquad \text{for } \mathbf{x} \in \Omega. \tag{5.2}$$

Consequently, we obtain, cf.(A.9),

$$\Big[a_{ijmn}\Big(\partial_{x_n} u_m^{(0)} + \partial_{y_n} u_m^{(1)}\Big)\Big] n_j^S = -p^{(0)}\, n_i^S \qquad \text{on} \quad \Gamma = \Gamma_A \cup \Gamma_B. \tag{5.3}$$

The set of equations (A.17) is satisfied provided that

$$u_m^{(1)}(\mathbf{x}, \mathbf{y}, t) = A_m^{(pq)}(\mathbf{x}, \mathbf{y}, t)\, \partial_{x_q} u_p^{(0)}(\mathbf{x}, t) + P_m(\mathbf{x}, (\mathbf{y}, t)\, p^{(0)}(\mathbf{x}, t) \quad \text{in } Y_S \tag{5.4}$$

and the functions $A_m^{(pq)}$ and P_m are Y-periodic solutions to the following local equations on Y_S:

$$\begin{aligned} \partial_{y_j}\Big[a_{ijpq} + a_{ijmn}\partial_{y_n} A_m^{(pq)}\Big] &= 0, \\ \partial_{y_j}\Big(a_{ijmn}\partial_{y_n} P_m + \delta_{ij}\Big) &= 0. \end{aligned} \tag{5.5}$$

By using the expression (5.4) and Eqs.(A.9) we get

$$\begin{aligned} \Big(a_{ijpq} + a_{ijmn}\partial_{y_n} A_m^{(pq)}\Big)\, n_j^S &= 0 \qquad \text{on } \Gamma, \\ \Big(a_{ijmn}\partial_{y_n} P_m + \delta_{ij}\Big)\, n_j^S &= 0 \qquad \text{on } \Gamma. \end{aligned} \tag{5.6}$$

5.1. Macroscopic constitutive relations

Applying asymptotic expansions to constitutive relation (4.3), comparing the terms linked with ε^0 and exploiting (5.2) we get

$$S_{ij}^{(0)} = \begin{cases} a_{ijmn}\Big(\partial_{x_n} u_m^{(0)} + \partial_{y_n} u_m^{(1)}\Big) & \text{in} \quad Y_S, \\ -p^{(0)}\delta_{ij} & \text{in} \quad Y_L = Y_A \cup Y_B. \end{cases} \tag{5.7}$$

We observe that according to the definitions of averages (3.1) we have

$$\langle S_{ij}^{(0)} \rangle = \langle S_{ij}^{(0)} \rangle_S + \langle S_{ij}^{(0)} \rangle_A + \langle S_{ij}^{(0)} \rangle_B, \tag{5.8}$$

or

$$\langle S_{ij}^{(0)} \rangle = \langle S_{ij}^{(0)} \rangle_S + \langle S_{ij}^{(0)} \rangle_L. \tag{5.9}$$

Using Eqs.(5.4) and (5.7) we get

$$\langle S_{ij}^{(0)} \rangle = a_{ijpq}^h \partial_{x_q} u_p^{(0)} + \Big(\langle a_{ijmn} \partial_{y_n} P_m \rangle_S - f \delta_{ij} \Big) p^{(0)}, \tag{5.10}$$

where

$$a_{ijpq}^h = \langle a_{ijpq} + a_{ijmn} \partial_{y_n} A_m^{(pq)} \rangle_S. \tag{5.11}$$

The functions $A_m^{(pq)}$ and P_m have to be determined from the local equations (5.5) and (5.6).

5.2. Mechanics of porous medium with biphasic liquid

From Eqs. (A.1) and (A.2), by comparing the terms linked with ε^0, we get

$$\begin{aligned}
\rho^S \ddot{u}_i^{(0)} &= F_i^S + \partial_{x_j} \Big[a_{ijmn} \Big(\partial_{x_n} u_m^{(0)} + \partial_{y_n} u_m^{(1)} \Big) \Big] \\
&\quad + \partial_{y_j} \Big[a_{ijmn} \Big(\partial_{x_n} u_m^{(1)} + \partial_{y_n} u_m^{(2)} \Big) \Big] \qquad \text{in } Y_S, \\
\rho^A \dot{v}_i^{A(0)} &= F_i^A - \Big(\partial_{x_i} p^{(0)} + \partial_{y_i} p^{A(1)} \Big) + \partial_{y_j} \Big(\eta_{ijmn}^A \partial_{y_n} v_m^{A(0)} \Big) \qquad \text{in } Y_A, \\
\rho^B \dot{v}_i^{B(0)} &= F_i^B - \Big(\partial_{x_i} p^{(0)} + \partial_{y_i} p^{B(1)} \Big) + \partial_{y_j} \Big(\eta_{ijmn}^B \partial_{y_n} v_m^{B(0)} \Big) \qquad \text{in } Y_B.
\end{aligned} \tag{5.12}$$

On the other hand, the terms linked with ε^1 in the interface condition (A.4) lead to the relations

$$\begin{aligned}
\Big[a_{ijmn} \Big(\partial_{x_n} u_m^{(1)} + \partial_{y_n} u_m^{(2)} \Big) \Big] n_j \Big|_S &= \Big(p^{A(1)} \delta_{ij} - \eta_{ijmn}^A \partial_{y_n} v_m^{A(0)} \Big) n_j \Big|_A, \\
\Big[a_{ijmn} \Big(\partial_{x_n} u_m^{(1)} + \partial_{y_n} u_m^{(2)} \Big) \Big] n_j \Big|_S &= \Big(p^{B(1)} \delta_{ij} - \eta_{ijmn}^B \partial_{y_n} v_m^{B(0)} \Big) n_j \Big|_B.
\end{aligned} \tag{5.13}$$

Integration of Eq. $(5.12)_1$ over Y_S, and $(5.12)_2$ and $(5.12)_3$ over Y_A and Y_B yields

$$(1-f)\rho^S \ddot{u}_i^{(0)} = \partial_{x_j}\langle a_{ijmn}\Big(\partial_{x_n}u_m^{(0)} + \partial_{y_n}u_m^{(1)}\Big)\rangle_S + \int\limits_{\partial Y_S}\Big[a_{ijmn}\Big(\partial_{x_n}u_m^{(1)} + \partial_{y_n}u_m^{(2)}\Big)\Big]n_j\,dS \quad \text{in } \Omega,$$

$$f_A\rho^A\langle \dot{v}_i^{A(0)}\rangle_A = f_A F_i^A - f_A\partial_{x_i}p^{(0)} + \int\limits_{\partial Y_A}\Big[-p^{A(1)}\delta_{ij} + \eta^A_{ijmn}\partial_{y_n}v_m^{A(0)}\Big]n_j\,dS \quad \text{in } \Omega, \tag{5.14}$$

$$f_B\rho^B\langle \dot{v}_i^{B(0)}\rangle_B = f_B F_i^B - f_B\partial_{x_i}p^{(0)} + \int\limits_{\partial Y_B}\Big[-p^{B(1)}\delta_{ij} + \eta^B_{ijmn}\partial_{y_n}v_m^{B(0)}\Big]n_j\,dS \quad \text{in } \Omega.$$

Adding Eqs.(5.14), using the interface relations (5.13) and taking into account Eqs. (5.7) and (5.8) we obtain

$$(1-f)\rho^S\ddot{u}_i^{(0)} + \rho^A\langle\dot{v}_i^{A(0)}\rangle_A + \rho^B\langle\dot{v}_i^{B(0)}\rangle_B = \partial_{x_j}\langle S_{ij}^{(0)}\rangle + (1-f)F_i^S + f_A F_i^A + f_B F_i^B. \tag{5.15}$$

This is the macroscopic equation of motion for the porous medium filled with the biphasic fluid.

5.3. Flow of biphasic fluid in porous medium

Equation (5.12) yield the following subsystem of equations posed in $\Omega \times Y_L$ describing the behaviour of the liquid part of the system:

$$\begin{aligned}\rho^A\dot{v}_i^{A(0)} &= F_i^A - \partial_{x_i}p^{(0)} - \partial_{y_i}p^{A(1)} + \partial_{y_j}\Big(\eta^A_{ijmn}\partial_{y_n}v_m^{A(0)}\Big),\\ \rho^B\dot{v}_i^{B(0)} &= F_i^B - \partial_{x_i}p^{(0)} - \partial_{y_i}p^{B(1)} + \partial_{y_j}\Big(\eta^B_{ijmn}\partial_{y_n}v_m^{B(0)}\Big),\end{aligned} \tag{5.16}$$

which can be rewritten as

$$\begin{aligned}\rho^A\dot{w}_i^{A(0)} &= F_i^A - \rho^A\ddot{u}_i^{(0)} - \partial_{x_i}p^{(0)} - \partial_{y_i}p^{A(1)} + \partial_{y_j}\Big(\eta^A_{ijmn}\partial_{y_n}w_m^{B(0)}\Big),\\ \rho^B\dot{w}_i^{B(0)} &= F_i^B - \rho^B\ddot{u}_i^{(0)} - \partial_{x_i}p^{(0)} - \partial_{y_i}p^{B(1)} + \partial_{y_j}\Big(\eta^B_{ijmn}\partial_{y_n}w_m^{B(0)}\Big)\end{aligned} \tag{5.17}$$

or

$$
\begin{aligned}
\rho^A \dot{w}_i^{A(0)} &= \Phi_i^{A(0)} - \partial_{y_i} p^{A(1)} + \partial_{y_j}\left(\eta^A_{ijmn}\partial_{y_n} v_m^{A(0)}\right),\\
\rho^B \dot{w}_i^{B(0)} &= \Phi_i^{B(0)} - \partial_{y_i} p^{B(1)} + \partial_{y_j}\left(\eta^B_{ijmn}\partial_{y_n} v_m^{B(0)}\right).
\end{aligned}
\tag{5.18}
$$

Here the relative velocities are defined by

$$
w_i^{A(0)} \equiv v_i^{A(0)} - \dot{u}_i^{(0)} \qquad \text{and} \qquad w_i^{B(0)} \equiv v_i^{B(0)} - \dot{u}_i^{(0)};
\tag{5.19}
$$

moreover,

$$
\begin{aligned}
\Phi_i^{A(0)} &= \Phi_i^{A(0)}(\mathbf{x},t) \equiv F_i^A - \partial_{x_i} p^{(0)} - \rho^A \ddot{u}_i^{(0)},\\
\Phi_i^{B(0)} &= \Phi_i^{B(0)}(\mathbf{x},t) \equiv F_i^B - \partial_{x_i} p^{(0)} - \rho^B \ddot{u}_i^{(0)}.
\end{aligned}
\tag{5.20}
$$

Since $u_i^{(0)} = u_i^{(0)}(\mathbf{x},t)$, therefore, cf. Eq. (5.1),

$$
\partial_{y_n} w_m^{A(0)} = \partial_{y_n} v_m^{A(0)},
$$

and similarly for $w_m^{B(0)}$ and $v_m^{B(0)}$. Note that in virtue of (A.10), we may write

$$
\dot{u}_i^{(0)}\Big|_S = v_i^{A(0)}\Big|_A \qquad \text{on } \Gamma_A \qquad \text{and} \qquad \dot{u}_i^{(0)}\Big|_S = v_i^{B(0)}\Big|_B \qquad \text{on } \Gamma_B.
$$

Hence

$$
\mathbf{w}^{A(0)} = \mathbf{0} \qquad \text{and} \qquad \mathbf{w}^{B(0)} = \mathbf{0} \quad \text{on } \Gamma.
\tag{5.21}
$$

To satisfy Eqs.(5.18) we set

$$
\begin{aligned}
p^{A(1)} &= \Phi_m^{A(0)}\gamma_m^{AA}(\mathbf{y},t) + \Phi_m^{B(0)}\gamma_m^{AB}(\mathbf{y},t) + \alpha^A(\mathbf{y},t),\\
p^{B(1)} &= \Phi_m^{A(0)}\gamma_m^{BA}(\mathbf{y},t) + \Phi_m^{B(0)}\gamma_m^{BB}(\mathbf{y},t) + \alpha^B(\mathbf{y},t).
\end{aligned}
\tag{5.22}
$$

The local functions $\gamma_m^{AB}(\mathbf{y},t)$, $\alpha^A(\mathbf{y},t)$ *etc.* are to be found. Here and further on, no summation over the capital indices.

Then Eqs.(5.18), posed in $\Omega \times Y_L$, take the form

$$
\begin{aligned}
\rho^A \dot{w}_i^{A(0)} &= \Phi_m^{A(0)}(\delta_{im} - \partial_{y_i}\gamma_m^{AA}) - \Phi_m^{B(0)}\partial_{y_i}\gamma_m^{AB}\\
&\qquad \partial_{y_i}\alpha_i^A + \partial_{y_j}\left(\eta^A_{ijmn}\partial_{y_n} w_m^{A(0)}\right),\\
\rho^B \dot{w}_i^{B(0)} &= \Phi_m^{B(0)}(\delta_{im} - \partial_{y_i}\gamma_m^{BB}) - \Phi_m^{A(0)}\partial_{y_i}\gamma_m^{BA} - \partial_{y_i}\alpha_i^B\\
&\qquad +\partial_{y_j}\left(\eta^B_{ijmn}\partial_{y_n} w_m^{B(0)}\right).
\end{aligned}
\tag{5.23}
$$

These equations are satisfied provided that $\mathbf{w}^{A(0)}$ and $\mathbf{w}^{B(0)}$ are given by the following time convolutions:

$$w_m^{A(0)} = w_m^{A(0)}(\mathbf{x},\mathbf{y},t) = \frac{1}{\varrho^A}\int_0^t \Big[\Phi_s^{A(0)}(\mathbf{x},\tau)\ \chi_{ms}^{AA}(\mathbf{y},t-\tau) + \Phi_s^{B(0)}(\mathbf{x},\tau)\ \chi_{ms}^{AB}(\mathbf{y},t-\tau)\Big]d\tau + \beta_m^A(\mathbf{y},t),$$

$$w_m^{B(0)} = w_m^{B(0)}(\mathbf{x},\mathbf{y},t) = \frac{1}{\varrho^B}\int_0^t \Big[\Phi_s^{A(0)}(\mathbf{x},\tau)\ \chi_{ms}^{BA}(\mathbf{y},t-\tau) + \Phi_s^{B(0)}(\mathbf{x},\tau)\ \chi_{ms}^{BB}(\mathbf{y},t-\tau)\Big]d\tau + \beta_m^B(\mathbf{y},t). \tag{5.24}$$

The functions $\gamma_n^{\alpha\beta} = \gamma_n^{\alpha\beta}(\mathbf{y},t)$ and $\chi_{ms}^{\alpha\beta} = \chi_{ms}^{\alpha\beta}(\mathbf{y},t)$, $\alpha,\beta \in \{A,B\}$ are Y-periodic solutions to the following local problems, cf. the last subsection of Appendix A,

$$\begin{aligned}
&\rho^A \frac{d}{dt}\chi_{is}^{AA}(\mathbf{y},t) - \Big(\delta_{is} - \partial_{y_i}\gamma_s^{AA}(\mathbf{y},t)\Big) - \partial_{y_j}\Big(\eta_{ijmn}^A \partial_{y_n}\chi_{ms}^{AA}\Big) = 0 && \mathbf{y}\in Y_A\times(0,T),\\
&\rho^A \frac{d}{dt}\chi_{is}^{AB}(\mathbf{y},t) + \partial_{y_i}\gamma_s^{AB}(\mathbf{y},t) - \partial_{y_j}\Big(\eta_{ijmn}^A \partial_{y_n}\chi_{ms}^{AB}\Big) = 0 && \mathbf{y}\in Y_A\times(0,T),\\
&\rho^B \frac{d}{dt}\chi_{is}^{BA}(\mathbf{y},t) + \partial_{y_i}\gamma_s^{BA}(\mathbf{y},t) - \partial_{y_j}\Big(\eta_{ijmn}^B \partial_{y_n}\chi_{ms}^{BA}\Big) = 0 && \mathbf{y}\in Y_B\times(0,T),\\
&\rho^B \frac{d}{dt}\chi_{is}^{BB}(\mathbf{y},t) - \Big(\delta_{is} - \partial_{y_i}\gamma_s^{BB}(\mathbf{y},t)\Big) - \partial_{y_j}\Big(\eta_{ijmn}^B \partial_{y_n}\chi_{ms}^{BB}\Big) = 0 && \mathbf{y}\in Y_B
\end{aligned} \tag{5.25}$$

$$\frac{\partial\chi_{ki}^{\alpha\beta}}{\partial y_i} = 0 \qquad \text{where} \quad \alpha,\beta = A,B. \tag{5.26}$$

The interface conditions completing Eqs. (5.25), (5.26) are given by formulae (A.23) and (A.27). After averaging of (5.24) we get

$$
\begin{aligned}
(5.27)\quad & \left\langle w_i^{A(0)} \right\rangle_A + \left\langle w_i^{B(0)} \right\rangle_B \\
& = \left\langle \frac{1}{\rho^A} \int_0^t \left[\Phi_s^A(\mathbf{x},\tau)\chi_{is}^{AA}(\mathbf{y},t-\tau) + \Phi_s^B(\mathbf{x},\tau)\chi_{is}^{AB}(\mathbf{y},t-\tau) \right] d\tau \right\rangle_A \\
& + \left\langle \frac{1}{\rho^B} \int_0^t \left[\Phi_s^A(\mathbf{x},\tau)\chi_{is}^{BA}(\mathbf{y},t-\tau) + \Phi_s^B(\mathbf{x},\tau)\chi_{is}^{BB}(\mathbf{y},t-\tau) \right] d\tau \right\rangle_B \\
& + \left\langle \int_0^t \beta_i^A(y,t)\, dt \right\rangle_A + \left\langle \int_0^t \beta_i^B(y,t) dt \right\rangle_B .
\end{aligned}
$$

The functions $\boldsymbol{\beta}^\alpha$ are solutions to Eqs. (A.24)–(A.27). In more elaborate models of two-phase flows comprising surface tension on the interface fluid-solid the last two integral vanish. After appropriate substitutions we have finally

$$
\begin{aligned}
(5.28)\quad & \langle v_i^{(0)} \rangle_L - \dot{u}_i^{(0)} = \left\langle \int_0^t \left[\chi_{is}^{AA}(\mathbf{y},\tau) \left(F_s^A - \rho^A \ddot{u}_s^{(0)} - \partial_{x_s} p^{(0)} \right)(\mathbf{x},t-\tau) \right.\right. \\
& \left. + \chi_{is}^{AB}(\mathbf{y},\tau) \left(F_s^B - \rho^B \ddot{u}_s^{(0)} \right) - \partial_{x_s} p^{(0)} \right)(\mathbf{x},t-\tau) \Big] d\tau \Big\rangle_A \\
& + \left\langle \int_0^t \left[\chi_{is}^{BA}(\mathbf{y},\tau) \left(F_s^A - \rho^A \ddot{u}_s^{(0)} - \partial_{x_s} p^{(0)} \right)(\mathbf{x},t-\tau) \right.\right. \\
& \left. + \chi_{is}^{BB}(\mathbf{y},\tau) \left(F_s^B - \rho^B \ddot{u}_s^{(0)} \right) - \partial_{x_s} p^{(0)} \right)(\mathbf{x},t-\tau) \Big] d\tau \Big\rangle_B \\
& + \left\langle \int_0^t \beta_i^A(y,t)\, dt \right\rangle_A + \left\langle \int_0^t \beta_i^B(y,t)\, dt \right\rangle_B .
\end{aligned}
$$

This is the Darcy equation describing the flow of biphasic liquid in a porous deformable body.

5.4. Consolidation equation

At $\varepsilon^{(0)}$ Eq. (A.3) yields for the Y_A part of the elementary cube

$$
(5.29)\qquad \partial_{x_i} v_i^{A(0)}(\mathbf{x},\mathbf{y},t) + \partial_{y_i} v_i^{A(1)}(\mathbf{x},\mathbf{y},t) = 0,
$$

and similarly for the Y_B part. Hence, after averaging,

$$\partial_{x_i}\langle v_i^{A(0)}\rangle_A = -\langle \partial_{y_i} v_i^{A(1)}\rangle_A \qquad \text{and} \qquad \partial_{x_i}\langle v_i^{B(0)}\rangle_A = -\langle \partial_{y_i} v_i^{B(1)}\rangle_B$$

or

$$\partial_{x_i}\langle v_i^{A(0)}(\mathbf{x},\mathbf{y},t)\rangle_A = -\frac{1}{|Y|}\int\limits_{\partial Y_A} v_i^{A(1)}(\mathbf{x},\mathbf{y},t)\; n_i^A\, dS,$$

(5.30)

$$\partial_{x_i}\langle v_i^{B(0)}(\mathbf{x},\mathbf{y},t)\rangle_B = -\frac{1}{|Y|}\int\limits_{\partial Y_B} v_i^{B(1)}(\mathbf{x},\mathbf{y},t)\; n_i^B\, dS.$$

Hence

$$\partial_{x_i}\left[\left\langle v_i^{A(0)}(\mathbf{x},\mathbf{y},t)\rangle_A + \langle v_i^{B(0)}(\mathbf{x},\mathbf{y},t)\right\rangle_B\right] \tag{5.31}$$

$$= \frac{1}{|Y|}\Big[\int\limits_{\partial Y_A} v_i^{A(1)} n_i^A(\mathbf{x},\mathbf{y},t)dS \;+ \int\limits_{\partial Y_B} v_i^{B(1)} n_i^B(\mathbf{x},\mathbf{y},t)dS\Big].$$

In virtue of (A.10) and (A.11) we have also

$$\partial_{x_i}\left[\left\langle v_i^{A(0)}(\mathbf{x},\mathbf{y},t)\rangle_A + \left\langle v_i^{B(0)}(\mathbf{x},\mathbf{y},t)\right\rangle_B\right] = \frac{1}{|Y|}\int\limits_{\partial Y_S} \dot{u}_i^{(1)}(\mathbf{x},\mathbf{y},t)\; n_i^S\, dS.$$

Since, from the definition of averages (3.1)

$$\langle v_i^{A(0)}(\mathbf{x},\mathbf{y},t)\rangle_A + \langle v_i^{B(0)}(\mathbf{x},\mathbf{y},t)\rangle_B = \langle v_i^{(0)}(\mathbf{x},\mathbf{y},t)\rangle_L,$$

therefore by (5.4) we have

$$\partial_{x_i}\langle v_i^{(0)}\rangle_L = \frac{1}{|Y|}\int\limits_{\partial Y_S} \frac{d}{dt}\Big[A_i^{(pq)}(\mathbf{x},\mathbf{y},t)\,\partial_{x_q} u_p^{(0)}(\mathbf{x},t) \tag{5.32}$$

$$+P_i(\mathbf{x},t)\,p^{(0)}(\mathbf{x},t)\Big]\; n_i^S\, dA.$$

As result, after use of the divergence theorem, we obtain

$$\partial_{x_i}\langle v_i^{(0)}\rangle_L \tag{5.33}$$

$$= \frac{d}{dt}\Big[\left\langle \partial_{y_m} A_m^{(pq)}(\mathbf{x},\mathbf{y},t)\right\rangle_S \partial_{x_q} u_p^{(0)}(\mathbf{x},t) + \left\langle \partial_{y_m} P_m(\mathbf{x},t)\right\rangle_S p^{(0)}(\mathbf{x},t)\Big]$$

where $\langle v_i^{(0)}\rangle_L$ is given by the Darcy law (5. 28). This is the result of Biot's type for nonstationary processes of seepage of incompressible biphasic liquid, identical with those for monophasic flow, cf. [14].

6. Justification of the asymptotic analysis by the two-scale convergence

The aim of this section is to rigorously justify the results obtained by the formal method of two-scale asymptotic expansions. To this end, we exploit the notion of the two-scale convergence, cf. [4, 69, 70]. Consider the following system of equations:

$$
\begin{aligned}
\rho_S \ddot{\mathbf{u}}_S^\varepsilon(x,t) &= \operatorname{div}\left(\mathbf{a}^\varepsilon \mathbf{e}(\mathbf{u}^\varepsilon(x,t))\right) + F^S(x,t) \qquad \text{in } \Omega_S^\varepsilon \times (0,T),\\
\rho_A \dot{\mathbf{v}}_A^\varepsilon(x,t) &= \mu_A \varepsilon^2 \Delta \mathbf{v}_A^\varepsilon(x,t) - \nabla p_A^\varepsilon(x,t) + F^A(x,t) \quad \text{in } \Omega_A \times (0,T),\\
\rho_B \dot{\mathbf{v}}_B^\varepsilon(x,t) &= \mu_B \varepsilon^2 \Delta \mathbf{v}_B^\varepsilon(x,t) - \nabla p_B^\varepsilon(x,t) + F^B(x,t) \quad \text{in } \Omega_B \times (0,T),\\
\operatorname{div} \mathbf{v}_A^\varepsilon &= 0 \quad \text{in } \Omega_A^\varepsilon \times (0,T),\\
\operatorname{div} \mathbf{v}_B^\varepsilon &= 0 \quad \text{in } \Omega_B^\varepsilon \times (0,T),\\
\mathbf{a}^\varepsilon \mathbf{e}(\mathbf{u}^\varepsilon)\mathbf{n} &= (-p_B^\varepsilon \mathbf{1} + \varepsilon^2 \mathbf{e}(\mathbf{v}_B^\varepsilon))\mathbf{n} \quad \text{on } \Gamma_{SB}^\varepsilon \times (0,T),\\
[\![-p^\varepsilon \mathbf{1} + \varepsilon^2 \mu \mathbf{e}(\mathbf{v}^\varepsilon)]\!]_{AB}\mathbf{n} &= \sigma H^\varepsilon \mathbf{n} \quad \text{on } \Gamma_{AB}^\varepsilon \times (0,T),\\
\dot{\mathbf{u}}^\varepsilon(x,t) &= \mathbf{v}_B^\varepsilon(x,t) \quad \text{on } \Gamma_{SB}^\varepsilon \times (0,T),\\
\mathbf{v}_A^\varepsilon(x,t) &= \mathbf{v}_B^\varepsilon(x,t) \quad \text{on } \Gamma_{AB}^\varepsilon \times (0,T),
\end{aligned}
\tag{6.1}
$$

and the initial conditions

$$
\mathbf{u}^\varepsilon(x,0) = \mathbf{u}_0(x) \quad \text{in } \Omega_S^\varepsilon, \tag{6.2}
$$

$$
\dot{\mathbf{u}}^\varepsilon(x,0) = \mathbf{u}_1(x) \quad \text{in } \Omega_S^\varepsilon, \tag{6.3}
$$

$$
\mathbf{v}^\alpha(x,0) = \mathbf{v}_0^\alpha(x) \quad \text{in } \Omega^\alpha;\ \alpha = A, B. \tag{6.4}
$$

We assume here that the function $H^\varepsilon(x) = H(\frac{x}{\varepsilon})$ is an εY-periodic function defined on the surface Γ_{AB}^ε. We can then formulate the following theorem.

THEOREM. *The sequence* $\{\mathbf{u}^\varepsilon, \mathbf{v}_A^\varepsilon, \mathbf{v}_B^\varepsilon, p_A^\varepsilon, p_B^\varepsilon\}_{\varepsilon>0}$ *of solutions of the system* (6.1)–(6.12) *is two-scale convergent to the solution*

$$
(\mathbf{u}^{(0)}(x,t), \mathbf{v}_A^{(0)}(x,y,t), \mathbf{v}_B^{(0)}(x,y,t), p_A^{(0)}(x,t), p_B^{(0)}(x,t))
$$

of the two-scale homogenized problem

$$(6.5)\quad (1-f)\rho^S \ddot{\mathbf{u}}^{(0)} + \rho^A \langle \dot{\mathbf{v}}_A^{(0)} \rangle_{Y_A} + \rho^B \langle \dot{\mathbf{v}}_B^{(0)} \rangle_{Y_B}$$
$$= \operatorname{div}_x \int\limits_{Y_S} \left[\mathbf{a}(\nabla_x \mathbf{u}^{(0)} + \nabla_y \mathbf{u}^{(1)}) \right] dy - \int\limits_{Y_A} \nabla_y p_A^{(1)}(x,y,t)\, dy$$
$$- \int\limits_{Y_B} \nabla_y p_B^{(1)}(x,y,t)\, dy - f_A \nabla_x p_A^{(0)}(x,t), -f_B \nabla_x p_B^{(0)}(x,t)$$
$$+ (1-f) F^S(x,t) + f_A F^A(x,t) + f_B F^B(x,t) \quad \text{in } \Omega \times (0,T),$$

$$(6.6)\quad \operatorname{div}_y [\mathbf{a}(\nabla_x \mathbf{u}^{(0)} + \nabla_y \mathbf{u}^{(1)})] = 0 \quad \text{in } \Omega \times Y_S \times (0,T),$$

$$(6.7)\quad \rho^A \dot{\mathbf{v}}_A^{\varepsilon}(x,y,t) = \mu_A \Delta_y \mathbf{v}_A^{(0)}(x,y,t)$$
$$- \nabla_x p_A^{(0)}(x,t) - \nabla_y p_A^{(1)}(x,y,t) + F^A(x,t) \quad \text{in } \Omega \times Y_A \times (0,T),$$

$$(6.8)\quad \rho^B \dot{\mathbf{v}}_B^{(0)}(x,y,t) = \mu_B \Delta \mathbf{v}_B^{(0)}(x,y,t) - \nabla_x p_B^{(0)}(x,t)$$
$$- \nabla_y p_B^{(1)}(x,y,t) + F^B(x,t) \text{ in } \Omega \times Y_B \times (0,T),$$

$$(6.9)\quad \operatorname{div}_y \mathbf{v}_A^{(0)} = 0 \quad \text{in } \Omega \times Y_A \times (0,T),$$

$$(6.10)\quad \operatorname{div}_y \mathbf{v}_B^{(0)} = 0 \quad \text{in } \Omega \times Y_B \times (0,T),$$

$$(6.11)\quad \operatorname{div}_x \int\limits_{Y_A} \mathbf{v}_A^{(0)}(x,y,t)\, dy = \int\limits_{Y_A} \operatorname{div}_y \mathbf{v}(1)_A(x,y,t),$$

$$(6.12)\quad \operatorname{div}_x \int\limits_{Y_B} \mathbf{v}_B^{(0)}(x,y,t)\, dy = \int\limits_{Y_B} \operatorname{div}_y \mathbf{v}_B^{(1)}(x,y,t),$$

$$(6.13)\quad [\![p^{(0)}]\!] = 0 \quad \text{on } \Gamma_{AB} \times (0,T),$$

$$(6.14)\quad [\![p^{(1)} \mathbf{1} + 2\mu \mathbf{e}(\mathbf{v}^{(0)})]\!] \mathbf{n} = \sigma H^{(1)} \mathbf{n} \quad \text{on } \Gamma_{AB} \times (0,T).$$

Sketch of the proof. By a standard procedure we show that there exists a constant $c > 0$ independent of ε such that

$$\|\mathbf{u}^\varepsilon\|_{H^1(\Omega)^3} \leq c, \ \|\mathbf{v}^\varepsilon\|_{L^2(\Omega)^3} \leq c, \ \varepsilon\|\nabla \mathbf{v}^\varepsilon\|_{L^2(\Omega,\mathbb{E}^N)} \leq c,$$

where $\mathbb{E}^N$ stands for the space of $N \times N$ matrices. For the definitions and properties of the Lebesgue and Sobolev spaces the reader is referred to ADAMS [1]. The two-scale limits of these sequences satisfy the following properties, cf. [4],

$$\operatorname{div}_y \mathbf{v}^{(0)_A}(x,y,t) = 0 \qquad \text{in} \qquad \Omega \times Y_B \times (0,T),$$

$$\operatorname{div}_x \mathbf{v}_A^{(0)}(x,y,t) + \operatorname{div}_y \mathbf{v}_A^{(1)}(x,y,t) = 0 \text{ in } \Omega \times Y_A \times (0,T),$$

$$\nabla_y \mathbf{u}^{(0)}(x,y,t) = 0, \qquad \text{or} \qquad \mathbf{u}^{(0)} = \mathbf{u}^{(0)}(x,t), \ t \in (0,T), \ x \in \Omega.$$

Similar equation is satisfied by the velocity $\mathbf{v}_B$ in $(0,T) \times \Omega \times Y_B$. The next conclusion, deduced from the two-scaled convergence, is that

$$\nabla_y p_A^{(0)}(x,y,t) = 0, \text{ or } p_A^{(0)} = p_A^{(0)}(x,t) \ (x,t) \in \Omega \times (0,T).$$

Similarly, for the pressure $p_B^{(0)}$ we write

$$\nabla_y p_B^{(0)}(x,y,t) = 0, \text{ or } p_B^{(0)} = p_B^{(0)}(x,t) \ (x,t) \in \Omega \times (0,T).$$

Let $\chi_S^\varepsilon, \chi_A^\varepsilon, \chi_B^\varepsilon$ be the characteristic functions and let $\phi = \phi(t) \in C^\infty(0,T)$ be such that $\phi(0) = \phi(T) = 0$. We also take a test function $\mathbf{\Phi}^\varepsilon(x)$ such that

$$\mathbf{\Phi}^\varepsilon(x) = \boldsymbol{\eta}(x) + \varepsilon \vartheta(x, \frac{x}{\varepsilon}),$$

where $\boldsymbol{\eta} \in \mathcal{D}(\Omega)^3$ and $\vartheta(x,y) \in \mathcal{D}[\Omega; C^\infty_{per}(Y)]^3$. Now the proof, rather lengthy, is an extension of the proof derived in [14] for a one-phase flow. However, difficulties which arise are due to the fact that interface Γ^ε_{AB} depends on time. We hope to present a detailed proof elsewhere.

7. Passage to the stationary case

To perform this passage we shall first reformulate the local problems and Darcy's law. To this end we set: $\boldsymbol{\chi}^{\alpha\beta} = \dot{\boldsymbol{\psi}}^{\alpha\beta}$, $\alpha, \beta \in \{A, B\}$, cf. [14],

PROBLEM P_1

Find the functions $\boldsymbol{\chi}^{\alpha\beta}$ and $\gamma^{AB(k)}$such that

$$\varrho^A \dot{\boldsymbol{\chi}}^{AA(k)}(y,t) = \eta^A \Delta_{yy} \boldsymbol{\chi}^{AA(k)}(y,t) - \nabla \gamma^{AA(k)}(y,t) + \mathbf{e}_k, \text{ in } Y_A \times (0,T),$$

$$\varrho^A \dot{\chi}^{AB(k)}(y,t) = \eta^A \Delta_{yy} \chi^{ABk)}(y,t) - \nabla \gamma^{ABk)}(y,t), \text{ in } Y_A \times (0,T),$$

$$\varrho^B \dot{\chi}^{BB(k)}(y,t) = \eta^B \Delta_{yy} \chi^{BB(k)}(y,t) - \nabla \gamma^{BB(k)}(y,t) + \mathbf{e}_k, \text{ in } Y_B \times (0,T),$$

$$\varrho^B \dot{\chi}^{BA(k)}(y,t) = \eta^B \Delta_{yy} \chi^{BA(k)}(y,t) - \nabla \gamma^{BA(k)}(y,t), \text{ in } Y_B \times (0,T),$$

$$\operatorname{div} \boldsymbol{\psi}^{AA(k)} = \operatorname{div} \boldsymbol{\psi}^{AB(k)} = 0, \quad \text{in } Y_A \times (0,T);$$

$$\operatorname{div} \boldsymbol{\psi}^{BB(k)} = \operatorname{div} \boldsymbol{\psi}^{BA(k)} = 0, \quad \text{in } Y_B \times (0,T);$$

$$\eta^A \mathbf{e}^y(\boldsymbol{\psi}^{AA(k)})\mathbf{n} - \gamma^{AA(k)}\mathbf{n} = \eta^B \mathbf{e}^y(\boldsymbol{\psi}^{BA(k)})\mathbf{n} - \gamma^{BA(k)}\mathbf{n}, \qquad \text{on } \Gamma_{AB},$$

$$\eta^A \mathbf{e}^y(\boldsymbol{\psi}^{AB(k)})\mathbf{n} - \gamma^{AB(k)}\mathbf{n} = \eta^B \mathbf{e}^y(\boldsymbol{\psi}^{BB(k)})\mathbf{n} - \gamma^{BB(k)}\mathbf{n}, \qquad \text{on } \Gamma_{AB},$$

$$\boldsymbol{\psi}^{AA(k)} - \boldsymbol{\psi}^{BA(k)} = 0, \ \boldsymbol{\psi}^{AB(k)} - \boldsymbol{\psi}^{BB(k)} = 0 \qquad \text{on } \Gamma_{AB}.$$

Moreover, homogeneous initial conditions and no-slip condition on the fluid-solid interface are assumed. Let us pass to the formulation of the second local problem.

LOCAL PROBLEM P_2

Find functions $\boldsymbol{\beta}^\alpha$ and π^α such that

$$\varrho^\alpha \dot{\boldsymbol{\beta}}^\alpha = \eta^\alpha \Delta_{yy} \boldsymbol{\beta}^\alpha - \nabla \pi^\alpha, \quad \text{in } Y_\alpha \times (0,T),$$

$$\operatorname{div}_y \boldsymbol{\beta}^\alpha = 0 \quad \text{in } Y_\alpha \times (0,T),$$

$$\boldsymbol{\beta}^A - \boldsymbol{\beta}^B = 0 \quad \text{on } \Gamma_{AB},$$

$$(\eta^A \mathbf{e}^y(\boldsymbol{\beta}^A) - \pi^A \mathbf{I})\mathbf{n} = (\eta^B \mathbf{e}^y(\boldsymbol{\beta}^B) - \pi^B \mathbf{I})\mathbf{n} + \sigma H \mathbf{n}, \text{ on } \Gamma_{AB},$$

$$\boldsymbol{\beta}^A = \boldsymbol{\beta}^B = \mathbf{0} \quad \text{on } \Gamma.$$

This system is completed by the homogeneous initial conditions. Then Darcy's law takes the form, cf. (5.27), where instead of $\boldsymbol{\chi}$ we write $\dot{\boldsymbol{\psi}}$. This law can be

written as follows:

$$(7.1)\quad \langle \bar{\mathbf{v}}^0 \rangle_L = \frac{1}{\varrho^A} \int_0^t \left\langle \dot{\psi}^{AA(k)}(y,s) \right\rangle_A (F_k^A - \varrho^A \ddot{\mathbf{u}}_k^{(0)} - \frac{\partial p^{A(0)}}{\partial x_k})(x, t-s)\, ds$$

$$+ \frac{1}{\varrho^A} \int_0^t \left\langle \dot{\psi}^{AB(k)}(y,s) \right\rangle_A (F_k^B - \varrho^B \ddot{\mathbf{u}}_k^{(0)} - \frac{\partial p^{B(0)}}{\partial x_k})(x, t-s)\, ds$$

$$+ \frac{1}{\varrho^B} \int_0^t \left\langle \dot{\psi}^{BB(k)}(y,s) \right\rangle_B (F_k^B - \varrho^B \ddot{\mathbf{u}}_k^{(0)} - \frac{\partial p^{B(0)}}{\partial x_k})(x, t-s)\, ds$$

$$+ \frac{1}{\varrho^B} \int_0^t \left\langle \dot{\psi}^{BA(k)}(y,s) \right\rangle_B (F_k^A - \varrho^A \ddot{\mathbf{u}}_k^{(0)} - \frac{\partial p^{A(0)}}{\partial x_k})(x, t-s)\, ds$$

$$+ \int_0^t \left\langle \dot{\boldsymbol{\beta}}^A(y, t-s) \right\rangle_A ds + \int_0^t \left\langle \dot{\boldsymbol{\beta}}^B(y, t-s) \right\rangle_B ds.$$

It may be rewritten as follows:

$$(7.2)\quad \langle \bar{\mathbf{v}}^0 \rangle_L = \int_0^t \left\{ \left[\frac{1}{\varrho^A} \left\langle \dot{\psi}^{AA(k)}(y,s) \right\rangle_A \right.\right.$$

$$\left.\left. + \frac{1}{\varrho^B} \left\langle \dot{\psi}^{BA(k)}(y,s) \right\rangle_B \right] (F_k^A - \varrho^A \ddot{\mathbf{u}}_k^{(0)} - \frac{\partial p^{A(0)}}{\partial x_k})(x, t-s) \right\} ds$$

$$\int_0^t \left\{ \left(\frac{1}{\varrho^A} \left\langle \dot{\psi}^{AB(k)}(y,s) \right\rangle_A \right.\right.$$

$$\left.\left. + \frac{1}{\varrho^B} \left\langle \dot{\psi}^{BB(k)}(y,s) \right\rangle_B \right] (F_k^B - \varrho^B \ddot{\mathbf{u}}_k^{(0)} - \frac{\partial p^{B(0)}}{\partial x_k})(x, t-s) \right\} ds$$

$$+ \int_0^t \left\langle \dot{\boldsymbol{\beta}}^A(y, t-s) \right\rangle_A ds + \int_0^t \left\langle \dot{\boldsymbol{\beta}}^B(y, t-s) \right\rangle_B ds.$$

The passage to the stationary case is enforced by assuming that the forcing terms $\mathbf{F}^A - \varrho^A \ddot{\mathbf{u}}^{(0)} - \nabla p^{A(0)}$ and $\mathbf{F}^B - \varrho^B \ddot{\mathbf{u}}^{(0)} - \nabla p^{B(0)}$ are time-independent. Next we

have to pass with time to infinity, cf. (BIELSKI and TELEGA [13]), HEYWOOD [55]. Consequently, since $\ddot{\mathbf{u}}^{(0)} = \mathbf{0}$ we get

$$(7.3)\quad \langle \bar{\mathbf{v}}^0 \rangle_L = \Big\{ \int_0^t \Big[\frac{1}{\varrho^A} \Big\langle \dot{\boldsymbol{\psi}}^{AA(k)}(y,s) \Big\rangle_A + \frac{1}{\varrho^B} \Big\langle \dot{\boldsymbol{\psi}}^{BA(k)}(y,s) \Big\rangle_B \Big] ds \Big\} \Big(F_k^A - \frac{\partial p^{A(0)}}{\partial x_k} \Big)(x)$$

$$+ \Big\{ \int_0^t \Big[\frac{1}{\varrho^A} \Big\langle \dot{\boldsymbol{\psi}}^{AB(k)}(y,s) | \Big\rangle_A + \frac{1}{\varrho^B} | \Big\langle \dot{\boldsymbol{\psi}}^{BB(k)}(y,s) \Big\rangle_B \Big] ds \Big\}$$

$$\Big(F_k^B - \frac{\partial p^{B(0)}}{\partial x_k} \Big)(x) + \int_0^t \Big\langle \dot{\mathbf{W}}^{\mathbf{A}}(y, t-s) \Big\rangle_A ds + \int_0^t \Big\langle \dot{\mathbf{W}}^{\mathbf{B}}(y, t-s) \Big\rangle_B ds.$$

Consider the first integral in the r.h.s of the last relation. We have

$$(7.4)\quad \int_0^t A_{ij}^A \big(t-s\big)\, ds = \frac{1}{\varrho_A |Y|} \int_{Y_A} \Big(\int_0^t \frac{\partial \boldsymbol{\psi}^{AA(i)}(t-s,y)}{\partial s}\, ds \Big) \cdot \mathbf{e}_j \, dy$$

$$+ \frac{1}{\varrho_B |Y|} \int_{Y_B} \Big(\int_0^t \frac{\partial \boldsymbol{\psi}^{BA(i)}(t-s,y)}{\partial s}\, ds \Big) \cdot \mathbf{e}_j \, dy.$$

Here A_{ij}^A is a part of the permeability tensor that corresponds to the forcing term $\mathbf{F}^A - \nabla_x p^{A(0)}$, i.e.,

$$\langle \mathbf{v}_A \rangle_A = \int_0^t A_{ij}(t-s)(\mathbf{F}^A - \nabla p^{A(0)}\, ds.$$

Performing the integration by parts in Eq. (7.4) we get

$$(7.5)\quad \int_0^t A_{ij}^A (t-s)\, ds = \frac{1}{\varrho^A |Y|} \int_{Y_A} \boldsymbol{\chi}^{AA(i)}(t,y) \cdot \mathbf{e}_j \, dy$$

$$+ \frac{1}{\varrho^B |Y|} \int_{Y_B} \boldsymbol{\psi}^{BA(i)}(t,y) \cdot \mathbf{e}_j \, dy.$$

Letting t to tend to infinity we find

$$\lim_{t\to\infty}\int_0^t A_{ij}^A(t-s)\,ds$$

$$= \frac{1}{\varrho^A|Y|}\int_{Y_A}\psi_\infty^{AA(i)}(y)\cdot\mathbf{e}_j\,dy + \frac{1}{\varrho_B|Y|}\int_{Y_B}\psi_\infty^{BA(i)}(y)\cdot\mathbf{e}_j\,dy = K_{ij}^A. \tag{7.6}$$

Similarly, the second integral on the r.h.s. of Eq. (7.3) yields

$$\lim_{t\to\infty}\int_0^t A_{ij}^A(t-s)\,ds$$

$$= \lim_{t\to\infty}\frac{1}{\varrho^A|Y|}\int_{Y_B}(\psi^{AA(i)}(t,y)\cdot\mathbf{e}_j\,dy + \frac{1}{\varrho^B|Y|}\int_{Y_B}\psi^{BA(i)}(t,y)\cdot\mathbf{e}_j\,dy = K_{ij}^B.$$

The third integral on the r.h.s. of Eq. (7.3) gives

$$\int_0^t \frac{1}{\varrho^A|Y|}\Big(\int_{Y_A}\frac{\partial\boldsymbol{\beta}^A(y,t-s)}{\partial s}\,dy\Big)\,ds = \frac{1}{\varrho^A|Y|}\int_{Y_A}\Big(\int_0^t\frac{\partial\boldsymbol{\beta}^A(y,t-s)}{\partial s}\,ds\Big)\,dy \tag{7.7}$$

$$= \frac{1}{\varrho^A|Y|}\int_{Y_A}\Big[-\boldsymbol{\beta}^A(y,0)+\boldsymbol{\beta}^A(y,t)\Big]\,dy.$$

By the initial condition we write $\boldsymbol{\beta}(y,0)=0$. Moreover, $\lim_{t\to\infty}\mathbf{W}^A(y,t)$ exists. We denote it by $\boldsymbol{\beta}_\infty^A(y)$, i.e.,

$$\lim_{t\to\infty}\boldsymbol{\beta}^A(y,t) = \boldsymbol{\beta}_\infty^A(y).$$

Finally, Darcy's law for the stationary two-phase flow assumes the following form

$$\langle\bar{\mathbf{v}}^{(0)}\rangle = K_{ij}^A(F_j^A - \frac{\partial p^{A(0)}}{\partial x_j}) + K_{ij}^B(F_j^B - \frac{\partial p^{B(0)}}{\partial x_j})$$

$$+ \frac{1}{|Y|}\int_{Y_A}\boldsymbol{\beta}^A(y)\,dy + \frac{1}{|Y|}\int_{Y_B}\boldsymbol{\beta}^B(y)\,dy.$$

This law is similar to the one derived in [74] for two-phase flow through undeformable porous medium provided that our symbols ψ are indentified with $\mathbf{V}$ in [74] and $\boldsymbol{\beta}_\infty$ with $\mathbf{W}$. The local problems for the determination of functions $\mathbf{V}$, $\mathbf{W}$, etc., are specified and studied in [74].

8. An example

As an example we consider one-dimensional stationary flow of two-phase liquid through a bundle of tubes in the direction z in the cylindrical coordinate system. We assume that the local problem has a cylindrical symmetry. Hence only the velocity in the z-direction does not vanish. For the sake of simplicity we assume that the fluid A occupies the pipe of radius R_A and is surrounded by the fluid B which forms a ring of the external radius R_B. Let us pass to the study of local problems derived from (7.6). For simplicity we wrrite $\chi^{\alpha\beta}$ instead of $\chi^{\alpha\beta}_{\infty}$; obviously now $\chi^{\alpha\beta} = \psi^{\alpha\beta}$.

LOCAL PROBLEM P_1

$$\eta_A \frac{1}{r}\frac{d}{dr}\left(r\frac{d\chi^{AA}(r)}{dr}\right) = \frac{d\gamma^{AA}(z)}{dz} + 1 = 0, \text{ for } 0 \le r \le R_A,$$
$$\eta_B \frac{1}{r}\frac{d}{dr}\left(r\frac{d\chi^{BA}(r)}{dr}\right) = \frac{d\gamma^{BA}(z)}{dz} = 0, \text{ for } R_A \le r \le R_B. \tag{8.1}$$

The interface conditions are now specified by

$$\chi^{AA}(R_A) = \chi^{BA}(R_A),\ \eta_A\frac{d\chi^{AA}}{dr}(R_A) = \eta_B\frac{d\chi^{BA}}{dr}(R_A),\ \chi^{AA}(R_B) = 0$$
$$\gamma^{AA} = \gamma^{BA} \quad \text{for } r = R_A. \tag{8.2}$$

Similar problems have to be formulated for $\chi^{BB}, \chi^{AB}, \gamma^{BB}$ and γ^{AB}. The solution ofproblemP_1 is given by

$$\chi^{AA}(r) = \frac{1}{4\eta_A}(r^2 - R_A^2) + \frac{1}{2\eta_B}R_A^2 \ln\frac{R_A}{R_B} \quad \text{for } 0 \le r \le R_A$$
$$\chi^{BA}(r) = \frac{1}{2\eta_B}R_A^2 \ln\frac{r}{R_B}, \quad \text{for } R_A \le r \le R_B. \tag{8.3}$$

The local functions χ^{BB} and χ^{AB} are specified by

$$\chi^{AB}(r) = \frac{1}{4\eta_B}(R_A^2 - R_B^2) - \frac{1}{2\eta_B}R_A^2 \ln\frac{R_A}{R_B}, \quad \text{if } 0 \le r \le R_A,$$
$$\chi^{BB}(r) = \frac{1}{4\eta_B}(r^2 - R_B^2) - \frac{1}{2\eta_B}R_A^2 \ln\frac{r}{R_B}, \quad \text{if } R_A \le r \le R_B. \tag{8.4}$$

LOCAL PROBLEM P_2

Now $\beta^A = (0, 0, \beta^A(r))$ and we have

$$\eta_A \frac{1}{r}\frac{d}{dr}\left(r\frac{d\beta^A(r)}{dr}\right) = \frac{d\pi^A(z)}{dz} = 0, \quad \text{for } 0 \le r \le R_A. \tag{8.5}$$

Similarly β^B is a solution to

$$\eta_B \frac{1}{r}\frac{d}{dr}\left(r\frac{d\beta^B(r)}{dr}\right) = \frac{d\pi^B(z)}{dz} = 0, \quad \text{for } R_A \leq r \leq R_B. \tag{8.6}$$

The boundary and interface conditions are:

$$\begin{gathered}\beta^A(R_A) = \beta^B(R_A), \ \eta_A \frac{d\beta^A}{dr}(R_A) = \eta_B \frac{d\beta^B}{dr}(R_A), \ \beta^B(R_B) = 0, \\ \pi^A = \pi^B + \frac{2\sigma}{R_A}, \quad \text{for } r = R_A.\end{gathered} \tag{8.7}$$

The solution of the local problem P_2 is trivial,

$$\beta^A(r) = \beta^B(r) = 0. \tag{8.8}$$

According to formula (7.6) Darcy's law assumes now the form

$$\begin{aligned}\left\langle v^{(0)}\right\rangle_L - f\dot{u} = \left\{\frac{\pi}{8\eta_A|Y|}R_A^4 + \frac{\pi}{2\eta_B|Y|}R_A^2\left(R_A^2 - R_B^2\right)\left(\frac{1}{2} - \ln R_B\right)\right\}\left(F_3^A - \frac{\partial p^{A(0)}}{\partial x_3}\right) \\ + \frac{\pi}{8\eta_B|Y|}\left(R_A^2 - R_B^2\right)^2\left(F_3^B - \frac{\partial p^{B(0)}}{\partial x_3}\right).\end{aligned}$$

We observe that a similar stationary flow was investigated by ZANOTTI and CARBONELL [83]. However, an explicit form of the Darcy law was not given by these authors. Moreover, homogenization was not used.

9. Final remarks

Essential feature of viscous flows through microperiodic porous media studied in the present paper and in [14, 15] is a linear elastic solid phase and Stokesian fluids. A challenging problem is to derive macroscopic flow for Navier-Stokes or other nonlinear fluids and more involved solid phases. We think of hyperelastic and inelastic phases. For instance, one can think of the solid phase made of elastic Ogden's material or elastic-plastic phases. Also, thermal flows are worth of examination.

Another open problem is to extend our results to the case of porous media with random distribution of micropores, cf. Sec. 2 of our paper for a brief discussion of simpler problems.

Darcy's law for nonstationary flows is nonlocal in time, also in the case of one-phase flow, cf. [14, 15]. Such a law is complicated and in general not directly applicable. Hence the need for elaboration of reliable approximate methods, the problem well known in micromechanics.

Acknowledgements

The authors were supported by the State Committee for Scientific Research (KBN - Poland) through the grant No 6 P04D 039 15. The second and the third author were also supported through the grant No 8 T11F 017 18.

Appendix A. Asymptotic analysis

Equations of motion$(4.1)_{1,2}$ and $(4.1)_3$ after substitution of expansions (4.4) take the form

$$\begin{aligned}(A.1)\quad & \rho^S\left[\ddot{u}_i^{(0)}(\mathbf{x},\mathbf{y},t)+\varepsilon\ddot{u}_i^{(1)}(\mathbf{x},\mathbf{y},t)+\varepsilon^2\ddot{u}_i^{(2)}(\mathbf{x},\mathbf{y},t)+...\right]\\ &=\left(\frac{\partial}{\partial x_j}+\frac{1}{\varepsilon}\frac{\partial}{\partial y_j}\right)\left\{a_{ijmn}\left(\frac{\partial}{\partial x_n}+\frac{1}{\varepsilon}\frac{\partial}{\partial y_n}\right)\left[u_m^{(0)}(\mathbf{x},\mathbf{y},t)\right.\right.\\ &\qquad\left.\left.+\varepsilon u_m^{(1)}(\mathbf{x},\mathbf{y},t)+\varepsilon^2u_m^{(2)}(\mathbf{x},\mathbf{y},t)+...\right]\right\}+F_i^S,\end{aligned}$$

$$\begin{aligned}(A.2)\quad & \rho^A\left[\dot{v}_i^{A(0)}(\mathbf{x},\mathbf{y},t)+\varepsilon\dot{v}_i^{A(1)}(\mathbf{x},\mathbf{y},t)+\varepsilon^2\dot{v}_i^{A(2)}(\mathbf{x},\mathbf{y},t)+...\right]\\ &=\left(\frac{\partial}{\partial x_j}+\frac{1}{\varepsilon}\frac{\partial}{\partial y_j}\right)\left\{\left[p^{A(0)}(\mathbf{x},\mathbf{y},t)+\varepsilon p^{A(1)}(\mathbf{x},\mathbf{y},t)\right.\right.\\ &\left.+\varepsilon^2p^{A(2)}(\mathbf{x},\mathbf{y},t)+...\right]\delta_{ij}+\varepsilon^2\eta_{ijmn}^A\left(\frac{\partial}{\partial x_n}+\frac{1}{\varepsilon}\frac{\partial}{\partial y_n}\right)\left[v_m^{A(0)}(\mathbf{x},\mathbf{y},t)\right.\\ &\qquad\left.\left.+\varepsilon v_m^{A(1)}(\mathbf{x},\mathbf{y},t)+\varepsilon^2v_m^{A(2)}(\mathbf{x},\mathbf{y},t)+...\right]\right\}+F_i^A,\end{aligned}$$

and

$$\begin{aligned}(A.3)\quad & \left(\frac{\partial}{\partial x_i}+\frac{1}{\varepsilon}\frac{\partial}{\partial y_i}\right)\left[v_i^{A(0)}(\mathbf{x},\mathbf{y},t)\right.\\ &\qquad\left.+\varepsilon v_i^{A(1)}(\mathbf{x},\mathbf{y},t)+\varepsilon^2v_i^{A(2)}(\mathbf{x},\mathbf{y},t)+...\right]=0.\end{aligned}$$

Similar relations held for $\mathbf{v}^B$, only the index A should be replaced by B. The interface conditions (4.2) read

$$
\begin{aligned}
(A.4)\quad & a_{ijmn}\left(\frac{\partial}{\partial x_n}+\frac{1}{\varepsilon}\frac{\partial}{\partial y_n}\right)\Big[u_m^{(0)}(\mathbf{x},\mathbf{y},t) \\
& \qquad +\varepsilon u_m^{(1)}(\mathbf{x},\mathbf{y},t)+\varepsilon^2 u_m^{(2)}(\mathbf{x},\mathbf{y},t)+\ldots\Big]\,n_j \\
& = \Big\{-\Big[p^{A(0)}(\mathbf{x},\mathbf{y},t)+\varepsilon p^{A(1)}(\mathbf{x},\mathbf{y},t)+\varepsilon^2 p^{A(2)}(\mathbf{x},\mathbf{y},t)+\ldots\Big]\,\delta_{ij} \\
& \qquad +\varepsilon^2\eta^A_{ijmn}\left(\frac{\partial}{\partial x_n}+\frac{1}{\varepsilon}\frac{\partial}{\partial y_n}\right)\Big[v_m^{A(0)}(\mathbf{x},\mathbf{y},t) \\
& \qquad +\varepsilon v_m^{A(1)}(\mathbf{x},\mathbf{y},t)+\varepsilon^2 v_m^{A(2)}(\mathbf{x},\mathbf{y},t)+\ldots\Big]\Big\}\,n_j \quad \text{on} \quad \Gamma,
\end{aligned}
$$

$$
\begin{aligned}
(A.5)\quad & \left(\dot{u}_i^{(0)}+\varepsilon\dot{u}_i^{(1)}+\varepsilon^2\dot{u}_i^{(2)}+\cdots\right)\Big|_S = \left(v_i^{A(0)}+\varepsilon v_i^{A(1)}+\varepsilon^2 v_i^{A(2)}+\cdots\right)\Big|_A \\
& \qquad \text{on } \Gamma_A \\
& \left(\dot{u}_i^{(0)}+\varepsilon\dot{u}_i^{(1)}+\varepsilon^2\dot{u}_i^{(2)}+\cdots\right)\Big|_S = \left(v_i^{B(0)}+\varepsilon v_i^{B(1)}+\varepsilon^2 v_i^{B(2)}+\cdots\right)\Big|_B \\
& \qquad \text{on } \Gamma_B
\end{aligned}
$$

$$
\begin{aligned}
(A.6)\quad & \left(v_i^{A(0)}+\varepsilon v_i^{A(1)}+\varepsilon^2 v_i^{A(2)}+\cdots\right)\Big|_A \\
& \qquad = \left(v_i^{B(0)}+\varepsilon v_i^{B(1)}+\varepsilon^2 v_i^{B(2)}+\cdots\right)\Big|_B \text{ on } \Gamma_{AB}
\end{aligned}
$$

and

$$
\begin{aligned}
(A.7)\quad & \Big\{-\Big[p^{A(0)}(\mathbf{x},\mathbf{y},t)+\varepsilon p^{A(1)}(\mathbf{x},\mathbf{y},t)+\varepsilon^2 p^{A(2)}(\mathbf{x},\mathbf{y},t)+\ldots\Big]\,\delta_{ij} \\
& \qquad +\varepsilon^2\eta^A_{ijmn}\left(\frac{\partial}{\partial x_n}+\frac{1}{\varepsilon}\frac{\partial}{\partial y_n}\right)\Big[v_m^{A(0)}(\mathbf{x},\mathbf{y},t)+\varepsilon v_m^{A(1)}(\mathbf{x},\mathbf{y},t) \\
& \qquad +\varepsilon^2 v_m^{A(2)}(\mathbf{x},\mathbf{y},t)+\ldots\Big]\Big\}\,n_j = \Big\{-\Big[p^{B(0)}(\mathbf{x},\mathbf{y},t)+\varepsilon p^{B(1)}(\mathbf{x},\mathbf{y},t) \\
& \qquad +\varepsilon^2 p^{B(2)}(\mathbf{x},\mathbf{y},t)+\ldots\Big]\,\delta_{ij}+\varepsilon^2\eta^B_{ijmn}\left(\frac{\partial}{\partial x_n}+\frac{1}{\varepsilon}\frac{\partial}{\partial y_n}\right)\Big[v_m^{B(0)}(\mathbf{x},\mathbf{y},t) \\
& \qquad +\varepsilon v_m^{B(1)}(\mathbf{x},\mathbf{y},t)+\varepsilon^2 v_m^{B(2)}(\mathbf{x},\mathbf{y},t)+\ldots\Big]\Big\}\,n_j+\varepsilon\sigma H_{ij}n_j \quad \text{on } \Gamma_{AB}.
\end{aligned}
$$

Analysis of terms of different orders of ε in equations at interfaces

From the interface condition (A.4) we find that at ε^{-1} appears the term

$$a_{ijmn}\partial_{y_n}u_m^{(0)}\, n_j = 0 \qquad \text{on } \Gamma \tag{A.8}$$

while the terms linked with ε^0 give

$$\begin{aligned}
&\Big[a_{ijmn}\Big(\partial_{x_n}u_m^{(0)} + \partial_{y_n}u_m^{(1)}\Big)\Big]n_j^S = -p^{A(0)}\, n_i^S \qquad \text{on} \quad \Gamma_A,\\
&\Big[a_{ijmn}\Big(\partial_{x_n}u_m^{(0)} + \partial_{y_n}u_m^{(1)}\Big)\Big]n_j^S = -p^{B(0)}\, n_i^S \qquad \text{on} \quad \Gamma_B.
\end{aligned} \tag{A.9}$$

Comparing the terms at different orders of ε in (A.5) we get

$$\begin{aligned}
&\dot{u}_i^{(0)}\Big|_S = v_i^{A(0)}\Big|_A, \quad \dot{u}_i^{(1)}\Big|_S = v_i^{A(1)}\Big|_A, \quad \dot{u}_i^{(2)}\Big|_S = v_i^{A(2)}\Big|_A \ \textit{etc.} \ \text{on}\,\Gamma_A,\\
&\dot{u}_i^{(0)}\Big|_S = v_i^{B(0)}\Big|_B, \quad \dot{u}_i^{(1)}\Big|_S = v_i^{B(1)}\Big|_B, \quad \dot{u}_i^{(2)}\Big|_S = v_i^{B(2)}\Big|_B \ \textit{etc.} \ \text{on}\,\Gamma_B,
\end{aligned} \tag{A.10}$$

and similarly in (A.6)

$$v_i^{A(0)}\Big|_A = v_i^{B(0)}\Big|_B \quad v_i^{A(1)}\Big|_A = v_i^{B(1)}\Big|_B \quad v_i^{A(2)}\Big|_A = v_i^{B(2)}\Big|_B \ \textit{etc.} \ \text{on}\,\Gamma_{AB}. \tag{A.11}$$

The terms at ε^0 in (A.7) give

$$p^{A(0)}(\mathbf{x},\mathbf{y},t) = p^{B(0)}(\mathbf{x},\mathbf{y},t) \qquad \text{on } \Gamma_{AB} \tag{A.12}$$

and at ε^1

$$\begin{aligned}
&-\Big[p^{A(1)}(\mathbf{x},\mathbf{y},t)\delta_{ij} + \eta_{ijmn}^A\, \partial y_n v_m^{A(0)}(\mathbf{x},\mathbf{y},t)\Big]\, n_j\\
&= -\Big[p^{B(1)}(\mathbf{x},\mathbf{y},t)\delta_{ij} + \eta_{ijmn}^B\, \partial y_n v_m^{A(0)}(\mathbf{x},\mathbf{y},t)\Big]\, n_j \;+\; \sigma H_{ij} n_j \quad \text{on } \Gamma_{AB}.
\end{aligned} \tag{A.13}$$

Analysis of terms of order ε^{-2} in equations of motion

Now we get

$$\partial_{y_j}\Big[a_{ijmn}\partial_{y_n}u_m^{(0)}\Big] = 0. \tag{A.14}$$

Multiplying (A.14) by $u_i^{(0)}$ and integrating by parts we get

$$\int\limits_{\partial Y_S} a_{ijmn}\partial_{y_n}u_m^{(0)}u_i^{(0)}n_j dA - \int\limits_{Y_S} a_{ijmn}(\partial_{y_j}u_i^{(0)})\partial_{y_n}u_m^{(0)} d\mathbf{y} = 0. \tag{A.15}$$

By virtue of the interface condition (A.8), the surface integral in the last equation vanishes and the rest implies, by positive definiteness of a_{ijmn}, that $\mathbf{u}$ depends on $\mathbf{x}$ and t only

$$u_i^{(0)} = u_i^{(0)}(\mathbf{x}, t) \tag{A.16}$$

but does not depend on $\mathbf{y}$.

Analysis of terms of order ε^{-1} in equations of motion

From Eq. (A.1) we get the following relation for $\mathbf{x} \in \Omega$ and $\mathbf{y} \in Y_S$:

$$\partial_{y_j}\left[a_{ijmn}\left(\partial_{x_n} u_m^{(0)} + \partial_{y_n} u_m^{(1)}\right)\right] = 0. \tag{A.17}$$

In turn, Eq. (A.2) for the fluid A and its counterpart for the fluid B give for $\mathbf{x} \in \Omega$ and $\mathbf{y} \in Y_L$

$$\partial_{y_i} p^{A(0)} = 0 \qquad \mathbf{y} \in Y_A \quad \text{and} \quad \partial_{y_i} p^{B(0)} = 0 \qquad \mathbf{y} \in Y_B. \tag{A.18}$$

Hence, taking account of (A.12) we obtain

$$p^{A(0)} = p^{B(0)} \equiv p^{(0)} = p^{(0)}(\mathbf{x}, t) \qquad \text{for } \mathbf{x} \in \Omega. \tag{A.19}$$

The incompressibility equation (A.3) yields

$$\partial_{y_i} v_i^{A(0)} = 0 \qquad \mathbf{y} \in Y_A \quad \text{and} \quad \partial_{y_i} v_i^{B(0)} = 0 \qquad \mathbf{y} \in Y_B \tag{A.20}$$

what means that the fields $\mathbf{v}^{A(0)}$ and $\mathbf{v}^{B(0)}$ are divergence-free with respect to for $\mathbf{y} \in Y_A$ and $\mathbf{y} \in Y_B$, respectively.

Local function for the flow problem

From (5.24) we get by the time differentiation

$$\begin{aligned}
\dot{w}_m^{A(0)} &= \frac{1}{\varrho^A} \int_0^t \Big[\Phi_s^A(\mathbf{x}, \tau)\, \frac{d}{dt}\, \chi_{ms}^{AA}(\mathbf{y}, t-\tau) \\
&+ \Phi_s^B(\mathbf{x}, \tau)\, \frac{d}{dt}\, \chi_{ms}^{AB}(\mathbf{y}, t-\tau)\Big] d\tau + \dot{\beta}_m^A(\mathbf{y}, t), \\
\dot{w}_m^{B(0)} &= \frac{1}{\varrho^B} \int_0^t \Big[\Phi_s^A(\mathbf{x}, \tau)\, \frac{d}{dt}\, \chi_{ms}^{BA}(\mathbf{y}, t-\tau) \\
&+ \Phi_s^B(\mathbf{x}, \tau)\, \frac{d}{dt}\, \chi_{ms}^{BB}(\mathbf{y}, t-\tau)\Big] d\tau + \dot{\beta}_m^B(\mathbf{y}, t),
\end{aligned} \tag{A.21}$$

where the following zero initial conditions for local functions were used in agreement with the initial condition (5.21) for the relative velocities $\mathbf{w}^A$ and $\mathbf{w}^B$,

$$\chi_{ms}^{AA}(\mathbf{y},0) = 0, \quad \chi_{ms}^{AB}(\mathbf{y},0) = 0, \quad \chi_{ms}^{BA}(\mathbf{y},0) = 0, \quad \chi_{ms}^{BB}(\mathbf{y},0) = 0. \tag{A.22}$$

Applying (5.24) to the interface condition (A.11) we find on Γ_{AB}

$$\begin{aligned} \chi_{ms}^{AA}(\mathbf{y},t)|_A &= \chi_{ms}^{BA}(\mathbf{y},t)|_B, \\ \chi_{ms}^{AB}(\mathbf{y},t)|_A &= \chi_{ms}^{BB}(\mathbf{y},t)|_B, \\ \beta_m^A(\mathbf{y},t)|_A &= \beta_m^B(\mathbf{y},t)|_B. \end{aligned} \tag{A.23}$$

Substituting (A.21) and (5.22) we obtain, apart from the system (5.25), the following local equations

$$\begin{aligned} &\rho^A \frac{d}{dt}\beta_i^A(\mathbf{y},t) + \partial_{y_i}\alpha_i^A(\mathbf{y},t) - \partial_{y_j}\left(\eta_{ijmn}^A \partial_{y_n}\beta_m^A\right) = 0 \qquad \mathbf{y} \in Y_A, \\ &\rho^B \frac{d}{dt}\beta_i^B(\mathbf{y},t) + \partial_{y_i}\alpha_i^B(\mathbf{y},t) - \partial_{y_j}\left(\eta_{ijmn}^B \partial_{y_n}\beta_m^B\right) = 0 \qquad \mathbf{y} \in Y_B. \end{aligned} \tag{A.24}$$

Substituting (5.24) into (A.20) with taking into account the definitions (5.19) and the propriety (A.16), we obtain

$$\begin{aligned} &\partial_{y_i}\chi_{ik}^{AA}(\mathbf{y},t) = 0, \qquad \partial_{y_i}\chi_{ik}^{AB}(\mathbf{y},t) = 0, \\ &\partial_{y_i}\chi_{ik}^{BA}(\mathbf{y},t) = 0, \qquad \partial_{y_i}\chi_{ik}^{BB}(\mathbf{y},t) = 0. \end{aligned} \tag{A.25}$$

and

$$\partial_{y_i}\beta_i^A(\mathbf{y},t) = 0, \qquad \partial_{y_i}\beta_i^B(\mathbf{y},t) = 0. \tag{A.26}$$

Finally, substitution of (5.22) and (5.24) into (A.13) yields the following conditions on the interface Γ_{AB} :

$$\begin{aligned} &\left[-\gamma_i^{AA}(\tau)\delta_{ij}\eta_{ijmn}^A \partial_{y_n}\chi_{ms}^{AA}(t-\tau)\right] n_j|_A \\ &\qquad = \left[-\gamma_i^{BA}(\tau)\,\delta_{ij}\eta_{ijmn}^B \partial_{y_n}\chi_{ms}^{BA}(t-\tau)\right] n_j|_B, \\ &\left[-\gamma_i^{AB}(\tau)\,\delta_{ij}\eta_{ijmn}^A \partial_{y_n}\chi_{ms}^{AB}(t-\tau)\right]\ n_j|_A \\ &\qquad = \left[-\gamma_i^{BB}(\tau)\delta_{ij}\eta_{ijmn}^B \partial_{y_n}\chi_{ms}^{BB}(t-\tau)\right]\ n_j|_B, \\ &\left[-\alpha_i^A(\tau)\delta_{ij}\eta_{ijmn}^A \partial_{y_n}\beta_m^A(t-\tau)\right]\ n_j|_A \\ &\qquad = \left[-\alpha_i^B(\tau)\delta_{ij}\eta_{ijmn}^B \partial_{y_n}\beta_m^B(t-\tau) + \sigma H_{ij}\right] n_j|_A. \end{aligned} \tag{A.27}$$

Appendix B. Scalling

According to Auriault *et al.* [6], one considers a relation Q between the pressure term ∇p and the viscosity term: $\eta \triangle \mathbf{v}$

$$Q \equiv \frac{|\nabla p|}{|\eta \triangle \mathbf{v}|}. \tag{B.1}$$

Those terms should be of the same order in the Stokes equation if the pressure and viscosity effect were meaningful in considered phenonemon

$$|\nabla p| = \mathcal{O}(|\eta \triangle \mathbf{v}|). \tag{B.2}$$

The estimation of the quotient (B. 1) may be written as

$$Q = \mathcal{O}\left(\frac{\frac{p}{L}}{\eta \frac{v}{L^2}}\right) = \mathcal{O}\left(\frac{p}{L}\frac{L^2}{\eta v}\right). \tag{B.3}$$

Since the pressure changes in the macroscopic scale, we have

$$\nabla p = \mathcal{O}\left(\frac{p}{L}\right). \tag{B.4}$$

However, the liquid velocity changes in the pore scale, thus we write

$$|\eta \triangle \mathbf{v}| = \mathcal{O}\left(\eta \frac{v}{l^2}\right). \tag{B.5}$$

Hence, instead of (B. 3) we obtain

$$\frac{p}{L} = \mathcal{O}\left(\eta \frac{v}{l^2}\right), \tag{B.6}$$

and

$$Q = \mathcal{O}\left(\frac{p}{L}\eta \frac{v}{L^2}\right) = \mathcal{O}\left(\frac{p}{L}\eta \frac{v^2}{l^2}\frac{l^2}{L^2}\right) = \mathcal{O}\left(\varepsilon^2\right). \tag{B.7}$$

The second scaling $\sigma \rightsquigarrow \varepsilon\sigma$ can be proved similarly. To this end we observe that now of the l.h.s of $(4.2)_2$, only the first derivative is present.

Acknowledgements

The authors were supported by the State Committee for Scientific Research (KBN - Poland) through the grant No 6 P04D 039 15. The second and the third author were also supported through the grant No 8 T11F 017 18.

References

1. R. A. ADAMS, *Sobolev spaces*, Academic Press, New York 1975.
2. P. M. ADLER, J.-F. THOVERT, *Real porous media: local geometry and macroscopic properties*, Appl. Mech. Reviews, **51**, 537-585, 1998.
3. G. ALLAIRE, *Homogenization of the unsteady Stokes equations in porous media*, [in]: Progress in partial differential equations - calculus of variations, applications, C. BANDLE, J. BEMELMANS, M. CHIPOT, J. SAINT JEAN PAULIN[Eds.], pp.109–123, Longman 1991.
4. G.ALLAIRE, *Homogenization and two-scale convergence*, SIAM J. Math. Anal., **23**, 1482–1518, 1992.
5. G. ALLAIRE, S. KOKH, *Simulating interfaces in two-phase flows, Preprint*, Laboratoire d'Analyse Numérique, Université Paris VI, 2000.
6. J.-L. AURIAULT, O. LEBAIGUE, G. BONNET, *Dynamics of two immiscible fluids flowing through deformable porous media*, Transp. Porous Media, **4**, 105–128, 1989.
7. J.-L. AURIAULT, E. SANCHEZ-PALENCIA, *Étude du comportement macroscopique d'un milieu poreux saturé déformable*, J. de Mécanique, **16**, 575–603, 1977.
8. J. L. AURIAULT, E. SANCHEZ-PALENCIA, *Remarques sur la loi de Darcy pour les écoulements biphasiques en milieu poreux*, J. de Méc. Théorique et Appl., (Special Issue), pp. 141–156, 1986.
9. A. BADEA, A. BOURGEAT, *Homogenization of two-phase flow through randomly heterogeneous porous media*, : Mathematical modelling of flow through porous media, A.P. BOURGEAT, C. CARASSO, S. LUCKHAUS, A. MIKELIĆ [Eds.], pp. 44-58, World Scientific, Singapore 1995.
10. J. BEAR, Y. BACHMAT, *Introduction to modelling of transport phenomena in porous media*, Kluwer Academic Publishers, Dordrecht 1991.
11. L.S. BENNETHUM, T. GIORGI, *Generalized Forchheimer equation for two-phase flow based on hybrid mixture thery*, Transp. Porous Media, **26**, 261-275, 1997.
12. Y. BERNABÉ, *On the measurement of permeability in anisotropic rocks*, in: Fault mechanics and transport properties of rocks, B. EVANS and T.- F. WONG [Eds.], pp. 147-167, Academic Press, London 1992.
13. W. BIELSKI, J. J. TELEGA, *Effective properties of geomaterials: rocks and porous media*, Publications of the Inst. of Geophys. Pol. Ac. Sci., **A – 26(285)**, Warszawa 1997.
14. W. R. BIELSKI, J. J. TELEGA, R. WOJNAR, *Macroscopic equations for nonstationary flow of Stokesian fluid through porous elastic skeleton*, Arch. Mech., **51**, 243–274, 1999.
15. W. R. BIELSKI, J. J. TELEGA, R. WOJNAR, *Nonstationary flow of a viscous fluid through a porous elastic medium: asymptotic analysis and two-scale convergence*, Mech. Res. Comm., **26**, 619–628, 1999.
16. W. R. BIELSKI, J. J. TELEGA, R. WOJNAR, *Nonstationary flow of diphasic viscous fluid through porous deformable medium*, Comput. Geosci., **26** [in press].
17. S. C. BLAIR, J. G. BERRYMAN, *Permeability and relative permeability in rocks*, in: Fault mechanics and transport properties of rocks, B. EVANS and T.-F. WONG [Ed.], pp.169–186, Academic Press, London 19.

18. R. DE BOER *Highlights in the historical development of the porous media theory: toward a consistent macroscopic theory*, Appl. Mech. Reviews, **49**, 201-262, 1996.

19. A. P. BOURGEAT, C. CARASSO, S. LUCKHAUS, A. MIKELIĆ [Eds.], *Mathematical modelling of flow through porous media*, World Scientific, Singapore 1995.

20. A. BOURGEAT, *Homogenized behavior of two-phase flows in naturally fractured reservoirs with uniform fractures distribution*, Comput. Meth. Appl. Mech. Eng., **47**, 205-216, 1984.

21. A. BOURGEAT *Two-phase flow, in: Homogenization and porous media*, U. HORNUNG [Ed]. pp. 95–127, Springer-Verlag, New York 1997.

22. A. BOURGEAT, M. PANFILOV *Effective two-phase flow through highly heterogeneous media: capillary nonequilbrium effects*, Comput. Geosci., **2**, 191-215, 1998.

23. A. BOURGEAT, A. HIDAMI, *Effective model of two-phase flow in a porous medium made of different rock types*, Applicable Anal., **58**, 1-29, 1995.

24. A. BOURGEAT, A. MIKELIĆ, S. WRIGHT, *Stochastic two-scale convergence in the mean and applications*, J. Reine Angew. Math., **456**, 19-51, 1994.

25. A. BOURGEAT, S. M. KOZLOV, A. MIKELIĆ, *Effective equations of two-phase flow in random media*, Calc. Variations, **3**, 385-406, 1995.

26. A. BOURGEAT, S. LUCKHAUS, A. MIKELIĆ, *Convergence of the homogenization process for a double-porosity model of immiscible two-phase flow*, SIAM J. Math. Anal., **27**, 1520-1543, 1996.

27. A. BOURGEAT, A. MIKELIĆ, *Homogenization of two-phase immiscible flow in one-dimensional porous medium*, Asymptotic Anal., **9**, 359-380, 1994.

28. H. BRENNER, D. A. EDWARDS, *Macrotransport processes*, Butterworth-Heinemann, Boston 1993.

29. R. BURRIDGE, J. B. KELLER, *Poroelasticity derived equations derived from microstructure*, J. Acoust. Soc. Am., **70**, 1140–1146, 1981.

30. G. CHAVENT, J. JAFFRÉ, S. JAN-JÉGOU, *Estimation of relative permeabilities in three-phase flow in porous media*, Inverse Probl., **15**, 33-39, 1999.

31. G. CHRISTAKOS, D. T. HRISTOPULOS, X. LI, *Multiphase flow in heterogeneous media from a stochastic differential geometry viewpoint*, Water Resources Res., **34**, 93-102, 1998.

32. G. N. CONSTANTINIDES, A. C. PAYATAKES, *A three-dimensional network model for consolidated porous media. Basic studies*, Chem. Eng. Comm., **81**, 55-81, 1989.

33. G. N. CONSTANTINIDES, A. C. PAYATAKES, *Network simulation of steady-state two-phase flow in consolidated porous media*, AIChE J., **42**, 369-382, 1996.

34. G. N. CONSTANTINIDES, A. C. PAYATAKES, *Effects of precursor wetting films in immiscible displacement through porous media*, Transp. Porous Media, **38**, 291-317, 2000.

35. O. COUSSY, *Mécanique des milieux poreux*, Editions Technip, Paris 1991.

36. J. M. CROLET, M. EL HATRI [Eds.], *Recent advances in problems of flow and transport in porous media*, Kluwer Academic Publishers, Dordrecht 1998.

37. J. H. CUSHMAN, *The physics of fluids in hierarchical porous media: angstroms to miles*, Kluwer Academic Publishers, Dordrecht 1997.

38. M. DALE, *Averaging of relative permeability in composite cores*, [in:] The mathematics of oil recovery [Ed.], P. R. KING, pp. 649-683, Clarendon Press, Oxford 1992.

39. M. DALE, *Darcy equations in heterogeneous porous media: interface conditions and uniqueness of periodic solutions*, Working paper from Stavanger College, School of Science and Technology, 43/1998.

40. J. T. DARTLEY, D. W. RUTH, *Relative permeabilility analysis of tube bundle models*, Transp. Porous Media, **36**, 161-187, 1999.

41. F. A. L. DULLIEN, *Porous media: fluid transport and pore structure*, Academic Press, San Diego 1992.

42. S. EKRANN, M. DALE, *Averaging of relative permeability in heterogeneous reservoirs*, in: The mathematics of oil recovery, P. R. KING, pp. 173-198, Clarendon Press, Oxford 1992.

43. EKRANN, M. DALE, K. LANGAAS, J. MYKKELTVEIT, *Capilary limit effective two-phase properties for 3D media*, SPE Int., Proc. European 3-D Reservoir Modelling Conf., Stavanger, Norway, 16-17 April 1996, pp. 119-129.

44. H. I. ENE, D. POLIŠEVSKI, *Thermal flow in porous media*, D. Reidel Publishing Company, Dordrecht 1987.

45. M. FIRDAOUSS, J.-L. GUERMOND, P. LE QUÉRE, *Nonlinear corrections to Darcy's law at low Reynolds numbers*, J. Fluid Mech., **343**, 331-350, 1997

46. G. FRAS, J. C. BENET, *Physical approach to averaging theorems on phase interfaces in a dispersed multiphase medium*, Transp. Porous Media, **15**, 209-227, 1994.

47. V. GANESAN, H. BRENNER, *A diffuse interface model of two-phase flow in porous media*, Proc. R. Soc. London, A **456**, 731-803, 2000.

48. W. G. GRAY, *Elements of a systematic procedure for the derivation of macroscale conservation equations for multi-phase flow in porous media*,in: Kinetic and continuum theories of granular and porous media,[Eds.] K. HUTTER AND K. WILMAŃSKI, pp. 67-129, Springer-Verlag, Wien-New York 1999.

49. W. G. GRAY, S. M. HASSANIZADEH, *Averaging theorems and averaged equations for transport of interface properties in multiphase systems*, Int. J. Multiphase Flow, **15**, 81-95, 1989.

50. W. G. GRAY, S. M. HASSANIZADEH, *Paradoxes and realities in unsaturated flow theory*, Water Resources Res., **27**, 1847-1854, 1991.

51. W. G. GRAY, S. M. HASSANIZADEH, *Unsaturated flow theory including interfacial phenomena*, Water Resources Res., **27**, 1855-1863, 1991.

52. W. G. GRAY, S. M. HASSANIZADEH, *Macroscale continuum mechanics for multiphase porous media flow including phases, interfaces, common lines, and common points*, Adv. Water Resources, **21**, 261-281, 1998.

53. T. HARTER, T. C. J. YEH, *Flow in unsaturated random porous media, nonlinear numerical analysis and comparison to analytical stochastic models*, Adv. Water Resources, **22**, 257-272, 1998.

54. S. M. HASSANIZADEH, W. G. GRAY, *Recent advances in theories of two-phase flow in porous media*, [in:] Fluid transport in porous media, P. DU PLESSIS[Ed.], pp.105–160, Computational Mechanics Publications, Southampton 1997.

55. J.G. HEYWOOD, *On convergence to steady state of solutions of parabolic equations in unbounded domains*, J. Diff. Eqs., **20**, 336–355, 1978.

56. U. HORNUNG [Ed.], *Homogenization and porous media*, Springer-Verlag, New York, 1997.

57. S. JEMIOŁO, J.J. TELEGA, *Modelling hyperelastic behaviour of soft tissues, Part I. Isotropy*, Eng. Trans., 2001, in press.

58. M. KAVIANY, *Principles of heat transfer in porous media*, Springer-Verlag, New York 1991.

59. M. KRAFCZYK, M. SCHULZ, E. RANK, *Lattice-gas simulations of two-phase flow in porous media*, Comm. Numer. Meth. Eng., **14**, 709-717, 1998.

60. J. KUBIK, M. CIESZKO, M. KACZMAREK, *Foundations of dynamics of saturated porous media*,in Polish,Biblioteka Mechaniki Stosowanej, Instytut Podstawowych Problemów Techniki PAN, ZTUREK, Warszawa 2000.

61. V.G. LEVICH, V. S. KRYLOV, *Surface-tension-driven phenomena*, Ann. Rev. Fluid Mech., **1**, 293–316, 1969.

62. R. W. LEWIS, B. A. SCHREFLER, *The finite element method in the static and dynamic deformation and consolidation of porous media*, John Wiley&Sons, Chichester 1998.

63. E. MARUŠIĆ-PALOKA, A. MIKELIĆ, *A derivation of a nonlinear filtration law including the inertia effects via homogenization*, Nonlinear Anal., **42**, 97-137, 2000.

64. A. MIKELIĆ, *A convergence theorem for homogenization of two-phase miscible flow through fractured reservoirs with uniform structure distribution*, Applicable Anal., **32**, 203-214, 1989.

65. A. MIKELIĆ, L. PAOLI, *On the derivation of the Buckley-Leverett model from the two fluid Navier-Stokes equation in a thin domain*, Comput. Geosci., **1**, 59-83, 1997.

66. C. T. MILLER, G. CHRISTAKOS, P. T. IMHOFF, J. F. C. MCBRIDE, J. A. PEDIT, J. A. TRANGENSTEIN, *Multiphase flow and transport modeling in heterogeneous porous media: challenges and approaches*, Advances in Water Resources, **21**, 77-120, 1998.

67. C. D. MONTEMAGNO, W. G. GRAY, *Photoluminescent volumetric imaging: A technique for the exploration of multiphase flow and transport in porous media*, Geoph. Res. Letters, **22**, 425-428, 1995.

68. L. W. MORLAND, *A simple constitutive theory for fluid-saturated porous solid*, J. Geoph. Res., **77**, 890–900, 1972.

69. G. NGUETSUNG, *A general convergence result for a functional related to the theory of homogenization*, SIAM J. Math. Anal., **20**, 608–623, 1989.

70. G. NGUETSUNG, *Asymptotic analysis for a stiff variational problem arising in mechanics*, SIAM J. Math. Anal., **21**, 1394–1414, 1990.

71. M. PANFILOV, *Macroscale models of flow through highly heterogeneous porous media*, Kluwer Academic Publishers, Dordrecht 2000.

72. P. DU PLESSIS[Ed.], *Fluid transport in porous media*, Computational Mechanics Publications, Southampton-Boston 1997.

73. M. RUDMAN, *One-field equations for two-phase flows*, J. Austral. Math. Soc., B**39**, 149-170, 1997.

74. J. SAINT JEAN PAULIN, K. TAOUS, *A generalized Darcy law. Homogenization of a diphasic flow problem in a porous medium*, Ric. Mat., **40**, 1991, 223–241.

75. E. SANCHEZ-PALENCIA, *Non-homogeneous media and vibration theory*, Springer, Berlin 1980.

76. M. SAHIMI, *Flow and transport in porous media and fractured rock: from classical methods to modern approaches*, VCH, Weinheim - New York, 1995.

77. B. R. SIMON, *Multiphase poroelastic finite element models for soft tissue structures*, Appl. Mech. Reviews, **45**, 191-218, 1992.

78. L. THIGGEN, J. G. BERRYMAN, *Mechanics of porous elastic materials containing multiphase fluid*, Int. J. Eng. Sci., **23**, 1203-1214, 1985.

79. G. C. TZIMAS, T. MATSUNRA, D. G. AVRAAM, W. VAN DER BRUGGHEN, G. N. CONSTANTINIDES, A. C. PAYATAKES, *The combined effect of the viscosity ratio and the wettability during forced imbibition through nonplanar porous media*, J. Colloid Interf. Sci., **189**, 27-36, 1997.

80. M. S. VALAVANIDES, G. N. CONSTANTINIDES, A. C. PAYATAKES, *Mechanistic model of steady-state two-phase flow in porous media based on ganglion dynamics*, Transp. Porous Media, **30**, 267-299, 1998.

81. S. WHITAKER, *The method of volume averaging*, Kluwer Academic Publishers, Dordrecht 1999.

82. L. P. YARIN, G. HETSRONI, *Turbulence intensity in dilute two-phase flows, - Part 1. Effect of particle-size distribution on the turbulence of the carrier fluid*, Int. J. Multiphase Flow, **20**, 1-15, 1994; *Part 2. Temperature fluctuations in particle-laden dilute flows, ibid.*, 17-25; *Part 3. ibid., 27-44.*

83. F. ZANOTTI, R. G. CARBONELL, *Development of transport equations for multiphase systems - I. General developments for two phase systems, Chem. Eng. Sci.*, **39**, *263-278, 1984; II. Application to one-dimensional axi-symmetric flows of two phases, ibid., 279-297; III. Application to heat transfer in packed beds, ibid., 299-311.*

84. D. Z. ZHANG, A. PROSPERETTI, *Averaged equations for inviscid disperse two-phase flow, J. Fluid Mech.*, **267**, *185-219, 1994.*

85. O. C. ZIENKIEWICZ, A. H. C. CHAN, M. PASTOR, B. A. SCHREFLER, T. SHIOMI, *Computational geomechanics with special reference to earthquake engineering, John Wiley&Sons, Chichester 1999.*

Received March 23, 2001; revised version June 1, 2001.

Arch. Mech., **53**, 4-5, pp. 367–384, Warszawa 2001

On the determination of residual stress distribution in plane elasticity

A. BLINOWSKI

University of Warmia and Mazury in Olsztyn,

PROBLEM OF THE DISTRIBUTION of incompatibilities in elastic solid in a quasi-plane stress state is discussed. It is assumed that the stress distribution can be measured at the boundary of a simply connected subregion of the body. Residual stress field must satisfy static equilibrium equations but, in general, the corresponding elastic strain field does not satisfy strain compatibility conditions. Taking the measured values of the stress components at the boundary of the region as the external boundary tractions and solving the corresponding boundary value problem of elasticity (including strain compatibility conditions), one can obtain a unique stress field, which, in general, differs from the actual one. It is reasonable to treat their difference as the residual stress field assigned to the region under consideration. Obviously, the values of residual stress defined in such a way (at given point of the region) depend on the choice of the region and do not depend on the external loading of the elastic body. Fourier series integral technique of determining such residual stress fields for simply connected circular regions are proposed. Some quantitative integral characteristics of residual stress fields are discussed.

1. Introduction

CONCEPTS OF THE RESIDUAL stresses of the first, second and third kind are widely used for the description of the state of polycrystalline metals. Despite the lack of rigorous definitions of these concepts there are no misunderstandings between the material engineering scientists owing to improper use of these notions corresponding to three scales of research: sub-micro- scale (electron microscope), micro-scale (optical microscope), and macro-scale (according to the newer terminology – micro-, meso- and macro-scale). This subdivision corresponds to the physical levels of the structure: defects in crystal lattice, granular structure of the real polycrystalline metals and alloys and the whole manufactured structure. Outside of these contexts these notions lose their meaning. Any considerations such as: "The residual stresses of the second kind are those, which are equilibrated within a structural element" have no meaning as long as the "structural element" is not defined rigorously and one does not know how the term "equili-

brate" should be understood – any static stress field in any region fulfills the equilibrium equations.

To describe residual stresses in any material, no matter: crystalline, amorphous or composite, one needs well-defined quantitative characteristics making it possible to compare the intensities and space distribution of the residual stress fields in any solid. In the present paper we consider the simplest case of the self-stressed body: a two-dimensional, linearly elastic isotropic homogeneous continuous medium. The author believes that such a model yields a fairly good approximate description of the plane subsurface layer in an unloaded 3-dimensional specimen. In our consideration we shall avoid the use of advanced geometric methods of description such as non-Euclidean material connection as well as the use of the concept of dislocation density tensor. For further considerations we shall adopt the Cartesian tensor notation and the summation convention.

2. Basic concepts

Let us consider a plane elastic state (no matter whether plane stress or strain) of the linearly elastic isotropic homogeneous body. In the absence of body forces (we shall assume they vanishing in all further considerations) one can introduce scalar parameters of incompatibility in terms of second derivatives of both elastic strain and stress field:

$$K_{(\varepsilon)} = \varepsilon_{ij,kl} e_{ik} e_{jl}, \tag{2.1}$$

$$K_{(\sigma)} = \sigma_{ii,kk}, \tag{2.2}$$

where $\boldsymbol{\varepsilon}$ and $\boldsymbol{\sigma}$ denote elastic strain and stress tensor respectively, while e_{ij} denotes representation of the unit skew-symmetric tensor ($e_{11} = e_{22} = 0$, $e_{12} = -e_{21} = 1$ in Cartesian co-ordinates). In the absence of residual stress both these quantities vanish. The conditions of vanishing of expressions (2.1) and (2.2) are equivalent under the above assumptions. In general (e.g. for the case material inhomogeneity), only vanishing of (2.1) ensures the local lack of residual stress.[1)]

If all the components of the two-dimensional stress (elastic strain) field were known exactly and were smooth enough, the appropriate area or contour integrals of the quantities defined by Eq. (2.1) and/or (2.2) could be used as good scalar measures of the residual stress associated with a chosen region. In reality,

[1)] This remains true also in the case of the unloaded surface of half-space (quasi-plane stress state). Moreover, simple count of the number of known fields at the surface shows that no other compatibility condition can be formulated in terms of these fields quantities which can be measured at the surface i.e. without knowledge of the normal components of the gradients of the stress components and/or strain tensors at the surface.

however, taking into account all the difficulties associated with the stress and/or elastic strain measurements, one can hardly expect to obtain sets of data dense enough to calculate reliable values of the second derivatives of the stress components. Moreover, the history of inelastic deformations producing the fields of residual stress is often restricted to some subdomains, thus even discontinuous stress fields may appear.

For better comprehension of the difficulties we shall consider three elementary, textbook examples of residual stress fields defined on the circular discs of radius r_2 in plane states in the absence of body forces and boundary tractions (c.f. [1]-[4]).

Example 1

Edge dislocation is introduced into the center of a circular region $0 \leqslant \rho \leqslant r_2$, internal region $0 \leqslant \rho \leqslant r_1$ is removed and disc of unstressed material is placed instead, ρ denotes polar co-ordinate (Fig. 1):

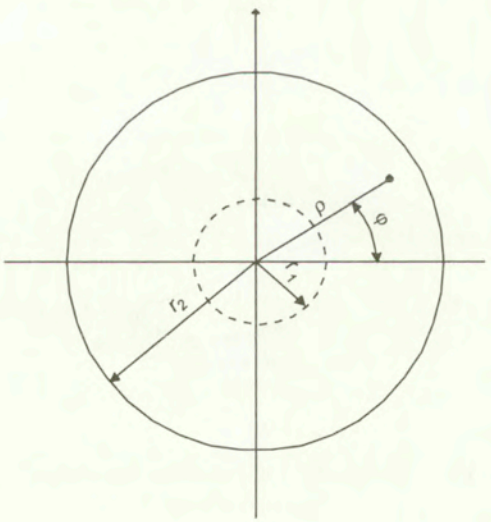

FIG. 1. Geometric scheme of the plane body.

The Airy stress function is written as

(2.3)
$$F(\rho,\varphi) = \begin{cases} -A\left(\rho \ln \frac{\rho}{r_2} - \frac{1}{2}\frac{\rho^3}{r_1^2+r_2^2} + \frac{1}{2}\frac{r_1^2 r_2^2}{r_1^2+r_2^2}\frac{1}{\rho}\right)\sin\varphi & \text{for } r_1 < \rho \leq r_2, \\ 0 & \text{for } 0 < \rho \leq r_1, \end{cases}$$

where A is an arbitrary constant (for plane strain state $A = \mu b/[2\pi(1-\nu)]$, where μ is the Lamé constant, ν denotes Poisson's ratio, b is a the length of the Burgers vector). For the stress field one obtains:

$$\sigma_{\rho\rho} \equiv \frac{1}{\rho}\frac{\partial F}{\partial \rho}+\frac{1}{\rho^2}\frac{\partial^2 F}{\partial \varphi^2} = \begin{cases} A\dfrac{\left(\rho^2-r_2^2\right)\left(\rho^2-r_1^2\right)}{\rho^3\left(r_1^2+r_2^2\right)} & \sin\varphi \quad \text{for } r_1 < \rho \leqslant r_2, \\ 0 & \text{for } 0 \leqslant \rho \leqslant r_1, \end{cases}$$

$$\sigma_{\varphi\varphi} \equiv \frac{\partial^2 F}{\partial \rho^2} = \begin{cases} A\dfrac{3\rho^4-\left(r_1^2+r_2^2\right)\rho^2-r_1^2 r_2^2}{\rho^3\left(r_1^2+r_2^2\right)} & \sin\varphi \quad \text{for } r_1 < \rho \leqslant r_2, \\ 0 & \text{for } 0 \leqslant \rho \leqslant r_1, \end{cases} \tag{2.4}$$

(compare Fig. 2).

$$\sigma_{\rho\varphi} \equiv -\frac{\partial}{\partial \rho}\left(\frac{1}{\rho}\frac{\partial F}{\partial \varphi}\right) = \begin{cases} A\dfrac{\left(\rho^2-r_2^2\right)\left(\rho^2-r_1^2\right)}{\rho^3\left(r_1^2+r_2^2\right)} & \cos\varphi \quad \text{for } r_1 < \rho \leqslant r_2, \\ 0 & \text{for } 0 \leqslant \rho \leqslant r_1. \end{cases}$$

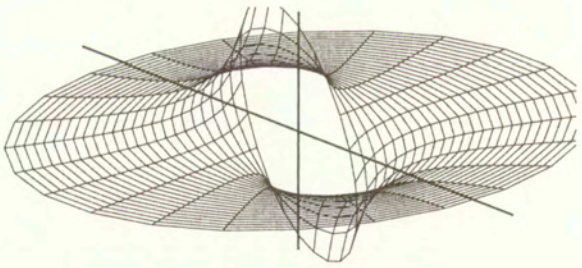

FIG. 2. An example of the residual stress distribution-transversal stress $\sigma_{\varphi\varphi}(r,\varphi)$arround edge dislocation.

Example 2

Angle disclination in the outer ring $r_1 < \rho \leqslant r_2$ and unstressed material in the internal disc $0 \leqslant \rho \leqslant r_1$:

Airy stress function

$$F(\rho,\varphi) = \begin{cases} \dfrac{1}{2}B\left(\rho^2-\dfrac{r_2^2\alpha^2}{1-\alpha^2}\ln\alpha^2\right)\left(\ln\dfrac{\rho^2}{r_2^2}+\dfrac{\alpha^2}{1-\alpha^2}\ln\alpha^2-1\right) & \text{for } r_1 < \rho \leq r_2, \\ 0 & \text{for } 0 \leqslant \rho \leqslant r_1, \end{cases} \tag{2.5}$$

where $\alpha \equiv r_1/r_2$, B is an arbitrary constant (for plane stress conditions $B = \frac{E\alpha}{8\pi}$, where α denotes the opening angle of disclination, E denotes the Young modulus).

Stress fields:

$$\sigma_{\rho\rho} = \begin{cases} B\left[\left(1 - \frac{r_2^2}{\rho^2}\right)\frac{\alpha^2}{1-\alpha^2}\ln\alpha^2 + \ln\frac{\rho^2}{r_2^2}\right] & \text{for} \quad r_1 < \rho \leqslant r_2, \\ 0 & \text{for} \quad 0 \leqslant \rho \leqslant r_1, \end{cases}$$

$$\sigma_{\varphi\varphi} = \begin{cases} B\left[\left(1 + \frac{r_2^2}{\rho^2}\right)\frac{\alpha^2}{1-\alpha^2}\ln\alpha^2 + \ln\frac{\rho^2}{r_2^2} + 2\right] & \text{for} \quad r_1 < \rho \leq r_2, \\ 0 & \text{for} \quad 0 \leqslant \rho \leqslant r_1, \end{cases} \tag{2.6}$$

$$\sigma_{\rho\varphi} = 0.$$

Example 3

Internal disc of the diameter $r_1 + \delta$, $\delta << (r_2 - r_1)$ inserted into initially unstrained outer ring $r_1 < \rho \leqslant r_2$ of the same material.

Airy stress function

$$F(\rho, \varphi) = \begin{cases} \frac{E\delta}{2r_1}\left(\frac{1}{2}\alpha^2\rho^2 - r_1^2\ln\frac{\rho}{r_1}\right) & \text{for} \quad r_1 < \rho \leqslant r_2, \\ \frac{E\delta}{2r_1}\left(\alpha^2 - 1\right)\rho^2 & \text{for} \quad 0 \leqslant \rho \leqslant r_1, \end{cases} \tag{2.7}$$

where E denotes the Young modulus. Stress fields are expressed as follows:

$$\sigma_{\rho\rho} = \begin{cases} \frac{E\delta}{2r_1}\left(\alpha^2 - \frac{r_1^2}{\rho^2}\right) & \text{for } r_1 < \rho \leqslant r_2, \\ \frac{E\delta}{2r_1}\left(\alpha^2 - 1\right) & \text{for } 0 \leqslant \rho \leqslant r_1, \end{cases}$$

$$\sigma_{\varphi\varphi} = \begin{cases} \frac{E\delta}{2r_1}\left(\alpha^2 + \frac{r_1^2}{\rho^2}\right) & \text{for} \quad r_1 < \rho \leqslant r_2, \\ \frac{E\delta}{2r_1}\left(\alpha^2 - 1\right) & \text{for } 0 \leqslant \rho \leqslant r_1, \end{cases} \tag{2.8}$$

$$\sigma_{\rho\varphi} = 0.$$

All three examples specified above are by no means "exotic", one can easily point out real production techniques leading to such residual stress fields or their linear combinations. It is not difficult to notice that in all three cases the incompatibility parameters defined by Eq. (2.1) and (2.2) vanish almost everywhere, except for the set of null surface measure – the contour $\Sigma : \{\rho = r_1\}$, where they are not defined. It is not difficult to notice that: any simply connected subbody Ω that doesn't intersect contour Σ is not a self-stressed body in the following sense: *if one removed at the boundary $\partial\Omega$ all contact forces of interaction with the remainder part of the body, then the stress field would vanish at all points of* Ω.

The above examples distinctly show that it would be impractical to look for such additive characteristics of the residual stress which can be obtained by integration of some density functions (e.g. such as defined by Eq. (2.1) and (2.2)) over the whole body or its part[2)] . In the course of further considerations we shall look for the characteristics of residual stress fields assigned rather to the domains of the body than to its individual points.

In accordance with the formulated above notion of the body free of residual stress we shall specify for further consideration an operational procedure of subdivision of the two-dimensional actual stress field $\sigma_A(\mathbf{x})$ on the simply connected sub-domain Ω of the body bounded by the closed contour $\partial\Omega$, into two parts: *residual* and *induced*[3)] .

1. Choose a material region Ω, measure the components of the actual stress tensor $\sigma_A(s)$ at the contour $\partial\Omega$ and find the contact forces $\mathbf{t}(s)$ of interaction of the sub-body Ω with the rest of the body across $\partial\Omega$, s denoting a parameter defining the closed curve $\partial\Omega : \{\mathbf{x} = \mathbf{x}(s)\}$.

2. Solve the plane elastic boundary value problem for initially unstrained body of the same material occupying region Ω and loaded with tractions $\mathbf{t}(s)$ at $\partial\Omega$, obtaining the *induced stress field* $\sigma_I(\mathbf{x})$defined on Ω.

3. Subtract on the region Ω the field $\sigma_I(\mathbf{x})$ from $\sigma_A(\mathbf{x})$ obtaining the *intrinsic residual stress field* $\sigma_R(\Omega, \mathbf{x})$ associated with the region Ω

$$\sigma_R(\Omega, \mathbf{x}) \stackrel{\text{df}}{=} \sigma_A(\mathbf{x}) - \sigma_I(\mathbf{x}), \quad \mathbf{x} \in \Omega. \tag{2.9}$$

Note that:

- Value of intrinsic residual stress field at a given point $\mathbf{x}$ essentially depends on the choice of the region Ω.
- From the superposition principle of linear elasticity it follows immediately that for given region Ω, the field $\sigma_R(\Omega, \mathbf{x})$ is insensitive to the change of

[2)] Such an approach, if possible at all, would lead us to rather inconvenient considerations concerning second derivatives of distributions (generalized functions).

[3)] Such an approach would be equivalent to the commonly used definition of the residual stress in terms of unloading, if the process of unloading were always purely elastic.

the external load applied to the body **outside** Ω, even if it causes inelastic deformations (up to the disintegration of the body), provided the material **inside** Ω remains in elastic state.

- Taking into account that real plastic deformations usually exceed considerably these which can be attained within elastic limits, one can expect that any inelastic deformation **inside** Ω may drastically change its intrinsic residual stress field.
- Residual stress field may not obey the limit state conditions, *actual* stress field is the only one, which must fulfill them. If this is the case, then a path of global elastic unloading of the body may not exist.

For practical applications it would be difficult to obtain the complete information about the *whole* intrinsic residual stress field for *all* parts of the body within reasonable accuracy limits. It is quite thinkable to perform measurements of the stress or elastic strain along a chosen curve, while performing such measurements for sufficiently dense set of internal points of two-dimensional region may turn out to be unreasonably time and/or money consuming. Some proposals of the choice of a limited number of parameters describing residual stress fields will be discussed in the next sections of the present paper, the problem however remains to be open for further investigations.

3. Circular domains

In this section we shall consider the simplest example of intrinsic residual stress distribution – residual stress fields in plane elastic state for the circular simply connected domains of the isotropic homogeneous material. All considerations of this section will be presented in terms of polar co-ordinates $\{\rho, \varphi\}$.

According to the E. Goursat theorem (c.f. [1] p. 322) any biharmonic function $F(x, y)$ defined in a simply connected region bounded by a smooth curve can be represented in the following form:

$$F(x, y) = Re[\bar{z} f(z) + g(z)] \tag{3.1}$$

where $f(z)$ and $g(z)$ are holomorphic functions of the complex variable $z = x + iy$, $\bar{z} \equiv x - iy$. Making use of the uniqueness of the power expansion of the holomorphic function and representing z^n as $\rho^n(\cos n\varphi + i \sin n\varphi)$, one can rewrite relation (10) in the following form:

$$F\left(\rho, \varphi\right) = \sum_{n=0}^{\infty} \left[\left(C_{(2)_n} \rho^{n+2} + C_{(0)_n} \rho^n \right) \cos n\varphi \right. \\ \left. + \left(S_{(2)_n} \rho^{n+2} + S_{(0)_n} \rho^n \right) \sin n\varphi. \right. \tag{3.2}$$

Taking $F(\rho, \varphi)$ as the Airy stress function and using well-known relations

$$\begin{aligned} \sigma_{\rho\rho} &= \frac{1}{\rho}\frac{\partial F}{\partial \rho} + \frac{1}{\rho^2}\frac{\partial^2 F}{\partial \varphi^2}, \\ \sigma_{\varphi\varphi} &= \frac{\partial^2 F}{\partial \rho^2}, \\ \sigma_{\rho\varphi} &= -\frac{\partial}{\partial \rho}\left(\frac{1}{\rho}\frac{\partial F}{\partial \varphi}\right), \end{aligned} \tag{3.3}$$

one obtains the following stress field:

$$\begin{aligned} \sigma_{\rho\rho} = 2C_{(2)0} - \sum_{n=1}^{\infty} \Big[& C_{(2)n}\big(n-2\big)\big(n+1\big)\rho^n \\ & + C_{(0)n}\big(n-1\big)\rho^{n-2}\Big]\cos n\varphi - \sum_{n=1}^{\infty}\Big[S_{(2)n}\big(n-2\big)\big(n+1\big)\rho^n \\ & + S_{(0)n}n\big(n-1\big)\rho^{n-2}\Big]\sin n\varphi, \end{aligned} \tag{3.4}$$

$$\begin{aligned} \sigma_{\varphi\varphi} = 2C_{(2)0} + \sum_{n=1}^{\infty} \Big[& C_{(2)n}\big(n+2\big)\big(n+1\big)\rho^n \\ & + C_{(0)n}\big(n-1\big)\rho^{n+2}\Big]\cos n\varphi + \sum_{n=1}^{\infty}\Big[S_{(2)n}\big(n-2\big)\big(n+1\big)\rho^n \\ & + S_{(0)n}n\big(n-1\big)\rho^{n-2}\Big]\sin n\varphi, \end{aligned} \tag{3.5}$$

$$\begin{aligned} \sigma_{\rho\varphi} = \sum_{n=1}^{\infty} \big[C_{(2)n}n\,(n+1)\,\rho^n + C_{(0)n}n\,(n-1)\,\rho^{n-2}\big]\sin n\varphi \\ - \sum_{n=1}^{\infty}\big[S_{(2)n}n\,(n+1)\,\rho^n + S_{(0)n}n\,(n-1)\,\rho^{n-2}\big]\cos n\varphi. \end{aligned} \tag{3.6}$$

This stress field corresponds to the stress distribution in a circular, initially unstressed disc Ω of radius R loaded at the boundary $\partial\Omega : \{\rho = R\}$ by the normal stress $t_n(\varphi)$ and the tangent stress $t_\tau(\varphi)$, where the following relations must be satisfied:

$$\begin{aligned} t_n(\varphi) &= \sigma_{\rho\rho}(R, \varphi), \\ t_\tau(\varphi) &= \sigma_{\rho\varphi}(R, \varphi), \end{aligned} \tag{3.7}$$

For the time being we shall assume, omitting technical details, that we are able to measure these quantities along the arbitrarily chosen circular contour $\partial\Omega$ inside the two-dimensional region occupied by the whole body.

Denoting:

$$
\begin{aligned}
&N_{Cn} = \frac{1}{\pi}\int_{-\pi}^{\pi} \sigma_{\rho\rho}\cos n\varphi\, d\varphi, \qquad N_{Sn} = \frac{1}{\pi}\int_{-\pi}^{\pi} \sigma_{\rho\rho}\sin n\varphi\, d\varphi,\\
&T_{Cn} = \frac{1}{\pi}\int_{-\pi}^{\pi} \sigma_{\rho\varphi}\cos n\varphi\, d\varphi, \qquad T_{Sn} = \frac{1}{\pi}\int_{-\pi}^{\pi} \sigma_{\rho\varphi}\sin n\varphi\, d\varphi,\\
&P_{Cn} = \frac{1}{\pi}\int_{-\pi}^{\pi} \sigma_{\varphi\varphi}\cos n\varphi\, d\varphi, \qquad P_{Sn} = \frac{1}{\pi}\int_{-\pi}^{\pi} \sigma_{\varphi\varphi}\sin n\varphi\, d\varphi,
\end{aligned}
\tag{3.8}
$$

where $\sigma_{\rho\rho}(\varphi)$, $\sigma_{\rho\varphi}(\varphi)$ and $\sigma_{\varphi\varphi}(\varphi)$ are the values of stress measured at the contour, and making use of (13) and (15), one obtains: for $n = 0$: $N_{C0} = 4C_{(2)0}$, and

$$
\begin{aligned}
N_{Cn} &= -n(n-1)\ C_{(0)n}R^{n-2} - (n+1)(n-2)\ C_{(2)n}R^{n},\\
N_{Sn} &= -n(n-1)\ S_{(0)n}R^{n-2} - (n+1)(n+2)\ S_{(2)n}R^{n}, \quad \text{for } n \geq 1.\\
T_{Cn} &= -n(n-1)\ S_{(0)n}R^{n-2} - n(n+1)\ S_{(2)n}R^{n},\\
T_{Sn} &= n(n-1)\ C_{(0)n}R^{n-2} + n(n+1)\ C_{(2)n}R^{n}.
\end{aligned}
\tag{3.9}
$$

Equations (3.9) can be solved with respect to $C_{(0)n}$, $C_{(2)n}$, $S_{(0)n}$ and $S_{(2)n}$ as follows[4] :

$$
\begin{aligned}
C_{(0)n} &= -\frac{nN_{(C)n} + (n-2)T_{(S)n}}{2R^{n-2}n(n-1)}, \quad C_{(2)n} = \frac{N_{(C)n} + T_{(S)n}}{2R^{n}(n+1)},\\
S_{(0)n} &= \frac{-nN_{(S)n} + (n-2)T_{(C)n}}{2R^{n-2}n(n-1)}, \quad S_{(2)n} = \frac{N_{(S)n} - T_{(C)n}}{2R^{n}(n+1)}.
\end{aligned}
\tag{3.10}
$$

Substituting values (3.10) into expressions (3.4), (3.5) and (3.6) we are able to express the formulae for the induced stress field $\sigma_I(\rho,\varphi)$ inside the circular region in terms of the Fourier coefficients of the tractions applied at the boundary:

[4] Expressions for $C_{(0)1}$ and $S_{(0)1}$ are not defined by Eq. (19); it is not difficult to notice however that these quantities can be taken arbitrarily since they don't contribute to the expressions for stress components.

$$(3.11)\quad \sigma_{I\rho\rho} = \frac{N_{(C)0}}{2} + \sum_{n=1}^{\infty}\left[\frac{nN_{(C)n} + \left(n-2\right)T_{(S)n}}{2R^{n-2}}\rho^{n-2} - \frac{\left(N_{(C)n} + T_{(S)n}\right)\left(n-2\right)}{2R^{n}}\rho^{n}\right]\cos n\varphi + \sum_{n=1}^{\infty}\left[\frac{nN_{(S)n} - \left(n-2\right)T_{(C)n}}{2R^{n-2}}\rho^{n-2} - \frac{\left(N_{(S)n} + T_{(C)n}\right)\left(n-2\right)}{2R^{n}}\rho^{n}\right]\sin n\varphi,$$

$$(3.12)\quad \sigma_{I\varphi\varphi} = \frac{N_{(C)0}}{2} - \sum_{n=1}^{\infty}\left[\frac{nN_{(C)n} + (n-2)\,T_{(S)n}}{2R^{n-2}}\rho^{n-2} - \frac{\left(N_{(C)n} + T_{(S)n}\right)(n+2)}{2R^{n}}\rho^{n}\right]\cos n\varphi - \sum_{n=1}^{\infty}\left[\frac{nN_{(S)n} - (n-2)\,T_{(C)n}}{2R^{n-2}}\rho^{n-2} - \frac{\left(N_{(S)n} + T_{(C)n}\right)(n+2)}{2R^{n}}\rho^{n}\right]\sin n\varphi$$

$$(3.13)\quad \sigma_{I\rho\varphi} = - \sum_{n=1}^{\infty}\left[\frac{nN_{(C)n} + (n-2)\,T_{(S)n}}{2R^{n-2}}\rho^{n-2} - \frac{\left(N_{(C)n} + T_{(S)n}\right)n}{2R^{n}}\rho^{n}\right]\sin n\varphi + \sum_{n=1}^{\infty}\left[\frac{nN_{(S)n} - (n-2)\,T_{(C)n}}{2R^{n-2}}\rho^{n-2} - \frac{\left(N_{(S)n} + T_{(C)n}\right)n}{2R^{n}}\rho^{n}\right]\cos n\varphi.$$

Subtracting these values from the measured actual values of stress components at an arbitrary internal point $\mathbf{x}$ of the Ω domain, one can easily obtain the values of residual stress component $\sigma_R(\Omega, \mathbf{x})$at this point associated with Ω. If $\sigma_R(\Omega, \mathbf{x})$ vanishes at all points of Ω (within the accuracy limits of the measuring techniques) then one may consider domain Ω as being free from residual stress. Obviously this remains true with respect to any subdomain $\Omega_i \subset \Omega$. On the contrary, for a larger domain $\Omega_e \supset \Omega$ it may occur that $\sigma_R(\Omega, \mathbf{x})$ does not vanish (compare *Example* 3). It is quite reasonable to consider the radius of such a domain for which the first non-vanishing residual stress field appears as the lower threshold of the range of residual stress. More detailed consideration on the estimate of the residual stress range we shall present in the next section.

For the time being we shall point out an interesting property of the induced stress fields defined on circular regions. Combining Eq. (3.11) and (3.12) and taking $\rho = R$ one obtains:

$$\frac{\sigma_{I\rho\rho} - \sigma_{I\varphi\varphi}}{2} = -\sum_{n=1}^{\infty} T_{(S)n} \cos n\varphi + \sum_{n=1}^{\infty} T_{(C)n} \sin n\varphi. \tag{3.14}$$

Thus, taking into account that at the boundary $\sigma_{I\rho\rho} = \sigma_{A\rho\rho}$ and $\sigma_{I\rho\varphi} = \sigma_{A\rho\varphi}$ we conclude that the only component of residual stress non-vanishing at the boundary can be expressed in terms of actual stress components as follows:

$$\sigma_{R\varphi\varphi} = \sigma_{A\varphi\varphi} - \sigma_{A\rho\rho} - 2\sum_{n=1}^{\infty} T_{(S)n} \cos n\varphi + 2\sum_{n=1}^{\infty} T_{(C)n} \sin n\varphi. \tag{3.15}$$

In the absence of residual stress, the right-hand side of Eq. (3.15) vanishes identically (compare Eqs. (3.4) – (3.6)). It is not difficult, however, to show an example of residual stress field non-vanishing in Ω for which this expression is equal to zero at the entire boundary of Ω[5]. Thus vanishing of the right-hand side of Eq. (3.15) at the boundary of some domain Ω of radius R is the necessary but not a sufficient condition of the absence of residual stress inside Ω.

Note that the value of $\sigma_{R\varphi\varphi}(\varphi)$ given by (3.15) describes the transversal component of residual stress at the circular contour of radius R **only for residual stress field associated with the circular region Ω of the same radius R.** Taking any larger concentric region Ω_1 of radius $R_1 > R$, one can use relation (3.12) and calculate $\sigma_{R\varphi\varphi}(\rho, \varphi)$ and then subtract it from $\sigma_{A\varphi\varphi}(\rho, \varphi)$ for $\rho = R$, obtaining (at the circle of radius R) the transversal component of **residual stress field associated with Ω_1.** In general **these quantities are different**[6]. In order to avoid possible misunderstandings, let us introduce new symbol $\kappa(R, \varphi)$ denoting **the value of residual transversal stress associated with the circular domain Ω of radius R taken at the boundary of the domain** (determined by the right-hand side of Eq. (24) for $\rho = R$).

Let us consider a domain Ω_0 of radius R_0. Assume that $\kappa(R, \varphi)$ vanishes for every circular domain Ω of radius $R \leqslant R_0$, concentric with Ω_0. We shall prove that such stress field is entirely load-induced and doesn't include residual constituent in Ω_0.

[5] One may take an arbitrary self-stressed body and surround it with unstressed material, then the right-hand side of Eq. (3.15) would identically vanish for any contour $\partial\Omega$ surrounding (but not touching) initial, self-stressed body, while the residual stress field associated with Ω doesn't vanish.

[6] It will turn out to be clear from the foregoing considerations that they are equal if the expression (24) vanishes for all concentric domains Ω' of intermediate radii $R < R' \leqslant R_1$.

Let us represent the stress function $\Phi(\rho, \varphi)$ as the following Fourier series:

$$\Phi(\rho,\varphi) = f_0(\rho) + \sum_{n=1}^{\infty} f_n(\rho)\cos n\varphi + \sum_{n=1}^{\infty} g_n(\rho)\sin n\varphi. \tag{3.16}$$

Calculating the stress components (using relations (3.3)) and substituting the results into Eq. (3.15), one obtains the following relation:

$$\begin{aligned}\kappa(R,\varphi) = \Bigg[& \frac{d^2 f_0(\rho)}{d\rho^2} - \frac{1}{\rho}\frac{df_0(\rho)}{d\rho}\frac{d^2 f_0(\rho)}{d\rho^2} - \frac{1}{\rho}\frac{df_0(\rho)}{d\rho} \\ & + \sum_{n=1}^{\infty}\left(\frac{d^2 f_n(\rho)}{d\rho^2} - \frac{2n+1}{\rho}\frac{df_n(\rho)}{d\rho} + \frac{n(n+1)}{\rho^2} f_n(\rho)\right)\cos n\varphi \\ & + \sum_{n=1}^{\infty}\left(\frac{d^2 g_n(\rho)}{d\rho^2} - \frac{2n+1}{\rho}\frac{dg_n(\rho)}{d\rho} + \frac{n(n+1)}{\rho^2} g_n(\rho)\right)\sin n\varphi \Bigg]_{\rho=R}.\end{aligned} \tag{3.17}$$

The right-hand side of Eq. (3.17) vanishes for every $R \leqslant R_0$ if and only if

$$\left.\begin{aligned} & \frac{d^2 f_0(\rho)}{d\rho^2} - \frac{1}{\rho}\frac{df_0(\rho)}{d\rho} = 0, \\ & \frac{d^2 f_n(\rho)}{d\rho^2} - \frac{2n+1}{\rho}\frac{df_n(\rho)}{d\rho} + \frac{n(n+1)}{\rho^2} f_n(\rho) = 0, \\ & \frac{d^2 g_n(\rho)}{d\rho^2} - \frac{2n+1}{\rho}\frac{dg_n(\rho)}{d\rho} + \frac{n(n+1)}{\rho^2} g_n(\rho) = 0, \end{aligned}\right\} \quad \text{for all } n = 1, 2, 3, \ldots \tag{3.18}$$

i.e. when

$$\left.\begin{aligned} f_0(\rho) &= A_0 + B_0\rho^2, \\ f_n(\rho) &= A_n\rho^n + B_n\rho^{n+2}, \\ g_n(\rho) &= C_n\rho^n + D_n\rho^{n+2}, \end{aligned}\right\} \quad \text{for all } n = 1, 2, 3, \ldots \tag{3.19}$$

where A_n, B_n, C_n, D_n are arbitrary constants. This means, however that the stress function $\Phi(\rho, \varphi)$ is biharmonic in Ω_0 (compare (3.2)). Therefore the entire stress field in Ω_0 is induced by the external load. QED.

The last result suggests that the intensity of $\kappa(R, \varphi)$ can serve as a convenient scalar characteristics of the magnitude and range of reach of residual stress fields.[7)]

[7)] Let us understand here all these notions in accordance with their colloquial meaning; we shall try to make them more precise later on.

4. Concluding propositions

Note that applying our operational procedure of determination of residual stress (compare Eq. (2.9)) beginning with the largest possible circle and gradually reducing its diameter, we act as "peeling" successively the original body (possibly "hardened" in advance to exclude inelastic behavior due to stress redistribution) and observing the resulting changes of the stress field. If for some range of R between R_1 and R_2, $(R_1 < R_2)$, our "stripping" does not change essentially the residual stress distribution, we would be inclined to claim that we do not observe significant internal stress of the range (scale) between R_1 and R_2 (on the level of intuitive understanding of all terms involved). On the contrary, if acting in such a way we change drastically the residual stress field magnitude and/or distribution, we would rather consider the *contribution of the residual stress of such a scale to the total stress distribution* as significant.

Let us try to express quantitatively these intuitive notions. To this end we shall define an integral characteristics of the residual stress distributions associated with the sequence of concentric circular regions:

$$I_1^2(R) \equiv \frac{1}{2\pi}\int_0^{2\pi} \kappa^2(R,\varphi)d\varphi. \tag{4.1}$$

We shall call $I_1(R)$ the *boundary intensity of residual stress*. It describes the mean value of the norm of residual stress tensor field (associated with the circular domain of radius R) calculated at the outline of the domain (circle of radius R).

For the description of the scale of reach of a residual stress field as well as its "coarseness" (or smoothness), not only the information on the intensity of residual stress can be useful – we have already seen that in some special cases the boundary residual stress intensity can vanish locally for large R while the specimen may be highly stressed inside. Also the "rate of change" of the boundary residual stress intensity during our imaginary process of "peeling" can be important. Thus we introduce another function of the domain radius R:

$$I_2(R) \equiv \frac{dI_1(R)}{dR}. \tag{4.2}$$

Before proceeding further in the description of residual stress distributions in terms of $I_1(R)$ and $I_2(R)$, we should try to examine their behavior in the case of the examples exposed in Sec. 2.

Ad *Example* 1

For the transversal component of residual stress in initial domain of radius r_2 one has:

$$(4.3)\quad \sigma_{R\varphi\varphi}(\rho,\varphi)=\begin{cases} A\dfrac{3\rho^4-\left(r_1^2+r_2^2\right)\rho^2-r_1^2r_2^2}{\rho^3\left(r_1^2+r_2^2\right)}\sin\varphi & \text{for } r_1<\rho\leqslant r_2,\\ 0 & \text{for } 0\leqslant\rho\leqslant r_1,\end{cases}$$

while

$$(4.4)\quad \kappa(R,\varphi)=\begin{cases} A\dfrac{2\left(R^2-r_1^2\right)}{R\left(R^2+r_1^2\right)}\sin\varphi & \text{for } r_1<R\leqslant r_2,\\ 0 & \text{for } 0<R\leqslant r_1,\end{cases}$$

thus:

$$(4.5)\quad \begin{cases}\left[A\dfrac{\sqrt{2}\left(R^2-r_1^2\right)}{R\left(R^2+r_1^2\right)}\right] & \text{for } r_1<R\leqslant r_2,\\ 0 & \text{for } 0<R\leqslant r_1,\end{cases}$$

and

$$(4.6)\quad I_2(R)=\begin{cases} -A\dfrac{\sqrt{2}\left(R^4-4R^2r_1^2-r_1^4\right)}{\left(R^2+r_1^2\right)^2R^2} & \text{for } r_1<R\leqslant r_2\\ 0 & \text{for } 0<R\leqslant r_1\end{cases}$$

(compare Fig. 3.)

Ad *Example 2*

$$(4.7)\quad \sigma_{\varphi\varphi}(\rho,\varphi)=\sigma_{\varphi\varphi}(\rho,)$$

$$=\begin{cases} 2B\left[\left(\alpha^2+\dfrac{r_1^2}{\rho^2}\right)\dfrac{\ln\alpha}{1-\alpha^2}+\ln\dfrac{\rho}{r_1}+\ln\alpha+1\right] & \text{for } r_1\leqslant\rho<r_2,\\ 0 & \text{for } 0\leq\rho<r_1,\end{cases}$$

$$(4.8)\quad \kappa(R,\varphi)=\kappa(R)=\begin{cases} 2B\left(\dfrac{2r_1^2}{R^2-r_1^2}\ln\dfrac{r_1}{R}+1\right) & \text{for } r_1,\leqslant R<r_2,\\ 0 & \text{for } 0\leqslant R<r_1,\end{cases}$$

$$(4.9)\quad I_1(R)=|\kappa(R)|=\begin{cases} 2|B|\left(\dfrac{2r_1^2}{R^2-r_1^2}\ln\dfrac{r_1}{R}+1\right) & \text{for } r_1\leqslant R<r_2,\\ 0 & \text{for } 0\leqslant R<r_1,\end{cases}$$

$$(4.10)\quad I_2(R) = \begin{cases} \left| \dfrac{-4|B|r_1^2}{R\left(R^2 - r_1^2\right)} \left(\dfrac{2R^2}{R^2 - r_1^2} \ln \dfrac{r_1}{R} + 1 \right) \right| & \text{for} \quad r_1 \leqslant R < r_2, \\ 0 & \text{for} \quad 0 \leqslant R < r_1. \end{cases}$$

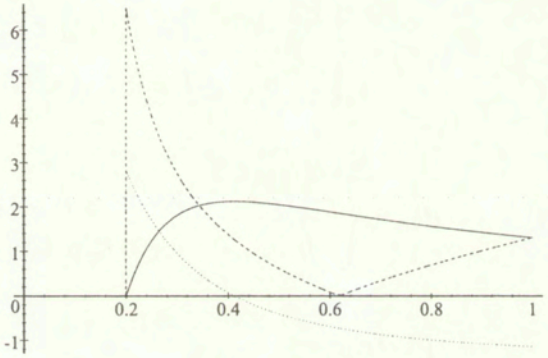

FIG. 3. Intensity of transversal stress $\sigma_{(i)\varphi\varphi}(\rho) \equiv \sqrt{\frac{1}{2\pi} \int\limits_{-\pi}^{\pi} \sigma_{\varphi\varphi}^2 \left(r, \varphi\right) d\varphi}$ - dashed line, intensity of boundary residual stress $I_1(\rho)$ - solid line, derivative of the intensity of boundary residual stress $\frac{dI_1(R)}{dR}$ - dotted line.

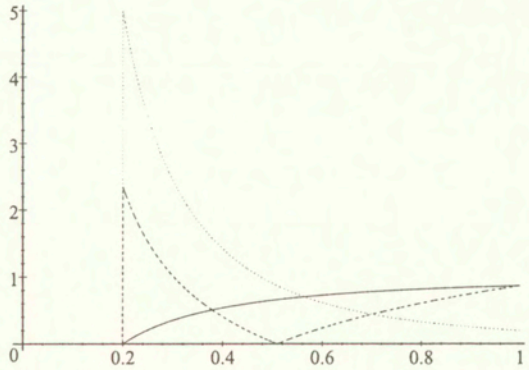

FIG. 4. Absolute value of transversal stress $|\sigma_{\varphi\varphi}(\rho)|$ - dashed line, intensity of boundary residual stress $I_1(\rho)$ - solid line, derivative of the intensity of boundary residual stress $\frac{dI_1(R)}{dR}$ - dotted line.

Ad *Example* 3

$$\sigma_{\varphi\varphi}(\rho,\varphi)=\sigma_{\varphi\varphi}(\rho)=\begin{cases}\dfrac{E\delta}{2r_1}\left(\alpha^2+\dfrac{r_1^2}{\rho^2}\right) & \text{for } r_1<\rho\leqslant r_2\\ \dfrac{E\delta}{2r_1}\left(\alpha^2-1\right) & \text{for } 0\leqslant\rho\leqslant r_1\end{cases} \tag{4.11}$$

$$\kappa(R,\varphi)=\kappa(R)=\begin{cases}\dfrac{E\delta\, r_1}{R^2} & \text{for } r_1<\rho\leqslant r_2\\ 0 & \text{for } 0\leqslant\rho\leqslant r_1\end{cases} \tag{4.12}$$

$$I_1(R)=|\kappa(R)|=\begin{cases}\dfrac{E|\delta|\, r_1}{R^2} & \text{for } r_1<\rho\leqslant r_2\\ 0 & \text{for } 0\leqslant\rho\leqslant r_1\end{cases} \tag{4.13}$$

$$I_2(R)=\begin{cases}-\dfrac{2E|\delta|\, r_1}{R^3} & \text{for } r_1<\rho\leqslant r_2\\ 0 & \text{for } 0\leqslant\rho\leqslant r_1\end{cases} \tag{4.14}$$

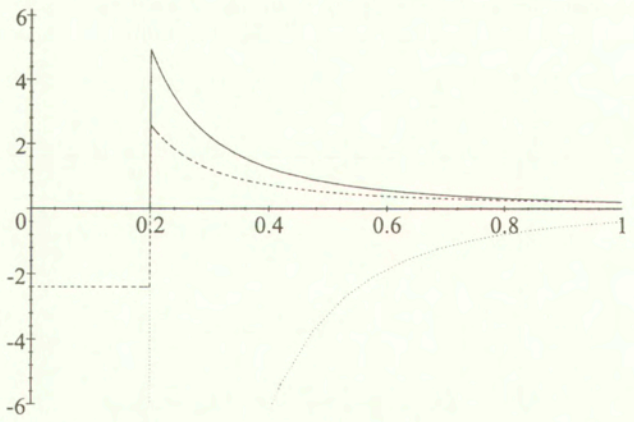

FIG. 5. Transversal stress $\sigma_{\varphi\varphi}(\rho)$ - dashed line, intensity of boundary residual stress $I_1(\rho)$ - solid line, derivative of the intensity of boundary residual stress $\frac{dI_1(R)}{dR}$ - dotted line.

Inspecting the curves describing the boundary residual stress intensity and their "rates" as the functions of the radius R, one can hardly point out (at

least concerning the examples under consideration) any characteristic numbers pointing out the scale of reach of the residual stress fields. Only in Fig. 3 at $R \cong 0.4$ one can observe a maximum of the boundary residual stress intensity. Figure 4 suggests that the whole specimen is involved in generation of residual stress. The curves in Fig. 5 indicate that the influence of the defect decreases rapidly with the distance from central inclusion. In the last case one can arbitrarily take some value of the stress intensity, say 10% of the maximal value, and consider the distance at which the stress intensity becomes lower than this threshold as the range of reach of the residual stress field caused by the inclusion. The proposed quantitative characteristics of the internal stress scale do not pretend to be the only possible, many other similar propositions can be discussed as well. Generally speaking, rather the information of the whole distribution profile of the boundary stress intensity and its gradient gives more or less complete information. Thus we should admit that our original goal consisting in defining a single parameter describing the reach of the residual stress has not been fully achieved. Instead we have proposed the way of description of the two-dimensional field of residual stress using functions of one variable obtained by the procedure based on the measurements along the contours only. In author's opinion the most important result of the considerations presented above consists in drastic reduction of the density of the measured points and the accuracy of measurements needed for the non-destructive evaluation of residual stress fields. It was achieved due to replacement of the differential operations by the integration along contours. It should be mentioned again, here, that the method proposed is insensitive to the external loading, making thus possible the interpretation of the results of *in situ* strain measurements on the elements of working construction. All the considerations assume the linearly elastic behavior of the material, the problem of the applicability of the results to real engineering situations is out of the scope of the present considerations and must be separately considered for each individual case.

Generalization of the considerations to the (plane) regions of arbitrary shape seems to be thinkable, while the other ways of generalization such as three-dimensional approach, anisotropy, inhomogeneity etc. do not seem to be straightforward.

As the last point of our consideration it is worthwhile to discuss briefly some technical details. At the present state of art of the stress measurement techniques, determination of all necessary data in the framework of the present approach may turn out to be unreasonably expensive and time-consuming. It is, however, the author's hope that the development of the automatic measurement procedures may change this situation in the near future. The fast computation methods based on the Fourier analysis are quite well advanced nowadays thus any thinkable amount of experimental data may be easily processed. The scarcity and low

accuracy of the experimental data combined with the powerful data processing capabilities may result in obtaining some "artifacts" such as (non-existing in reality) short range stress fields obtained in calculations, due to the experimental data scattering. Thus, certain precautions must be recommended, e.g. the number of the Fourier terms taken into considerations must be much less than the number of measuring points at the circular boundary.

Acknowledgement

The results reported were obtained in the framework of the Research Project of the Committee of the Scientific Research 7 TO7A 032 12.

References

1. W. NOWACKI, *Theory of Elasticity* (in Polish), PWN, Warszawa, 1970.
2. B.N. ZHEMOCHKIN, *Theory of elasticity* (in Russian), Gosstroyizdat, Moskva 1957.
3. R.W. LARDNER, *Mathematical theory of dislocations and fracture*, Univ. of Toronto Press, Toronto, 1974.
4. A. BLINOWSKI, *Mechanics of elastic and plastic bodies* (in Polish), vol.1, Ed. Polit. Białost., Białystok, 1989.

Received March 23, 2000.

Arch. Mech., **53**, 4-5, pp. 385–420, Warszawa 2001

Transport phenomena in saturated porous media undergoing liquid-solid phase change

C. GEINDREAU and J.-L. AURIAULT

Laboratoire "Sols, Solides, Structures" (3S)
UJF, INPG, UMR CNRS 5521,
BP 53X 38041 Grenoble Cedex 09, France.

THE MACROSCOPIC MODELLING of transport phenomena occurring during the solidification process in porous media is revisited in this paper. The particular case of binary phase change in metallic alloys is considered. Continuum models for momentum, mass, heat and species transport in metallic saturated porous media undergoing liquid-solid phase change are derived from the description at the pore scale by using an upscaling technique. We use the method of multiple scale expansions which gives rigorously the macroscopic behaviour. Different macroscopic descriptions are derived in function of the orders of magnitude of dimensionless numbers that characterize the dominating phenomena and the physical properties of the constituents at the microscopic scale. Among the distinct homogenizable situations, the three richest cases are presented in this paper. The domains of validity of the micro-macrosegregation models, i.e lever-rule type models and Scheil type models, are shown by means of the order of magnitude of dimensionless numbers. The continuous passage between the different models is investigated.

Key words: porous media; heat transfer; mass transport; species transport; phase change; metallic materials, solidification, homogenisation.

Notations

$\mathbf{b}$	pore vector field
C_p^s, C_p^f	solid and fluid thermal capacities [J/(kg.K)]
D^s, D^f	solid and fluid diffusion coefficients [m^2/s]
D, K, M, Q, H, W	dimensionless numbers
$\mathbf{D}^*$	effective diffusion tensors [m^2/s]
$\mathbf{D}^{**}$	effective dispersion tensors [m^2/s]
f^s, f^f	solid and fluid volume fractions [dimensionless]
FT^s, FT^f	solid and fluid thermal Fourier numbers [dimensionless]
FS^s, FS^f	solid and fluid solutal Fourier numbers [dimensionless]
$k(T^*)$	equilibrium partition ratio [dimensionless]
$\mathbf{k}, \mathbf{K}$	microscopic and macroscopic permeability tensors [m^2]
l	characteristic microscopic length [m]
L^{fs}	latent heat of fusion [J/kg]

L	characteristic macroscopic length [m]
Le^s, Le^f	solid and fluid Lewis numbers [dimensionless]
$\mathbf{N}$	unit outward vector of Γ
p^f	fluid pressure [Pa]
PT^f	thermal Péclet number of the fluid phase [dimensionless]
PS^f	solutal Péclet number of the fluid phase [dimensionless]
Re	Reynolds number [dimensionless]
REV	Representative Elementary Volume
t	time [s]
T^s, T^f	solid and liquid temperatures [K]
$\mathbf{v}^s, \vec{v}^f$	solid and fluid velocities [m/s]
$\mathbf{w}$	liquid-solid interface velocity [m/s]
$\mathbf{X}$	physical space variable [m]
$\mathbf{x}$	macroscopic (or slow) space variable [dimensionless]
$\mathbf{y}$	microscopic (or fast) space variable [dimensionless]

Greek letters

β, φ, χ	pore vector fields
Γ	boundary between Ω^s and Ω^f
δ	unit tensor
λ^{eff}	effective thermal conductivity tensor [J/(m.K.s)]
ε	parameter of scale separation [dimensionless]
λ^s, λ^f	solid and fluid thermal conductivity [J/(m.K.s)]
μ^f	solid and fluid viscosity [Pa.s]
ρ^s, ρ^f	solid and fluid densities [kg/m^3]
ϕ, Φ	complex functions
ω^s, ω^f	fluid and solid mass fractions [dimensionless]
Ω	total volume of the periodic cell [m^3]
Ω^f, Ω^s	solid and fluid volumes of the periodic cell [m^3]
∇	gradient operator
$\nabla\cdot$	divergence operator

Subscripts

c	characteristic quantities related to the physical phenomenon
l	dimensionless number using l as reference length
x	macroscopic variable in use for derivation
y	microscopic variable in use for derivation

Superscripts

$*$	interfacial value (Γ)
s	value defined in Ω^s
f	value defined in Ω^f

1. Introduction

THE STUDY OF SOLID-LIQUID phase change in fluid-saturated porous media that involve coupled mass transport, heat transfer, fluid flow and species transport processes, spans a range of scientific and engineering domains, including metallurgy, material sciences and earth sciences. For example, such research is necessary to predict the formation of defects in mechanical components due to micro- or macrosegregation occurring during casting processes [9,26,25,15,20], or to describe the formation of the various igneous rocks in geological systems [14,7,13]. In nuclear engineering, it is also fundamental to describe correctly the solidification of a molten pool, namely the corium, that can be found in a nuclear vessel during a hypothetical accident [32].

The solidification of melts of many types of materials, as metals and igneous rocks, leads to the formation of a mushy zone [9] which separates the fully solidified and melted regions during solidification. The mushy zone is composed of solid dendrites and interdendritic liquid. In most solidification models, the mushy zone is viewed as a saturated porous medium undergoing liquid-solid phase change [20]. In order to simulate solidification processes, two different approaches have been adopted in the past: the multi-domain approach and the single-domain approach. In the multi-domain approach, the conservation equations for the solid phase and the fluid phase are solved separately with appropriate boundary conditions over the moving solid-liquid interface [28,29,23,31]. Due to the complex interfacial geometry that characterizes the solidification of multi-component systems, it is usually difficult to solve the problem without any questionable hypothesis. For these reasons, the single-domain approach is usually preferred. In this approach, the multi-component system is viewed as a continuum material described by a single set of conservation equations for the whole domain comprising the solid, the mush and the fluid domains. In the last two decades, several continuum transport models have been developed using the mixture theory [14,5,12,30,21] and the volume average method [4,10,22,19]. Most of them concern the binary phase change such as in metallic alloys and have been applied to simulate solidification processes such as casting or welding. It is well known that macroscopic description of the solidification process strongly depends on the physical properties of each phase and on the physical processes at the microscopic scale [20]. Hence, the macroscopic description can take different forms according to the intensity of the phenomena occurring at the microscopic scale. Although the mixture theory and the volume average approach allow to capture some microscopic information at the macroscopic scale, macroscopic prerequisites are sometimes required for deriving the different macroscopic description. Moreover, the domain of validity of the derived macroscopic models and homoge-

nisability conditions, i.e conditions under which an equivalent macroscopic description exists, are not expressly stated.

The macroscopic modelling of transport phenomena occurring during the solidification process in porous media is revisited in this paper by using the homogenisation method of multiple scale expansions [6,24,1]. The particular case of binary phase change in metallic alloys is considered. The upscaling technique we are using allows to derive the macroscopic behaviour from the description of the physical mechanisms at the microscopic scale without any prerequisite of the form of the macroscopic equations. The basic assumption of the method is the existence of a Representative Elementary Volume (REV) of the medium, which is large enough to be a representative of the heterogeneity scale and small in comparison with the macroscopic volume. We also assume the medium to be periodic. In a periodic medium, the periodic cell represents the REV. Let l be the characteristic length of the REV and L be the characteristic macroscopic dimension. The key parameter of the upscaling method is the small parameter

$$\varepsilon = \frac{l}{L} \ll 1. \tag{1.1}$$

ε is the parameter of scale separation. The separation of scales must also be verified regarding the phenomenon. Under these conditions, the corresponding macroscopic descriptions are intrinsic to the geometry of the medium and the phenomenon. They are also independent of the macroscopic boundary conditions. In this study, we follow the approach suggested in [1].It enables to obtain the macroscopic laws, their domain of validity and also the effective parameters. Homogenisability conditions are also expressly stated. The methodology is based on the definition and estimation of dimensionless numbers that characterize the dominating phenomena and the physical properties of the constituents at the microscopic scale. The domain of validity of the derived macroscopic description is given by means of orders of magnitude of the local dimensionless numbers.

The existence of a REV plus a scale separation are the necessary conditions for the existence of an equivalent macroscopic description. Although the dendritic skeleton is nonuniform and anisotropic in the the mushy zone [20], we will admit these two conditions to be fulfilled. If they are not verified, there is no possible equivalent macroscopic description.

The physics at the microscopic scale of a binary-alloy solidification system is presented in Sec. 2. Section 3 is devoted to the estimations of the dimensionless numbers arising from the description at the microscopic scale with respect to the scale ratio ε. The homogenisation technique of multiple scale expansions for periodic structures is then applied in Sec. 4 to derive the macroscopic coupled equations of momentum, mass, heat and species transports. Among the different homogenisable situations, the three most fruitful cases are presented. The con-

tinuous passage between the different macroscopic models is investigated in the conclusion.

2. Description at the microscopic scale

The homogenisation method for periodic structures is applied to the solidification of a binary alloy A-B. Although the dendritic skeleton is nonuniform and anisotropic [20], the mushy zone (Fig. 1) is considered to be a periodic porous medium with a space period Ω.

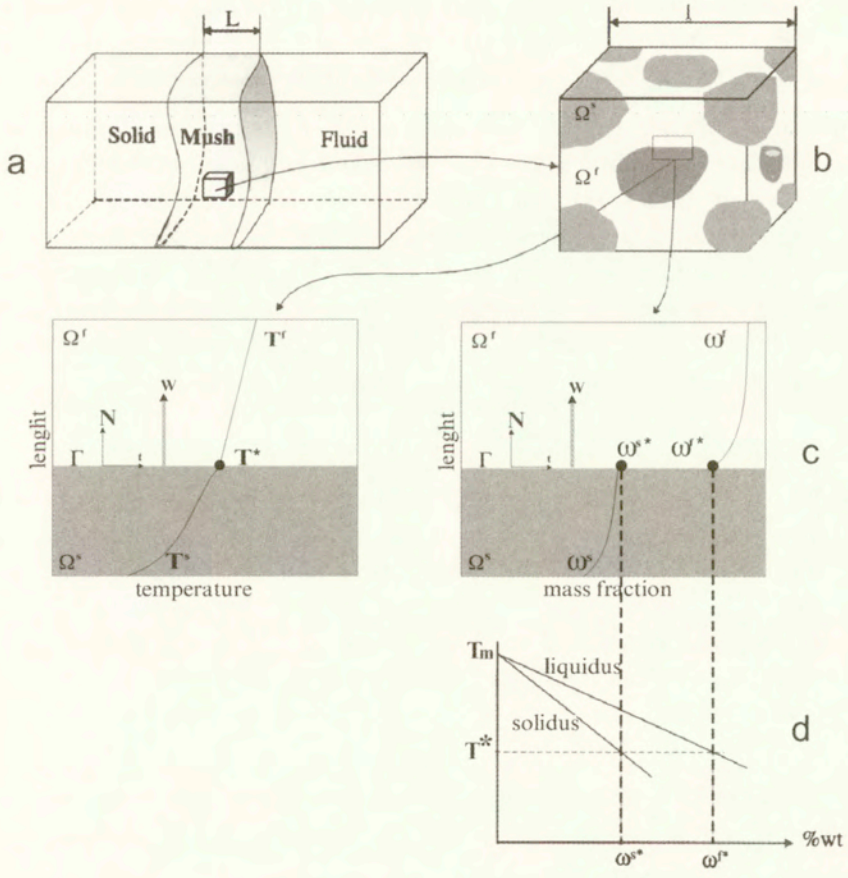

FIG. 1. (**a**) Macroscopic mushy zone with a large number of Representative Elementary Volumes or periodic cell. (**b**) Representative Elementary Volume or periodic cell Ω. (**c**) Schematic representation of the different boundary conditions on Γ. (**d**) Equilibrium phase diagram of a binary system.

This assumption is actually not a restriction [1,16]. The characteristic length of the period l is of about the same order of magnitude as the dimension of the pores or dendritic particles, while the scale L reveals the dimension of the mushy zone. Under typical solidification conditions in a metallic alloy system, a characteristic value of l is $l \approx 10^{-4}$m while $L \approx 10^{-1}$m, therefore $\varepsilon \approx 10^{-3}$. In the analysis to follow, this value for the separation of scales is adopted. Ω^s and Ω^f are the domains occupied by the solid phase (^{s}) and the fluid phase (^{f}), respectively. Each phase is assumed to be connected. The common boundary between solid and fluid is denoted Γ. At the microscopic scale, i.e at the REV scale, the medium is assumed to be composed of a fluid and of a rigid solid with phase change through which heat and species are diffused and are convected. The physical phenomena are governed by the following equations.

Momentum balance: At the microscopic scale, the solid skeleton is incompressible and usually follows a non-linear viscous law such as the Odqvist law. It has been shown that the motion of the solid network can play a key role in the fluid segregation, depending on the contrast of the mechanical properties of the solid and the fluid phases [11]. For the sake of simplicity, we assume in this study that the solid network is rigid ($\mathbf{v}^s = 0$). The fluid is considered to be an incompressible Newtonian fluid of viscosity μ^f. In the pores, the steady state fluid flow is governed by the usual Stokes equation,

$$\mu^f \triangle \mathbf{v}^f - \nabla p^f - \rho^f (\mathbf{v}^f \cdot \nabla)\mathbf{v}^f = 0. \tag{2.1}$$

$\mathbf{v}^f$ is the fluid velocity, p^f is the fluid pressure and ρ^f is the density of the fluid. In practice, μ^f and ρ^f depend on the temperature and the mass fraction of the different species (A-B). In this study, they are assumed to be constant.

Mass balance: The density of the solid phase, ρ^s ($\rho^s > \rho^f$), is also supposed to be constant. The incompressibility of the fluid is given by

$$\nabla \cdot \mathbf{v}^f = 0. \tag{2.2}$$

Energy balance: The heat transfer is governed by conduction in the solid phase whereas it is governed by conduction and convection in the fluid phase,

$$\rho^s C_p^s \frac{\partial T^s}{\partial t} - \nabla \cdot (\lambda^s \nabla T^s) = 0, \tag{2.3}$$

$$\rho^f C_p^f \frac{\partial T^f}{\partial t} + \rho^f C_p^f \vec{v}^f \cdot \nabla T^f - \nabla \cdot (\lambda^f \nabla T^f) = 0. \tag{2.4}$$

T^s and T^f are the temperature of the solid phase and the fluid phase, respectively. C_p^α and λ^α are the thermal capacity and the thermal conductivity of the

phase α ($\alpha = s, f$). In the following, C_p^α and λ^α are supposed to be independent of the temperature and of the mass fractions of the different species (A-B).

Species balance: Species transport is governed by diffusion in the solid phase and by diffusion and convection in the fluid phase,

$$\rho^s \frac{\partial \omega^s}{\partial t} - \nabla \cdot (\rho^s D^s \nabla \omega^s) = 0, \tag{2.5}$$

$$\rho^f \frac{\partial \omega^f}{\partial t} + \rho^f \mathbf{v}^f \cdot \nabla \omega^f - \nabla \cdot (\rho^f D^f \nabla \omega^f) = 0. \tag{2.6}$$

ω^α and D^α are the mass fraction and the diffusion coefficient of a given species (A or B) in the phase α ($\alpha = s, f$).

Conditions on the solid-liquid interface Γ**:** The following interfacial conditions are illustrated in Fig. 1.

- *Continuity of tangential velocities:*

$$\mathbf{v}^f \cdot \mathbf{t} = 0, \tag{2.7}$$

$\mathbf{t}$ is the unit tangential vector of Γ.

- *Continuity of mass fluxes:*

$$\rho^f (\mathbf{v}^f - \mathbf{w}) \cdot \mathbf{N} = -\rho^s \mathbf{w} \cdot \mathbf{N}, \tag{2.8}$$

where $\mathbf{N}$ is a unit outward vector of Γ and $\mathbf{w}$ is the velocity of the interface.

- *Continuity of temperatures:*

$$T^s = T^f = T^*. \tag{2.9}$$

A state of thermodynamic equilibrium is assumed. T^* is the equilibrium temperature on the interface.

- *Continuity of heat fluxes:*

$$\left(\lambda^s \nabla T^s - \lambda^f \nabla T^f\right) \cdot \mathbf{N} = L^{fs} \rho^s \mathbf{w} \cdot \mathbf{N}, \tag{2.10}$$

L^{fs} is the latent heat of fusion.

- *Continuity of species fluxes:*

$$\left(\rho^s D^s \nabla \omega^s - \rho^f D^f \nabla \omega^f\right) \cdot \mathbf{N} = (\rho^f \omega^{f*} - \rho^s \omega^{s*}) \mathbf{w} \cdot \mathbf{N}. \tag{2.11}$$

Under the assumption of thermodynamic equilibrium, the fluid mass fraction ω^{f*} and the solid mass fraction ω^{s*} on the interface Γ are related through the equilibrium phase diagram,

$$\omega^{s*} = k(T^*) \omega^{f*}, \tag{2.12}$$

where $k(T^*)$ is the equilibrium partition ratio. In this study, a linearised phase diagram is supposed, thus $k(T^*) = k$.

At the microscopic scale, the coupling between mass, heat and species transports is ensured by equations (2.8), (2.10)-(2.11) and the equilibrium phase diagram (2.12).

3. Homogenisation process

3.1. Normalisation

An important step of the homogenisation process is the normalisation of all equations. The above microscopic description (2.1)-(2.12) introduces fourteen dimensionless numbers that will measure the relative influence of the phenomena under consideration. From Eq. (2.1), we can define the Reynolds number Re and the dimensionless number Q^f,

$$Re = \frac{|\rho^f(\mathbf{v}^f \cdot \nabla)\mathbf{v}^f|}{|\mu^f \triangle \mathbf{v}^f|}, \qquad Q^f = \frac{|\nabla p^f|}{|\mu^f \triangle \mathbf{v}^f|}.$$

Eqs. (2.3)-(2.4) introduce two thermal Fourier numbers FT^s and FT^f, and the thermal Péclet number of the fluid phase PT^f,

$$FT^s = \frac{|\nabla \cdot (\lambda^s \nabla T^s)|}{\left|\rho^s C_p^s \dfrac{\partial T^s}{\partial t}\right|}, \quad FT^f = \frac{|\nabla \cdot (\lambda^f \nabla T^f)|}{\left|\rho^f C_p^f \dfrac{\partial T^f}{\partial t}\right|}, \quad PT^f = \frac{|\rho^f C_p^f \mathbf{v}^f \cdot \nabla T^f|}{|\nabla \cdot (\lambda^f \nabla T^f)|}.$$

Similarly, Eqs.(2.5)-(2.6) introduce two solutal Fourier numbers FS^s and FS^f, and the solutal Péclet number of the fluid phase PS^f,

$$FS^s = \frac{|\nabla \cdot (\rho^s D^s \nabla \omega^s)|}{\left|\rho^s \dfrac{\partial \omega^s}{\partial t}\right|}, \; FS^f = \frac{|\nabla \cdot (\rho^f D^f \nabla \omega^f)|}{\left|\rho^f \dfrac{\partial \omega^f}{\partial t}\right|}, \; PS^f = \frac{|\rho^f \mathbf{v}^f \cdot \nabla \omega^f|}{|\nabla \cdot (\rho^f D^f \nabla \omega^f)|}.$$

Now, from the continuity equation of mass fluxes (2.8) we obtain

$$M = \frac{|\mathbf{v}^f \cdot \mathbf{N}|}{|\mathbf{w} \cdot \mathbf{N}|}, \qquad R = \frac{\rho^s}{\rho^f}.$$

From the continuity equation of heat fluxes (2.10), we get the following two dimensionless numbers

$$K = \frac{\lambda^s}{\lambda^f}, \qquad H = \frac{|L^{fs}\rho^s \mathbf{w} \cdot \mathbf{N}|}{|\lambda^f \nabla T^f \cdot \mathbf{N}|}.$$

Finally, from the continuity equation of species fluxes (2.11), we have

$$D = \frac{D^s}{D^f}, \qquad W = \frac{|(\rho^f \omega^{f*} - \rho^s \omega^{s*})\mathbf{w} \cdot \mathbf{N}|}{|\rho^f D^f \nabla \omega^f \cdot \mathbf{N}|}.$$

Note that Re, Q^f, FT^s, FT^f, PT^f, FS^s, FS^f, PS^f are defined in the bulk of each phase whereas M, R, K, H, D and W are defined on the solid-liquid interface Γ.

3.2. Estimation of the dimensionless numbers

According the methodology presented in [1], the next important step of the homogenisation process consists in estimating these different dimensionless numbers arising from the description at the microscopic scale with respect to the key parameter ε of the process. In practice, ε is varying in time and in space because the mushy zone is expanding during the processes which changes l and L. Therefore estimation of dimensionless numbers may vary in time and space. Although we may consider several values of ε, we assume for simplicity in this study that $\varepsilon \approx 10^{-3}$, which corresponds to the situation of the greatest interest. Remark that macroscopic models already proposed are actually based on this typical value [20]. Let us consider l as the reference characteristic length. Thus, the microscopic point of view is adopted and the dimensionless numbers will be denoted by the subscript l. Notice that this choice does not affect the final result. Dimensionless numbers R_l, K_l, D_l can easily be estimated from the physical properties of the constituents. For example, from the material properties of a Pb-Sn alloy (Table 1), we have: $R_l = O(1)$, $K_l = O(1)$ and $D_l = O(\varepsilon)$. In the particular case of a Fe-C alloy (Table 1), R_l, K_l and D_l are $O(1)$. For the other dimensionless numbers, several orders of magnitude leading to several homogenisable situations may be considered. These numbers are expressed by means of characteristics quantities (denoted by the subscript c) that are related to the physical phenomenon (pressure drop, fluid velocity, solidification time ...).

The fluid flow and the mass balance depends on three dimensionless numbers,

$$Re = \frac{|\rho^f (\mathbf{v}^f \cdot \nabla)\mathbf{v}^f|}{|\mu^f \triangle \mathbf{v}^f|} \quad \Longrightarrow \quad Re_l = O\left(\frac{\rho_c^f v_c^f l}{\mu_c^f}\right),$$

$$Q^f = \frac{|\nabla p^f|}{|\mu^f \triangle \mathbf{v}^f|}. \quad \Longrightarrow \quad Q_l^f = O\left(\frac{p_c^f \; l}{\mu_c^f v_c^f}\right),$$

$$M = \frac{|\mathbf{v}^f \cdot \mathbf{N}|}{|\mathbf{w} \cdot \mathbf{N}|} \quad \Longrightarrow \quad M_l = O\left(\frac{v_c^f}{w_c}\right)_\Gamma.$$

Table 1. Physical properties of metallic alloys

Physical properties	Pb-Sn [15]	Fe-C [18]
ρ^s [kg/m^3]	10800	7300
ρ^f [kg/m^3]	10000	7300
μ^f [Pa.s]	10^{-3}	10^{-3}
C_p^f [J/(kg.K)]	177	800
C_p^s [J/(kg.K)]	154	800
D^s [m^2/s]	2.10^{-12}	10^{-10}
D^f [m^2/s]	10^{-9}	10^{-9}
λ^f [J/(m.K.s)]	22.9	30
λ^s [J/(m.K.s)]	39.7	30
^{fs} [J/kg]	30162	270000

Usually, the range of the fluid velocity in the mushy zone that is encountered in castings is between 10^{-7} m/s and 10^{-3} m/s. This corresponds to a variation of the Reynolds number from 0.001 to 1: $O(\varepsilon) \leq Re_l \leq O(1)$. For sufficiently low Reynolds numbers, $Re_l \approx O(\varepsilon)$, the steady state flow of an incompressible fluid through porous media is described by Darcy's law: the fluid velocity is linearly related to the gradient of the fluid pressure. As the Reynolds number increases, non-linearities appear and the drag law becomes nonlinear at the macroscopic scale [17, 27]. In this study, we will simply assume that Reynolds number is very small $Re_l \approx O(\varepsilon)$. On the other hand, it can be shown by a simple physical reasoning [1] that the problem is homogenisable if $Q_l^f = O(\varepsilon^{-1})$ and if the interfacial velocity is small or very small compared to the fluid velocity [3], i.e $M_l \geq O(\varepsilon^{-1})$.

Concerning the thermal problem, the microscopic description introduces four dimensionless numbers which can be estimated as follows

$$FT^s = \frac{|\nabla \cdot (\lambda^s \nabla T^s)|}{\left|\rho^s C_p^s \dfrac{\partial T^s}{\partial t}\right|} \quad \Longrightarrow \quad FT_l^s = O\left(\frac{\lambda_c^s \; t_c}{\rho_c^s \; C_{pc}^s \; l^2}\right),$$

$$FT^f = \frac{|\nabla \cdot (\lambda^f \nabla T^f)|}{\left|\rho^f C_p^f \dfrac{\partial T^f}{\partial t}\right|} \quad \Longrightarrow \quad FT_l^f = O\left(\frac{\lambda_c^f \; t_c}{\rho_c^f \; C_{pc}^f \; l^2}\right),$$

$$PT^f = \frac{|\rho^f C_p^f \, \mathbf{v}^f \cdot \nabla T^f|}{|\nabla \cdot (\lambda^f \nabla T^f)|} \quad \Longrightarrow \quad PT_l^f = O\left(\frac{\rho_c^f \; C_{pc}^f \; v_c^f \; l}{\lambda_c^f}\right),$$

$$H = \frac{|L^{fs} \rho^s \mathbf{w} \cdot \mathbf{N}|}{|\lambda^f \nabla T^f \cdot \mathbf{N}|} \quad \Longrightarrow \quad H_l = O\left(\frac{L_c^{fs} \; \rho_c^s \; w_c \; \delta_T^f}{\lambda_c^f \; \delta T^f}\right)_\Gamma .$$

t_c is the characteristic solidification time, δ_T^f is the fluid thermal diffusion layer thickness and $\delta T^f = |T^f - T^*|$ stands for the temperature increment in the boundary layer. Assuming that during castings, the range of the characteristic solidification time is typically between 10^2 s and 10^6 s, we have: $O(\varepsilon^{-2}) \leq FT_l^s \simeq FT_l^f \leq O(\varepsilon^{-3})$. The range of the fluid velocity implies that the thermal Péclet number of the fluid phase is small: $O(\varepsilon) \geq PT_l^f \geq O(\varepsilon^2)$. Consider now H_l. It has been shown [3] that the interface velocity must be small compared to the fluid velocity: $w_c \leq O(\varepsilon\, v_c^f)$. The fluid thermal-diffusion length δ_T is, in general, a complicated function of the microstructure, the solid volume fraction, interface velocities and curvatures, the time, melt flow conditions ... If we consider that $\delta_T^f \leq 10^{-5}$ m $\leq l$ and $\delta T^f \approx 10$ K, we get: $O(\varepsilon^3) \leq H_l \leq O(\varepsilon)$.

The microscopic dimensionless description of the species transport introduces four dimensionless numbers:

$$FS^s = \frac{|\nabla \cdot (\rho^s D^s \nabla \omega^s)|}{\left|\rho^s \dfrac{\partial \omega^s}{\partial t}\right|} \quad \Longrightarrow \quad FS_l^s = O\left(\frac{D_c^s\ t_c}{l^2}\right),$$

$$FS^f = \frac{|\nabla \cdot (\rho^f D^f \nabla \omega^f)|}{\left|\rho^f \dfrac{\partial \omega^f}{\partial t}\right|} \quad \Longrightarrow \quad FS_l^f = O\left(\frac{D_c^f\ t_c}{l^2}\right),$$

$$PT^f = \frac{|\rho^f \mathbf{v}^f \cdot \nabla \omega^f|}{|\nabla \cdot (\rho^f D^f \nabla \omega^f)|} \quad \Longrightarrow \quad PT_l^f = O\left(\frac{v_c^f\ l}{D_c^f}\right),$$

$$W = \frac{|(\rho^f \omega^{f*} - \rho^s \omega^{s*})\mathbf{w} \cdot \mathbf{N}|}{|\rho^f D^f \nabla \omega^f \cdot \mathbf{N}|} \quad \Longrightarrow \quad W_l = O\left(\frac{(\rho_c^f \omega_c^{f*} - \rho_c^s \omega_c^{s*})\ \delta_D^f\ w_c}{\rho_c^f\ D_c^f\ \delta\omega_c^f}\right)_\Gamma.$$

δ_D^f is the fluid-species diffusion length and $\delta\omega_c^f = |\omega^f - \omega^{f*}|$ stands for the fluid mass fraction increment in the boundary layer. Solutal dimensionless numbers can be related to thermal dimensionless numbers by introducing the fluid and the solid Lewis numbers defined as the ratio of the thermal diffusivity to the solutal diffusivity,

$$Le_l^f = O\left(\frac{\lambda_c^f}{\rho_c^f\ C_{pc}^f\ D_c^f}\right) = O(\varepsilon^{-1}),$$

$$Le_l^s = O\left(\frac{\lambda_c^s}{\rho_c^s\ C_{pc}^s\ D_c^s}\right) = O(Le_l^f\ D_l^{-1}).$$

Taking into account these results, we obtain: $O(\varepsilon^{-1}) \leq FS_l^f \simeq Le_l^{f-1}\ FT_l^f \leq O(\varepsilon^{-2})$, $FS_l^s \simeq D_l\ FS_l^f$ and $O(1) \geq PS_l^f \simeq Le_l^f\ PT_l^f \geq O(\varepsilon)$. It has been shown [2] that the problem is not homogenisable, i.e. an equivalent macroscopic

description does not exist, if $PS_l^f \geq O(\varepsilon^{-1})$. On the interface Γ, the fluid and solid mass fractions are related to the temperature through the equilibrium phase diagram. Thus, we get: $O(\varepsilon^2) \leq W_l \simeq Le_l^f \; H_l \leq O(1)$.

The above analysis shows that the dimensionless numbers arising from the description at the microscopic scale can take different orders of magnitude according to the physical properties of the constituents and to the characteristic quantities that are related to the physical phenomenon at the microscopic scale. Therefore, when applying the homogenisation process to the local description, it turns out that several macroscopic descriptions can be derived from the microscopic description according to the order of magnitude of these dimensionless numbers. Among the different homogenisable situations in which $PS_l^f < O(\varepsilon^{-1})$, $FS_l^f \geq O(\varepsilon^{-1})$ and $M_l \geq O(\varepsilon^{-1})$, only the three most fruitful cases (cases A, B and C) are presented in this paper. These three cases of interest (Fig. 2) correspond to different orders of dimensionless numbers, which are summarized in Table 2. Practical situations in which $PS_l^f \geq O(\varepsilon^{-1})$, $FS_l^f < O(\varepsilon^{-1})$ and $M_l < O(\varepsilon^{-1})$ can occur. However, in these cases an equivalent macroscopic description does not exist [1].

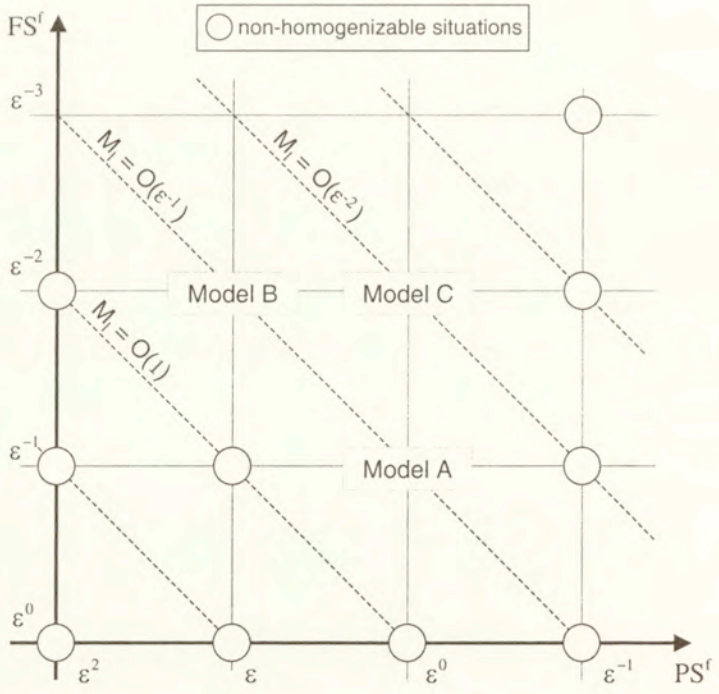

FIG. 2. Homogenizable and non-homogenizable situations with respect to the orders of magnitude of the three dimensionless numbers: M_l, FS_l^f and PS_l^f.

We are now able to write Eqs. (2.1)-(2.12) in the dimensionless form. For the sake of simplicity, we keep the same notations, but all quantities are now dimensionless quantities:

$$(3.1)\quad \mu^f \triangle \mathbf{v}^f - (Q^f)\,\nabla p^f - (Re)\,\rho^f(\mathbf{v}^f\cdot\nabla)\mathbf{v}^f = 0 \qquad \text{in } \Omega^f,$$

$$(3.2)\quad \nabla\cdot\mathbf{v}^f = 0 \qquad \text{in } \Omega^f,$$

$$(3.3)\quad (FT^s)^{-1}\,\rho^s C_p^s \frac{\partial T^s}{\partial t} - \nabla\cdot(\lambda^s\nabla T^s) = 0 \qquad \text{in } \Omega^s,$$

$$(3.4)\quad (FT^f)^{-1}\,\rho^f C_p^f \frac{\partial T^f}{\partial t} + (PT^f)\,\rho^f C_p^f \mathbf{v}^f\cdot\nabla T^f - \nabla\cdot(\lambda^f\nabla T^f) = 0 \qquad \text{in } \Omega^f,$$

$$(3.5)\quad (FS^s)^{-1}\,\rho^s \frac{\partial \omega^s}{\partial t} - \nabla\cdot(\rho^s D^s\nabla\omega^s) = 0 \qquad \text{in } \Omega^s,$$

$$(3.6)\quad (FS^f)^{-1}\,\rho^f \frac{\partial \omega^f}{\partial t} + (PS^f)\,\rho^f \mathbf{v}^f\cdot\nabla\omega^f - \nabla\cdot(\rho^f D^f\nabla\omega^f) = 0 \qquad \text{in } \Omega^f,$$

$$(3.7)\quad \mathbf{v}^f\cdot\mathbf{t} = 0 \qquad \text{on } \Gamma,$$

$$(3.8)\quad \rho^f((M)\,\mathbf{v}^f - \mathbf{w})\cdot\mathbf{N} = -(R)\,\rho^s\mathbf{w}\cdot\mathbf{N} \qquad \text{on } \Gamma,$$

$$(3.9)\quad T^s = T^f = T^* \qquad \text{on } \Gamma,$$

$$(3.10)\quad \Big((K)\,\lambda^s\nabla T^s - \lambda^f\nabla T^f\Big)\cdot\mathbf{N} = (H)\,L^{fs}\rho^s\mathbf{w}\cdot\mathbf{N} \qquad \text{on } \Gamma,$$

$$(3.11)\quad \Big((D)(R)\,\rho^s D^s\nabla\omega^s - \rho^f D^f\nabla\omega^f\Big)\cdot\mathbf{N} = (W)(\rho^f\omega^{f*} - \rho^s\omega^{s*})\mathbf{w}\cdot\mathbf{N} \quad \text{on } \Gamma$$

$$(3.12)\quad \omega^{s*} = k\,\omega^{f*} \qquad \text{on } \Gamma$$

3.3. Homogenisation method of double scale expansions

The condition of separation of scales (1.1) enables us to use the homogenisation method of double scale expansions for periodic structures [6, 24, 1]. Both characteristic lengths L and l introduce two dimensionless space variables,

$$\mathbf{y} = \frac{\mathbf{X}}{l}, \qquad \mathbf{x} = \frac{\mathbf{X}}{L},$$

Table 2. Orders of magnitude of the dimensionless numbers corresponding to the three cases of interest: model A, B and C

	Model A	Model B	Model C
R_l	$O(1)$	$O(1)$	$O(1)$
K_l	$O(1)$	$O(1)$	$O(1)$
D_l	$O(1)$ or $O(\varepsilon)$	$O(1)$ or $O(\varepsilon)$	$O(1)$ or $O(\varepsilon)$
Re_l	$O(\varepsilon)$	$O(\varepsilon)$	$O(\varepsilon)$
Q_l^f	$O(\varepsilon^{-1})$	$O(\varepsilon^{-1})$	$O(\varepsilon^{-1})$
M_l	$O(\varepsilon^{-1})$	$O(\varepsilon^{-1})$	$O(\varepsilon^{-2})$
$FT_l^s \simeq FT_l^f$	$O(\varepsilon^{-2})$	$O(\varepsilon^{-3})$	$O(\varepsilon^{-3})$
PT_l^f	$O(\varepsilon)$	$O(\varepsilon^2)$	$O(\varepsilon)$
H_l	$O(\varepsilon^2)$	$O(\varepsilon^3)$	$O(\varepsilon^3)$
FS_l^f	$O(\varepsilon^{-1})$	$O(\varepsilon^{-2})$	$O(\varepsilon^{-2})$
$FS_l^s \simeq D_l FS_l^f$	$O(\varepsilon^{-1})$ or $O(1)$	$O(\varepsilon^{-2})$ or $O(\varepsilon^{-1})$	$O(\varepsilon^{-2})$ or $O(\varepsilon^{-1})$
PS_l^f	$O(1)$	$O(\varepsilon)$	$O(1)$
W_l	$O(\varepsilon)$	$O(\varepsilon^2)$	$O(\varepsilon^2)$

where $\mathbf{X}$ is the physical space variable. The variable $\mathbf{x}$ is the macroscopic (or slow) space variable and $\mathbf{y}$ is the microscopic (or fast) space variable. The unknown fields at the microscopic scale of a given boundary value problem appear as functions of these two dimensionless space variables and are looked for in the following forms,

$$\phi(\mathbf{x},\mathbf{y},t = \phi^{(0)}(\mathbf{x},\mathbf{y},t) + \varepsilon\phi^{(1)}(\mathbf{x},\mathbf{y},t) + \varepsilon^2\phi^{(2)}(\mathbf{x},\mathbf{y},t) + \cdots, \tag{3.13}$$

where $\phi(\mathbf{x},\mathbf{y},t) = p^f, \mathbf{v}^f, \mathbf{w}, T^f, T^s, \omega^f, \omega^s$ and the $\phi^{(i)}$ are periodic functions or vectors of period Ω with respect to space variable $\mathbf{y}$. Since l is the reference characteristic length, the corresponding dimensionless space variable is $\mathbf{y}$ and $\mathbf{x} = \varepsilon\mathbf{y}$. Thus, the gradient operator ∇ is now written $(\nabla_y + \varepsilon\nabla_x)$ where subscripts x and y denote the variable for the derivative. The methodology of the homogenisation consists in introducing the asymptotic expansions (3.13) in the dimensionless local description (3.1)-(3.12). Solving the boundary-value problems arising at the successive orders of ε leads to the macroscopic description.

4. Description at the macroscopic scale

4.1. Model A

We consider here the orders of magnitude of dimensionless numbers given in Table 2 for model A. The first order macroscopic description derived from the

microscopic equations is presented below. The detailed calculus is itemized in Appendix A.

Fluid flow and mass balance: At the first order of approximation, the fluid pressure (A.14) is constant over the periodic cell and the macroscopic fluid pressure gradient $\nabla_x p^{f(0)}$ is acting as a driving force for the local flow (A.19):

$$p^{f(0)} = p^{f(0)}(\mathbf{x}, t), \qquad \mathbf{v}^{f(0)} = -\mathbf{k}(\mathbf{y}, t)\nabla_x p^{f(0)}.$$

$\mathbf{k}(\mathbf{y}, t)$ is the microscopic permeability tensor solution of the boundary value problem (A.21)-(A.23). The macroscopic fluid velocity which is obtained by volume averaging follows the Darcy's law,

$$\langle \mathbf{v}^{f(0)} \rangle = -\mathbf{K}\nabla_x p^{f(0)}, \quad K_{ij} = \frac{1}{\Omega}\int_{\Omega^f} k_{ij}(\mathbf{y}, t)\, d\Omega, \tag{4.1}$$

where $\mathbf{K}$ is the macroscopic permeability tensor of the porous medium. The first order macroscopic volume balance takes the classical form (A.30),

$$\nabla_x \cdot \langle \mathbf{v}^{f(0)} \rangle + \left(\frac{\rho^s}{\rho^f} - 1\right)\frac{df^s}{dt} = 0, \tag{4.2}$$

where f^s is the solid volume fraction. The first term and the second term of this equation are equal to the fluid flux and the shrinkage due to the solidification process, respectively (open system). Let us remark that the shrinkage due to the solidification process appears at the macroscopic scale although the metallic fluid is incompressible at the microscopic scale (2.2).

Heat transfer: At the first order of approximation, we have only one temperature field which is constant over the periodic cell: $T^{s(0)} = T^{f(0)} = T^{*(0)} = T^{(0)}(\mathbf{x}, t)$. The macroscopic heat transfer is governed by Eq.(A.48),

$$(\rho C_p)^{\text{eff}}\,\frac{\partial T^{(0)}}{\partial t} + \rho^f C_p^f \mathbf{V}_T^{\text{eff}} \cdot \nabla_x T^{(0)} - \nabla_x \cdot \left(\boldsymbol{\lambda}^{\text{eff}} \nabla_x T^{(0)}\right) - L^{fs}\rho^s \frac{df^s}{dt} = 0. \tag{4.3}$$

$(\rho C_p)^{\text{eff}}$ and $\boldsymbol{\lambda}^{\text{eff}}$ are the effective thermal capacity and the effective thermal conductivity tensor of the mixture, respectively. $\mathbf{V}_T^{\text{eff}}$ is an effective fluid velocity which is different from the Darcy velocity (4.2) and which accounts for heat effects. Such velocity was already introduced in previous works [8]. These effective

parameters characterize the average properties of the medium at the macroscopic scale. They are defined as follows:

$$(\rho C_p)^{\text{eff}} = f^s \rho^s C_p^s + f^f \rho^f C_p^f, \tag{4.4}$$

$$\boldsymbol{\lambda}^{\text{eff}} = \frac{1}{\Omega} \int_{\Omega^f} \lambda^f \left(\nabla_y \boldsymbol{\chi} + \boldsymbol{\delta}\right) d\Omega + \frac{1}{\Omega} \int_{\Omega^s} \lambda^s \left(\nabla_y \boldsymbol{\chi} + \boldsymbol{\delta}\right) d\Omega, \tag{4.5}$$

$$\mathbf{V}_T^{\text{eff}} = \frac{1}{\Omega} \int_{\Omega^f} \mathbf{v}^{f(0)} \left(\nabla_y \boldsymbol{\chi} + \boldsymbol{\delta}\right) d\Omega. \tag{4.6}$$

where $\boldsymbol{\chi}(\mathbf{y}, t)$ is the solution to the boundary value problem (A.41)-(A.43). The macroscopic heat transfer is governed by conduction and convection incorporating a heat flux due the solidification process over the solid-liquid interface. The above macroscopic description corresponds to the most general regime and reveals a coupling between heat and mass transfer. The structure of the macroscopic model is similar to the structure of the macroscopic heat transfer model already derived by NI and BECKERMANN [19] using the volume average method.

Species transport:

CASE. $D_l = O(1)$ and $FS_l^s = O(\varepsilon^{-1})$: In this case (Fe-C alloy), the solute is completely mixed in the fluid and the solid phases, i.e. we recover a lever-rule type model. The macroscopic species transport (A.63) is governed by convection and also contains a species flux due to the solidification process over the solid-liquid interface,

$$\rho^s \frac{\partial (f^s k\, \omega^{f(0)})}{\partial t} + \rho^f \frac{\partial ((1 - f^s)\omega^{f(0)})}{\partial t} + \rho^f \langle \mathbf{v}^{f(0)} \rangle \cdot \nabla_x \omega^{f(0)} = 0, \tag{4.7}$$

$\omega^{s(0)}$ and $\omega^{f(0)}$ which are completely mixed in the fluid and the solid phases respectively, are related to the temperature $T^{(0)}$ through the equilibrium phase diagram and satisfy $\omega^{s(0)}(\mathbf{x}, t) = k\, \omega^{f(0)}(\mathbf{x}, t)$. Thus the system (4.1), (4.2), (4.3) and (4.7) is closed.

CASE. $D_l = O(\varepsilon)$ and $FS_l^s = O(1)$: In this case (Sn-Pb alloy), the solute is completely mixed in the fluid phase only, i.e. we recover a Scheil-type behaviour: $\omega^{f(0)} = \omega^{f(0)}(\mathbf{x}, t)$ and $\omega^{s(0)} = \omega^{s(0)}(\mathbf{x}, \mathbf{y}, t)$. The macroscopic species transport is now given by equation (A.73),

$$\rho^s \left(\left\langle \frac{\partial \omega^{s(0)}}{\partial t} \right\rangle + \frac{\mathrm{d} f^s}{\mathrm{d} t} \omega^{s*(0)} \right) + \rho^f \frac{\partial \left((1 - f^s)\omega^{f(0)} \right)}{\partial t} + \rho^f \langle \mathbf{v}^{f(0)} \rangle \cdot \nabla_x \omega^{f(0)} = 0, \tag{4.8}$$

where

$$\left\langle \frac{\partial \omega^{s(0)}}{\partial t} \right\rangle = \frac{1}{\Omega} \int_{\Omega^s} \frac{\partial \omega^{s(0)}(\mathbf{x}, \mathbf{y}, t)}{\partial t} \, d\Omega = \frac{1}{\Omega} \int_{\Omega^s} \nabla_y \cdot \left(D^s \nabla_y \omega^{s(0)} \right) \, d\Omega. \tag{4.9}$$

$\omega^{s*(0)}$ and $\omega^{f(0)}$ are also related to the temperature $T^{(0)}$ through the equilibrium phase diagram and satisfy $\omega^{s*(0)}(\mathbf{x}, t) = k \; \omega^{f(0)}(\mathbf{x}, t)$. Thus the system (4.1), (4.2), (4.3) and (4.8) is closed. The macroscopic species transport is governed by convection and solute "back diffusion" within the solid phase (4.9) which, in contrast with what is usually assumed, is not negligible. The macroscopic description also contains a species flux due to the solidification process over the solid-liquid interface. The solute "back diffusion" within the solid phase (4.9), i.e. the memory effects, can be expressed as follows

$$\left\langle \frac{\partial \omega^{s(0)}}{\partial t} \right\rangle = F^{-1}(\Phi(\omega)) * \omega^{f(0)} \tag{4.10}$$

where $F^{-1}(\Phi(\omega))$ in the inverse Fourier transform of $\Phi(\omega)$ and $*$ is the convolution product. $\Phi(\omega)$ is a complex effective coefficient given by Eq.(A.74),

$$\Phi(\omega) = \frac{1}{\Omega} \int_{\Omega^s} i \; \omega \; \phi(\omega, \mathbf{y}) \; d\Omega \tag{4.11}$$

where $\phi(\omega, \mathbf{y})$ is the $\mathbf{y}$-periodic solution of the boundary value problem (A.69)-(A.70)

The above analysis shows that the macroscopic species transport equation takes two different forms according to the order of magnitude of the solutal Fourier number of the solid phase FS_l^s. This solutal Fourier number is estimated with respect to the parameter of scale separation, ε. The macroscopic description is given by a Scheil type model (4.8) and by a lever-rule type model (4.7) for small and large solutal Fourier number of the solid phase, respectively. In contrast with the macroscopic descriptions already proposed [9,5,22,19], the derived first order macroscopic models (4.7) and (4.8) do not contain the term $\rho^f \omega^{f(0)} \nabla_x \cdot \langle \mathbf{v}^{f(0)} \rangle$, although the shrinkage due to the solidification process appears at the macroscopic scale (4.2). This term characterizes the second order effects ($O(\varepsilon^2)$) in Eqs.(4.7) and (4.8). This result is due to the homogenisability condition: $M_l \geq O(\varepsilon^{-1})$. Practical situations in which $M_l < O(\varepsilon^{-1})$ can occur. However, in these cases an equivalent macroscopic description does not exist [3].

4.2. Model B

We now assume that the fluid velocity and the solidification process are very slow. Under such conditions, the three dimensionless numbers, Re_l, Q_l^f

and M_l are unchanged. Fourier numbers (FT_l^s, FT_l^f, FS_l^s, FS_l^f) are increased by an order of magnitude whereas Péclet numbers (PT_l^f, PS_l^f) and interfacial dimensionless numbers (H_l, W_l) are decreased by an order of magnitude (see Table 2 and Fig. 2). The derived macroscopic description is presented below.

Fluid flow and mass balance: The problem concerning the fluid flow and the mass balance is the same as in Model A. Once again, the fluid flow follows Darcy's law (4.1) and the macroscopic volume balance is given by Eq. (4.2).

Heat transfer: By following the same route as in Appendix A, it can be shown that the first-order macroscopic heat transfer is now governed by conduction only,

$$\nabla_x \cdot \left(\boldsymbol{\lambda}^{\text{eff}} \nabla_x T^{(0)}\right) = 0, \tag{4.12}$$

where $\boldsymbol{\lambda}^{\text{eff}}$ is the effective thermal conductivity tensor of the mixture already defined by Eq.(4.5)

Species transport:

CASE. $D_l = O(1)$ and $FS_l^s = O(\varepsilon^{-2})$ (Fe-C alloy): Under such conditions, the first order macroscopic description (Appendix B) is given by a lever-type model. The macroscopic species transport is now governed by diffusion and convection incorporating a species flux due to the solidification process over the solid-liquid interface,

$$\rho^s \frac{\partial(f^s k\, \omega^{f(0)})}{\partial t} + \rho^f \frac{\partial((1-f^s)\omega^{f(0)})}{\partial t} + \rho^f \mathbf{V}_S^{\text{eff}} \cdot \nabla_x \omega^{f(0)} - \nabla_x \cdot \left((\rho \mathbf{D}^\star) \nabla_x \omega^{f(0)}\right) = 0, \tag{4.13}$$

$\omega^{f(0)}$ and $\omega^{s(0)}$ are related to the temperature $T^{(0)}$ through the equilibrium phase diagram and satisfy $\omega^{s(0)}(\mathbf{x}, t) = k\ \omega^{f(0)}(\mathbf{x}, t)$. Thus the system (4.1), (4.2), (4.12) and (4.13) is closed. $\mathbf{V}_S^{\text{eff}}$ is an effective fluid velocity which is different from the Darcy velocity (4.1) and which accounts for solutal effects. The effective fluid velocity $\mathbf{V}_S^{\text{eff}}$ and the effective diffusion tensor $(\rho \mathbf{D}^\star)$ of the mixture are defined as follows:

$$\mathbf{V}_S^{\text{eff}} = \frac{1}{\Omega} \int_{\Omega^f} \mathbf{v}^{f(0)} \left(\nabla_y \boldsymbol{\beta}^f + \boldsymbol{\delta}\right) d\Omega,$$

$$(\rho \mathbf{D}^\star) = \frac{1}{\Omega} \int_{\Omega^f} \rho^f D^f \left(\nabla_y \boldsymbol{\beta}^f + \boldsymbol{\delta}\right) d\Omega \frac{1}{\Omega} \int_{\Omega^s} \rho^s D^s k\ \left(\nabla_y \boldsymbol{\beta}^s + \boldsymbol{\delta}\right) d\Omega.$$

$\boldsymbol{\beta}^s(\mathbf{y},t)$ and $\boldsymbol{\beta}^f(\mathbf{y},t)$ are the solutions to the boundary-value problem (B.16 - B.19). Once again, the homogenisability condition, $M_l \geq O(\varepsilon^{-1})$, implies that the term $\rho^f \omega^{f(0)} \nabla_x \cdot \mathbf{V}_S^{\text{eff}}$ does not appear in the first order derived macroscopic description (4.13).

CASE. $D_l = O(\varepsilon)$ and $FS_l^s = O(\varepsilon^{-1})$ (Sn-Pb alloy): It can be shown that macroscopic species transport is also given by Eq. (4.13). But now, the effective diffusion tensor is written,

$$(\rho \mathbf{D}^\star) = \frac{1}{\Omega} \int_{\Omega^f} \rho^f D^f \left(\nabla_y \boldsymbol{\beta}^f + \boldsymbol{\delta} \right) d\Omega.$$

4.3. Model C

In this last case, the solidification process is assumed to be very slow whereas the fluid velocity is increased by an order of magnitude. Consequently, the interfacial dimensionless number M_l and Péclet numbers (PT_l^f, PS_l^f) are increased by one order of magnitude whereas other dimensionless numbers remain unchanged (see Table 2 and Fig. 2 : model C). Under such conditions, the first-order macroscopic description is written as follows.

Fluid flow and mass balance: At the macroscopic scale, the fluid flow is always described by the Darcy law (4.1). The interface velocity is now very small compared to the fluid velocity ($M_l = O(\varepsilon^{-2})$). Therefore, the macroscopic volume balance takes the form

$$\nabla_x \cdot \langle \mathbf{v}^{f(0)} \rangle = 0. \tag{4.14}$$

The shrinkage due the solidification process does not appear at the macroscopic scale at the first order of approximation (closed system).

Heat transfer: By following the same route as in Appendix A, we obtain the first-order macroscopic description. The macroscopic heat transfer is governed by both conduction and convection,

$$\rho^f C_p^f \mathbf{V}_T^{\text{eff}} \cdot \nabla_x T^{(0)} - \nabla_x \cdot \left(\boldsymbol{\lambda}^{\text{eff}} \nabla_x T^{(0)} \right) = 0. \tag{4.15}$$

$\boldsymbol{\lambda}^{\text{eff}}$ and $\mathbf{V}_T^{\text{eff}}$ are the effective conductivity tensor of the mixture (4.5) and the effective fluid velocity (4.6), respectively.

Species transport:

CASE. $D_l = O(1)$ and $FS_l^s = O(\varepsilon^{-2})$ (Fe-C alloy): The solidification process is very slow. Thus, at the first order of approximation, the solute is completely mixed in the fluid and in the solid phase, i.e. we obtain a lever-type behaviour

(see Appendix C). The macroscopic species transport is governed by convection only,

$$\rho^f \langle \mathbf{v}^{f(0)} \rangle \cdot \nabla_x \omega^{f(0)} = 0, \tag{4.16}$$

with $\omega^{s(0)}(\mathbf{x},t) = k\ \omega^{f(0)}(\mathbf{x},t)$. In contrast with models A and B, the evolution of the solid volume fraction during the solidification process can not be deduced from the above macroscopic description at the first order of approximation. The evolution of the solid fraction may be derived from the second order macroscopic equation (C.26) governing the average fluid mass fraction $\langle \omega^f \rangle$ which is given by

$$\varepsilon\ \rho^s \frac{\partial (f^s k\ \langle \omega^f \rangle)}{\partial t} + \varepsilon\ \rho^f \frac{\partial ((1-f^s)\langle \omega^f \rangle)}{\partial t} + \rho^f \langle \mathbf{v}^f \rangle \cdot \nabla_x \langle \omega^f \rangle - \varepsilon\ \nabla_x \cdot \Big((\rho \mathbf{D}^{\star\star}) \nabla_x \langle \omega^f \rangle \Big) = 0. \tag{4.17}$$

$\langle \omega^s \rangle$ and $\langle \omega^f \rangle$ are related to the macroscopic temperature $T^{(0)}$ through the equilibrium phase diagram and satisfy $\langle \omega^s \rangle = k\ \langle \omega^f \rangle$. Thus the system (4.2), (4.15), (4.16) and (4.18) is closed. $(\rho \mathbf{D}^{\star\star})$ is the effective dispersion tensor of the mixture,

$$(\rho \mathbf{D}^{\star\star}) = \frac{1}{\Omega} \int_{\Omega^f} \rho^f D^f \left(\nabla_y \boldsymbol{\varphi}^f + \delta \right) d\Omega + \frac{1}{\Omega} \int_{\Omega^f} \rho^f \mathbf{k} \nabla_x p^{f(0)} \cdot \boldsymbol{\varphi}^f\ d\Omega + \frac{1}{\Omega} \int_{\Omega^s} \rho^s D^s k\ \left(\nabla_y \boldsymbol{\varphi}^s + \delta \right) d\Omega,$$

where $\boldsymbol{\varphi}^f(\mathbf{y}, \nabla_x p^{f(0)}, t)$ and $\boldsymbol{\varphi}^s(\mathbf{y}, \nabla_x p^{f(0)}, t)$ are the solutions to the bounda- ry-value problem (C.17)-(C.20). The dispersive character of $(\rho \mathbf{D}^{\star\star})$ appears through its dependence on the macroscopic gradient of fluid pressure $\nabla_x p^{f(0)}$, i.e. the fluid velocity. $(\rho \mathbf{D}^{\star\star})$ is, in general, positive definite but it is nonsymmetric [2].

CASE. $D_l = O(\varepsilon)$ and $FS_l^s = O(\varepsilon^{-1})$ (Sn-Pb alloy): The macroscopic species transport is also given by equation (4.17). But now, the effective dispersion tensor is written in the form:

$$(\rho \mathbf{D}^{\star\star}) = \frac{1}{\Omega} \int_{\Omega^f} \rho^f D^f \left(\nabla_y \boldsymbol{\varphi}^f + \delta \right) d\Omega + \frac{1}{\Omega} \int_{\Omega^f} \rho^f \mathbf{k} \nabla_x p^{f(0)} \cdot \boldsymbol{\varphi}^f\ d\Omega.$$

5. Conclusion

Continuum models for momentum, mass, heat and species transport in metallic saturated porous media undergoing liquid-solid phase change have been rigorously derived from the description at the pore scale by using an upscaling

technique, namely the method of multiple scale expansions. Among the several homogenisable situations, the three most fruitful cases are presented. Their domain of validity is given by means of orders of magnitude of the dimensionless numbers characterizing the dominating phenomena and the physical properties of the constituents at the microscopic scale (Fig.2). In practical situations, knowledge of the order of magnitude of these dimensionless numbers will clearly indicate which model should be chosen for describing the physical processes.

In model A, fluid flow obeys Darcy's law and shrinkage effects due to the solidification process appear at the macroscopic scale (open system). Heat transfer is governed by conduction and convection incorporating a heat flux due to the liquid-solid phase change. We have shown that the species transport equation may take two different forms with respect to the orders of magnitude of the ratio of the solid diffusivity to the fluid diffusivity (D_l), i.e the solutal Fourier number of the solid phase (FS^s). For small solutal Fourier number of the solid phase, the macroscopic description is given by a Scheil type model: the species transport is governed by convection and solute "back diffusion" within the solid phase. It also contains a species flux due to the solidification process over the solid-liquid interface. For large solutal Fourier number of the solid phase, the macroscopic species transport follows a lever-rule type model.

In contrast with model A, we assume in model B that the solidification process and the fluid velocity are very slow. Under such conditions, the fluid flow follows Darcy's law and shrinkage effects due to the solidification process are still present at the macroscopic scale. The macroscopic heat transfer is governed by conduction only. For small and large solutal Fourier number of the solid phase, the macroscopic species transport follows a lever-rule type model and is governed by convection and diffusion.

In model C, the solidification process is considered to be very slow whereas the fluid velocity is increased by one order of magnitude. At the first order of approximation, the fluid flow obeys Darcy's law whereas shrinkage effects due the solidification process do not appear at the macroscopic scale (closed system). The macroscopic heat transfer is governed by conduction and convection. For small and large solutal Fourier number of the solid phase, the first order macroscopic species transport is governed by convection only. The evolution of the solid mass fraction can be deduced from the macroscopic description at the second order of approximation. In this case, the macro-segregation equation that governs the average fluid mass fraction contains both convection and dispersion terms.

There is a possible continuous passage from the mass transport models A and B to model C by increasing M_l (Fig. 2). Similarly, it can be shown that there exist continuous passages from heat transfer model A to models C and B. Model A corresponds to the most general regime. Concerning species transport, the only possible continuous passage is from model B to model C by increasing

the solutal Péclet number of the fluid phase PS^f and the dimensionless number M_l simultaneously (Fig. 2).

It should be mentioned that it is relatively straightforward to extend the models proposed in this paper to other solid-liquid systems (igneous rocks) and to more than two phases. For example, it would be very interesting to take into account the presence of a gas phase to describe correctly the formation of hot tears.

Appendix A. Model A

Taking into account the order of magnitude of the dimensionless numbers (see Table 2), the dimensionless description at the microscopic scale given by Eqs.(3.7)-(3.18), takes the form:

$$\mu^f \triangle \mathbf{v}^f - \varepsilon^{-1} \nabla p^f - \varepsilon \rho^f (\mathbf{v}^f \cdot \nabla)\mathbf{v}^f = 0 \qquad \text{in } \Omega^f, \tag{A.1}$$

$$\nabla \cdot \mathbf{v}^f = 0 \qquad \text{in } \Omega^f, \tag{A.2}$$

$$\varepsilon^2 \rho^s C_p^s \frac{\partial T^s}{\partial t} - \nabla \cdot (\lambda^s \nabla T^s) = 0 \qquad \text{in } \Omega^s, \tag{A.3}$$

$$\varepsilon^2 \rho^f C_p^f \frac{\partial T^f}{\partial t} + \varepsilon \rho^f C_p^f \mathbf{v}^f \cdot \nabla T^f - \nabla \cdot (\lambda^f \nabla T^f) = 0 \qquad \text{in } \Omega^f, \tag{A.4}$$

$$(FS_l^s)^{-1} \rho^s \frac{\partial \omega^s}{\partial t} - \nabla \cdot (\rho^s D^s \nabla \omega^s) = 0 \qquad \text{in } \Omega^s, \tag{A.5}$$

$$\varepsilon \rho^f \frac{\partial \omega^f}{\partial t} + \rho^f \mathbf{v}^f \cdot \nabla \omega^f - \nabla \cdot (\rho^f D^f \nabla \omega^f) = 0 \qquad \text{in } \Omega^f, \tag{A.6}$$

$$\mathbf{v}^f \cdot \mathbf{t} = 0 \qquad \text{on } \Gamma, \tag{A.7}$$

$$\rho^f (\varepsilon^{-1} \mathbf{v}^f - \mathbf{w}) \cdot \mathbf{N} = -\rho^s \mathbf{w} \cdot \mathbf{N} \qquad \text{on } \Gamma, \tag{A.8}$$

$$T^s = T^f = T^* \qquad \text{on } \Gamma, \tag{A.9}$$

$$\left(\lambda^s \nabla T^s - \lambda^f \nabla T^f\right) \cdot \mathbf{N} = \varepsilon^2 L^{fs} \rho^s \mathbf{w} \cdot \mathbf{N} \qquad \text{on } \Gamma, \tag{A.10}$$

$$\left((D_l)\ \rho^s D^s \nabla \omega^s - \rho^f D^f \nabla \omega^f\right) \cdot \mathbf{N} = \varepsilon(\rho^f \omega^{f*} - \rho^s \omega^{s*}) \mathbf{w} \cdot \mathbf{N} \qquad \text{on } \Gamma, \tag{A.11}$$

$$\omega^{s*} = k\ \omega^{f*} \qquad \text{on } \Gamma, \tag{A.12}$$

Fluid flow and mass balance: Introducing the asymptotic expansions (3.13) in Eqs. (A.1)-(A.2) and (A.7)-(A.8), the first order problem to be solved is given by

$$\nabla_y p^{f(0)} = 0 \qquad \text{in } \Omega^f, \tag{A.13}$$

where the unknown $p^{f(0)}$ is $\mathbf{y}$-periodic. Thus, from Eq. (A.13) we get

$$p^{f(0)} = p^{f(0)}(\mathbf{x}, t). \tag{A.14}$$

Taking into account this result, the second order problem is given by

$$\mu^f \triangle_y \mathbf{v}^{f(0)} - \nabla_y p^{f(1)} - \nabla_x p^{f(0)} = 0 \qquad \text{in } \Omega^f, \tag{A.15}$$

$$\nabla_y \cdot \mathbf{v}^{f(0)} = 0 \qquad \text{in } \Omega^f, \tag{A.16}$$

$$\mathbf{v}^{f(0)} \cdot \mathbf{t} = 0 \qquad \text{on } \Gamma, \tag{A.17}$$

$$\mathbf{v}^{f(0)} \cdot \mathbf{N} = 0 \qquad \text{on } \Gamma, \tag{A.18}$$

This is a boundary-value problem for the $\mathbf{y}$-periodic unknowns $p^{f(1)}$ and $\mathbf{v}^{f(0)}$. From Eq. (A.15)-(A.18), it has been shown [1] that the fluid velocity $\mathbf{v}^{f(0)}$ and the pressure $p^{f(1)}$ can be put in the form

$$\mathbf{v}^{f(0)} = -\mathbf{k}(\mathbf{y}, t) \nabla_x p^{f(0)}, \tag{A.19}$$

$$p^{f(1)} = \mathbf{b}(\mathbf{y}, t) \cdot \nabla_x p^{f(0)} + \overline{p}^{f(1)}(\mathbf{x}, t), \tag{A.20}$$

where $\mathbf{k}(\mathbf{y}, t)$ is the microscopic permeability tensor. The fluid pressure $p^{f(1)}$ is a linear function of the macroscopic gradient $\nabla_x p^{f(0)}$, modulo an arbitrary function $\overline{p}^{f(1)}(\mathbf{x}, t)$. The vector $\mathbf{b}(\mathbf{y}, t)$ is $\mathbf{y}$-periodic and average to zero, $\langle \mathbf{b} \rangle = 0$. The latter condition ensures the uniqueness of $\mathbf{b}$. The microscopic permeability tensor $\mathbf{k}$ and the pore vector field $\mathbf{b}$ are the solutions of the following boundary value problem,

$$\mu^f \triangle_y \mathbf{k} - \nabla_y \mathbf{b} - \boldsymbol{\delta} = 0 \qquad \text{in } \Omega^f, \tag{A.21}$$

$$\nabla_y \cdot \mathbf{k} = 0 \qquad \text{in } \Omega^f, \tag{A.22}$$

$$\mathbf{k} = 0 \qquad \text{on } \Gamma, \tag{A.23}$$

where $\boldsymbol{\delta}$ is the unit tensor.The macroscopic fluid velocity $\langle \mathbf{v}^{f(0)} \rangle$ follows Darcy's law,

$$\langle \mathbf{v}^{f(0)} \rangle = -\mathbf{K} \nabla_x p^{f(0)}, \quad K_{ij} = \frac{1}{\Omega} \int_{\Omega^f} k_{ij}(\mathbf{y}, t) \, d\Omega, \tag{A.24}$$

where $\mathbf{K}$ is the macroscopic permeability tensor. We consider now equations,

$$\nabla_y \cdot \mathbf{v}^{f(1)} + \nabla_x \cdot \mathbf{v}^{f(0)} = 0 \qquad \text{in } \Omega^f, \tag{A.25}$$

$$\mathbf{v}^{f(1)} \cdot \mathbf{t} = 0 \qquad \text{on } \Gamma, \tag{A.26}$$

$$\rho^f (\mathbf{v}^{f(1)} - \mathbf{w}^{(0)}) \cdot \mathbf{N} = -\rho^s \mathbf{w}^{(0)} \cdot \mathbf{N} \qquad \text{on } \Gamma, \tag{A.27}$$

where the unknown $\mathbf{v}^{f(1)}$ is $\mathbf{y}$-periodic. Integrating equation (A.25) over Ω^f and then using the divergence theorem, boundary condition (A.27) and the period-

icity on $\partial\Omega \cap \partial\Omega^f$, we obtain

$$\rho^f \nabla_x \cdot \langle \mathbf{v}^{f(0)} \rangle = -\frac{1}{\Omega} \int_{\Gamma \cup (\partial\Omega \cap \partial\Omega^f)} \rho^f \mathbf{v}^{f(1)} \cdot \mathbf{N} d\Gamma \tag{A.28}$$

$$= -(\rho^f - \rho^s) \frac{1}{\Omega} \int_{\Gamma} \mathbf{w}^{(0)} \cdot \mathbf{N} d\Gamma,$$

with

$$\frac{1}{\Omega} \int_{\Gamma} \mathbf{w}^{(0)} \cdot \mathbf{N} d\Gamma = \frac{d}{dt}\left(\frac{\Omega^f}{\Omega}\right) = \frac{df^f}{dt} = -\frac{df^s}{dt}. \tag{A.29}$$

f^s and f^f are the solid volume fraction and the fluid volume fraction, respectively. Therefore, the macroscopic volume balance takes the form

$$\nabla_x \cdot \langle \mathbf{v}^{f(0)} \rangle + \left(\frac{\rho^s}{\rho^f} - 1\right) \frac{df^s}{dt} = 0. \tag{A.30}$$

Heat transfer: Introducing the asymptotic expansions (3. 13) in Eq. (A.3)-(A.4) and (A.9)-(A. 10), the lower order problem to be solved is given by

$$\nabla_y \cdot \left(\lambda^s \nabla_y T^{s(0)}\right) = 0 \qquad \text{in } \Omega^s, \tag{A.31}$$

$$\nabla_y \cdot \left(\lambda^f \nabla_y T^{f(0)}\right) = 0 \qquad \text{in } \Omega^f, \tag{A.32}$$

$$T^{s(0)} = T^{f(0)} = T^{*(0)} \qquad \text{on } \Gamma, \tag{A.33}$$

$$\left(\lambda^s \nabla_y T^{s(0)} - \lambda^f \nabla_y T^{f(0)}\right) \cdot \mathbf{N} = 0 \qquad \text{on } \Gamma, \tag{A.34}$$

where the unknowns $T^{s(0)}$ and $T^{f(0)}$ are $\mathbf{y}$-periodic. It can be shown that the obvious solution of the above boundary value problem (A.31)-(A.34) is given by

$$T^{s(0)} = T^{f(0)} = T^{*(0)} = T^{(0)}(\mathbf{x}, t). \tag{A.35}$$

It means that the first order solution is independent of the microscopic variable $\mathbf{y}$ and that we have only one temperature field at the first order of approximation. Taking into account the preceding results, we get the following second-order problem:

$$\nabla_y \cdot \left[\lambda^s \left(\nabla_y T^{s(1)} + \nabla_x T^{(0)}\right)\right] = 0 \qquad \text{in } \Omega^s, \tag{A.36}$$

$$\nabla_y \cdot \left[\lambda^f \left(\nabla_y T^{f(1)} + \nabla_x T^{(0)}\right)\right] = 0 \qquad \text{in } \Omega^f, \tag{A.37}$$

$$T^{s(1)} = T^{f(1)} = T^{*(1)} \qquad \text{on } \Gamma, \tag{A.38}$$

$$\left[\lambda^s \left(\nabla_y T^{s(1)} + \nabla_x T^{(0)}\right) - \lambda^f \left(\nabla_y T^{f(1)} + \nabla_x T^{(0)}\right)\right] \cdot \mathbf{N} = 0 \qquad \text{on } \Gamma, \tag{A.39}$$

where the unknowns $T^{s(1)}$ and $T^{f(1)}$ are $\mathbf{y}$-periodic. The solution of the set of equations (A.36)-(A.39) appears as a linear function of the macroscopic thermal gradient of $T^{(0)}$, modulo an arbitrary function $\overline{T}^{(1)}(\mathbf{x},t)$:

$$T^{(1)} = \boldsymbol{\chi}(\mathbf{y},t)\cdot\nabla_x T^{(0)} + \overline{T}^{(1)}(\mathbf{x},t). \tag{A.40}$$

$T^{(1)}$ stands for $T^{s(1)}$ in Ω^s and $T^{f(1)}$ in Ω^f. The vector $\boldsymbol{\chi}(\mathbf{y},t)$ is $\mathbf{y}$-periodic, average to zero, and it is a solution of the following boundary-value problem:

$$\nabla_y\cdot\left[\lambda^s\left(\nabla_y\boldsymbol{\chi}+\boldsymbol{\delta}\right)\right]=0 \qquad \text{in } \Omega^s, \tag{A.41}$$

$$\nabla_y\cdot\left[\lambda^f\left(\nabla_y\boldsymbol{\chi}+\boldsymbol{\delta}\right)\right]=0 \qquad \text{in } \Omega^f, \tag{A.42}$$

$$\lambda^s\left(\nabla_y\boldsymbol{\chi}+\boldsymbol{\delta}\right)\cdot\mathbf{N}=\lambda^f\left(\nabla_y\boldsymbol{\chi}+\boldsymbol{\delta}\right)\cdot\mathbf{N} \qquad \text{on } \Gamma, \tag{A.43}$$

The third order problem is given by

$$\rho^s C_p^s\frac{\partial T^{(0)}}{\partial t}-\nabla_y\cdot\left[\lambda^s\left(\nabla_y T^{s(2)}+\nabla_x T^{s(1)}\right)\right] - \nabla_x\cdot\left[\lambda^s\left(\nabla_y T^{s(1)}+\nabla_x T^{(0)}\right)\right]=0 \quad \text{in} \quad \Omega^s, \tag{A.44}$$

$$\rho^f C_p^f\frac{\partial T^{(0)}}{\partial t}+\rho^f C_p^f\mathbf{v}^{f(0)}\cdot\left(\nabla_y T^{f(1)}+\nabla_x T^{(0)}\right)-\nabla_y\cdot\left[\lambda^f\left(\nabla_y T^{f(2)} +\nabla_x T^{f(1)}\right)\right]-\nabla_x\cdot\left[\lambda^f\left(\nabla_y T^{f(1)}+\nabla_x T^{(0)}\right)\right]=0 \quad \text{in} \quad \Omega^f, \tag{A.45}$$

$$T^{s(2)}=T^{f(2)}=T^{*(2)} \qquad \text{on} \quad \Gamma, \tag{A.46}$$

$$\left[\lambda^s\left(\nabla_y T^{s(2)}+\nabla_x T^{s(1)}\right)-\lambda^f\left(\nabla_y T^{f(2)}+\nabla_x T^{f(1)}\right)\right]\cdot\mathbf{N} = L^{fs}\rho^s\mathbf{w}^{(0)}\cdot\mathbf{N} \quad \text{on} \quad \Gamma, \tag{A.47}$$

where the $\mathbf{y}$-periodic unknowns are $T^{s(2)}$ and $T^{f(2)}$. The fluid velocity $\mathbf{v}^{f(0)}$ follows the law (A.19). Integrating (A.44) over Ω^s and (A.45) over Ω^f and then using the divergence theorem, the condition of periodicity on $\partial\Omega\cap\partial\Omega^f$ and $\partial\Omega\cap\partial\Omega^s$ and the boundary condition (A.47) leads to first order macroscopic description:

$$(\rho C_p)^{\text{eff}}\frac{\partial T^{(0)}}{\partial t}+\rho^f C_p^f\mathbf{V}_T^{\text{eff}}\cdot\nabla_x T^{(0)}-\nabla_x\cdot\left(\boldsymbol{\lambda}^{\text{eff}}\nabla_x T^{(0)}\right)-L^{fs}\rho^s\frac{df^s}{dt}=0. \tag{A.48}$$

$(\rho C_p)^{\text{eff}}$ and $\boldsymbol{\lambda}^{\text{eff}}$ are the effective thermal capacity and the effective conductivity tensor of the mixture respectively, and $\mathbf{V}_T^{\text{eff}}$ is the effective fluid velocity. These different effective parameters are defined as follows

$$(\rho C_p)^{\text{eff}} = f^s \rho^s C_p^s + f^f \rho^f C_p^f, \tag{A.49}$$

$$\boldsymbol{\lambda}^{\text{eff}} = \frac{1}{\Omega} \int_{\Omega^f} \lambda^f \left(\nabla_y \boldsymbol{\chi} + \boldsymbol{\delta}\right) d\Omega + \frac{1}{\Omega} \int_{\Omega^s} \lambda^s \left(\nabla_y \boldsymbol{\chi} + \boldsymbol{\delta}\right) d\Omega, \tag{A.50}$$

$$\mathbf{V}_T^{\text{eff}} = \frac{1}{\Omega} \int_{\Omega^f} \mathbf{v}^{f(0)} \left(\nabla_y \boldsymbol{\chi} + \boldsymbol{\delta}\right) d\Omega. \tag{A.51}$$

Species transport:

CASE. $D_l = O(1)$ and $FS_l^s = O(\varepsilon^{-1})$ (Fe-C alloy): Introducing the asymptotic expansions (3.13) in Eqs. (A.5)-(A.6) and (A.11)-(A.12), the first order problem to be solved takes the forms

$$\nabla_y \cdot \left(\rho^s \; D^s \nabla_y \omega^{s(0)}\right) = 0 \qquad \text{in } \Omega^s, \tag{A.52}$$

$$\rho^f \mathbf{v}^{f(0)} \cdot \nabla_y \omega^{f(0)} - \nabla_y \cdot \left(\rho^f \; D^f \nabla_y \omega^{f(0)}\right) = 0 \qquad \text{in } \Omega^f, \tag{A.53}$$

$$\left(\rho^s D^s \nabla_y \omega^{s(0)} - \rho^f D^f \nabla_y \omega^{f(0)}\right) \cdot \mathbf{N} = 0 \qquad \text{on } \Gamma, \tag{A.54}$$

$$\omega^{s*(0)} = k \; \omega^{f*(0)} \qquad \text{on } \Gamma, \tag{A.55}$$

where the unknowns $\omega^{s(0)}$ and $\omega^{f(0)}$ are $\mathbf{y}$-periodic. The fluid $\mathbf{v}^{f(0)}$ velocity follows the law (A.19). From Eqs. (A.52)-(A.55), we get

$$\begin{aligned} \omega^{f(0)} &= \omega^{f*(0)} = \omega^{f(0)}(\mathbf{x}, t), \\ \omega^{s(0)} &= \omega^{s*(0)} = \omega^{s(0)}(\mathbf{x}, t) = k\omega^{f(0)}. \end{aligned} \tag{A.56}$$

At the first order of approximation, the fluid and the solid mass fraction are independent of the microscopic variable $\vec{y}$, i.e. they are constant over the cell. We consider now the following equations that are obtained at a higher order:

$$\rho^s \frac{\partial \omega^{s(0)}}{\partial t} - \nabla_y \cdot \left[\rho^s \; D^s \left(\nabla_y \omega^{s(1)} + \nabla_x \omega^{s(0)}\right)\right] = 0 \qquad \text{in} \quad \Omega^s \tag{A.57}$$

$$\begin{aligned} \rho^f \frac{\partial \omega^{f(0)}}{\partial t} + \rho^f \mathbf{v}^{f(0)} \cdot \left(\nabla_y \omega^{f(1)} + \nabla_x \omega^{f(0)}\right) \\ - \nabla_y \cdot \left[\rho^f \; D^f \left(\nabla_y \omega^{f(1)} + \nabla_x \omega^{f(0)}\right)\right] = 0 \quad \text{in} \quad \Omega^f, \end{aligned} \tag{A.58}$$

$$\left[\rho^s D^s \left(\nabla_y \omega^{s(1)} + \nabla_x \omega^{s(0)}\right) - \rho^f D^f \left(\nabla_y \omega^{f(1)} + \nabla_x \omega^{f(0)}\right)\right] \cdot \mathbf{N} = (\rho^f \omega^{f*(0)} - \rho^s \omega^{s*(0)}) \mathbf{w}^{(0)} \cdot \mathbf{N} \quad \text{on} \quad \Gamma, \tag{A.59}$$

where the unknowns $\omega^{f(1)}$ and $\omega^{s(1)}$ are $\mathbf{y}$-periodic. Integrating (A.57) over Ω^s and (A.58) over Ω^f and then using the divergence theorem, the condition of periodicity on $\partial\Omega \cap \partial\Omega^f$ and $\partial\Omega \cap \partial\Omega^s$ leads to

$$|\Omega^s| \rho^s \frac{\partial \omega^{s(0)}}{\partial t} - \int_\Gamma \rho^s \; D^s \left(\nabla_y \omega^{s(1)} + \nabla_x \omega^{s(0)}\right) \cdot \mathbf{N} d\Gamma = 0, \tag{A.60}$$

$$|\Omega^f| \rho^f \frac{\partial \omega^{f(0)}}{\partial t} + \rho^f \int_{\Omega^f} \mathbf{v}^{f(0)} \cdot \left(\nabla_y \omega^{f(1)} + \nabla_x \omega^{f(0)}\right) d\Omega - \int_\Gamma \rho^f \; D^f \left(\nabla_y \omega^{f(1)} + \nabla_x \omega^{f(0)}\right) \cdot \mathbf{N} d\Gamma = 0. \tag{A.61}$$

By considering the fluid incompressibility (A.16) and the boundary condition (A.18), and by using the divergence theorem and the periodicity on $\partial\Omega \cap \partial\Omega^f$, we get

$$\int_{\Omega^f} \mathbf{v}^{f(0)} \cdot \nabla_y \omega^{f(1)} d\Omega = 0. \tag{A.62}$$

Therefore, from Eqs. (A.60)-(A.61) and the boundary condition (A.59), we obtain the following first order macroscopic description

$$\rho^s \frac{\partial \left(f^s k \; \omega^{f(0)}\right)}{\partial t} + \rho^f \frac{\partial \left((1 - f^s) \omega^{f(0)}\right)}{\partial t} + \rho^f \langle \mathbf{v}^{f(0)} \rangle \cdot \nabla_x \omega^{f(0)} = 0, \tag{A.63}$$

where $\langle \mathbf{v}^{f(0)} \rangle = -\mathbf{K} \; \nabla_x p^{f(0)}$ and $\omega^{s(0)}(\mathbf{x}, t) = k \; \omega^{f(0)}(\mathbf{x}, t)$.

CASE. $D_l = O(\varepsilon)$ and $FS_l^s = O(1)$ (Sn-Pb alloy): The first order problem to be solved takes now the forms:

$$\rho^s \frac{\partial \omega^{s(0)}}{\partial t} - \nabla_y \cdot \left(\rho^s \; D^s \nabla_y \omega^{s(0)}\right) = 0 \qquad \text{in } \Omega^s, \tag{A.64}$$

$$\rho^f \mathbf{v}^{f(0)} \nabla_y \omega^{f(0)} - \nabla_y \cdot \left(\rho^f \; D^f \nabla_y \omega^{f(0)}\right) = 0 \qquad \text{in } \Omega^f, \tag{A.65}$$

$$\rho^f D^f \nabla_y \omega^{f(0)} \cdot \mathbf{N} = 0 \qquad \text{on } \Gamma, \tag{A.66}$$

$$\omega^{s*(0)} = k \; \omega^{f*(0)} \qquad \text{on } \Gamma, \tag{A.67}$$

where the unknowns $\omega^{s(0)}$ and $\omega^{f(0)}$ are $\mathbf{y}$-periodic. The fluid $\mathbf{v}^{f(0)}$ velocity follows the law (A.19). Once again, from Eqs. (A.65)-(A.66), we get: $\omega^{f(0)} = \omega^{f*(0)} = \omega^{f(0)}(\mathbf{x}, t)$. At the first order of approximation, the fluid mass fraction is independent of the microscopic variable $\mathbf{y}$. In contrast with $\omega^{f(0)}$, the solid mass fraction is $\mathbf{y}$-dependent. Consider a solid mass fraction in the form $\omega^{s(0)}(\mathbf{x}, \mathbf{y}, t) = \overline{\omega}^{s(0)}(\mathbf{x}, \mathbf{y})\, e^{i\omega t}$ and the Fourier transform of Eqs. (A.64) and (A.67). The Fourier transform $\overline{\omega}^{s(0)}$ of $\omega^{s(0)}$ appears as a linear function of the fluid mass fraction,

$$\overline{\omega}^{s(0)} = \phi(\omega, \mathbf{y})\ \omega^{f(0)}(\mathbf{x}, t). \tag{A.68}$$

The complex function $\phi(\omega, \mathbf{y})$ is the $\mathbf{y}$-periodic solution of the following boundary value problem:

$$-\rho^s i\ \omega\ \phi - \nabla_y \cdot (\rho^s\ D^s \nabla_y \phi) = 0 \qquad \text{in } \Omega^s, \tag{A.69}$$

$$\phi = k \qquad \text{on } \Gamma. \tag{A.70}$$

We consider now the following equations that are obtained at a higher order:

$$\rho^f \frac{\partial \omega^{f(0)}}{\partial t} + \rho^f \mathbf{v}^{f(0)} \cdot \left(\nabla_y \omega^{f(1)} + \nabla_x \omega^{f(0)}\right) - \nabla_y \cdot \left[\rho^f\ D^f \left(\nabla_y \omega^{f(1)} + \nabla_x \omega^{f(0)}\right)\right] = 0 \quad \text{in } \Omega^f, \tag{A.71}$$

$$\left[\rho^s D^s \nabla_y \omega^{s(0)} - \rho^f D^f \left(\nabla_y \omega^{f(1)} + \nabla_x \omega^{f(0)}\right)\right] \cdot \mathbf{N} = \rho^f \omega^{f*(0)} - \rho^s \omega^{s*(0)}) \mathbf{w}^{(0)} \cdot \mathbf{N} \quad \text{on } \Gamma, \tag{A.72}$$

where the unknown $\omega^{f(1)}$ is $\mathbf{y}$-periodic. The relation (A.62) remains valid. Therefore, integrating (A.64) over Ω^s and (A.71) over Ω^f and then using the divergence theorem, the condition of periodicity on $\partial\Omega \cap \partial\Omega^f$ and on $\partial\Omega \cap \partial\Omega^s$ and the boundary condition (A.72) leads to the following first order macroscopic description:

$$\rho^s \left(\left\langle \frac{\partial \omega^{s(0)}}{\partial t} \right\rangle + \frac{\mathrm{d}f^s}{\mathrm{d}t} \omega^{s*(0)}\right) + \rho^f\ \frac{\partial \left((1 - f^s)\omega^{f(0)}\right)}{\partial t} + \rho^f \langle \mathbf{v}^{f(0)} \rangle \cdot \nabla_x \omega^{f(0)} = 0, \tag{A.73}$$

where $\langle \mathbf{v}^{f(0)} \rangle = -\mathbf{K}\ \nabla_x p^{f(0)}$ and $\omega^{s*(0)}(\mathbf{x}, t) = k\ \omega^{f(0)}(\mathbf{x}, t)$. We have

$$F\left(\left\langle \frac{\partial \omega^{s(0)}}{\partial t} \right\rangle\right) = \frac{1}{\Omega} \int_{\Omega^s} i\ \omega \phi(\omega, \mathbf{y})\ d\Omega\ .\omega^{f(0)} = \Phi(\omega).\omega^{f(0)} \tag{A.74}$$

where $F\left(\left\langle \frac{\partial \omega^{s(0)}}{\partial t} \right\rangle\right)$ is the Fourier transform of $\left\langle \frac{\partial \omega^{s(0)}}{\partial t} \right\rangle$. $\Phi(\omega)$ is a complex effective coefficient. From Eq. (A.74), it follows

$$\left\langle \frac{\partial \omega^{s(0)}}{\partial t} \right\rangle = F^{-1}(\Phi(\omega)) * \omega^{f(0)} \tag{A.75}$$

where $F^{-1}(\Phi(\omega))$ in the inverse Fourier transform of $\Phi(\omega)$ and $*$ is the convolution product.

Appendix B. Model B

Species transport: We now consider the order of magnitude of dimensionless numbers given in Table 2 for model B. The dimensionless description concerning the species transport takes the forms

$$(FS_l^s)^{-1}\ \rho^s \frac{\partial \omega^s}{\partial t} - \nabla \cdot (\rho^s D^s \nabla \omega^s) = 0 \qquad \text{in } \Omega^s, \tag{B.1}$$

$$\varepsilon^2\ \rho^f \frac{\partial \omega^f}{\partial t} + \varepsilon \rho^f \vec{v}^f \cdot \nabla \omega^f - \nabla \cdot (\rho^f D^f \nabla \omega^f) = 0 \qquad \text{in } \Omega^f, \tag{B.2}$$

$$\left((D_l)\rho^s D^s \nabla \omega^s - \rho^f D^f \nabla \omega^f\right) \cdot \mathbf{N} = \varepsilon^2 (\rho^f \omega^{f*} - \rho^s \omega^{s*}) \mathbf{w} \cdot \mathbf{N} \qquad \text{on } \Gamma, \tag{B.3}$$

$$\omega^{s*} = k\ \omega^{f*} \qquad \text{on } \Gamma. \tag{B.4}$$

Consider the case $D_l = O(1)$ and $FS_l^s = O(\varepsilon^{-2})$ (Fe-C alloy). Introduction of the asymptotic expansions (3.13) in Eqs. (B.1)-(B.4), yields at the lower order problem:

$$\nabla_y \cdot \left(\rho^s D^s \nabla_y \omega^{s(0)}\right) = 0 \qquad \text{in } \Omega^s, \tag{B.5}$$

$$\nabla_y \cdot \left(\rho^f D^f \nabla_y \omega^{f(0)}\right) = 0 \qquad \text{in } \Omega^f, \tag{B.6}$$

$$\left(\rho^s D^s \nabla_y \omega^{s(0)} - \rho^f D^f \nabla_y \omega^{f(0)}\right) \cdot \mathbf{N} = 0 \qquad \text{on } \Gamma, \tag{B.7}$$

$$\omega^{s*(0)} = k\ \omega^{f*(0)} \qquad \text{on } \Gamma. \tag{B.8}$$

where the unknowns $\omega^{s(0)}$ and $\omega^{f(0)}$ are $\mathbf{y}$-periodic. From Eqs. (B.5)-(B.8), we get

$$\begin{aligned} \omega^{f(0)} &= \omega^{f*(0)} = \omega^{f(0)}(\mathbf{x}, t), \\ \omega^{s(0)} &= \omega^{s*(0)} = \omega^{s(0)}(\mathbf{x}, t) = k\ \omega^{f(0)}(\mathbf{x}, t). \end{aligned} \tag{B.9}$$

At the first order, the solid and the fluid mass fraction are constant over the periodic cell (lever-rule type model). The second order problem to be solved

takes the form:

$$\nabla_y \cdot \left[\rho^s \; D^s \left(\nabla_y \omega^{s(1)} + \nabla_x \omega^{s(0)}\right)\right] = 0 \quad \text{in } \Omega^s \tag{B.10}$$

$$\nabla_y \cdot \left[\rho^f \; D^f \left(\nabla_y \omega^{f(1)} + \nabla_x \omega^{f(0)}\right)\right] = 0 \quad \text{in } \Omega^f, \tag{B.11}$$

$$\left[\rho^s D^s \left(\nabla_y \omega^{s(1)} + \nabla_x \omega^{s(0)}\right) - \rho^f D^f \left(\nabla_y \omega^{f(1)} + \nabla_x \omega^{f(0)}\right)\right] \cdot \mathbf{N} = 0 \quad \text{on } \Gamma, \tag{B.12}$$

$$\omega^{s*(1)} = k \; \omega^{f*(1)} \quad \text{on } \Gamma, \tag{B.13}$$

where the unknowns $\omega^{s(1)}$ and $\omega^{f(1)}$ are $\mathbf{y}$-periodic. The solutions of the set of Eqs. (B.10)-(B.13) appear as a linear function of the macroscopic solutal gradient of $\omega^{f(0)}$, modulo an arbitrary function,

$$\omega^{f(1)} = \boldsymbol{\beta}^f(\mathbf{y}, t) \cdot \nabla_x \omega^{f(0)} + \overline{\omega}^{f(1)}(\mathbf{x}, t), \tag{B.14}$$

$$\omega^{s(1)} = k \; \boldsymbol{\beta}^s(\mathbf{y}, t) \cdot \nabla_x \omega^{f(0)} + \overline{\omega}^{s(1)}(\mathbf{x}, t). \tag{B.15}$$

$\boldsymbol{\beta}^f(\mathbf{y}, t)$ and $\boldsymbol{\beta}^s(\mathbf{y}, t)$ are $\mathbf{y}$-periodic, average to zero, and are solutions of the following boundary-value problem:

$$\nabla_y \cdot [\rho^s D^s k \; (\nabla_y \boldsymbol{\beta}^s + \delta)] = 0 \quad \text{in } \Omega^s, \tag{B.16}$$

$$\nabla_y \cdot \left[\rho^f D^f \left(\nabla_y \boldsymbol{\beta}^f + \delta\right)\right] = 0 \quad \text{in } \Omega^f, \tag{B.17}$$

$$\rho^s D^s k \; (\nabla_y \boldsymbol{\beta}^s + \delta) \cdot \mathbf{N} = \rho^f D^f \left(\nabla_y \boldsymbol{\beta}^f + \delta\right) \cdot \mathbf{N} \quad \text{on } \Gamma. \tag{B.18}$$

$$\boldsymbol{\beta}^s = \boldsymbol{\beta}^f \quad \text{on } \Gamma, \tag{B.19}$$

The third order order problem to be solved is given by

$$\rho^s \frac{\partial \omega^{s(0)}}{\partial t} - \nabla_y \cdot \left[\rho^s D^s \left(\nabla_y \omega^{s(2)} + \nabla_x \omega^{s(1)}\right)\right] - \nabla_x \cdot \left[\rho^s D^s \left(\nabla_y \omega^{s(1)} + \nabla_x \omega^{s(0)}\right)\right] = 0 \quad \text{in } \Omega^s, \tag{B.20}$$

$$\text{(B.21)}\quad \rho^f \frac{\partial \omega^{f(0)}}{\partial t} + \rho^f \mathbf{v}^{f(0)} \cdot \left(\nabla_y \omega^{f(1)} + \nabla_x \omega^{f(0)}\right) - \nabla_y \cdot \left[\rho^f D^f \left(\nabla_y \omega^{f(2)} + \nabla_x \omega^{f(1)}\right)\right] - \nabla_x \cdot \left[\rho^f D^f \left(\nabla_y \omega^{f(1)} + \nabla_x \omega^{f(0)}\right)\right] = 0 \quad \text{in } \Omega^f,$$

$$\text{(B.22)}\quad \left[\rho^s D^s \left(\nabla_y \omega^{s(2)} + \nabla_x \omega^{s(1)}\right) - \rho^f D^f \left(\nabla_y \omega^{f(2)} + \nabla_x \omega^{f(1)}\right)\right] \cdot \mathbf{N} = (\rho^f \omega^{f*(0)} - \rho^s \omega^{s*(0)}) \mathbf{w}^{(0)} \cdot \mathbf{N} \quad \text{on } \Gamma.$$

Integrating (B.20) over Ω^s and (B.21) over Ω^f, using the divergence theorem, the condition of periodicity on $\partial\Omega \cap \partial\Omega^f$ and $\partial\Omega \cap \partial\Omega^s$, and then taking into account the boundary condition (B.22), leads to the following first order macroscopic description

$$\text{(B.23)}\quad \rho^s \frac{\partial \left(f^s k\, \omega^{f(0)}\right)}{\partial t} + \rho^f \frac{\partial \left((1 - f^s)\omega^{f(0)}\right)}{\partial t} + \rho^f \mathbf{V}_S^{\text{eff}} \cdot \nabla_x \omega^{f(0)} - \nabla_x \cdot \left((\rho \mathbf{D}^\star) \nabla_x \omega^{f(0)}\right) = 0.$$

with $\omega^{s(0)}(\mathbf{x}, t) = k\, \omega^{f(0)}(\mathbf{x}, t)$. The effective diffusion tensor $(\rho \mathbf{D}^\star)$ of the mixture and the effective fluid velocity $\mathbf{V}_S^{\text{eff}}$ are defined as follows:

$$\text{(B.24)}\quad \mathbf{V}_S^{\text{eff}} = \frac{1}{\Omega} \int_{\Omega^f} \mathbf{v}^{f(0)} \left(\nabla_y \boldsymbol{\beta}^f + \boldsymbol{\delta}\right) d\Omega,$$

$$\text{(B.25)}\quad (\rho \mathbf{D}^\star) = \frac{1}{\Omega} \int_{\Omega^f} \rho^f D^f \left(\nabla_y \boldsymbol{\beta}^f + \boldsymbol{\delta}\right) d\Omega + \frac{1}{\Omega} \int_{\Omega^s} \rho^s D^s \left(\nabla_y \boldsymbol{\beta}^s + k\, \boldsymbol{\delta}\right) d\Omega.$$

Appendix C. Model C

Species transport: We now consider the order of magnitude of dimensionless numbers given in Table 2, model C. The set of dimensionless equations takes the form:

$$\text{(C.1)}\quad (FS_l^s)^{-1}\, \rho^s \frac{\partial \omega^s}{\partial t} - \nabla \cdot (\rho^s D^s \nabla \omega^s) = 0 \quad \text{in } \Omega^s,$$

$$\text{(C.2)}\quad \varepsilon^2\, \rho^f \frac{\partial \omega^f}{\partial t} + \rho^f \mathbf{v}^f \cdot \nabla \omega^f - \nabla \cdot (\rho^f D^f \nabla \omega^f) = 0 \quad \text{in } \Omega^f,$$

$$\text{(C.3)}\quad \left((D_l)\, \rho^s D^s \nabla \omega^s - \rho^f D^f \nabla \omega^f\right) \cdot \mathbf{N} = \varepsilon^2 (\rho^f \omega^{f*} - \rho^s \omega^{s*}) \mathbf{w} \cdot \mathbf{N} \quad \text{on } \Gamma,$$

$$\text{(C.4)}\quad \omega^{s*} = k\, \omega^{f*} \quad \text{on } \Gamma.$$

Consider the case $D_l = O(1)$ and $FS_l^s = O(\varepsilon^{-2})$ (Fe-C alloy). Introducing the asymptotic expansions (3.13) in Eqs. (C.1)-(C.4), the first order problem to be solved takes the form

$$\nabla_y \cdot \left(\rho^s D^s \nabla_y \omega^{s(0)}\right) = 0 \qquad \text{in } \Omega^s, \tag{C.5}$$

$$\rho^f \mathbf{v}^{f(0)} \cdot \nabla_y \omega^{f(0)} - \nabla_y \cdot \left(\rho^f D^f \nabla_y \omega^{f(0)}\right) = 0 \qquad \text{in } \Omega^f, \tag{C.6}$$

$$\left(\rho^s D^s \nabla_y \omega^{s(0)} - \rho^f D^f \nabla_y \omega^{f(0)}\right) \cdot \mathbf{N} = 0 \qquad \text{on } \Gamma, \tag{C.7}$$

$$\omega^{s*(0)} = k\ \omega^{f*(0)} \qquad \text{on } \Gamma, \tag{C.8}$$

where the unknowns $\omega^{s(0)}$ and $\omega^{f(0)}$ are $\mathbf{y}$-periodic. The fluid $\mathbf{v}^{f(0)}$ velocity is given by Eq. (A.19). From Eqs. (C.5)-(C.8), we get

$$\omega^{f(0)} = \omega^{f*(0)} = \omega^{f(0)}(\mathbf{x}, t), \qquad \omega^{s(0)} = \omega^{s*(0)} = \omega^{s(0)}(\mathbf{x}, t). \tag{C.9}$$

At the lower order, the fluid and the solid mass fractions are constant over the cell. We consider now the next order,

$$\nabla_y \cdot \left[\rho^s D^s \left(\nabla_y \omega^{s(1)} + \nabla_x \omega^{s(0)}\right)\right] = 0 \quad \text{in } \Omega^s \tag{C.10}$$

$$\rho^f \mathbf{v}^{f(0)} \cdot \left(\nabla_y \omega^{f(1)} + \nabla_x \omega^{f(0)}\right) - \nabla_y \cdot \left[\rho^f D^f \left(\nabla_y \omega^{f(1)} + \nabla_x \omega^{f(0)}\right)\right] = 0 \quad \text{in } \Omega^f, \tag{C.11}$$

$$\left[\rho^s D^s \left(\nabla_y \omega^{s(1)} + \nabla_x \omega^{s(0)}\right) - \rho^f D^f \left(\nabla_y \omega^{f(1)} + \nabla_x \omega^{f(0)}\right)\right] \cdot \mathbf{N} = 0 \quad \text{on } \Gamma, \tag{C.12}$$

$$\omega^{s*(1)} = k\ \omega^{f*(1)} \quad \text{on } \Gamma, \tag{C.13}$$

where the unknowns $\omega^{f(1)}$ and $\omega^{s(1)}$ are $\mathbf{y}$-periodic. Integrating (C.10) over Ω^s and (C.11) over Ω^f, the condition of periodicity, the boundary condition (C.12) and the fluid incompressibility (A.16) we obtain the following first order macroscopic description,

$$\rho^f \langle \mathbf{v}^{f(0)} \rangle \cdot \nabla_x \omega^{f(0)} = 0. \tag{C.14}$$

From Eqs.(C.10)-(C.11), we get

$$\omega^{f(1)} = \boldsymbol{\varphi}^f(\mathbf{y}, \nabla_x p^{f(0)}, t) \cdot \nabla_x \omega^{f(0)} + \overline{\omega}^{f(1)}(\mathbf{x}, t), \tag{C.15}$$

$$\omega^{s(1)} = k\ \boldsymbol{\varphi}^s(\mathbf{y}, \nabla_x p^{f(0)}, t) \cdot \nabla_x \omega^{f(0)} + \overline{\omega}^{s(1)}(\mathbf{x}, t). \tag{C.16}$$

$\boldsymbol{\varphi}^f$ and $\boldsymbol{\varphi}^s$ depend on the macroscopic pressure gradient $\nabla_x p^{f(0)}$. They are $\mathbf{y}$-periodic, average zero and are solutions of the following boundary-value problem:

$$\nabla_y \cdot [\rho^s D^s k\ (\nabla_y \boldsymbol{\varphi}^s + \delta)] = 0 \qquad \text{in } \Omega^s, \tag{C.17}$$

$$\mathbf{v}^{f(0)} \cdot \left(\nabla_y \boldsymbol{\varphi}^f + \delta\right) - \nabla_y \cdot \left[\rho^f D^f \left(\nabla_y \boldsymbol{\varphi}^f + \delta\right)\right] = 0 \qquad \text{in } \Omega^f, \tag{C.18}$$

$$\left[\rho^s D^s k\,(\nabla_y \boldsymbol{\varphi}^s + \delta) - \rho^f D^f \left(\nabla_y \boldsymbol{\varphi}^f + \delta\right)\right] \cdot \mathbf{N} = 0 \qquad \text{on } \Gamma, \tag{C.19}$$

$$\boldsymbol{\varphi}^s = \boldsymbol{\varphi}^f \qquad \text{on } \Gamma. \tag{C.20}$$

The next problem to be solved takes the form

$$\rho^s \frac{\partial \omega^{s(0)}}{\partial t} - \nabla_y \cdot \left[\rho^s D^s \left(\nabla_y \omega^{s(2)} + \nabla_x \omega^{s(1)}\right)\right] - \nabla_x \cdot \left[\rho^s D^s \left(\nabla_y \omega^{s(1)} + \nabla_x \omega^{s(0)}\right)\right] = 0 \quad \text{in } \Omega^s, \tag{C.21}$$

$$\rho^f \frac{\partial \omega^{f(0)}}{\partial t} + \rho^f \mathbf{v}^{f(0)} \cdot \left(\nabla_y \omega^{f(2)} + \nabla_x \omega^{f(1)}\right) + \rho^f \mathbf{v}^{f(1)} \cdot \left(\nabla_y \omega^{f(1)} + \nabla_x \omega^{f(0)}\right) - \nabla_y \cdot \left[\rho^f D^f \left(\nabla_y \omega^{f(2)} + \nabla_x \omega^{f(1)}\right)\right] - \nabla_x \cdot \left[\rho^f D^f \left(\nabla_y \omega^{f(1)} + \nabla_x \omega^{f(0)}\right)\right] = 0 \quad \text{in } \Omega^f, \tag{C.22}$$

$$\left[\rho^s D^s \left(\nabla_y \omega^{s(1)} + \nabla_x \omega^{s(0)}\right) - \rho^f D^f \left(\nabla_y \omega^{f(2)} + \nabla_x \omega^{f(1)}\right)\right] \cdot \mathbf{N} = (\rho^f \omega^{f*(0)} - \rho^s \omega^{s*(0)}) \mathbf{w}^{(0)} \cdot \mathbf{N} \quad \text{on } \Gamma. \tag{C.23}$$

Integrating (C.21) over Ω^s and (C.22) over Ω^f, then using the divergence theorem, the condition of periodicity and then taking into account the boundary condition (C.23), we obtain the first order correction to the macroscopic description (C.14),

$$\rho^s \frac{\partial \left(f^s k\ \omega^{f(0)}\right)}{\partial t} + \rho^f \frac{\partial \left((1 - f^s)\omega^{f(0)}\right)}{\partial t} + \rho^f \langle \mathbf{v}^{f(0)} \rangle \cdot \nabla_x \overline{\omega}^{f(1)} + \rho^f \langle \mathbf{v}^{f(1)} \rangle \cdot \nabla_x \omega^{f(0)} - \nabla_x \cdot \left((\rho \mathbf{D}^{\star\star}) \nabla_x \omega^{f(0)}\right) = 0. \tag{C.24}$$

$(\rho\mathbf{D}^{\star\star})$ is the effective dispersion tensor of the mixture,

$$(\text{C.25}) \quad (\rho\mathbf{D}^{\star\star}) = \frac{1}{\Omega}\int_{\Omega^f}\left(\rho^f D^f\left(\nabla_y\boldsymbol{\varphi}^f + \boldsymbol{\delta}\right) + \rho^f k\nabla_x p^{f(0)}\cdot\boldsymbol{\varphi}^f\right)\,d\Omega$$

$$+\frac{1}{\Omega}\int_{\Omega^s}\rho^s D^s k\;\left(\nabla_y\boldsymbol{\varphi}^s + \boldsymbol{\delta}\right)d\Omega.$$

By adding, member to member, Eqs. (C.14) and (C.24) multiplied by ε, we get the second order macroscopic equation governing the average fluid mass fraction $\langle\omega^f\rangle = \langle\omega^{f(0)}\rangle + \varepsilon\langle\omega^{f(1)}\rangle$,

$$(\text{C.26}) \quad \varepsilon\,\rho^s\frac{\partial\left(f^s k\,\langle\omega^f\rangle\right)}{\partial t} + \varepsilon\,\rho^f\frac{\partial\left((1-f^s)\langle\omega^f\rangle\right)}{\partial t} + \rho^f\langle\mathbf{v}^f\rangle\cdot\nabla_x\langle\omega^f\rangle$$

$$-\varepsilon\,\nabla_x\cdot\left((\rho\mathbf{D}^{\star\star})\nabla_x\langle\omega^f\rangle\right) = 0$$

with $\langle\omega^s\rangle = k\,\langle\omega^f\rangle$.

References

1. J.-L. AURIAULT, *Heterogeneous medium is an equivalent description possible?* Int. J. Engng. Sci., **29**, 785–795, 1991.
2. J.-L. AURIAULT and P.M. ADLER, *Taylor dispersion in porous media. Analysis by multiple sacle expansions,* Advances in Water Resources., **18**, 217–226, 1995.
3. J.-L. AURIAULT, *Non saturated deformable porous media: Quasistatics,* Transport in Porous Media, **2**, 45–64, 1987.
4. C. BECKERMANN and R. VISKANTA, *Natural convection solid/liquid phase change in porous media,* Int. J. Heat Mass Transfer, **31**, 35–46, 1988.
5. W. D. BENNON and F. P. INCROPERA, *A continuum model fo momentum, heat and species transport in binary solid-liquid phase change systems. - I. Model formulation,* Int. J. Heat. Mass. Transfer, **30**, 2161–2170, 1987.
6. A. BENSOUSSAN, J.L. LIONS, and G. PAPANICOLAOU, *Asymptotic analysis for periodic structures,* North-Holland, Amsterdam 1978.
7. G. W. BERGANTZ, *Conjugate solidification and melting in multicomponent open and closed system,* Int. J. Heat Mass Transfer, **35**, 533–543, 1992.
8. A. BOUDDOUR, J.-L. AURIAULT, M. MHAMDI-ALAOUI, and J.-F. BLOCH, *Heat and mass transfer in wet porous media in presence of evaporation-condensation,* Int. J. Heat Mass Transfer, **41**, 2263–2277, 1998.
9. M. C. FLEMINGS, *Solidification Processing,* McGraw Hill, New-York 1974.
10. S. GANESAN and D. R. POIRIER, *Conservation of mass and momentum for the flow of interdendritic liquid during solidification,* Metall. Trans. B, **21B**, 173–180, 1990.

11. C. GEINDREAU and J.-L. AURIAULT, *Investigation of the mechanical behaviour of alloys in the semi-solid state by homogenization,* Mech. Mater., **31**, 535–551, 1999.

12. R. HILL, D. LOPER, and P. ROBERTS, *A thermodynamically consistent model of a mushy zone,* Q. J. Mech. Appl. Math., **36**, 505–539, 1983.

13. M. D. JACKSON and M. J. CHEADLE, *A continuum model for the transport of heat, mass and momentum in deformable multicomponent mush, undergoing solid-liquid phase change,* Int. J. Heat Mass Transfer, **41**, 1035–1048, 1998.

14. I. KECECIOGLU and B. RUBINSKY, *A continuum model for propagation of discrete phase-change fronts in porous media in the presence of coupled heat flow, fluid flow and species transport processes,* Int. J. Heat Mass Transfer, **32**, 1111–1130, 1989.

15. M. J. M. KRANE and F. P. INCROPERA, *Analysis of the effect of shrinkage on macrosegregation in alloy solidification,* Metall. and Mater. Trans. A, **26A**, 2329–2388, 1995.

16. S. LE CORRE, D. CAILLERIE, D. FAVIER and L. ORGEAS, *Overall behaviour of a truss of fibres linked by viscous joints,* [in:] FRC 2000 - Composites for the Millenium, A. G. GIBSON [Ed.] Woodhead Publishing Limited vol:1, 303-310, 2000.

17. C. C. MEI and J. L. AURIAULT, *The effect of inertia on flow through porous medium,* J. Fluid. Mech., **222**, 647–663, 1991.

18. I. NASTAC and D. M. STEFANESCU, *Macrotransport solidification kinetics modeling of equiaxed dendritic growth : Part i. Model development and discussion,* Metall. and Mater. Trans. A, **27A**, 4061–4074, 1996.

19. J. NI and C. BECKERMANN, *A volume averaged two-phase model for transport phenomena during solidification,* Metall. Trans. B, **22B**, 349–361, 1991.

20. P. J. PRESCOTT and F. P. INCROPERA, *Convection heat and mass transfer in alloy solidification,* Advances in Heat Transfer, **28**, 231–337, 1996.

21. P. J. PRESCOTT, F. P. INCROPERA, and W. D. BENNON, *Modeling of dendritic solidification systems : Reassessment of the continuum momentum equation,* Int. J. Heat Mass Transfer, **34**, 2351–2359, 1991.

22. M. RAPPAZ and V. VOLLER, *Modeling of micro-macrosegregation in solidification processes,* Metall. Trans. A, **21A**, 749–753, 1990.

23. S. RIDDER, S. KOU, and R. MEHRABIAN, *Effect of fluid flow on macrosegregation in axisymmetric lingots,* Met. Trans. B, **12B**, 435–447, 1981.

24. E. SANCHEZ-PALENCIA. *Non-homogeneous media and vibration theory,* [in:] Lectures Notes in Physics, Vol. 127, Springer-Verlag, Berlin 1980

25. M. C. SCHNEIDER and C. BECKERMANN, *Formation of macrosegregation by multicomponent thermosolutal convection during the solidification of steel,* Metal. Mater. Trans. A, **26A**, 2373–2388, 1995.

26. M. C. SCHNEIDER and C. BECKERMANN, *A numerical study of the combined effects of microsegregation, mushy zone permeability and flow, caused by volume contraction and thermosolutal convection, on macrosegregation and eutectic formation in binary alloy solidification,* Int. J. Heat Mass Transfer, **38**, 3455–3473, 1995.

27. E. SKJETNE and J.-L. AURIAULT, *High-velocity laminar and turbulent flow in porous media,* Transport in Porous Media, **36**, 131–147, 1999.

28. J. SZEKELY and A. JASSAL, *An experimental and analytical study of the solidification of a binary dendritic system,* Metal. Trans. B, **9B**, 389–398, 1978.

29. R. VISKANTA and C. BECKERMANN, *Mathematical modeling of solidification,* Proc. symp. on interdisciplinary issues in materials processing and manufacturing, Boston 1987.

30. V. R. VOLLER, A. D. BRENT, and C. PRAKASH, *The modelling of heat, mass and solute transport in solidification systems,* Int. J. Heat Mass Transfer, **32**, 1719–1731, 1989.

31. M. WORSTER, *Natural convection in a mushy layer,* J. Fluid. Mech., **224**, 335–359, 1991.

32. R. WRIGHT, *Core melt progression : Status of current understanding and principal uncertainties,* U.K. J. ROGERS [Ed.] Heat and Mass Transfer in Severe Nuclear Reactor Accidents, Begell House, New York, Wallingford 1996.

Received March 20, 2001; revised version June 6, 2001.

Arch. Mech., **53**, 4-5, pp. 421–437, Warszawa 2001

The dispacement discontinuity technique in fracture mechanics: the subsurface crack problem

S. K. KOURKOULIS[1] and G. E. EXADAKTYLOS[2]

[1] *National Technical University of Athens,*
Department of Mechanics,
Zografou Campus, Theocaris Building,
157 73 Zografou, Athens, Greece.

[2] *Technical University of Crete,*
Department of Mineral Resources Engineering
731 00 Chania, Crete, Greece.

THE DISPLACEMENT DISCONTINUITY technique is employed for the determination of the critical conditions causing propagation of a preexisting finite fracture that lies close to the free boundary of a semi-infinite medium. The technique is applied by using a suitably adapted commercial indirect boundary element code, permitting the determination of the displace-ment, strain and stress fields in multiply-connected elastic bodies. The critical conditions are then determined by employing a suitable failure criterion. The results of the numerical analysis are compared with the respective ones obtained from a series of experiments with pre-cracked specimens simulating the semi-infinite medium. The agreement is proved to be satisfactory.

1. Introduction

ALTHOUGH FRACTURE MECHANICS is accepted nowadays as one of the most reliable tools for the prediction of failure conditions of engineering structures containing defects, and many problems of practical interest related to the influence of crack-type defects on the strength and structural integrity of structures have been solved, a number of important problems related to cracked bodies of finite dimensions remain yet unanswered. The main reason is the fact that the analytical determination of the strain and stress fields in case of finite or semi-infinite cracked bodies is very difficult, preventing the application of fracture mechanics criteria for the prediction of the conditions of catastrophic crack propagation. In such cases, uncertainties in fracture mechanics analyses appear in the determination of fracture toughness, stress and strain fields, stress intensity factors etc. [1]. It seems that for these problems, the numerical methods and

techniques constitute a unique means for an, at least approximate, solution of the problem.

Such a problem that reappeared recently in the limelight and attracted the interest of engineers due to its broad field of applications in Structural- as well as in Geotechnical- and Earthquake Engineering, is that of a slightly inclined, finite subsurface crack in a semi-infinite medium. This is because strong indications exist that the relative configuration simulates in a satisfactory manner the behaviour of shallow geological faults under the influence of seismic loading, and the critical conditions leading to catastrophic crack propa-gation could provide useful information on the conditions causing activation of such faults.

It is clear that the exact full-field solution of the problem is very complicated even for a purely elastic material, due to the interaction of the crack with the free boundary of the medium. For this reason, the main qualitative features of the problem are explored here numerically, by performing plane-stress displacement discontinuity calculations. The method adopted is the Displacement Discontinuity Technique introduced originally by Crouch [2]. The technique is based on a solution that expresses the displacements and stresses at a point of the loaded cracked elastic body due to a constant displacement discontinuity over a line segment within an elastic body. The constant displacement discontinuity elements have the advantage of simplicity and are widely used for analyzing various engineering problems.

The efficiency of the technique in treating the crack problems was verified in the present work, by employing either already known closed-form solutions (cracks in infinite media [3]), or well established numerical analyses (single edge-notched specimens of finite dimensions [4]). The criterion adopted for the prediction of the critical conditions (load causing crack initiation and initial angle of crack propagation) is the T-criterion of failure [5]. The agreement between the existing results and those of the present analysis was very satisfactory, supporting the decision to use the technique for the solution of the finite subsurface crack within a semi-infinite medium.

However, and in order to verify further the results of this analysis, series of experiments were executed using specimens of suitable configuration that simulated the semi-infinite medium with a sub-surface crack. Specific configurations were selected concerning the crack inclination, in order to draw conclusions useful for the geotechnical community. As it will be seen, the experimental results for both critical quantities (load and angle) are very close to the results obtained from the numerical analysis.

2. Numerical analysis

The problem considered is demonstrated in Fig. 1: A stationary crack, AB, of length 2a is located close to the free boundary of a semi-infinite plane elastic medium. The crack is inclined with respect to the free boundary by an angle β and its mid-point is located at a distance y_0 from the boundary. The system is subjected to a uniformly applied remote tensile load P parallel to the free boundary. According to the Displacement Discontinuity Technique, the natural crack with parallel lips is considered as a linear mathematical discontinuity and the solution of the problem of a cracked semi-infinite body is obtained on the basis of the corresponding one for an infinite cracked body.

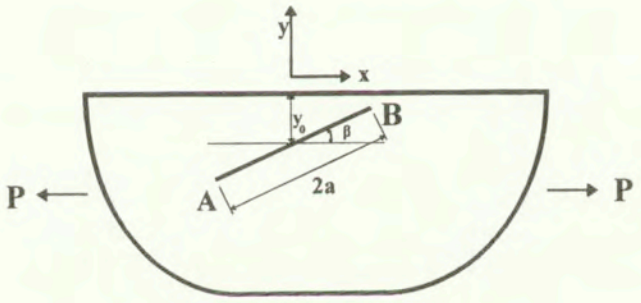

FIG. 1. Configuration of the problem.

Consider first a crack within an infinite homogeneous medium, located, for simplicity, along the y=0 line at -a⩽x⩽a (for inclined cracks, a simple coordinates transformation is performed). The crack is divided into N elementary segments and the displacements due to each segment are calculated at any point of the body, so that the general solution of the static problem is obtained a the sum of the respective elementary displacements. Practically the technique is applied in three discrete steps: (i) The coordinates of all boundary elements are defined and the respective boundary conditions are prescribed. (ii) The boundary influence coefficients are calculated and the algebraic system of equations is formulated and solved. (iii) The values of the unknown displacements and stresses are calculated in each boundary element and the analysis is extended to cover any point of the studied body.

The displacement caused by each elementary segment is written as:

$$D_i = u_i(x_i, 0_-) - u_i(x_i, 0_+), \quad \text{for } y = 0, \ i = x, y. \tag{2.1}$$

Crouch [2, 6] proved that in such a case, the displacements are given by the formula:

$$
\begin{aligned}
u_x &= D_x[2(1-\nu) f_{,y} - y f_{,xx}] + D_y[-(1-2\nu) f_{,x} - y f_{,xy}], \\
u_y &= D_x[(1-2\nu) f_{,x} - y f_{,xy}] + D_y[2(1-\nu) f_{,y} - y f_{,yy}],
\end{aligned} \tag{2.2}
$$

while the stress field is described by the following set of equations:

$$
\begin{aligned}
\sigma_{xx} &= 2GD_x(2f_{,xy} + y f_{,xyy}) + 2GD_y(f_{,yy} + y f_{,xyy}), \\
\sigma_{yy} &= 2GD_x(-y f_{,xy}) + 2GD_y(f_{,yy} - y f_{,xyy}), \\
\sigma_{xy} &= 2GD_x(2f_{,yy} + y f_{,xyy}) + 2GD_y(-y f_{,xyy}),
\end{aligned} \tag{2.3}
$$

where G and ν are the shear modulus and Poisson's ratio of the material, respectively, and the indices after the comma denote partial differentiation. Concerning the factor $f(x,y)$, it holds:

$$
\begin{aligned}
f(x,y) = \frac{-1}{4\pi(1-\nu)} \Bigg[& y\left(\arctan\frac{y}{x-a} - \arctan\frac{y}{x+a}\right) \\
& -(x-a)\ell n\sqrt{(x-a)^2+y^2} + (x+a)\ell n\sqrt{(x+a)^2+y^2}\Bigg],
\end{aligned} \tag{2.4}
$$

By superposition, the stress at the mid-point of the i-th crack element, due to displacement discontinuities at all N-elements, will be equal to:

$$
\sigma_{yy}(x^i, 0) = \sigma^i_{yy} = \sum_{j=1}^{N} \overset{ij}{A}\, \overset{j}{D}_y, \tag{2.5}
$$

where the matrix is the respective coefficient of influence and is equal to

$$
\overset{ij}{A} = \frac{-G}{\pi(1-\nu)} \frac{\overset{j}{a}}{\left(\overset{i}{x} - \overset{j}{x}\right)^2 - \overset{j}{\alpha}^2}. \tag{2.6}
$$

The coefficient $\overset{ij}{A}$ for example, gives the actual normal stress at the midpoint of the i-th segment due to a constant unit normal displacement discontinuity applied to the j-th segment ($\overset{j}{D}_y = 1$). For the case of uniformly pressurized straight crack, the stress is specified by the following system of N simultaneous linear equations in N unknowns:

$$\overset{i}{\sigma}_{yy} = -p = \sum_{j=1}^{N} \overset{ij}{A} \overset{j}{D}_y, \quad i = 1 \quad \text{to} \quad N. \tag{2.7}$$

These equations can be solved for $\overset{i}{D}_y$, i=1 to N, by standard methods of numerical analysis.

The solution for the case of an infinite cracked body being known, the problem of the semi-infinite medium with a subsurface crack can be solved by treating the surface-line of the half plane like any other boundary line and dividing it into elements following the usual process. The analytical solution to this problem can be obtained by using a procedure known as the method of images which is based on the principle of superposition. According to this method, the solution to the problem is obtained in two stages:

• An infinite plate is considered containing two symmetric cracks, as it is shown in Fig. 2. The first one is located on the negative half-plane and corresponds to the real crack, the coordinates of its mid-point being (x_0, y_0), while the second one is located on the positive half-plane and is symmetric to the first one with respect to the x-axis, i.e. the free boundary. Due to the symmetry of the configuration, the shear stresses σ_{xy} along the x-axis are zero.

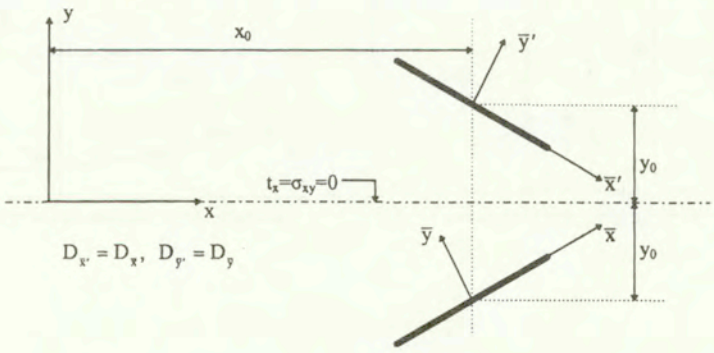

FIG. 2. Schematic representation of the method of images.

• The normal stress σ_{yy} along the x-axis is cancelled out by superimposing an additional assumption related to the elastic half-plane with prescribed tractions, t_x=0, $t_y \neq 0$. Accordingly, and denoting the displacements and stresses due to the actual displacement discontinuity u_i^A and σ_{ij}^A those due to its image u_i^I and σ_{ij}^I, and the ones resulting from the supplementary retraction solution $u\,i^S$ and

σ_{ij}^S, the complete solution for the half-plane $y \leqslant 0$ becomes:

$$u_i = u_i^A + u_i^I + u_i^S,$$
$$\sigma_{ij} = \sigma_{ij}^A + \sigma_{ij}^I + \sigma_{ij}^S. \tag{2.8}$$

The results of the numerical analysis concerning the strain distribution have been plotted in Fig. 3(a,b) for an external load level P equal to 80% of the final fracture load. The configuration studied corresponds to a crack of length equal to 2a=20 mm, inclined by an angle β=10^o with respect to the free boundary, the mid-point of which is located at a distance $|y_0|$=20 mm from the free surface (Fig. 1). The specific configuration is chosen since most geological faults, either normal or the thrust ones, are relatively slightly inclined with respect to the Earth's surface. Since from the point of view of geotechnical engineering, the interest is focussed mainly on the variation of strains along the directions parallel

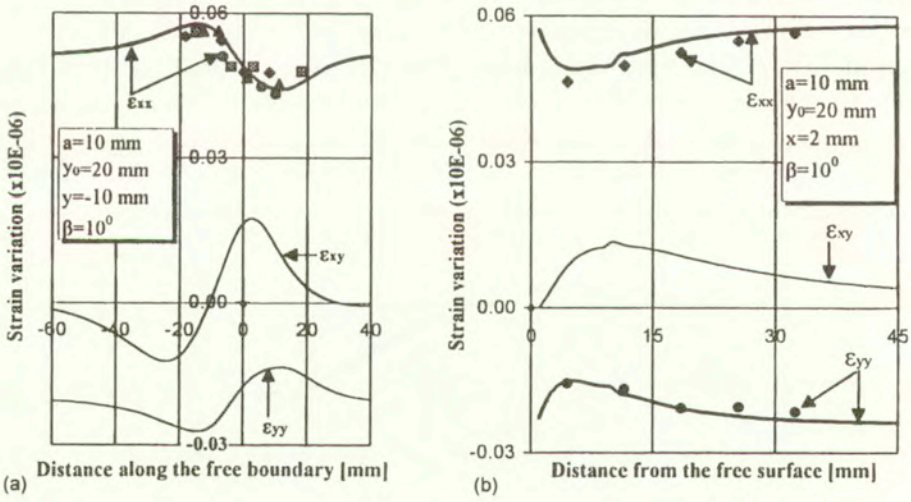

FIG. 3. Strain distribution along a line.

and perpendicular to the free surface, the familiar in Fracture Mechanics polar plot of the strain distribution around the crack tip is avoided in the present work. Thus, all three strain components are plotted in Fig. 3a along a line parallel to the free surface of the medium at a distance y=-10 mm from it, while in Fig. 3b the respective quantities are plotted along a line perpendicular to the free surface at a distance x=2mm from the tip nearest to the boundary (tip B in Fig. 2). In the same figures, the corresponding experimental results have been plotted. Although analytical discussion of the experimental results follows in

the next section, it can be said that the agreement between the numerical and experimental results is satisfactory.

It can be seen from Fig. 3a that the disturbance of the strain field due to the free boundary is of dominant importance, since the symmetry of distribution for all three strain components disappears. On the other hand, it is observed that the strain components show clearly the extreme values (maximum or minimum) as the crack tips are approached, but it is to be emphasized that the points where the maximum values are reached are not located exactly above the crack tips. A similar conclusion is drawn from Fig. 3b, especially for the shear strain ε_{xy}, the maximum value of which does not correspond to the point straight forward along the axis of the crack.

In the next Fig. 4, the polar distribution of the stress components according to the numerical analysis is plotted for the same configuration ($2a$=20 mm and β=10^0) and for both crack tips: thick lines correspond to the tip A while the thinner ones to the tip B

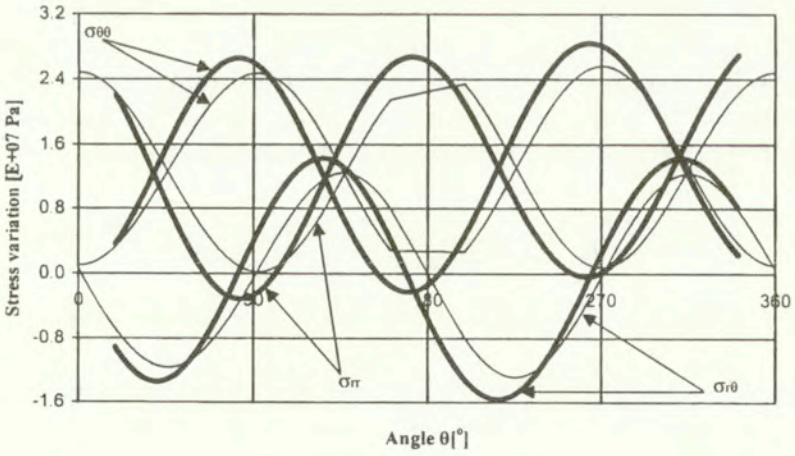

FIG. 4. Polar distribution of the stress components around tip A (thick lines) and tip B (thin lines).

It is again obvious that the two sets of lines are not identical as it should be expected in case of an infinite medium, exactly due to the presence of the free boundary. From this figure one could obtain directly the expected crack initiation angle according to the maximum tangential stress criterion (σ_θ-criterion) as $\theta_{A,\sigma}$=86^o and $\theta_{B,\sigma}$=93^o, which, as it will be seen in next section, are slightly higher than the respective experimental values $\theta_{A,\text{exp}}$=81^o and $\theta_{B,\text{exp}}$=87^o.

3. The failure criterion and the critical conditions

The stress and strain fields having been calculated, a failure criterion is required to predict the onset of crack propagation and the initial propagation angle. A number of criteria have been proposed towards this direction during the past decades. For the purposes of the present study the T-criterion of failure was used [5], mainly due to its clear physical meaning and the fact that its predictions for the critical load and for the initiation angle have been found to be in a very good agreement with the experimental evidence, both for centrally cracked and single-edge notched specimens [7]. For comparison reasons, the σ_θ-criterion (maximum tangential stress criterion [8]) was also used together with the T-criterion, in some cases.

The T-criterion of failure is based on the following assumptions: (i) The crack propagates towards the direction θ_o of the maximum value of the density of the elastic dilatational strain energy T_V. The propagation starts when this maximum value exceeds a critical limit $T_{V,0}$. (ii) The polar distribution of T_V around the crack-tip is calculated along the elastic-plastic boundary, where the distortional strain energy density, T_D, is constant, equal to a critical value $T_{D,0}$ and finally (iii) Both $T_{V,0}$ and $T_{D,0}$ are considered as material constants determined experimentally, according to the procedure described in [9].

Mathematically speaking, and for plane stress conditions, like the ones prevailing in the present study, the criterion is expressed as follows:

$$T_V\left(r\left(\vartheta\right),\vartheta\right)\big|_{\vartheta=\vartheta_o} \geqslant T_{V,0} = \text{const.} \tag{3.1}$$

$$\left.\frac{\partial T_V\left(r\left(\vartheta\right),\vartheta\right)}{\partial\vartheta}\right|_{\vartheta=\vartheta_o} = 0, \quad \left.\frac{\partial^2 T_V\left(r\left(\vartheta\right),\vartheta\right)}{\partial\vartheta^2}\right|_{\vartheta=\vartheta_o} \leqslant 0, \tag{3.2}$$

$$T_D = \frac{1+\nu}{3E}\sigma_\Delta^2 = T_{D,0} = \text{const.} \tag{3.3}$$

The polar variation of the quantity controlling the crack initiation according to the T-criterion, namely the elastic dilatational strain energy density, T_v is plotted in Fig. 5, for both tips A and B of the crack, for β=10^0, y_0=20 mm and $2a$=20 mm. The main characteristic is that the distortion of the shape of the distribution, inevitably caused by the inclination of the crack, is balanced by the influence of the free boundary. Since this influence is more pronounced at the tip B, the distribution of the elastic dilatational strain energy density at this tip is almost circular. Such a balance is not possible for tip A, since its distance from

the free surface is greater. From the same figure it is also concluded that the expected angles of crack initiation according to the T-criterion, are $\theta_{A,T}=83^o$ and $\theta_{B,T}=89^o$, for tips A and B respectively, which are close enough to the experimental results.

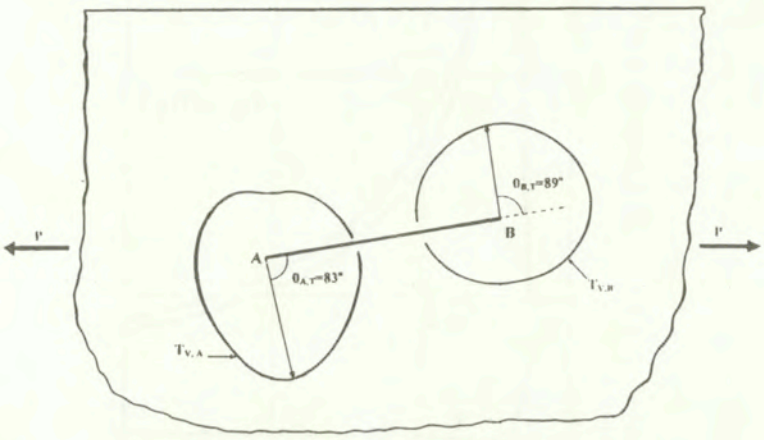

FIG. 5. Polar distribution of the elastic dilatational strain energy density around the two crack tips.

Concerning the critical load, what is most important is the detection of the configuration for which the crack is either most eager or most reluctant to propagate. For this purpose, the variation of the square root of the elastic dilatational strain energy density, reduced over the respective quantity for an infinite medium, is plotted in Fig. 6, versus the reduced distance of the mid-point of the crack, y_0, from the free boundary, since this quantity is directly related to the critical fracture load. The configuration corresponds again to $\beta=10^0$, $2a = 20$ mm while the position of the mid-point of the crack varies from $y_c = a\sin\beta$, corresponding to a single-edge notched configuration, to $y_c = 12a$, corresponding to a configuration which starts resembling the infinite medium. It is concluded from this figure that the critical condition is first fulfilled at the tip A, i.e. the one most remote from the free boundary. This tendency is decreased as the crack moves towards the interior of the medium, since the influence of the boundary becomes weaker and the displacement distribution around the two tips becomes symmetric.

However, what is most interesting, and perhaps astonishing, from the analysis of the variation of the square root of the elastic dilatational strain energy density versus the position of the crack, is that this function is not a monotonic one. Specific configurations exist for which the crack appears to be most reluctant

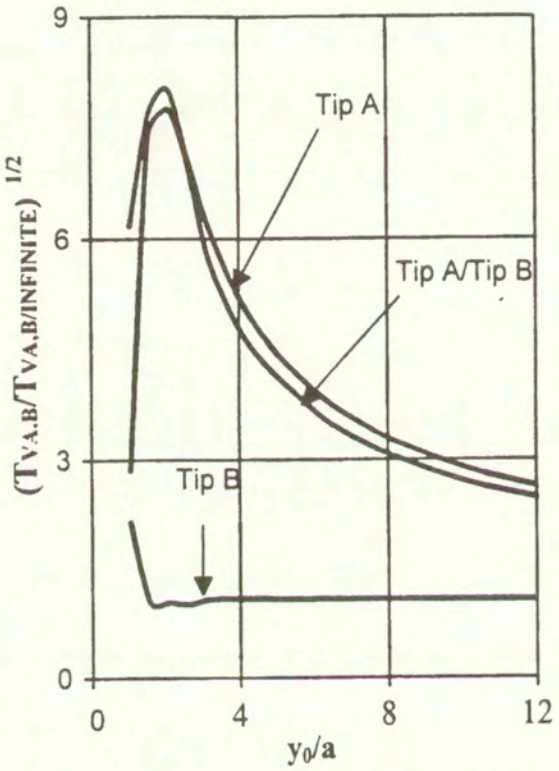

FIG. 6. Variation of the reduced elastic dilatational strain energy density around the two crack tips versus the position of the crack.

to propagate. For example, for the case studied in Fig. 6, the relative function shows a clear maximum for cracks located at a distance $y_c \cong 2a$ from the free boundary. It means that such a geometry is much more stable compared to both the centrally cracked finite or infinite medium and the single-edge notched geometry. Such a conclusion, perhaps contradicting the common sense, was the main motive for an extended experimental analysis of the phenomenon, the results of which are presented in the next section.

4. Experimental procedure and results

Series of uniaxial tension tests were carried out using the specimens, shown schematically in Fig. 7, i.e. internally cracked plates of dimensions 0.300 x 0.275 x 0.002 m^3. Two crack inclinations were selected: One with $\beta=10^0$, i.e. cracks

that are sub-parallel to the free boundary, fulfilling the demands of geotechnical engineers, for the case of geological faults that are slightly dipping with respect to the surface of the earth, and one with $\beta=90^0$, i.e. faults that dip 90^0, for comparison reasons. The length of the cracks was $2a = 20$ mm and their location varied from single-edge notched specimens to centrally cracked ones.

As it is seen from Fig. 7, the dimensions of the specimens were selected in such a way, that the geometry simulated satisfactorily the semi-infinite body with a subsurface crack. Special attention was paid to ensure that the stress waves reflected from the three boundaries, other than the one closest to the crack, arrived to the crack-tips after the crack emanating from tip B had reached the free boundary (ff). On the other hand, the very small thickness of the plate ensured that the loading conditions could be safely considered as plane-stress ones.

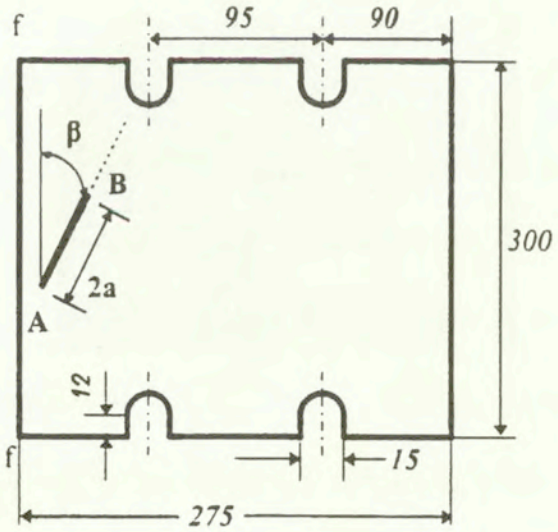

FIG. 7. Geometry of the specimens

The material used in the experimental study was Polymethylmethylate (PM MA), known under the commercial name Plexiglas. The reason for this choice is that the specific material is extremely brittle and behaves in a linear elastic manner from the very early loading steps up to almost the final failure. Since the mechanical properties of this material vary significantly, depending on its exact chemical composition, the properties of the batch used were determined with the aid of a preliminary series of standardized uniaxial tension tests. From

these experiments it was concluded that the assumptions of Linear Elastic Fracture Mechanics, adopted in the previous sections, were absolutely justified. The results of these tests are summarized in Table 1.

Table 1. The mechanical properties of Plexiglas (PMMA).

Elasticity modulus, E	3.8 GPa
Shear Modulus, G	1.5 GPa
Poisson's ratio, ν	0.35
Fracture Stress, σ_f	88.0 MPa
Velocity of longitudinal waves, c_l	2730 m/s
Velocity of transverse waves, c_t	1430 m/s

FIG. 8. A fractured specimen with the arrangement of strain gauges.

The experiments were carried out with the aid of an Instron loading frame with maximum loading capacity $25\text{x}10^4$ N. Taking into account that the maximum fracture load recorded during the whole series of tests did not exceed in any case the level of $2\text{x}10^4$ N, it is concluded that the stiffness of the frame could be considered infinite. The load was applied statically and it was parallel to the free boundary (ff) of the specimen. For each geometry (crack inclination, β, and initial crack length, $2a$), seven different classes of tests were carried out, with the free parameter, the distance of the center of the crack from the free boundary of the specimen, y_0. Five to ten specimens were tested for each class, depending on the repeatability of the results. The characteristics recorded during each test were the critical load causing crack initiation, P_{cr}, and the angle

(a)

(b)

FIG. 9. Fractured specimens with $\beta = 10^0$ and (a) $y_0 = 2a$ (b) $y_0 = 6a$.

of the initial crack propagation from the two tips A and B, θ_A and θ_B, respectively. In a number of tests, the variation of the strain field in the vicinity of the crack tips was also recorded during the loading procedure, using a system of six to ten orthogonal strain rosettes, suitably attached at various strategic points of the specimens. The gauges were arranged along a line either parallel or normal to the free boundary of the specimens. In Fig. 8, a characteristic photograph of a fractured specimen is shown indicating both the arrangement of the strain gauges and the branching phenomenon that accompanied systematically the fracture process. In Fig. 9 (a,b), two characteristic fractured specimens are shown corresponding to $\beta=10^0$ and $y_0 = 2a$ mm (Fig. 9a) and $y_0 = 6a$ (Fig. 9b).

The experimental results obtained from the strain gauge rosettes have already been plotted in Fig. 3(a, b). The agreement between the numerically obtained values for the strain components and the respective experimental quantities is very satisfactory, indicating the validity of the technique used for the numerical solution.

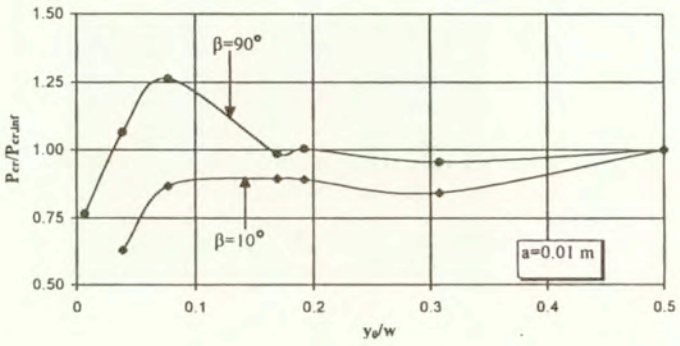

FIG. 10. Reduced critical load versus the position of the crack.

In Fig. 10 the experimentally obtained critical load, P_{cr}, is plotted versus the distance of the center of the crack from the free boundary, y_0, for both the tested configurations, i.e. β=90^o and β=10^o. The values of the critical load are reduced over the respective value for the case of a centrally cracked specimen of the same geometry, while the geometric parameter, y_0, is reduced over the width of the plate, w. It can be seen from this figure that for both configurations, the critical load is not a monotonous function of the distance of the crack from the free boundary, exactly as it was indicated by the numerical analysis of the previous section. A characteristic weak minimum is observed at $x_c \cong 0.3w$. However, the most astonishing observation is the existence of a global maximum in the case of β=10^o, located at about $y_0^* \cong 0.075w$, which means that the specific configuration corresponds to specimens with higher resistance to fracture compared to the centrally cracked ones. Taking into account the dimensions of the crack and the width of the specimens it is concluded that the location of the global maximum is identical to that detected by the numerical analysis and the T-criterion, namely equal to $y_0^* = 2a$ (the initial crack length). It should be mentioned, however, that the scattering of the experimental results for the specific specimen's class varied around 18% while the scattering for all other classes did not exceed 5%. Motivated by this difference, additional tests were carried out for the specific configuration. Both phenomena, i.e. the high scattering and the existence of the total maximum, were consistently repeated indicating that a more thorough study is necessary in order to understand the natural basis of such a type of inherent instability.

In Fig. 11 the experimentally obtained crack initiation angles are plotted, again versus the reduced distance of the center of the crack from the free boundary, y_0, for both crack tips and for crack inclination angle β=10^o. The influence of the free boundary is again of dominant importance. For the tip closer to the free surface (tip B), the initiation angle is considerably higher as compared to

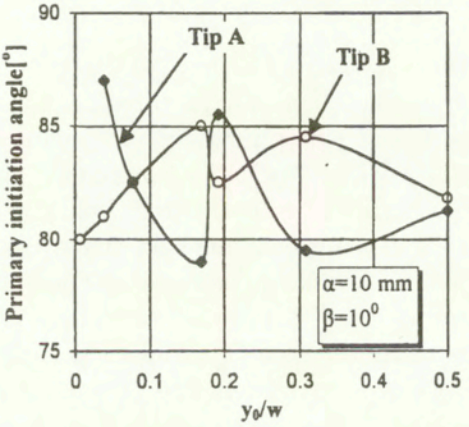

FIG. 11. Initiations angles for tips A and B.

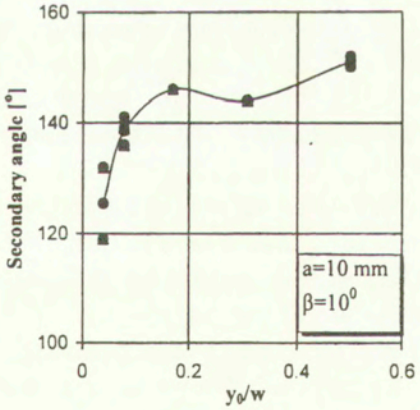

FIG. 12. Initiation angle of the secondary cracks occasionally emanating from tip A.

the respective one of the remote tip (tip A) for low y_0 values. The strong fluctuation of the values of the initiation angles should also be emphasized as well as the fact that for $y_0 = 0.5w$ the experimental values for the two tips become equal as it should be expected for symmetry reasons.

Finally, in Fig. 12 the values of the secondary (after failure) initiation angles, occasionally emanating from tip A, are plotted for the same crack inclination. The influence of the free boundary for this quantity is again dramatic.

5. Discussion and conclusions

The problem of the conditions causing catastrophic propagation of a pre-existing sub-surface crack in a semi-infinite medium was studied in the present paper, both numerically and experimentally. The main qualitative features of the problem were explored by using the displacement discontinuity technique in conjunction with a suitably adapted indirect boundary element code for the determination of the displacement, strain and stress fields around cracks in a semi-infinite, isotropic, linearly elastic half-space. The T-criterion of failure was adopted for the determination of the critical conditions at the moment of crack initiation. The results obtained from the numerical analysis were compared to the respective ones obtained experimentally. Special attention was given to a specific configuration of the specimens, i.e. those with cracks very slightly inclined with respect to the free boundary, since this configuration is supposed to simulate the geometry of a number of shallow, gently dipping geological faults, responsible for a number of catastrophic earthquakes in the Mediterranean basin. The agreement between the numerical results and the experimental evidence for the strain distribution was satisfactory. The same was true for the predictions of the T-criterion of failure, for both the critical load and the crack initiation angle.

The main advantage of the Displacement Discontinuity Technique is that it is very flexible and if it is supplemented with a suitable fracture criterion, it can be used both for the prediction of the initiation angle of a stationary crack in an elastic medium of finite dimensions as well as for the estimation of the strength of the body, i.e. the critical load that causes initiation of the crack.

However, the most attractive conclusion of the present study was that the load required to cause initiation of the crack is not a monotonic function of the distance of the center of the crack from the free boundary. Specific configurations were detected for which the crack initiation load was maximized, the conclusion contradicting perhaps the common sense. Depending on the crack inclination angle, this optimum distance varied between 2 and 2.5 times the initial semi-length of the crack. Such a conclusion, associated with a significant increase of the scattering of the experimental results, in other words with an inherent instability of the phenomenon, is not easily explainable. Further experimental study is required, for a wider class of materials, before definite conclusions are drawn.

Acknowledgements

The authors gratefully acknowledge the assistance of Mr P.-J. R. Goycoechea in the execution of the experiments.

References

1. A. R. ROSENFIELD AND C. W. MARSCHALL, *Engineering fracture mechanics,* **45**(3), 333-338, 1993.
2. S. L. CROUCH, *Solution of plane elasticity problems by the displacement discontinuity method,* International Journal of Numerical Methods in Engineering, **10,** 301-343, 1976.
3. G. R. IRWIN, *Analysis of stresses and strain near the end of a crack traversing a plate,* Journal of Applied Mechanics, **24**, 361-364, 1957.
4. Y. MURAKAMI, (editor), *Stress Intensity Factors Handbook,* Pergamon Press, Vol.**II**, p. 916, 1981.
5. N. P. ANDRIANOPOULOS and P. S. THEOCARIS, *The Griffith-Orowan fracture theory revisited: The T-criterion,* International Journal of Mechanical Science, **27**, 793-801 1985.
6. S. L. CROUCH and A. M. STARFIELD, *Boundary Element Methods in Solid Mechanics,* Allen & Unwin, London 1983.
7. P. S. THEOCARIS, N. P. ANDRIANOPOULOS and S. K. KOURKOULIS, *The angle of initiation and propagation of cracks in ductile media,* Experimental Mechanics, **27**, 120-125, 1987.
8. E. H. YOFFE, *The moving Griffith crack,* Philosophical Magazine, **42**, pp. 739-750, 1951.
9. N. P. ANDRIANOPOULOS and S. K. KOURKOULIS, *FLDs for modern Al and Al-Li alloys and MMCs,* 10^{th} Int. Conf. on Exp. Mech., J.F.GOMEZ [Ed.], Balkema, 995-1000, Rotterdam 1994.

Received November 2, 2000.

Arch. Mech., **53**, 4-5, pp. 439–456, Warszawa 2001

The influence of cracks on the mechanical behaviour of particulate MMCs: an experimental study

S. K. KOURKOULIS

National Technical University of Athens,
Department of Mechanics,
Zografou Campus, Theocaris Building,
157 73 Zografou, Athens, Greece

THE DETERIORATION OF THE MECHANICAL PROPERTIES of particulate Metal Matrix Composites (MMCs) caused by macroscopic cracks is studied, experimentally, in comparison to the behaviour of the respective matrix alloys. Two Al-based MMCs, reinforced with fine SiC particles, extensively used in aerospace engineering, are employed. The study is focused on the influence of cracks on the fracture strength of MMCs and on the variation of the critical Crack Opening Displacement (COD) versus the inclination of the crack with respect to the loading direction. The role of the plastic anisotropy induced during manufacturing is also investigated.

1. Introduction

THE STRENGTH AND THE STIFFNESS of ceramic particle reinforced MMCs is considerably increased compared to the respective quantities of the unreinforced matrix alloys. This is attributed to the presence of the stiffer particles and the thermal expansion mismatch between the matrix and the reinforcement, which causes a high density of dislocations during the cooling process [1]. Taking also into account that particulate MMCs can be mechanically processed using classical manufacturing technologies developed for monolithic alloys [2], as well as their improved and attracting thermal and mechanical properties, such as low sensitivity to thermal shocks and temperature changes, high surface durability, high thermal and electrical conductivity and high absorption of plastic deformation under impact (in case of ductile metal matrices), one would expect that MMCs could substitute conventional alloys in practical applications. However, and beyond their advantages, the use of MMCs is yet rather restricted, since both their ductility and fracture toughness are considerably lower than the respective quantities of the unreinforced alloy [3]. Similar conclusions are drawn concerning the plastic anisotropy induced during manufacturing, which appears to reduce

considerably the strength of cracked composite material while its influence on the respective cracked matrix alloy is almost negligible [4].

In general, it is known that in particulate matrix composites the primary load-bearing element is the matrix material. Especially, in the case of a ductile matrix, the role of the reinforcing particles is to block the motion and slip of dislocations limiting in this way the plastic deformation of the composite material. According to Kelly's theory [5], the maximum strengthening achieved is controlled by the shear modulus of the matrix and the fineness of the particle dispersion. However it is clear, that a much more detailed investigation of the mechanisms responsible for the deterioration of the mechanical properties of MMCs in presence of macroscopic cracks is essential, if one aims at the development of new materials with improved damage tolerance. It was only very recently, that POZA and LLORCA [6] investigated experimentally and numerically the strength and ductility of Al-Li/SiC composites and concluded that the progressive fracture of the reinforcing particles reduced the strain-hardening rate of the composite, precipitating the onset of plastic instability and failure. Unfortunately, the relative literature, especially for modern MMCs, is limited and extensive experimental study of the above phenomena is necessary, in order to quantify them.

Towards this direction, a series of experimental results are presented in the next section, concerning the fracture stress and the critical COD of MMCs' specimens, cracked at various inclinations with respect to the loading direction. Two pairs of materials were tested, namely the 8090 and 2124 matrix alloys and MMCs. Both materials are produced by BP with the aid of a novel powder metallurgy process. An aluminum-based matrix (Al-Li and Al-Cu, respectively) is used, reinforced with 20% per volume of fine silicon carbide (SiC) particulates of diameter $\sim 3\text{x}10^{-6}$ m. According to the process adopted by the manufacturer, the raw materials, i.e. the atomized aluminum alloy powder and the silicon carbide microgrit, are bought-in to an internal specification covering chemistry and size. The powders are then processed and blended to a homogeneous mixture. The mixed powders are then canned, degassed and hot isostatically pressed to full density using conventional aluminum powder metallurgy practices. The hot-pressed billets are decanned and converted to wrought product using standard metal working equipment and techniques. The materials were available in the form of rolled sheets of thickness equal to 1 mm and a special heat treatment was applied to the specimens prior to testing, according to the manufacturer's instructions, in order to obtain their optimum mechanical properties. The treatment included gradual heating of the specimens up to 505°C, keeping the temperature constant for 90 minutes, and immediately cold water quenching, as it is described in the respective Processing Handbook [7]. No visible distortion or surface cracking of the specimens was observed due to the quenching.

The mechanical properties of the materials were determined with the aid of preliminary standardized tension tests and are recapitulated in Table 1. It is clear from this table that the composite materials show increased stiffness compared to their matrix alloys by almost 25% for both "pairs" of materials (where the term "pair" denotes the combination of the MMC material with its respective matrix alloy). On the other hand, the tensile strength of the 8090 MMC composite is 34% higher than that of the matrix alloy while for the case of 2124 pair, the improvement is about 43% . On the contrary, and as it was expected, the ductility of the MMCs, is reduced by 11% in the case of the 8090 pair and by 27% in the case of the 2124 pair. The higher the gain in stiffness and strength, the higher the loss in ductility! However, in case of macroscopically cracked specimens, the above conclusions are not any more valid, and the use of MMCs does not appear to be advantageous, as it will become evident in the next section.

Table 1. The mechanical properties of the materials used in the present study.

		8090			2124	
	Alloy	MMC	Change [%]	Alloy	MMC	Change [%]
Modulus of elasticity [GPa]	92.5	114.0	23	80.0	109.9	37
Tensile strength[MPa]	428	575	34	435	622	43
Ductility [%]	4.5	4.0	-11	6.7	4.9	-27

2. Mechanical behaviour of MMCs in presence of cracks

The dramatic changes in the stress and strain fields in a specimen or in a structure due to macroscopic cracks and the complications imposed are of such a nature that an almost independent branch of Mechanics, the Fracture Mechanics, was developed, devoted exclusively to their study. The fracture toughness, K_{IC} and the critical COD are the two simplest and most widely used concepts for the description of the critical conditions leading an initially stationary crack to growth and finally to catastrophic propagation. Although it is not likely that a single parameter can serve as a complete failure criterion [8], K_{IC} and critical COD are widely applied in Fracture Mechanics, mainly due to their simplicity. Besides the fact that the independence of these quantities of the geometry of the specimens used for their measure is still under discussion [9] and a lot of disagreements and ambiguities concerning the correct method of their measure are stated, the critical COD (and a number of other single-parameter fracture

criteria like the J – integral and the K_{IC} ones) is considered, even today, to be a unique tool for the in-situ inspection and fracture safety assessment of cracked structural members already in function. For this reason, experimental results concerning these parameters are presented here, in an effort to enlighten the change of the behaviour of MMCs caused by macroscopic cracks.

2.1. Fracture strength of cracked MMCs and their matrix alloys

Four series of uniaxial tension tests were carried out using specimens made from each one of the materials under study. The specimens were rectangular Single Edge Notched (SEN) plates of length l =100 mm, width b=50 mm and thickness d=1mm (Fig. 1). The cracks, of length a_0=10 mm, were artificially machined at one side of the specimens, at a distance $h = l/2$ from their lower edge, using an extra thin cutting disc (thickness δ_0=0.2 mm). The tips of the cracks were smoothened using a diamond wire of diameter 0.2 mm in order to eliminate the double singularity existing in case of artificial cracks (see further Fig. 3a). The inclination of the cracks varied between $\beta = 90°$ to $\beta = 10°$ with respect to the load direction, which was parallel to the long dimension of the specimens (Fig. 1). For each crack inclination angle, three to ten tests were executed depending on the repeatability and scattering of the results. The results of these experiments are shown in Fig. 2, in which the variation of the fracture strength is plotted versus the crack inclination angle, β, for both pairs of materials. The fracture strength of each material is reduced over the fracture strength of the respective intact material.

It can be seen from Fig. 2 that in the case of the 8090 pair, the composite material is of higher strength only for cracks tending to become parallel to the loading direction ($\beta \leq 30°$). For crack inclinations between 30° and 90° the two materials have almost the same reduced strength, which varies between 25% and 30% of the strength of the intact specimens. The absolute values of the fracture strength are recapitulated in Tables 2 and 3. It is evident from Table 2, that for cracks perpendicular to the load direction (β=90°), the matrix alloy is of slightly superior absolute strength (about 2%) compared to the respective reinforced MMC, while for cracks with β=10° the absolute strength of the reinforced material is by about 17% higher than that of the matrix alloy.

Table 2. The fracture strength of cracked 8090 Alloy and MMC specimens in MPa.

Material ↓/ Crack Inclination →	90°	70°	30°	10°
8090 Alloy	132.5	119.6	144.1	210.2
8090 MMC	129.8	120.7	146.2	245.5

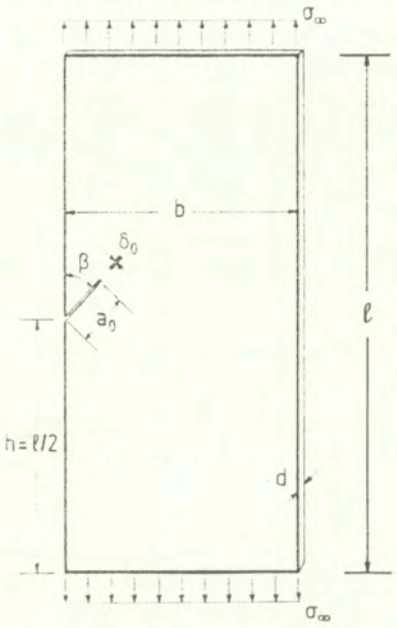

FIG. 1. The geometry of the specimens and the loading configuration.

Table 3. The fracture strength of cracked 2124 Alloy and MMC specimens in MPa.

Material ↓ /Crack Inclination→	90°	70°	50°	25°	10°
2124 Alloy	182.7	206.6	217.5	261.5	287.1
2124 MMC	187.1	186.6	180.4	248.8	357.7

The next characteristic of Fig. 2, which deserves attention, is that the fracture stress for specimens with crack inclinations about $\beta \cong 60°$ is clearly lower compared to that of specimens with $\beta = 90°$, both for the alloy and the reinforced material. In other words and contrary to common sense, a cracked specimen with $\beta \cong 60°$, is at a worst position and the crack is most prone to propagate compared to a specimen containing a crack with $\beta = 90°$, i.e. perpendicular to the load. This phenomenon was already observed experimentally by SIH and KIPP [10] from early seventies. Later it was predicted theoretically by THEOCARIS and ANDRIANOPOULOS [11] for relatively brittle materials, using a modified strain energy-density criterion. A similar experimental result is mentioned by THEOCARIS *et al.* [12], who observed that for dynamic crack propagation, and in case the branching phenomenon was suppressed, the crack tended to place itself in an

optimum direction, corresponding to an inclination of about $\beta = 70°$. However, a unified explanation of these phenomena and a soundness interpretation of them in physical terms is still pending.

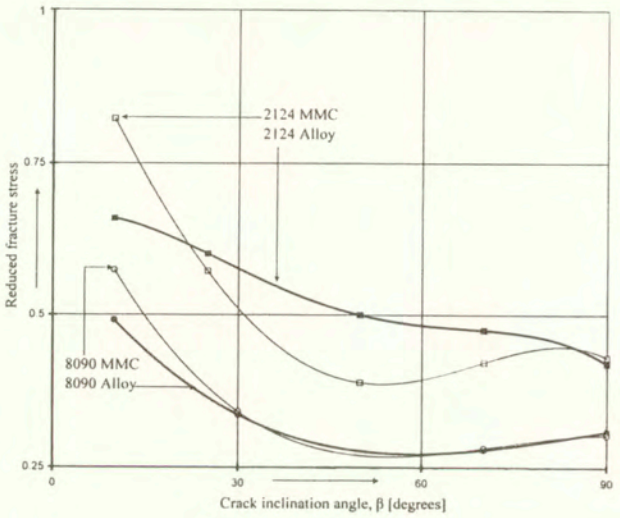

FIG. 2. The fracture stress of the 8090 and 2124 matrix alloys and MMCs reduced over the respective fracture stress of the intact material, versus the inclination of the crack, β.

The conclusions drawn from Fig. 2 for the 2124 pair are of the same nature. However, in this case the matrix alloy appears to be of superior reduced strength for the whole band of crack inclinations between $\beta = 20°$ and $\beta = 90°$. Only for cracks with $\beta \leq 20°$ the composite material excels with respect to the matrix alloy. Moreover, and as it is concluded from Table 3, the matrix alloy has significantly higher absolute fracture stress (about 17% for $\beta = 50°$) compared to the reinforced material. As far as it concerns the variation of the fracture strength versus the crack inclination angle, the anomaly observed for $\beta = 60°$ in the behaviour of the 8090 pair of materials, is not detected at all for the matrix material, while for the composite one it is weak. Such a behaviour is justified, according to what is mentioned in [11], since the 2124 matrix alloy is relatively ductile compared to all three other materials.

2.2. Crack Opening Displacement and its critical value

The COD method of test is standardized according to the ASTM as well as according to the British Standards, either in the form of compact specimens or in the form of three-point-bend specimens. However, it is doubtless that the reliable measure is a very difficult task. The techniques that have been devel-

oped, varying from the infiltration technique to the empirical extrapolation of clip gauge measurements, may be considered satisfactory for the case of conventional metallic materials, but are difficult to be applied in the case of MMCs, because their brittleness results in very small absolute values of the COD and the experimental "noise" covers the main phenomenon. The δ_5 procedure proposed recently by HELLMANN and SCHWALBE [13] is the one widely used today for MMCs. The main restriction of the conventional standardized methods is that they have been developed for cracks either perpendicular (compact specimens)or parallel to the loading direction (three-point-bending specimens).

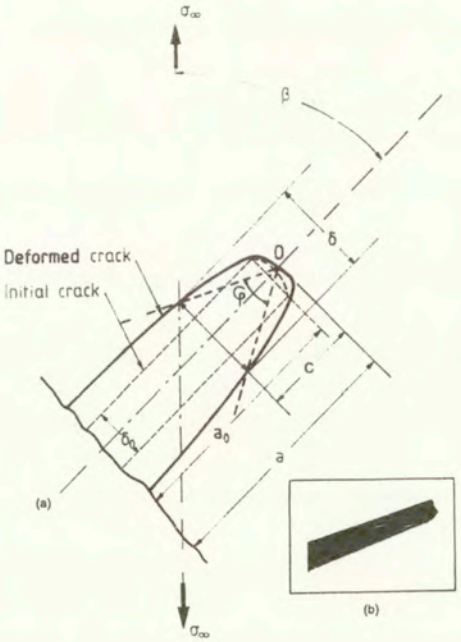

FIG. 3. (a) Schematic representation of the distorted crack tip area and the method adopted for measuring the COD. (b) The distorted crack tip area in case of a crack with $\beta = 70°$ in a specimen made from 8090 alloy, just before failure.

In Fig. 3a the method adopted in the present study for the measurement of the COD ($\equiv \delta$) is explained. The angle φ was not a-priori defined since it depends on the technique followed and it varies between 30° and 45°[14]. However, it was indicated by KNAUF and RIEDEL [14] that the exact point of measurement seems to be unimportant for the final results, as long as the measurement is executed within the distance from the crack tip for which the HRR-field dominates the deformation field. Thus, for the purposes of the present study and taking into account the dimensions of the initial crack, it can be proved that it is sufficient

to execute the measurement of COD at a distance c from the current crack tip position, defined from the relation $c/a \approx c/a_0$=0.2 (Fig. 3a), as it is analytically described in [8] (the crack-tip blunting is ignored).

The additional problems confronted in case of cracks inclined with respect to the loading direction, rendering the conventional standardized methods inapplicable, are the following two ones:

i. The loss of symmetry of the crack configuration and the lack of symmetry axis, since prior to its initiation the crack is not developed in a self-similar manner. This is schematically shown in Fig. 3a and, also, in Fig. 3b in which the tip of a crack with β=70° in a specimen made from 8090 alloy is shown, just before catastrophic crack propagation. The same phenomenon is shown, also, in Figs. 4(a,b), in which the asymmetrically blunted tip of an inclined crack is shown, together with its initial symmetric configuration prior to the loading process, as it was obtained with the aid of a scanning electron microscopy.

ii. The rigid-body rotation, inevitably accompanying the blunting of the crack-tip [15, 16].

Concerning the geometry and specimen-size dependence of the critical COD, it has been shown by COWLING and HANCOCK [17] that the onset of crack growth does not occur always at a unique critical value of COD even for a given thickness of the specimens. This phenomenon is attributed to the difference in triaxiality. However, for practical applications the critical COD concept is widely used as a useful lower limit of the fracture behaviour [9].

Having in mind the above-mentioned restrictions, series of uniaxial tension tests were carried out, using SEN specimens with crack-length to specimen-width ratio equal to 0.2. The dimensions of the specimens were again of 100 mm length, 50 mm width and 1mm thickness (Fig.1). Specimens with cracks both perpendicular and inclined with respect to the loading direction were tested. An Instron loading frame was used (maximum loading capacity 250 kN) for the execution of the tests. During the loading procedure, the area around the crack tip was monitored using a high-speed video camera. The COD was measured afterwards using suitable computer image processing software and a series of successive photographs of the crack configuration. The critical COD value was detected from the load versus clip gauge displacement plot as it is described by LANDES and MCCABE [18]. Four series of tests were carried out, one for each material. For each configuration the value of the critical COD reported is the outcome of three to ten tests, depending on the repeatability of the results.

Characteristic results of the above series of experiments have been plotted in Figs. 5 - 7, for the 2124 pair of materials. In these figures, the reduced COD is plotted versus the reduced applied stress. The reduction for the COD was realized by dividing the difference δ-δ_0 (i.e. the current value of COD, δ, minus the initial

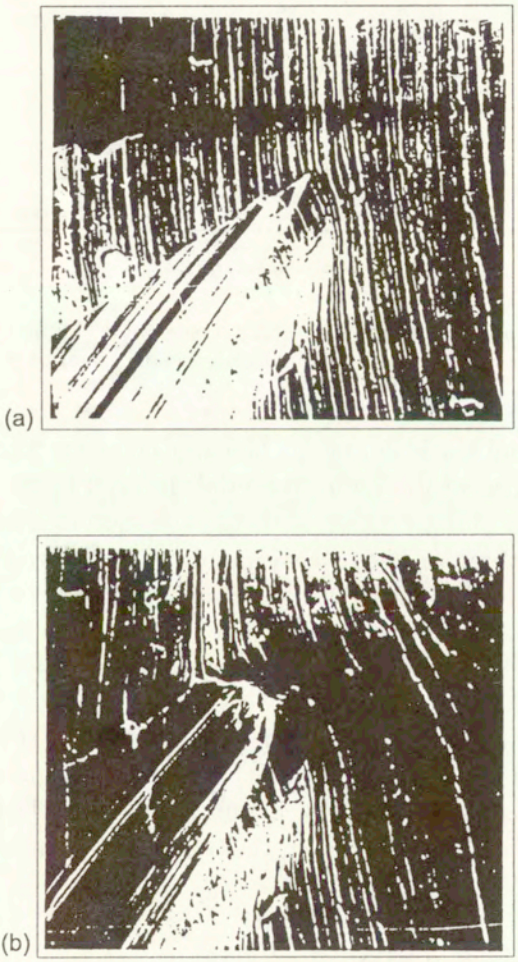

FIG. 4. Asymmetrically blunted crack in a copper specimen, prior and during loading, as it is obtained with the aid of Scanning Electron Microscopy (Magnification: x 1000) (a) Configuration prior to loading. (b) Configuration during loading, for a load equal to 75% of the failure load. (Courtesy: V.Kytopoulos, Microscopy Laboratory, LTM/NTUA)

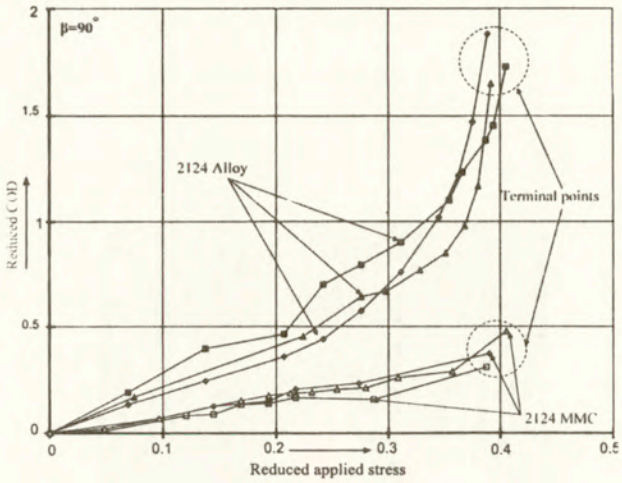

FIG. 5. Experimental results for the reduced COD versus reduced applied stress for the 2124 pair of materials and for crack inclination angle equal to $\beta = 90°$

thickness of the artificial crack, δ_0) by δ_0. The applied stress was reduced over the respective fracture stress of the intact material. In each figure the results of six characteristic tests are plotted, three of them corresponding to the matrix alloy (filled symbols) and three of them corresponding to the reinforced composite (empty symbols). In Fig. 5 the crack inclination is equal to β=90°, in Fig. 6 it is β=50°, while in Fig. 7 it is β=10°. For comparison, the same quantities are plotted in Figure 8 for the 8090 pair of materials and for the configuration corresponding to β=90°.

It can be seen from these figures that the variation of the COD versus the applied stress is initially almost linear and then it increases more or less abruptly (exponentially), up to the critical crack initiation point. Extensive numerical study of the results of the tests indicated that the best-fit curve is an exponential one of the form:

$$\frac{COD - \delta_0}{\delta_0} = m \left(\frac{\sigma}{\sigma_f} \right)^n \tag{2.1}$$

where σ_f is the fracture stress of the intact material and m, n are numerically determined constants, the values of which are recapitulated in Tables 4 and 5, for the 8090 and 2124 pairs respectively. The scattering of the results is not significant for all four materials and all different configurations employed in the experimental procedure.

In Figs. 9 and 10 the critical reduced COD, δ^*, is plotted versus the crack inclination angle, β. The value of the critical COD is obtained as the average of

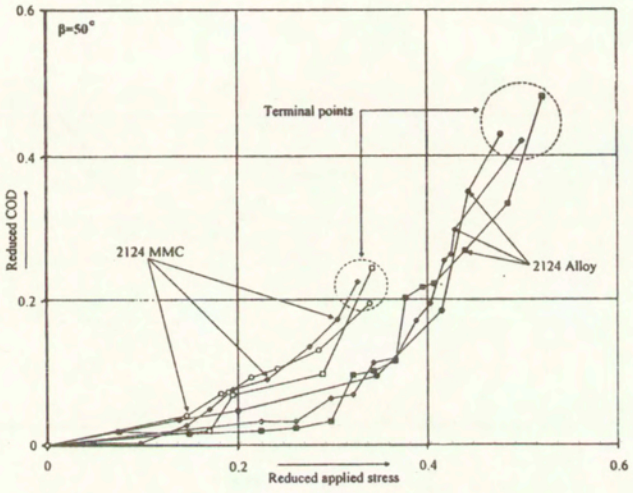

FIG. 6. Experimental results for the reduced COD versus reduced applied stress for the 2124 pair of materials and for crack inclination angle equal to $\beta = 50°$

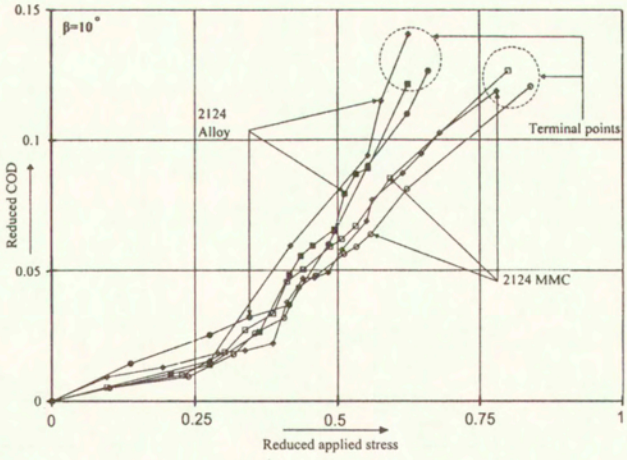

FIG. 7. Experimental results for the reduced COD versus reduced applied stress for the 2124 pair of materials and for crack inclination angle equal to $\beta = 10°$

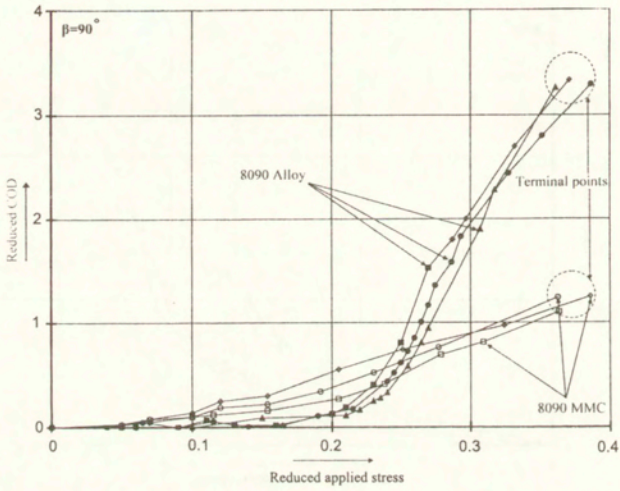

FIG. 8. Experimental results for the reduced COD versus reduced applied stress for the 8090 pair of materials and for crack inclination angle equal to $\beta = 90°$

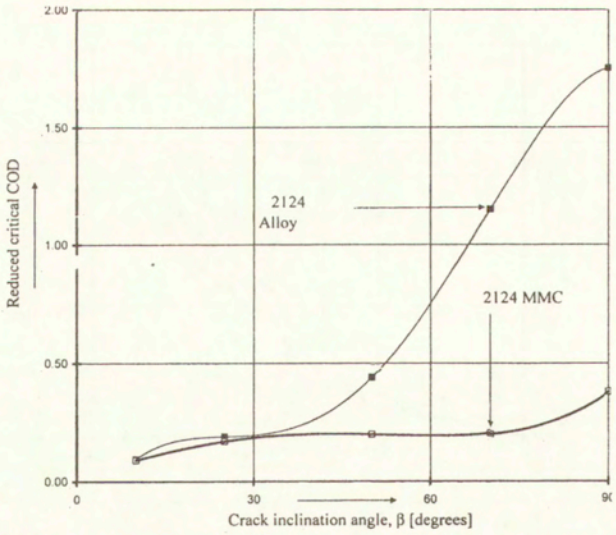

FIG. 9. The critical COD, reduced over the thickness of the initial crack, versus the inclination of the crack for the 2124 pair of materials.

Table 4. The constants m and n of Eq.(2.1) for the 8090 pair of materials.

	Alloy			MMC	
β [°]	m	n	β[°]	m	n
90	64480	8.341	90	15.31	1.903
70	3167	5.991	70	333.5	3.695
30	187.3	4.711	50	95.62	3.336
20	45.04	3.555	25	4.601	1.737
10	9.433	3.296	10	4.008	1.628
			8	1.661	2.487

Table 5. The constants m and n of Eq.(2.1) for the 2124 pair of materials.

	Alloy			MMC	
β[°]	m	n	β[°]	m	n
90	13.11	2.360	90	7.122	2.407
70	5.884	2.458	70	2.660	2.308
50	7.664	4.032	50	33.29	3.770
25	0.943	4.128	25	0.859	1.848
10	0.351	2.304	10	0.351	2.579

all "terminal points" encircled with a dotted line in Figs. 5 - 8. It is observed from Figs. 9 and 10 that the function $\delta^*=\delta^*(\beta)$ is relatively smooth, dividing the (δ^*, β) space into two regions: one corresponding to safe combinations of the COD and crack inclination, and one to combinations leading to failure. Obviously, once the function $\delta^*=\delta^*(\beta)$ is available from a simple series of experiments, like the one described in the present section, it represents a powerful tool for the in-situ inspection of structural elements already in function: one can decide about the remaining life of the element without knowing the value of the applied load but only its relative direction with respect to the crack.

A slight deviation of the above referenced smooth variation is detected for the 8090 matrix alloy and for crack inclinations of about 20°. Indeed, for this geometry the critical COD appears to be higher compared to that corresponding to the configuration with β=30°. The same deviation is also observed for the respective composite material but in this case it is considerably weaker. An explanation of this peculiar experimental observation is not yet available and additional experimental data for other materials are required before definite conclusions are drawn.

An additional anomaly, worth to be mentioned, is the one observed in the behaviour of the $\delta^*=\delta^*(\beta)$ function for the 8090 MMC and for crack inclinations

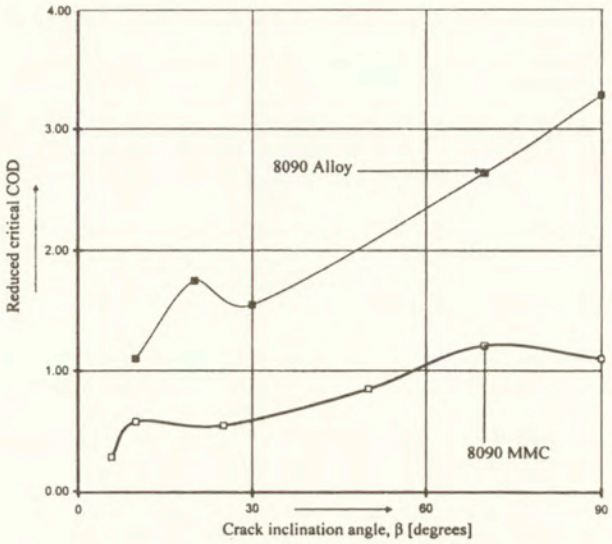

FIG. 10. The critical COD, reduced over the thickness of the initial crack, versus the inclination of the crack for the 8090 pair of materials.

roughly equal to 70°. Indeed, as it can be seen from Fig. 8, the reduced critical COD-value for β=70° exceeds slightly the respective value for the geometry with β=90°. This anomaly is, possibly, related to the respective one mentioned in the previous paragraph for the variation of the fracture stress of cracked materials with respect to the crack inclination. However, and besides the two anomalies just mentioned, the main conclusion from this paragraph is, again, that the influence of macroscopic cracks on the reinforced composite materials is of completely different nature and much more dramatic compared to the influence of macroscopic cracks on the unreinforced matrix alloys.

2.3. Influence of anisotropy on the strength of cracked MMCs

Among the advantages of the MMCs obtained through Powder Metallurgy processes (as it is the case of the BP 8090 and 2124 MMCs of the present study) is the fact that they are more or less homogeneous and isotropic materials, although their density is sometimes variable within the volume of the final product. However, after manufacturing, either by using hot or cold forming processes, the material obtains an oriented texture and exhibits significant anisotropy. It is exactly the purpose of the present paragraph to study the influence of this type of anisotropy on the strength of cracked MMCs, in comparison, again, to the behaviour of their matrix alloys.

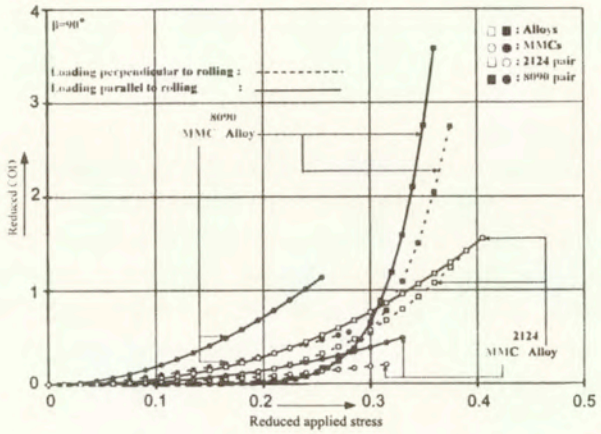

FIG. 11. Best fit curves for specimens loaded parallel and perpendicular to the loading direction for all four materials and crack inclination angle $\beta = 90°$

In order to achieve this target two types of SEN specimens, with cracks oriented perpendicular to the loading direction (i.e. β=90°), were subjected to tensile loading up to fracture. In the first type of specimens the load was applied parallel to the rolling direction (in other words, the initial cracks were machined perpendicular to the rolling direction), while in the second type of specimens the load was applied perpendicular to the rolling direction (and the cracks were machined parallel to the rolling direction).

The results of these series of experiments are shown in Fig. 11, where the reduced values of the COD have been plotted versus the reduced stress for the two types of specimens and for both pairs of materials. The heavy lines correspond to the first type of specimens (load // rolling) while the dotted lines correspond to the second type (load $\perp$ rolling). The filled symbols correspond to the 8090 pair of materials while the empty ones correspond to the 2124 pair. The curves denoted by rectangular symbols (empty and filled) describe the behaviour of the two matrix alloys while the curves denoted by circular symbols (empty and filled) describe the behaviour of the respective reinforced composite materials. To avoid confusion, only the lines obtained as best fit curves from the numerical elaboration of the experimental results have been plotted in this figure, since the variation of the individual tests is identical to that observed in previous series of tests plotted in Figs. 3 - 6.

It is seen from Fig. 11 that the critical COD-value in the case of the MMC materials are considerably lower if the crack is oriented perpendicularly to the rolling direction. For example, for the 8090 MMC, the reduced critical COD-value changes from about 1.25, when the load is applied parallel to the rolling

direction to about 0.4, when the load is applied perpendicular to the rolling direction, which correspond to a change of about 210% ! On the other hand, the reduced critical stress changes considerably from about 0.235 to about 0.275 respectively, which corresponds to a change of about 16% . On the contrary, in the case of the respective matrix alloy, the critical COD-value changes by only $\sim$ 25% (from $\sim$ 3.75 to $\sim$ 2.80) and the critical stress remains essentially constant (reduced by less than 5%). The conclusions for the second pair of materials are of similar qualitative nature, although not so impressive quantitatively.

Both observations imply, again, that SiC particles play a profound role in ultimate behaviour of 8090 MMC, which is completely different compared to the behaviour of their matrix alloys.

3. Discussion and conclusions

The primary conclusion of the present experimental study is that the presence of macroscopic cracks deteriorates the strength advantages of MMCs and their respective matrix alloys appear to be more attractive for mechanical applications. The example of the 2124 MMC for which the gain in strength versus its matrix alloy is less than 3% in the presence of cracks perpendicular to the loading direction is characteristic, especially if one considers the gain in strength on the case of intact specimens which is about 43% ! On the other hand, specific configurations (crack inclinations) were detected for which the unreinforced material appears to be stronger than the reinforced one. Only as the crack tends to become parallel to the external load (which means that the influence of the crack tends to disappear), the MMC appears to be again of superior strength.

This behaviour can be explained if it is taken into account that the fracture processes in the case of particulate reinforced MMCs are significantly influenced by the presence of particles, even if they are in the form of platelets, as it happens with both MMCs studied in the present work. Indeed it has been proved by IBRAHIM *et al.* [19] that for such materials the critical step for failure is void nucleation rather than void coalescence. Voids are generated when the local stresses exceed the stress necessary to decompose the particle. When the local plastic relaxation, that relieves stress concentration becomes difficult, as in case of pre-cracked materials, where the plastic relaxation is concentrated in the immediate vicinity of the tip of the macroscopic crack, then the final failure occurs at rather low strains.

As far as it concerns the COD and the class of failure criteria based on the critical COD concept, various drawbacks have been reported in scientific literature, ranging from uncertainties concerning the most representative point of measuring it to the relationship between COD and other critical mechanical quantities (like K_C or J_C) serving as crack initiations indices. However, in spite

of these drawbacks, COD appears to be irreplaceable especially for in-situ applications, mainly due to its simplicity. Towards this direction the relationship between critical COD and crack inclination, extracted from the present series of experiments, constitutes an extremely useful tool for the determination of the remaining life of cracked structural members, since the knowledge of the exact value of the load level is not necessary. The only piece of information required, beyond COD, is a rough estimation of the inclination of the crack with respect to the loading direction.

Last but not least, it was concluded that the anisotropy induced during manufacturing affects considerably the mechanical behaviour of reinforced composite materials. The coexistence of plastically induced anisotropy and macroscopic cracks transforms completely the characteristics of MMCs and almost eliminates their advantages concerning both the critical COD and the fracture stress. The respective influence on the matrix materials is very small if it exists at all.

Acknowledgement

The author acknowledges the assistance of Professor N. P. ANDRIANOPOULOS for the critical interpretation of the experimental findings and the help of MR S. SARAGAS in the execution of the experiments.

References

1. G. HENESS, L. GAN, B. BEN-NISSAN, D. DAVIDSON and Y.W. MAI, *An experimental and finite element analysis of the effect of particle shape on the constraint in metal matrix composites.* 4^{th} *Int. Conf. on Composite Materials*, Corfu, Greece, S. A. PAIPETIS AND A. G. YOUTSOS [Eds.], Univ. of Patras Publications, Patras, pp. 297-302, 1995.

2. F.J. HUMPHREYS, W.S. MILER and M.R. DJAZEB, *Microstructural development during thermomechanical processing of particulate metal matrix composites,* Material Science and Technology, **6**, 1157-1166, 1990.

3. G. HENESS, L. GAN and Y.W. MAI, *Effect of particle morphology on matrix constraint in metal matrix composites*, 9^{th} Int. Conf. Fracture, Sydney, Australia, B. L. KARIHALOO [Ed.], Pergamon Press, **1**, 759-765, New York 1997.

4. S.K. KOURKOULIS and N.P. ANDRIANOPOULOS, *Plastically induced anisotropy on metal matrix composites,* Mechanics of Composite, Materials and Structures, **7**, 1, 1-18, 2000.

5. A. KELLY, *The strengthening of metals by dispersed particles,* Proceedings of the Royal Society, **A282**, 63-79, 1964.

6. P. POZA and J. LLORCA, *An experimental and numerical analysis of the strength and ductility of Al-Li/Sic composites.* 9^{th} Int. Conf. of Fracture, Sydney, Australia, B. L. KARIHALOO [Ed.], Pergamon Press, Vol.1, 775-782, New York 1997.

7. *Particulate Metal Matrix Composite Processing Handbook,* Issue 1, BP Metal Composites, Farnborough, United Kingdom, 1991.

8. N.P. ANDRIANOPOULOS, S.K. KOURKOULIS and S. SARAGAS, *COD measurements and optimum exploitation of MMCs for aerospace applications,* Engineering Fracture Mechanics, **57**, 5, 565-576, 1997.

9. C.E TURNER, *Methods for post-yield fracture safety assessment. Post-yield fracture mechanics*, D.G.H. LATZKO *et al.* [Eds.], Elsevier Applied Science Publications, London, 2nd edition, 25-221, 1984.

10. G.C. SIH and M.E. KIPP, *Fracture under complex stress - The angled crack problem,* International Journal of Fracture, **10**, 261-265, 1974.

11. P.S. THEOCARIS and N.P. ANDRIANOPOULOS, *A modified strain-energy density criterion applied to crack propagation.* Journal of Applied Mechanics, **49**, 81-86, 1982.

12. P.S. THEOCARIS, N.P. ANDRIANOPOULOS and S.K. KOURKOULIS, *Brittle curving and branching under high dynamic loading.* Int. J. Pres.Ves. & Piping, **46**, 149-166, 1991.

13. D. HELLMANN and K.-H. SCHWALBE *Geometry and size effects on J-R and δ-R curves under plane stress conditions,* ASTM STP 833, 577-605, 1984.

14. G. KNAUF and H. RIEDEL, *A comparative study on different methods to measure the crack opening displacement* Advances in Fracture Research, D. FRANCOIS [Ed.], Pergamon Press, Vol.5, 2547-2553, New York 1981.

15. P.S. THEOCARIS, N.P. ANDRIANOPOULOS and S.K. KOURKOULIS, *The angle of initiation and propagation of cracks in ductile media,* Experimental Mechanics, **27**, 120-125, 1987.

16. P.S. THEOCARIS, D. PAZIS and B.D. KONSTANTELLOS, *Elastic displacements along the flanks of internal cracks in rubber,* Experimental Mechanics, **29**, 33-45, 1989.

17. M.J. COWLING and J.W. HANCOCK, *Ductile failure criteria for blunting cracks,* Fracture 1977 ICF4, University of Waterloo, 3171-3175, 1977.

18. J.D. LANDES and D.E. MCCABE, *Experimental methods for post-yield fracture toughness determinations.* Post-yield fracture mechanics, D.G.H. LATZKO *et al.* [Eds.], Elsevier Applied Science Publications, London, 2nd edition, 223-284, 1984.

19. I.A. IBRAHIM, F.A. MOHAMED and E.J. LAVERNIA, *Particulate reinforced metal matrix composites - A review,* J. Material Science, **26**, 1137-1156, 1991.

Received November 02, 2000; revised version January 30, 2001.

Arch. Mech., **53**, 4-5, pp. 457–485, Warszawa 2001

Michell-like grillages and structures with locking

T. LEWIŃSKI[1] and J. J. TELEGA[2]

[1] *Warsaw University of Technology,*
Faculty of Civil Engineering,
Armii Ludowej 16, 00-637 Warsaw, Poland,
e-mail: T.Lewinski@il.pw.edu.pl

[2] *Institute of Fundamental Technological Research,*
Polish Academy of Sciences,
Świętokrzyska 21, 00-049 Warsaw, Poland,
e-mail: jtelega@ippt.gov.pl

THE PAPER GENERALIZES THE MICHELL theory of plane pseudo-continua to the anti-plane problems in which the loading is perpendicular to the plane of the structure. The starting point is the minimum compliance problem for a two-phase Kirchhoff plate. Upon relaxation, one of the materials can be degenerated to a void (or microvoids) and by imposing the condition of the volume being small, one arrives at the Michell-like problem for a locking plate. The locking locus B is determined explicitly; it tends to a square if the Poisson ratio tends to 1. In the last case the locking locus coincides with that used in the Rozvany-Prager theory of optimal grillages. A theory of perfectly-locking and elastic-locking plates and shells, not necessarily isotropic, is formulated. Dual extremum and existence theorems are also given.

1. Introduction

MICHELL STRUCTURES REPRESENT solutions to the following optimum design problem:

$$(\mathrm{P}_1) \qquad \inf\left\{\int_\Omega \left(|\sigma_I| + |\sigma_{II}|\right)dx \;\middle|\; \boldsymbol{\sigma} \in S_1(\Omega)\right\}.$$

Here σ_I, σ_{II}, $\sigma_I \geq \sigma_{II}$, are principal stresses of $\boldsymbol{\sigma}$ and $S_1(\Omega)$ stands for the set of statically admissible stresses within a bounded plane domain Ω. This domain is parametrized by a Cartesian system $(x_1, x_2); x = (x_1, x_2) \in \Omega$. The loading of

density $\mathbf{p}=\mathbf{p}(x)$ is applied on $\Gamma_1 \subset \partial\Omega$. Thus

$$S_1(\Omega) = \{\boldsymbol{\sigma} \in L^2(\boldsymbol{\Omega}, \mathbb{E}_2^s) \mid \int_\Omega \sigma^{\alpha\beta} v_{\alpha,\beta}\, dx = \int_{\Gamma_1} \mathbf{p} \cdot \mathbf{v}\, ds \quad \forall\, \mathbf{v} \in V_1(\Omega)\},$$

and

$$V_1(\Omega) = \{\mathbf{v} \in H^1(\Omega)^2 \quad \mid \mathbf{v} = \mathbf{0} \quad \text{on} \quad \partial\Omega \setminus \Gamma_1\}.$$

$\mathbb{E}_2^s$ represents the space of symmetric 2×2 matrices and $H^1(\Omega)^2 = [H^1(\Omega)]^2$. The problem (P_1) can be found in ROZVANY [17, p.48] and was developed by STRANG and KOHN [18]. The problem dual to (P_1) is equivalent to the original MICHELL setting [14].

A natural counterpart of the above plane elasticity problem for the antiplane case, where the structure should carry a loading perpendicular to its plane, reads

$$(P_2) \qquad \inf \left\{ \int_\Omega (|M_I| + |M_{II}|) dx \quad \mid \mathbf{M} \in S_2(\Omega) \right\}$$

where $S_2(\Omega)$ represents a set of statically admissible moments $\mathbf{M}$ or

$$S_2(\Omega) = \{\mathbf{M} \in L^2(\Omega; \mathbb{E}_2^s) \mid \int_\Omega M^{\alpha\beta} v_{,\alpha\beta}\, dx + \int_{\Gamma_1} (Q^0 v - M^0 \frac{\partial v}{\partial \mathbf{n}}) ds = 0 \ \forall v \in V_2(\Omega)\}$$

where

$$V_2(\Omega) = \left\{ v \in H^2(\Omega) \mid \quad v = 0, \quad \frac{\partial v}{\partial \mathbf{n}} = 0 \quad \text{on} \quad \partial\Omega \setminus \Gamma_1 \right\}.$$

Here $\mathbf{n}$ is a unit vector outward normal to $\partial\Omega$. The boundary loading Q^0, M^0 is assumed here along $\Gamma_1 \subset \Omega$ and the plate is clamped on $\Gamma_0 = \partial\Omega \setminus \Gamma_1$.

Several exact solutions to the problem (P_2) have been found by Prager, Rozvany and their collaborators, see ROZVANY[17].

In 1993 ALLAIRE and KOHN [1] showed that the problem (P_1) can be obtained by admitting the volume of a structure to be smaller and smaller in the minimum compliance shape design within the linear elasticity framework. This passage to a limit leads to the formulation (P_1) free of any elastic characteristics, see Remark 28.4.2 in LEWIŃSKI and TELEGA [11].

The above results suggest that the problem (P_2) can be achieved by imposing the condition of the volume being small in the shape design problem for a thin

plate. But this is not the case. The present authors proved in Sec. 26.9 of [11] that the condition of the volume being small results in a new formulation

$$(P_3) \qquad \inf\left\{\int_\Omega \left[\frac{1-\nu}{1+\nu}(\mathrm{tr}\mathbf{M})^2 + (|M_I| + |M_{II}|)^2\right]^{\frac{1}{2}} dx \,|\, \mathbf{M} \in S_2(\Omega)\right\},$$

where ν represents the Poisson ratio. It is seen that only for $\nu = 1$ the problem (P_3) assumes the form (P_2) Note, however, that in both the formulations (P_2) and (P_3) the integrand is of linear growth.

All the available analytical and numerical solutions to the problems (P_1), (P_2) are based on the formulations dual to them. The formulation dual to (P_1) reads, see STRANG and KOHN [18],

$$(P_1^*) \qquad \sup\{\int_{\Gamma_1} \mathbf{p}\cdot\mathbf{v}\, ds \quad |\boldsymbol{\epsilon}(\mathbf{v}) \in B_1\}$$

where

$$B_1 = \{\boldsymbol{\epsilon} \in \mathbb{E}_s^2 \Big| \quad |\epsilon_I| \leq 1, \quad |\epsilon_{II}| \leq 1\}$$

and $\boldsymbol{\epsilon}(\mathbf{v}) = (\epsilon_{\alpha\beta}(\mathbf{v}))$, where

$$(1.1) \qquad \epsilon_{\alpha\beta}(\mathbf{v}) = \frac{1}{2}\left(\frac{\partial v_\alpha}{\partial x_\beta} + \frac{\partial v_\beta}{\partial x_\alpha}\right).$$

Thus B_1 is a square in the $(\epsilon_I, \epsilon_{II})$-plane. By analogy, the problem (P_2^*) assumes the form

$$(P_2^*) \qquad \sup\{\int_{\Gamma_1} (Q^\circ v - M^\circ \frac{\partial v}{\partial \mathbf{n}})ds \quad | \quad \boldsymbol{\kappa}(v) \in B_2\}$$

with

$$B_2 = \{\boldsymbol{\kappa} \in \mathbb{E}_s^2 \Big| \quad |\kappa_I| \leq 1, \quad |\kappa_{II}| \leq 1\},$$

and

$$(1.2) \qquad \kappa_{\alpha\beta}(v) = -\frac{\partial^2 v}{\partial x_\alpha \partial x_\beta}.$$

The aim of the present paper is to derive the dual problem (P_3^*). Since the integrand in (P_3) is of linear growth, it is clear that the dual formulation should

be similar to (P_2^*) but with the set B_2 replaced with a new set B. Just this convex set B will be explicitly constructed.

The problem (P_3^*) constructed in this manner can be viewed as a locking problem, see ČYRAS [4], DEMENGEL AND SUQUET [7] , JEMIOŁO and TELEGA [9]. The aim of the present paper is also to exploit the locking nature of the problem (P_3) thus showing its new physical interpretation and proving its well-posedness. This naturally leads to perfectly-locking and elastic-locking plates. We will also propose a theory of such shells. Our considerations imply that in the problem (P_1) the quantities $(\sigma^{\alpha\beta})$ denote not the stress tensor but the stress rate tensor, a fact usually overlooked in the relevant literature. Similarly in (P_2) and (P_3) the quantity $\mathbf{M} = (M^{\alpha\beta})$ is to be viewed as the rate of couple resultants. Our first results on plates of small volume were announced in [22], [20]. The results formulated in these two contributions need refinements, particularly the form of B.

2. Two-phase layout optimization of thin elastic plates

The classical layout problem for thin elastic plates consists in looking for an in-plane optimal distribution of *two isotropic materials*, of prescribed volumes, that realizes minimum of the total compliance. To be more specific, let us assume that the α-th material is characterized by the bulk and shear moduli $\hat{k}_\alpha, \hat{\mu}_\alpha, \alpha = 1, 2$. Let the thickness of the plate h be fixed. Thus the bending stiffness tensor of the α-th phase assumes the form

$$\mathbf{D}_\alpha = 2k_\alpha \mathbf{I}_1 + 2\mu_\alpha \mathbf{I}_2, \tag{2.1}$$

where

$$k_\alpha = \frac{h^3}{12}\hat{k}_\alpha, \quad \mu_\alpha = \frac{h^3}{12}\hat{\mu}_\alpha \tag{2.2}$$

and the tensors $\mathbf{I}_\alpha$ are defined by

$$I_1^{\alpha\beta\lambda\mu} = \frac{1}{2}\delta^{\alpha\beta}\delta^{\lambda\mu}, \qquad I_2^{\alpha\beta\lambda\mu} = \frac{1}{2}(\delta^{\alpha\lambda}\delta^{\beta\mu} + \delta^{\alpha\mu}\delta^{\beta\lambda} - \delta^{\alpha\beta}\delta^{\lambda\mu}). \tag{2.3}$$

The compliance tensor $\mathbf{C}_\alpha = \mathbf{D}_\alpha^{-1}$ is represented by

$$\mathbf{C}_\alpha(x) = \frac{1}{2}K_\alpha(x)\mathbf{I}_1 + \frac{1}{2}L_\alpha(x)\mathbf{I}_2 \tag{2.4}$$

where

$$K_\alpha = 1/k_\alpha, \qquad L_\alpha = 1/\mu_\alpha. \tag{2.5}$$

For simplicity, the assumption of ordering is usually assumed

$$k_2 > k_1, \qquad \mu_2 > \mu_1, \tag{2.6}$$

hence the terms $\mathbf{D}_2 - \mathbf{D}_1$ and $\mathbf{C}_1 - \mathbf{C}_2$ are positive definite and invertible. Assume that the α-th material covers the domain Ω_α, hence $\bar{\Omega}_1 \cup \bar{\Omega}_2 = \bar{\Omega}, \Omega_1 \cap \Omega_2 = \varnothing$. Let $\chi_\alpha(x) = \chi_{\Omega_\alpha}(x)$ be the characteristic function of Ω_α. The bending stiffness tensor has the form

$$\mathbf{D}(x) = \chi_1(x)\mathbf{D}_1 + \chi_2(x)\mathbf{D}_2. \tag{2.7}$$

Let us impose the isoperimetric condition

$$|\Omega_2| = \int_\Omega \chi_2(x)dx = c_2 \tag{2.8}$$

and $|\Omega_1| = |\Omega| - c_2$. Assume that the plate is subjected along Γ_1 to the transverse boundary loading $Q^0(s)$ and the boundary moment $M^0(s)$, (s) being the natural parameter of $\Gamma = \partial\Omega$.

Let us define the linear form, being the loading functional, by

$$f(v) = \int_{\Gamma_1} \left(M_n^0 \left(-\frac{\partial v}{\partial \mathbf{n}} \right) + Q^0 v \right) ds. \tag{2.9}$$

One can also assume that $\Gamma_1 = \partial\Omega$ and then we additionally assume that

$$f(v) = 0 \qquad \forall v \in \mathcal{R}$$

with

$$\mathcal{R} = \{v| \qquad v = v_\circ + \alpha_1 x_1 + \alpha_2 x_2\}, \qquad v_\circ, \alpha_1, \alpha_2, \in \mathbb{R}.$$

Note that $\boldsymbol{\kappa}(v) = \mathbf{0}$ for $v \in \mathcal{R}$; here $\boldsymbol{\kappa}(v) = (\kappa_{\alpha\beta}(v))$, see Eq.(1.2). Let us define the bilinear form

$$a(w, v) = \int_\Omega \kappa_{\alpha\beta}(w) D^{\alpha\beta\lambda\mu}(x) \kappa_{\lambda\mu}(v) dx, \tag{2.10}$$

with $\mathbf{D}$ being given by (2.7). Let w_{χ_2} be a solution to the equilibrium problem

$$(\mathrm{P}_{\chi_2}) \qquad \left| \quad a(w_{\chi_2}, v) = f(v) \qquad \forall v \in V_2(\Omega). \right.$$

The minimum compliance problem reads:

Find $\bar{\chi}_2$ such that

$$(\mathrm{P}) \qquad f(w_{\bar{\chi}_2}) = \min\{f(w_{\chi_2}) |\ w_{\chi_2} \text{ solves } (P_{\chi_2}) \text{ with } \int_\Omega \chi_2(x)dx = c_2\}.$$

It is well-known that the above problem needs a relaxation, see LIPTON [12], TELEGA and LEWIŃSKI [21], LEWIŃSKI and TELEGA [11]. The relaxation means replacing:

$$\chi_\alpha \text{ by } m_\alpha \in L^\infty(\Omega; [0,1]) \quad \text{and } \mathbf{D} \text{ by } \mathbf{D}_h,$$

where $\mathbf{D}_h$ represents the effective bending stiffness tensor of a composite plate in which the area fractions of both materials are equal to m_1 and m_2 , respectively. Moreover, the isoperimetric condition (2.8) is replaced by

$$\int_\Omega m_2(x)dx = c_2. \tag{2.11}$$

The stiffness tensor $\mathbf{D}_h$ is determined by the formula of homogenization. Moreover, one can prove that $\mathbf{D}_h$ is fully characterized by periodic composites, see RAITUMS [15] and LEWIŃSKI and TELEGA [11]. This feature makes the formula for $\mathbf{D}_h$ explicit and, consequently, makes it possible to introduce the relaxed formulation $(\tilde{\mathrm{P}})$ of (P) in a constructive manner. Since all details of posing the relaxed problem $(\tilde{\mathrm{P}})$ can be found in LEWIŃSKI and TELEGA [11, Secs. 26.2, 26.3] there is no need to rewrite the details. It is sufficient to recall that in the first step we apply the Castigliano theorem and then reformulate the problem by the translation method of GIBIANSKY and CHERKAEV, see [11].

The relaxed formulation of the minimum compliance problem for two-phase thin plates assumes eventually the form

$$(\tilde{\mathrm{P}}) \qquad \min\{F(m_2) + \lambda \int_\Omega m_2(x)dx \,|\, m_2 \in L^\infty(\Omega; [0,1])\}.$$

Here λ is a multiplier associated with the isoperimetric condition (2.11) and

$$F(m_2) = 2 \min_{\mathbf{M} \in S_2(\Omega)} \int_\Omega \mathcal{W}^*(\mathbf{M}(x), m_2(x))dx. \tag{2.12}$$

The potential $\mathcal{W}^*$ is defined as follows:

$$\mathcal{W}^*(\mathbf{M}, m_2) = \begin{cases} \dfrac{1}{4} I^2(\mathbf{M}) H(\zeta_M) & \text{if } \ I(\mathbf{M}) \neq 0, \\ \dfrac{1}{4} \{L\}_m II^2(\mathbf{M}) & \text{if } \ I(\mathbf{M}) = 0. \end{cases} \tag{2.13}$$

The following notation has been introduced:

$$I(\mathbf{M}) = \frac{1}{\sqrt{2}}\mathrm{tr}(\mathbf{M}), \quad II(\mathbf{M}) = \frac{1}{\sqrt{2}}[(\mathrm{tr}(\mathbf{M}))^2 - 4\det\mathbf{M}]^{1/2}, \tag{2.14}$$

$$\{L\}_m = (m_1 L_1^{-1} + m_2 L_2^{-1})^{-1}, \tag{2.15}$$

$$\zeta_M = \frac{II(\mathbf{M})}{|I(\mathbf{M})|} \tag{2.16}$$

or

$$\zeta_M = \frac{|M_I - M_{II}|}{|M_I + M_{II}|}.$$

The function $H(\zeta)$ is defined as follows:

$$H(\zeta) = \begin{cases} H_L(\zeta) & \text{if} \quad \zeta \in [0, \zeta_2], \\ H_i(\zeta) & \text{if} \quad \zeta \in [\zeta_2, \zeta_1], \\ H_R(\zeta) & \text{if} \quad \zeta \geq \zeta_1. \end{cases} \tag{2.17}$$

Here

$$\zeta_1 = \frac{[L]_m \triangle K}{[K]_m \triangle L}, \quad \zeta_2 = \frac{m_2 \triangle K}{[K]_m + L_2}, \tag{2.18}$$

and

$$[f]_m = m_1 f_2 + m_2 f_1, \quad \triangle f = |f_2 - f_1|, \quad f \in \{K, L\}. \tag{2.19}$$

Moreover,

$$H_L(\zeta) = a_L + c_L\zeta^2, \quad H_R(\zeta) = a_R + c_R\zeta^2,$$

$$\begin{aligned} H_i(\zeta) &= H_L(\zeta) + A_L(\zeta - \zeta_2)^2, \\ H_i(\zeta) &= H_R(\zeta) + A_R(\zeta - \zeta_1)^2, \end{aligned} \tag{2.20}$$

where

$$a_L = \frac{< K >_m L_2 + K_1 K_2}{L_2 + [K]_m}, \quad a_R = \{K\}_m, \quad c_L = L_2, \quad c_R = \{L\}_m, \tag{2.21}$$

$$\begin{aligned} A_L &= \frac{m_1 \triangle L (L_2 + [K]_m)}{[K]_m + [L]_m}, \\ A_R &= \frac{m_1 m_2 (\triangle L)^2 [K]_m}{[L]_m ([K]_m + [L]_m)}, \end{aligned} \tag{2.22}$$

and

$$< f >_m = m_1 f_1 + m_2 f_2, \quad f \in \{K, L\}.$$

Let us note that (2.12) may be viewed as an equilibrium problem of a non-linearly elastic plate with a smooth potential $\mathcal{W}^*$.

3. Shape design of a thin plate

The notion of *shape design* means that only one material is at our disposal and we should arrange a given amount of this material to form the stiffest plate. Thus it suffices to put $k_1 = 0$ and $\mu_1 = 0$ into the problem $(\tilde{\mathrm{P}})$ and observe that this substitution is admissible. Then we obtain

$$\mathcal{W}^*(\mathbf{M}, m_2) = \begin{cases} \dfrac{1}{4} I^2(\mathbf{M}) H_0(\zeta_M) & \text{if} \quad I(\mathbf{M}) \neq 0, \\ \dfrac{1}{4m_2} L_2 II^2(\mathbf{M}) & \text{if} \quad I(\mathbf{M}) = 0, \end{cases} \tag{3.1}$$

where

$$H_0(\zeta) = \begin{cases} \dfrac{1}{m_2}(K_2 + m_1 L_2) + L_2 \zeta^2 & \text{if} \quad \zeta \in [0, 1], \\ \dfrac{1}{m_2}(K_2 + L_2 \zeta^2) & \text{if} \quad \zeta \geq 1. \end{cases} \tag{3.2}$$

Note that the conditions

$$\zeta_M \in [0, 1], \quad \zeta_M \geq 1, \tag{3.3}$$

are equivalent to

$$\det \mathbf{M} \geq 0, \quad \det \mathbf{M} \leq 0. \tag{3.4}$$

The function $H(\zeta)$ was smooth but $H_0(\zeta)$ is not. It is continuous but has a cusp at $\zeta = 1$.

The formula (3.1) can be expressed by a concise formula

$$\mathcal{W}^*(\mathbf{M}, m_2) = \mathcal{W}_0^*(\mathbf{M}) + \frac{1 - m_2}{4\, m_2}[K_2 I^2(\mathbf{M}) + L_2 u(\mathbf{M})] \tag{3.5}$$

where $\mathcal{W}_0^*(\mathbf{M})$ given by

$$\mathcal{W}_0^*(\mathbf{M}) = \frac{1}{4} K_2 I^2(\mathbf{M}) + \frac{1}{4} L_2 II^2(\mathbf{M}), \tag{3.6}$$

represents the potential of a virgin plate and the function $u(\mathbf{M})$ is defined by

$$u(\mathbf{M}) = \begin{cases} II^2(\mathbf{M}) & \text{if} \quad \det(\mathbf{M}) \leq 0, \\ I^2(\mathbf{M}) & \text{if} \quad \det(\mathbf{M}) \geq 0, \end{cases} \tag{3.7}$$

or

$$u(\mathbf{M}) = \frac{1}{2}(|M_I| + |M_{II}|)^2. \tag{3.8}$$

Thus the expression(3.5) can be rearranged to the form

$$\mathcal{W}^*(\mathbf{M}, m_2) = \mathcal{W}_0^*(\mathbf{M}) + \frac{1 - m_2}{2\, m_2} g(\mathbf{M}), \tag{3.9}$$

with

$$g(\mathbf{M}) = \frac{1}{4} K_2 (M_I + M_{II})^2 + \frac{1}{4} L_2 (|M_I| + |M_{II}|)^2. \tag{3.10}$$

Let us put (3.9) into $(\tilde{P})$ and interchange the order of minima. One finds

$$\min_{\mathbf{M} \in S_2(\Omega)} \int_{\Omega} F_\lambda(\mathbf{M}) dx \tag{3.11}$$

where

$$F_\lambda(\mathbf{M}) = \min_{0 \leq m_2 \leq 1} [2\mathcal{W}^*(\mathbf{M}, m_2) + \lambda m_2]. \tag{3.12}$$

Minimization over m_2 can be performed analytically. Finally we arrive at

$$F_\lambda(\mathbf{M}) = 2\mathcal{W}_0^*(\mathbf{M}) + \begin{cases} 2[\lambda g(\mathbf{M})]^{1/2} - g(\mathbf{M}) & \text{if} \quad g(\mathbf{M}) \leq \lambda, \\ \lambda & \text{if} \quad g(\mathbf{M}) \geq \lambda. \end{cases} \tag{3.13}$$

The minimization problem (3.11) with the integrand of the form (3.13) is well-posed; its solution exists, see LEWIŃSKI and TELEGA [11, Sec.26.7].

4. Shape design of thin plates of small volume

The relaxed formulation (3.11) of the shape design problem of thin plates can serve as a starting point for finding the shape design formulation of plates of very small volume. The compliance minimization assumes a peculiar form. In such a case the material tries to carry the loading by very thin, continuously distributed ribs.

4.1. Compliance minimization problem

The solutions to the problem (3.11) become exteremely interesting if the given amount of the material is very small. In such a case the optimum plates degenerate to grillages forming ribbed structures or fans. The condition of small volume implies that the multiplier λ is very large. Thus the region $g(\mathbf{M}) > \lambda$ will be absent and for large values of λ, the main term of $F_\lambda(\mathbf{M})$ has the form

$$F_\lambda(\mathbf{M}) = 2\lambda^{1/2}[g(\mathbf{M})]^{1/2}. \tag{4.1}$$

Since only one material is at our disposal, we shall simplify the notation by writing $k_2 = k, \quad \mu_2 = \mu, \quad \nu_2 = \nu, \quad K_2 = K, \quad L_2 = L.$

Consequently, the problem (3.11) assumes the form

$$(\hat{\mathrm{P}}) \qquad \inf_{\mathbf{M}\in S_2(\Omega)} \int_\Omega [K(M_I + M_{II})^2 + L(|M_I| + M_{II}|)^2]^{1/2} dx.$$

We set

$$G(\mathbf{M}) = [K(M_I + M_{II})^2 + L(|M_I| + |M_{II}|)^2]^{1/2}, \quad \mathbf{M} \in \mathbb{E}_2^s.$$

A straightforward calculation shows that

$$G_\infty(\mathbf{M}) = G(\mathbf{M}), \ \mathbf{M} \in \mathbb{E}_2^s,$$

where G_∞ denotes the so-called recession function of G defined by, cf. LEWIŃSKI and TELEGA [11], ROCKAFELLAR [16],

$$G(\mathbf{M}) := \lim_{t\to\infty} \frac{1}{t} G(t\mathbf{M}).$$

It means that the stiffest plate of small volume exhibits perfectly-locking behaviour. Since $K/L = \mu/k$ and $\nu = (k-\mu)/(k+\mu)$ one finds: $K/L = (1-\nu)/(1+\nu)$ and the problem $(\hat{\mathrm{P}})$ assumes the form (P_3) mentioned in the Introduction.

Let us consider the level lines of the integrand of $(\hat{\mathrm{P}})$ in the plane (M_I, M_{II}). Let us introduce the polar representation

$$M_I = r\cos\vartheta, \quad M_{II} = r\sin\vartheta \tag{4.2}$$

into the condition

$$\left[\frac{1-\nu}{1+\nu}(M_I + M_{II})^2 + (|M_I| + |M_{II}|)^2\right]^{1/2} = \text{const.} \tag{4.3}$$

Hence we find

$$M_I = M_0 \frac{\cos\vartheta}{\left[1 + \frac{1-\nu}{1+\nu}(1+\sin 2\vartheta) + |\sin 2\vartheta|\right]^{1/2}}, \tag{4.4}$$

$$M_{II} = M_0 \frac{\sin\vartheta}{\left[1 + \frac{1-\nu}{1+\nu}(1+\sin 2\vartheta) + |\sin 2\vartheta|\right]^{1/2}},$$

and M_0 is a constant. Assume that $M_0 = 1$. For $\nu = 1$ the contour (4.4) forms a square, of the side $\sqrt{2}$, rotated by $\pi/4$, see Fig.1. For each $\nu \in [0,1]$ the contours in the quarters $M_I M_{II} > 0$ are straight lines parallel to the line: $M_I + M_{II} = 1$.

For $\nu = 0$ the contour (4.4), in the quarters $M_I M_{II} < 0$, becomes a circle of radius $\sqrt{2}/2$, see Fig.1.

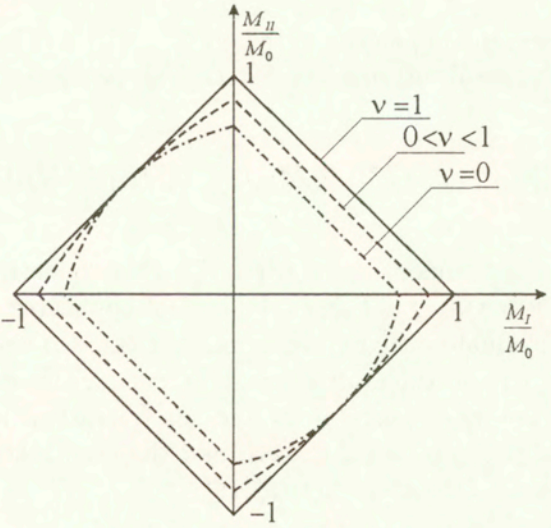

FIG. 1. Level lines of the integrand of problem $(\hat{\mathrm{P}})$

4.2. Dual formulation of ($\hat{\mathrm{P}}$)

It is highly convenient to rearrange the problem ($\hat{\mathrm{P}}$) to its dual form involving kinematic variables. Note first that $\hat{\mathrm{P}}$ represents a locking problem in which $\mathbf{M}$ is not a moment field but rather a moment rate.

Let us disclose the equilibrium equation concealed in $S_2(\Omega)$ in a standard manner:

$$\inf_{\mathbf{M}\in L^2(\Omega;\mathbb{E}_2^s)} \sup_{v\in V_2} \left\{ \int_\Omega \{[K(M_I+M_{II})^2 + L(|M_I|+|M_{II}|)^2]^{1/2}\}dx - \int_\Omega \mathbf{M} : \boldsymbol{\kappa}(v)dx + f(v) \right\} \tag{4.5}$$

where $\mathbf{M} : \boldsymbol{\kappa}(v) = M^{\alpha\beta}\kappa_{\alpha\beta}$. Note that v plays simultaneously two roles: it is a trial field of the variational equilibrium equation and the Lagrangian multiplier. The operations inf and sup can be formally interchanged and thus we arrive at

$$\sup_{v\in V_2(\Omega)} \{f(v) + \int_\Omega R(\boldsymbol{\kappa}(v))dx\} \tag{4.6}$$

with

$$R(\boldsymbol{\kappa}) = \inf_{\mathbf{M}\in\mathbb{E}_2^s} \{[K(M_I+M_{II})^2 + L(|M_I|+|M_{II}|)^2]^{1/2} - \mathbf{M} : \boldsymbol{\kappa}\}. \tag{4.7}$$

Since the integrand appearing in the problem ($\hat{\mathrm{P}}$) is of linear growth therefore inf $\hat{\mathrm{P}}$ is not, in general, attained in $S_2(\Omega)$. The problem ($\hat{\mathrm{P}}$) is convex but the functional

$$J(\mathbf{M}) = \int_\Omega [K(M_I+M_{II})^2 + L(|M_I|+|M_{II}|)^2]^{1/2}dx$$

is not lower semicontinuous over $L^2(\Omega,\mathbb{E}_2^s)$ Consequently, minimax theorems expounded in EKELAND and TEMAM [8] are not applicable to our case. However, one can apply the duality theory presented in EKELAND and TEMAM [8] directly to the problem ($\hat{\mathrm{P}}$) and then, after standard calculation, we get (4.6) and (4.7). In this manner the interchange of inf and sup operations is justified. Note that the integrand of ($\hat{\mathrm{P}}$) is of linear growth and the dual function $R(\boldsymbol{\kappa})$ must have the following form, cf. ROCKAFELLAR [16],

$$R(\boldsymbol{\kappa}) = \begin{cases} 0 & \text{if } \boldsymbol{\kappa}\in B, \\ -\infty & \text{otherwise.} \end{cases} \tag{4.8}$$

Here B is a convex set containing $\boldsymbol{\kappa} = \mathbf{0}$ in its interior. This set, defining the locking locus, can be explicitly constructed. The construction is the subject of the next section.

Thus the problem (4.6) takes the form

$$(\hat{\mathrm{P}}^*) \qquad \sup\{f(v) | v \in V_2(\Omega), \quad \boldsymbol{\kappa}(v(x)) \in B \quad \text{for a.e.} \quad x \in \Omega\}.$$

Existence theorems, for the problems $\hat{\mathrm{P}}$ and $\hat{\mathrm{P}}^*$, will be formulated in Sec.5.

4.3. Geometry of the set B

The aim of this section is to analyze the problem (4.7) and find the explicit form of the set B.

STEP 1. We show first that minimum in (4.7) is attained by a matrix $\mathbf{M}$ of principal directions (x_α^M) coinciding with the principal directions (x_α^κ) of the tensor $\boldsymbol{\kappa}$. We consider three coordinate systems: $(x_1, x_2), (x_1^\kappa, x_2^\kappa), (x_1^M, x_2^M)$, see Fig. 2, where the angles α_κ and α_M are depicted.

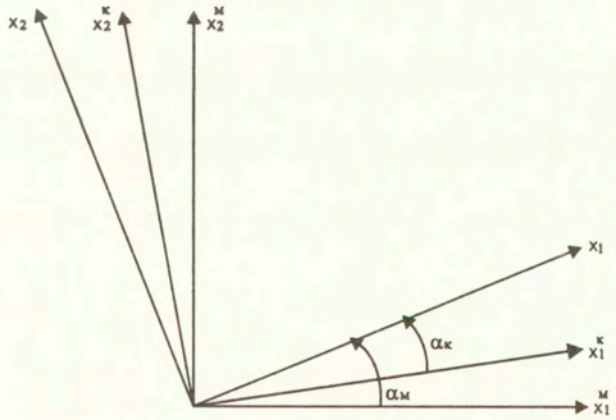

FIG. 2. The axes x_α versus principal directions of $\boldsymbol{\kappa}$ and $\mathbf{M}$

The components of $\boldsymbol{\kappa}$ are represented by the classical formulae

$$\kappa_{11} = \frac{1}{2}[(\kappa_I + \kappa_{II}) + (\kappa_1 - \kappa_{II}) \cos 2\alpha_\kappa],$$

$$\kappa_{22} = \frac{1}{2}[(\kappa_I + \kappa_{II}) - (\kappa_1 - \kappa_{II}) \cos 2\alpha_\kappa], \tag{4.9}$$

$$\kappa_{12} = -\frac{1}{2}(\kappa_I - \kappa_{II}) \sin 2\alpha_\kappa,$$

and the components M^{11}, M^{22}, M^{12} are represented similarly, in terms of M_I, M_{II} and α_M. We assume: $\kappa_I \geq \kappa_{II}, M_I \geq M_{II}$. We calculate

$$\mathbf{M} : \boldsymbol{\kappa} = M^{\alpha\beta}\kappa_{\alpha\beta} = \kappa_I M_I + \kappa_{II} M_{II} - \sin^2(\alpha_M - \alpha_\kappa)(M_I - M_{II})(\kappa_I - \kappa_{II}). \tag{4.10}$$

Thus (4.7) can be expressed as follows:

$$R(\boldsymbol{\kappa}) = \min_{M_I, M_{II}} \Big\{ \min_{\alpha_M} \{[K(M_I + M_{II})^2 + L(|M_I| + |M_{II}|)^2]^{1/2} - (\kappa_I M_I + \kappa_{II} M_{II}) + \sin^2(\alpha_M - \alpha_\kappa)(M_I - M_{II})(\kappa_I - \kappa_{II})\} \Big\}. \tag{4.11}$$

Minimum over α_M is attained for $\alpha_M = \alpha_\kappa$ since $(M_I - M_{II})(\kappa_I - \kappa_{II}) > 0$. Thus the principal directions of $\mathbf{M}$ coincide with the principal directions of $\boldsymbol{\kappa}$.

STEP 2. The function $R(\boldsymbol{\kappa})$ can be put in the form

$$R(\boldsymbol{\kappa}) = \min_{\bar{x}, \bar{y} \in \mathbb{R}} \{[K(\bar{x} + \bar{y})^2 + L(|\bar{x}| + |\bar{y}|)^2]^{1/2} - \bar{x}\kappa_I - \bar{y}\kappa_{II}\} \tag{4.12}$$

since now it is unimportant that M_I, M_{II} in (4.11) are principal values of a certain matrix of $\mathbb{E}_2^s$.

Let us change the variables

$$\sqrt{L}\,\bar{x} = x, \quad \sqrt{L}\,\bar{y} = y, \quad \kappa_I/\sqrt{L} = \varkappa_I, \quad \kappa_{II}/\sqrt{L} = \varkappa_{II}, \tag{4.13}$$

to obtain

$$R(\sqrt{L}\boldsymbol{\varkappa}) = \min_{x, y \in \mathbb{R}} \{[\gamma(x + y)^2 + (|x| + |y|)^2]^{1/2} - x\varkappa_I - y\varkappa_{II}\}, \tag{4.14}$$

where

$$\gamma = K/L, \quad \gamma = \frac{1 - \nu}{1 + \nu}, \quad \nu \in [0, 1]. \tag{4.15}$$

Let us introduce the polar representation

$$\begin{aligned} x &= r\cos\vartheta, \quad y = r\sin\vartheta, \quad r \geq 0, \\ \varkappa_I &= k\cos\varphi, \quad \varkappa_{II} = k\sin\varphi, \quad k \geq 0. \end{aligned} \tag{4.16}$$

Let $R(\sqrt{L}\boldsymbol{\varkappa}) = \tilde{R}(k, \varphi)$,where

$$\tilde{R}(k, \varphi) = \min_{\substack{r \geq 0 \\ \vartheta \in \mathbb{R}}} r\{[1 + \gamma(1 + \sin 2\vartheta) + |\sin 2\vartheta|]^{1/2} - k\cos(\vartheta - \varphi)\} \tag{4.17}$$

Further we introduce an auxiliary function

$$h(\varphi) = \min_{\vartheta \in \mathbb{R}} \frac{[1 + \gamma(1 + \sin 2\vartheta) + |\sin 2\vartheta|]^{1/2}}{|\cos(\vartheta - \varphi)|}. \tag{4.18}$$

Here γ is treated as a parameter. We note that

$$\tilde{R}(k, \varphi) = \begin{cases} 0 & \text{if} \quad k \leq h(\varphi)|, \\ -\infty & \text{otherwise.} \end{cases} \tag{4.19}$$

Consequently,

$$R(\boldsymbol{\kappa}) = \begin{cases} 0 & \text{if} \quad \|\boldsymbol{\kappa}\| \leq \sqrt{L}\, h(\varphi) \\ -\infty & \text{otherwise,} \end{cases} \tag{4.20}$$

where $\|\boldsymbol{\kappa}\| = \sqrt{(\kappa_I)^2 + (\kappa_{II})^2}$ and $\varphi = \operatorname{arctg}(\kappa_{II}/\kappa_I)$. Thus we have

$$R(\boldsymbol{\kappa}) = \begin{cases} 0 & \text{if} \quad \boldsymbol{\kappa} \in B \\ -\infty & \text{otherwise,} \end{cases} \tag{4.21}$$

and the locking locus observed in the plane (κ_I, κ_{II}), denoted by $\tilde{B}$, has the form

$$\tilde{B} = \{(\kappa_I, \kappa_{II}) \;\Big|\; \| \boldsymbol{\kappa} \| \leq r(\varphi), \quad \varphi = \operatorname{arctg}(\frac{\kappa_{II}}{\kappa_I})\} \tag{4.22}$$

and

$$r(\varphi) = \sqrt{L}\, h(\varphi), \quad r(\varphi) = \sqrt{L + K}\, \tilde{h}(\varphi), \tag{4.23}$$

with

$$\tilde{h}(\varphi) = \Big(\frac{L}{L + K}\Big)^{1/2} h(\varphi). \tag{4.24}$$

The function $\tilde{h}(\varphi)$ assumes the form (a detailed derivation is given in the Appendix)

$$\tilde{h}(\varphi) = \begin{cases} \dfrac{1}{\sin \varphi} & \text{if} \quad \dfrac{\pi}{4} \leq \varphi \leq \dfrac{\pi}{2} + \beta, \\ \left[\dfrac{1 - \nu^2}{1 + \nu \sin 2\varphi}\right]^{1/2} & \text{if} \quad \dfrac{\pi}{2} + \beta \leq \varphi \leq \dfrac{3}{4}\pi, \end{cases} \tag{4.25}$$

where $\operatorname{tg}\beta = \nu$ or $\beta = \operatorname{arctg}\nu$.

Note that for $\frac{\pi}{4} \leq \varphi \leq \frac{\pi}{2} + \beta$ the contour of $\tilde{B}$ is a line $\kappa_{II} = \sqrt{L+K}$. For greater φ the contour becomes a curve. For $\varphi = \frac{3}{4}\pi$ we have $\tilde{h} = \sqrt{1+\nu}$. For all $\nu \in [0,1]$ the relevant locking locus has a corner at $\kappa_I = \kappa_{II}$ and is smooth for $\varphi = \frac{\pi}{2} + \beta$. Indeed, one can check that

$$
\begin{aligned}
&\tilde{h}\left((\frac{\pi}{2}+\beta)^-\right) = \tilde{h}\left((\frac{\pi}{2}+\beta)^+\right) = \sqrt{1+\nu^2}, \\
&\frac{d\tilde{h}}{d\varphi}\left((\frac{\pi}{2}+\beta)^-\right) = \frac{d\tilde{h}}{d\varphi}\left((\frac{\pi}{2}+\beta)^+\right) = \nu\sqrt{1+\nu^2},
\end{aligned} \tag{4.26}
$$

which confirms that stitching at $\varphi = \frac{\pi}{2} + \beta$ is smooth. For the limit case $\nu = 0$ we have $\beta = 0$ and hence

$$
\tilde{h}(\varphi) = \begin{cases} \dfrac{1}{\sin\varphi} & \text{if} \quad \dfrac{\pi}{4} \leq \varphi \leq \dfrac{\pi}{2}, \\ 1 & \text{if} \quad \dfrac{\pi}{2} \leq \varphi \leq \dfrac{3}{4}\pi. \end{cases} \tag{4.27}
$$

For the limit case $\nu = 1$ we get

$$
\tilde{h}(\varphi) = \frac{1}{\sin\varphi}, \quad \frac{\pi}{4} \leq \varphi \leq \frac{3}{4}\pi. \tag{4.28}
$$

Those two extreme shapes of $\tilde{B}$ are depicted in Fig.3, where $\tilde{\kappa}_\alpha = \kappa_\alpha (L+K)^{-1/2}, \alpha = I, II$.

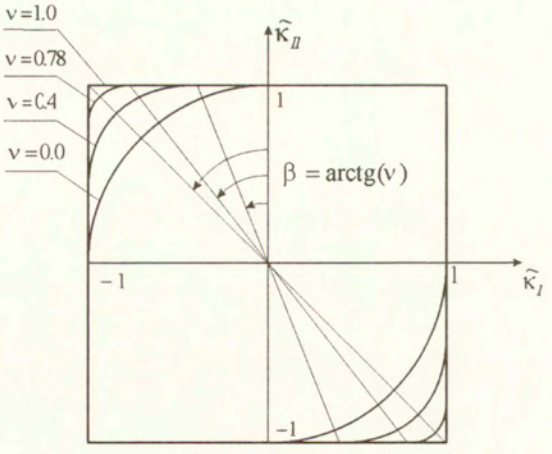

FIG. 3. Shapes of the locking loci $\tilde{B}$ for various values of ν

The contours of Figs. 1 and 3 are reciprocal. We note that for $\nu = 0$ the arcs of a circle transform into the same arcs. For $\nu = 1$ we note that the corners in Fig.1 transform into the sides of the square and vice versa, a well-known result of the duality theory. Transformation of the intermediate contours for $0 < \nu < 1$ is more complicated, but is still found analytically.

A correct qualitative characterization of the set B has already been given in TELEGA *et al.* [22]. However, the contours of $\tilde{B}$ for $\det \boldsymbol{\kappa} < 0$ were found there incorrectly. Figure 3 constitutes a refinement of Fig. 1 in [22, 20].

4.4. Mutually dual constitutive relations

The locking locus $\tilde{B}$ is bounded, convex and closed in the space of principal strain measures κ_I, κ_{II}. Similar properties characterize the locking locus B in the space of strain measures $\kappa_{\alpha\beta}$, since $I_B = G^*$. Moreover, $\boldsymbol{\kappa} = \mathbf{0}$ lies in the interior of B ($\mathbf{0} \in \operatorname{int} B$). The constitutive relation for the problem $(\hat{\mathrm{P}}^*)$ of Sec. 4.2 can be put in the subdifferential form

$$\mathbf{M} \in \partial I_B(\boldsymbol{\kappa}), \tag{4.29}$$

where I_B denotes the indicator function of the set B, see EKELAND and TEMAM [8], ROCKAFELLAR [16],

$$I_B(\boldsymbol{\kappa}) = \begin{cases} 0 & \text{if} \quad \boldsymbol{\kappa} \in B, \\ \infty & \text{otherwise.} \end{cases} \tag{4.30}$$

The inverse constitutive relationship is given by

$$\boldsymbol{\kappa} \in \partial \mathrm{G}(\mathbf{M}). \tag{4.31}$$

In (4.29) and (4.31) ∂ denotes subdifferentiation, cf.[16]. We recall that the function $G(\mathbf{M})$ is the integrand of the functional appearing in the problem $(\hat{\mathrm{P}})$, cf. Sec. 4.1 Moreover, by Eq.(3.10), we write $G(\mathbf{M}) = 2\sqrt{g(\mathbf{M})}$. Since λ in Eq.(4.1) is positive, therefore we may write

$$\boldsymbol{\kappa} \in \partial F_\lambda(\mathbf{M}) \qquad <=> \qquad \boldsymbol{\kappa} \in \partial G(\mathbf{M}).$$

Elementary, we also have, cf [16],

$$G(\mathbf{M}) = \sup\{\mathbf{M} : \boldsymbol{\kappa} | \boldsymbol{\kappa} \in B\}, \tag{4.32}$$

which links both the formulations $(\hat{\mathrm{P}})$ and $(\hat{\mathrm{P}})^*$.

Let us pass now to the basic properties of the function G. They are given by

(i) $$G(\mathbf{0}) = 0.$$

(ii) There exist constants $C_1 > C_0 > 0$ such that

$$\forall \mathbf{M} \in \mathbb{E}_2^s, \quad C_0|\mathbf{M}| \leq G(\mathbf{M}) \leq C_1(1 + |\mathbf{M}|).$$

(iii) G is positively homogeneous, i.e. ,

$$G(a\mathbf{M}) = aG(\mathbf{M}) \text{ if } a > 0.$$

Here $|\mathbf{M}| = \sum_{\beta,\alpha=1}^{2} M^{\alpha\beta} M^{\alpha\beta}$.

The proof of properties (i)-(iii) is similar to the procedure used in perfect plasticity for the study of the dissipation density, cf. LEWIŃSKI and TELEGA [11], TEMAM [23].

In the existence study which is the subject of the next section, a particular form of locking locus is not required. General assumptions on a locking locus, still denoted by B, are

(a) $B \subset \mathbb{E}_s^2$ is convex and closed.

(b) There exist $0 < r_1 < r_2 < +\infty$ such that $K(0, r_1) \subset B \subset K(0, r_2)$ where $K(0, r)$ denotes the ball with the centre at zero and with radius r.

The sets B and $\tilde{B}$ derived in Sec.4.3 satisfy (a) and (b). In the general case, the support function G of B is determined by the relation of type (4.32).

5. Existence theorems

In the case of plates with locking extremal problems cannot be formulated in standard manner, as for elastic plates. Let us first solve the problem of existence of transverse displacements. The primal problem is formulated as follows, cf. the problem $(\hat{\mathrm{P}})^*$,

$$(\mathcal{P}) \qquad \sup\{f(w) \,|w \in U, \, \kappa(w(x)) \in B \text{ a.e. } x \in \Omega\}$$

where

$$U = \{w \in V(\Omega) | w = \tilde{u}a_1, \, \partial w/\partial \mathbf{n} = \tilde{u}a_2 \text{ on } \Gamma_1\}$$

Here a_α, $\alpha = 1, 2$, are prescribed functions of $s \in \Gamma_1$ whilst $\tilde{u}$, possibly depending on s, denotes the intensity of generalized boundary displacements $(w, \partial w/\partial \mathbf{n})$. One parameter problem is a specific case, where $m = \tilde{u} \in \mathbb{R}$ is simply a load parameter. In the functional f, Q^0 and M_n^0 are to be viewed as fields of weight multipliers, cf. ČYRAS [4].

THEOREM 1. *Under the assumptions (a) and (b), the maximization problem* $(\mathcal{P})$ *possesses a solution* $\bar{w} \in U$ *provided that*

$$\int_{\Gamma_1} (Q^0 a_1 - M_n^0 a_2)\, ds \neq 0. \tag{5.1}$$

P r o o f. The proof follows the approach used in Demengel and Suquet [7], Demengel [6] for 3D problems. Therefore it suffices to sketch the proof for the plates with locking. Applying the duality theory we prove

$$\sup \mathcal{P} = \inf \mathcal{P}^*, \tag{5.2}$$

where

$$(\mathcal{P}^*) \quad \inf \Big\{ \int_\Omega G(\mathbf{M})\, dx | \mathbf{M} \in L^2(\Omega, \mathbb{E}_2^s),\ \operatorname{divdiv}\mathbf{M} = 0 \text{ a.e. in } \Omega;$$

$$Q = Q^0, M_n = M_n^0 \quad \text{on } \Gamma_1 \Big\},$$

where $M_n = M^{\alpha\beta} n_\alpha n_\alpha$ and Q is the rate of the KIRCHHOFF shear force. To simplify the remaining part of the proof we consider the case of one parameter loading: $w = mw^0$ and $\partial w/\partial \mathbf{n} = mw^1$ on Γ_1. We set, see the formula (5.9) below,

$$U_{ad}(m) = \big\{ w \in H^2(\Omega) | w = 0, \quad \partial w/\partial \mathbf{n} = 0 \quad \text{on} \quad \Gamma_0; \tag{5.3}$$

$$w = mw^0, \quad \partial w/\partial \mathbf{n} = mw^1 \quad \text{on } \Gamma_1 \big\},$$

$$\mathcal{S}_0(\Omega) = \{ \mathbf{M} \in \mathcal{Z}(\Omega, \mathbb{E}_2^s) |\ \operatorname{divdiv}\mathbf{M} = 0 \text{ a.e. in } \Omega \}, \tag{5.4}$$

$$B_g = \big\{ w \in H^2(\Omega) |\quad \boldsymbol{\kappa}(w(x)) \in B \text{ a.e. } x \in \Omega \big\}. \tag{5.5}$$

The locking limit analysis problems assume now the following form:

$$\sup \{ m | B_g \cap U_{ad}(m) \neq \varnothing \}, \tag{Q}$$

$$\inf \Big\{ \int_\Omega G(\mathbf{M})\, dx | \mathbf{M} \in \mathcal{S}_0, \int_{\Gamma_1} (Qw^0 - M_n w^1) ds = 1 \Big\}. \tag{Q*}$$

It can be shown that

$$\sup Q = \inf Q^*.$$

Under the assumption (5.1), which now means that there exists $\tilde{\mathbf{M}} \in \mathcal{S}_0$ such that

$$\int_{\Gamma_1} (\tilde{Q}w^0 - \tilde{M}_n w^1) ds \neq 0, \tag{5.6}$$

we have

$$m_l = \inf Q^* = \sup Q < +\infty. \tag{5.7}$$

Here m_l is the locking limit load. Indeed, it can be shown that if (5.6) is not satisfied then $\inf Q^* = \sup Q = +\infty$. To assess the equality between $\sup Q$ and $\inf Q^*$ one can apply a penalty method, cf. DEMENGEL and SUQUET [7].To this end we introduce the following perturbed problem:

$$\inf \left\{ -m + \frac{1}{\delta} d(\boldsymbol{\kappa}(w), B_d) \,|m \in \mathbb{R}, w \in U_{ad}(m) \right\}, \tag{Q_δ}$$

where

$$B_d = \left\{ \boldsymbol{\varepsilon} \in L^2(\Omega, \mathbb{E}^2_s) | \boldsymbol{\varepsilon}(x) \in B \text{ a.e. } x \in \Omega \right\}.$$

The dual problem means evaluating

$$\sup \left\{ -\int_\Omega G(\mathbf{M})\, ds | \mathbf{M} \in \mathcal{S}_0, \int_{\Gamma_1} (Qw^0 - M_n w^1)\, ds = 1, ||\mathbf{M}||_{L^2(\Omega, \mathbb{E}^s_2)} \leq \frac{1}{\delta} \right\}. \tag{Q^*_δ}$$

Under (5.6) we have

(i) $\inf Q_\delta = \sup Q^*_\delta > -\infty$,

(ii) Q_δ admits a solution,

(iii) $-\inf Q_\delta$ converges to $\sup Q$.

The functional

$$J_\delta(m, w) = -m + \frac{1}{\delta} d(\boldsymbol{\kappa}(w), B_d)$$

is coercive on $H^2(\Omega) \cap U_{ad}(m)$. Consequently, there exists at least one solution (m_δ, w_δ) to the problem (Q_δ). The sequence $\{(m_\delta, w_\delta)\}_{\delta > 0}$ is bounded in $\mathbb{R} \times$

$H^2(\Omega)$ and we can extract a subsequence $\{(m_{\delta'}, w_{\delta'})\}_{\delta'>0}$ such that $m_{\delta'} \to \bar{m}$ in $\mathbb{R}$, $w_{\delta'} \rightharpoonup \bar{w}$ weakly in $H^2(\Omega)$ when $\delta' \to 0$. Finally

$$\limsup(-\inf Q_{\delta'}) = \liminf(-\inf Q_{\delta'}) = \sup Q = \inf Q^* = \bar{m} = m_l.$$

REMARK 1. In fact, the function $\bar{w}$ solving the primal problem $(\mathcal{P})$ or (Q) belongs to a nonreflexive Banach space, cf. DEMENGEL [6],

$$V^\infty(\Omega) = \{v \in L^\infty(\Omega) | \kappa_{\alpha\beta}(v) \in L^\infty(\Omega)\}.$$

□

Let us pass to the study of dual problem (Q*). We introduce the following nonreflexive Banach space:

$$\mathcal{S}(\Omega) = \{\mathbf{M} \in \mathcal{Z}(\Omega, \mathbb{E}_2^s) | \ \mathrm{divdiv}\mathbf{M} \in \mathbb{M}_b(\Omega)\}, \tag{5.8}$$

where $\mathbb{M}_b(\Omega)$ denotes the space of bounded measures on Ω and, cf. DEMENGEL [6],

$$\mathcal{Z}(\Omega, \mathbb{E}_2^s) = \{\mathbf{M} \in \mathbb{M}_b(\Omega, \mathbb{E}_2^s) | \mathrm{div}\mathbf{M} \in L^2(\Omega)^2\}. \tag{5.9}$$

Now the function G is a convex function of the measure, cf. BOUCHITTÉ and VALADIER [3]. We also introduce the relaxed problem

$$\inf\left\{ \int_\Omega G(\mathbf{M})\, dx + m_l \Big| \int_{\Gamma_1} (Qw^o - M_n w^1)\, ds - 1 \Big|, \ \mathbf{M} \in \mathcal{S}(\Omega), \right. \tag{RQ*}$$

$$\left. \mathrm{divdiv}\mathbf{M} = 0 \ \text{ in } \Omega \right\}.$$

THEOREM 2. *From each minimizing sequence of* (Q*) *or* (RQ*) *one can extract a subsequence weak-* convergent in* $\mathbb{M}_b(\Omega, \mathbb{E}_2^s)$ *to a solution of* (RQ*).

To prove the last theorem it suffices to follow the approach elaborated by DEMENGEL [6].

REMARK 2. Let γ be a sufficiently smooth curve in Ω, for instance dividing Ω into subdomains Ω^+ and Ω^- such that $\Omega = \Omega^+ \cup \Omega^- \cup \gamma$. If $\mathbf{M} \in \mathcal{S}(\Omega)$, there exists a couple $(\mathbf{M}_1, \xi) \in L^2(\Omega, \mathbb{E}_2^s) \times HB(\Omega)$ such that, cf. DEMENGEL [6],

(i) $\mathbf{M} = \mathbf{M}_1 + (\mathrm{cof} \bigtriangledown^2 \xi)^t$,

(ii) the mass of $\mathbf{M}$ on γ takes the form $\left[\frac{\partial \xi}{\partial \mathbf{n}}\right] \mathbf{t} \otimes \mathbf{t}$, and

$$M_n = \frac{\partial^2 \xi}{\partial s^2} - \frac{1}{R}\frac{\partial \xi}{\partial \mathbf{n}}, \qquad [M_n] = \frac{1}{R}\left[\frac{\partial \xi}{\partial \mathbf{n}}\right], \tag{5.10}$$

$$M^{\alpha\beta} n_\alpha t_\beta = \frac{\partial}{\partial s}\left(\frac{\partial \xi}{\partial \mathbf{n}}\right) + \frac{1}{R}\frac{\partial \xi}{\partial s}, \qquad [M^{\alpha\beta} n_\alpha t_\beta] = \left[\frac{\partial}{\partial s}\left(\frac{\partial \xi}{\partial \mathbf{n}}\right)\right]. \tag{5.11}$$

Here R is the curvature radius of γ and $\mathbf{t}$ denotes a unit tangent vector, and [q] denotes the jump of q across γ. Obviously, $(\mathrm{cof}\mathbf{A})^t$ is the transpose matrix of the cofactor matrix of $\mathbf{A}$, cf. DACOROGNA [5]. If γ is a line interval then $[M_n] = 0$. Further, if R is bounded then $[M_n] \in L^1(\gamma)$. Particularly, γ can be a part of Γ. Anyway, the moment stress rate tensor $\bar{\mathbf{M}}$ solving problem (RQ*) exhibits discontinuities.

6. Theory of perfectly-locking thin plates and shells

Let $S \subset \mathbb{R}^3$ denote a sufficiently regular middle surface of a thin shell [2]. Its deformation is determined by the displacement vector $(\mathbf{u}, w)$, where $\mathbf{u} = (u_a)$. By $\boldsymbol{\gamma} = (\gamma_{\alpha\beta})$ and $\boldsymbol{\rho} = (\rho_{\alpha\beta})$ we denote the linear deformation measures. The locking locus is now contained in the space $\mathbb{E}^2_s \times \mathbb{E}^2_s$, i.e. $B \subset \mathbb{E}^2_s \times \mathbb{E}^2_s$. For instance, once the locking condition

$$l(x, \boldsymbol{\gamma}, \boldsymbol{\rho}) \leq 0, \quad x = (x_i) \in S, \quad i = 1, 2, 3, \tag{6.1}$$

is known, then

$$B(x) = \{(\boldsymbol{\gamma}, \boldsymbol{\rho}) \in \mathbb{E}^2_s \times \mathbb{E}^2_s |\ l(x, \boldsymbol{\gamma}, \boldsymbol{\rho}) \leq 0, \quad x \in S\}. \tag{6.2}$$

The strains measures the for linear Koiter's shell are given by Eqs.(6.6) below.

We observe that no assumption of isotropy is required. A specific case of B for thin plates has been given in Sec.4.3. For homogeneous materials B does not depend on x. General assumptions on B are specified by:

(A_1) $B(x) \subset \mathbb{E}^2_s \times \mathbb{E}^2_s$ is convex and closed.

(A_2) There exist $0 < r_1 < r_2 < +\infty$ such that, $K(0, r_1) \subset B \subset K(0, r_2)$, where $K(0, r)$ denotes the ball with the centre at zero (in $\mathbb{E}^2_s \times \mathbb{E}^2_s$) and with radius r.

The constitutive relationship is assumed in the subdifferential form, cf. (4.29),

$$(\mathbf{N}, \mathbf{M}) \in \partial I_{B(x)}(\boldsymbol{\gamma}, \boldsymbol{\rho}). \tag{6.3}$$

As we already know, for perfectly-locking shells $\mathbf{N}, \mathbf{M}$ denote the rates of the stress resultants and couple resultants, respectively.

The support function of B is now given by, cf. Eq.(4.32),

$$G(x, \mathbf{N}, \mathbf{M}) = \sup\{N^{\alpha\beta}\gamma_{\alpha\beta} + M^{\alpha\beta}\rho_{\alpha\beta} | (\boldsymbol{\gamma}, \boldsymbol{\rho}) \in B(x)\}. \tag{6.4}$$

The function G is a counterpart of the density of plastic dissipation. Now, however, it does not describe the dissipation since the locking response is reversible. The constitutive relationship inverse to (6.3) is given by

$$(\boldsymbol{\gamma}, \boldsymbol{\rho}) \in \partial G(x, \mathbf{N}, \mathbf{M}), \quad x \in S. \tag{6.5}$$

The function $G(x, ., .)$ has linear growth and satisfies:

(i) $G(x, \mathbf{0}, \mathbf{0}) = 0$,

(ii) there exist constants $C_1 > C_0 > 0$ such that

$$\forall\ (\mathbf{N}, \mathbf{M}) \in \mathbb{E}_2^s \times \mathbb{E}_2^s, C_0(|\mathbf{N}| + |\mathbf{M}|) \leq G(x, \mathbf{N}, \mathbf{M}) \leq C_1(1 + |\mathbf{N}| + |\mathbf{M}|),$$

(iii) $G(x, ., .)$ is positively homogeneous

$$G(x, a\mathbf{N}, a\mathbf{M}) = aG(x, \mathbf{N}, \mathbf{M}) \text{ if } a > 0.$$

Dependence of B on $x \in S$ is not arbitrary. After BOUCHITTÉ and VALADIER [3] we make the following assumption, cf. also Remark 13.2.1 in LEWIŃSKI and TELEGA [11],

$$\forall \boldsymbol{\Phi} \in C_0(S, \mathbb{E}_s^2 \times \mathbb{E}_s^2), \boldsymbol{\Phi}(x) \in B(x) \text{ almost everywhere} \Rightarrow \boldsymbol{\Phi}(x) \in B(x) \text{ everywhere.}$$

Locking limit analysis

Let the boundary ∂S of the shell middle surface S consist of two disjoint parts denoted by ∂S_0 and ∂S_1. For KOITER's shells the strain measures are, cf.[2],

$$\begin{aligned} \gamma_{\alpha\beta}(\mathbf{u}, w) &= \frac{1}{2}(u_{\alpha\|\beta} + u_{\beta\|\alpha}) - b_{\alpha\beta}w, \\ \rho_{\alpha\beta}(\mathbf{u}, w) &= -w \|_{\alpha\beta} - b^{\gamma}_{\alpha\|\beta}u_{\gamma} - b^{\gamma}_{\alpha}u_{\gamma\|\beta} - b^{\gamma}_{\beta}u_{\gamma\|\alpha} + c_{\alpha\beta}w. \end{aligned} \tag{6.6}$$

The meaning of (6.6) is standard in the linear shell theory. Now we introduce the spaces of kinematically admissible fields and of statically admissible fields as

follows, cf. (5.3-5.5),

$$\mathcal{U}_{ad}(m) = \Big\{(\mathbf{u}, w) \in \big[H^1(S)\big]^2 \times H^2(S) \mid \mathbf{u} = m\mathbf{u}^0,\ w = mw^0,\ \frac{\partial w}{\partial \mathbf{n}} = mw^1 \text{ on } \partial S_1\Big\},$$

$$\mathcal{B}_g = \Big\{(\mathbf{u}, w) \in \big[H^1(S)\big]^2 \times H^2(S) \mid [\boldsymbol{\gamma}(\mathbf{u}(x), w(x)),\ \boldsymbol{\rho}(\mathbf{u}(x), w(x))] \in B(x), \text{a.e. } x \in S\Big\},$$

$$\mathcal{S}_o(S) = \big\{(\mathbf{N}, \mathbf{M}) \in L^2(S, \mathbb{E}_2^s) \times L^2(S, \mathbb{E}_2^s) \mid$$

$$eq_1 := N^{\alpha\beta}{}_{\|\beta} - 2b^\alpha_\sigma M^{\sigma\beta}_{\ \ \|\beta} - b^\alpha_{\sigma\|\beta} M^{\sigma\beta} = 0,$$

$$eq_2 := b_{\alpha\beta} N^{\alpha\beta} + M^{\alpha\beta}_{\|\alpha\beta} - c_{\alpha\beta} M^{\alpha\beta} = 0 \text{ in } S,$$

$$\tilde{N}^a = (N^{\alpha\beta} - b^\alpha_\lambda M^{\lambda\beta}) n_\beta - b^\alpha_\beta M^{\lambda\beta} n_\lambda = 0 \text{ on } \partial S_0,$$

$$T = M^{\alpha\beta}_{\ \ \|\beta} n_\alpha + \partial/\partial s (M^{\alpha\beta} t_\alpha n_\beta) = 0,\ M_n = M^{\alpha\beta} n_\alpha n_\beta = 0 \text{ on } \partial S_o\Big\}.$$

The locking limit analysis is formulated in the form of two dual problems:

$$(\mathcal{R}) \qquad \sup\{m \mid B_g \cap U_{ad}(m) \neq \varnothing\}$$

$$(\mathcal{R}^*) \qquad \inf\Big\{\int_S G(x, \mathbf{N}, \mathbf{M}) dS \mid (\mathbf{N}, \mathbf{M}) \in \mathcal{S}_o(S),\ \int_{\partial S_1} (\tilde{N}^a u^0_\alpha + Tw^0 - M_n w^1) ds = 1\Big\}.$$

Similarly to the previous section we get

$$m_l = \inf \mathcal{R}^* = \sup \mathcal{R} < +\infty,$$

where m_l denotes the locking limit load multiplier.

7. Elastic-perfectly locking thin shells

Let us introduce a model of such shells, being a counterpart of the deformational theory of plasticity. Now we have

$$(7.1) \qquad \mathbf{N} = \mathbf{N}_e + \mathbf{N}_l, \quad \mathbf{M} = \mathbf{M}_e + \mathbf{M}_l.$$

Here the subscripts e, l denote the elastic and locking parts, respectively. For the elastic parts linear elastic behavior is assumed. The locking parts obey the following rule, cf. (6.3),

$$(\mathbf{N}_l, \mathbf{M}_l) \in \partial I_{B(x)}(\boldsymbol{\gamma}, \boldsymbol{\rho}). \tag{7.2}$$

The locking locus $B(\mathrm{x})$ has the properties (A_1) and (A_2) specified in Sec.6. We observe, however, that in contrast to plasticity, only some components of $(\mathbf{N}(x), \mathbf{M}(x))$ can be constrained by $B(x)$. The density of the strain energy (elastic-locking potential) is given by

$$j^*(x, \boldsymbol{\gamma}, \boldsymbol{\rho}) = \frac{1}{2}(A^{\alpha\beta\lambda\mu}\gamma_{\alpha\beta}\gamma_{\lambda\mu} + D^{\alpha\beta\lambda\mu}\rho_{\alpha\beta}\rho_{\lambda\mu}) + I_{B(x)}(\boldsymbol{\gamma}, \boldsymbol{\rho}), \tag{7.3}$$

where $(\boldsymbol{\gamma}, \boldsymbol{\rho}) \in \mathbb{E}_s^2 \times \mathbb{E}_s^2$. Its conjugate (dual) function $j(x, ., .)$ satisfies, cf. LEWIŃSKI and TELEGA [11], TEMAM [23],

$$\exists\, \tilde{c}_0, \tilde{c}_1 > 0,\ \tilde{c}_0(|\mathbf{N}| + |\mathbf{M}| - 1) \leq j(x, \mathbf{N}, \mathbf{M}) \leq \tilde{c}_1(|\mathbf{N}| + |\mathbf{M}| + 1), \tag{7.4}$$

where $(\mathbf{N}, \mathbf{M}) \in \mathbb{E}_2^s \times \mathbb{E}_2^s$. The loading functional is assumed in the following form :

$$\hat{F}(\mathbf{u}, w) = \int_S (q^\alpha u_\alpha + qw)dS + \int_{\partial S_0} \left(N_\alpha^0 u_\alpha + T^0 w - M_n^0 \frac{\partial w}{\partial \mathbf{n}} \right) ds. \tag{7.5}$$

We are now in a position to formulate a pair of dual extremum principles characterizing the displacements and generalized stresses in the elastic-locking shell.

$$(\mathcal{P}_1) \qquad \inf \left\{ \int_S j^*(x, \boldsymbol{\gamma}(\mathbf{u}, w),\ \boldsymbol{\rho}(\mathbf{u}, w))dS - \hat{F}(\mathbf{u}, w) | (\mathbf{u}, w) \in \mathcal{U}_{ad} \right\},$$

$(\mathcal{P}^*)$

$$\sup \left\{ -\int_S j(x, \mathbf{N}, \mathbf{M})dS + \int_{\partial S_1} (\tilde{N}^a \hat{u}_\alpha + T\hat{w} - M_n \hat{w}^1)\, ds | (\mathbf{N}, \mathbf{M}) \in \mathcal{S}_{ad} \right\}.$$

Here

$$\mathcal{U}_{ad} = \left\{ (\mathbf{u}, w) \in [H^1(S)]^2 \times H^2(S) | \mathbf{u} = \hat{\mathbf{u}},\ w = \hat{w},\ \partial w/\partial \mathbf{n} = \hat{w}^1 \quad \text{on} \quad \partial S_1 \right\}$$

$$\mathcal{S}_{ad} = \big\{ (\mathbf{N}, \mathbf{M}) \in L^2(S, \mathbb{E}_2^s) \times L^2(S, \mathbb{E}_2^s) | eq_1 + \mathbf{q} = \mathbf{0},\ eq_2 + q = 0 \text{ in } S;$$

$$\tilde{N}^\alpha = N_\alpha^0,\ T = T^0,\ M_n = M_n^0 \text{ on } \partial S_0 \big\}.$$

Problem $(\mathcal{P}_1)$ admits a solution provided that $B_g \cap \mathcal{U}_{ad} \neq \varnothing$ It means that the loading functional $\hat{F}$ cannot be arbitrary.

REMARK 3. The model of elastic-locking plates is a specific case of the model proposed for shells.

8. Final remarks

We have shown that the shape optimization problem of plates of small volume leads to plates with locking. This fact has been established for isotropic plates. Whether a similar statement holds for anisotropic plates and shells, not necessarily isotropic, remains an open problem. Nevertheless, a general theory of perfectly-locking and elastic-locking plates and shells has been proposed. The elastic-locking model is a counterpart of the deformational theory of plasticity.

Acknowledgement

The work was supported by the Polish Committee for Scientific Research (KBN) through the grant No 7 T07A 04318.

Appendix

Te aim of the Appendix is to derive the formula (4.25) defining the contour of the set $\tilde{B}$. To find $h(\varphi)$ given by (4.18) we represent it in the form

$$h(\varphi) = \left[\min_{\vartheta} f_{\varphi}(\vartheta)\right]^{\frac{1}{2}}, \tag{A.1}$$

where

$$f_{\varphi}(\vartheta) = \frac{1 + \gamma(1 + \sin 2\vartheta) + |\sin 2\vartheta|}{\cos^2(\vartheta - \varphi)}. \tag{A.2}$$

Let us show that the lines

$$\kappa_I = \pm\kappa_{II} \tag{A.3}$$

are symmetry axes of $\tilde{B}$. It is sufficient to show that

$$h(\varphi_1) = h(\varphi_2), \quad h(\varphi_3) = h(\varphi_4), \tag{A.4}$$

for $\varphi_2 = \dfrac{\pi}{2} - \varphi_1$, $\varphi_1 \in [0, \pi/2]$, and for $\varphi_4 = \pi - \left(\varphi_3 - \dfrac{\pi}{2}\right)$, $\varphi_3 \in \left[\dfrac{\pi}{2}, \pi\right]$.

We have

$$h\left(\frac{\pi}{2}-\varphi\right)=\left[\min_{\vartheta} f_{\frac{\pi}{2}-\varphi}(\vartheta)\right]^{1/2}.$$

Note that

$$f_{\frac{\pi}{2}-\varphi}(\vartheta)=\frac{1+\gamma(1+\sin 2\vartheta')+|\sin 2\vartheta'|}{\cos^2(\vartheta'-\varphi)},$$

where $\vartheta'=\frac{\pi}{2}-\vartheta$. Hence $f_{\frac{\pi}{2}-\varphi}(\vartheta)=f_{\varphi}(\vartheta')$. Thus

$$\min_{\vartheta} f_{\frac{\pi}{2}-\varphi}(\vartheta)=\min_{\vartheta'} f_{\varphi}(\vartheta')=\min_{\vartheta} f_{\varphi}(\vartheta).$$

Therefore, $h(\frac{\pi}{2}-\varphi)=h(\varphi)$, which proves (A4). We conclude that in order to find the contour of $\tilde{B}$, it is suffcient to find this contour for $\varphi\in\left[\frac{\pi}{4},\frac{3}{4}\pi\right]$.

We proceed further to find the contour of $\tilde{B}$ for $\varphi\in\left[\frac{\pi}{4},\frac{3}{4}\pi\right]$. We note that the formula (A2) can be rearranged to the form

(A.5) $$f_{\varphi}(\vartheta)=\hat{f}_{\varphi}(\mathrm{tg}\vartheta),$$

(A.6) $$\hat{f}_{\varphi}(x)=\frac{1+\gamma}{\sin^2\varphi}\,g_{\varphi}(x).$$

with

(A.7) $$g_{\varphi}(x)=\begin{cases}\dfrac{1-2\nu x+x^2}{(x+\mathrm{ctg}\varphi)^2} & \text{if} \quad x\leq 0,\\[2ex] \left(\dfrac{1+x}{x+\mathrm{ctg}\varphi}\right)^2 & \text{if} \quad x\geq 0.\end{cases}$$

The results above lead to

(A.8) $$h(\varphi)=\frac{\sqrt{1+\gamma}}{\sin\varphi}\left[\min_{x\in\mathbb{R}} g_{\varphi}(x)\right]^{1/2}$$

and the variable ϑ is no longer necessary. To find $\min\limits_{x} g_{\varphi}(x)$ we shall make use of two elementary results:

(a) $$\min_{x\geq 0}\left|\frac{x+1}{x+\mathrm{ctg}\varphi}\right|=1 \quad \text{if} \quad \varphi\in\left[\frac{\pi}{4},\frac{3}{4}\pi\right],$$

(b) $$\min\frac{1-2bx+x^2}{(x-p)^2}=\frac{1-b^2}{1-2bp+p^2} \quad \text{if} \quad b<1,\ p\in\mathbb{R}.$$

The minimum in (b) is attained at

$$x_0 = \frac{1-bp}{b-p}, \tag{A.9}$$

To find $\min_x g(x)$ one should consider the case of $x_0 \leq 0$ and

$$\frac{1-b^2}{1-2bp+p^2} \leq 1, \tag{A.10}$$

for $b = \nu$, $p = -\mathrm{ctg}\varphi$. Let us note that

$$1 - \frac{1-b^2}{1-2bp+p^2} = \frac{(b-p)^2}{1-2bp+p^2}.$$

Thus the condition (A10) is satisfied provided that $x_0 \leq 0$. Let $\Psi = \varphi - \pi/2$. Then $\mathrm{ctg}\varphi = -\mathrm{tg}\Psi$.

The condition $x_0 \leq 0$ implies

$$\beta \leq \Psi \leq \frac{\pi}{2} - \beta \tag{A.11}$$

where $\beta = \mathrm{arctg}\nu$ and for such φ the minimum in (b) is attained. Thus the final result has the form

$$\min_{x\in\mathbb{R}} g_\varphi(x) = \begin{cases} 1 & \text{if } \frac{\pi}{4} \leq \varphi \leq \frac{\pi}{2} + \beta, \\ \dfrac{1-\nu^2}{1+2\nu\mathrm{ctg}\varphi + \mathrm{ctg}^2\varphi} & \text{if } \frac{\pi}{2} + \beta \leq \varphi \leq \frac{3}{4}\pi. \end{cases} \tag{A.12}$$

Now we use (A.8) and come back to (4.23), (4.24) to find $r(\varphi) = \sqrt{L+K}\,\tilde{h}(\varphi)$, where $\tilde{h}(\varphi)$ is given by (4.25).

References

1. G. ALLAIRE, and R.V. KOHN, *Optimal design for minimum weight and compliance in plane stress using extremal microstructures.*, Eur. J. Mech., A/Solids, **12**, 839-878, 1993.
2. M. BERNADOU, *Finite Element Methods for Thin Shell Problems.*, J. Wiley & Sons, Chichester; Masson, Paris 1996.
3. G. BOUCHITTÉ and M. VALADIER, *Integral representation of convex functionals on a space of measures,* J. Funct., Anal. **80**, 398-420, 1988.
4. A. ČYRAS, *Optimization theory of perfectly locking bodies,* Arch. Mech., **24**, 203-210, 1972.
5. B. DACOROGNA, *Direct Methods in the Calculus of Variations,* Springer, Berlin 1989.
6. F. DEMENGEL, *Relaxation et existence pour le problème des matériaux à blockage,* Math. Modell. and Numer. Anal., **19**, 351-395, 1985.

7. F. DEMENGEL and P. SUQUET, *On locking materials,* Acta Appl. Math., **6** 185-211, 1986.

8. I. EKELAND and R. TEMAM, *Convex Analysis and Variational Problems,* North-Holland, Amsterdam 1976.

9. S. JEMIOŁO and J. J. TELEGA , *Fabric tensor and constitutive equations for a class of plastic and orthotropic materials,* Arch. Mech., **49**, 1041-1067, 1997.

10. T. LEWIŃSKI and J.J. TELEGA, *Elastic plates and shells of minimal compliance.* In: Proc. WCSMO-2, Second World Congress of Structural and Multidisciplinary Optimization. Zakopane 26-30 May 1997, Poland, W. GUTKOWSKI and Z. MRÓZ. [Ed.] vol.2, pp.841-846, 1997.

11. T. LEWIŃSKI and J.J. TELEGA, *Plates, Laminates and Shells. Asymptotic Analysis and Homogenization,* World Scientific, Series on Advances in Mathematics for Applied Sciences- vol.**52**., Singapore, New Jersey, London, Hong Kong 2000.

12. R. LIPTON, *A saddle point theorem with application to structural optimization,* J. Optimiz. Theory Appl., **81**, 549-568, 1994.

13. K.A. LURIE and A.V. CHERKAEV, *Effective characteristics of composite materials and optimum design of structural members* (in Russian), Adv. Mech., **9**, 3-81, 1986.

14. A.G.M. MICHELL, *The limits of economy of material in frame structures,* Phil.Mag., **8**, 589-597, 1904.

15. U. RAITUMS, *On the local representation of G-closure,* Report No 206, Institute of Mathematics and Computer Science, University of Latvia, Riga 1999.

16. R.T. ROCKAFELLAR, *Convex Analysis,* Princeton University Press, Princeton 1970.

17. G.I.N. ROZVANY, *Optimal Design of Flexural Systems: Beams, Grillages, Slabs, Plates and Shells,* Pergamon Press, Oxford 1976.

18. G. STRANG and R.V. KOHN, *Hencky-Prandtl nets and constrained Michell trusses,* Comp. Meth. Appl. Mech. Engrg., **36**, 207-222, 1983.

19. J.J.TELEGA and S.JEMIOŁO, *Macroscopic behaviour of locking materials with microstructure. Part I. Primal and dual locking potential. Relaxation,* Bull.Polon.Acad.Sci, Tech.Sci, **46**, 265-276, 1998.

20. J.J. TELEGA and T. LEWIŃSKI, *Theory of plates and shells with locking and application to optimization,* [In:] Theoretical Foundations of Civil Engineering-VII. Ed. By W. Szcześniak, pp. 319-330, Oficyna Wydawnicza PW, Warszawa 2000.

21. J.J. TELEGA and T. LEWIŃSKI, *On a saddle-point theorem in minimum compliance design, J.Optimiz.Theory and Appl.,* **106**, 441-450, 2000.

22. J.J. TELEGA, T. LEWIŃSKI and G. DZIERŻANOWSKI, *Minimization of compliance of two-phase plates of small volume,* Proc. 3rd World Congress of Structural and Multidisciplinary Optimization (WCSMO-3), Univ. at Buffalo, Niagara Falls/Amherst, NY. 17-21 May 1999, CD ROM, 2000.

23. R. TEMAM, *Mathematical Problems in Plasticity,* Gauthier-Villars, Paris 1985.

Received March 23, 2001.

Arch. Mech., **53**, 4-5, pp. 487–499, Warszawa 2001

Material modeling of concrete subjected to multiaxial loading: application to pull-out analyses

P. PIVONKA, R. LACKNER, and H. A. MANG

Institute for Strength of Materials
Vienna University of Technology, Vienna, Austria

THIS PAPER DEALS with the application of 3D-constitutive models for concrete to simulations of pull-out experiments [1]. Two different models are considered:

- The first material model is formulated within the framework of multi-surface plasticity. It consists of three Rankine yield surfaces for the simulation of cracking and a Drucker-Prager yield surface for the description of compressive failure of concrete. The Drucker-Prager surface is reformulated in order to account for the influence of confinement on the compressive strength and the ductility of concrete.
- The formulation of the second model, the Extended Leon Model (ELM) [4], is based on one yield function for description of compressive and tensile failure of concrete. It accounts for the influence of the Lode angle on the material strength. The simulation of ductile behavior of concrete is controlled by means of a pressure-dependent ductility function.

The predictive capability of the models is demonstrated by means of a finite element (FE) analysis of a pull-out test [1]. The influence of confinement on the peak load and the failure mode is investigated.

Key words: concrete, triaxial loading, pull-out analyses, multi-surface plasticity, Drucker-Prager, Rankine, Extended Leon Model, confinement

1. Introduction

THE USE OF NUMERICAL tools such as the FEM allows simulation of real-life structures characterized by complex geometric properties and loading conditions. As regards the simulation of concrete structures, sophisticated material models are required in order to provide an appropriate description of the mechanical behavior of concrete. Such material models should account for crack opening in the case of tensile loading, crushing in the case of compressive loading, and compaction of concrete when subjected to hydrostatic pressure.

In the context of plasticity theory, failure may be described either by one failure criterion (single-surface plasticity) or by a combination of several failure criteria (multi-surface plasticity). As regards single-surface models, the ELM [4] was developed in order to give realistic results for tensile, compressive, and confined compressive states of loading. It is characterized by relating the main parameters of the model such as, e.g., ductility and fracture energy to the confinement of the material. The hydrostatic pressure is used as the measure for confinement.

In multi-surface plasticity, each failure criterion is used to describe a certain mode of material failure. For the simulation of cracking, the Rankine criterion gives the best results. In the compressive loading regime, the Drucker-Prager surface is commonly employed (see, e.g., [5][10]). The compaction of concrete may be considered by means of an additional cap (see, e.g., [7]).

In this paper, two material models developed for the simulation of the mechanical behavior of concrete, the Extended Leon Model [2] and a multi-surface plasticity model consisting of the Drucker-Prager criterion and the Rankine criterion, are considered. As regards the Drucker-Prager criterion, a reformulation is proposed in order to extend its range of applicability. The influence of this reformulation on the numerical results is demonstrated by means of a finite element analysis of a pull-out test.

In the following section, both material models are briefly presented and the proposed modification of the Drucker-Prager criterion is described. However, the main part of the paper is devoted to the numerical analysis of a pull-out test. The respective results are contained in Sec. 3.

2. 3D plasticity models for plain concrete

Concrete is a composite material, made of cement, aggregates, and water. In continuum mechanics, however, concrete is treated as homogeneous material. The respective scale of observation is referred to as macro-level. Stress-strain relations formulated at the macro-level relate macro-stresses to macro-strains. However, the mechanical behavior observed at the macro-level is associated with phenomena occurring at the micro-level of the material. E.g., inelastic macro-strains arise from micro-cracking of hydrates. For the description of phenomena at the micro-level, so-called internal variables $\boldsymbol{\alpha}$ are introduced in the material model. They are used to describe the microstructural change of the material. The energetically conjugated thermodynamic quantities are the hardening/softening forces $\mathbf{q}$. They are related to the internal variables via the state equation $\mathbf{q}=\mathbf{q}(\boldsymbol{\alpha})$. The hardening forces represent the actual strength of the material, defining the space of admissible stress states, $\mathbf{C}_E$

$$\boldsymbol{\sigma} \in \mathbf{C}_E \;\Leftrightarrow\; f_k = f_k(\boldsymbol{\sigma},\mathbf{q}(\boldsymbol{\alpha})) \leq 0 \quad \forall \quad k \in [1,2,\ldots,N], \tag{2.1}$$

where f_k denotes the k-th yield function. In definition (2.1), the general case of multi-surface plasticity is considered. N denotes the number of employed yield functions.

The internal variables and the respective deformations related to plastic material response are obtained by means of evolution equations, reading

$$\dot{\boldsymbol{\alpha}} = \sum_{k \in J_{act}} \dot{\gamma}_k \frac{\partial H_k}{\partial \mathbf{q}}, \quad \dot{\boldsymbol{\varepsilon}}^p = \sum_{k \in J_{act}} \dot{\gamma}_k \frac{\partial Qk}{\partial \boldsymbol{\sigma}}, \tag{2.2}$$

where γ_k denotes the plastic multiplier of the k-th yield function. Q_k and H_k are potentials which, in general, depend on $\boldsymbol{\sigma}$ and $\mathbf{q}$.

The first material model considered in this paper is formulated within the framework of multi-surface plasticity theory. It consists of four yield surfaces (N=4): a Drucker-Prager (DP) yield surface for the description of concrete when subjected to compressive loading and three Rankine (RK) surfaces for the description of tensile failure. In the principal stress space, the failure criteria read

$$f_{DP}(\boldsymbol{\sigma}, q_{DP}) = \sqrt{J_2} - \kappa_{DP} I_1 - \frac{\bar{q}_{DP}}{\beta_{DP}} \quad \text{with} \quad \bar{q}_{DP} = f_{cy} - q_{DP}, \tag{2.3}$$

and

$$f_{RK,A}(\sigma_A, q_{RK}) = \sigma_A - \bar{q}_{RK}, \quad \text{with} \quad \bar{q}_{RK} = f_{tu} - q_{RK}, \tag{2.4}$$

where the subscript "A"(A=1,2,3) refers to one of the three principal axes. f_{tu} is the tensile strength and f_{cy} represents the elastic limit of concrete under uniaxial compressive loading. κ_{DP} and β_{DP} are constant material parameters.

For the description of microstructural changes of concrete, two internal variables are employed: α_{RK} and α_{DP}. They are computed according to associated hardening/softening laws, i.e., $H_{RK,A}$=$f_{RK,A}$ and H_{DP}=f_{DP}, reading

$$\dot{\alpha}_{RK} = \sum_{A=1}^{3} \dot{\gamma}_{RK,A} \frac{\partial f_{RK,A}}{\partial q_{RK}}, \quad \dot{\alpha}_{DP} = \dot{\gamma}_{DP} \frac{\partial f_{DP}}{\partial q_{DP}}. \tag{2.5}$$

Cracking of concrete is characterized by a continuous decrease of the tensile strength, $\bar{q}_{RK}$. Accordingly, an exponential softening law is chosen, reading

$$\bar{q}_{RK} = f_{tu} \exp[-\alpha_{RK}/\alpha_{RK,u}], \tag{2.6}$$

where $\alpha_{RK,u}$ is a calibration parameter. Under compressive loading, however, the behavior of concrete is characterized by hardening as well as softening behavior. The chosen hardening/softening curve for the compressive strength, $\bar{q}_{DP}$, is depicted in Fig. 1a. Commonly, the Drucker-Prager criterion is calibrated by

means of uniaxial and biaxial compression tests, giving β_{DP} and κ_{DP} (see, e.g., [11]). For the application of the Drucker-Prager criterion experiencing mainly biaxial stress states, this mode of calibration is appropriate. For confined stress states, however, large deviations between the experimental data and the numerical results were reported in [13]. Experimental data indicate an influence of confinement on both the compressive strength, described by the ultimate and the residual strengths, $\bar{q}_{DP,p}$ and $\bar{q}_{DP,r}$, and the ductility [14]. The proposed modification of the Drucker-Prager criterion accounts for this influence by relating $\bar{q}_{DP,p}$, $\bar{q}_{DP,r}$, and $\alpha_{DP,m}$ to the actual level of confinement. Confinement is represented by the major principal stress σ_1, with $\sigma_1 \geq \sigma_2 \geq \sigma_3$, yielding $\bar{q}_{DP,p} = \bar{q}_{DP,p}(\sigma_1)$, $\bar{q}_{DP,r} = \bar{q}_{DP,r}(\sigma_1)$, and $\alpha_{DP,m} = \alpha_{DP,m}(\sigma_1)$ (see Fig. 1b and 1c). $\bar{q}_{DP,p}$ and $\bar{q}_{DP,r}$ are computed by means of the Drucker-Prager criterion, $f_{DP} = 0$, using the stress state $\boldsymbol{\sigma}^T = [\sigma_1, \sigma_1, \sigma_3(\sigma_1)]$ (for details, see [13]).

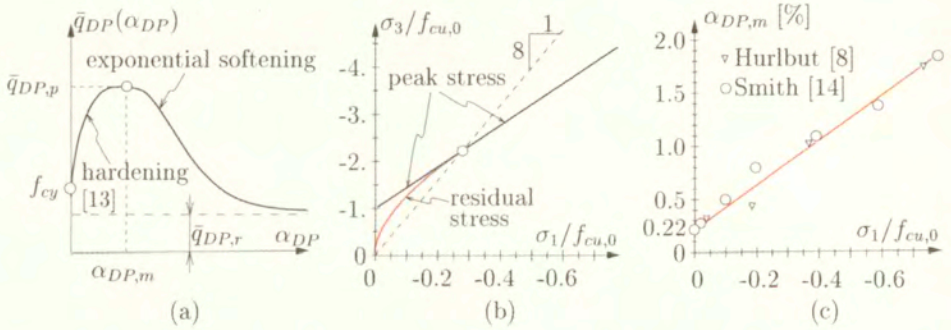

FIG. 1. Multi-surface model: (a) employed hardening/softening curve for the Drucker-Prager criterion; influence of confinement on (b) the peak and residual stress (related to $\bar{q}_{DP,p}$ and $\bar{q}_{DP,r}$) and (c) the ductility $\alpha_{DP,m}$. The level of confinement is represented by the maximum principal stress σ_1 (f_{cy}: elastic limit under uniaxial compressive loading, f_{cu}: uniaxial compressive strength of concrete)

The second material model considered in this paper is the Extended Leon Model (ELM) [2]. It belongs to the class of single-surface models, i.e., $N=1$. The yield function is given by

$$f_{ELM}(p,r,\theta;q_h,q_s) = \left\{\left(1-\frac{\bar{q}_h}{f_{cu}}\right)\left[\frac{p}{f_{cu}}+\frac{rg(\theta,e)}{\sqrt{6}f_{cu}}\right]^2+\sqrt{\frac{3}{2}}\frac{rg(\theta,e)}{f_{cu}}\right\}^2 + \left(\frac{\bar{q}_h}{f_{cu}}\right)^2 m(q_s)\left[\frac{p}{f_{cu}}+\frac{rg(\theta,e)}{\sqrt{6}f_{cu}}\right] - \left(\frac{\bar{q}_h}{f_{cu}}\right)^2\frac{\bar{q}_s}{f_{tu}} = 0, \tag{2.7}$$

with

$$\bar{q}_h = f_{cy} - q_h \quad \text{and} \quad \bar{q}_s = f_{tu} - q_s. \tag{2.8}$$

In Eq. (2.7), p is the hydrostatic pressure, r is the deviatoric radius, and θ denotes the Lode angle. f_{cu} and f_{tu} denote the uniaxial compressive and tensile strength, respectively. The deviatoric shape of the loading surface is described by the elliptic function $g(\theta, e)$ (see [15]), where the parameter e is referred to as eccentricity, describing the out-off roundness of the deviatoric meridian. $m(q_s)$ is a frictional parameter. The ELM is used for the simulation of hardening as well as softening material response. Hence, two hardening/softening forces, q_h and q_s, are contained in the yield function (2.7). The internal variables, α_h and α_s, are employed to monitor the respective changes of the material at the micro-level. The evolution equations for α_h and α_s are given as [13]

$$\dot{\alpha}_h = \dot{\gamma} \frac{\partial H_{ELM,h}}{\partial q_h} = \frac{1}{x_h(p)} \dot{\epsilon}_h^p \quad \text{with} \quad \dot{\epsilon}_h^p = \dot{\gamma} \, \| \frac{\partial Q_{ELM}}{\partial \boldsymbol{\sigma}} \|, \tag{2.9}$$

$$\dot{\alpha}_s = \dot{\gamma} \frac{\partial H_{ELM,s}}{\partial q_s} = \frac{1}{x_s(p)} \dot{\epsilon}_s^p \quad \text{with} \quad \dot{\epsilon}_s^p = \dot{\gamma} \, \| \langle \frac{\partial Q_{ELM}}{\boldsymbol{\sigma}} \rangle \|. \tag{2.10}$$

In Eq. (2.10), the McAuley operator $\langle \bullet \rangle = (\bullet + |\bullet|)/2$ extracts the positve eigenvalues of the principal components of $\partial Q_{ELM}/\partial \boldsymbol{\sigma}$ [12]. x_h and x_s are pressure-dependent ductility functions in the hardening and the softening regime, respectively. The influence of the ductility function on the hardening and softening material behavior is illustrated in Fig. 2.

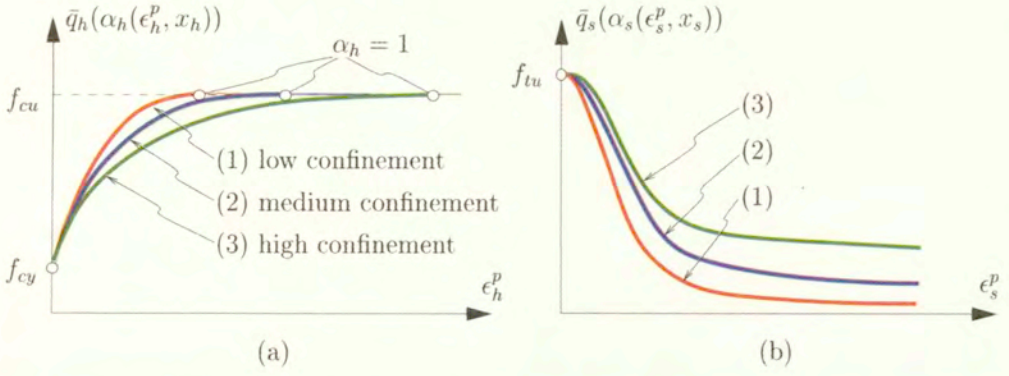

FIG. 2. Extended Leon Model: illustration of the influence of (a) the ductility function x_h on the increase of the compressive strength $\bar{q}_h$ and (b) the ductility function x_s on the decrease of the residual strenght $\bar{q}_s$ (f_{cy}: elastic limit under compresive loading, with $f_{cy} = 0.2 \, f_{cu}$)

3. Failure analysis of pull-out test

The focus of the present paper is on the influence of the underlying material model on the numerical results obtained from failure analyses of anchor bolts in concrete, referred to as the pull-out test. For this purpose, analyses on the basis of both material models described in Sec. 2 were performed. Moreover, the influence of confinement on the peak load and on the failure mode is investigated.

3.1. Geometric dimensions and material properties

Figure 3 contains the experimental setup of the considered pull-out test (Round-Robin test [1]). It shows the geometric dimensions as well as the support conditions of the specimen. Further, the material properties of concrete and steel are given.

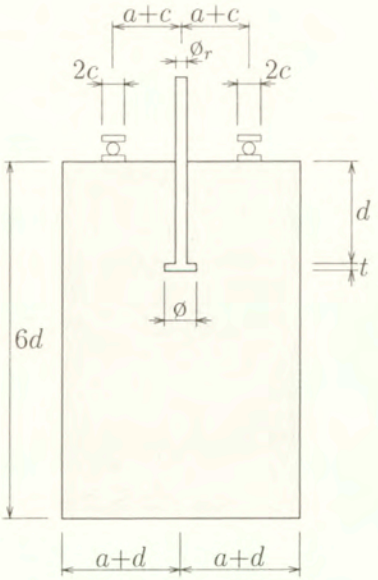

dimensions:
d=150 mm a=150 mm
t=15 mm c=22.5 mm
ø=45 mm $ø_r$=24 mm

concrete:
Young's modulus: E_c=30000 N/mm^2
Poisson's ratio: ν_c=0.2
uniaxial compressive strength: f_{cu}=40 N/mm^2
uniaxial tensile strength: f_{tu}=3 N/mm^2
fracture energy: G_f^I=0.1 Nmm/mm^2
fracture energy: G_f^{II}=50G_f^I

steel:
Young's modulus: E_s=210000 N/mm^2
Poisson's ratio: ν_s=0.3

FIG. 3. Pull-out analysis: geometric dimensions and material properties

3.2. Numerical analysis

In the numerical analysis, the material behavior of the steel bolt is assumed to be linear elastic. For the description of concrete, the two previously described material models are used.

Because of symmetry of the geometric dimensions and the loading conditions, the problem is solved by means of axisymmetric analyses. Fig. 4 shows

the employed FE mesh consisting of 677 four-node finite elements. As regards the mechanical model of the anchor bolt, only the anchor head is discretized. At the contact line between the anchor head and the concrete, no slip is considered. The analyses are performed displacement-driven. The displacement at the nodes of the anchor head located at the axis of symmetry is prescribed (see Fig. 4).

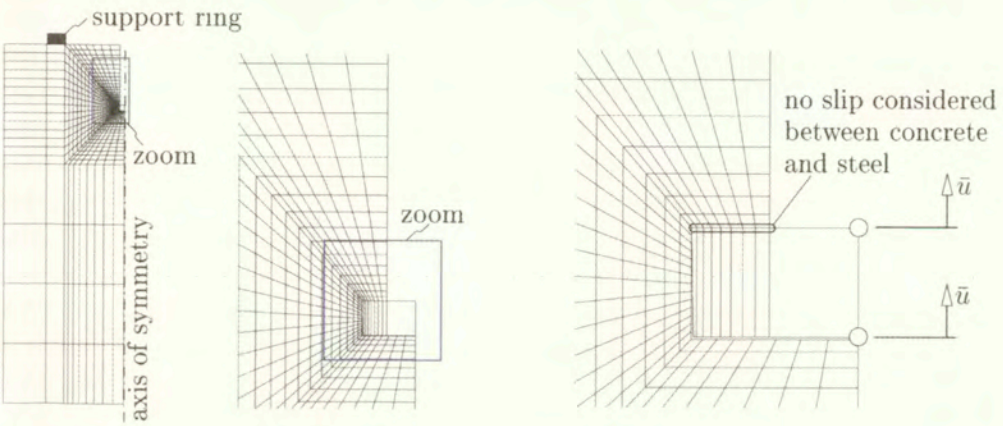

FIG. 4. Pull-out analysis: FE discretization

Softening functions appearing in the formulations of both models were calibrated according to the fictitious crack concept [6]. The application of the fictitious crack concept to the simulation of radial cracks in axisymmetric analyses requires the input of the expected number of radial cracks (for details, see [9]). In the present analyses, four radial cracks are assumed to develop.

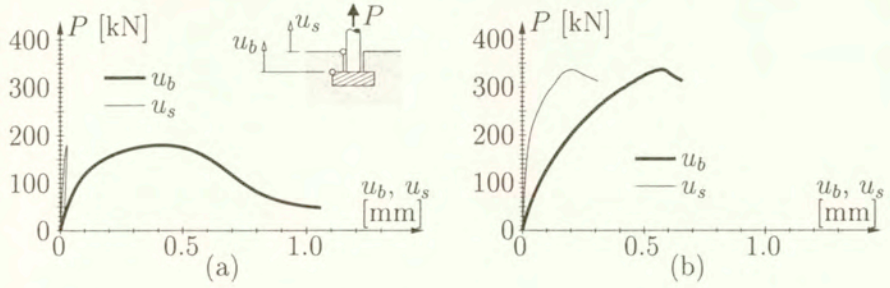

FIG. 5. Pull-out analysis: (a) load-displacement curves obtained from multi-surface model with (a) *original* and (b) *modified* Drucker-Pager criterion

Figure 5 contains the load-displacement curves obtained from the multi-surface model. The peak load obtained from the Drucker-Prager criterion characterized by consideration of confinement (*modified* model) was found to be 340 kN.

Neglection of the influence of confinement within the Drucker-Prager criterion (*original* model), i.e., setting $\bar{q}_{DP,p}$=const., $\bar{q}_{DP,r}$=const., and $\alpha_{DP,m}$=0.0022, led to a reduction of the peak load by 47% (see Fig. 5a). The difference between the displacement at the anchor head and the concrete surface, $u_b - u_s$, is an indicator for compressive failure of concrete over the anchor head. An almost constant evolution of $u_b - u_s$ indicates a rigid body motion in consequence of formation of a cone-like failure mode (see, e.g., Fig. 8a). Small values of u_s together with continuously increasing values of $u_b - u_s$ indicate local failure of concrete over the anchor head. This failure mode was obtained from the analysis based on the *original* multi-surface model (see Fig. 5a). The underestimation of compressive strength and ductility by neglecting the influence of confinement resulted in compressive failure of concrete over the anchor head. The respective $P - u_b$ curve shows similar characteristics as the underlying hardening/softening curve used for the Drucker-Prager criterion (see Fig. 1a). Moreover, failure of concrete over the anchor head resulted in an unloading of the remaining part of the structure. This is reflected by the decrease of u_s in the post-peak regime. Consideration of confinement by the *modified* multi-surface model led to an increase of the compressive strength over the anchor head. The almost constant evolution of $u_b - u_s$ in the post-peak regime indicates the development of a cone-like failure mode (see Fig. 8a).

The distribution of α_{DP} is given in Fig. 6 for both analyses at the respective peak loads. The compressive failure over the anchor head obtained from the *original* model is reflected by softening material behavior (see Fig. 6a).

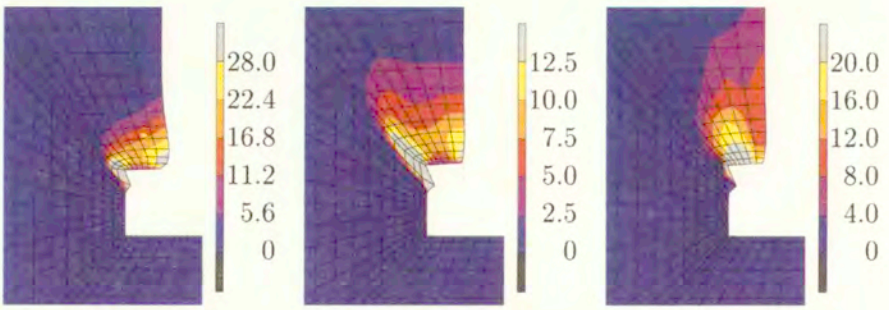

(a) $10^3 \cdot \alpha_{DP}$ (b) $10^3 \cdot \alpha_{DP}$ (c) $10^3 \cdot \alpha_{DP,m}$

FIG. 6. Pull-out analysis: distribution of the internal hardening/softening variable of the Drucker-Prager criterion, α_{DP}, at peak load obtained from (a) *original* and (b) *modified* multi-surface model; (c) distribution of $\alpha_{DP,m}$ at peak load obtained from *modified* multi-surface model (10-fold magnification of displacements)

Softening is characterized by $\alpha_{DP} > \alpha_{DP,m}$=0.0022. On the other hand, the confinement considered in the simulation based on the *modified* multi-surface

model resulted in an increase of $\alpha_{DP,m}$ over the anchor head (see Fig. 6c). The distribution of α_{DP} is shown in Fig. 6b. The values of α_{DP} are lower than the respective values of $\alpha_{DP,m}$ indicating that the compressive strength in this area has not reached the ultimate strength $\bar{q}_{DP,p}$ (hardening regime). The strong influence of confinement on the obtained numerical results is a consequence of large compressive stresses over the anchor head. For the multi-surface model, the major principal stress is used as a measure for confinement. If the major principal stress is positive, no confinement is considered. Fig. 7 shows the distribution of the two principal stresses in the axisymmetric plane, denoted as σ_{min} and σ_{max}, and the circumferential stress σ_{circ} at peak load obtained from the analysis based on the *modified* multi-surface model. Over the anchor head, negative stresses are observed for all three principal stresses. Hence, $\sigma_1 < 0$, resulting in an increase of the compressive strength and the ductility (see Fig. 1b and 1c).

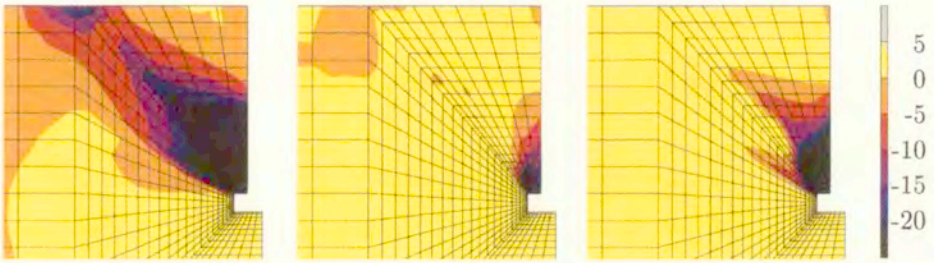

(a) σ_{min} (b) σ_{max} (c) σ_{circ}

FIG. 7. Pull-out analysis: distribution of principal stresses in the axisymmetric plane, σ_{min} and σ_{max}, and the stress component in the circumferential direction, σ_{circ}, at peak load obtained from *modified* multi-surface model (in [N/mm^2])

The distribution of the minimum in-plane principal stress σ_{min} (see Fig. 7a) provides insights into the load-carrrying behavior of the concrete specimen. The applied load at the anchor head is transferred by a compressive strut from the confined area over the anchor head to the support ring (see [3] for similar results). The respective maximum principal stress in this strut resulted in the development of a circumferential crack. This crack started to open at the anchor head propagating towards the support ring, finally causing a cone-shaped failure of the specimen. The crack pattern obtained at peak load on the basis of the *modified* multi-surface model is shown in Fig. 8a by means of the distribution of the maximum plastic strain in the axisymmetric plane, ε^p_{max}. In addition to the circumferential crack, radial cracks developed, starting from the corner at the concrete surface and propagating into the interior of the concrete block. Recall, four radial cracks were assumed to open in the context of the fictitious crack

concept. In Fig. 8b, the location of these radial cracks is shown by means of the respective circumferential plastic strain, ε^p_{circ}.

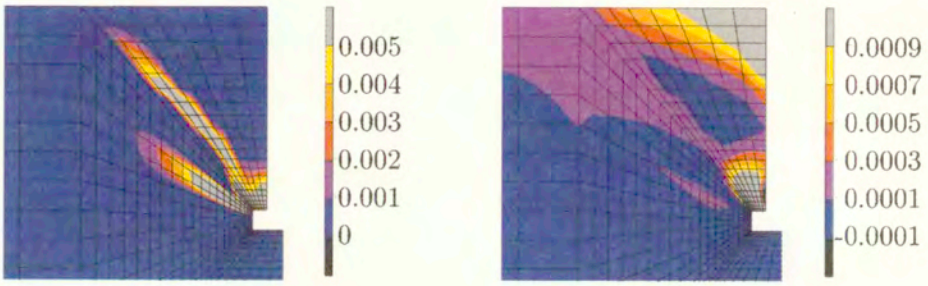

(a) ε^p_{max} (b) ε^p_{circ}

FIG. 8. Pull-out analysis: distribution of the maximum plastic strain in axisymmetric plane, ε^p_{max}, and of the circumferential plastic strain ε^p_{circ} at peak load obtained from *modified* multi-surface model

The load displacement curve obtained from the analysis based on the single-surface model is shown in Fig. 9. The peak load was computed as 312 kN. The continuously increasing value of $u_b - u_s$ in the pre-peak regime indicates plastic material response over the anchor head. However, the actual failure occurs in consequence of circumferential cracks resulting in a cone-like failure surface. Similar to the analysis based on the *modified* multi-surface model, an almost constant evolution of $u_b - u_s$ is observed in the post-peak regime indicating this mode of failure.

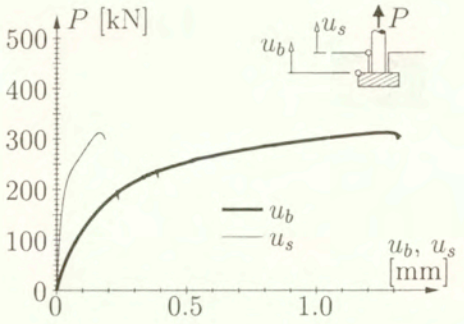

FIG. 9. Pull-out analysis: load displacement curve obtained from single-surface model

The distribution of α_h at peak load is shown in Fig. 10a. α_h describes the state of the yield surface in the hardening regime. $\alpha_h = 0$ refers to the initial yield surface defined by $\bar{q}_h = f_{cy}$ (see Fig. 2a.) If $\alpha_h = 1$, the failure surface is reached ($\bar{q}_h = f_{cu}$) and softening or ideally-plastic behavior is initiated. Whether or not

softening will take place depends on the level of confinement. For the single-surface model, confinement is represented by the hydrostatic pressure. For a hydrostatic pressure p, with $p = -(\sigma_1 + \sigma_2 + \sigma_3)/3$, lower than the hydrostatic pressure related to the so-called transition point TP, p_{TP}, softening occurs. For stress states characterized by $p > p_{TP}$, ideally-plastic material behavior is assumed. The transition point TP is equal to the stress point on the failure surface characterized by a confined stress state given as $\sigma_1 = \sigma_2$, $\sigma_3 = 8\sigma_1$ [14]. Based on the material parameters given in Fig. 3, the hydrostatic pressure at the TP is computed as p_{TP}=44.3 N/mm^2.

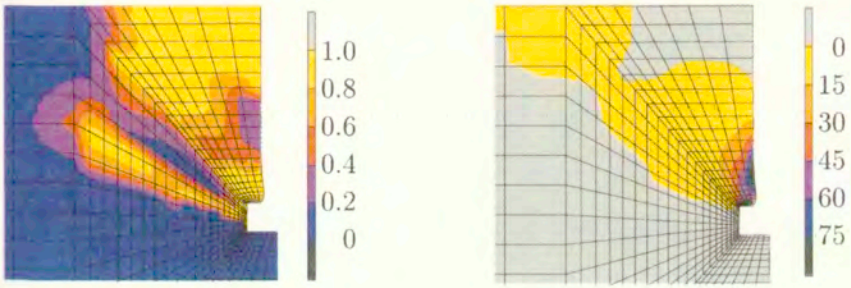

FIG. 10. Pull-out analysis: distribution of (a) the internal hardening variable α_h and (b) the hydrostatic pressure p, with $p = -(\sigma_1 + \sigma_2 + \sigma_3)/3$, (in [N/mm^2]) at peak load obtained from single-surface model (5-fold magnification of displacements)

The distribution of the hardening variable α_h at peak load shown in Fig. 10a is characterized by several zones with $\alpha_h = 1$. As regards the zone over the anchor head, the respective hydrostatic pressure is greater than the hydrostatic pressure at the transition point, i.e., $p > p_{TP}$. This resulted in ideally-plastic material response and, hence, in plastic deformations already observed by the evolution of $u_b - u_s$ depicted in Fig. 9. Based on this ideally-plastic material response no local failure mode over the anchor head developed. The remaining regions characterized by $\alpha_h = 1$ show low values for the hydrostatic pressure resulting in softening material behavior. Similar to the crack pattern obtained from the multi-surface model (Fig. 8), these regions refer to two circumferential cracks starting at the anchor head, and radial cracks propagating from the concrete surface into the interior of the concrete block.

4. Conclusions

In this paper, structural failure of anchor bolts placed in concrete was investigated. For this purpose, two material models for plain concrete were used.

One of them was a single-surface and the other one a multi-surface model. The latter model was originally proposed by MESCHKE [10] (it is referred to as *original* model). This model was reformulated in order to account for the influence of confinement. The reformulated model is referred to as *modified* multi-surface model. From the numerical simulations, the following conclusions concerning the structural response of the concrete specimen can be drawn:

- the concrete located between the anchor head and the support ring is subjected to strong non-uniform triaxal stress states, characterized by
  - hydrostatic pressure over the anchor head,
  - a compressive strut from the anchor head to the support ring, and
  - circumferential cracking caused by tensile loading perpendicular to this strut;
- the underlying material model has a crucial influence on the predicted failure mode characterized either
  - by local compressive failure over the anchor head, or
  - by a cone-shaped failure surface in consequence of the development of circumferential cracks.

The cone-shaped failure surface, which presumably represents the correct failure mode, was obtained by the *modified* multi-surface model and the single-surface model. The respective peak loads deviated by 8%. Disregard of the influence of confinement on the material strength and ductility in the context of the *original* multi-surface model resulted in local compressive failure of concrete over the anchor head. The peak load related to this presumably incorrect failure mode was found to be significantly lower than the peak loads obtained from the analyses characterized by cone-shaped failure.

References

1. L. ELFGREN, *Fracture mechanics of concrete structures,* Technical report, RILEM, Technical Committee 90, 1990.
2. G. ETSE, *Theoretische und numerische Untersuchung zum diffusen und lokalisierten Versagen in Beton,* [in German], PhD thesis, Universität Karlsruhe, Karlsruhe, 1992.
3. G. ETSE, *Finite element analysis of failure response behavior of anchor bolts in concrete,* Int. Journal of Nuclear Engineering and Design, 179, 245–252, 1998.
4. G. ETSE and K. WILLAM, *Fracture energy formulation for inelastic behavior of plain concrete,* Journal of Engineering Mechanics (ASCE), 120, 1983–2011, 1994.
5. CH. HELLMICH, F.-J. ULM, and H. A. MANG. *Consistent linearization in finite element analysis of coupled chemo-thermal problems with exo- or endothermal reactions,* Computational Mechanics, **24**, 4 238–244, 1999.
6. A. HILLERBORG, M. MODEER, and P.E. PETERSSON, *Analysis of crack formation and crack growth in concrete by means of fracture mechanics and finite elements,* Cement and Concrete Research, **6**, 773–782, 1976.

7. G. HOFSTETTER, J.C. SIMO, and R.L. TAYLOR, *A modified cap model: closest point solution algorithms,* Computers & Structures, **46**, 2, 203–214, 1993.

8. B. HURLBUT, *Experimental and computational investigation of strain-softening in concrete,* Master's thesis, University of Colorado, Boulder, USA, 1985.

9. H.A. MANG, R. LACKNER, P. PIVONKA, and CH. SCHRANZ, *Selected topics in computational structural mechanics,* In W.A. Wall, K.-U. Bletzinger, and K. Schweizerhof, editors, Trends in Computational Structural Mechanics, Lake Constance, Austria / Germany, pages 1–25, 2001.

10. G. MESCHKE, *Consideration of aging of shotcrete in the context of a 3D viscoplastic material model,* International Journal for Numerical Methods in Engineering, **39**, 3123–3143, 1996.

11. G. MESCHKE, R. LACKNER, and H.A. MANG, *An anisotropic elastoplastic-damage model for plain concrete,* International Journal for Numerical Methods in Engineering, **42**, (4):703–727, 1998.

12. M. ORTIZ, *A constitutive theory for the inelastic behavior of concrete,* Mech. of Materials, **4**; 67–93, 1985.

13. P. PIVONKA, R. LACKNER, and H. MANG, *Numerical analysis of concrete subjected to triaxial compressive loading,* [in:] CD-ROM Proceedings of the European Congress on Computational Methods in Applied Sciences and Engineering, Barcelona, Spain, 2000.

14. S. SMITH, *On fundamental aspects of concrete behavior,* Master's thesis, University of Colorado, Boulder, USA, 1987.

15. K. WILLAM and E. WARNKE, *Constitutive models for the triaxial behavior of concrete,* [in:] Int. Assoc. Bridge Struct. Eng. Sem. Concr. Struct. Subjected Triaxial Stresses, volume 19, pages 1–30, Bergamo, Italy, 1975. Int. Assoc. Bridge Struct. Eng. Proc.

Received May 20, 2001.

Arch. Mech., **53**, 4-5, pp. 501–518, Warszawa 2001

Generalized proper states for anisotropic elastic materials

J. OSTROWSKA-MACIEJEWSKA [(1)], J. RYCHLEWSKI [(2)]

[(1)] *Institute of Fundamental Technological Research, Polish Academy of Sciences,*

[(2)] *University of Warmia and Mazury in Olsztyn*

THE MAIN AIM OF THIS PAPER is to determine all the unit stresses $\omega(\omega \cdot \omega = 1)$ for which the stored elastic energy $\Phi(\omega)$ has the local extrema in some classes of stresses. Our consideration is restricted to two classes: $\mathcal{K}_1$ – uniaxial tensions and then the directions for which the Young modulus assumes its extremal value are determined, and $\mathcal{K}_2$ – pure shears in physical space. The problem is then reduced to the determination of the planes of minimal and maximal shear modulus. The idea of a generalized proper state for Hooke's tensor is introduced. It is shown that a mathematical treatment of the considered problem comes down to the problem of the generalized proper elastic states for the compliance tensor $\mathbf{C}$. The problem has been effectively solved for cubic symmetry.

1. Introduction

MOST MODERN MATERIALS are, or can be considered anisotropic. Composites have these properties due to the production technology, while the natural and biological bodies such as wood, bones, tissues, rock structures, can also be considered anisotropic.

Designation of the optimal structure needs some clear criteria for forming the properties of composite materials.

The aim of this paper is to provide clear criteria for controlling the properties of composite materials by a proper choice of the stiffness and /or compliance tensor at a given material point. The rules of this choice could be based upon the determination of the directions for which the Young modulus assumes its minimal and maximal values, as well as on the determination of the plane of minimal and maximal shear modulus, the Kirchhoff modulus.

It is convenient to make use of the qualitative description of the properties of the stiffness and the compliance tensors of anisotropic bodies developed by J. Rychlewski [1].

The problem considered is reduced to the problem of generalized proper elastic states for the compliance tensor. For cubic isotropy, the problem can be effectively solved. The solution obtained in the paper offers some new possibilities of approaching the problem of optimal formation of the internal structure of materials, eg. the direction of reinforcement of fibrous composites.

2. Formulation of the problem

We are discussing the classical materials, with linear elasticity, in which the infinitesimal strain $\boldsymbol{\varepsilon}$ causes the stress $\boldsymbol{\sigma}$ according to *Hooke's law*

$$\boldsymbol{\sigma} = \mathbf{S} \cdot \boldsymbol{\varepsilon}, \qquad \boldsymbol{\varepsilon} = \mathbf{C} \cdot \boldsymbol{\sigma}, \tag{2.1}$$

where $\mathbf{S}$ is the *stiffness tensor* and $\mathbf{C}$ is the *compliance tensor*. They are connected by the relation

$$\mathbf{S}^{-1} = \mathbf{C}, \quad \mathbf{S} \circ \mathbf{C} = \mathbf{C} \circ \mathbf{S} = \mathbb{I}_{\mathcal{S}}, \tag{2.2}$$

$$\mathbb{I}_S \cdot \boldsymbol{\sigma} = \boldsymbol{\sigma}.$$

The anisotropic form of Hooke's law written in indicial notation is given in the Appendix.

For the stress tensor $\boldsymbol{\sigma} \in \mathcal{S}$, the quadratic form

$$\Phi(\boldsymbol{\sigma}) = \boldsymbol{\sigma} \cdot \mathbf{C} \cdot \boldsymbol{\sigma} \tag{2.3}$$

is the doubled work of stress $\boldsymbol{\sigma}$. It is also called the complementary energy function or stored elastic energy function.

PROBLEM

We are looking for all unit stress states $\boldsymbol{\omega} \in \mathcal{K} \subset S$ $(\boldsymbol{\omega} \cdot \boldsymbol{\omega} = 1)$ for which the stored elastic energy has a local extremum. It means that

$$\Phi(\boldsymbol{\omega}) = \boldsymbol{\omega} \cdot \mathbf{C} \cdot \boldsymbol{\omega} = ext$$

for $\boldsymbol{\omega} \in \mathcal{K}$.

Our considerations are restricted to the two classes of stresses: $\mathcal{K}_1$ and $\mathcal{K}_2$. For these classes the solution of the problem is obtained in analytical form.

a) Uniaxial tensions $\boldsymbol{\sigma}$ in any direction $\mathbf{n}$ in the physical space are considered as the subspace $\mathcal{K}_1 \subset \mathcal{S}$

$$\mathcal{K}_1 : \{\boldsymbol{\omega} \in \mathcal{S};\ \boldsymbol{\omega} = \mathbf{n} \otimes \mathbf{n} \equiv \boldsymbol{\sigma}\}, \quad \mathbf{n} \cdot \mathbf{n} = 1. \tag{2.4}$$

In this case the stored elastic energy (2.3) may be rewritten as:

$$\Phi(\boldsymbol{\omega}) = \frac{1}{\lambda(\boldsymbol{\omega})} = \frac{1}{E(\boldsymbol{\sigma})} \tag{2.5}$$

and the local extremum of the *Young modulus* E is sought for.

b) Pure shears $\boldsymbol{\tau}$ in the plane $\mathbf{n}_1$, $\mathbf{n}_2$ in the physical space are forming the subspace $\mathcal{K}_2 \subset \mathcal{S}$

$$\mathcal{K}_2 \; : \; \{\boldsymbol{\omega} \in \mathcal{S}; \;\; \boldsymbol{\omega} = \frac{\sqrt{2}}{2}(\mathbf{n}_1 \otimes \mathbf{n}_2 + \mathbf{n}_2 \otimes \mathbf{n}_1) \equiv \boldsymbol{\tau}\}, \tag{2.6}$$

$$\mathbf{n}_1 \cdot \mathbf{n}_1 \; = \; \mathbf{n}_2 \cdot \mathbf{n}_2 = 1, \quad \mathbf{n}_1 \cdot \mathbf{n}_2 = 0.$$

The stored elastic energy (2.3) for pure shears has the following form:

$$\Phi(\boldsymbol{\omega}) = \frac{1}{\lambda(\boldsymbol{\omega})} = \frac{1}{2G(\boldsymbol{\tau})} \tag{2.7}$$

and the local extremum of *shear modulus* G is looked for.

From the definition of tensors $\boldsymbol{\sigma}$ (2.4) and from the definition of tensor $\boldsymbol{\tau}$ (2.6) it is evident that the subspaces $\mathcal{K}_1$ and $\mathcal{K}_2$ constitute the orbits, the group of rotations $\mathcal{O}$ in the space $\mathcal{S}$

$$\mathcal{K}_1 : \{\boldsymbol{\sigma} \in \mathcal{S}; \;\; \operatorname{tr}\boldsymbol{\sigma} = 1, \;\; \operatorname{tr}\boldsymbol{\sigma}^2 = 1, \;\; \operatorname{tr}\boldsymbol{\sigma}^3 = 1\}, \tag{2.8}$$

$$\mathcal{K}_2 : \{\boldsymbol{\tau} \in \mathcal{S}; \;\; \operatorname{tr}\boldsymbol{\tau} = 0, \;\; \operatorname{tr}\boldsymbol{\tau}^2 = 1, \;\; \operatorname{tr}\boldsymbol{\tau}^3 = 0\}. \tag{2.9}$$

3. Generalized proper states

Mathematical treatment of the above problem is the well-known Lagrange condition for the local extremum with constrains. The necessary extremum condition defines the generalized proper states problem for the compliance tensor $\mathbf{C}$.

We will call *Hooke's tensor* any Euclidean tensor of the fourth order $\mathbf{H}$ which realises a symmetric linear transformation of the space of symmetric second-order tensors $\mathcal{S}$ into itself. The space $\mathcal{S}$ is six-dimensional. Tensor $\mathbf{H}$ has the following internal symmetries:

$$H_{ijkl} = H_{jikl} = H_{klij} = H_{ijlk}. \tag{3.1}$$

DEFINITION 1. *For each Hooke's tensor* $\mathbf{H}$ *(3.1), the second order tensor* $\boldsymbol{\omega} \in \mathcal{S}$ $(\boldsymbol{\omega} \cdot \boldsymbol{\omega} = 1)$ *is called* the generalized proper state *of this tensor if there exists such parameters* α, β *and* γ *that*

$$\mathbf{H} \cdot \boldsymbol{\omega} = \alpha(\mathbf{H}, \boldsymbol{\omega})\mathbf{1} + \beta(\mathbf{H}, \boldsymbol{\omega})\boldsymbol{\omega} + \gamma(\mathbf{H}, \boldsymbol{\omega})\boldsymbol{\omega}^2. \tag{3.2}$$

The scalar functions α, β and γ can be obtained from the set of the linear equations:

$$\begin{aligned} \mathbf{1} \cdot \mathbf{H} \cdot \boldsymbol{\omega} &= 3\alpha + \operatorname{tr} \boldsymbol{\omega} \cdot \beta + \gamma, \\ \boldsymbol{\omega} \cdot H \cdot \boldsymbol{\omega} &= \operatorname{tr} \boldsymbol{\omega} \cdot \alpha + \beta + \operatorname{tr} \boldsymbol{\omega}^3 \cdot \gamma, \\ \boldsymbol{\omega}^2 \cdot \mathbf{H} \cdot \boldsymbol{\omega} &= \alpha + \operatorname{tr} \boldsymbol{\omega}^3 \cdot \beta + \operatorname{tr} \boldsymbol{\omega}^4 \cdot \gamma. \end{aligned} \tag{3.3}$$

When $\alpha = \gamma = 0$, the classical proper state problem is obtained

$$\mathbf{H} \cdot \boldsymbol{\omega} = \beta \boldsymbol{\omega}. \tag{3.4}$$

If as a tensor $\mathbf{H}$ the tensor $\mathbf{C}$ is considered, then $\boldsymbol{\omega}$ is a proper elastic state for compliance tensor $\mathbf{C}$ and $\lambda = \frac{1}{\beta}$ is the Kelvin modulus (see J. Rychlewski [1]). The equation

$$\mathbf{C} \cdot \boldsymbol{\omega} = \frac{1}{\lambda} \boldsymbol{\omega} \tag{3.5}$$

is the necessary condition for local extremum of the stored elastic energy (2.3) on unit sphere $\mathcal{K}$ in the stress space $\mathcal{S}$. It means that

$$\mathcal{K} : \{\boldsymbol{\omega} \in \mathcal{S}; \quad \boldsymbol{\omega} \cdot \boldsymbol{\omega} = 1\} \tag{3.6}$$

and $\mathcal{K}_1 \subset \mathcal{K}$ and $\mathcal{K}_2 \subset \mathcal{K}$.

3.1. Uniaxial tension

Mathematical treatment of the local extemum problem for (2.5) by the Lagrange multipliers method leads to the following necessary condition for $\boldsymbol{\sigma} \in \mathcal{K}_1$ (2.8):

$$\mathbf{C} \cdot \boldsymbol{\sigma} = \frac{1}{2}(\mathbf{1} \cdot \mathbf{C} \cdot \boldsymbol{\sigma} - \boldsymbol{\sigma} \cdot \mathbf{C} \cdot \boldsymbol{\sigma})\mathbf{1} + \frac{1}{2}(3\boldsymbol{\sigma} \cdot \mathbf{C} \cdot \boldsymbol{\sigma} - \mathbf{1} \cdot \mathbf{C} \cdot \boldsymbol{\sigma})\boldsymbol{\sigma}. \tag{3.7}$$

It is not difficult to notice that the above equation has the form of the Eq.(3.2) for a generalized proper state when $\gamma = 0$.

From the definition of the class $\mathcal{K}_1$ (2.4) it follows that the direction $\mathbf{n}$ is a proper vector for $\boldsymbol{\sigma}$

$$\boldsymbol{\sigma} \cdot \mathbf{n} = (\mathbf{n} \otimes \mathbf{n}) \cdot \mathbf{n} = \mathbf{n}. \tag{3.8}$$

Substituting the relation (3.8) into (3.7) after multiplying by $\mathbf{n}$ we obtain the following result:

$$(\mathbf{C}\cdot\boldsymbol{\sigma})\cdot\mathbf{n}=(\boldsymbol{\sigma}\cdot\mathbf{C}\cdot\boldsymbol{\sigma})\mathbf{n}. \tag{3.9}$$

It means that

$$[\mathbf{C}\cdot(\mathbf{n}\otimes\mathbf{n})]\cdot\mathbf{n}=[(\mathbf{n}\otimes\mathbf{n})\cdot\mathbf{C}\cdot(\mathbf{n}\otimes\mathbf{n})]\,\mathbf{n}. \tag{3.10}$$

According to the paper by S. C. Cowin, M. M. Mehrabadi [2], condition (3.10) is the necessary condition for the vector $\mathbf{n}$ to be normal to a plane of symmetry of a material of given compliance $\mathbf{C}$.

Any material which is not entirely anisotropic, like for example crystals of triclinic system, was called by A. Blinowski and J. Rychlewski [3] a symetric elastic material. They proved that every symmetric elastic material has at least one plane of elastic symmetry. Hence every symmetric elastic material has at least one direction with extremal Young modulus.

3.2. Pure shear

We now apply the Lagrange method for searching the local extremum of stored elastic energy (2.7). The necessary condition for $\boldsymbol{\tau}\in\mathcal{K}_2$ (2.9) has the following form:

$$\mathbf{C}\cdot\boldsymbol{\tau}=(\mathbf{1}\cdot\mathbf{C}\cdot\boldsymbol{\tau})\mathbf{1}+(\boldsymbol{\tau}\cdot\mathbf{C}\cdot\boldsymbol{\tau})\,\boldsymbol{\tau}+2(3\boldsymbol{\tau}^2\cdot\mathbf{C}\cdot\boldsymbol{\tau}-\mathbf{1}\cdot\mathbf{C}\cdot\boldsymbol{\tau})\,\boldsymbol{\tau}^2. \tag{3.11}$$

It is easy to see that a main direction of $\boldsymbol{\tau}$ is a main direction of $\mathbf{C}\cdot\boldsymbol{\tau}$, but not conversely. From the definition of $\boldsymbol{\tau}$ (2.6) we obtain that

$$\boldsymbol{\tau}^2=\frac{1}{2}(\mathbf{n}_1\otimes\mathbf{n}_1+\mathbf{n}_2\otimes\mathbf{n}_2).$$

For the plane tensors, the general description of the material can be significantly simplified. The same results obtained for the theory of plane elasticity are of self-contained value, more convenient for formulation and interpretation. For the two-dimensional case, the problem of local extrema of the stored elastic energy has been effectively solved in the paper by J. OSTROWSKA-MACIEJEWSKA, J. RYCHLEWSKI [4]. The solution obtained was discused in terms of energy limitations. The final solution depended strongly on the type and degree of anisotropy.

In a general three-dimensional case, the above problems are reduced, as it was shown, to the problem of generalized proper elastic states for the compliance tensor $\mathbf{C}$. The solution of the Eqs. (3.7) and (3.11) can be obtained only for some classes of symmetry.

4. Cubic isotropy

For quick orientation and to form an intuition in the presented approach, let us examine the simplest anisotropy, that is when the material has a cubic symmetry [7].

The spectral decomposition of compliance tensor $\mathbf{C}$ for cubic symmetry was given in the paper by J. OSTROWSKA-MACIEJEWSKA and J. RYCHLEWSKI [5] and has the form:

$$\mathbf{C} = \frac{1}{3\lambda_1}\mathbf{1}\otimes\mathbf{1}+\frac{1}{\lambda_2}(\mathbf{K}-\frac{1}{3}\mathbf{1}\otimes\mathbf{1})+\frac{1}{\lambda_3}(\mathbb{I}_{L_S}-\mathbf{K}), \tag{4.1}$$

where λ_1, λ_2, λ_3 are the essentially different Kelvin moduli for the three mutually orthogonal subspaces of the proper elastic states $\mathcal{P}_1, \mathcal{P}_2$ and $\mathcal{P}_3$

$$\mathcal{S} = \mathcal{P}_1 \dotplus \mathcal{P}_2 \dotplus \mathcal{P}_3. \tag{4.2}$$

If the directions $\mathbf{k}$, $\mathbf{l}$ and $\mathbf{m}$ coincide with the crystal axes for cubic isotropy (Fig. 1), the fourth-order tensor $\mathbf{K}$ may be represented in the form

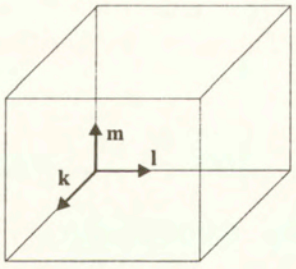

FIG. 1. Crystal axes $\mathbf{k}$, $\mathbf{l}$, $\mathbf{m}$.

$$\mathbf{K} = \mathbf{k}\otimes\mathbf{k}\otimes\mathbf{k}\otimes\mathbf{k}+\mathbf{l}\otimes\mathbf{l}\otimes\mathbf{l}\otimes\mathbf{l}+\mathbf{m}\otimes\mathbf{m}\otimes\mathbf{m}\otimes\mathbf{m}. \tag{4.3}$$

The space $\mathcal{P}_1$ is the one-dimensional subspace of spherical tensors:

$$\boldsymbol{\omega} \sim \begin{pmatrix} p & 0 & 0 \\ 0 & p & 0 \\ 0 & 0 & p \end{pmatrix}, \tag{4.4}$$

the space $\mathcal{P}_2$ is the two-dimensional subspace of deviators of diagonal form:

$$\boldsymbol{\omega} \sim \begin{pmatrix} u & 0 & 0 \\ 0 & v & 0 \\ 0 & 0 & -u-v \end{pmatrix}, \tag{4.5}$$

and the space $\mathcal{P}_3$ is the three-dimensional subspace of deviators of extradiagonal form:

$$\boldsymbol{\omega} \sim \begin{pmatrix} 0 & p & r \\ p & 0 & q \\ r & q & 0 \end{pmatrix} \tag{4.6}$$

in the crystal axes.

From the spectral decomposition (4.1) and the definitions of $\boldsymbol{\sigma}$ (2.8) and $\boldsymbol{\tau}$ (2.9), we obtain that

$$\mathbf{C} \cdot \boldsymbol{\sigma} = \frac{1}{3}\left(\frac{1}{\lambda_1} - \frac{1}{\lambda_2}\right)\mathbf{1} + \frac{1}{\lambda_3}\boldsymbol{\sigma} + \left(\frac{1}{\lambda_2} - \frac{1}{\lambda_3}\right)\mathbf{K} \cdot \boldsymbol{\sigma} \tag{4.7}$$

and

$$\mathbf{C} \cdot \boldsymbol{\tau} = \frac{1}{\lambda_3}\boldsymbol{\tau} + \left(\frac{1}{\lambda_2} - \frac{1}{\lambda_3}\right)\mathbf{K} \cdot \boldsymbol{\tau}. \tag{4.8}$$

It is easy to see from (4.7) that if $\boldsymbol{\sigma}$ is a proper state of $\mathbf{K}$ (4.3) then it is not a proper state of $\mathbf{C}$. Quite a different situation is for $\boldsymbol{\tau}$ (4.8): each proper state of $\mathbf{K}$ is a proper state of $\mathbf{C}$.

The stored elastic energy (2.5) and (2.7) for both classes of stresses $\mathcal{K}_1$ (2.4) and $\mathcal{K}_2$ (2.6) now may be rewritten as:

$$\Phi(\boldsymbol{\sigma}) = \frac{1}{E(\boldsymbol{\sigma})} = \boldsymbol{\sigma} \cdot \mathbf{C} \cdot \boldsymbol{\sigma} = \frac{1}{3}\left(\frac{1}{\lambda_1} - \frac{1}{\lambda_2} + \frac{3}{\lambda_3}\right) + \left(\frac{1}{\lambda_2} - \frac{1}{\lambda_3}\right)\boldsymbol{\sigma} \cdot \mathbf{K} \cdot \boldsymbol{\sigma}, \tag{4.9}$$

$$\Phi(\boldsymbol{\tau}) = \frac{1}{2G(\boldsymbol{\tau})} = \boldsymbol{\tau} \cdot \mathbf{C} \cdot \boldsymbol{\tau} = \frac{1}{\lambda_3} + \left(\frac{1}{\lambda_2} - \frac{1}{\lambda_3}\right)\boldsymbol{\tau} \cdot \mathbf{K} \cdot \boldsymbol{\tau}. \tag{4.10}$$

Let us denote by $E_1 = E_2 = E_3 = \mathrm{E}$ the Young moduli for the directions of the axes of crystal $\mathbf{k}, \mathbf{l}$ and $\mathbf{m}$, by $G_{12} = G_{13} = G_{23} = \mathrm{G}$ the shear moduli, and by $\nu_{12} = \nu_{13} = \nu_{23} = \nu$ the Poisson coefficients for the planes connected with the axes of the crystal; then the relation between these two sets of material constants $\mathrm{E}, \mathrm{G}, \nu$ and λ_1, λ_2, λ_3 are as follows:

$$\lambda_1 = \frac{\mathrm{E}}{1 - 2\nu}, \quad \lambda_2 = \frac{\mathrm{E}}{1 + \nu}, \quad \lambda_3 = 2\mathrm{G} \tag{4.11}$$

or

$$\mathrm{E} = \frac{3\lambda_1\lambda_2}{2\lambda_1 + \lambda_2}, \quad \nu = \frac{\lambda_1 - \lambda_2}{2\lambda_1 + \lambda_2}, \quad \mathrm{G} = \frac{\lambda_3}{2}. \tag{4.12}$$

The anisotropy tensor $\mathbf{C}$ (4.1) decomposes the space $\mathcal{S}$ into three mutually orthogonal subspaces $\mathcal{P}_1$, $\mathcal{P}_2$, $\mathcal{P}_3$ (4.2). Any state of stress $\boldsymbol{\omega}$ can be projected on

these subspaces and given as a sum of these portions. In the three-dimensional set of orthogonal coordinates connected with the subspaces of the proper states (4.2), the stored elastic energy (2.3) can be presented as a closed surface

$$\Phi(\boldsymbol{\omega}) = \boldsymbol{\omega} \cdot \mathbf{C} \cdot \boldsymbol{\omega} = \frac{\cos^2\theta\cos^2\varphi}{\lambda_1} + \frac{\cos^2\theta\sin^2\varphi}{\lambda_2} + \frac{\sin^2\theta}{\lambda_3}. \tag{4.13}$$

In order to draw this surface some material of cubic isotropy must be chosen.

For copper which is a typical material of cubic symmetry, moduli λ_i are given in the paper S. Sutcliffe [6], and they are as follows:

$$\lambda_1 = 41.6, \quad \lambda_2 = 4.7, \quad \lambda_3 = 15. \tag{4.14}$$

The succession of eigenvalues for copper is typical of most cubic isotropy metals with the lowest eigenvalue associated with the two-dimensional eigenspace $\mathcal{P}_2$ (4.5). The surface of the stored elastic energy for copper is shown in Fig. 2.

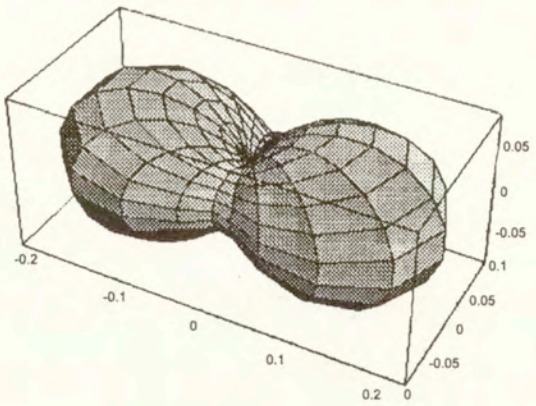

FIG. 2. Stored elastic energy in the space of proper elastic subspaces $\mathcal{P}_1, \mathcal{P}_2, \mathcal{P}_3$.

According to the paper by J. RYCHLEWSKI [1], the local extrema of the stored elastic energy on a unit sphere (3.6) are located on the axes of coordinates. Intersection of the surface (4.13) by the cone $\boldsymbol{\omega} = \mathbf{n} \otimes \mathbf{n}$ gives us the class of stresses $\mathcal{K}_1$ (2.4), but intersection by the plane of deviators describes the class $\mathcal{K}_2$ (2.6).

The surface of the stored elastic energy for the class of stresses $\mathcal{K}_1$ (2.8) is described by the Eq.(2.5). Since

$$\frac{1}{E(\boldsymbol{\sigma})} = \frac{1}{E(\mathbf{n} \otimes \mathbf{n})} = \frac{1}{E(\mathbf{n})}, \tag{4.15}$$

then this surface may be drawn in the physical space. Using the crystal axes $\mathbf{k}$, $\mathbf{l}$, $\mathbf{m}$, any direction $\mathbf{n}$ may be given as

$$\mathbf{n} = n_1\mathbf{k} + n_2\mathbf{l} + n_3\mathbf{m} \tag{4.16}$$

and the stress tensor $\boldsymbol{\sigma}$ (2.4) has the form

$$\begin{aligned}\boldsymbol{\sigma} = \mathbf{n}\otimes\mathbf{n} = n_1^2\mathbf{k}\otimes\mathbf{k} + n_2^2\mathbf{l}\otimes\mathbf{l} + n_3^2\mathbf{m}\otimes\mathbf{m} + \\ + n_1n_2(\mathbf{k}\otimes\mathbf{l} + \mathbf{l}\otimes\mathbf{k}) + n_1n_3(\mathbf{k}\otimes\mathbf{m} + \mathbf{m}\otimes\mathbf{k}) + n_2n_3(\mathbf{l}\otimes\mathbf{m} + \mathbf{m}\otimes\mathbf{l}).\end{aligned} \tag{4.17}$$

From the definition of tensor $\mathbf{K}$ (4.3) and the above form of $\boldsymbol{\sigma}$, it follows that

$$\boldsymbol{\sigma}\cdot\mathbf{K}\cdot\boldsymbol{\sigma} = (\mathbf{n}\otimes\mathbf{n})\cdot\mathbf{K}\cdot(\mathbf{n}\otimes\mathbf{n}) = n_1^4 + n_2^4 + n_3^4 = 1 - 2(n_1^2n_2^2 + n_2^2n_3^2 + n_3^2n_1^2) \tag{4.18}$$

and the formula for the stored elastic energy (4.9) for uniaxial tension takes the form

$$\begin{aligned}\frac{1}{E(\mathbf{n})} &= \frac{2\lambda_1 + \lambda_2}{3\lambda_1\lambda_2} + 2\frac{\lambda_2 - \lambda_3}{\lambda_2\lambda_3}(n_1^2n_2^2 + n_2^2n_3^2 + n_3^2n_1^2) \\ &= \frac{2\lambda_1 + \lambda_2}{3\lambda_1\lambda_2} + \frac{\lambda_2 - \lambda_3}{2\lambda_2\lambda_3}(\cos^4\theta\sin^2 2\varphi + \sin^2 2\theta).\end{aligned} \tag{4.19}$$

For computational purposes, the eigenvalues for copper (4.14) were used. The surface (4.19) for copper is shown in the Fig. 3.

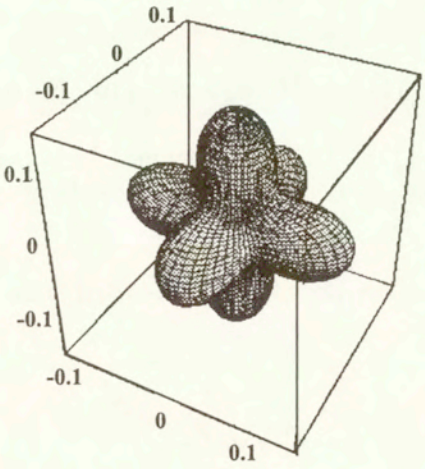

FIG. 3. Stored elastic energy under uniaxial tension in the physical space.

5. Local extrema of the Young modulus and the shear modulus for cubic isotropy.

In order to find the local extrema of the stored elastic energy for two classes of stresses $\mathcal{K}_1$ (2.4) and $\mathcal{K}_2$ (2.6), we have to come back to two equations for the generalized proper states of $\mathbf{C}$ (3.7) and (3.11).

For cubic isotropy, taking into account the spectral decomposition (4.1), the Eq.(3.7) and (3.11) may be rewritten as

$$\mathbf{K}\cdot\boldsymbol{\sigma} = \frac{1}{2}(1-\boldsymbol{\sigma}\cdot\mathbf{K}\cdot\boldsymbol{\sigma})\mathbf{1}+\frac{1}{2}(3\boldsymbol{\sigma}\cdot K\cdot\boldsymbol{\sigma}-1)\boldsymbol{\sigma}, \tag{5.1}$$

$$\mathbf{K}\cdot\boldsymbol{\tau} = (-2\tau^2\cdot\mathbf{K}\cdot\boldsymbol{\tau})\mathbf{1}+(\boldsymbol{\tau}\cdot\mathbf{K}\cdot\boldsymbol{\tau})\boldsymbol{\tau}+(6\tau^2\cdot\mathbf{K}\cdot\boldsymbol{\tau})\tau^2. \tag{5.2}$$

Please note that the obtained equations are the equations for generalised proper states of tensor $\mathbf{K}$ (4.3).

5.1. Young modulus

Let us begin with the class of stresses $\mathcal{K}_1$ (2.4) – uniaxial tension. Equation (5.1) is the necessery condition for the local extrema of Young's modulus. In order to determine the solution of the Eq. (5.1) we have to note that the tensor $\mathbf{K}\cdot\boldsymbol{\sigma}$ has a diagonal form in the crystal axes

$$\mathbf{K}\cdot\boldsymbol{\sigma} = n_1^2\mathbf{k}\otimes\mathbf{k}+n_2^2\mathbf{l}\otimes\mathbf{l}+n_3^2\mathbf{m}\otimes\mathbf{m}. \tag{5.3}$$

Equation (5.1) may be rewritten in the form

$$\mathbf{K}\cdot\boldsymbol{\sigma}-\frac{1}{2}(1-\boldsymbol{\sigma}\cdot\mathbf{K}\cdot\boldsymbol{\sigma})\,\mathbf{1} = \frac{1}{2}(3\boldsymbol{\sigma}\cdot\mathbf{K}\cdot\boldsymbol{\sigma}-1)\boldsymbol{\sigma}. \tag{5.4}$$

The left-hand side of the Eq. (5.4) has a diagonal form because of (5.3). It means that the right-hand side has to be diagonal as well. It will happen if tensor $\boldsymbol{\sigma}$ has the diagonal form

$$\boldsymbol{\sigma} = n_1^2\mathbf{k}\otimes\mathbf{k}+n_2^2\mathbf{l}\otimes\mathbf{l}+n_3^2\mathbf{m}\otimes\mathbf{m}, \tag{5.5}$$

or when

$$3\boldsymbol{\sigma}\cdot\mathbf{K}\cdot\boldsymbol{\sigma} = 1. \tag{5.6}$$

a) If Eq. (5.5) is satisfied, then from (5.3) we have

$$\mathbf{K}\cdot\boldsymbol{\sigma} = \boldsymbol{\sigma}, \text{ and } \boldsymbol{\sigma}\cdot\mathbf{K}\cdot\boldsymbol{\sigma} = \operatorname{tr}\sigma^2 = 1. \tag{5.7}$$

It means that $\boldsymbol{\sigma}$ is the proper state of $\mathbf{K}$ and from (4.7) it follows that

$$\mathbf{C}\cdot\boldsymbol{\sigma}=\frac{1}{3}\left(\frac{1}{\lambda_1}-\frac{1}{\lambda_2}\right)\mathbf{1}+\frac{1}{\lambda_2}\boldsymbol{\sigma} \tag{5.8}$$

and $\boldsymbol{\sigma}$ is a generalized proper state of $\mathbf{C}$. See (3.2) with $\gamma=0$.

The stored elastic energy (4.9) may be rewritten as

$$\Phi_a(\boldsymbol{\sigma})=\frac{1}{E(\boldsymbol{\sigma})}=\frac{2\lambda_1+\lambda_2}{3\lambda_1\lambda_2}. \tag{5.9}$$

The stress tensor $\boldsymbol{\sigma}$ (4.17) will have the form (5.5) if

$$n_1n_2=0,\quad n_1n_3=0,\quad n_2n_3=0. \tag{5.10}$$

It means that the direction $\mathbf{n}$ has to coincide with the directions of the crystal axes

$$\mathbf{n}=\mathbf{k},\quad \boldsymbol{\sigma}=\mathbf{k}\otimes\mathbf{k},$$

$$\mathbf{n}=\mathbf{l},\quad \boldsymbol{\sigma}=\mathbf{l}\otimes\mathbf{l}, \tag{5.11}$$

$$\mathbf{n}=\mathbf{m},\quad \boldsymbol{\sigma}=\mathbf{m}\otimes\mathbf{m}.$$

Hence the Young modulus has the local extrema in the direction of the crystal axes.

b) In the case when the condition (5.6) is satified, then

$$\boldsymbol{\sigma}\cdot\mathbf{K}\cdot\boldsymbol{\sigma}=\frac{1}{3}, \tag{5.12}$$

and from Eq. (5.4) we conclude

$$\mathbf{K}\cdot\boldsymbol{\sigma}=\frac{1}{3}\mathbf{1}=\frac{1}{3}(\mathbf{k}\otimes\mathbf{k}+\mathbf{l}\otimes\mathbf{l}+\mathbf{m}\otimes\mathbf{m}). \tag{5.13}$$

According to (5.3), the above formula means that

$$n_1^2=n_2^2=n_3^2=\frac{1}{3}. \tag{5.14}$$

Using (5.13), Eq. (4.7) may be rewritten as follows:

$$\mathbf{C}\cdot\boldsymbol{\sigma}=\frac{1}{3}\left(\frac{1}{\lambda_1}-\frac{1}{\lambda_3}\right)\mathbf{1}+\frac{1}{\lambda_3}\boldsymbol{\sigma}. \tag{5.15}$$

It is not difficult to notice that tensor $\boldsymbol{\sigma}$ is not a proper state for $\mathbf{C}$, but it is a generalized proper state of $\mathbf{C}$. Moreover, among eight possible forms, one of them may be presented as

$$\boldsymbol{\sigma} = \frac{1}{3}(\mathbf{k}+\mathbf{l}+\mathbf{m}) \otimes (\mathbf{k}+\mathbf{l}+\mathbf{m}). \tag{5.16}$$

The direction $\mathbf{n}$ (4.16) is hence perpendicular to the octahedral plane.

The Young moduli have local extrema for these directions. The stored elastic energy (4.9) in this case is as follows

$$\Phi_b = \frac{1}{E(\boldsymbol{\sigma})} = \frac{2\lambda_1 + \lambda_3}{3\lambda_1\lambda_3}. \tag{5.17}$$

If $\lambda_2 < \lambda_3$ (note that this situation occurs for copper (4.14)) then the following inequality is satisfied (Fig. 3)

$$\Phi_a(\boldsymbol{\sigma}) > \Phi_b(\boldsymbol{\sigma}). \tag{5.18}$$

5.2. Shear - Kirchhoff modulus

The necessary condition for the local extemum of the stored elastic energy for the class $\mathcal{K}_2$ (2.6) has the form (5.2). This fomula may be rewritten as

$$\mathbf{K}\cdot\boldsymbol{\tau}+2(\boldsymbol{\tau}^2\cdot\mathbf{K}\cdot\boldsymbol{\tau})\mathbf{1} = (\boldsymbol{\tau}\cdot\mathbf{K}\cdot\boldsymbol{\tau})\boldsymbol{\tau} + \mathbf{6}(\boldsymbol{\tau}^2\cdot\mathbf{K}\cdot\boldsymbol{\tau})\boldsymbol{\tau}^2. \tag{5.19}$$

The left-hand side of the above equation has diagonal representation in the system of crystal axes. The right-hand side will have the diagonal form if

a) tensor $\boldsymbol{\tau}$ has a diagonal form

$$\boldsymbol{\tau} \sim \begin{pmatrix} \tau_{11} & 0 & 0 \\ 0 & \tau_{22} & 0 \\ 0 & 0 & \tau_{33} \end{pmatrix}. \tag{5.20}$$

From the definition of tensor $\mathbf{K}$ (4.3) it follows that

$$\mathbf{K}\cdot\boldsymbol{\tau} = \boldsymbol{\tau}. \tag{5.21}$$

Tensor $\boldsymbol{\tau} \in \mathcal{K}_2$ (2.9). It means that the following conditions are satistfied:

$$\boldsymbol{\tau}\cdot\mathbf{K}\cdot\boldsymbol{\tau} = \operatorname{tr}\boldsymbol{\tau}^2 = 1, \qquad \boldsymbol{\tau}^2\cdot\mathbf{K}\cdot\boldsymbol{\tau} = \operatorname{tr}\boldsymbol{\tau}^3 = 0. \tag{5.22}$$

Note that τ is a proper state of $\mathbf{K}$ (5.21) and it follows immediately from (4.8) that it is the proper state of $\mathbf{C}$

$$\mathbf{C} \cdot \boldsymbol{\tau} = \frac{1}{\lambda_2} \boldsymbol{\tau}. \tag{5.23}$$

Comparing (5.20) with (4.5) we note that $\boldsymbol{\tau} \in \mathcal{P}_2$. Because $\boldsymbol{\tau} \in \mathcal{K}_2$ (2.9), then the following equations

$$\det \boldsymbol{\tau} = \tau_{11} \cdot \tau_{22} \cdot \tau_{33} = 0, \tag{5.24}$$

$$\operatorname{tr} \boldsymbol{\tau} = \tau_{11} + \tau_{22} + \tau_{33} = 0, \tag{5.25}$$

have to be satisfied. It means that one and only one term at the diagonal must be equal to zero. Without any loss of generality we can assume, for instance, that

$$\boldsymbol{\tau} \sim \frac{1}{\sqrt{2}} \begin{pmatrix} 1 & 0 & 0 \\ 0 & -1 & 0 \\ 0 & 0 & 0 \end{pmatrix}. \tag{5.26}$$

Tensor $\boldsymbol{\tau}$ (5.20) will have the above representation if

$$\mathbf{n}_1 = \frac{1}{\sqrt{2}}(\mathbf{k} - \mathbf{l}), \qquad \mathbf{n}_2 = \frac{1}{\sqrt{2}}(\mathbf{k} + \mathbf{l}); \tag{5.27}$$

then from the definition of $\boldsymbol{\tau}$ (2.6) we have

$$\boldsymbol{\tau} = \frac{1}{\sqrt{2}}(\mathbf{n}_1 \otimes \mathbf{n}_2 + \mathbf{n}_2 \otimes \mathbf{n}_1) = \frac{1}{\sqrt{2}}(\mathbf{k} \otimes \mathbf{k} - \mathbf{l} \otimes \mathbf{l}). \tag{5.28}$$

The stored elastic energy (4.10) in the case when $\boldsymbol{\tau}$ has the representation (5.20) is the following:

$$\Phi_a(\boldsymbol{\tau}) = \frac{1}{2G(\boldsymbol{\tau})} = \frac{1}{\lambda_2}. \tag{5.29}$$

Hence the shear modulus has a local extremum in the plane described by the directions (5.27).

b) Coming back to Eq. (5.19) we see that the right-hand side of that equation will have the diagonal form if

$$\mathbf{K} \cdot \boldsymbol{\tau} = \mathbf{0}. \tag{5.30}$$

It means that tensor $\boldsymbol{\tau}$ has now an extradiagonal form in the system of crystal axes

$$\boldsymbol{\tau} \sim \begin{pmatrix} 0 & \tau_{12} & \tau_{13} \\ \tau_{12} & 0 & \tau_{23} \\ \tau_{13} & \tau_{23} & 0 \end{pmatrix}. \tag{5.31}$$

From (5.30) it follows that

$$\boldsymbol{\tau} \cdot \mathbf{K} \cdot \boldsymbol{\tau} = 0 \quad \text{and} \quad \boldsymbol{\tau}^2 \cdot \mathbf{K} \cdot \boldsymbol{\tau} = 0. \tag{5.32}$$

Substituting (5.30) to (4.8) we obtain that $\boldsymbol{\tau}$ is a proper state of $\mathbf{C}$, namely

$$\mathbf{C} \cdot \boldsymbol{\tau} = \frac{1}{\lambda_3} \boldsymbol{\tau} \tag{5.33}$$

and according to (4.10), the stored elastic energy is now as follows:

$$\Phi_b(\boldsymbol{\tau}) = \frac{1}{2G(\boldsymbol{\tau})} = \frac{1}{\lambda_3}. \tag{5.34}$$

Tensor $\boldsymbol{\tau}$ (5.31), in view of its extradiagonal form, belongs to $\mathcal{P}_3$ (4.6). Definition $\mathcal{K}_2$ (2.6) implies that

$$\det \boldsymbol{\tau} = 2\tau_{12} \cdot \tau_{13} \cdot \tau_{23} = 0. \tag{5.35}$$

It means that at least one of the terms in the matrix representation (5.31)has to be equal to zero. Let us assume that $\tau_{23} = 0$; then $\boldsymbol{\tau}$ has the following form:

$$\boldsymbol{\tau} \sim \begin{pmatrix} 0 & \tau_{12} & \tau_{13} \\ \tau_{12} & 0 & 0 \\ \tau_{13} & 0 & 0 \end{pmatrix}, \tag{5.36}$$

or may be rewritten as

$$\boldsymbol{\tau} = \tau_{12}(\mathbf{k} \otimes \mathbf{l} + \mathbf{l} \otimes \mathbf{k}) + \tau_{13}(\mathbf{k} \otimes \mathbf{m} + \mathbf{m} \otimes \mathbf{k}). \tag{5.37}$$

From the definition of $\boldsymbol{\tau}$ (2.6) we obtain that $\boldsymbol{\tau}$ will have the form (5.37) for

$$\mathbf{n}_1 = \mathbf{k}, \quad \text{and} \quad \mathbf{n}_2 = \sqrt{2}(\tau_{12}\mathbf{l} + \tau_{13}\mathbf{m}). \tag{5.38}$$

The terms τ_{12} and τ_{13} are not independent. Hence $\boldsymbol{\tau} \in \mathcal{K}_2$ and then

$$\operatorname{tr} \boldsymbol{\tau}^2 = 2(\tau_{12}^2 + \tau_{13}^2) = 1. \tag{5.39}$$

In the limiting cases we have

$$\begin{aligned} &\tau_{13} = 0, \quad \tau_{12}^2 = \frac{1}{2} \quad \text{and} \quad \mathbf{n}_1 = \mathbf{k}, \ \mathbf{n}_2 = \pm\mathbf{l}, \\ &\tau_{12} = 0, \quad \tau_{13}^2 = \frac{1}{2} \quad \text{and} \quad \mathbf{n}_1 = \mathbf{k}, \ \mathbf{n}_2 = \pm\mathbf{m}. \end{aligned} \tag{5.40}$$

It means that there is the family of planes with the same value of shear modulus (5.34).

Changing the order of the crystal axes we will obtain other planes with extremal value (5.34) of the shear modulus.

c) The equation (5.19) may have another solution than the one mentioned above. Let us now assume that $\boldsymbol{\tau}$ has a full matrix representation in the system of crystal axes

$$\boldsymbol{\tau} \sim \begin{pmatrix} \tau_{11} & \tau_{12} & \tau_{13} \\ \tau_{12} & \tau_{22} & \tau_{23} \\ \tau_{13} & \tau_{23} & \tau_{33} \end{pmatrix}. \tag{5.41}$$

According to the definition of $\mathcal{K}_2$ (2.9), the following equations have to be satisfied:

$$\begin{aligned} &\operatorname{tr}\boldsymbol{\tau} = \tau_{11} + \tau_{22} + \tau_{33} = 0, \\ &\operatorname{tr}\boldsymbol{\tau}^2 = \tau_{11}^2 + \tau_{22}^2 + \tau_{33}^2 + 2\tau_{12}^2 + 2\tau_{13}^2 + 2\tau_{23}^2 = 1, \\ &\frac{1}{3}\operatorname{tr}\boldsymbol{\tau}^3 = \det\boldsymbol{\tau} = \tau_{11}\tau_{22}\tau_{33} + 2\tau_{12}\tau_{13}\tau_{23} - \tau_{11}\tau_{23}^2 - \tau_{22}\tau_{13}^2 - \tau_{33}\tau_{12}^2 = 0. \end{aligned} \tag{5.42}$$

Tensor $\mathbf{K}\cdot\boldsymbol{\tau}$ has a diagonal form

$$\mathbf{K}\cdot\boldsymbol{\tau} \sim \begin{pmatrix} \tau_{11} & 0 & 0 \\ 0 & \tau_{22} & 0 \\ 0 & 0 & \tau_{33} \end{pmatrix}$$

and from this we see at once that

$$\operatorname{tr}(\mathbf{K}\cdot\boldsymbol{\tau}) = (\mathbf{1}\cdot\mathbf{K}\cdot\boldsymbol{\tau}) = \operatorname{tr}\boldsymbol{\tau} = 0$$

and

$$\boldsymbol{\tau}\cdot\mathbf{K}\cdot\boldsymbol{\tau} = \tau_{11}^2 + \tau_{22}^2 + \tau_{33}^2, \tag{5.43}$$

$$(\mathbf{K}\cdot\boldsymbol{\tau})\cdot(\mathbf{K}\cdot\boldsymbol{\tau}) = \tau_{11}^2 + \tau_{22}^2 + \tau_{33}^2. \tag{5.44}$$

Combining (5.44) with $(5.42)_2$ we conclude that

$$0 \leqslant \tau_{11}^2 + \tau_{22}^2 + \tau_{33}^2 \leqslant 1. \tag{5.45}$$

Substituting (5.44) by (4.10) we can rewrite (4.10) as

$$\Phi_c(\boldsymbol{\tau}) = \frac{1}{2G(\boldsymbol{\tau})} = \boldsymbol{\tau}\cdot\mathbf{C}\cdot\boldsymbol{\tau} = \frac{1}{\lambda_3} + (\frac{1}{\lambda_2} - \frac{1}{\lambda_3})(\tau_{11}^2 + \tau_{22}^2 + \tau_{33}^2). \tag{5.46}$$

We may now turn to the assumption $\lambda_2 < \lambda_3$ (it is valid for copper (4.14)). In this case it is easy to see that

$$\frac{1}{\lambda_3} \leqslant \Phi_c(\boldsymbol{\tau}) \leqslant \frac{1}{\lambda_2}. \tag{5.47}$$

Substituting (5.29) and (5.34) by (5.47) we obtain

$$\Phi_b(\boldsymbol{\tau}) \leqslant \Phi_c(\boldsymbol{\tau}) \leqslant \Phi_a(\boldsymbol{\tau}). \tag{5.48}$$

When tensor $\boldsymbol{\tau}$ has the form (5.41), the equations (5.42) together with (5.19) form a set of nine equations for six components of $\boldsymbol{\tau}$ (5.41). It means that the set in general has no solution. From (5.19) it is easy to conclude that

$$(\mathbf{K}\cdot\boldsymbol{\tau})\cdot(\mathbf{K}\cdot\boldsymbol{\tau}) = (\boldsymbol{\tau}\cdot\mathbf{K}\cdot\boldsymbol{\tau})^2 + 6(\boldsymbol{\tau}^2\cdot\mathbf{K}\cdot\boldsymbol{\tau})^2. \tag{5.49}$$

Substituting (5.43) and (5.44) by (5.49) we get

$$3(\boldsymbol{\tau}^2\cdot\mathbf{K}\cdot\boldsymbol{\tau})^2 = (\tau_{11}^2 + \tau_{22}^2 + \tau_{33}^2)(\tau_{12}^2 + \tau_{13}^2 + \tau_{23}^2). \tag{5.50}$$

It means that

$$\boldsymbol{\tau}^2\cdot\mathbf{K}\cdot\boldsymbol{\tau} = 0$$

if and only if $\boldsymbol{\tau}$ is a proper state of $\mathbf{C}$. On the other hand, using the definition $\boldsymbol{\tau}^2$ and $\mathbf{K}\cdot\boldsymbol{\tau}$ and the property of $\boldsymbol{\tau}$ (5.42), we obtain

$$\boldsymbol{\tau}^2\cdot\mathbf{K}\cdot\boldsymbol{\tau} = 2(\tau_{11}\tau_{22}\tau_{33} - \tau_{12}\tau_{13}\tau_{23}). \tag{5.51}$$

There are solutions of (5.19) for which

$$\boldsymbol{\tau}^2\cdot\mathbf{K}\cdot\boldsymbol{\tau} \neq 0.$$

For instance, if we make the following assumption:

$$\tau_{23} = 0, \qquad \tau_{11}\tau_{22}\tau_{33} \neq 0$$

then we find from (5.19) and (5.42) that

$$\tau_{11}^2 = \tau_{22}^2 = \tau_{12}^2 = \frac{1}{8}, \quad \tau_{33}^2 = \frac{1}{2}, \quad \tau_{13} = \tau_{23} = 0, \tag{5.52}$$

$$\tau_{11} = \tau_{22}, \qquad \tau_{33} = -(\tau_{11} + \tau_{22}).$$

Substituting (5.52) by (5.43) we get

$$\boldsymbol{\tau} \cdot \mathbf{K} \cdot \boldsymbol{\tau} = \tau_{11}^2 + \tau_{22}^2 + \tau_{33}^2 = \frac{3}{4}. \tag{5.53}$$

If tensor $\boldsymbol{\tau}$ is taken as

$$\boldsymbol{\tau} \sim \frac{1}{\sqrt{8}} \begin{pmatrix} 1 & 1 & 0 \\ 1 & 1 & 0 \\ 0 & 0 & -2 \end{pmatrix} \tag{5.54}$$

then it satisfies (5.52) and the vectors $\mathbf{n}_1$, $\mathbf{n}_2$ (2.6) are as follows:

$$\mathbf{n}_1 = \frac{1}{2}(\mathbf{k} + \mathbf{l} + \sqrt{2}\mathbf{m}), \qquad \mathbf{n}_2 = \frac{1}{2}(\mathbf{k} + \mathbf{l} - \sqrt{2}\mathbf{m}).$$

The stored elastic energy (4.10) in this case has the form

$$\Phi_c(\boldsymbol{\tau}) = \frac{1}{2G(\boldsymbol{\tau})} = \frac{\lambda_2 + 3\lambda_3}{4\lambda_2\lambda_3}. \tag{5.55}$$

It is easy to see that for copper

$$\Phi_b(\boldsymbol{\tau}) \leqslant \Phi_c(\boldsymbol{\tau}) \leqslant \Phi_a(\boldsymbol{\tau}),$$

and there are no local extrema of the stored elastic energy at this $\boldsymbol{\tau}$.

In this same manner we can consider the following assumption:

$$\tau_{33} = 0, \ \tau_{12} \cdot \tau_{13} \cdot \tau_{23} \neq 0.$$

An easy computation shows that there is no solution (5.19) of the above form.

The obtained results show that for cubic isotropy, the Young modulus has local extrema in the directions of the axes of crystal and the directions perpendicular to the octahedral planes. Uniaxial tension $\boldsymbol{\sigma} = \mathbf{n} \otimes \mathbf{n}$ is a generalized proper state of the compliance tensor $\mathbf{C}$. There is quite a different situation for the shear modulus. The Kirchhoff modulus has local extrema for some deviatoric proper states of $\mathbf{C}$ with the constraint $\det \boldsymbol{\tau} = 0$.

Appendix. Notation

For readers more accustomed to the usual Cartesian index notation, we shall add a convenient rephrasing of formulae:

$$\boldsymbol{\sigma} = \mathbf{S} \cdot \boldsymbol{\varepsilon} \leftrightarrow \sigma_{ij} = S_{ijkl}\varepsilon_{kl}, \quad \boldsymbol{\varepsilon} = \mathbf{C} \cdot \boldsymbol{\sigma} \leftrightarrow \varepsilon_{mn} = C_{mnij}\sigma_{ij},$$

$$\mathbf{S} \circ \mathbf{C} = \mathbf{C} \circ \mathbf{S} = \mathbb{I}_{\mathcal{S}} \leftrightarrow S_{ijkl}C_{klmn} = C_{ijkl}S_{klmn} = \frac{1}{2}(\delta_{im}\delta_{jn} + \delta_{in}\delta_{jm}),$$

$$\boldsymbol{\sigma}\cdot\mathbf{C}\cdot\boldsymbol{\sigma}\leftrightarrow C_{pqrs}\sigma_{pq}\sigma_{rs},\qquad \boldsymbol{\omega}\cdot\boldsymbol{\omega}\leftrightarrow\omega_{ij}\omega_{ij},$$

$$\mathbf{1}\leftrightarrow\delta_{ij}\ \text{(Kronecker's symbol)},$$

$$\mathbf{n}\otimes\mathbf{n}\leftrightarrow n_in_j,$$

$$\mathbf{1}\cdot\mathbf{H}\cdot\boldsymbol{\omega}\leftrightarrow H_{pprs}\omega_{rs},$$

$$\mathbf{C}\cdot(\mathbf{n}\otimes\mathbf{n})\leftrightarrow C_{ijkl}n_kn_l,$$

$$\boldsymbol{\tau}^2\cdot\mathbf{C}\cdot\boldsymbol{\tau}\leftrightarrow C_{ijkl}\tau_{im}\tau_{mj}\tau_{kl},$$

$$\operatorname{tr}\boldsymbol{\sigma}=\mathbf{1}\cdot\boldsymbol{\sigma}=\sigma_{pp},\quad \operatorname{tr}\boldsymbol{\sigma}^2=\sigma_{pq}\sigma_{pq},\quad \operatorname{tr}\boldsymbol{\sigma}^3=\sigma_{pq}\sigma_{qr}\sigma_{rp},$$

$$\begin{aligned}\mathbf{K} &= \mathbf{k}\otimes\mathbf{k}\otimes\mathbf{k}\otimes\mathbf{k}+\mathbf{l}\otimes\mathbf{l}\otimes\mathbf{l}\otimes\mathbf{l}+\mathbf{m}\otimes\mathbf{m}\otimes\mathbf{m}\otimes\mathbf{m},\\ K_{pqrs} &= k_pk_qk_rk_s+l_pl_ql_rl_s+m_pm_qm_rm_s.\end{aligned}$$

Acknowledgements

Most of the results reported in the paper were obtained in the framework of the research supported by the Project of the Committee of the Scientific Research (KBN) No.7 T07A 032 12.

References

1. J. RYCHLEWSKI, *Unconventional approach to linear elasticity,* Arch. Mech., **47,** 2, 149-171, 1995.
2. S. C. COWIN AND M. M. MEHRABADI, *On the identification of material symmetry for anisotropic elastic materials,* Quart. J. Mech. Appl. Math. 40, 451-476, 1987.
3. A. BLINOWSKI, J. RYCHLEWSKI, *Pure shears in the mechanics of materials,* Math. and Mech. of Solids **4,** 471-503, 1998.
4. J. OSTROWSKA-MACIEJEWSKA, J. RYCHLEWSKI, *On the minimal and maximal stiffness moduli of anisotropic media in the two-dimensional case,* (to be published).
5. J. OSTROWSKA-MACIEJEWSKA, J. RYCHLEWSKI, *Plane elastic and limit states in anisotropic solids,* Arch. Mech., **40,** 379-386, 1988.
6. S. SUTCLIFFE, *Spectral decomposition of the elasticity tensor,* J. Appl. Mech. Trans. of ASME, 59, 762-774, 1992.
7. JU. I. SIROTIN, M. P. SASKOLSKAJA, *Foundations of crystal physics* [in Russian], Izd. "Nauka", Moskva 1975.

Received February 9, 2001.

Arch. Mech., **53**, 4-5, pp. 519–539, Warszawa 2001

Physical reasons for abandoning plastic deformation measures in plasticity and viscoplasticity theory

M.B. RUBIN

Faculty of Mechanical Engineering Technion
Israel Institute of Technology
32000 Haifa, Israel
e-mail: mbrubin@tx.technion.ac.il

CONSTITUTIVE EQUATIONS, which characterize the response of a material to future loadings, must depend on state variables that, in principle, can be measured without any prior knowledge of the past history of deformation of the material. This notion of state is consistent with that proposed by ONAT [3] and it is consistent with GILMAN'S comment [4] on physical problems with using total strain as a state variable in plasticity theory. Within the context of this notion of state, elastic strain is a state variable, whereas the total strain and plastic strains are not state variables since they are measured with respect to an arbitrary reference configuration. Alternative constitutive equations which are formulated in terms of elastic deformation measures have been discussed in the literature for finite deformations of elastically isotropic and anisotropic elastic-plastic and elastic-viscoplastic materials. These constitutive equations have the physical properties that they are independent of the choice of the reference configuration, and they do not utilize any measures of total deformation or plastic deformation. The main objectives of this paper are to discuss physical reasons for abandoning total and plastic deformation measures in plasticity and viscoplasticity theory, and to present an alternative small deformation theory which is formulated in terms of elastic strain. Also, aspects of alternative finite deformation theories are reviewed.

1. Introduction

THE MAIN OBJECTIVES of this paper are to discuss physical reasons for abandoning total and plastic deformation measures in plasticity and viscoplasticity theory and to present an alternative small deformation theory which is formulated in terms of elastic strain. This point of view is motivated by the notion that deformation measures are, by definition, relative measures which depend explicitly on the choice of the reference from which they are defined. More specifically, total strain is a measure of the deformation of the body from a fixed, but arbitrary reference configuration. Consequently, the total strain measure depends explicitly on the choice of the reference configuration and thus inherits all of the

arbitrariness of this choice. Similarly, plastic deformation and strain measures are also defined relative to the reference configuration so they too inherit certain arbitrariness. Some ideas related to this perspective have been presented in [1,2].

To be more specific, it is emphasized that given a sample of material in its present configuration, there is no set of experiments that can be used to determine completely the past history of deformation of the material or the arbitrary choice of the reference configuration. Moreover, the physical response of a material, which is characterized by its constitutive equation, cannot depend on the arbitrary choice of the reference configuration. Consequently, such constitutive equations must depend on variables which characterize the state of the material. To avoid arbitrariness, these state variables should have the property that, in principle, they can be measured (given enough identical samples of the material in its present configuration) without any prior knowledge of the past history of deformation of the material. This notion of state is consistent with that proposed by ONAT [3] and it is consistent with GILMAN'S comment [4] on physical problems using the strain as a state variable in plasticity theory:

> "It seems very unfortunate to me that the theory of plasticity was ever cast into a mold of stress-strain relations because 'strain' in the plastic case has no physical meaning that is related to the *material* of the body in question. It is rather like trying to deduce some properties of a liquid from the shape of the container that holds it. The plastic behaviour of a body depends on its structure (crystalline and defect), and on the system of stresses that is applied to it."

Further in this regard, it is noted that some quantities like position, velocity, temperature, force and stress on the outer surface of a body are presumed to be measurable directly. Whereas, other quantities like a hardening variable in plasticity theory are presumed to be measurable indirectly by interpreting the results of experimental data using a general but specific constitutive equation. Moreover, since only constitutive equations for simple materials are considered, it is sufficient to confine attention to the response of uniform, homogeneous materials. Also, the complications of analyzing a sample of material which has been subjected to inhomogeneous deformations and which can have residual stresses, is not considered here.

An outline of this paper is as follows. Section 2 distinguishes between the notions of material states and configurations and it describes some properties of a thermoelastic solid. Section 3 presents a dissipation inequality for the purely mechanical theory and Sec. 4 discusses the main ideas of this paper within the context of the small deformation theory. Then, Sec. 5 and 6 briefly review alternative constitutive equations for finite deformations of elastically isotropic and elastically anisotropic materials, respectively, and Sec. presents conclusions.

Throughout the text, vectors and tensors are denoted by bold- faced symbols; $\mathbf{a} \cdot \mathbf{b}$ denotes the usual dot product of two vectors $\mathbf{a}$ and $\mathbf{b}$;$\mathbf{A} \cdot \mathbf{B} = \mathrm{tr}(\mathbf{A}\mathbf{B}^{\mathrm{T}})$ denotes the dot product of two second order tensors; $\mathrm{tr}(\mathbf{A})$ denotes the trace of $\mathbf{A}$; $\mathbf{B}^{\mathrm{T}}$ denotes the transpose of $\mathbf{B}$; $\mathbf{A}^{-1}$ denotes the inverse of $\mathbf{A}$; $\mathbf{a}\otimes\mathbf{b}$ denotes the tensor product of $\mathbf{a}$ and $\mathbf{b}$; and $\mathbf{I}$ is the unit second order tensor. Also, the usual summation convention is implied over all repeated indices except (e,p,m) which are used to denote elastic, plastic, and microstructural quantities, respectively.

2. Material states, configurations and a thermoelastic solid

The notion of a material state is both mathematical and physical. From the mathematical point of view, a material state is the collection of all variables that are needed to predict the response of the material to future mechanical and thermal loadings. On the other hand, from the physical point of view, these state variables are restricted only to those variables which can be measured, in principle, by experiments on identical samples of the material. For the present discussion, it is convenient to introduce the notion of the *Reference State*.

> The *Reference State* of a material is any state of the material when it is stress-free and at absolute reference temperature θ_0.

Here, a thermoelastic solid is assumed to have a unique shape in its *Reference State*. Consequently, since the stress and temperature can be measured, it is always possible to determine this reference shape by unloading the material to its *Reference State*. This also means that it is natural to introduce a measure of elastic strain from this reference shape. Thus, the elastic strain and the absolute temperature θ are the state variables which characterize a thermoelastic solid. Moreover, by definition, the elastic strain vanishes whenever the material is in its *Reference State*.

The notion of a configuration is a mathematical mapping of the position of all material points onto the physical space, as well as a mapping of all of the state variables onto an appropriately dimensioned vector space. In particular, with reference to a fixed origin, a material point Y is mapped onto the position vector $\mathbf{X}$ in the fixed reference configuration and the same material point is mapped onto the position vector $\mathbf{x}$ in the present configuration at time t.

Consequently, a configuration is a mathematical representation of the physical state of the material. Moreover, since the notion of the *Reference State* fixes only the values of the stress and the temperature, there are an infinite number of configurations of a body in its *Reference State*. These configurations include all superposed rigid body motions as well as a group of homogeneously deformed configurations for elastic-plastic materials.

3. Rate of material dissipation in the purely mechanical theory

To present the physical argument in its simplest terms, it is convenient to focus attention on the purely mechanical theory for which θ equals the reference temperature θ_0. More specifically, with reference to the present configuration, it is convenient to consider a material region P with smooth closed surface ∂P. Now, the rate of material dissipation $\mathcal{D}$ can be defined by the equation

$$\int_P \mathcal{D} dv = \mathcal{W} - \dot{\mathcal{K}} - \dot{\mathcal{U}}, \tag{3.1}$$

where a superposed dot denotes material time differentiation, $\mathcal{W}$ is the rate of work due to the specific (per unit mass) external body force $\mathbf{b}$ and the surface tractions $\mathbf{t}$, $\mathcal{K}$ is the kinetic energy, and $\mathcal{U}$ is the internal strain energy due to the specific strain energy function Σ, which are defined by

$$\mathcal{W} = \int_P \rho \mathbf{b} \cdot \mathbf{v} dv + \int_{\partial P} \mathbf{t} \cdot \mathbf{v} da, \quad K = \int_P \frac{1}{2} \rho \mathbf{v} \cdot \mathbf{v} dv, \quad U = \int_P \rho \Sigma dv. \tag{3.2}$$

In these formulas, ρ is the present value of the mass density, $\mathbf{v}$ is the absolute velocity of a material point, dv is the present element of volume and da is the present element of area.

Next, using the conservation of mass, the balances of linear and angular momentum, the fact that the traction vector is related to the Cauchy stress $\mathbf{T}$ and the outward unit normal vector $\mathbf{n}$ to ∂P by the formula $\mathbf{t}=\mathbf{Tn}$, and using standard continuity assumptions, it can be shown that the local form of the dissipation $\mathcal{D}$ becomes

$$\mathcal{D} = \mathbf{T} \cdot \mathbf{D} - \rho \dot{\Sigma} \geq 0. \tag{3.3}$$

In this expression, $\mathbf{D}$ is the symmetric part of the velocity gradient $\mathbf{L}=\partial \mathbf{v}/\partial \mathbf{x}$ and $\mathbf{W}$ is its skew-symmetric part, which are defined by

$$\mathbf{L} = \mathbf{D} + \mathbf{W}, \quad \mathbf{D} = \frac{1}{2}(\mathbf{L} + \mathbf{L}^T), \quad \mathbf{W} = \frac{1}{2}(\mathbf{L} - \mathbf{L}^T). \tag{3.4}$$

Moreover it is assumed that the rate of material dissipation $\mathcal{D}$ must be non-negative for all motions.

4. Small deformation theory of elastic-viscoplastic materials

A review of the small deformation theory of plasticity and thermoplasticity can be found in [5]. Within the context of this theory, the plastic strain $\boldsymbol{\varepsilon}_p$ can be introduced through an evolution equation for its rate of the form

$$\dot{\boldsymbol{\varepsilon}} = \mathbf{D}_p, \quad \mathbf{D}_p = \Gamma \bar{\mathbf{D}}_p, \quad \Gamma \geq 0, \quad \bar{\mathbf{D}}_p^T = \bar{\mathbf{D}}_p, \tag{4.1}$$

where $\mathbf{D}_p$ represents the relaxation effects of plasticity on the stress. In this equation, the symmetric second order tensor $\bar{\mathbf{D}}_p$ controls the direction of plastic strain rate and the non-negative scalar Γ influences the magnitude of plastic strain rate. Also, it is common to introduce hardening variables which control both the isotropic hardening and directional hardening [6]. However, here, it suffices to consider only isotropic hardening κ which is determined by integrating the evolution equation

$$\dot{\kappa} = \Gamma K, \tag{4.2}$$

where K requires a constitutive equation. Moreover, for nonporous metals, it is usually assumed that plastic deformation is isochoric so that $\bar{\mathbf{D}}_p$ must satisfy the restriction

$$\bar{\mathbf{D}}_p \cdot \mathbf{I} = 0, \tag{4.3}$$

which causes $\boldsymbol{\varepsilon}_p$ to be a deviatoric tensor. Furthermore, it can be observed from the evolution equations (4.1) and (4.2) that when Γ vanishes, both the plastic strain rate and hardening rate vanish, so the material response becomes elastic.

If both of the evolution equations (4.1) and (4.2) are homogeneous of order one in time, then the constitutive equations characterize rate-insensitive plasticity. Otherwise, the constitutive equations characterize rate-sensitive viscoplasticity. For plasticity theory with a yield function [5], the scalar Γ in (4.1) is determined by a consistency condition in both the stress-space and strain-space [7] formulations. For the overstress formulation of viscoplasticity [8,9], the yield function is retained but the consistency condition is no longer enforced. Also, an alternative unified formulation of viscoplasticity can be proposed which does not use either a yield function or the consistency condition [10-12].

Total strain $\boldsymbol{\varepsilon}$ is a measure of the deformation of the material from a specified fixed reference configuration. Within the context of the small deformation theory, the total strain can be separated into a pure measure of dilatation ε and a deviatoric tensor $\boldsymbol{\varepsilon}'$, which is a pure measure of distortion, such that

$$\boldsymbol{\varepsilon} = \frac{\varepsilon}{3}\mathbf{I} + \boldsymbol{\varepsilon}', \quad \varepsilon = \boldsymbol{\varepsilon} \cdot \mathbf{I}, \quad \boldsymbol{\varepsilon}' \cdot \mathbf{I} = 0. \tag{4.4}$$

Moreover, these quantities can be obtained by integrating equations for their rates which can be approximated by the formulas

$$\dot{\varepsilon} = \mathbf{D} \cdot \mathbf{I}, \quad \dot{\boldsymbol{\varepsilon}} = \mathbf{D}' = \mathbf{D} - \frac{1}{3}(\mathbf{D} \cdot \mathbf{I})\mathbf{I}, \tag{4.5}$$

where $\mathbf{D}'$ is the deviatoric part of $\mathbf{D}$.

For an elastic material, it is common to express the stress as a unique function of the total strain $\boldsymbol{\varepsilon}$ that is insensitive to the history of loading. In contrast, the

response of an elastic-plastic material depends on the history of loading and the stress can have different values for the same value of total strain. One of the reasons for introducing the plastic strain $\boldsymbol{\varepsilon}_{\mathrm{p}}$ in plasticity theory is to account for this history-dependence. Also, since it is usually assumed that stress depends on elastic strain $\boldsymbol{\varepsilon}_{\mathrm{e}}$, it is necessary to introduce an additional definition of elastic strain as a function of total strain and plastic strain. In the small deformation theory this definition is simply the difference between the total and plastic strains

$$\boldsymbol{\varepsilon}_e = \boldsymbol{\varepsilon} - \boldsymbol{\varepsilon}_p \tag{4.6}$$

Furthermore, using the fact that $\boldsymbol{\varepsilon}_{\mathrm{p}}$ is a deviatoric tensor, it follows that the elastic strain can be represented in the form

$$\boldsymbol{\varepsilon}_e = \frac{\varepsilon_e}{3}\mathbf{I} + \boldsymbol{\varepsilon}'_e, \quad \varepsilon_e = \varepsilon, \quad \boldsymbol{\varepsilon}'_e = \boldsymbol{\varepsilon}' - \boldsymbol{\varepsilon}_p, \tag{4.7}$$

where ε_e is a measure of elastic dilatation and $\boldsymbol{\varepsilon}'_e$ is a measure of elastic distortion.

Next, it is assumed that the stress $\mathbf{T}$ and the strain energy Σ are functions of the elastic strains only

$$\mathbf{T} = \mathbf{T}(\varepsilon_e, \boldsymbol{\varepsilon}'_e), \quad \Sigma = \Sigma(\varepsilon_e, \boldsymbol{\varepsilon}'_e), \tag{4.8}$$

and that the constitutive equation for stress satisfies the restriction that

$$\mathbf{T}(0,0) = 0. \tag{4.9}$$

It then follows from (4.5) and (4.7) that the dissipation inequality (3.3) reduces to

$$\mathcal{D} = \left[\mathbf{T} - \rho\frac{\partial\Sigma}{\partial\varepsilon_e}\mathbf{I} - \rho\frac{\partial\Sigma}{\partial\boldsymbol{\varepsilon}'_e}\right] \cdot \mathbf{D} + \rho\frac{\partial\Sigma}{\partial\boldsymbol{\varepsilon}'_e} \cdot \mathbf{D}_p \geq 0. \tag{4.10}$$

For plasticity theory with a yield function [5,7], it can be shown by considering elastic response or elastic unloading, that the stress must be determined by derivatives of the strain energy function such that

$$\mathbf{T} = -p\mathbf{I} + \mathbf{T}', \quad p = -\rho\frac{\partial\Sigma}{\partial\varepsilon_e}, \quad \mathbf{T}' = \rho\frac{\partial\Sigma}{\partial\boldsymbol{\varepsilon}'_e}, \tag{4.11}$$

where p is the pressure and $\mathbf{T}'$ is the deviatoric stress. Thus, the dissipation inequality reduces to

$$\mathcal{D} = \mathbf{T}' \cdot \mathbf{D}_p \geq 0, \tag{4.12}$$

This condition places a restriction on the tensor $\bar{\mathbf{D}}_p$ which ensures that plasticity is dissipative. Next, for viscoplasticity, with or without a yield function, the

stress is assumed to be given by the expressions (4.11) for all motions so that the dissipation inequality again reduces to (4.12). Moreover, it is noted that more general constitutive equations which include dependence of the energy on the hardening variables can be considered without difficulty [13,14].

Within the context of this formulation, it is necessary to specify initial conditions for the variables

$$(\varepsilon,\ \varepsilon',\ \varepsilon_p,\ \kappa), \tag{4.13}$$

in order to integrate the evolution equations (4.1), (4.2) and (4.5). The main objective of this paper is to emphasize that total strain and plastic strain are not state variables that can be measured in the present configuration, so that an alternative formulation of plasticity theory is required which depends only on measurable quantities.

To this end, it is noted that in the present loaded configuration it is possible to measure the force acting on a surface and its surface area, so that it is possible to measure the traction vector acting on an arbitrary surface of the body. Since attention is confined to homogeneous deformations with homogeneous states of stress, it follows that all components of the stress tensor $\mathbf{T}$ can be determined by measuring the traction vector on three planes whose normals are linearly independent.

Next, it is emphasized that the constitutive equation for stress (4.11) depends only on the elastic strains ε_e and ε'_e. Thus, assuming that this functional form is invertible, it is possible to determine the values of $(\varepsilon_e, \varepsilon'_e)$ as functions of the stress $\mathbf{T}$. Consequently, the current values$(\varepsilon_e, \varepsilon'_e)$ of elastic strain can be determined indirectly by measuring the current value of stress $\mathbf{T}$. In this regard, it is important to emphasize that in contrast with the stress $\mathbf{T}$, which can be determined by direct measurements, the values $(\varepsilon_e, \varepsilon'_e)$ of elastic strain are determined only indirectly because they depend on the specific choice of the constitutive equations. This fundamental difference between quantities that are determined by direct measurements and other quantities that are determined only by indirect measurements is a consequence of the essential physical fact that different materials respond differently to the same stress state. More specifically, the elastic strains for rubber and steel are different when the two materials are subjected to the same stress state.

The hardening variable κ is another example of a quantity that depends on specific constitutive assumptions and can only be determined by indirect measurements. For example, in the simplest theory with a yield function based on the von Mises stress, the value of κ determines the current value of the yield strength. Given a specific definition of yielding (either based on a specified amount of inelastic deformation or based on a specified amount of change in stiffness), experiments can be performed on a finite set of identical samples to

determine the current value of the yield strength. For a more general theory, the hardening variable κ measures the resistance to plastic flow and usually appears in the scalars Γ and K in (4.2). Again, by comparing the predictions of a specified set of constitutive equations with experimental data (on a finite set of identical samples), it is possible to determine the initial value of hardening that is consistent with the proposed set of constitutive equations.

Physically, the above discussion indicates that the values of the elastic strains ε_e and $\boldsymbol{\varepsilon}'_e$, and the value of κ can be measured, in principle, in the present configuration. In particular, the initial values of these variables

$$(\varepsilon_e, \boldsymbol{\varepsilon}'_e, \kappa), \tag{4.14}$$

can be measured without any prior knowledge of the past history of loading. Thus, these quantities are state variables in the sense described in the Introduction.

In contrast, it follows from the definition $(4.7)_3$ that only the difference between the total deviatoric strain $\boldsymbol{\varepsilon}'$and the plastic stain $\boldsymbol{\varepsilon}_p$ can be measured. More specifically, it is obvious that the elastic strain and the stress remain unaffected by the transformation that subtracts an arbitrary deviatoric tensor $\bar{\boldsymbol{\varepsilon}}'$ from both the total deviatoric strain $\boldsymbol{\varepsilon}'$ and the plastic strain $\boldsymbol{\varepsilon}_p$ such that

$$\boldsymbol{\varepsilon}'^{*} = \boldsymbol{\varepsilon}' - \bar{\boldsymbol{\varepsilon}}', \quad \boldsymbol{\varepsilon}^{*}_p = \boldsymbol{\varepsilon}_p - \bar{\boldsymbol{\varepsilon}}', \tag{4.15}$$

and the elastic strain $\boldsymbol{\varepsilon}'^{*}_e$ associated with these transformed variables becomes

$$\boldsymbol{\varepsilon}'^{*}_e = \boldsymbol{\varepsilon}'^{*} - \boldsymbol{\varepsilon}^{*}_p = \boldsymbol{\varepsilon}' - \boldsymbol{\varepsilon}_p = \boldsymbol{\varepsilon}'_e. \tag{4.16}$$

Physically, this means that the initial values for $\boldsymbol{\varepsilon}'$ and $\boldsymbol{\varepsilon}_p$ can never be measured without prior knowledge of the past history of deformation since they always include the arbitrariness of the deviatoric tensor $\bar{\boldsymbol{\varepsilon}}'$. Consequently, the initial values of these variables, which are required in the integrate the evolution equations $(4.5)_2$ and $(4.1)_1$, cannot be determined uniquely.

In other words, only the difference between the total deviatoric strain $\boldsymbol{\varepsilon}'$ and the plastic strain $\boldsymbol{\varepsilon}_p$ influences the response of the material. Consequently, the individual actual values of these quantities have no physical meaning, as was clearly stated by GILMAN [4]. This also means that the notions of total strain and plastic strain should be abandoned in the formulation of plasticity theories.

For the small deformation theory, it is quite easy to formulate constitutive equations for plasticity and viscoplasticity which are free from these physical inconsistencies. In particular, it is possible to differentiate equations $(4.7)_{2,3}$ with respect to time and to use the expressions $(4.1)_1$ and (4.5) to develop evolution equations for the elastic strains ε_e and $\boldsymbol{\varepsilon}'_e$ directly of the forms

$$\dot{\varepsilon}_e = \mathbf{D} \cdot \mathbf{I}, \quad \dot{\boldsymbol{\varepsilon}}'_e = \mathbf{D}' - \mathbf{D}_p. \tag{4.17}$$

Now, since the elastic strains ε_e and ε'_e are state variables, which can be measured in the present configuration, the initial conditions which are required to integrate these evolution equations can be determined without arbitrariness. The resulting theory is characterized by the constitutive equations for the strain energy $(4.8)_2$, the stress (4.11), the rate of plastic dissipation $\mathbf{D}_p$, the expression for the hardening rate K (4.2), and the evolution equations (4.2) and (4.17). This theory has the properties that it is independent of the choice of the reference configuration, and it does not utilize any measures of total deformation or plastic deformation. The influence of plastic deformation only enters the constitutive equations through the rate of relaxation $\mathbf{D}_p$, which is a function of state variables that can be determined in the present configuration only. Also, when Γ vanishes, the plastic deformation rate vanishes and the constitutive equations characterize the usual small deformation theory of elastic materials.

A rather standard set of constitutive equations for an elastically isotropic material can be obtained by specifying

$$\rho\Sigma = \frac{1}{2}k\varepsilon_e^2 + \mu\varepsilon'_e \cdot \varepsilon'_e, \quad \bar{\mathbf{D}}_p = \varepsilon'_e, \quad K = m(Z_1 - \kappa), \tag{4.18}$$

where the material constants k and μ are the bulk modulus and the shear modulus, respectively, m is a material constant that controls the rate of hardening, and Z_1 controls the saturated value of hardening. It then follows from (4.11) and $(4.1)_2$ that

$$p = -k\varepsilon_e, \quad \mathbf{T}' = 2\mu\varepsilon'_e, \quad \mathbf{D}_p = \Gamma\varepsilon'_e = \frac{\Gamma}{2\mu}\mathbf{T}', \tag{4.19}$$

which shows that the rate of relaxation $\mathbf{D}_\mathrm{p}$ is consistent with the classical Prandtl-Reuss form. SWEGLE and GRADY [15,16] have developed an overstress model for modeling viscoplasticity in shock waves which is equivalent to specifying Γ in the form

$$\Gamma = \Gamma_0 \frac{< \sigma_e - \kappa >^2}{\kappa_0^2}, \quad \sigma_e^2 = \frac{3}{2}\mathbf{T}' \cdot \mathbf{T}', \tag{4.20}$$

where Γ_0 is a material constant controlling the strain-rate sensitivity, κ_0 is the annealed value of hardening, σ_e is the von Mises effective stress, and the McAuley brackets are defined by

$$< x >= \frac{x + |x|}{2}. \tag{4.21}$$

Alternatively, a modified version of the Bodner-Partom viscoplasticity model without a yield function can be obtained by taking Γ in the form [17]

$$\Gamma = \Gamma_0 \exp\left[-\frac{1}{2}\{\frac{\kappa}{\sigma_e}\}^{2n}\right]. \tag{4.22}$$

For large values of stress ($\sigma_e >> \kappa$) or very high strain rates, the rate-dependence of the material is controlled almost entirely by the material constant Γ_0. On the other hand, at lower stresses ($\sigma_e < \kappa$) or lower strain rates, the rate-dependence of the material is controlled mainly by the material constant n. Both of the functions (4.20) and (4.22) cause the evolution equation $(4.17)_2$ to be a stiff differential equation which requires special numerical methods that have been developed in [18-20].

5. Finite deformation of elastically isotropic elastic-viscoplastic materials

ECKART [21] seems to have been the first to develop a properly invariant theory of elastically isotropic inelastic solids which does not depend on the choice of the reference configuration or any measure of total or plastic deformations. LEONOV [22], independently, developed the same theory for describing the response of polymeric liquids. The main idea in this theory is to propose an evolution equation directly for an elastic deformation tensor. Specifically, the symmetric tensor $\mathbf{B}_e$ is introduced as a measure of elastic deformation which is determined by the evolution equation

$$\dot{\mathbf{B}}_e = \mathbf{L}\mathbf{B}_e + \mathbf{B}_e\mathbf{L}^T - 2\mathbf{D}_p, \quad \mathbf{D}_p = \Gamma\bar{\mathbf{D}}_p, \tag{5.1}$$

where Γ and $\bar{\mathbf{D}}_p$ have the same physical meanings as those quantities related to $(4.1)_2$. Next, a pure measure of elastic dilation J_e is defined by the formula

$$J_e = [\det\mathbf{B}_e]^{1/2}, \tag{5.2}$$

so that

$$\dot{J}_e = \frac{1}{2}J_e\left[\dot{\mathbf{B}}_e \cdot \mathbf{B}_e^{-1}\right] = J_e[\mathbf{D}\cdot\mathbf{I} - \Gamma\bar{\mathbf{D}}_p \cdot \mathbf{B}_e^{-1}]. \tag{5.3}$$

Consequently, the condition that plastic deformation rate is isochoric and does not influence the elastic dilation, requires $\bar{\mathbf{D}}_p$ to satisfy the restriction that

$$\bar{\mathbf{D}}_p \cdot \mathbf{B}_e^{-1} = 0. \tag{5.4}$$

Thus, it is possible to use the notions proposed by Flory [23] to define a pure measure of elastic distortional deformation $\mathbf{B}'_e$ as a unimodular symmetric tensor

$$\mathbf{B}'_e = J_e^{-2/3}\mathbf{B}_e, \quad \det\mathbf{B}'_e = 1. \tag{5.5}$$

Then, the evolution equations for the pure measure of elastic dilation J_e and the pure measure of elastic distortional deformation $\mathbf{B}'_e$ can be written in the forms

$$\dot{J}_e = J_e \mathbf{D} \cdot \mathbf{I}, \quad \dot{\mathbf{B}}'_e = \mathbf{L}\mathbf{B}'_e + \mathbf{B}'_e\mathbf{L}^T - \frac{2}{3}(\mathbf{D} \cdot \mathbf{I})\mathbf{B}'_e - 2\Gamma\bar{\mathbf{D}}_p. \tag{5.6}$$

Moreover, a specific form for $\bar{\mathbf{D}}_p$ and a numerical procedure for integrating the evolution equation $(5.6)_2$ can be found in [20].

Under superposed rigid body motions (SRBM) it is well known that the mass density ρ in the present configuration and the kinematic quantities $\mathbf{D}$ and $\mathbf{W}$ transform to the values ρ^+, $\mathbf{D}^+$, $\mathbf{W}^+$ in the superposed configuration such that

$$\rho^+ = \rho, \quad \mathbf{D}^+ = \mathbf{Q}\mathbf{D}\mathbf{Q}^T, \quad \mathbf{W}^+ = \mathbf{Q}\mathbf{W}\mathbf{Q}^T + \boldsymbol{\Omega}, \tag{5.7}$$

where $\mathbf{Q}(t)$ is an arbitrary proper orthogonal tensor function of time only characterizing the rigid rotation, and $\boldsymbol{\Omega}(t)$ is the skew-symmetric tensor function of time related to $\dot{\mathbf{Q}}$

$$\mathbf{Q}^T\mathbf{Q} = \mathbf{I}, \quad \det\mathbf{Q} = 1, \quad \dot{\mathbf{Q}} = \boldsymbol{\Omega}\mathbf{Q}, \quad \boldsymbol{\Omega}^{\mathrm{T}} = -\boldsymbol{\Omega}. \tag{5.8}$$

Also, the stress $\mathbf{T}$ and the strain energy Σ transform by the formulas

$$\mathbf{T}^+ = \mathbf{Q}\mathbf{T}\mathbf{Q}^T, \quad \Sigma^+ = \Sigma. \tag{5.9}$$

Next, with the help of the assumption that $\Gamma, \bar{\mathbf{D}}_p$ and K satisfy the transformation relations

$$\Gamma^+ = \Gamma, \quad \bar{\mathbf{D}}_p^+ = \mathbf{Q}\bar{\mathbf{D}}_p\mathbf{Q}^T, \quad K^+ = K, \tag{5.10}$$

it follows that $\mathbf{B}_e, J_e, \mathbf{B}'_e$ and κ transform under SRBM by

$$\mathbf{B}_e^+ = \mathbf{Q}\mathbf{B}_e\mathbf{Q}^{\mathbf{T}}, \quad J_e^+ = J_e, \quad \mathbf{B}_e^{'+} = \mathbf{Q}\mathbf{B}_e^{'}\mathbf{Q}^T, \quad K^+ = K. \tag{5.11}$$

Here, and throughout the text, a superposed $(^+)$ is added to any variable to denote its value in the superposed configuration.

Furthermore, the stress and the strain energy are functions of elastic deformation quantities

$$\mathbf{T} = \mathbf{T}(J_e, \mathbf{B}'_e), \quad \Sigma = \Sigma, (J_e, \mathbf{B}'_e) \tag{5.12}$$

where the constitutive equation for stress satisfies the restriction

$$\mathbf{T}(1, \mathbf{I}) = 0 \tag{5.13}$$

However, since Σ must remain unaltered by SRBM, it can be a function of $\mathbf{B}'_e$ only through its two nontrivial invariants, which can be expressed in the forms

$$\alpha_1 = \mathbf{B}'_e \cdot \mathbf{I}, \quad \alpha_2 = \mathbf{B}'_e \cdot \mathbf{B}'_e, \tag{5.14}$$

so that Σ becomes

$$\Sigma = \Sigma(J_e, \alpha_1, \alpha_2). \tag{5.15}$$

Next, using the evolution equation $(5.6)_2$, it can be shown that

$$\dot{\alpha}_1 = 2\left[\mathbf{B}'_e - \frac{1}{3}(\mathbf{B}'_e \cdot \mathbf{I})\mathbf{I}\right] \cdot \mathbf{D} - 2\Gamma \bar{\mathbf{D}}_p \cdot \mathbf{I}, \tag{5.16}$$

$$\dot{\alpha}_2 = 4\left[\mathbf{B}'^2_e - \frac{1}{3}(\mathbf{B}'_e \cdot \mathbf{B}'_e)\mathbf{I}\right] \cdot \mathbf{D} - 4\Gamma \bar{\mathbf{D}}_p \cdot \mathbf{B}'_e.$$

Thus, the constitutive equations

$$p = -\rho_0 \frac{\partial \Sigma}{\partial J_e},$$

$$\mathbf{T}' = 2\rho \frac{\partial \Sigma}{\partial \alpha_1}\left[\mathbf{B}'_e - \frac{1}{3}(\mathbf{B}'_e \cdot \mathbf{I})\mathbf{I}\right] + 4\rho \frac{\partial \Sigma}{\partial \alpha_2}\left[\mathbf{B}'^2_e - \frac{1}{3}(\mathbf{B}'_e \cdot \mathbf{B}'_e)\mathbf{I}\right], \tag{5.17}$$

can be used to reduce the dissipation inequality (3.3) to the form

$$\mathcal{D} = 2\Gamma\left[\rho \frac{\partial \Sigma}{\partial \alpha_1}\mathbf{I} + 2\rho \frac{\partial \Sigma}{\partial \alpha_2}\mathbf{B}'_e\right] \cdot \bar{\mathbf{D}}_p \geq 0, \tag{5.18}$$

which restricts the tensor $\bar{\mathbf{D}}_p$. Also, in $(5.17)_1$, use has been made of the conservation law of of mass which relates the density ρ to the density ρ_0 in the *Reference State*

$$\rho J_e = \rho_0. \tag{5.19}$$

This theory for elastically isotropic elastic-viscoplastic materials is characterized by the constitutive equations for the strain energy (5.15), the stress (5.17), the rate of plastic dissipation $(5.1)_2$, the expression for the hardening rate K (4.2), and the evolution equations (4.2) and (5.6). Assuming that the stress is an invertible function of the elastic deformation quantities J_e and $\mathbf{B}'_e$, it follows that

$$\{J_e, \mathbf{B}'_e, \kappa\}, \tag{5.20}$$

are state variables since they can be measured, in principle, without any prior knowledge of the past history of deformation of the material. In particular, the initial values of these quantities, which are required to integrate the evolution equations (4.2) and (5.6), can be measured without arbitrariness. Also, when Γ vanishes, the plastic deformation rate vanishes and the constitutive equations characterize general elastically isotropic materials, with $\mathbf{B}_e$ reducing to the left Cauchy-Green deformation tensor $\mathbf{B}$.

A simple specific set of constitutive equations can be obtained by specifying the strain energy Σ and the plastic deformation rate tensor $\bar{\mathbf{D}}_p$ in the forms [13,14]

$$\rho_0\Sigma = k[1 - J_e - \ln(\mathrm{J_e})] + \frac{1}{2}\mu(\alpha_1 - 3), \quad 2\bar{\mathbf{D}}_{\mathrm{p}} = \mathbf{B'}_{\mathrm{e}} - \frac{3}{\mathbf{B'}_{\mathrm{e}}^{-1}\cdot\mathbf{I}}\mathbf{I}, \tag{5.21}$$

where again the material constants k and μ are the bulk modulus and the shear modulus, respectively. It then follows from (5.17) and (5.19) that stresses become

$$p = k\left[\frac{1}{J_e} - 1\right], \quad \mathbf{T'} = J_e^{-1}\mu\left[\mathbf{B'}_e - \frac{1}{3}(\mathbf{B'}_e\cdot\mathbf{I})\mathbf{I}\right]. \tag{5.22}$$

Also, the constitutive equation for K is given by $(4.18)_3$, Γ can be taken in the forms (4.20) or (4.21), and the numerical methods developed in [18-20] remain applicable to this finite deformation theory.

6. Finite deformation of elastically anisotropic elastic-viscoplastic materials

A critical review of finite deformation theories of elastically anisotropic elastic-plastic materials has been presented by NAGHDI [24]. In order to model anisotropic response, these theories are usually formulated in terms of deformation tensors that are related to the reference configuration and hence are trivially invariant under SRBM. However, as has been previously discussed, the specific choice of the reference configuration is a part of the history of the material that can never be determined by experiments on identical samples of the material in its present state. Consequently, it is necessary to consider an alternative formulation that is capable of describing the material anisotropy. One such formulation has been motivated by the physical discussion presented by BESSELING [25] and has been developed in terms of physically based microstructural variables [13,14].

The response of a material that is elastically anisotropic depends on the orientation of the material relative to the loading direction. This means that there are specific material directions which are related to the microstructure of the material and which can be determined by experiments. Within the context

of this alternative formulation of plasticity theory [13,14], these microstructural directions in the present configuration are represented by a triad of linearly independent vectors $\mathbf{m}_i (i = 1, 2, 3)$, which characterize the present state of the material. In this theory, it is convenient to introduce the metric

$$m_{ij} = \mathbf{m}_i \cdot \mathbf{m}_j, \tag{6.1}$$

which measures deformation of the microstructure relative to the *Reference State* of the material. Moreover, the vectors $\mathbf{m}_i$ can be normalized so that $\mathbf{m}_i$ become an orthonormal set of vectors whenever the material is in its *Reference State*

$$m_{ij} = \delta_{ij} \quad \text{in the } \textit{Reference State}, \tag{6.2}$$

where δ_{ij} is the Kronecker delta symbol. However, for a general material state, the metric m_{ij} attains the values different from δ_{ij}.

The general theory requires evolution equations for the vectors $\mathbf{m}_i$. In order to motivate the forms of these evolution equations, it is recalled that the rate of change of a macroscopic material line element $d\mathbf{x}$ in the present configuration can be expressed in the form

$$d\dot{\mathbf{x}} = \mathbf{L}\, d\mathbf{x}. \tag{6.3}$$

An important physical characteristic of the vectors $\mathbf{m}_i$ is that, in general, they characterize the elastic deformation of the microstructure which is not directly connected with the deformation of macroscopic material line elements $d\mathbf{x}$. To model this physical distinction between the evolution of the microstructure and the macroscopic total deformation rate, the evolution equations for $\mathbf{m}_i$ are specified by modifying (6.3), such that

$$\dot{\mathbf{m}}_i = \mathbf{L}_m \mathbf{m}_i, \quad \mathbf{L}_m = \mathbf{L} - \mathbf{L}_p. \tag{6.4}$$

In these equations, $\mathbf{L}_m$ denotes the microstructural deformation rate, and $\mathbf{L}_p$ is a second order tensor that characterizes the relaxation effects of plasticity. In general, $\mathbf{L}_p$ has a symmetric part $\mathbf{D}_p$ and a skew-symmetric part $\mathbf{W}_p$

$$\mathbf{L}_p = \mathbf{D}_p + \mathbf{W}_p, \quad \mathbf{D}_p = \frac{1}{2}(\mathbf{L}_p + \mathbf{L}_p^T), \quad \mathbf{W}_p = \frac{1}{2}(\mathbf{L}_p - \mathbf{L}_p^T), \tag{6.5}$$

and $\mathbf{D}_p$ and $\mathbf{W}_p$ can be expressed in the forms

$$\mathbf{D}_p = \Gamma \bar{\mathbf{D}}_p, \quad \mathbf{W}_p = \Gamma \bar{\mathbf{W}}_p, \tag{6.6}$$

where $\Gamma, \bar{\mathbf{D}}_p$ and $\mathbf{W}_p$ require constitutive equations. In this regard it should be mentioned that the term $\mathbf{W}_p$, which is currently referred to as the plastic spin in

crystal plasticity [26], is not new and was required in the constitutive equations for elastically anisotropic material response proposed by BESSELING [25].

Since $\mathbf{m}_i$ are normalized vectors that measure the deformation relative to the *Reference State*, it is possible to introduce the dilatation J_e and a pure measure of distortional deformation m_{ij}, both measured relative to the *Reference State*, through the definitions

$$J_e = \mathbf{m}_1 \times \mathbf{m}_2 \cdot \mathbf{m}_3 > 0, \quad m'_{ij} = J_e^{-2/3} m_{ij}. \tag{6.7}$$

Moreover, by using (6.4), it can be shown that

$$\dot{J}_e = J_e[\mathbf{D} \cdot \mathbf{I} - \mathbf{D}_p \cdot \mathbf{I}]. \tag{6.8}$$

Consequently, the condition that plastic deformation rate is isochoric and does not influence the elastic dilation requires $\bar{\mathbf{D}}_p$ to satisfy the condition that

$$\bar{\mathbf{D}}_p \cdot \mathbf{I} = 0. \tag{6.9}$$

Also, it is possible to express the derivatives of J_e and m'_{ij} in the forms

$$\dot{J}_e = J_e \mathbf{D} \cdot \mathbf{I}, \quad \dot{m}'_{ij} = 2\left[\mathbf{m}'_i \otimes \mathbf{m}'_j - \frac{1}{3} m'_{ij} \mathbf{I}\right] \cdot \mathbf{D} - 2[\mathbf{m}'_i \otimes \mathbf{m}'j] \cdot \mathbf{D}_p, \tag{6.10}$$

where the vectors $\mathbf{m}'_i$ are defined by

$$\mathbf{m}'_i = J_e^{-1/3} \mathbf{m}_i. \tag{6.11}$$

Thus, it follows from (6.4) and $(6.10)_2$ that spin tensor $\mathbf{W}_p$ affects only the orientation of the vectors $\mathbf{m}_i$, and specifically does not influence the rate of change of the elastic distortional deformation tensor m'_{ij}.

These constitutive equations are properly invariant under SRBM provided that the constitutive equation for $\mathbf{L}_p$ satisfies the transformation relations

$$\mathbf{L}_p^+ = \mathbf{Q} \mathbf{L}_p \mathbf{Q}^T. \tag{6.12}$$

Consequently, various other quantities transform under SRBM as follows:

$$\Gamma^+ = \Gamma, \quad \bar{\mathbf{D}}_p^+ = \mathbf{Q} \bar{\mathbf{D}}_p \mathbf{Q}^T, \quad \bar{\mathbf{W}}_p^+ = \mathbf{Q} \bar{\mathbf{W}}_p \mathbf{Q}^T, \tag{6.13}$$

$$\mathbf{m}_i^+ = \mathbf{Q} \mathbf{m}_i, \quad \mathbf{m}'^+_i = \mathbf{Q} \mathbf{m}'_i,$$

$$J_e^+ = J_e, \quad m_{ij}^+ = m_{ij}, \quad m'^+_{ij} = m'_{ij}.$$

Since J_e and m'_{ij} measures of elastic deformation from the *Reference State*, it follows that the stress and the strain energy are functions of the forms

$$\mathbf{T} = \mathbf{T}(J_e, m'_{ij}, \mathbf{m}'_i), \quad \Sigma = \Sigma(J_e, \mathbf{m}'_i), \tag{6.14}$$

where the constitutive equation for stress satisfies the condition

$$\mathbf{T}(1, \delta_{ij}, \mathbf{m}'_i) = 0. \tag{6.15}$$

However, since Σ must remain unaltered by SRBM, it can be a function of $\mathbf{m}'_i$ only through the metric m'_{ij} so that Σ becomes

$$\Sigma = \Sigma(J_e, m'_{ij}). \tag{6.16}$$

Thus, with the help of (6.10), it can be shown that the constitutive equations

$$p = -\rho_0 \frac{\partial \Sigma}{\partial J_e}, \quad \mathbf{T}' = 2\rho \frac{\partial \Sigma}{\partial m'_{ij}} \left[\mathbf{m}'_i \otimes \mathbf{m}'_j - \frac{1}{3} m'_{ij} \mathbf{I} \right], \tag{6.17}$$

and the condition(6.9) can be used to reduce the dissipation inequality (3.3) to the form

$$D = \Gamma \mathbf{T}' \cdot \bar{\mathbf{D}}_p \geq 0, \tag{6.18}$$

which restricts the tensor $\bar{\mathbf{D}}_p$. Also, in $(6.17)_1$ use has been made of the law of conservation of mass (5.19).

This theory for elastically anisotropic elastic-viscoplastic materials is characterized by the constitutive equations for the strain energy (6.16), the stress (6.17), the relaxation effects of plasticity (6.5), (6.6), the definitions (6.7), the expression for the hardening rate K (4.2), and the evolution equations (4.2) and $(6.4)_1$. In this theory, the microstructural vectors $\mathbf{m}_i$ are state variables since they can be measured, in principle, without any prior knowledge of the past history of deformation of the material. When Γ vanishes, the relaxation effects of plasticity vanish and the constitutive equations characterize general elastically anisotropic materials.

For a general anisotropic response, the initial values of $\mathbf{m}_i$ which are required to integrate the evolution equations $(6.4)_1$, can be measured. Moreover, $\mathbf{m}_i$ are directly connected to identifiable directions in the microstructure of the material. Depending on the symmetry properties of the specific material under consideration, there can be some degree of arbitrariness in the determination of the initial values of $\mathbf{m}_i$. However, any such arbitrariness must be reflected in corresponding restrictions on the symmetry of the strain energy function which cause the resulting material response to be uninfluenced by this arbitrariness. For example, if the material is elastically isotropic, then there is no physical experiment that can distinguish between the directions $\mathbf{m}_1$, $\mathbf{m}_2$ and $\mathbf{m}_3$. For this case, the strain energy function must depend on m'_{ij} only through its two invariants, which are related to the elastic deformation tensor $\mathbf{B}'_e$ by the equations

$$\mathbf{B}'_e = \mathbf{m}'_i \otimes \mathbf{m}'_i, \quad \alpha_1 = \mathbf{B}'_e \cdot \mathbf{I} = m'_{ii}, \quad \alpha_2 = \mathbf{B}'_e \cdot \mathbf{B}'_e = m'_{ij} m'_{ij}. \tag{6.19}$$

Due to the summation over the repeated indices in these expressions, it is obvious that these variables cannot distinguish between the 1, 2 and 3 directions in the material's microstructure.

Since J_e and m'_{ij} are trivially invariant under SRBM, the strain energy function can be an arbitrary function of its arguments which satisfies restrictions related to (6.15). Moreover, the tensors $\bar{\mathbf{D}}_p$ and $\bar{\mathbf{W}}_p$ are properly invariant under SRBM (6.13) if they are expressed in terms of components relative to $\mathbf{m}_i$ of the forms

$$\bar{\mathbf{D}}_p = \bar{D}^p_{ij}(\mathbf{m}_i \otimes \mathbf{m}_j), \quad \bar{\mathbf{W}}_p = \bar{W}^p_{ij}(\mathbf{m}_i \otimes \mathbf{m}_j), \tag{6.20}$$

where $\bar{D}^p_{ij}$ and $\bar{W}^p_{ij}$ are arbitrary functions (which remain unaltered by SRBM) of the state variables $\{J_e, m'_{ij}\}$. Specific examples of these tensors can be developed to incorporate standard expressions used in crystal plasticity [26] without difficulty.

7. Conclusions

The discussion in this paper emphasizes the notion that neither total strain nor plastic strain are measurable quantities in the present configuration of an elastic-plastic material. Consequently, total strain and plastic strain are not state variables and therefore should be abandoned in the formulation of constitutive equations. An alternative approach to the development of constitutive equations for elastically isotropic response of inelastic materials [21, 22] has been reviewed in both the small deformation and the large deformation contexts. Within the context of this alternative approach, evolution equations are proposed directly for elastic deformation quantities and hardening (4.14) or (5.20), instead of for total deformation, plastic deformation and hardening (4.13). Moreover, since Cauchy stress is measurable in the present configuration, the elastic deformations can be obtained by inverting the constitutive equations for stress (4.19) or (5.22), so the initial conditions for the evolution equations (4.17) for (5.6) can be determined without ambiguity. In contrast, the initial conditions for the evolutions of total strain (4.5) and plastic strain (4.1) cannot be determined without arbitrariness which has no physical relevance to the prediction of subsequent material response.

An alternative formulation for elastically anisotropic inelastic materials has also been discussed which introduces evolution equations (6.4) for three vectors characterizing the absolute orientation and elastic deformation of the microstructure. Again, the initial values of these vectors are measurable so the evolution equations can be integrated without ambiguity. Also, these vectors are used to determine the stress by constitutive equations of the form (6.17). This alternative method should be contrasted with the more standard methods (discussed in

[13]), such as the one used for crystal plasticity [26], which requires integration of the evolution equations for the total deformation gradient $\mathbf{F}$ and the plastic deformation tensor $\mathbf{F}_p$

$$\dot{\mathbf{F}} = \mathbf{L}\mathbf{F}, \quad \dot{\mathbf{F}}_p = \mathbf{\Lambda}_p \mathbf{F}_p, \tag{7.1}$$

and which includes a definition of elastic deformation $\mathbf{F}_e$

$$\mathbf{F}_e = \mathbf{F}\,\mathbf{F}_p^{-1}, \tag{7.2}$$

where the function $\mathbf{\Lambda}_p$ requires a constitutive equation. For elastically anisotropic response the Cauchy stress depends on both $\mathbf{F}$ and $\mathbf{F}_p$, neither of which can be measured without arbitrariness in the present configuration [13].

Within the context of the formulation associated with (7.1) and (7.2), it is common to define the symmetric tensors $\mathbf{C}_e$ and $\mathbf{B}_e$ by

$$\mathbf{C}_e = \mathbf{F}_e^T \mathbf{F}_e, \quad \mathbf{B}_e = \mathbf{F}_e \mathbf{F}_e^T. \tag{7.3}$$

Then, it can be shown that these tensors are determined by the evolution equations

$$\dot{\mathbf{F}}_e = \mathbf{L}\mathbf{F}_e - \mathbf{F}_e \mathbf{\Lambda}_p, \tag{7.4a}$$

$$\dot{\mathbf{C}}_e = 2\mathbf{F}_e^T \mathbf{D}\,\mathbf{F}_e - \mathbf{\Lambda}_p^T \mathbf{C}_e - \mathbf{C}_e \mathbf{\Lambda}_p, \tag{7.4b}$$

$$\dot{\mathbf{B}}_e = \mathbf{L}\,\mathbf{B}_e + \mathbf{B}_e \mathbf{L}^T - \mathbf{F}_e(\mathbf{\Lambda}_p + \mathbf{\Lambda}_p^T)\mathbf{F}_e^T. \tag{7.4c}$$

In particular, notice that unless $\mathbf{\Lambda}_p$ is specified in a special form, these evolution equations depend on $\mathbf{F}_e$, so that it is still necessary to integrate the evolution equation (7.4a) for $\mathbf{F}_e$ and there is no advantage of the evolution equations (7.4b,c). As a special case, $\mathbf{\Lambda}_p$ can be specified in the form

$$\mathbf{\Lambda}_p = \mathbf{F}_e^{-1} \mathbf{L}_p \mathbf{F}_e, \tag{7.5}$$

to obtain the theory of BESSELING [25] for elastically anisotropic response which focuses attention on an evolution equation for the elastic deformation

$$\dot{\mathbf{F}}_e = (\mathbf{L} - \mathbf{L}_p)\mathbf{F}_e. \tag{7.6}$$

Also, when $\mathbf{\Lambda}_p$ satisfies the condition

$$\mathbf{\Lambda}_p + \mathbf{\Lambda}_p^T = 2\mathbf{F}_e^{-1} \mathbf{D}_p \mathbf{F}_e^{-T}, \tag{7.7}$$

then the evolution equation (5.1) is consistent with the theories of ECKART [21] and LEONOV [22] for elastically isotropic response.

The advantages of the alternative method are not emphasized in the small deformation theory because the difference between the total deviatoric strain $\boldsymbol{\varepsilon}'$and the plastic strain $\boldsymbol{\varepsilon}_p$ (which is deviatoric) is measurable. Consequently, the arbitrariness of $\boldsymbol{\varepsilon}'$ and $\boldsymbol{\varepsilon}_p$ which influences the material response can be easily removed. However, for large deformations, one standard approach requires the Cauchy stress $\mathbf{T}$ to be a function of both $\mathbf{F}$ and $\mathbf{F}_p$ in order to be properly invariant under the superposed rigid body motions. Consequently, the arbitrariness which is associated with the determination of the initial values of $\mathbf{F}$ and $\mathbf{F}_p$ cannot be removed in general and can cause an unphysical influence on the response of elastically anisotropic inelastic materials. Additional differences between the alternative theories reviewed in this paper and the more classical theories associated with (7.6) and (7.7) have been discussed in [13].

The alternative constitutive equations discussed here not only have the conceptual advantage that the required initial conditions can be measured; they also have a practical advantage for computations. In particular, it has been shown [20] that the formulation of Section 5 can be implemented into standard wave propagation codes by using the Cauchy stress $\mathbf{T}$ to determine the elastic deformation, so that there is no need to store $\mathbf{F}$ and $\mathbf{F}_p$ as history-dependent variables. Moreover, one standard approach for elastically anisotropic inelastic materials requires the calculation of the two tensors $\mathbf{F}$ and $\mathbf{F}_p$. In contrast, for the alternative equations of Section 6, the microstructural vectors $\mathbf{m}_i$ (9 independent quantities) can be stored instead of the two tensors $\mathbf{F}$ and $\mathbf{F}_p$ (18 independent quantities).

This paper has emphasized that the total strain associated with the current state of a material cannot be measured because it is dependent on an arbitrary choice of the reference configuration. Nevertheless, the total strain which is measured relative to a reference configuration which an experimenter specifies, is certainly a useful parameter for monitoring the history of total deformations of a specimen. This measured total strain is similar to time, in the sense that both are measured relative to an arbitrary reference state, and both they cannot appear explicitly in constitutive equations.

Acknowledgements

This work was partially supported by the Fund for Promotion of Research at the Technion. The author would also like to acknowledge helpful discussions with S.R. Bodner, and constructive comments of an anonymous reviewer.

References

1. M.B. RUBIN, *On the treatment of elasticdeformation in finite elastic-viscoplastic theory,* Int. J. Plasticity, **12**, 951-965, 1996.
2. M.B. RUBIN, *Unphysical features of plasticity theories which depend on total and plastic deformations, in Proceedings of the fourth international conference on constitutive laws for engineering materials,* Rensselaer, New York (eds. R.C. Picu and E. Krempl), 27-30 July 1999, 184-187 1996.
3. E.T. ONAT, *The notion of state and its implications in thermodynamics of inelastic solids, Proc. of the IUTAM Symposium on irreversible aspects of continuum mechanics and transfer of physical characteristics in moving fluids, Vienna.* (Eds. H. Parkus and L. I. Sedov), Springer-Verlag, Wien, 1968, 292-314, 1996.
4. J.J. GILMAN, *Physical nature of plastic flow and fracture, Plasticity, Proceedings of the second symposium on naval structural mechanics,* (Eds. Lee, E. H. and Symonds, P.S.) Pergamon Press, New York, 43-99, 1996.
5. P.M. NAGHDI, *Stress-strain relations in plasticity and thermoplasticity, Proceedings of the second symposium on naval structural mechanics,* Pergamon Press, 121-167, 1960.
6. S.R. BODNER, *Review of unified elastic-viscoplastic theory,* Unified Constitutive Equations for Creep and Plasticity, ed. A.K. Miller, Elsevier Applied Science Pub. Barking, England, 273-301, 1987.
7. P.M. NAGHDI AND J.A. TRAPP, *The significance of formulating plasticity theory with reference to loading surfaces in strain space,* Int. J. Engng. Sci., **13**, 785-797, 1975.
8. L.E. MALVERN, *The propagation of longitudinal waves of plastic deformation in a bar of material exhibiting a strain-rate effect,* ASME J. Appl. Mech., **18**, 203-208, 1951.
9. P. PERZYNA, *The constitutive equations for rate-sensitive plastic materials,* Quarterly of Appl. Math.,**20**, 321-332, 1963.
10. S.R.BODNER, *Constitutive equations for dynamic material behavior, in Mechanical Behavior of Materials Under Dynamic Loads*, ed. U.S. Lindholm, Springer-Verlag, New York, 176-190, 1968.
11. S.R. BODNER AND Y. PARTOM, *A large deformation elastic-viscoplastic analysis of a thick-walled spherical shell,* ASME J. Appl. Mech. **39**, 751-757, 1972.
12. S.R. BODNER AND Y. PARTOM, *Constitutive equations for elastic-viscoplastic strain-hardening materials*, ASME J. Appl.Mech., **42**, 385-389, 1975.
13. M.B. RUBIN , *Plasticity theory formulated in terms of physically based microstructural variables - Part I: Theory,* Int. J. Solids Structures, **31**, 2615-2634, 1994.
14. M.B. RUBIN, *Plasticity theory formulated in terms of physically based microstructural variables – Part II: Examples*, Int. J. Solids Structures, **31**, 2635-2652, 1994.
15. J.W. SWEGLE AND D.E. GRADY , *Shock viscosity and the prediction of shock wave rise times,* J. Appl. Phys., **58**, 692-701, 1985.
16. J.W. SWEGLE AND D.E. GRADY, *Shock viscosity and the calculation of steady shock wave profiles,* In: Gupta, Y.M. Ed. Shock Waves in Condensed Matter. Plenum, New York, 353-357, 1986.

17. M.B. RUBIN, *An elastic-viscoplastic model exhibiting continuity of solid and fluid states,* Int. J. Engng. Sci., **25**, 1175-1191, 1987.

18. M.B. RUBIN, *A time integration procedure for plastic deformation in elastic-viscoplastic metals,* J. Appl. Math. Phys. (ZAMP), **40**, 846-871, 1989.

19. M.B. RUBIN, *Efficient time integration of a viscoplastic model for shock waves,* J. Appl. Phys.,**68**, 1356-1358, 1990.

20. M.B. RUBIN AND A. ATTIA, *Calculation of hyperelastic response of finitely deformed elastic-viscoplastic materials,* Int. J. for Numer. Meth. in Engng., **39**, 309-320, 1996.

21. C. ECKART, *The thermodynamics of irreversible processes. IV. The theory of elasticity and anelasticity,* Physical Review, **73**, 373-382, 1948.

22. A.I. LEONOV, *Nonequilibrium thermodynamics and rheology of viscoelastic polymer media,* Rheologica Acta, **15**, 85-98, 1996.

23. P. FLORY, *Thermodynamic relations for highly elastic materials,* Trans. Faraday Soc., **57**, 829-838, 1961.

24. P.M. NAGHDI, *A critical review of the state of finite plasticity,* J. Appl. Math. and Phys.(ZAMP), **41**, 315-394, 1990.

25. J.F. BESSELING, *A thermodynamic approach to rheology,* Proc. of the IUTAM Symposium on irreversible aspects of continuum mechanics and transfer of physical characteristics in moving fluids, Vienna. Eds. H. Parkus and L.I. Sedov, Springer-Verlag, Wien, 1968, 16-53, 1996.

26. R.J. ASARO, *Micromechanics of crystals and polycrystals, Advances in Applied Mechanics,* **23**, 1-115, 1983.

Received February 15, 2000; revised version April 6, 2001.

Arch. Mech., **53**, 4-5, pp. 541–564, Warszawa 2001

A dynamic asymptotic model of linear elastic orthotropic plates: first and second-order terms

A. SŁAWIANOWSKA and J. J. TELEGA

Institute of Fundamental Technological Research,
Polish Academy of Sciences,
Świętokrzyska 21, 00-049 Warsaw, Poland,
e-mail : aslawian@ippt.gov.pl; jtelega@ippt.gov.pl

BY USING the asymptotic method combined with variational approach a new dynamic model of elastic orthotropic plates is derived. This model accounts for rotational inertia and takes into account second order terms $\mathbf{U}^2$ and $\boldsymbol{\sigma}^2$ in the asymptotic expansions of displacements and stresses. To avoid the boundary layer analysis, the boundary conditions for $\mathbf{U}^2$ are satisfied in a suitable averaged sense. Convergence theorem is formulated. Influence of the second-order terms on plate response in the static case is investigated.

1. Introduction

IN OUR RECENT PAPERS [19, 20] we derived a new static model of thin, linear elastic orthotropic plates. In essence, this model takes into account the second-order terms $\mathbf{U}^2$, and $\boldsymbol{\sigma}^2$ of the asymptotic expansions of displacements and stresses. For clamped plates the term $\mathbf{U}^2$ does not satisfy the boundary condition $\mathbf{U}^2 = 0$ on that part of the boundary where the plate is clamped. To overcome this inherent difficulty Destuynder investigated the boundary layer, cf. also DAUGE and GRUAIS [4]. An alternative approach was proposed by RAOULT [15, 16] for isotropic plates. To cope with the second-order term $\mathbf{U}^2$ of the asymptotic expansion, this author appropriately defined the boundary conditions. Their precise, average form appears in the definition of the set X of admissible displacements, cf. formulae (3.2), (3.3). In this manner one avoids the study of boundary layer. In our papers [19, 20] the approach due to RAOULT [16] is extended to orthotropic plates in the static case.

The asymptotic approach to construction of models of rods, beams, plates and shells is usually confined to finding the zero-order terms, which correspond to equations obtained in a more standard manner in engineering literature, cf. [2, 5, 12-20, 23]. However, even in this case no a priori assumptions, like the Kirchhoff – Love hypotheses, are needed. The asymptotic approach to modelling of

structures has already a long history, cf. the comments in [2, 10, 13, 17, 22]. The book by LEWIŃSKI and TELEGA [13] summarizes the research on finding effective models of linear and nonlinear structures with microstructures. In this case the asymptotic methods also play a crucial role.

In the present contribution the static model elaborated in [19,20] is extended so as to include the inertia term. A new dynamic model of linear elastic orthotropic plates is derived. An important feature of the model is that the second-order terms $\mathbf{U}^2$ and $\boldsymbol{\sigma}^2$ of asymptotic expansions of displacements and stresses are taken into account. We follow the procedure exploited in the static case thus avoiding the analysis typical for the study of boundary layer. Anyway, our approach is an alternative one. The formal asymptotic procedure is justified by proving a convergence theorem. To exhibit a significant influence of second-order terms on the plate response, the circular isotropic plate is investigated in the static case.

2. Basic equations and scalings

Let $\Omega \subset \mathbb{R}^2$ be the mid-plane of the plate and 2ε its thickness. Here $\varepsilon > 0$ is treated as a small parameter. In the underformed state the plate occupies the region $\overline{\mathcal{B}^\varepsilon} = \overline{\Omega} \times [-\varepsilon, \varepsilon]$. We set: $\Gamma = \partial\Omega$, $\Gamma_0^\varepsilon = \Gamma \times [-\varepsilon, \varepsilon]$, $\Gamma_\pm^\varepsilon = \Omega \times \{\pm\varepsilon\}$. Throughout the paper the Cartesian coordinate system is used, except Sec.8.

It is assumed that the plate is made of a linear elastic material with the density ${}^\varepsilon\varrho$. In the case of orthotropy the elasticity tensor $\mathbf{C} = (C_{ijkl})$ is such that $C_{iijj} \neq 0$, $C_{klkl} \neq 0$ for $k \neq l$; (no summation over repeated indices), the remaining coefficients C_{ijkl} vanish. Roman indices take values in $\{1, 2, 3\}$. The basic equations are given by

$$ {}^\varepsilon\varrho\, {}^\varepsilon U_i'' = \partial_j\, {}^\varepsilon\sigma_{ij} + {}^\varepsilon f_i \qquad \text{in } \mathcal{B}^\varepsilon \times [0,T], \tag{2.1} $$

$$ {}^\varepsilon\sigma_{ij} = C_{ijkl}\, \gamma_{kl}({}^\varepsilon\mathbf{U}), \tag{2.2} $$

$$ \gamma_{ij}({}^\varepsilon\mathbf{U}) = \frac{1}{2}(\partial_i\, {}^\varepsilon U_j + \partial_j\, {}^\varepsilon U_i), \tag{2.3} $$

$$ {}^\varepsilon\mathbf{U} = \mathbf{0} \qquad \text{on } \Gamma_0^\varepsilon \times [0,T], \tag{2.4} $$

$$ {}^\varepsilon\mathbf{U}(\mathbf{x}, 0) = {}^\varepsilon\widetilde{\mathbf{U}}(\mathbf{x}), \qquad {}^\varepsilon\mathbf{U}'(\mathbf{x}, 0) = {}^\varepsilon\widetilde{\mathbf{V}}(\mathbf{x}), \qquad \mathbf{x} \in \mathcal{B}^\varepsilon, \tag{2.5} $$

$$ {}^\varepsilon\sigma_{i3} = \pm {}^\varepsilon g_i \qquad \text{on } \Gamma_\pm^\varepsilon \times [0,T]. \tag{2.6} $$

The quantities ${}^{\varepsilon}\sigma_{ij}$, ${}^{\varepsilon}\mathbf{U}$ and $\gamma_{ij}({}^{\varepsilon}\mathbf{U})$ denote the stress tensor, the displacement vector and the linearized strain tensor, respectively. Obviously, these quantities depend on the space coordinate $\mathbf{x}$ and time t. Here $(\cdot)' = \partial(\cdot)/\partial t$, etc. The initial data ${}^{\varepsilon}\widetilde{\mathbf{U}}$, ${}^{\varepsilon}\widetilde{\mathbf{V}}$ are prescribed. To use the method of asymptotic expansion, [2,3,12-20], it is convenient to work with the fixed domain, say $\mathcal{B} = \Omega \times (-1,1)$. To this end, for $\varepsilon > 0$ we define the mapping, cf. [3],

$$F^{\varepsilon} : \mathbf{x} = (x^1, x^2, x^3) \in \mathcal{B} \longrightarrow F^{\varepsilon}(\mathbf{x}) = (x^1, x^2, \varepsilon x^3) = \mathbf{x}^{\varepsilon} \in \mathcal{B}^{\varepsilon}. \tag{2.7}$$

Let us introduce a composition $(\varphi \circ F^{\varepsilon}) : \mathcal{B} \longrightarrow \mathbb{R}^3$ defined as follows

$$\forall \mathbf{x}^{\varepsilon} = F^{\varepsilon}(\mathbf{x}), \qquad (\varphi \circ F^{\varepsilon})(\mathbf{x}) = \varphi(\mathbf{x}^{\varepsilon}), \quad \text{where} \quad \varphi : \mathcal{B}^{\varepsilon} \longrightarrow \mathbb{R}^3. \tag{2.8}$$

One can easily verify that the quantities $\boldsymbol{\sigma}^{\varepsilon}$, $\mathbf{U}^{\varepsilon}$, etc., defined in $\mathcal{B}$, are interrelated with ${}^{\varepsilon}\boldsymbol{\sigma}$, ${}^{\varepsilon}\mathbf{U}$, etc., defined in $\mathcal{B}^{\varepsilon}$, as follows:

$$U_{\alpha}^{\varepsilon} = {}^{\varepsilon}U_{\alpha} \circ F^{\varepsilon}, \qquad U_3^{\varepsilon} = \varepsilon\,({}^{\varepsilon}U_3 \circ F^{\varepsilon}), \qquad \varrho = \varepsilon^{-2}\,({}^{\varepsilon}\varrho \circ F^{\varepsilon}), \tag{2.9}$$

$$\sigma_{\alpha\beta}^{\varepsilon} = {}^{\varepsilon}\sigma_{\alpha\beta} \circ F^{\varepsilon}, \qquad \sigma_{\alpha 3}^{\varepsilon} = \varepsilon^{-1}\,({}^{\varepsilon}\sigma_{\alpha 3} \circ F^{\varepsilon}), \qquad \sigma_{33}^{\varepsilon} = \varepsilon^{-2}\,({}^{\varepsilon}\sigma_{33} \circ F^{\varepsilon}), \tag{2.10}$$

$$\begin{aligned} f_{\alpha}^{o} &= {}^{\varepsilon}f_{\alpha} \circ F^{\varepsilon}, \qquad f_3^{o} = \varepsilon^{-1}\,({}^{\varepsilon}f_3 \circ F^{\varepsilon}), \\ g_{\alpha}^{o} &= \varepsilon^{-1}\,({}^{\varepsilon}g_{\alpha} \circ F^{\varepsilon}), \qquad g_3^{o} = \varepsilon^{-2}\,({}^{\varepsilon}g_3 \circ F^{\varepsilon}). \end{aligned} \tag{2.11}$$

Throughout the paper Greek indices take values in $\{1,2\}$. In the ε-independent domain $\mathcal{B}$ we write $\mathbf{U}^{\varepsilon}(\mathbf{x},t)$ and $\boldsymbol{\sigma}^{\varepsilon}(\mathbf{x},t)$ for displacements and stresses.

3. The variational formulation of the plate dynamics

Prior to passing to the variational formulation, we introduce the spaces of stresses and displacements, cf. [15, 16, 19, 20],

$$\Sigma = L^2(\mathcal{B}, \mathbb{E}_s^3), \tag{3.1}$$

$$X = X_{12} \times X_3, \tag{3.2}$$

where

$$\begin{aligned} X_{12} &= \{\mathbf{V} \in H^1(\mathcal{B})^2 : \int_{-1}^{1} V_{\alpha}\, dx_3 = 0, \quad \int_{-1}^{1} x_3\, V_{\alpha}\, n_{\alpha}\, dx_3 = 0 \quad \text{on } \Gamma\}, \\ X_3 &= \{V_3 \in H^1(\mathcal{B}) : \int_{-1}^{1} (1 - x_3^2)\, V_3\, dx_3 = 0 \quad \text{on } \Gamma\}, \qquad \alpha = 1,2. \end{aligned} \tag{3.3}$$

Here $\mathbb{E}_s^3$ denotes the space of symmetric 3×3 matrices and $H^1(\mathcal{B})^3 = [H^1(\mathcal{B})]^3$.

For a function $f(\mathbf{x}, t)$ $(\mathbf{x} \in \mathcal{B})$ we shall often write $f(t) = \{f(\mathbf{x}, t) | \mathbf{x} \in \mathcal{B}\}$ and similarly if $\mathbf{x} \in \Omega$, cf. [16]. Such a notation is common in mathematical studies of evolution problems.

Throughout the paper it is assumed that $f_\alpha^0(\mathbf{x}, t) = f_\alpha^0(x_1, x_2, t)$.

Let $(\mathbf{x}, t) \in \mathcal{B} \times (0, T)$, where $\mathcal{B} = \Omega \times (-1, 1)$. After rescaling (2.9) – (2.11), problem (2.1) – (2.6) is formulated in the variational form, see [16, 20].

PROBLEM $(\mathcal{P}^\varepsilon)$

Find $(\boldsymbol{\sigma}^\varepsilon, \mathbf{U}^\varepsilon) \in L^\infty(0, T; \Sigma \times X)$, such that $\mathbf{U}^{\varepsilon\prime} \in L^\infty(0, T; L^2(\mathcal{B})^3)$ and

$$\forall \boldsymbol{\tau} \in \Sigma, \quad A^\varepsilon(\boldsymbol{\sigma}^\varepsilon, \boldsymbol{\tau}) + B(\boldsymbol{\tau}, \mathbf{U}^\varepsilon) = 0, \tag{3.4}$$

$$\forall \mathbf{V} \in X, \quad -\varrho\,(U_3^{\varepsilon\prime\prime}, V_3) - \varrho\,\varepsilon^2\,(U_\alpha^{\varepsilon\prime\prime}, V_\alpha) + B(\boldsymbol{\sigma}^\varepsilon, \mathbf{V}) = F^0(\mathbf{V}), \tag{3.5}$$

$$\mathbf{U}^\varepsilon(\mathbf{x}, 0) = \widetilde{\mathbf{U}}^\varepsilon(\mathbf{x}), \qquad \mathbf{U}^{\varepsilon\prime}(\mathbf{x}, 0) = \widetilde{\mathbf{V}}^\varepsilon(\mathbf{x}), \qquad \mathbf{x} \in \mathcal{B}. \tag{3.6}$$

Here $(\cdot, \cdot)$ denotes the duality $(\mathcal{D}'(0, T; L^2(\mathcal{B})), L^2(\mathcal{B}))$. For the definition and properties of functional spaces used in this paper the reader is referred to the book by ADAMS [1].

If $U_\alpha^{\varepsilon\prime\prime}(\cdot, t) \in L^2(\mathcal{B})$ then

$$(U_\alpha^{\varepsilon\prime\prime}, V_\alpha) = \int_{\mathcal{B}} U_\alpha^{\varepsilon\prime\prime} V_\alpha \, d\mathbf{x}. \tag{3.7}$$

The forms A^ε and B are defined as follows, cf. [16, 19, 20],

$$\forall \{\boldsymbol{\sigma}, \boldsymbol{\tau}\} \in \Sigma \times \Sigma, \qquad A^\varepsilon(\boldsymbol{\sigma}, \boldsymbol{\tau}) = A^0(\boldsymbol{\sigma}, \boldsymbol{\tau}) + \varepsilon^2 A^2(\boldsymbol{\sigma}, \boldsymbol{\tau}) + \varepsilon^4 A^4(\boldsymbol{\sigma}, \boldsymbol{\tau}), \tag{3.8}$$

$$\forall \boldsymbol{\sigma} \in \Sigma, \quad \forall \mathbf{V} \in H^1(\mathcal{B})^3, \qquad B(\boldsymbol{\sigma}, \mathbf{V}) = -\int_{\mathcal{B}} \gamma_{ij}(\mathbf{V})\, \sigma_{ij} \, d\mathbf{x}, \tag{3.9}$$

where $\mathbf{A} = \mathbf{C}^{-1}$. The functional F^0 of external forces is given by

$$F^0(\mathbf{V}) = -\int_{\mathcal{B}} f_i^0 V^i \, d\mathbf{x} - \int_{\Gamma_\pm} g_i^0 V^i \, d\Gamma. \tag{3.10}$$

Obviously, the initial data $\widetilde{\mathbf{U}}^\varepsilon$ and $\widetilde{\mathbf{V}}^\varepsilon$ are prescribed, and $\Gamma_\pm = \Omega \times \{\pm 1\}$.

The bilinear form A^ε is easily derived from a bilinear form defined on the $\mathcal{B}^\varepsilon$ and using Eqs. (2.9), (2.10), cf. [16, 19, 20].

It can easily be shown that

$$A^0(\boldsymbol{\sigma}, \boldsymbol{\tau}) = (A_{\alpha\beta\gamma\delta}\,\sigma_{\gamma\delta}, \tau_{\alpha\beta}), \qquad A^4(\boldsymbol{\sigma}, \boldsymbol{\tau}) = (A_{3333}\,\sigma_{33}, \tau_{33}),$$

(3.11)

$$A^2(\boldsymbol{\sigma}, \boldsymbol{\tau}) = (A_{\alpha\beta 33}\,\sigma_{33}, \tau_{\alpha\beta}) + 2(A_{\alpha 3\delta 3}\,\sigma_{3\delta}, \tau_{3\alpha}) + (A_{33\gamma\delta}\,\sigma_{\gamma\delta}, \tau_{33}).$$

Here $(\cdot, \cdot)$ denotes the scalar product in $L^2(\mathcal{B})$.

Similarly to the static case we assume the asymptotic expansions of $\{\boldsymbol{\sigma}^\varepsilon, \mathbf{U}^\varepsilon\}$ as follows:

$$\boldsymbol{\sigma}^\varepsilon = \boldsymbol{\sigma}^0 + \varepsilon^2\,\boldsymbol{\sigma}^2 + \cdots, \tag{3.12}$$

$$\mathbf{U}^\varepsilon = \mathbf{U}^0 + \varepsilon^2\,\mathbf{U}^2 + \cdots. \tag{3.13}$$

Performing now the asymptotic analysis, i.e. substituting (3.12) into (3.4) and (3.5), we arrive at problem $(\mathcal{P}^0)$, linked with $\{\boldsymbol{\sigma}^0, \mathbf{U}^0\}$, and problem $(\mathcal{P}^2)$, linked with $\{\boldsymbol{\sigma}^2, \mathbf{U}^2\}$, cf. [15, 16, 19, 20].

The solution $\{\boldsymbol{\sigma}^2, \mathbf{U}^2\}$ of problem $(\mathcal{P}^2)$ yields the *first corrector* to $\{\boldsymbol{\sigma}^0, \mathbf{U}^0\}$. It is well-known that $\mathbf{U}^2$ does not satisfy, in general, the homogeneous boundary condition on Γ_0^1, [4, 16, 19]. We recall that $\mathbf{U}^0$ vanishes on $\Gamma_0^1 = \Gamma \times [-1, 1]$.

In subsequent sections we shall examine both the problem $(\mathcal{P}^0)$ and the problem $(\mathcal{P}^2)$. The choice of the space X for kinematically admissible displacements will prove to be crucial. We observe that the boundary conditions involved in definition (3.2),(3.3) of the space X are satisfied only in an averaged sense.

REMARK 1. Let us assume that $f_i^0 \in L^2(0, T; L^2(\mathcal{B}))$ and $g_i^{0\pm} \in L^2(0, T; L^2(\Gamma_\pm))$, $\widetilde{\mathbf{U}}^\varepsilon \in X$, $\widetilde{\mathbf{V}}^\varepsilon \in L^2(\mathcal{B})^3$. Then the solution $\{\mathbf{U}^\varepsilon, \boldsymbol{\sigma}^\varepsilon\}$ of problem $(\mathcal{P}^\varepsilon)$ exists and is unique; moreover, $\mathbf{U}^{\varepsilon\,\prime\prime} \in L^2(0, T; X')$, where X' denotes the dual space of X. For the proof the reader is referred to [6].

4. Study of Problem $(\mathcal{P}^0)$

Identifying the terms linked with ε^0 in problem $(\mathcal{P}^\varepsilon)$ we obtain problem $(\mathcal{P}^0)$, which includes a classical dynamic problem for orthotropic plates. The plate problem reads:

Find $\{\boldsymbol{\sigma}^0, \mathbf{U}^0\} \in L^\infty(0, T; \Sigma \times X)$ such that $U_3^{0\prime} \in L^\infty(0, T; L^2(\mathcal{B}))$ and

$$\forall\, \boldsymbol{\tau} \in \Sigma, \quad A^0(\boldsymbol{\sigma}^0, \boldsymbol{\tau}) + B(\boldsymbol{\tau}, \mathbf{U}^0) = 0, \tag{4.1}$$

$$\forall\, \mathbf{V} \in X, \quad -\varrho\,(U_3^{0\prime\prime}, V_3) + B(\boldsymbol{\sigma}^0, \mathbf{V}) = F^0(\mathbf{V}), \tag{4.2}$$

$$U_3^0(0) = \widetilde{U}_3^0, \qquad U_3^{0\prime}(0) = \widetilde{V}_3^0. \tag{4.3}$$

We recall that $\mathbf{U}^0 = (U_\alpha^0, U_3^0)$. The in-plane displacements U_α^0 are specified below. To proceed further, we introduce two spaces

$$X_{KL} = \{\, \mathbf{U} \mid \quad \gamma_{\alpha 3}(\mathbf{U}) = 0, \quad \gamma_{33}(\mathbf{U}) = 0 \,\}, \tag{4.4}$$

$$S = \{\, \boldsymbol{\tau} \in \Sigma \mid \ \tau_{\alpha 3} = 0, \quad \tau_{33} = 0 \,\}. \tag{4.5}$$

The existence result for problem $(\mathcal{P}^0)$ is classical, cf. [16].

PROPOSITION 1. If $F^0(\mathbf{V})$ is given by (3.10) and if

$$f_3^0 \in H^1(0,T;L^2(\mathcal{B})), \quad f_\alpha^0 \in L^\infty(0,T;\, L^2(\Omega)), \quad g_i^0 \in H^1(0,\, T; L^2(\Gamma_+ \cup \Gamma_-)),$$

then problem $(\mathcal{P}^0)$ has a unique solution $\{\mathbf{U}^0, \boldsymbol{\sigma}^0\}$. □

Now we consider problem $(\mathcal{P}^0 f)$, that is a particular case of $(\mathcal{P}^0)$ where $\{\boldsymbol{\sigma}^0, \mathbf{U}^0\} \in L^\infty(0,T; S \times X_{KL})$. From Eqs. (4.1) – (4.3), proceeding similarly to the static case, we find

$$U_3^0 \in L^\infty(0,\, T; H_0^2(\Omega)), \quad U_3^{0\prime} \in L^\infty(0,\, T; L^2(\Omega)),$$

$$2\varrho\, U_3^{0\prime\prime} + \frac{2}{3} D_{\alpha\beta\gamma\delta}\, \partial_{\alpha\beta\gamma\delta}\, U_3^0 = \int_{-1}^{1} f_3^0\, dx_3 + g_3^{0+} + g_3^{0-} + \partial_\alpha (g_\alpha^{0+} - g_\alpha^{0-}); \tag{4.6}$$

$$\alpha, \beta, \gamma, \delta = 1, 2,$$

$$U_3^0(0) = \widetilde{U}_3^0, \qquad U_3^{0\prime}(0) = \widetilde{V}_3^0, \tag{4.7}$$

$$U_\alpha^0 = u_\alpha^0 - x_3\, \partial_\alpha U_3^0, \tag{4.8}$$

where

$$D_{\alpha\beta\gamma\delta} = C_{\alpha\beta\gamma\delta} - C_{\alpha\beta 33}\, C_{3333}^{-1}\, C_{33\gamma\delta}. \tag{4.9}$$

Here $\mathbf{u}^0$ is the unique solution of the plane problem:

find $\mathbf{u}^0 \in L^\infty(0,T; H_0^1(\Omega)^2)$ such that

$$[K\, \mathbf{u}^0,\, \mathbf{v}] = F^0(-\mathbf{v},\, 0), \qquad \forall \mathbf{v} \in L^\infty(0,T; H_0^1(\Omega)^2), \tag{4.10}$$

where

$$[K\,\mathbf{u},\,\mathbf{v}] := 2\,[D_{\alpha\beta\gamma\delta}\,\gamma_{\gamma\delta}(\mathbf{u}),\,\gamma_{\alpha\beta}(\mathbf{v})], \tag{4.11}$$

and $[\cdot,\cdot]$ denotes the scalar product on $L^2(\Omega)$.

We observe that in the case of transverse homogeneity, the problem $(\mathcal{P}^0)$ (and problem $(\mathcal{P}^2)$ as well) splits into a plane elasticity problem and a plate problem, similarly to the static case considered in [16, 19, 20].

From Eq.(4.1) we conclude that

$$\sigma^0_{\alpha\beta} = D_{\alpha\beta\lambda\delta}\,\gamma_{\lambda\delta}(\mathbf{U}^0). \tag{4.12}$$

Passing to the full problem $(\mathcal{P}^0)$ we have to find the formulas for $\sigma^0_{\alpha 3}$ and σ^0_{33}. To this end we use *Lemma A*, formulated in the Appendix. In the dynamic problem considered, the inertia term $(-\varrho U_3^{0\prime\prime})$ is to be added to f_3^0, the third component of the body force vector $\mathbf{f}^0$. Proceeding then similarly to the static case we finally get

$$\sigma^0_{\alpha 3} = -\frac{1}{2}(1-x_3^2)\,D_{\alpha\beta\lambda\delta}\,\partial_{\beta\lambda\delta}\,U_3^0 + \frac{(1+x_3)}{2}g_\alpha^{0+} - \frac{(1-x_3)}{2}g_\alpha^{0-}, \tag{4.13}$$

$$\begin{aligned}\sigma^0_{33} = \varrho U_3^{0\prime\prime}\frac{(x_3^3-x_3)}{2} - \int_{-1}^{x_3} f_3^0\,dx_3 + \frac{2+3x_3-x_3^3}{4}\int_{-1}^{1} f_3^0\,dx_3 \\ + \frac{g_3^{0+}-g_3^{0-}}{2} + \frac{(3x_3-x_3^3)(g_3^{0+}+g_3^{0-})}{4} \\ + \frac{(1-x_3^2)}{4}\,\partial_\alpha(g_\alpha^{0+}+g_\alpha^{0-}) + x_3\frac{(1-x_3^2)}{4}\,\partial_\alpha(g_\alpha^{0+}-g_\alpha^{0-}).\end{aligned} \tag{4.14}$$

Formula (4.13) for the stresses $\sigma^0_{\alpha 3}$ is formally similar to the static case; however, now U_3^0 and $\sigma^0_{\alpha 3}$ depend also on time. If $U_3^{0\prime\prime}$ vanishes then we recover the formula for σ^0_{33} known from the static analysis, [16, 19, 20].

5. Study of Problem $(\mathcal{P}^2 f)$

Identifying the terms of $A^\varepsilon(\boldsymbol{\sigma}^\varepsilon, \boldsymbol{\tau})$ linked with ε^2 in $(\mathcal{P}^\varepsilon)$ we get problem $(\mathcal{P}^2)$ and its truncated form $(\mathcal{P}^2 f)$, cf. [15, 6, 19, 20]. Here we limit ourselves to the second problem.

Find $(\boldsymbol{\sigma}^2, \mathbf{U}^2) \in L^\infty(0,T;\,S\times X)$ such that $U_3^{2\prime} \in L^\infty(0,\,T;\,L^2(\mathcal{B}))$ and

$$\forall\,\boldsymbol{\tau}\in\Sigma, \qquad A^0(\boldsymbol{\sigma}^2,\boldsymbol{\tau}) + B(\boldsymbol{\tau},\mathbf{U}^2) = -A^2(\boldsymbol{\sigma}^0,\boldsymbol{\tau}), \tag{5.1}$$

$$(5.2)\qquad \forall \mathbf{V} \in X_{KL}, \qquad -\varrho(U_3^{2\prime\prime}, V_3) + B^2(\boldsymbol{\sigma}^2, \mathbf{V}) = \varrho(U_\alpha^{0\prime\prime}, V_\alpha),$$

$$(5.3)\qquad U_3^2(0) = \widetilde{U}_3^2, \qquad U_3^{2\prime}(0) = \widetilde{V}_3^2.$$

We observe that for $\boldsymbol{\sigma}^2 \in S$ and $\boldsymbol{\sigma}^0 \notin S$ we have

$$A^0(\boldsymbol{\sigma}^2, \boldsymbol{\tau}) = (D_{\alpha\beta\gamma\delta}{}^{-1}\, \boldsymbol{\sigma}_{\gamma\delta}^2, \boldsymbol{\tau}_{\alpha\beta}),$$

$$A^2(\boldsymbol{\sigma}^0, \boldsymbol{\tau}) = (A_{\alpha\beta 33}\, \boldsymbol{\sigma}_{33}^0, \boldsymbol{\tau}_{\alpha\beta}),$$

provided that $\boldsymbol{\tau} \in S$.

Let us pass to characterization of problem $(\mathcal{P}^2 f)$. If the external forces $\{\mathbf{f}^0, \mathbf{g}^0\}$ are sufficiently regular, see Sec.6, and if the initial conditions are of the form

$$(5.4)\quad \widetilde{U}_3^2 = \widetilde{w}^2 + A_{33\alpha\beta}\, D_{\alpha\beta\gamma\delta}\left[x_3\, \gamma_{\gamma\delta}(\mathbf{u}^0(0)) - \frac{1}{2}\, x_3^2\, \partial_{\gamma\delta}\, \widetilde{w}^0\right], \qquad \widetilde{w}^2 \equiv \widetilde{u}_3^2,$$

$$(5.5)\qquad \widetilde{V}_3^2 = \widetilde{v}_3^2 + A_{33\alpha\beta}\, D_{\alpha\beta\gamma\delta}\left[x_3\, \gamma_{\gamma\delta}(\mathbf{u}^{0\prime}(0)) - \frac{1}{2}\, x_3^2\, \partial_{\gamma\delta}\, \widetilde{v}_3^0\right],$$

with, see [19, 20],

$$(5.6)\qquad \widetilde{w}^2 \in H^2(\Omega), \quad \widetilde{w}^2 = \frac{1}{10}\, D_{\alpha\beta\lambda\mu}\, A_{33\alpha\beta}\, \partial_{\lambda\mu}\widetilde{w}^0 \qquad \text{on } \Gamma \times (0, T),$$

$$(5.7)\quad \partial_n \widetilde{w}^2 = \frac{1}{10}\, A_{33\alpha\beta}\, D_{\alpha\beta\lambda\mu}\, \partial_n\, \partial_{\lambda\mu}\widetilde{w}^0 - \frac{8}{10} \sum_{\alpha=1,2} A_{\alpha 3\alpha 3}\, D_{\alpha\alpha\gamma\delta}\, \partial_n\, \partial_{\gamma\delta}\, \widetilde{w}^0$$

$$\text{on } \Gamma \times (0, T),$$

then there exists the unique solution $\{\boldsymbol{\sigma}^2, \mathbf{U}^2\} \in L^\infty(0, T; S \times X)$, $U_3^{2\prime} \in L^\infty(0, T; L^2(\mathcal{B}))$ of problem $(\mathcal{P}^2 f)$.

The displacement (U_α^2, U_3^2) is given by

$$(5.8)\qquad U_3^2 = w^2 + A_{33\alpha\beta}\, D_{\alpha\beta\gamma\delta}\left[x_3\, \gamma_{\gamma\delta}(\mathbf{u}^0) - \frac{1}{2}\, x_3^2\, \partial_{\gamma\delta}\, w^0\right], \qquad w^2 \equiv u_3^2,$$

$$(5.9)\quad U_\alpha^2 = u_\alpha^2 - x_3\, \partial_\alpha\, w^2 - A_{\alpha 3\delta 3}\, (x_3 - \frac{1}{3}\, x_3^3)\, D_{\delta\beta\gamma\kappa}\, \partial_{\beta\gamma\kappa}\, w^0$$

$$- \frac{1}{2}\, A_{33\xi\zeta}\, D_{\xi\zeta\gamma\delta}\, [x_3^2\, \partial_\alpha\, \gamma_{\gamma\delta}(\mathbf{u}^0) - \frac{1}{3}\, x_3^3\, \partial_{\alpha\gamma\delta}\, w^0],$$

where $w^2 \in L^\infty(0,T;\, H^2(\Omega))$ and $w^{2\prime} \in L^\infty(0,T; L^2(\Omega))$.

Formally, the formulas for the components of displacement vector $\mathbf{U}^2$ are the same as in the static case, [19, 20]. Now, however,all quantities describing the dynamic problem depend also on time.

For the membrane components of the stress tensor we have the expression, cf. [20],

$$\sigma^2_{\gamma\delta} = D_{\alpha\beta\gamma\delta}\,\gamma_{\alpha\beta}(\mathbf{U}^2) - A_{\alpha\beta 33}\,D_{\alpha\beta\gamma\delta}\,\sigma^0_{33}. \tag{5.10}$$

Substituting (5.8) into (5.2) and integrating the obtained equation twice by parts, we get the formulation of the plate bending equation in problem $(\mathcal{P}^2 f)$ in the form

$$\begin{aligned} &2\varrho\, w^{2\prime\prime} + \frac{2}{3}\,D_{\alpha\beta\gamma\delta}\,\partial_{\alpha\beta\gamma\delta}\,w^2 \\ &\quad = -\Big(\frac{3}{10}\,D_{\alpha\beta\gamma\delta}\,A_{\gamma\delta 33} + \frac{8}{10}\sum_{\gamma=1,2} D_{\alpha\beta\gamma\gamma}\,A_{\gamma 3\gamma 3}\Big)\,\partial_{\alpha\beta}\Big[\int_{-1}^{1} f_3^0 + g_3^{0+} + g_3^{0-} \\ &\qquad + \partial_\alpha(g_\alpha^{0+} - g_\alpha^{0-})\Big] + D_{\alpha\beta\gamma\delta}\,A_{\gamma\delta 33}\,\partial_{\alpha\beta}\int_{-1}^{1} x_3\,dx_3 \int_{-1}^{x_3} f_3^0\,d\tilde{x}_3 + \frac{2}{3}\,\varrho\,\partial_{\alpha\alpha} w^{0\prime\prime} \\ &\qquad + \varrho\,\partial_{\alpha\beta} w^{0\prime\prime}\Big[\frac{4}{15}\,D_{\alpha\beta\gamma\delta}\,A_{\gamma\delta 33} + \frac{8}{5}\sum_{\gamma=1,2} D_{\alpha\beta\gamma\gamma}\,A_{\gamma 3\gamma 3}\Big] \quad \text{in } \Omega\times(0,T), \end{aligned} \tag{5.11}$$

where the boundary and initial conditions are

$$w^2 = \frac{1}{10}\,D_{\alpha\beta\lambda\mu}\,A_{33\alpha\beta}\,\partial_{\lambda\mu} w^0 \qquad \text{on } \Gamma\times(0,T), \tag{5.12}$$

$$\partial_n w^2 = \frac{1}{10} A_{33\alpha\beta} D_{\alpha\beta\lambda\mu}\partial_n\,\partial_{\lambda\mu} w^0 - \frac{8}{10}\sum_{\alpha=1,2} A_{\alpha 3\alpha 3}\,D_{\alpha\alpha\gamma\delta}\partial_n\,\partial_{\gamma\delta}\,w^0 \qquad \text{on } \Gamma\times(0,T), \tag{5.13}$$

$$w^2(0) = \tilde{w}^2, \qquad w^{2\prime}(0) = \tilde{v}_3^2. \tag{5.14}$$

The dynamic membrane problem resulting from $(\mathcal{P}^2 f)$ means finding

$$\mathbf{u} \in L^\infty(0, T; H^1(\Omega)^2)$$

such that

$$K\,\mathbf{u}^2 = -2\varrho\,\mathbf{u}^{0\,\prime\prime} + \frac{1}{3}\,A_{33\xi\zeta}\,D_{\xi\zeta\gamma\delta}\,\partial_\beta \triangle\,\gamma_{\gamma\delta}(\mathbf{u}^0) + A_{\gamma\delta 33}\,D_{\alpha\beta\gamma\delta}\,\partial_\beta \int_{-1}^{1} \sigma_{33}^0\,\delta_{\alpha\beta}\,dx_3, \tag{5.15}$$

$$\mathbf{u}^2 \in L^\infty(0,T;\, H^1(\Omega)^2), \qquad u_\alpha^2 = \frac{1}{6}\,A_{33\lambda\mu}\,D_{\lambda\mu\gamma\delta}\,\partial_\alpha\,\gamma_{\gamma\delta}(\mathbf{u}^0) \quad \text{on } \Gamma \times (0,T). \tag{5.16}$$

6. Convergence study

The aim of this section is to prove the second-order convergence of displacements and stresses. Precise meaning of such a convergence follows from Theorem 1. Primarily, however, we formulate the following result, being a slight modification of Corollary 2 proved in Raoult [16].

PROPOSITION 2. Let

$$\psi = \int_{-1}^{1} f_3^0\,dx_3 + g_3^{0+} + g_3^{0-} + \partial_\alpha\,(g_\alpha^{0+} - g_\alpha^{0-}), \tag{6.1}$$

(i) $$f_\alpha^0 \in H^3(0,T;\, H^1(\Omega)), \quad g_\alpha^{0+} \in H^3(0,T;\, H^1(\Gamma^+)), \quad g_\alpha^{0-} \in H^3(0,T;\, H^1(\Gamma^-)),$$

(ii) $$f_3^0 \in H^3(0,T;\, L^2(\mathcal{B})), \quad g_3^{0+} \in H^3(0,T;\, L^2(\Gamma^+)), \quad g_3^{0-} \in H^3(0,T;\, L^2(\Gamma^-)),$$

(*iii*) $$\widetilde{U}_3^0 \in H^4(\Omega) \cap H_0^2(\Omega),$$

(*iv*), $$\psi(x,0) - \frac{2}{3}\,D_{\alpha\beta\lambda\mu}\,\partial_{\alpha\beta\lambda\mu}\,\widetilde{U}_3^0 \in H^3(\Omega) \cap H_0^2(\Omega),$$

(v) $$\widetilde{V}_3^0 \in H^4(\Omega) \cap H_0^2(\Omega),$$

(vi) $$\psi'(x,0) - \frac{2}{3} D_{\alpha\beta\lambda\mu}\, \partial_{\alpha\beta\lambda\mu}\, \widetilde{V}_3^0 \in H_0^1(\Omega),$$

then

(a) $$U_3^0 \in C^1(0,T; H^4(\Omega) \cap H_0^2(\Omega)), \quad U_3^{0\,\prime\prime} \in C^0(0,T; H^3(\Omega) \cap H_0^2(\Omega)),$$
$$U_3^{0\,\prime\prime\prime} \in C^0(0,T; H_0^1(\Omega)),$$

(b) $$u_\alpha^0 \in H^3(0,T;\ H^3(\Omega) \cap H_0^1(\Omega).$$ □

In the proof of convergence we shall also exploit a priori estimates.

PROPOSITION 3. Under the assumptions of Proposition 2. and if the initial data of problems $(\mathcal{P}^\varepsilon)$ and $(\mathcal{P}^0)$ are such that

(6.2) $$\|(\sigma_{\alpha\beta}^\varepsilon - \sigma_{\alpha\beta}^0)(0)\| \leq C\varepsilon^2, \quad \|(\sigma_{\alpha 3}^\varepsilon - \sigma_{\alpha 3}^0)(0)\| \leq C\varepsilon, \quad \|\sigma_{33}^\varepsilon(0)\| \leq C,$$

(6.3) $$\|U_3^{\varepsilon\,\prime}(0) - w^{0\,\prime}(0)\| \leq C\varepsilon^2, \quad \|U_\alpha^{\varepsilon\,\prime}(0) - U_\alpha^{0\,\prime}(0)\| \leq C\varepsilon,$$

where $\|\cdot\| = \|\cdot\|_{L^2}$ and C is a generic positive constant, then

(6.4) $\varepsilon^{-2}(\sigma_{\alpha\beta}^\varepsilon - \sigma_{\alpha\beta}^0)$, $\varepsilon^{-1}(\sigma_{\alpha 3}^\varepsilon - \sigma_{\alpha 3}^0)$, σ_{33}^ε are bounded in $L^\infty(0,T; L^2(\mathcal{B}))$,

(6.5) $$\varepsilon^{-2}(\mathbf{U}^\varepsilon - \mathbf{U}^0) \quad \text{is bounded in } L^\infty(0,T;X),$$

(6.6) $\varepsilon^{-2}(U_3^{\varepsilon\,\prime} - w^{0\,\prime})$, $\varepsilon^{-1}(U_\alpha^{\varepsilon\,\prime} - U_\alpha^{0\,\prime})$ are bounded in $L^\infty(0,T; L^2(\mathcal{B}))$.

P r o o f. The proof does not differ from a similar one performed by RAOULT [15, 16] for isotropic plates.

REMARK 2. The assumptions appearing in Proposition 3. can be formulated exclusively in terms of the data of problems $(\mathcal{P}^\varepsilon)$ and $(\mathcal{P}^0)$. More precisely, by using the constitutive equations involved in these problems and if the initial data are such that

(6.7) $$\|\widetilde{\mathbf{U}}^\varepsilon - \mathbf{U}^0(0)\|_{H^1} \leq C\varepsilon^2,$$

(6.8) $$\|\varepsilon^{-2}\gamma_{\alpha 3}(\widetilde{\mathbf{U}}^{\varepsilon}) - A_{\alpha 3\alpha 3}\sigma^0_{\alpha 3}(w^0(0))\|_{L^2} \leq C\varepsilon, \text{ (no summation over } \alpha),$$

where

$$\sigma^0_{\alpha 3}(w^0) = -\frac{(1-x_3^2)}{2} D_{\alpha\beta\lambda\mu}\,\partial_{\beta\lambda\mu}\,w^0 + \frac{(1+x_3)}{2}\,g^{0+}_{\alpha} - \frac{(1-x_3)}{2}\,g^{0-}_{\alpha},$$

(6.9) $$\|\varepsilon^{-2}\gamma_{33}(\widetilde{\mathbf{U}}^{\varepsilon}) - \gamma_{33}(w^0(0))\|_{L^2} \leq C\varepsilon^2,$$

where

$$\gamma_{33}(w^0(0)) = -C^{-1}_{3333}\sum_{\mu=1,2} C_{\mu\mu 33}\,\gamma_{\mu\mu}(\mathbf{u}^0(0)),$$

(6.10) $$\|\widetilde{V}^{\varepsilon}_3 - w^{0\,\prime}(0)\|_{L^2} \leq C\varepsilon^2, \quad \|\widetilde{V}^{\varepsilon}_{\alpha} - U^{0\,\prime}_{\alpha}(0)\|_{L^2} \leq C\varepsilon,$$

then (6.4) – (6.6) are satisfied. □

After these preparations we can formulate the second-order convergence theorem.

THEOREM 1. *Under the assumptions of Proposition 2. and if the data of problems* $(\mathcal{P}^{\varepsilon})$ *and* $(\mathcal{P}^0)$ *are such that*

(i) $$\varepsilon^{-2}(\widetilde{\mathbf{U}} - \mathbf{U}^0(0))$$

converges in $H^1(\mathcal{B})^3$ *to an element* $\mathbf{U}^2$ *of the form*

(6.11) $$\widetilde{U}^2_3 = \widetilde{w}^2 + A_{33\alpha\beta}\,D_{\alpha\beta\gamma\delta}\left[x_3\,\gamma_{\gamma\delta}(\mathbf{u}^0(0)) - \frac{1}{2}\,x_3^2\,\partial_{\gamma\delta}\,\widetilde{w}^0\right],$$

with $\widetilde{w}^2 \in H^2(\Omega)$, *and*

$$\widetilde{w}^2 = \frac{1}{10}\,D_{\alpha\beta\lambda\mu}\,A_{33\alpha\beta}\,\partial_{\lambda\mu}\widetilde{U}^0_3 \qquad \text{on } \Gamma,$$

$$\partial_n\widetilde{w}^2 = \frac{1}{10}\,A_{33\alpha\beta}\,D_{\alpha\beta\lambda\mu}\,\partial_n\,\partial_{\lambda\mu}\widetilde{U}^0_3 - \frac{8}{10}\sum_{\alpha=1,2} A_{\alpha 3\alpha 3}\,D_{\alpha\alpha\gamma\delta}\,\partial_n\,\partial_{\gamma\delta}\,\widetilde{U}^0_3$$

on Γ,

(6.12) $$\widetilde{U}^2_{\alpha} = \widetilde{u}^2_{\alpha} - x_3\,\partial_{\alpha}\,w^2 - A_{\alpha 3\delta 3}\,(x_3 - \frac{1}{3}\,x_3^3)\,D_{\delta\beta\gamma\kappa}\,\partial_{\beta\gamma\kappa}\,w^0$$
$$- \frac{1}{2}\,A_{33\xi\zeta}\,D_{\xi\zeta\gamma\delta}\left[x_3^2\,\partial_{\alpha}\,\gamma_{\gamma\delta}(\mathbf{u}^0) - \frac{1}{3}\,x_3^3\,\partial_{\alpha\gamma\delta}\,w^0\right],$$

where $\widetilde{u}_\alpha^2 \in H^1(\Omega)$ *is given by*

$$(6.13)\quad K\widetilde{\mathbf{u}}^2 = -2\varrho\,\mathbf{u}^{0\prime\prime} + \frac{1}{3}\,A_{33\xi\zeta}\,D_{\xi\zeta\gamma\delta}\,\partial_\beta\,\triangle\,\gamma_{\gamma\delta}(\mathbf{u}^0) + A_{\gamma\delta 33}\,D_{\alpha\beta\gamma\delta}\,\partial_\beta \int_{-1}^{1} \sigma_{33}^0\,\delta_{\alpha\beta}\,dx_3 \quad \text{in } \Omega,$$

with

$$\widetilde{\mathbf{u}}_\alpha^2 = \frac{1}{6}\,A_{33\lambda\mu}\,D_{\lambda\mu\gamma\delta}\,\partial_\alpha\,\gamma_{\gamma\delta}(\mathbf{u}^0(0) \quad \text{on } \Gamma,$$

(ii)
$$\varepsilon^{-1}(\sigma_{\alpha 3}^\varepsilon(0) - \sigma_{\alpha 3}^0(0)) \longrightarrow 0 \quad \text{in } L^2(\mathcal{B}),$$
$$\sigma_{33}^\varepsilon(0) \longrightarrow \sigma_{33}^0(0) \quad \text{in } L^2(\mathcal{B}),$$

(iii)
$$\varepsilon^{-1}(\widetilde{V}_\alpha^\varepsilon - U_\alpha^{0\prime}(0)) \longrightarrow 0 \quad \text{in } L^2(\mathcal{B}),$$
$$\varepsilon^{-2}(\widetilde{V}_3^\varepsilon - \widetilde{V}_3^0) \longrightarrow \widetilde{V}_3^2 \quad \text{in } L^2(\mathcal{B}),$$

with $\widetilde{V}_3^2$ *of the form*

$$(6.14)\quad \widetilde{V}_3^2 = \widetilde{v}_3^2 + A_{33\alpha\beta}\,D_{\alpha\beta\gamma\delta}\left[x_3\,\gamma_{\gamma\delta}(\mathbf{u}^{0\prime}(0)) - \frac{1}{2}\,x_3^2\,\partial_{\gamma\delta}\,\widetilde{v}_3^0\right],$$

then we have

$$\varepsilon^{-2}(\mathbf{U}^\varepsilon - \mathbf{U}^0) \longrightarrow \mathbf{U}^2 \quad \text{in } L^2(0,T;\,X),$$

$$\varepsilon^{-1}(U_\alpha^\varepsilon - U_\alpha^0)' \longrightarrow 0 \quad \text{in } L^2(0,T;\,L^2(\mathcal{B})),$$

$$\varepsilon^{-2}(U_3^\varepsilon - U_3^0)' \longrightarrow U_3^{2\prime} \quad \text{in } L^2(0,T;\,L^2(\mathcal{B})),$$

$$\varepsilon^{-2}(\sigma_{\alpha\beta}^\varepsilon - \sigma_{\alpha\beta}^0) \longrightarrow \sigma_{\alpha\beta}^2 \quad \text{in } L^2(0,T;\,L^2(\mathcal{B})),$$

$$\varepsilon^{-1}(\sigma_{\alpha 3}^\varepsilon - \sigma_{\alpha 3}^0) \longrightarrow 0 \quad \text{in } L^2(0,T;\,L^2(\mathcal{B})),$$

$$(\sigma_{33}^\varepsilon - \sigma_{33}^0) \longrightarrow 0 \quad \text{in } L^2(0,T;\,L^2(\mathcal{B})),$$

where $((\sigma_{\alpha\beta}^2,\,0,\,0),\,\mathbf{U}^2)$ *is the unique solution to problem* $(\mathcal{P}^2 f)$ *with the initial data* $\widetilde{U}_3^2,\,\widetilde{V}_3^2$.

P r o o f. It is divided into two major steps. First, one establishes the weak convergence by using Proposition 3. Next the strong convergence is demonstrated by showing the convergence of norms, i.e.,

$$\int_0^T \Big[\varrho\varepsilon^{-4}\|\overline{U}_3^{\varepsilon\prime}\|_{L^2}^2 + \varrho\varepsilon^{-2}\|\overline{U}_\alpha^{\varepsilon\prime}\|_{L^2}^2 + A(\tilde{\boldsymbol{\sigma}}^\varepsilon, \tilde{\boldsymbol{\sigma}}^\varepsilon)\Big]dt \longrightarrow \int_0^T \Big[\varrho\|U_3^{2\prime}\|_{L^2}^2 + A(\tilde{\boldsymbol{\sigma}}^2, \tilde{\boldsymbol{\sigma}}^2)\Big]dt,$$

where

$$A(\boldsymbol{\sigma}, \boldsymbol{\tau}) = (A^0 + A^2 + A^4)(\boldsymbol{\sigma}, \boldsymbol{\tau}),$$

$$\overline{\mathbf{U}}^\varepsilon = \mathbf{U}^\varepsilon - \mathbf{U}^0, \qquad \overline{\boldsymbol{\sigma}}^\varepsilon = \boldsymbol{\sigma}^\varepsilon - \boldsymbol{\sigma}^0,$$

$$\tilde{\boldsymbol{\sigma}}^\varepsilon = (\varepsilon^{-2}\overline{\sigma}_{\alpha\beta}^\varepsilon,\ \varepsilon^{-1}\overline{\sigma}_{\alpha 3}^\varepsilon,\ \overline{\sigma}_{33}^\varepsilon), \quad \tilde{\boldsymbol{\sigma}}^2 = (\sigma_{\alpha\beta}^2,\ 0,\ 0).$$

Otherwise the proof runs similarly to the one devised by RAOULT [16] for isotropic plates. However, formula (148) in [16] is to be replaced by

$$2\,w^{2\prime}(0) - \frac{1}{3}A_{33\gamma\delta}\,D_{\gamma\delta\alpha\beta}\,\partial_{\alpha\beta}\,U_3^{0\prime}(0) = 2\,\tilde{v}_3^2 - \frac{1}{3}A_{33\gamma\delta}\,D_{\gamma\delta\alpha\beta}\,\partial_{\alpha\beta}\tilde{V}_3^0,$$

where $U_3^{2\prime}(0) = \tilde{V}_3^2$.

REMARK 3. Conditions (6.13 (ii)) can be formulated in terms of the data of problems $(\mathcal{P}^\varepsilon)$ and $(\mathcal{P}^0)$ as follows:

$$\varepsilon^{-1}\,[\varepsilon^{-2}\gamma_{\alpha 3}(\tilde{\mathbf{U}}^\varepsilon) - \gamma_{\alpha 3}(\tilde{\mathbf{U}}^0)] \longrightarrow 0,$$

where $\gamma_{\alpha 3} = A_{\alpha 3\alpha 3}\,\sigma_{\alpha 3}^0(U_3^0)$ (no summation over α),

$$\varepsilon^{-2}\Big[\sum_{\mu=1,2} C_{\mu\mu 33}\,\gamma_{\mu\mu}(\tilde{\mathbf{U}}^\varepsilon) + \varepsilon^{-2}\,C_{3333}\,\gamma_{33}(\tilde{U}_3^\varepsilon)\Big] \longrightarrow -\frac{x_3^3 - x_3}{6}D_{\alpha\beta\gamma\delta}\,\partial_{\alpha\beta\gamma\delta}\,\tilde{U}_3^0$$

$$+\left\{\frac{(x_3+1)}{2}\int_{-1}^{1} f_3^0 - \int_{-1}^{x_3} f_3^0 + \frac{(1-x_3^2)}{4}\,\partial_\alpha(g_\alpha^{0+} + g_\alpha^{0-}) + \frac{g_3^{0+} - g_3^{0-}}{2} + \frac{x_3(g_3^{0+} + g_3^{0-})}{2}\right\}(0).$$

7. Interpretation of the asymptotic approach for the dynamic problem

Let ${}^{\varepsilon}\varrho = \varepsilon^2 \varrho$, ${}^{\varepsilon}g_3^+ = \varepsilon^2 g_3^+$, see [20]. According to (2.9) we write

$$ {}^{\varepsilon}U_3 (x_1, x_2, \varepsilon x_3, t) = \varepsilon^{-1} U_3^{\varepsilon} (x_1, x_2, x_3, t). $$

Consequently, for sufficiently small ε we have:

$$ \varepsilon^{-2}({}^{\varepsilon}U_3 - Z_3^0)(x_1, x_2, 0, t) \simeq z_3^2 (x_1, x_2, t), \quad z_3^0(x_1, x_2, t) = Z_3^0(x_1, x_2, 0, t). $$

Here Z_3^0 is the deflection in the real plate with the thickness $2h$. Such a plate is subjected to the gravity forces with the density ${}^{h}\varrho$ and the load ${}^{h}g_3^+$, acting on the upper face. The mid-plane deflection is

$$ (7.1) \quad {}^{h}r_3 = z_3^0 + h^2 z_3^2, \qquad \text{where } z_3^0 = z_3^0 (x_1, x_2, t), \qquad z_3^2 = z_3^2 (x_1, x_2, t). $$

The following dynamic plate equations are satisfied by ${}^{h}r$:

$$ (7.2) \quad 2h\, {}^{h}\varrho\, {}^{h}r_3'' + \frac{2}{3} h^3 D_{\alpha\beta\gamma\delta}\, \partial_{\alpha\beta\gamma\delta}\, {}^{h}r_3 - {}^{h}\varrho\, h^3 \Big[\frac{2}{3} \triangle z_3^{0\prime\prime} + \partial_{\alpha\beta} z_3^{0\prime\prime} \Big(\frac{4}{15} D_{\alpha\beta\gamma\delta} A_{\gamma\delta 33} + \frac{8}{5} D_{\alpha\beta\gamma\gamma} A_{\gamma 3\gamma 3}\Big)\Big] = -2h\, {}^{h}\varrho + {}^{h}g_3^+, \text{ in } \Omega \times (0, T). $$

The term in rectangular brackets is the *corrector term*. The boundary conditions implied by the analysis of the second-order term $\{\boldsymbol{\sigma}^2, \mathbf{U}^2\}$ are:

$$ (7.3) \qquad {}^{h}r_3 = \frac{1}{10} h^2 D_{\alpha\beta\lambda\mu} A_{33\alpha\beta}\, \partial_{\lambda\mu} z_3^0 \qquad \text{on } \Gamma \times (0, T), $$

$$ (7.4) \quad \partial_n\, {}^{h}r_3 = \frac{1}{10} h^2 A_{33\alpha\beta}\, D_{\alpha\beta\lambda\mu}\, \partial_n\, \partial_{\lambda\mu} z_3^0 - \frac{8}{10} h^2 \sum_{\alpha=1,2} A_{\alpha 3\alpha 3}\, D_{\alpha\alpha\gamma\delta}\, \partial_n\, \partial_{\gamma\delta} z_3^0 \quad \text{on } \Gamma \times (0, T). $$

Obviously, $z_3^0 \in L^{\infty}(0, T; H_0^2(\Omega))$ is a solution to

$$ (7.5) \quad 2h\, {}^{h}\varrho\, z_3^{0\prime\prime} + \frac{2}{3} h^3\, D_{\alpha\beta\lambda\mu}\, \partial_{\alpha\beta\lambda\mu}\, z_3^0 = -2h\, {}^{h}\varrho + {}^{h}g_3^+ \qquad \text{in } \Omega \times (0, T), $$

$$ (7.6) \qquad z_3^0(0) = \widetilde{Z}_3^0, \quad z_3^{0\prime}(0) = 0 \qquad \text{in } \Omega. $$

We have additionally assumed that the initial velocity of all points of the plate is zero, or ${}^{e}\widetilde{\mathbf{V}} = \mathbf{0}$. The initial conditions for Eq.(7.2) are specified by

$$(7.7) \qquad {}^{h}r_3(0) = \widetilde{Z}_3^0 + h^2\widetilde{z}_3^2, \qquad {}^{h}r_3'(0) = 0.$$

The initial data $\widetilde{Z}_3^0$ and $\widetilde{Z}_3^2$ are determined by performing the static analysis, see (5.6). Thus we assume that at the beginning of a dynamic process, i.e. for $t = 0$, we have

$$(7.8) \qquad \begin{aligned} &{}^{h}A({}^{h}\boldsymbol{\sigma}(0), \boldsymbol{\tau}) + {}^{h}B(\boldsymbol{\tau}, {}^{h}\mathbf{U}(0)) = 0, \\ &{}^{h}B({}^{h}\boldsymbol{\sigma}(0), \mathbf{V}) = {}^{h}F(0)(\mathbf{V}). \end{aligned}$$

Now, to find $\widetilde{Z}_3^0$ we have to solve the problem

$$(7.9) \qquad \widetilde{Z}_3^0 \in H_0^2(\Omega), \qquad \frac{2}{3} D_{\alpha\beta\gamma\delta}\, \partial_{\alpha\beta\gamma\delta}\, \widetilde{Z}_3^0 = -2\varrho + g_3^{0+}(0).$$

To get the initial quantity $\widetilde{z}_3^2$, we have to consider the boundary-value problem

$$(7.10) \qquad \frac{2}{3} D_{\alpha\beta\gamma\delta}\, \partial_{\alpha\beta\gamma\delta}\, \widetilde{z}_3^2 = 0 \quad \text{in } \Omega,$$

$$(7.11) \qquad \widetilde{z}_3^2 = \frac{1}{10} D_{\alpha\beta\lambda\mu} A_{33\alpha\beta} \partial_{\lambda\mu} \widetilde{Z}_3^0 \qquad \text{on } \Gamma,$$

$$(7.12) \qquad \partial_n \widetilde{z}_3^2 = \frac{1}{10} A_{33\alpha\beta}\, D_{\alpha\beta\lambda\mu}\, \partial_n\, \partial_{\lambda\mu} \widetilde{Z}_3^0 - \frac{8}{10} \sum_{\alpha=1,2} A_{\alpha 3\alpha 3}\, D_{\alpha\alpha\gamma\delta}\, \partial_n\, \partial_{\gamma\delta} \widetilde{Z}_3^0 \quad \text{on } \Gamma.$$

In the case of isotropic plates, Eqs.(7.2)-(7.6) reduce to those derived earlier by RAOULT [16]

$$(7.13) \qquad 2\,{}^{h}\varrho\, h\, {}^{h}r_3'' + \frac{2}{3} \frac{E}{1-\nu^2} h^3 \triangle^2 {}^{h}r_3 = -2h\,{}^{h}\varrho + {}^{h}g_3^{+} + {}^{h}\varrho h^3 \frac{34 - 14\nu}{15(1-\nu)} \triangle z_3^{0\prime\prime} \quad \text{in } \Omega \times (0, T),$$

$$(7.14) \qquad {}^{h}r_3 = -h^2 \frac{\nu}{10(1-\nu)} \triangle z_3^0 \qquad \text{on } \Gamma \times (0, T),$$

$$\partial_n {}^h r_3 = -h^2 \frac{8+\nu}{10(1-\nu)} \partial_n \triangle z_3^0 \qquad \text{on } \Gamma \times (0, T), \tag{7.15}$$

$$ {}^h r_3(0) = \widetilde{Z}_3^0 + h^2 \widetilde{z}_3^2, \qquad {}^h r_3'(0) = 0. \tag{7.16}$$

Here $z_3^0 \in L^\infty(0,T; H_0^2(\Omega))$ is a solution to

$$2h\, {}^h\varrho\, z_3^{0\prime\prime} + \frac{2}{3} \frac{E}{1-\nu^2} h^3 \triangle^2 z_3^0 = -2h\, {}^h\varrho + {}^h g_3^+ \quad \text{in } \Omega \times (0, T), \tag{7.17}$$

$$z_3^0(0) = \widetilde{Z}_3^0, \quad z_3^{0\prime}(0) = 0 \quad \text{in } \Omega. \tag{7.18}$$

In this simple case of loading, the in-plane components of the displacement in the real plate vanish. Indeed, in such a case Eq. (4.5) yields $u_\alpha^0 = 0$, and since $[K\,\mathbf{u}^2, \mathbf{v}] = 0$, we conclude that $u_\alpha^2 = 0$, $\alpha = 1, 2$.

8. Illustrative example: evaluation of the influence of the first corrector in the static case

In the present section we shall illustrate quantitatively the influence of the second-order asymptotic term or the *first corrector* on the plate deflection. We shall analyse only the static boundary-value problem for circular plates. Thus all variables do not depend on time and the inertial terms are neglected. Also, initial conditions are obviously absent.

The asymptotic theory is applied to a circular *isotropic* plate of thickness $2h$, of the radius R, and subjected to the uniform vertical load g_3 acting on Γ_+^h. Let $r_3(\rho)$ be the deflection of the plate mid-plane accounting for the *corrector*. In the polar coordinates (ρ, θ) we have

$$r_3(\rho, x_3)_{|x_3=0} = r_3(\rho, 0) = r_3 = w^0(\rho, 0) + h^2 w^2(\rho, 0). \tag{8.1}$$

To find r^3 we have to solve the following boundary-value problem:

$$D \frac{1}{\rho} \frac{d}{d\rho} \Big\{ \rho \frac{d}{d\rho} \Big[\frac{1}{\rho} \frac{d}{d\rho} \Big(\rho \frac{d r_3}{d\rho} \Big) \Big] \Big\} = g_3 \qquad \text{in } \Omega, \tag{8.2}$$

$$r_3 = -\frac{h^2 \nu}{10(1-\nu)} \Big(\frac{d^2}{d\rho^2} + \frac{1}{\rho} \frac{d}{d\rho} \Big) w^0 \qquad \text{on } \Gamma, \tag{8.3}$$

$$\partial_n r_3 = -\frac{h^2(8+\nu)}{10(1-\nu)} \partial_n \Big(\frac{d^2}{d\rho^2} + \frac{1}{\rho} \frac{d}{d\rho} \Big) w^0 \qquad \text{on } \Gamma. \tag{8.4}$$

Here E is the the Young modulus, ν denotes the Poisson ratio, $D = \dfrac{2Eh^3}{3(1-\nu^2)}$, ρ is the radial running coordinate in the polar coordinate system.

First, we solve the classical bending problem

$$D\frac{1}{\rho}\frac{d}{d\rho}\left\{\rho\frac{d}{d\rho}\left[\frac{1}{\rho}\frac{d}{d\rho}\left(\rho\frac{dw^0}{d\rho}\right)\right]\right\} = g_3 \qquad \text{in } \Omega, \tag{8.5}$$

$$w^0 = 0, \qquad \frac{dw^0}{d\rho} = 0 \qquad \text{on } \Gamma. \tag{8.6}$$

It is known that the solution of Eqs.(8.5),(8.6) has the form [22]

$$w^0 = \frac{g_3\,(R^2-\rho^2)^2}{64D}. \tag{8.7}$$

Taking into account (8.7) in (8.3) and (8.4) we get

$$r_3 = -\frac{h^2\nu}{10(1-\nu)} \cdot \frac{g_3\,R^2}{8D} \qquad \text{on } \Gamma, \tag{8.8}$$

$$\partial_n r_3 = -\frac{h^2(8+\nu)}{10(1-\nu)} \cdot \frac{g_3 R}{2D} \qquad \text{on } \Gamma, \tag{8.9}$$

since $\left(\dfrac{d^2}{d\rho^2} + \dfrac{1}{\rho}\dfrac{d}{d\rho}\right)w^0 = \dfrac{g_3\,R^2}{8D}$ on Γ.

Finally, solving Eq.(8.2) with the boundary conditions (8.8) and (8.9), we obtain

$$r_3 = r_3(\rho) = \frac{g_3\,(R^2-\rho^2)^2}{64D} + \frac{g_3\,h^2}{80D(1-\nu)}[R^2(16+\nu) - 2\rho^2(8+\nu)]. \tag{8.10}$$

For the central point of the plate, where $\rho = 0$, we get the following formulae:

$$r_3 = r_3(\rho) = \frac{g_3\,R^4}{64D} + \frac{g_3\,h^2R^2(16+\nu)}{80D(1-\nu)}, \tag{8.11}$$

$$w^0(0) = \frac{3R^4(1-\nu^2)}{128\,h^3} \cdot g_3/E, \tag{8.12}$$

$$h^2\,w^2(0) = \frac{3R^2(1+\nu)(16+\nu)}{160\,h} \cdot g_3/E. \tag{8.13}$$

Table 1. Influence of the *first corrector* on deflection of clamped circular isotropic plate, $\rho = 0$ (centre of the plate)

h/R	$\frac{h^2 w^2}{w^0}$ if $\nu = 0.3$	$\frac{h^2 w^2}{w^0}$ if $\nu = 0.45$
1/20	4.7%	6.0%
1/15	8.3%	10.6%
1/10	18.6%	23.9%

Let us present the above results in the form of Table 1. This table shows a relative participation of the *first corrector* included in $r_3(0)$.

For $\rho = R$ the boundary conditions for the deflections w^0, and w^2, are specified by

$$w^0 = 0, \qquad w^2 = -\frac{g_3 R^2}{80D} \cdot \frac{\nu}{(1-\nu)} \neq 0 \quad \text{on } \Gamma.$$

From Table 1 we conclude that the influence of w^2 may be significant, depending on the Poisson ratio, the thickness and the radius of the plate.

9. Comments on related papers

Refined theories of plates can be derived either with the use of asymptotic expansions or by assuming suitable displacements or stress hypotheses. The aim of this section is to perform a comparison of our results with the approaches used in the papers [7, 8, 9, 11, 21]. In our case the displacement distribution is obtained by using asymptotics. In contrast to the approach used in [9,11,21], the asymptotic method does not require any assumptions on the kinematics.

The papers [9, 21] are devoted to dynamics of thick and moderately thick plates, respectively. In [9] the kinematical assumptions due to Hencky are used:

$$(9.1)\quad u_\alpha(x_i, t) = x_3\, \phi_\alpha(x_\beta, t), \quad u_3(x_i, t) = w(x_\alpha, t), \quad \alpha, \beta = 1, 2, \quad i = 1, 2, 3,$$

where ϕ_α denotes rotation of the plate cross-sections. In the equations describing the free vibrations plate problem appears the term: $-4\,\varrho\, h^3/3(1-\nu) \cdot A\, \triangle w''$. It coincides with the rotational inertia term obtained in our paper for the isotropic case, see Eq.(7.13), provided that $A = (17 - 7\nu)/10$. We observe that in [9] four alternate values of A are cited, for which the obtained solution was discussed.

In [21] a special form for shear stresses (not for displacements) was assumed. Moderately thick plate on an elastic foundation yields the equation describing

free vibrations of the plate. In this governing equation, a term similar to our second order term(the *corrector*)

$$\frac{34-14\nu}{15(1-\nu)}\varrho h^3 \triangle z_3^{0\prime\prime} \tag{9.2}$$

is involved. However, in [21] the numerator is equal to $34-12\nu$.

In the paper [11] Jemielita's kinematical assumptions are admitted. The dynamic problem for thick, isotropic plate is analysed starting from the Hamilton variational principle. First, the energy-consistent model is derived. Then, rational simplifications of the three functionals used yield, in the static case, Reissner equations. In the equation of motion obtained in [11] for the averaged plate deflection the term (9.2) appears. However, in the model studied, also other terms are present in this equation. Such a difference is due to the fact that in [11] the kinematical hypothesis has been a priori assumed.

The developments of the paper [7] are based on using some averaged values in Reissner's sense. Finally, one derives a Kármán-Reissner nonlinear anisotropic plate model and its linear approximation. The elastic anisotropic material is described by means of engineering coefficients, E_i, ν_{ij}.

In [8] the refined 2-D dynamic equations of an isotropic thin plate are derived from 3-D equations of elasticity with the use of asymptotic method. The small parameter λ is defined as follows: $\lambda = \varepsilon^{1/q}$, $\varepsilon = h/l$, $2h$ – the thickness, where l is the characteristic plate dimension, and $r = p/q$, p, q – integers. The asymptotic expansions for displacements are admitted in the form:

$$v_x = \varepsilon^{3r-3}\sum_{s=0}^{\infty}\lambda^s v_x^{(s)}, \quad v_z = \varepsilon^{4r-4}\sum_{s=0}^{\infty}\lambda^s v_z^{(s)}, \quad v_x = u_x/h, \quad v_z = u_z/h. \tag{9.3}$$

The formula for v_y is similar to Eq.$(9.3)_1$. The coefficients $v_x^{(s)}$, $v_z^{(s)}$ involve expansions:

$$v_z^{(s)} = \sum_{k=0}^{K}\zeta^k v_{zk}^{(s)}, \quad v_x^{(s)} = \sum_{k=0}^{K+1}\zeta^k v_{xk}^{(s)}, \quad \zeta = z/h,$$

where $K = s/q$, if it is an even number, and $K = (s/q-1)$ in the opposite case. For the quantities $v_{zk}^{(s)}, v_{xk}^{(s)}$ the recurrence formulas are derived in [8].

For various approximations, various dynamical models are obtained. For instance, if $s < 6q - 6p$ then in the dynamical equation the following term is present:

$$\frac{17-7\nu}{15(1-\nu)}\frac{\partial^2}{\partial\tau^2}\triangle v_{z0}^{(s-2q-2p)}, \tag{9.4}$$

where $\tau = t/t_0$, $t_0 = l\,\varepsilon^{\omega-1}\sqrt{\varrho/E}$. In this theory an important role is played by the parameter $\omega = 2r$ characterising the time-dependence of stresses. If $\omega < 0$, the quasistatic deformation is described. The remaining two classes of this theory are characterised by: $0 \leq \omega < 2$ and $\omega \geq 2$. The second class contains the 3-D dynamic deformation.

At the end of the comments given above, we want to mention that an useful introduction to engineering approaches of formulations of refined plate models may be offered by the monograph [14].

Comparing our results with other contributions we conclude that second order terms (the *correctors*) also appear in refined engineering models. However, these terms are not always exactly the same, though very similar. Also, in our case the *corrector* has been rigorously derived and justified.

Appendix

The following lemma was formulated in [16].

LEMMA A.

Let Y be a space such that $\{v \in H^1(\mathcal{B}) \mid v = 0 \text{ on } \Gamma_0^1\} \subset Y \subset H^1(\mathcal{B})$ and let G be a linear form on Y given by

$$\forall\, v \in Y, \quad G(v) = (p\ ,\ v) - (q_\alpha, \partial_\alpha w) + \int\limits_\Omega \Big[rw(1) + sw(-1)\Big]\,dx_1\,dx_2$$

with $p,\ q_\alpha,\ \partial_\alpha q_\alpha \in L^2(\mathcal{B})$ and $r,\ s \in L^2(\Omega)$. Then the problem

$$\sigma \in L^2(\mathcal{B}), \quad \forall\, v \in Y, \quad (\sigma\ , \partial_3 v) = G(v)$$

has a solution if and only if the following compatibility conditions are satisfied:

$$(C_1) \qquad \int\limits_{-1}^{1} (p + \partial_\alpha q_\alpha)\,dx_3 \ + \ r \ + \ s = 0,$$

$$(C_2) \qquad \forall\, v \in Y, \qquad \int\limits_{\Gamma_0^1} q_\alpha\, n_\alpha\, v\, d\Gamma = 0.$$

The solution σ is given by

$$\sigma = \int\limits_{-1}^{x_3} (-p - \partial_\alpha q_\alpha)\,dx_3 \ + \ \frac{1}{2}\int\limits_{-1}^{1} (p + \partial_\alpha q_\alpha)\,dx_3 \ + \ \frac{1}{2}(r - s).$$

Similarly, let $\mathcal{Z}$ be such that $\{(v_\alpha) \in H^1(\mathcal{B})^2 \mid v_\alpha = 0 \text{ on } \Gamma_0^1\} \subset \mathcal{Z} \subset H^1(\mathcal{B})^2$ and let G be a linear form on $\mathcal{Z}$ given by

$$\forall\, (v_\alpha) \in \mathcal{Z}, \quad G_1(v_\alpha) = (p_\alpha, v_\alpha) - (q_{\alpha\beta}, \partial_\alpha v_\beta) + \int_\Omega [r_\alpha v_\alpha(1) + s_\alpha v_\alpha(-1)]\, dx_1 dx_2$$

with $p_\alpha,\ q_{\alpha\beta},\ \partial_\beta q_{\alpha\beta} \in L^2(\mathcal{B})$, and $r_\alpha,\ s_\alpha \in L^2(\Omega)$.

Then the problem

$$\sigma_\alpha \in L^2(\mathcal{B}), \quad \forall v_\alpha \in \mathcal{Z}, \quad (\sigma_\alpha\ ,\ \partial_3 v_\alpha) = G_1(v_\alpha)$$

has a solution if and only if the following compatibility conditions are satisfied:

$$(D_1) \qquad \int_{-1}^{1} (p_\alpha + \partial_\beta q_{\alpha\beta})\, dx_3 \ + \ r_\alpha \ + \ s_\alpha = 0,$$

$$(D_2) \qquad \forall\, v_\alpha \in \mathcal{Z}, \qquad \int_{\Gamma_0^1} q_{\alpha\beta}\, n_\beta\, v_\alpha\, d\Gamma = 0.$$

The solution σ_α $(\alpha = 1, 2)$ is given by

$$\sigma_\alpha = \int_{-1}^{x_3} (-p_\alpha - \partial_\beta q_{\alpha\beta})\, dx_3 \ + \ \frac{1}{2} \int_{-1}^{1} (p_\alpha + \partial_\beta q_{\alpha\beta})\, dx_3 \ + \ \frac{1}{2}(r_\alpha - s_\alpha).$$

Acknowledgement

The authors are grateful to the Referee for useful comments on the earlier version of the paper. The second author was partially supported by the State Committee for Scientific Research CKBN, Poland, through the grant No 7 T07A 043 18.

References

1. R. A. ADAMS, *Sobolev spaces,* Academic Press, New York 1975.
2. P. G. CIARLET, *Mathematical elasticity, vol.II: Theory of plates,* North-Holland, Amsterdam 1997.

3. P. G. CIARLET, P. DESTUYNDER, *A justification of the two-dimensional linear plate model*, J. Méc., **18**, 315-344, 1979.

4. M. DAUGE, I. GRUAIS, *Asymptotics of arbitrary order for a thin elastic clamped plate, I. Optimal error estimates*, Asymptotic Anal., **13**,167-197, 1996; *II. Analysis of the boundary layer term, ibid.*, **16**, 99-124, 1998.

5. H. LE DRET, *Problèmes variationnels dans le multi-domaines. Modélisation des jonctions et applications*, Masson, Paris 1991.

6. G. DUVAUT, J. L. LIONS, *Inequalities in mechanics and physics*, Springer-Verlag, Berlin, Heidelberg, New York 1976.

7. R. P. GILBERT, T. S. VASHAKMADZE, *A two-dimensional nonlinear theory of anisotropic plates*, Math. Comp. Model., **32**, 855-875, 2000.

8. M. I. GUSEIN-ZADE, *Asymptotic analysis of three-dimensional dynamical equations of a thin plate*(in Russian), Prikl. Mat. Mekh. **38**, 1072-1078, 1974.

9. G. JEMIELITA, *Free vibrations of an isotropic cube and a thick plate*(in Polish), Arch. Civ. Eng., **23**,511-525, 1977.

10. G. JEMIELITA, *Exact equations theory of plates* (in Polish), Warsaw University of Technology Publications, Civil Engineering, No 124, 1993.

11. T. LEWIŃSKI, *On refined plate models based on kinematical assumptions*, Ing.-Arch., **57**, 133-146, 1987.

12. T. LEWIŃSKI, *Effective models of composite periodic plates - I. Asymptotic solution*, Int. J. Solids Struct., **27**, 1155-1172, 1991; *II. Simplifications due to symmetries, ibid.*, 1173-1184; *III. Two-dimensional approaches, ibid.*, 1185-1203.

13. T. LEWIŃSKI, J. J. TELEGA, *Plates, laminates and shells: asymptotic analysis and homogenization*, World Scientific, Series on Advances in Mathematics for Applied Sciences, **52**, Singapore 2000.

14. S. ŁUKASIEWICZ, *Local loads on plates and shells* (in Polish), P. S. P., Warsaw 1976.

15. A. RAOULT, *Contributions a l'étude des modèles d'évolution des plaques et à l'approximation d'équation d'évolution linéaires du second ordre par les méthodes multipas*, Thèse 3ème cycle, Université Pierre et Marie Curie, Paris 1980.

16. A. RAOULT, *Construction d'un modèle d'évolution de plaques avec terme d'inertie de rotation*, Annali Mat. pura appl., **139**, 361-400, 1985.

17. J. SANCHEZ-HUBERT, E. SANCHEZ-PALENCIA, *Coques élastiques minces: proprietés asymptotiques*, Masson, Paris 1997.

18. A. SŁAWIANOWSKA, J. J. TELEGA, *Asymptotic analysis of anisotropic nonlinear elastic membranes*, Bull. Pol. Acad. Sci., Tech. Sci., **47**,115-126, 1999.

19. A. SŁAWIANOWSKA, J. J. TELEGA, *Second-order model of linear elastic orthotropic plates*, Mech. Res. Comm., **27**, 659-668, 2000.

20. A. SŁAWIANOWSKA, J. J. TELEGA, *An asymptotic model of linear elastic orthotropic plates*, Bull. Pol. Acad. Sci., Tech. Sci., **49**, 1-16, 2001, (in press).

21. W. SZCZEŚNIAK, *Influence of two-parameter elastic foundation on free vibrations of a plate of moderate thickness* (in Polish), Eng. Trans., **37**, 87-115, 1989.

22. S. TIMOSHENKO, W. WOINOWSKY-KRIEGER, *Theory of plates and shells*, Mc-Graw-Hill, 1959.

23. L. TRABUCHO, J. M. VIAÑO, *Mathematical modelling of rods*, [in:] Handbook of numerical analysis, Vol. IV, P. G. CIARLET, J. L. LIONS (Eds.), 487-973, North Holland, Amsterdam 1996.

Received March 23, 2001; revised version May 11, 2001.

Arch. Mech., **53**, 4-5, pp. 565–597, Warszawa 2001

Gradient formulation in coupled damage-plasticity

G. Z. VOYIADJIS and R. J. DORGAN

Department of Civil and Environmental Engineering,
Louisiana State University
Baton Rouge, LA 70803 USA

THIS WORK PROVIDES a consistent and systematic framework for the gradient approach in coupled damage-plasticity that enables one to better understand the effects of material inhomogeneity on the macroscopic behavior and the material instabilities. The idea of multiple scale effects is made more general and complete by introducing damage and plasticity internal state variables and the corresponding gradients at both the macro and mesoscale levels. The mesoscale gradient approach allows one to obtain more precise characterization of the nonlinearity in the damage distribution; to address issues such as lack of statistical homogeneous state variables at the macroscale level such as debonding of fibers in composite materials, crack, voids, etc., and to address nonlocal influences associated with crack interaction. The macroscale gradients allow one to address non-local behavior of materials and interpret the collective behavior of defects such as dislocations and cracks. The development of evolution equations for plasticity and damage is treated in a similar mathematical approach and formulation since both address defects such as dislocations for the former and cracks/voids for the latter. Computational issues of the gradient approach are introduced in a form that can be applied using the finite element approach.

1. Introduction

ENGINEERING MATERIALS contain defects that lead in some cases to specific pattern formation due to a coupling of inelastic mechanisms of microcrack and microvoid growth with plastic flow and fracture. Initially, loading of heterogeneous materials causes non-interacting microcracks and microvoids; however, experimental observations indicate that further loading will cause failure mechanisms to occur at localized zones of plasticity and damage where a lot of interaction and coalescence of microcracks and microvoids take place. These interactions lead to a degradation of the global stiffness and to a subsequent decrease of the load carrying capacity of the material. As damage localizes over a narrow region of the continuum, the characteristic length scale governing the variations of damage falls far below the scale of the state variables of strain and damage used to describe the response of the continuum. This leads to the case where the

wavelength of the damage distribution is predicted to be much smaller than the size of the material heterogeneities [1].

The classical local approach does not adequately capture a decreased length scale, and it is therefore necessary to look for alternative strategies for the solution of the problem such as micromechanical characterization, Cosserat continua, and nonlocal approaches. In the case of the nonlocal approach, a common procedure is to introduce the nonlocal terms either through an integral equation [2] or through a gradient equation [3].

Localization problems due to plasticity and damage can be handled by using the gradient approach at the macroscale. However, it is observed that for a given value of macroscopic damage variable variation, the macroscale response function associated with the representative volume elements (RVE) consisting of different distributions of defects are attributable to the differences in the size, orientation, and spatial distribution of defects within the RVEs. These are important factors that make the evolution function statistically inhomogeneous below the RVE scale. Macroscale strain and damage gradient approaches cannot capture this sub-representative volume element (SRVE) length-scale effect. Lacy *et. al.* [4] proposed a mesoscale gradient approach in order to obtain more precise characterization of the nonlinearity in the damage distribution, nonlocal influences associated with crack interaction, and statistical inhomogeneity of the evolution related damage variables.

Damage and plasticity internal state variables and the corresponding gradients at both the macro and mesoscale levels are introduced. By including both internal state variables of plasticity and damage, this work provides sufficient details of defects and their interaction to characterize physically the material behavior. By incorporating the gradient of these internal state variables, this work also addresses the non-local effects. The combined coupled concept of introducing gradients at the mesoscale and macroscale enables one to address two issues simultaneously. The mesoscale gradients allow one to address such issues as lack of statistical homogeneous state variables at the macroscale level such as debonding of fibers in composite materials, crack, voids, etc. On the other hand, the macroscale gradients allow one to address non-local behavior of materials and interpret the collective behavior of defects such as dislocations and cracks. This coupled proposed gradients formulation allows one to model size-dependent behavior of the materials together with localization.

2. Gradient model using non-local internal state variables

In order to introduce long-range microstructural interaction, the stress response at a material point is assumed to depend on the state of its neighborhood in addition to the state of the point itself. The use of nonlocal continua theory is

made in order to achieve that. KUHL *et. al.* [5] and MÜHLHAUS and AIFANTIS [6] have derived a gradient continuum enhancement as a special case of the general concept of nonlocal continua. At the position $\mathbf{x}$, the nonlocal tensor $\bar{\mathbf{A}}$ can be expressed as the weighted average of its local counterpart $\mathbf{A}$ over a surrounding volume V at a small distance $|\zeta| \leq L_c$ from $\mathbf{x}$ such that

$$\bar{\mathbf{A}} = \frac{1}{V} \int_V \mathbf{h}(\zeta)\mathbf{A}(\mathbf{x}+\zeta)dV \tag{2.1}$$

where L_c is an internal characteristic length [6] and $\mathbf{h}(\zeta)$ is a weight function that decays smoothly with distance and in this work is given by $\mathbf{h}(\zeta) = \mathbf{I}\,h(\zeta)$where $\mathbf{I}$ is an identity tensor. However, the identity tensor $\mathbf{I}$ may be suitably substituted by another tensor in order to induce further anisotropic behavior of the material.

The local tensor $\mathbf{A}$ in Eq. (2.1) can be approximated by a Taylor expansion at $\zeta = 0$ such that:

$$\mathbf{A}(\mathbf{x}+\zeta) = \mathbf{A}(\mathbf{x}) + \nabla\mathbf{A}(\mathbf{x})\zeta + \frac{1}{2!}\nabla^2\mathbf{A}(\mathbf{x})\zeta\zeta + \frac{1}{3!}\nabla^3\mathbf{A}(\mathbf{x})\zeta\zeta\zeta + \quad \ldots \quad . \tag{2.2}$$

where ∇^i denotes the i-th order gradient operator. Assuming only an isotropic influence of the averaging equation, the integrals of the odd terms in Eq. (2.2) vanish. Furthermore, making use of Eqs. (2.1) and (2.2) and truncating the TAYLOR series after the quadratic term, leads to the following expression for the nonlocal tensor $\bar{\mathbf{A}}$ [5]:

$$\bar{\mathbf{A}} = \frac{1}{V}\int_V h(\zeta)\mathbf{A}(\mathbf{x})\,dV + \frac{1}{2!V}\int_V h(\zeta)\nabla^2\mathbf{A}(\mathbf{x})\zeta\zeta\,dV. \tag{2.3}$$

This relation can be expressed as a partial differential equation such that [5]:

$$\bar{\mathbf{A}} = \mathbf{A} + \left(\frac{1}{2!V}\int_V [h(\zeta)]\zeta\zeta dV\right)\nabla^2\mathbf{A} = \mathbf{A} + a\nabla^2\mathbf{A} \tag{2.4}$$

where $\frac{1}{V}\int_V [h(\zeta)]dV = 1$. In Eq. (2.4), a is a constant proportional to a length squared and weights each component of the gradient term identically. If one assumes a more general tensorial character for $\mathbf{h}$ not necessarily confined to the expression in terms of an identity tensor, then one obtains a different weighting of the individual coefficients. This will give a weighting function with a tensorial nature a containing several different integration constants a_{ij}. We have thus introduced the gradient term $a\nabla^2\mathbf{A}$ as an approximation of the difference between the nonlocal tensor $\bar{\mathbf{A}}$ at $\mathbf{x}$ and the local tensor A at $\mathbf{x}$.

A similar expression for the non-local internal variable $\bar{\mathbf{A}}$ may be obtained at the mesoscale to characterize interface damage such as debonding of the fiber from the matrix such that $\bar{\hat{\mathbf{A}}} = \hat{\mathbf{A}} + a\hat{\nabla}^2\hat{\mathbf{A}}$. This allows one to describe $\bar{\hat{\mathbf{A}}}$ at a SRVE where the internal variable can only be statistically homogeneous at a subvolume of the RVE and $\hat{\nabla}^2\hat{\mathbf{A}}$ is its corresponding gradient.

3. Representative volume and sub-volume elements

The internal state variables are divided into two categories. The first category is statistically homogeneous at the RVE, while the second is statistically homogeneous at the SRVE. The definition of the RVE and SRVE is detailed in the work of NEMAT-NASSER and HORI [9].

In the literature, the RVE is the necessary minimum observation window that is used for the determination of the statistically homogenous elastic stiffness. The RVE is considered to be a cube with dimension L_{RVE} such that the following conditions are fulfilled:

$$\frac{d}{L_{RVE}} \ll 1, \qquad L_c \leq L_{RVE} \leq L, \qquad \left|\frac{\partial \sigma_{ij}^0}{\partial x_k}\right| L_{RVE} \ll |\sigma_{ij}^0|, \tag{3.1}$$

where d is a characteristic size of the micro-constituents, L_C is the heterogeneity correlation length, L is the characteristic macroscopic structural dimension, σ_{ij}^0 is the mean field stress and x_1, x_2, are x_3 the components of the Cartesian coordinates. The RVE implied in this work is the matrix with a single fiber in the middle of the RVE (Fig. 1).

The other category of internal state variables are those that can only be statistically homogenous at a subvolume of the RVE. For an RVE made of two

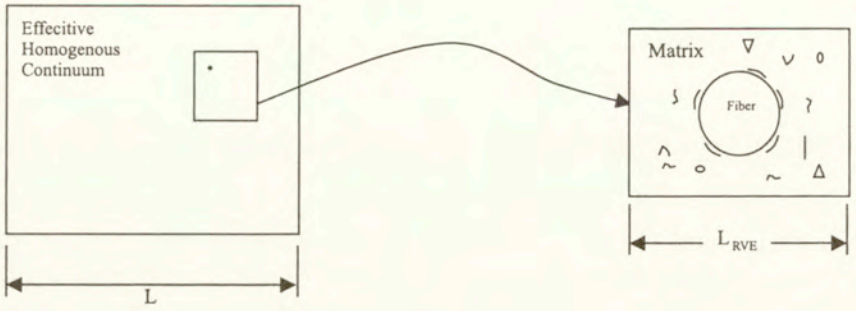

FIG. 1. Schematic representation of RVE

phase materials, the defect in each constituent and in the interphase (debonding) cannot be categorized as statistically homogenous for the RVE unless a very low order of measure of these defects is used to characterize damage or plasticity. The subvolume characterization of damage and plasticity at a level below the RVE allows one to adequately characterize the details of these defects. This SRVE definition for the composite material in the case of multi-scale analysis is introduced by defining an equivalent minimum observation window for each constituent of the composite where the response function of each constituent is statistically homogenous within the equivalent RVEs (Fig. 2). Then the sub-RVE damage distribution of each constituent can be characterized at a point within the corresponding RVEs.

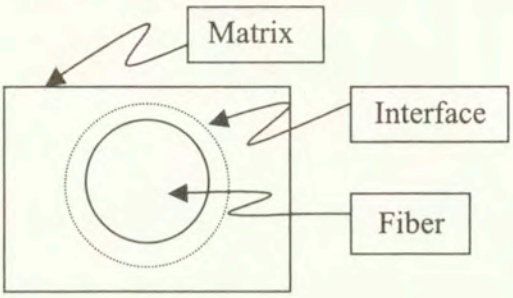

FIG. 2. Sub-RVEs for multiscale composite materials

4. Macroscale-mesoscale coupled plasticity and damage gradient theory using nonlocal internal state variables

The thermoelastic Helmoltz free energy may be expressed in terms of the nonlocal internal state variables as

$$(4.1)\quad \Psi = \Psi({}^{(e)}\varepsilon_{ij},\, T, {}^{(p)}\bar{\alpha}_{ij},\, {}^{(p)}\bar{p},\, {}^{(d)}\bar{\phi}_{ij}^{(u)}, {}^{(d)}\bar{\gamma}_{ij}, {}^{(u)}, {}^{(d)}\bar{\kappa}^{(u)}) \quad \text{where } u = m, f, i,$$

where the subscribed letters after the variables indicate the tensorial nature of the variables. To the left of the variables, the bracketed superscript e implies elasticity-related internal state variable, p implies plasticity-related internal state variables, and d refers to the damage related internal state variables. The superscribed letter u to the right of the variables indicates that the different internal state variables are used to characterize the types of damages associated with the different material constituents. The composite material is divided into three components: matrix (m), fiber (f), and interface (i).

In the above equations, the nonlocal internal state variables $\bar{p}$ and $\bar{\alpha}_{ij}$ variables characterize the isotropic and kinematic hardening flux variables in plastic-

ity, respectively; the nonlocal internal state variables $\bar{\kappa}_{(u)}$ and $\bar{\gamma}_{ij}^{(u)}$ characterize the isotropic and kinematic hardening flux variables in damage, respectively. We define the kinematic hardening of the yield surface to be the cumulative effect from the flux-related backstresses. The $\bar{\phi}$ is the nonlocal damage second order tensor. Additive decomposition of the strain is assumed with $\varepsilon_{ij}^{'}$ being the elastic component and $\varepsilon_{ij}^{''}$ being the corresponding plastic component such that:

$$\varepsilon_{ij} = \varepsilon_{ij}^{'} + \varepsilon_{ij}^{''}. \tag{4.2}$$

The components of the macroscale gradient terms and the averaged mesoscale gradient terms of the macroscale internal state variables of both plasticity and damage may be used as additional higher order internal variables. In lieu of Section 1, with regard to using gradients to describe the non-local behavior of the material, the following relations are given here in a form similar to that given by Eqs. (5.1) and (5.2) such that:

$$\bar{\alpha}_{ij} = \alpha_{ij} + {}^{(p)}_{(2)}A\,\nabla^2\alpha_{ij} + {}^{(p)}_{(3)}A\widehat{\hat{\nabla}^2\hat{\alpha}_{ij}}, \tag{4.3}$$

$$\bar{p} = p + {}^{(p)}_{(2)}B\,\nabla^2 p + {}^{(p)}_{(3)}B\,\widehat{\hat{\nabla}^2\hat{p}}, \tag{4.4}$$

$$\bar{\gamma}_{ij}^{(u)} = \gamma_{ij}^{(u)} + {}^{(d)}_{(2)}A^{(u)}\ \nabla^2\gamma_{ij}^{(u)} + {}^{(d)}_{(3)}A^{(u)}\ \widehat{\hat{\nabla}^2\hat{\gamma}_{ij}^{(u)}}, \tag{4.5}$$

$$\bar{\kappa}^{(u)} = \kappa^{(u)} + {}^{(d)}_{(2)}B^{(u)}\ \nabla^2\kappa^{(u)} + {}^{(d)}_{(3)}B^{(u)}\ \widehat{\hat{\nabla}^2\hat{\kappa}^{(u)}}, \tag{4.6}$$

$$\bar{\phi}_{ij}^{(u)} = \phi_{ij}^{(u)} + {}^{(d)}_{(2)}C^{(u)}\ \nabla^2\phi_{ij}^{(u)} + {}^{(d)}_{(3)}C^{(u)}\ \widehat{\hat{\nabla}^2\hat{\phi}_{ij}^{(u)}}. \tag{4.7}$$

The constants ${}^{(p)}_{(r)}A$, ${}^{(p)}_{(r)}B$, ${}^{(d)}_{(r)}A^{(u)}$, ${}^{(d)}_{(r)}B^{(u)}$, and ${}^{(d)}_{(r)}C^{(u)}$ are constants similar to the constant a given by Eq. (2.4). If one chooses the same weight function $h(\zeta)$ for both the plasticity and damage macro-related internal variables, then one obtains

$${}^{(p)}_{(2)}A = {}^{(p)}_{(2)}B = {}^{(d)}_{(2)}A^{(u)} = {}^{(d)}_{(2)}B^{(u)} = {}^{(d)}_{(2)}C^{(u)} = A. \tag{4.8}$$

However, this will not be the case for the micro-related internal variables since the region of the sub-volume will change for different internal variables.

The isotropic hardening variable of plasticity, p, is a scalar quantity and is expressed in terms of the second order tensor, $\dot{\varepsilon}''_{ij}$ describing the plastic strain rate. The gradient terms of p characterize measures of the dislocation density [7]. The gradient terms referring to the backstress characterizes the internal embedded stress variations introduced by dislocation pile-ups, etc. The average mesoscale gradients of kinematic and isotropic hardening in plasticity may be used to characterize discrete dislocations in the formulation, if that is paramount to the analysis.

For the case of damage, the second order tensor, ϕ_{ij} characterizes a kinematic measure of damage due to volume or surface reduction associated with the evolution of voids or cracks, respectively [10-12]. The eigen values of define the Jacobian that describes the change in volume due to the micro-cracks and the micro-cavities. The damage is characterized through the individual damages of the matrix, $\phi_{ij}^{(m)}$ the fiber, $\phi_{ij}^{(f)}$ and the interface, $\phi_{ij}^{(i)}$ The gradients of the damages can also be used in this analysis. For the case of matrix damage, $\nabla^2\phi_{ij}^{(m)}$ is used, while for fiber damage, $\nabla^2\phi_{ij}^{(f)}$ is used. However, for the interface damage, the averaged mesoscale gradient $\widehat{\hat{\nabla}^2\hat{\phi}_{ij}^{(i)}}$ is used which is averaged at the sub-volume of the RVE. The overall damage is obtained directly from VOYIADJIS and PARK [13].

The cohesive zone concept [14] applied to metal matrix composites is one of these processes that attempt to use evolution equations at the mesoscale and averaged at the macroscale level. To address the evolution behavior of such SRVE internal variables one must follow one of two approaches. The first and most robust one is to use evolution equations at the SRVE level to obtain the current state of characterization of these defects. These defects are then used to obtain gradients of these internal state variables that are averaged over a domain of subvolumes in order to recover the internal state variables at the macroscale. The alternative and more efficient but less precise approach is to integrate the evolution relations over the SRVE sectionally in order to obtain the evolution relations at the macroscale.

To simplify the formulations, a new notation for the internal state variables used in the Helmholtz free energy can be defined as follows [4]:

$$\underset{(1)}{\overset{(r)}{\mathbf{f}}} = \mathbf{f} = \frac{1}{V_{RVE}} \int_{V_{RVE}} \underset{(1)}{\overset{(r)}{\hat{\mathbf{f}}}} dV_{RVE} \tag{4.9}$$

$$\underset{(2)}{\overset{(r)}{\mathbf{f}}} = \nabla^2 \underset{(1)}{\overset{(r)}{\mathbf{f}}} \tag{4.10}$$

$$(4.11) \qquad {}^{(r)}_{(3)}\mathbf{f} = \widehat{\hat{\nabla}^2 {}^{(r)}_{(1)}\hat{\mathbf{f}}}$$

where the ${}^{(r)}_{(1)}\mathbf{f} = \mathbf{f}$ in these equations represent an RVE-averaged internal state variable evaluated using the macroscale coordinate system $\mathbf{x}$ and may be a tensor of any order. ${}^{(r)}_{(1)}\hat{\mathbf{f}}$ represents the local sub-RVE internal state variable evaluated using the mesoscale coordinate system $\hat{\mathbf{x}}$, and ${}^{(r)}_{(3)}\mathbf{f}$ represents an RVE average of a mesoscale internal state variable which measures the mesostructural variability within the RVE [4]. The gradient operators ∇ and $\hat{\nabla}$ involve spatial derivatives at the macroscale and mesoscale, respectively. The macroscale internal state variables given by Eq. (4.9) as well as the corresponding gradient terms given by Eqs. (4.10) and (4.11) are regarded as independent internal state variables with respect to each other. Consequently, independent evolution equations should be obtained with respect to each of these internal state variables that are subject to the appropriate boundary conditions for the corresponding internal state variable.

Incorporating the relations given by Eq. (4.8) - (4.11) into Eqs. (4.3) to (4.7) gives the following relations:

$$(4.12) \qquad \bar{\alpha}_{ij} = {}^{(p)}_{(1)}\alpha_{ij} + A^{(p)}_{(2)}\alpha_{ij} + {}^{(p)}_{(3)}A^{(p)}_{(3)}\alpha_{ij},$$

$$(4.13) \qquad \bar{p} = {}^{(p)}_{(1)}p + A^{(p)}_{(2)}p + {}^{(p)}_{(3)}B^{(p)}_{(3)}p,$$

$$(4.14) \qquad \bar{\gamma}^{(u)}_{ij} = {}^{(d)}_{(1)}\gamma^{(u)}_{ij} + A^{(d)}_{(2)}\gamma^{(u)}_{ij} + {}^{(d)}_{(3)}A^{(u)}{}^{(d)}_{(3)}\gamma^{(u)}_{ij},$$

$$(4.15) \qquad \bar{\kappa}^{(u)} = {}^{(d)}_{(1)}\kappa^{(u)} + A^{(d)}_{(2)}\kappa^{(u)} + {}^{(d)}_{(3)}B^{(u)}{}^{(d)}_{(3)}\kappa^{(u)},$$

$$(4.16) \qquad \bar{\phi}^{(u)}_{ij} = {}^{(d)}_{(1)}\phi^{(u)}_{ij} + A^{(d)}_{(2)}\phi^{(u)}_{ij} + {}^{(d)}_{(3)}C^{(u)}{}^{(d)}_{(3)}\phi^{(u)}_{ij}.$$

5. Macroscale-mesoscale coupled plasticity and damage gradient theory using local internal state variables

In this paper, the terms $\mathbf{A}$ and $\nabla^2\mathbf{A}$ given in Eq. (2.4) are regarded as two independent internal state variables with different physical interpretations and

initial conditions. This approach is used since certain internal variables such as the dislocation density expressed through $\nabla^2 p$ and the accumulated plastic strain, p, do not necessarily have the same evolution equation. They each have a different physical interpretation that guides one to use different evolution equations for $\nabla^2 p$ and p. Using the non-local internal variable $\bar{p}$ similar to Eq. (4.4) such that

$$\bar{p} = p + {}^{(p)}B\nabla^2 p, \tag{5.1}$$

will enforce both internal variables to have a single evolution expression. However, the term p is physically a macroscale measure obtained through the plastic strain rate while the term $\nabla^2 p$ is interpreted as a macroscale measure comparable to the mesoscale measure identified as the dislocation density [7]. This term maybe obtained computationally through the use of discrete dislocations and continuum plasticity. Similar arguments may be used for the flux-related back-stress plasticity tensor:

$$\bar{\alpha}_{ij} = \alpha_{ij} + {}^{(p)}A\nabla^2 \alpha_{ij}. \tag{5.2}$$

FLECK and HUTCHINSON [8] incorporated the measure of the average dislocation density into the flow strength. Allowing α_{ij} and $\nabla^2 \alpha_{ij}$ to be independent internal state variables instead of the single quantity $\bar{\alpha}_{ij}$ allows one to introduce computationally the independent macro and mesoscales. It also allows these two different physical phenomena to be identified separately with different evolution equations.

Equation (4.1) may now be expressed in terms of both the macroscale internal state variables and the averaged mesoscale gradients as

$$\Psi = \Psi({}^{(e)}\varepsilon_{ij}, T, {}^{(p)}_{(k)}\alpha_{ij}, {}^{(p)}_{(k)}p, {}^{(d)}_{(k)}\phi^{(u)}_{ij}, {}^{(d)}_{(k)}\gamma^{(u)}_{ij}, {}^{(d)}_{(k)}\kappa^{(u)}_{ij}), \quad k = 1, 2, 3. \tag{5.3}$$

We use Eq. (5.3) because Eq. (4.1) will lead to coupling terms of the nature $\alpha_{ij}\nabla^2(\alpha_{ij})$, etc. These coupling terms may not have a physical interpretation in material behavior. In this work, the authors do not introduce gradient effects directly through the strains and stresses by introducing terms such as $\bar{\varepsilon}_{ij}$ and $\bar{\sigma}_{ij}$. They are introduced only through the internal state variables associated with plasticity and damage. Stresses and strains are macro-variables that maybe computed using the macro-, meso-, and micro-structure internal state variables of the material.

Since the internal state variables are selected independently of one another, one can express the analytical form of the Helmholtz free energy given by Eq. (4.1) as the quadratic form in terms of its gradient-dependent internal state

variables as:

$$\rho\Psi = \frac{1}{2}\left(\varepsilon_{ij} - \varepsilon''_{ij}\right) E_{ijkl}\left(\varepsilon_{kl} - \varepsilon''_{kl}\right) + \sum_{k=1}^{3}\left(\frac{1}{2}{}^{(p)}_{(k)}a\,{}^{(p)}_{(k)}\alpha_{ij}\,{}^{(p)}_{(k)}b\,{}^{(p)}_{(k)}p\,{}^{(p)}_{(k)}p\right)$$

$$+ \sum_{u=m,f,i}\sum_{k=1}^{3}\left(\frac{1}{2}{}^{(d)}_{(k)}a^{(u)}\,{}^{(d)}_{(k)}\gamma^{(u)}_{ij}\,{}^{(d)}_{(k)}\gamma^{(u)}_{ij} + \frac{1}{2}{}^{(d)}_{(k)}b^{(u)}\,{}^{(d)}_{(k)}\kappa^{(u)}\,{}^{(d)}_{(k)}\kappa^{(u)}\right), \tag{5.4}$$

where the matrix $E_{ijkl} = E_{ijkl}\left(\bar{\phi}^{(u)}_{ij}\right)$ is the fourth-order damaged elastic stiffness tensor. In Eq. (5.4), the coefficients are dependent on material and geometrical properties of the composite. In the case of composites, the geometrical properties may include size, shape, and spacing of the fibers. In the case of the gradient theory these coefficients become also dependent on the gradient of the fiber size and fiber spacing variation. The functional dependence of these coefficients can be obtained by studying the interaction problem of an inclusion embedded in an infinite homogeneous matrix subjected to a macroscopic stress rate and the corresponding strain rate at infinity [7].

One can express the time derivative of Eq. (5.3) as follows:

$$\dot{\Psi} = \frac{\partial\Psi}{\partial\varepsilon'_{ij}}\dot{\varepsilon}'_{ij} + \frac{\partial\Psi}{\partial T}\dot{T} + \sum_{k=l}^{3}\left(\frac{\partial\Psi}{\partial^{(p)}_{(k)}\alpha_{ij}}\,{}^{(p)}_{(k)}\dot{\alpha}_{ij} + \frac{\partial\Psi}{\partial^{(p)}_{(k)}p}\,{}^{(p)}_{(k)}\dot{p}\right)$$

$$+ \sum_{u=m,f,i}\sum_{k=1}^{3}\left(\frac{\partial\Psi}{\partial^{(d)}_{(k)}\gamma^{(u)}_{ij}}\,{}^{(d)}_{(k)}\dot{\gamma}^{(u)}_{ij} + \frac{\partial\Psi}{\partial^{(d)}_{(k)}\kappa^{(u)}}\,{}^{(d)}_{(k)}\dot{\kappa}^{(u)} + \frac{\partial\Psi}{\partial^{(d)}_{(k)}\phi^{(u)}_{ij}}\,{}^{(d)}_{(k)}\dot{\phi}^{(u)}_{ij}\right). \tag{5.5}$$

By substituting of Eq. (5.5) into the Clausus-Duhem inequality one obtains

$$\left(\sigma_{ij} - \rho\frac{\partial\Psi}{\partial\varepsilon'_{ij}}\right)\dot{\varepsilon}'_{ij} - \rho\left(\frac{\partial\Psi}{\partial T} + s\right)\dot{T} + \sigma_{ij}\dot{\varepsilon}''_{ij} - \frac{q_{ij}}{T}\cdot\nabla T$$

$$- \sum_{k=1}^{3}\left(\rho\frac{\partial\Psi}{\partial^{(p)}_{(k)}\alpha_{ij}}\,{}^{(p)}_{(k)}\dot{\alpha}_{ij} + \rho\frac{\partial\Psi}{\partial^{(p)}_{(k)}p}\,{}^{(p)}_{(k)}\dot{p}\right)$$

$$- \sum_{u=m,f,i}\sum_{k=1}^{3}\left(\rho\frac{\partial\Psi}{\partial^{(d)}_{(k)}\gamma^{(u)}_{ij}}\,{}^{(d)}_{(k)}\dot{\gamma}^{(u)}_{ij} + \rho\frac{\partial\Psi}{\partial^{(d)}_{(k)}\kappa^{(u)}}\,{}^{(d)}_{(k)}\dot{\kappa}^{(u)} + \rho\frac{\partial\Psi}{\partial^{(d)}_{(k)}\phi^{(u)}_{ij}}\,{}^{(d)}_{(k)}\dot{\phi}^{(u)}_{ij}\right) \geq 0 \tag{5.6}$$

from which the thermodynamic state laws given in Table 1 are obtained. In this table, ${}^{(p)}_{(k)}X_{ij}$, ${}^{(p)}_{(k)}R$, ${}^{(d)}_{(k)}Y^{(u)}_{ij}$, ${}^{(p)}_{(k)}\Gamma^{(u)}_{ij}$, and ${}^{(d)}_{(k)}K^{(u)}$ are defined as the thermodynamic

conjugate forces corresponding to the internal state flux variables, respectively ${}^{(p)}_{(k)}\alpha_{ij}$, ${}^{(p)}_{(k)}p$, ${}^{(d)}_{(k)}\phi^{(u)}_{ij}$, ${}^{(d)}_{(k)}\gamma^{(u)}_{ij}$, and ${}^{(d)}_{(k)}\kappa^{(u)}$.

Using the equations in Table 1 along with Eq. (5.4), the definitions for the thermodynamic conjugate forces shown in Table 2 can be obtained.

Table 1. Thermodynamic State Laws

Thermoelastics Laws	Elastic deformation	$\sigma_{ij} = \rho\left(\partial\Psi/\partial\varepsilon'_{ij}\right)$
	Thermal entropy	$s = -\partial\Psi/\partial T$
Plasticity	Kinematic hardening	${}^{(p)}_{(k)}X_{ij} = \rho\left(\partial\Psi/\partial {}^{(p)}_{(k)}\alpha_{ij}\right)$
	Isotropic hardening	${}^{(p)}_{(k)}R = \rho\left(\partial\Psi/\partial {}^{(p)}_{(k)}p\right)$
Damage	Damage tensor	${}^{(d)}_{(k)}Y^{(u)}_{ij} = \rho\left(\partial\Psi/\partial {}^{(d)}_{(k)}\phi^{(u)}_{ij}\right)$
	Kinematic hardening	${}^{(d)}_{(k)}\Gamma^{(u)}_{ij} = \rho\left(\partial\Psi/\partial {}^{(d)}_{(k)}\gamma^{(u)}_{ij}\right)$
	Isotropic hardening	${}^{(d)}_{(k)}K^{(u)} = \rho\left(\partial\Psi/\partial {}^{(d)}_{(k)}\kappa^{(u)}\right)$

The value of the thermodynamic conjugate forces can be obtained through the evolution relations of the internal state variables. They are obtained by assuming the physical existence of the dissipation potential at the macroscale. With regard to the evolution equations for the averaged mesoscale based gradients, discrete elements, or micromechanical based models may be used to develop such relations.

The total power of dissipation can now be expressed as the sum of the plastic dissipation and damage dissipation as follows:

$$\Pi = \Pi^p + \Pi^d \tag{5.7}$$

where the dissipation processes are given as the sum of the products of the thermodynamic conjugate forces with the respective flux variables as follows:

$$\Pi^p = \sigma_{ij}\dot{\varepsilon}''_{ij} - \sum_{k=1}^{3}\left({}^{(p)}_{(k)}X_{ij}\ {}^{(p)}_{(k)}\dot{\alpha}_{ij} + {}^{(p)}_{(k)}R\ {}^{(p)}_{(k)}\dot{p}\right), \tag{5.8}$$

$$\Pi^d = -\sum_{u=m,f,i}\sum_{k=1}^{3}\left({}^{(d)}_{(k)}\Gamma^{(u)}_{ij}\ {}^{(d)}_{(k)}\dot{\gamma}^{(u)}_{ij} + {}^{(d)}_{(k)}K^{(u)}\ {}^{(d)}_{(k)}\dot{\kappa}^{(u)} + {}^{(d)}_{(k)}Y^{(u)}_{ij}\ {}^{(d)}_{(k)}\dot{\phi}^{(u)}_{ij}\right). \tag{5.9}$$

Table 2. Thermodynamic Conjugate Forces

Plasticity	Kinematic hardening	${}^{(p)}_{(k)}X_{ij} = {}^{(p)}_{(k)}a \; {}^{(p)}_{(k)}\alpha_{ij}$
	Isotropic hardening	${}^{(p)}_{(k)}R = {}^{(p)}_{(k)}b \; {}^{(p)}_{(k)}p$
Damage	Damage tensor	${}^{(d)}_{(k)}Y^{(u)}_{ij} = \frac{1}{2}\frac{\partial}{\partial\, {}^{(d)}_{(k)}\phi^{(u)}_{ij}}\left\{\left(\varepsilon_{ij} - \varepsilon''_{ij}\right)E_{ijkl}\left(\varepsilon_{kl} - \varepsilon''_{kl}\right)\right\}$
	Kinematic hardening	${}^{(d)}_{(k)}\Gamma^{(u)}_{ij} = {}^{(d)}_{(k)}a^{(u)} \; {}^{(d)}_{(k)}\gamma^{(u)}_{ij}$
	Isotropic hardening	${}^{(d)}_{(k)}K^{(u)} = {}^{(d)}_{(k)}b^{(u)} \; {}^{(d)}_{(k)}\kappa^{(u)}$

Since the plastic strain rate will be developed in the current deformed and damaged configuration, its corresponding evolution equation will be a function of the damage tensor. Similarly, the evolution equation of the conjugate force due to damage will be a function of the stress. The evolution equations for the plastic strain and the damage are interdependent [12], and therefore the two dissipative mechanisms shown above are implicitly interdependent through the stress and the conjugate forces due to damage.

The total power of dissipation can also be expressed by the sum of the dissipation mechanism due to plasticity and the dissipation mechanisms due to damage in each of the material constituents as follows:

$$\Pi = \Pi^{p} + \Pi^{d^{(m)}} + \Pi^{d^{(f)}} + \Pi^{d^{(i)}} \tag{5.10}$$

where the dissipation processes for each constituent are given as follows:

$$\Pi^{d^{(m)}} = -\sum_{k=1}^{3}\left({}^{(d)}_{(k)}\Gamma^{(m)}_{ij} \; {}^{(d)}_{(k)}\dot{\gamma}^{(m)}_{ij} + {}^{(d)}_{(k)}K^{(m)} \; {}^{(d)}_{(k)}\dot{\kappa}^{(m)} + {}^{(d)}_{(k)}Y^{(m)}_{ij} \; {}^{(d)}_{(k)}\dot{\phi}^{(m)}_{ij}\right), \tag{5.11}$$

$$\Pi^{d^{(f)}} = -\sum_{k=1}^{3}\left({}^{(d)}_{(k)}\Gamma^{(f)}_{ij} \; {}^{(d)}_{(k)}\dot{\gamma}^{(f)}_{ij} + {}^{(d)}_{(k)}K^{(f)} \; {}^{(d)}_{(k)}\dot{\kappa}^{(f)} + {}^{(d)}_{(k)}Y^{(f)}_{ij} \; {}^{(d)}_{(k)}\dot{\phi}^{(f}_{ij})\right), \tag{5.12}$$

$$\Pi^{d^{(i)}} = -\sum_{k=1}^{3}\left({}^{(d)}_{(k)}\Gamma^{(i)}_{ij} \; {}^{(d)}_{(k)}\dot{\gamma}^{(i)}_{ij} + {}^{(d)}_{(k)}K^{(i)} \; {}^{(d)}_{(k)}\dot{\kappa}^{(i)} + {}^{(d)}_{(k)}Y^{(i)}_{ij} \; {}^{(d)}_{(k)}\dot{\phi}^{(i)}_{ij}\right). \tag{5.13}$$

The dissipation potentials of the damage in each of the constituents are interdependent through dependence of the damage tensors on the stress.

In this work, the evolution equations of the macroscale internal state variables are obtained through the use of the generalized normality rule of thermodynamics. In this regard the macroscale dissipation potential is defined in terms of the gradient-dependent internal state variables as a continuous and convex scalar-valued function of the flux variables [12]:

$$\Theta = \Theta\Big(\dot{\varepsilon}''_{ij},\ T,\ {}^{(p)}_{(k)}\dot{\alpha}_{ij},\ {}^{(p)}_{(k)}\dot{p},\ {}^{(p)}_{(k)}\dot{\phi}^{(u)}_{ij},\ {}^{(p)}_{(k)}\dot{\gamma}^{(u)}_{ij},\ {}^{(p)}_{(k)}\dot{\kappa}^{(u)}\Big). \tag{5.14}$$

By using the Legendre-Fenchel transformation of the dissipation potential $\Theta^{(u)}$, one can obtain complementary laws in the form of the evolution laws of flux variables as functions of the dual variables which can be decoupled into the plastic and damage dissipation potential parts as follows:

$$\begin{aligned}\Theta^* &= \Theta^*\Big(\sigma_{ij}, {}^{(p)}_{(k)}X_{ij}, {}^{(p)}_{(k)}R, {}^{(d)}_{(k)}Y^{(u)}_{ij}, {}^{(d)}_{(k)}K^{(u)}, {}^{(d)}_{(k)}\Gamma^{(u)}_{ij}\Big) \\ &= F\Big(\sigma_{ij}, {}^{(p)}_{(k)}R, {}^{(p)}_{(k)}X_{ij}\Big) + \sum_{m,f,i} G^{(u)}\Big({}^{(d)}_{(k)}Y^{(u)}_{ij}, {}^{(d)}_{(k)}K^{(u)}, {}^{(d)}_{(k)}\Gamma^{(u)}_{ij}\Big).\end{aligned} \tag{5.15}$$

As noted previously for the dissipation mechanisms, there is an implicit coupling between the plastic and damage dissipation potentials through the stress and the conjugate damage force.

6. Gradient-dependent thermodynamic conjugate forces

Assuming a similar definition for the nonlocal conjugate forces as for the conjugate forces given in Table 2, one obtains the following relations:

$$\bar{X}_{ij} = {}^{(p)}\bar{a}\,\bar{\alpha}_{ij} = {}^{(p)}\bar{a}\Big(\alpha_{ij} + A\nabla^2\alpha_{ij} + {}^{(p)}_{(3)}A\,\widehat{\hat{\nabla}^2\hat{\alpha}_{ij}}\Big), \tag{6.1}$$

$$\bar{R} = {}^{(p)}\bar{b}\,\bar{p} = {}^{(p)}\bar{b}\Big(p + A\,\nabla^2 p + {}^{(p)}_{(3)}B\,\widehat{\hat{\nabla}^2\hat{p}}\Big), \tag{6.2}$$

$$\bar{\Gamma}^{(u)}_{ij} = {}^{(d)}\bar{a}^{(u)}\,\bar{\gamma}^{(u)}_{ij} = {}^{(d)}\bar{a}^{(u)}\Big(\gamma^{(u)}_{ij} + A\,\nabla^2\gamma^{(u)}_{ij} + {}^{(d)}_{(3)}A^{(u)}\,\widehat{\hat{\nabla}^2\hat{\gamma}^{(u)}_{ij}}\Big), \tag{6.3}$$

$$\bar{K}^{(u)} = {}^{(d)}\bar{b}^{(u)}\bar{\kappa}^{(u)} = {}^{(d)}\bar{b}^{(u)}\Big(\kappa^{(u)} + A\,\nabla^2\kappa^{(u)} + {}^{(d)}_{(3)}B^{(u)}\,\widehat{\hat{\nabla}^2\hat{\kappa}^{(u)}}\Big). \tag{6.4}$$

One now makes use of the relations in Table 2 to obtain

$$\bar{X}_{ij} = {}^{(p)}_{(1)}\tilde{A}\,{}^{(p)}_{(1)}X_{ij} + {}^{(p)}_{(2)}\tilde{A}\,{}^{(p)}_{(2)}X_{ij} + {}^{(p)}_{(3)}\tilde{A}\,{}^{(p)}_{(3)}X_{ij}, \tag{6.5}$$

$$\bar{R} = {}^{(p)}_{(1)}\tilde{B}\,{}^{(p)}_{(1)}R + {}^{(p)}_{(2)}\tilde{B}\,{}^{(p)}_{(2)}R + {}^{(p)}_{(3)}\tilde{B}\,{}^{(p)}_{(3)}R, \tag{6.6}$$

$$\bar{\Gamma}^{(u)}_{ij} = {}^{(d)}_{(1)}\tilde{A}^{(u)}\,{}^{(d)}_{(1)}\Gamma^{(u)}_{ij} + {}^{(d)}_{(2)}\tilde{A}^{(u)}\,{}^{(d)}_{(2)}\Gamma^{(u)}_{ij} + {}^{(d)}_{(3)}\tilde{A}^{(u)}\,{}^{(d)}_{(3)}\Gamma^{(u)}_{ij}, \tag{6.7}$$

$$\bar{K}^{(u)} = {}^{(d)}_{(1)}\tilde{B}^{(u)}\,{}^{(d)}_{(1)}K^{(u)} + {}^{(d)}_{(2)}\tilde{B}^{(u)}\,{}^{(d)}_{(2)}K^{(u)} + {}^{(d)}_{(3)}\tilde{B}^{(u)}\,{}^{(d)}_{(3)}K^{(u)}, \tag{6.8}$$

where the constants are given by

$${}^{(r)}_{(k)}\tilde{A} = {}^{(r)}\bar{a}\frac{{}^{(r)}_{(k)}A}{{}^{(r)}_{(k)}a} \qquad \left({}^{(r)}_{(1)}A = 1,\ {}^{(r)}_{(2)}A = A\right), \tag{6.9}$$

$${}^{(r)}_{(k)}\tilde{B} = {}^{(r)}\bar{b}\frac{{}^{(r)}_{(k)}B}{{}^{(r)}_{(k)}b} \qquad \left({}^{(r)}_{(1)}B = 1,\ {}^{(r)}_{(2)}B = A\right). \tag{6.10}$$

In the above equations, $r = d$ for damage and $r = p$ for plasticity.

Here it is assumed that the relationship between the nonlocal thermodynamic force for damage and the nonlocal damage tensor is a linear relationship in the same form as Eqs. (6.1) to (6.4), which gives the following equations:

$$\bar{Y}^{(u)}_{ij} = {}^{(d)}\bar{c}\,\bar{\phi}^{(u)}_{ij} = {}^{(d)}\bar{c}\left(\phi^{(u)}_{ij} + A\,\nabla^2\phi^{(u)}_{ij} + {}^{(p)}_{(3)}A\,\hat{\bar{\nabla}}^2\,\hat{\phi}^{(u)}_{ij}\right), \tag{6.11}$$

$$\bar{Y}^{(u)}_{ij} = {}^{(d)}_{(1)}\tilde{C}^{(u)}\,{}^{(d)}_{(1)}Y^{(u)}_{ij} + {}^{(d)}_{(2)}\tilde{C}^{(u)}\,{}^{(d)}_{(2)}Y^{(u)}_{ij} + {}^{(d)}_{(3)}\tilde{C}^{(u)}\,{}^{(d)}_{(3)}Y^{(u)}_{ij}, \tag{6.12}$$

where the constants are given by

$${}^{(d)}_{(k)}\tilde{C} = {}^{(d)}\bar{c}\frac{{}^{(d)}_{(k)}C}{{}^{(d)}_{(k)}c} \qquad \left({}^{(d)}_{(1)}C = 1,\ {}^{(d)}_{(2)}C = A\right). \tag{6.13}$$

7. Evolution equations for the internal state variables

The theory of functions of several variables is used with the Lagrange multipliers $\dot{\lambda}_p$ and $\dot{\lambda}_d$ to construct the objective function Ω in the following form:

The theory of functions of several variables is used with the Lagrange multipliers and to construct the objective function in the following form:

$$\Omega = \Pi^p + \Pi^{d^{(m)}} + \Pi^{d^{(f)}} + \Pi^{d^{(i)}} - \dot{\lambda}_p F - \dot{\lambda}_d \left(G^{(m)} + G^{(f)} + G^{(i)}\right) \tag{7.1}$$

where F and $G^{(u)}$ are plastic and damage potential functions, respectively, and will be defined in subsequent sections. In order to obtain the plastic strain rate and the damage rate, the following conditions are used to extremize the objective function:

$$\frac{\partial \Omega}{\partial \sigma} = 0, \tag{7.2}$$

$$\frac{\partial \Omega}{\partial^{(d)}_{(k)} Y^{(u)}_{ij}} = 0. \tag{7.3}$$

From these conditions for the case when $F \geq 0$ and $G^{(u)} \geq 0$, the corresponding coupled evolution equations for the plastic strain and the damage are given as:

$$\dot{\varepsilon}''_{ij} = \dot{\lambda}_p \frac{\partial F}{\partial \sigma_{ij}} + \dot{\lambda}_d \left(\frac{\partial G^{(m)}}{\partial \sigma_{ij}} + \frac{\partial G^{(f)}}{\partial \sigma_{ij}} + \frac{\partial G^{(i)}}{\partial \sigma_{ij}} \right), \tag{7.4}$$

$$\overset{(d)}{(1)}\dot{\phi}^{(u)}_{ij} = -\dot{\lambda}_p \frac{\partial F}{\partial^{(d)}_{(1)} Y^{(u)}_{ij}} - \dot{\lambda}_d \frac{\partial G^{(u)}}{\partial^{(d)}_{(1)} Y^{(u)}_{ij}} = \overset{(d)}{(1)}\tilde{C}^{(u)} \left(-\dot{\lambda}_p \frac{\partial F}{\partial \bar{Y}^{(u)}_{ij}} - \dot{\lambda}_d \frac{\partial G^{(u)}}{\partial \bar{Y}^{(u)}_{ij}} \right), \tag{7.5}$$

$$\overset{(d)}{(2)}\dot{\phi}^{(u)}_{ij} = -\dot{\lambda}_p \frac{\partial F}{\partial^{(d)}_{(2)} Y^{(u)}_{ij}} - \dot{\lambda}_d \frac{\partial G^{(u)}}{\partial^{(d)}_{(2)} Y^{(u)}_{ij}} = \overset{(d)}{(2)}\tilde{C}^{(u)} \left(-\dot{\lambda}_p \frac{\partial F}{\partial \bar{Y}^{(u)}_{ij}} - \dot{\lambda}_d \frac{\partial G^{(u)}}{\partial \bar{Y}^{(u)}_{ij}} \right), \tag{7.6}$$

$$\overset{(d)}{(3)}\dot{\phi}^{(u)}_{ij} = -\dot{\lambda}_p \frac{\partial F}{\partial^{(d)}_{(3)} Y^{(u)}_{ij}} - \dot{\lambda}_d \frac{\partial G^{(u)}}{\partial^{(d)}_{(3)} Y^{(u)}_{ij}} = \overset{(d)}{(3)}\tilde{C}^{(u)} \left(-\dot{\lambda}_p \frac{\partial F}{\partial \bar{Y}^{(u)}_{ij}} - \dot{\lambda}_d \frac{\partial G^{(u)}}{\partial \bar{Y}^{(u)}_{ij}} \right). \tag{7.7}$$

However, plastic strain is assumed to occur only in the matrix. Therefore, the evolution of the plastic strain given by Eq. (7.4) is reduced to:

$$\dot{\varepsilon}''_{ij} = \dot{\lambda}_p \frac{\partial F}{\partial \sigma_{ij}} + \dot{\lambda}_d \frac{\partial G^{(m)}}{\partial \sigma_{ij}}. \tag{7.8}$$

However, one can still use Eq. (7.4) by insisting that fiber damage and damage due to debonding can produce permanent non-recoverable strains that should be added to the plastic strain.

Taking the time derivative of the definition for the non-local damage tensor $\bar{\phi}^{(u)}_{ij}$ given by Eq. (4.15) results in the following formula:

$$\dot{\bar{\phi}}^{(u)}_{ij} = {}^{(d)}_{(1)}\dot{\phi}^{(u)}_{ij} + A\, {}^{(d)}_{(2)}\dot{\phi}^{(u)}_{ij} + {}^{(d)}_{(3)}C^{(u)}\, {}^{(d)}_{(3)}\dot{\phi}^{(u)}_{ij}. \tag{7.9}$$

Substitution of Eqs. (7.5) to (7.7) into this equation gives the evolution of the damage tensor as:

$$\begin{aligned} \dot{\bar{\phi}}^{(u)}_{ij} = &-\dot{\lambda}_p \left(\frac{\partial F}{\partial {}^{(d)}_{(1)}Y^{(u)}_{ij}} + A \frac{\partial F}{\partial {}^{(d)}_{(2)}Y^{(u)}_{ij}} + {}^{(d)}_{(3)}C^{(u)} \frac{\partial F}{\partial {}^{(d)}_{(3)}Y^{(u)}_{ij}} \right) \\ &- \dot{\lambda}_d \left(\frac{\partial G^{(u)}}{\partial {}^{(d)}_{(1)}Y^{(u)}_{ij}} + A \frac{\partial G^{(u)}}{\partial {}^{(d)}_{(2)}Y^{(u)}_{ij}} + {}^{(d)}_{(3)}C^{(u)} \frac{\partial G^{(u)}}{\partial {}^{(d)}_{(3)}Y^{(u)}_{ij}} \right) \end{aligned} \tag{7.10}$$

which from Eq. (6.12) becomes:

$$\dot{\bar{\phi}}^{(u)}_{ij} = -\left(\dot{\lambda}_p \frac{\partial f}{\partial \bar{Y}^{(u)}_{ij}} + \dot{\lambda}_d \frac{\partial g^{(u)}}{\partial \bar{Y}^{(u)}_{ij}} \right) \left({}^{(d)}_{(1)}\tilde{C}^{(u)} + A\, {}^{(d)}_{(2)}\tilde{C}^{(u)} + {}^{(d)}_{(3)}C^{(u)}\, {}^{(d)}_{(3)}\tilde{C}^{(u)} \right). \tag{7.11}$$

Coupling occurs between the evolution equations of the damage tensor and plastic strain due to the dependence of σ_{ij} on $\bar{\phi}^{(u)}_{ij}$ and $\bar{Y}^{(u)}_{ij}$ on σ_{ij}. It can be seen that if $F \leq 0$ or, $G^{(u)} \leq 0$, the evolution equations for the plastic strain and the damage will become decoupled [12].

7.1. Thermodynamic Potential of Plasticity and Yield Criterion

In order to obtain evolution equations for the internal state variables, a proper analytical form of the potentials that are defined in Eq. (5.15) needs to be obtained. In order to satisfy the generalized normality rule of thermodynamics, the following form of the plastic potential function, F, is defined here:

$$F = f + \frac{k_p}{2} \bar{X}_{ij}\, \bar{X}_{ij}. \tag{7.12}$$

In Eq. (7.12), k_p is a constant used to adjust the units of the equation, and f is the yield function and can be defined such that

$$f = \left\{ \frac{3}{2}(s_{ij} - \bar{X}_{ij})(s_{ij} - \bar{X}_{ij}) \right\}^{1/2} - \left[\sigma_{yp} + \bar{R} \right] \equiv 0 \tag{7.13}$$

in terms of the non-local conjugate forces $\bar{X}_{ij}$ and $\bar{R}$ where is the deviatoric component of the stress tensor σ_{ij}.

Gradient-dependent evolution equations of the internal state variables for plasticity can be obtained using the generalized normality rule of thermodynamics along with Eqs. (7.12) and (7.13)

$$\overset{(p)}{(1)}\dot{\alpha}_{ij} = -\dot{\lambda}_p \frac{\partial F}{\partial \overset{(p)}{(1)}X_{ij}} = -\dot{\lambda}_p \overset{(p)}{(1)}\tilde{A} \left\{ \frac{\partial f}{\partial \bar{X}_{ij}} + k_p \bar{X}_{ij} \right\}, \tag{7.14}$$

$$\overset{(p)}{(2)}\dot{\alpha}_{ij} = -\dot{\lambda}_p \frac{\partial F}{\partial \overset{(p)}{(2)}X_{ij}} = -\dot{\lambda}_p \overset{(p)}{(2)}\tilde{A} \left\{ \frac{\partial f}{\partial \bar{X}_{ij}} + k_p \bar{X}_{ij} \right\}, \tag{7.15}$$

$$\overset{(p)}{(3)}\dot{\alpha}_{ij} = -\dot{\lambda}_p \frac{\partial F}{\partial \overset{(p)}{(3)}X_{ij}} = -\dot{\lambda}_p \overset{(p)}{(3)}\tilde{A} \left\{ \frac{\partial f}{\partial \bar{X}_{ij}} + k_p \bar{X}_{ij} \right\}, \tag{7.16}$$

$$\overset{(p)}{(1)}\dot{p} = -\dot{\lambda}_p \frac{\partial F}{\partial \overset{(p)}{(1)}R} = -\dot{\lambda}_p \overset{(p)}{(1)}\tilde{B} \frac{\partial f}{\partial \bar{R}} = \dot{\lambda}_p \overset{(p)}{(1)}\tilde{B}, \tag{7.17}$$

$$\overset{(p)}{(2)}\dot{p} = -\dot{\lambda}_p \frac{\partial F}{\partial \overset{(p)}{(2)}R} = -\dot{\lambda}_p \overset{(p)}{(2)}\tilde{B} \frac{\partial f}{\partial \bar{R}} = \dot{\lambda}_p \overset{(p)}{(2)}\tilde{B}, \tag{7.18}$$

$$\overset{(p)}{(3)}\dot{p} = -\dot{\lambda}_p \frac{\partial F}{\partial \overset{(p)}{(3)}R} = -\dot{\lambda}_p \overset{(p)}{(3)}\tilde{B} \frac{\partial f}{\partial \bar{R}} = \dot{\lambda}_p \overset{(p)}{(3)}\tilde{B}. \tag{7.19}$$

An alternate approach to evolution Eqs. (7.15) and (7.16) is to obtain an evolution equation for α_{ij} only using the potential, F, as indicated by Eq. (7.12). The evolution equation for the corresponding gradient term of α_{ij} specifically, $\nabla^2\dot{\alpha}_{ij}$, is to be obtained directly by operating on $\dot{\alpha}_{ij}$ with the laplacian. An evolution equation for the averaged mesoscale gradient term, $\overline{\hat{\nabla}^2\hat{\alpha}_{ij}}$, is to be derived

at the mesoscale level using $\hat{\alpha}_{ij}$ through crystal plasticity, etc. and averaged over the RVE instead of Eq. (7.16). The same arguments apply for the subsequent evolution equations of plasticity and damage.

The plastic multiplier, $\dot{\lambda}_p$ can be obtained using the consistency condition for plasticity such ($\dot{f} = 0$) that

$$\dot{f} \equiv \frac{\partial f}{\partial \sigma_{ij}} : \dot{\sigma}_{ij} + \frac{\partial f}{\partial \bar{\phi}_{ij}} : \dot{\bar{\phi}}_{ij} + \frac{\partial f}{\partial \bar{X}_{ij}} : \dot{\bar{X}}_{ij} + \frac{\partial f}{\partial \bar{R}} \dot{\bar{R}} = 0. \tag{7.20}$$

7.2. Thermodynamic potential of damage

The following form of the damage potentials for a composite is defined here:

$$G^{(u)} = g^{(u)} + \frac{k_d}{2} \bar{\Gamma}_{ij}^{(u)} \bar{\Gamma}_{ij}^{(u)}. \tag{7.21}$$

Similar to Eq. (7.12), k_d is a constant to adjust the units of the equation, and $g^{(u)}$ represents the non-local, gradient-dependent damage criterion and is defined as follows

$$g^{(u)} = \left(\bar{Y}_{ij}^{(u)} - \bar{\Gamma}_{ij}^{(u)}\right) \bar{P}_{ijkl}^{(u)} \left(\bar{Y}_{kl}^{(u)} - \bar{\Gamma}_{kl}^{(u)}\right) - 1 \leq 0. \tag{7.22}$$

The fourth order tensor $\bar{P}_{ijkl}$ describes the anisotropic nature of the damage growth and the initiation of damage. Its form is given as a function of the hardening tensor $\tilde{h}$:

$$\bar{P}_{ijkl}^{(u)} = \tilde{h}_{ij}^{(u)^{-1}} \tilde{h}_{kl}^{(u)^{-1}}, \tag{7.23}$$

$\tilde{h}_{kl}^{(u)^{-1}}$ is the inverse of the tensor $\tilde{h}^{(u)}$,

$$\tilde{h}_{ij}^{(u)} = \left(\lambda\eta\left(\frac{\bar{\kappa}^{(u)}}{\lambda}\right)^{\xi} \bar{\phi}_{ij}^{(u)} + \delta_{ij}\lambda v^2\right) \tag{7.24}$$

where ξ, η, λ, and v are material parameters related to damage [12] and the non-local damage term $\bar{\kappa}^{(u)}$ is defined by Eq. (4.16).

Using the generalized and normality rule of thermodynamics, the evolution equations can be defined for the internal state variables for damage as follows:

$$\overset{(d)}{(1)}\dot{\kappa}^{(u)} = -\dot{\lambda}_d \frac{\partial G^{(u)}}{\partial \overset{(d)}{(1)} K^{(u)}} = -\dot{\lambda}_d \overset{(d)}{(1)} \tilde{B}^{(u)} \frac{\partial g^{(u)}}{\partial \bar{K}^{(u)}}, \tag{7.25}$$

$$\overset{(d)}{(2)}\dot{\kappa}^{(u)} = -\dot{\lambda}_d \frac{\partial G^{(u)}}{\partial \overset{(d)}{(2)} K^{(u)}} = -\dot{\lambda}_d \overset{(d)}{(2)} \tilde{B}^{(u)} \frac{\partial g^{(u)}}{\partial \bar{K}^{(u)}}, \tag{7.26}$$

$$(7.27) \qquad \overset{(d)}{(3)}\dot{\kappa}^{(u)} = -\dot{\lambda}_d \frac{\partial G^{(u)}}{\partial \overset{(d)}{(3)} K^{(u)}} = -\dot{\lambda}_d \overset{(d)}{(3)}\tilde{B}^{(u)} \frac{\partial g^{(u)}}{\partial \bar{K}^{(u)}},$$

$$(7.28) \qquad \overset{(d)}{(1)}\dot{\gamma}_{ij}^{(u)} = -\dot{\lambda}_d \frac{\partial G^{(u)}}{\partial \overset{(d)}{(1)}\Gamma_{ij}^{(u)}} = -\dot{\lambda}_d \overset{(d)}{(1)}\tilde{A}^{(u)} \left\{ \frac{\partial g^{(u)}}{\partial \bar{\Gamma}_{ij}^{(u)}} + k_d \bar{\Gamma}_{ij}^{(u)} \right\},$$

$$(7.29) \qquad \overset{(d)}{(2)}\dot{\gamma}_{ij}^{(u)} = -\dot{\lambda}_d \frac{\partial G^{(u)}}{\partial \overset{(d)}{(2)}\Gamma_{ij}^{(u)}} = -\dot{\lambda}_d \overset{(d)}{(2)}\tilde{A}^{(u)} \left\{ \frac{\partial g^{(u)}}{\partial \bar{\Gamma}_{ij}^{(u)}} + k_d \bar{\Gamma}_{ij}^{(u)} \right\},$$

$$(7.30) \qquad \overset{(d)}{(3)}\dot{\gamma}_{ij}^{(u)} = -\dot{\lambda}_d \frac{\partial G^{(u)}}{\partial \overset{(d)}{(3)}\Gamma_{ij}^{(u)}} = -\dot{\lambda}_d \overset{(d)}{(3)}\tilde{A}^{(u)} \left\{ \frac{\partial g^{(u)}}{\partial \bar{\Gamma}_{ij}^{(u)}} + k_d \bar{\Gamma}_{ij}^{(u)} \right\},$$

The damage multiplier $\dot{\lambda}_d$ can be obtained using the consistency condition for damage ($\dot{g} = 0$). The damage consistency condition is given as follows:

$$(7.31) \qquad \dot{g}^{(u)} = \frac{\partial g^{(u)}}{\partial \sigma} : \dot{\sigma} + \frac{\partial g^{(u)}}{\partial \bar{Y}_{ij}^{(u)}} : \dot{\bar{Y}}_{ij}^{(u)} + \frac{\partial g^{(u)}}{\partial \bar{K}^{(u)}} \dot{\bar{K}}^{(u)} + \frac{\partial g^{(u)}}{\partial \bar{\Gamma}_{ij}^{(u)}} : \dot{\bar{\Gamma}}_{ij}^{(u)} = 0.$$

8. Computational issues of the gradient approach

In this work, for the specific examination of interfacial damage, the internal state variables are reduced as will be discussed. The remaining set of differential equations involve macroscale second order gradients of the internal state variables for both plasticity and damage, and a mesoscale second order gradient of the damage tensor. In order to solve such a higher order problem, the finite element approach is used here. Both the yield and damage conditions can be only satisfied in the weak form respectively.

8.1. Thermodynamic potential (augmented by some gradient terms)

In the formulation presented here the internal state variables are augmented as shown in Table 3. The average mesoscale gradients of kinematic and isotropic hardening in plasticity are eliminated since no analysis at the mesoscale level will be conducted for discrete dislocations. The average mesoscale gradients of kinematic and isotropic hardening in damage are discarded from the analysis

since no mesostructure will be used for the analysis of these variables. Also, only interface damage will be incorporated in this work such that $\bar{\phi}_{ij} = \bar{\phi}_{ij}^{(i)} = \phi_{ij}^{(i)} + {}^{(d)}C\widehat{\hat{\nabla}^2\hat{\phi}_{ij}^{(i)}}$ in order to simplify the formulation.

Eqs. (4.3) to (4.7) can now be written as follows:

$$\bar{\alpha}_{ij} = \alpha_{ij} + A\nabla^2\alpha_{ij}, \tag{8.1}$$

$$\bar{p} = p + A\nabla^2 p, \tag{8.2}$$

$$\bar{\gamma}_{ij} = \gamma_{ij}^{(i)} + A\nabla^2\gamma_{ij}^{(i)}, \tag{8.3}$$

$$\bar{\kappa} = \kappa^{(i)} + A\nabla^2\kappa^{(i)}, \tag{8.4}$$

$$\bar{\phi}_{ij} = \bar{\phi}_{ij}^{(i)} + C^{(i)}\,\widehat{\hat{\nabla}^2\hat{\phi}_{ij}^{(i)}}. \tag{8.5}$$

Table 3. Reduced internal state flux variables

		Macroscale Variables in RVE	Macroscale Gradient in RVE	Averaged Mesoscale Gradient in SRVE
Elastic Internal Variable	Elastic strain	${}^{(e)}\varepsilon_{ij} = \varepsilon'_{ij}$		
Plasticity Internal Flux Variables	Kinematic hardening	${}^{(p)}_{(1)}\alpha_{ij} = \alpha_{ij}$	${}^{(p)}_{(2)}\alpha_{ij} = \nabla^2\alpha_{ij}$	
	Isotropic hardening	${}^{(p)}_{(1)}p = p$	${}^{(p)}_{(2)}p = \nabla^2 p$	
Damage Internal	Damage tensor	${}^{(d)}_{(1)}\phi_{ij}^{(i)} = \phi_{ij}^{(i)}$		${}^{(d)}_{(3)}\phi_{ij}^{(i)} = \widehat{\hat{\nabla}^2\phi_{ij}^{(i)}}$
	Kinematic hardening	${}^{(d)}_{(1)}\alpha_{ij}^{(i)} = \alpha_{ij}^{(i)}$	${}^{(d)}_{(2)}\alpha_{ij}^{(i)} = \nabla^2\alpha_{ij}^{(i)}$	
	Isotropic hardening	${}^{(d)}_{(1)}\kappa^{(i)} = \kappa^{(i)}$	${}^{(d)}_{(2)}\kappa^{(i)} = \nabla^2\kappa^{(i)}$	

8.2. Discretization of the displacement field

Starting with the displacement field discretization one can write [15]:

$$\int \delta\mathbf{u}^T(\mathbf{L}^T\sigma_{j+1})dV = 0, \tag{8.6}$$

where the superscript T is the transpose symbol, denotes the variation of a term, and $\mathbf{L}$ is a differential operator given as follows:

$$\mathbf{L}^T = \begin{bmatrix} \frac{\partial}{\partial x} & 0 & 0 & \frac{\partial}{\partial y} & 0 & \frac{\partial}{\partial z} \\ 0 & \frac{\partial}{\partial y} & 0 & \frac{\partial}{\partial x} & \frac{\partial}{\partial z} & 0 \\ 0 & 0 & \frac{\partial}{\partial z} & 0 & \frac{\partial}{\partial y} & \frac{\partial}{\partial x} \end{bmatrix}. \tag{8.7}$$

σ_{j+1} contains the stress components and can be decomposed as $\sigma_j + d\sigma$ where $d\sigma$ is defined as follows [12]:

$$d\sigma = \mathbf{E}d\varepsilon' + \frac{\partial \mathbf{M}^{-1}}{\partial \bar{\phi}} \dot{\bar{\phi}} \tilde{\mathbf{E}} \varepsilon', \tag{8.8}$$

where $\mathbf{E}$ is the damaged elastic stiffness tensor and $\tilde{\mathbf{E}}$ is the undamaged elastic stiffness tensor. $\mathbf{M}$ is an overall damage effect tensor such that

$$\tilde{\sigma} = \mathbf{M}\sigma \tag{8.9}$$

where $\tilde{\sigma}$ is the undamaged stress tensor. VOYIADJIS and PARK [13] have shown that the fourth order tensor for damage $\mathbf{M}^{(u)}$ for each constituent may be expressed in terms of the second order damage tensor $\bar{\phi}^{(u)}$ where u=m,f,i. Also, VOYIADJIS and PARK [13] have shown that the total damage tensor $\mathbf{M}$ may be expressed in terms of the individual damages as:

$$\mathbf{M} = \left(\tilde{c}^{(m)} \mathbf{M}^{(m)} \tilde{\mathbf{B}}^{(m)} + \tilde{c}^{(f)} \mathbf{M}^{(f)} \tilde{\mathbf{B}}^{(f)} \right) \mathbf{M}^{(i)} \tag{8.10}$$

where $\tilde{\mathbf{B}}^{(m)}$ and $\tilde{\mathbf{B}}^{(f)}$ denote the effective undamaged configuration stress concentration tensors for the matrix and fiber, respectively, and $\tilde{c}^{(m)}$ and $\tilde{c}^{(f)}$ denote the effective undamaged configuration volume fractions for the matrix and fiber, respectively. Since we are just considering interfacial damage here, the overall damage effect tensor is given as:

$$\mathbf{M} = \left(\tilde{c}^{(m)} \mathbf{I} \tilde{\mathbf{B}}^{(m)} + \tilde{c}^{(f)} \mathbf{I} \tilde{\mathbf{B}}^{(f)} \right) \mathbf{M}^{(i)} = \mathbf{I}\mathbf{M}^{(i)} = \mathbf{M}^{(i)} \tag{8.11}$$

where $\mathbf{I}$ is the identity tensor. One can now obtain $\bar{\phi}$ from M and use $\bar{\phi}$ in Eq. (8.8) to obtain $d\sigma$.

Substitution of the evolution equations given by Eqs. (7.8) and (7.11) with the appropriate simplifications gives:

$$(8.12)\quad d\sigma = \mathbf{E}\left(d\varepsilon - \dot{\lambda}_p \frac{\partial f}{\partial \sigma}\right) - \frac{\partial \mathbf{M}^{-1}}{\partial \bar{\phi}}\left(\dot{\lambda}_p \frac{\partial f}{\partial \bar{\mathbf{Y}}^{(i)}} + \dot{\lambda}_d \frac{\partial g^{(i)}}{\partial \bar{\mathbf{Y}}^{(i)}}\right) \left(\begin{matrix}{}^{(d)}_{(1)}\tilde{C}^{(i)} + {}^{(d)}_{(3)}C^{(i)}\,{}^{(d)}_{(3)}\tilde{C}^{(i)}\end{matrix}\right)\tilde{\mathbf{E}}\varepsilon'$$

which can be written as follows:

$$(8.13)\qquad d\sigma = \mathbf{E}\left(d\varepsilon - \dot{\lambda}_p \chi_p\right) - \dot{\lambda}_d \chi_d,$$

where the following tensors have been introduced:

$$(8.14)\qquad \chi_p = \frac{\partial f}{\partial \sigma} + \frac{\partial \mathbf{M}^{-1}}{\partial \bar{\phi}} \frac{\partial f}{\partial \bar{\mathbf{Y}}^{(i)}} \left(\begin{matrix}{}^{(d)}_{(1)}\tilde{C}^{(i)} + {}^{(d)}_{(3)}C^{(i)}\,{}^{(d)}_{(3)}\tilde{C}^{(i)}\end{matrix}\right)\tilde{\mathbf{E}}\varepsilon',$$

$$(8.15)\qquad \chi_d = \frac{\partial \mathbf{M}^{-1}}{\partial \bar{\phi}} \frac{\partial g^{(i)}}{\partial \bar{\mathbf{Y}}^{(i)}} \left(\begin{matrix}{}^{(d)}_{(1)}\tilde{C}^{(i)} + {}^{(d)}_{(3)}C^{(i)}\,{}^{(d)}_{(3)}\tilde{C}^{(i)}\end{matrix}\right)\sigma.$$

The standard boundary conditions and small deformation strains, ε are defined in the following equations [15]:

$$(8.16)\qquad \Sigma \nu_s = \mathbf{t}, \qquad \mathbf{u} = \mathbf{u}_s,$$

$$(8.17)\qquad \varepsilon = \mathbf{L}\mathbf{u},$$

where Σ is the stress tensor in matrix form, ν_s is the outward normal to a surface S and $\mathbf{t}$ is the boundary traction vector.

Integrating by parts and using the standard boundary conditions, Eq. (8.6) can be rewritten as follows [15]

$$(8.18)\qquad \int_V \delta\varepsilon^T\, d\sigma\, dV = \int_S \delta\mathbf{u}^T\, \mathbf{t}_{j+1}\, dS - \int_V \delta\varepsilon^T\, \sigma_j dV.$$

where $\mathbf{t}_{j+1}$ are the tractions on the boundary. Using Eq. (8.13) in Eq. (8.18) one can obtain the following relation:

$$\int_V \delta\varepsilon^T \left\{ \mathbf{E}\left(d\varepsilon - \dot{\lambda}_p \chi_p\right) - \dot{\lambda}_d \chi_d \right\} dV = \int_S \delta \mathbf{u}^T \mathbf{t}_{j+1} dS - \int_V \delta\varepsilon^T \sigma_j dV. \tag{8.19}$$

The discretization procedure for the displacement field $\mathbf{u}$ requires C^0 continuous interpolation functions assembled in the shape function $\mathbf{N}$, such that

$$\mathbf{u} = \mathbf{N}\mathbf{a} \tag{8.20}$$

where $\mathbf{a}$ is the nodal displacement vector. The discretization of the strain from the linear kinematic relation is given as follows

$$\varepsilon = \mathbf{B}\mathbf{a} = \mathbf{L}\mathbf{N}\mathbf{a}, \tag{8.21}$$

where $\mathbf{B}$ is a matrix that relates the strain and the displacement.

The discretization of the multipliers, λ_p and λ_d, requires the C^1 continuous shape function contained in $\mathbf{h}$

$$\dot{\lambda}_p = \mathbf{h}^T \dot{\Lambda}_p, \qquad \dot{\lambda}_p = \mathbf{h}^T \dot{\Lambda}_d, \tag{8.22}$$

where Λ_p and Λ_d denote vectors of the nodal degrees of freedom for the plastic and damage multiplier field, respectively.

The discretization of the gradients of the multipliers will require the matrices $\mathbf{p} = \nabla\mathbf{h}$ and $\mathbf{q} = \nabla^2\mathbf{h}$ so that [15]:

$$\nabla d\lambda_p = \mathbf{p}^T d\Lambda_p, \qquad \nabla d\lambda_d = \mathbf{p}^T d\Lambda_d, \tag{8.23}$$

$$\nabla^2 d\lambda_p = \mathbf{q}^T d\Lambda_p, \qquad \nabla^2 d\lambda_d = \mathbf{q}^T d\Lambda_d. \tag{8.24}$$

Using Eqs. (8.21) and (8.22) in Eq. (8.19), the discretized equilibrium equation can be written as follows:

$$\delta\mathbf{a}^T \int_V \mathbf{B}^T \left\{ \mathbf{E}\mathbf{B}\dot{\mathbf{a}} - \mathbf{E}\chi_p \mathbf{h}^T \dot{\Lambda}_p - \chi_p \mathbf{h}^T \dot{\Lambda}_d \right\} dV = \delta\mathbf{a}^T \left\{ \int_S \mathbf{N}^T \mathbf{t}_{j+1} dS - \int_V \mathbf{B}^T \sigma_j dV \right\}. \tag{8.25}$$

8.3. Discretization of the yield condition

A second set of linear system of equations may be obtained by using the yield condition that is satisfied in a distributed sense such that

A second set of linear system of equations may be obtained by using the yield condition that is satisfied in a distributed sense such that

$$\int_V \delta\lambda_p F\left(\sigma_{j+1},\, p_{j+1},\, \nabla^2 p_{j+1},\, \alpha_{j+1},\, \nabla^2\alpha_{j+1}\right) dV = 0. \tag{8.26}$$

One can expand the yield potential, F_{j+1}, around $[\sigma_j, p_j, \nabla^2 p_j, \alpha_j, \nabla^2\alpha_j]$ by using the Taylor series in the following form:

$$F_{j+1} = F_j + \left(\frac{\partial F}{\partial \sigma}\right)_j^T d\sigma + \frac{\partial F}{\partial p}\, dp + \frac{\partial F}{\partial \nabla^2 p}\, d\nabla^2 p + \left(\frac{\partial f}{\partial \alpha}\right)_j^T d\alpha + \left(\frac{\partial F}{\partial \nabla^2 \alpha}\right)_j^T d\nabla^2\alpha. \tag{8.27}$$

The evolution equations for the isotropic and kinematic hardening terms and the corresponding gradients are given here from Eqs. (7.14)-(7.15) and (7.17)-(7.18) as

$$d\alpha = -d\lambda_p \, {}^{(p)}_{(1)}\tilde{A}\left\{\frac{\partial f}{\partial \bar{\bar{\mathbf{X}}}} + k_p\, \bar{\mathbf{X}}\right\}, \qquad dp = d\lambda_p \, {}^{(p)}_{(1)}\tilde{B}. \tag{8.28}$$

$$\nabla^2 d\alpha = -d\lambda_p \, {}^{(p)}_{(2)}\tilde{A}\left\{\frac{\partial f}{\partial \bar{\bar{\mathbf{X}}}} + k_p\, \bar{\mathbf{X}}\right\}, \qquad \nabla^2 dp = d\lambda_p \, {}^{(p)}_{(2)}\tilde{B}. \tag{8.29}$$

Alternatively, the evolution equations for the gradient terms can be obtained directly by operating on Eqs. (8.28) with the laplacian. Thus, the evolution equations are given as

$$d\alpha = d\lambda_p\, \eta_1^p, \tag{8.30}$$

$$\nabla^2 d\alpha = \eta_1^p \nabla^2 d\lambda_p + 2\nabla d\lambda_p \nabla\eta_1^p + d\lambda_p \nabla^2 \eta_1^p, \tag{8.31}$$

$$dp = d\lambda_p \eta_2^p, \tag{8.32}$$

$$\nabla^2 dp = \eta_2^p \nabla^2 d\lambda_p, \tag{8.33}$$

where

$$\eta_1^p = -{}^{(p)}_{(1)}\tilde{A}\left\{\frac{\partial f}{\partial \bar{\mathbf{X}}} + k_p \bar{\mathbf{X}}\right\}, \tag{8.34}$$

$$\eta_2^p = {}^{(p)}_{(1)}\tilde{B}. \tag{8.35}$$

Using Eqs. (8.30) to (8.33), the discretized yield potential in Eq. (8.27) can be rewritten in terms of the plastic multiplier, $d\lambda_p$ in the following way:

$$F_{j+1} = F_j + \left(\frac{\partial F}{\partial \sigma}\right)_j^T d\sigma + \eta_2^p \left\{\left(\frac{\partial F}{\partial p}\right)_j d\lambda_p + \left(\frac{\partial F}{\partial \nabla^2 p}\right)_j \nabla^2 d\lambda_p\right\} + \left\{\left(\frac{\partial F}{\partial \alpha}\right)_j^T \eta_1^p d\lambda_p + \left(\frac{\partial F}{\partial \nabla^2 \alpha}\right)_j^T \left\{\eta_1^p \nabla^2 d\lambda_p + 2\nabla \eta_1^p \nabla d\lambda_p \nabla^2 \eta_1^p\right\}\right\}. \tag{8.36}$$

Equation (8.36) may be rewritten in terms of the plastic multiplier and its gradients such that

$$F_{j+1} = F_j + \mathbf{m}_p^T \mathbf{E} d\varepsilon + \left(n_p + \mathbf{g}_p + \mathbf{g}'_{p1} - \mathbf{m}_p^T \mathbf{E} \chi_p\right) d\lambda_p + \mathbf{g}'_{p2} \nabla d\lambda_p + \left(n'_p + \mathbf{g}'_{p3}\right) \nabla^2 d\lambda_p - \mathbf{m}_p^T \chi_d d\lambda_d, \tag{8.37}$$

where,

$$\mathbf{m}_p = \left(\frac{\partial F}{\partial \sigma}\right)_j, \tag{8.38}$$

$$n_p = \eta_2^p \left(\frac{\partial F}{\partial \sigma}\right)_j, \tag{8.39}$$

$$n'_p = \eta_2^p \left(\frac{\partial F}{\partial \nabla^2 p}\right), \tag{8.40}$$

$$\mathbf{g}_p = \left(\frac{\partial F}{\partial \alpha}\right)_j^T \eta_1^p, \tag{8.41}$$

$$\mathbf{g}'_{p1} = \left(\frac{\partial F}{\partial \nabla^2 \alpha}\right)_j^T \nabla^2 \eta_1^p, \qquad \mathbf{g}'_{p2} = 2\left(\frac{\partial F}{\partial \nabla^2 \alpha}\right)_j^T \nabla^2 \eta_1^p,$$

(8.42)

$$\mathbf{g}'_{p3} = \left(\frac{\partial F}{\partial \nabla^2 \alpha}\right)_j^T \eta_1^p.$$

Substituting Eqs. (8.21) - (8.24) and (8.37) in Eq. (8.37), one can obtain the discretized yield condition in the following form:

$$(8.43) \quad -\delta\Lambda_p^T \int_V \mathbf{h}\Big\{\Big[\Big(n_p + \mathbf{g}_p + \mathbf{g}'_{p1} - \mathbf{m}_p^T \mathbf{E}\chi_p\Big)\mathbf{h}^T + \mathbf{g}'_{p2}\mathbf{p}^T$$

$$+ \Big(n'_p + \mathbf{g}'_{p3}\Big)\mathbf{q}^T\Big] d\Lambda_p + \mathbf{m}_p^T \mathbf{E}\mathbf{B} d\mathbf{a} - \mathbf{m}_p^T \chi_d \mathbf{h}^T d\Lambda_d\Big\} dV = \delta\Lambda_p^T \int \mathbf{h} F_j dV,$$

which is valid provided that the nonstandard boundary conditions for plasticity given in the following expressions [15]:

$$(8.44) \qquad \delta\lambda_p = 0, \qquad \text{or} \qquad (\nabla d\lambda_p)\,\nu_p = 0$$

are valid on the elastic-plastic boundary S_p. The detailed explanation for the nonstandard boundary conditions of plasticity is given by [2] and [15].

8.4. Discretization of the damage condition

A third set of linear system of equations may be obtained by using the discretized damage condition

$$(8.45) \qquad \int_V \delta\lambda_d G\Big(\phi_{j+1},\ \overline{\hat{\nabla}^2 \hat{\phi}_{j+1}},\ \kappa_{j+1},\ \nabla^2\kappa_{j+1},\ \gamma_{j+1},\ \nabla^2\gamma_{j+1}\Big) dV = 0.$$

One can expand Eq. (8.45) around $[\phi_j \widehat{\hat{\nabla}^2 \hat{\phi}_j}, \kappa_j, \nabla^2\kappa_j, \gamma_j, \nabla^2\gamma_j]$ by using the Taylor series in the following way:

$$(8.46) \quad G_{j+1} = G_j + \left(\frac{\partial G}{\partial \sigma}\right)_j^T d\sigma + \left(\frac{\partial G}{\partial \phi}\right)_j^T d\phi + \left(\frac{\partial G}{\partial \overline{\hat{\nabla}^2 \hat{\phi}}}\right)_j^T d\widehat{\hat{\nabla}^2 \hat{\phi}_j}$$

$$+ \left(\frac{\partial G}{\partial \kappa}\right)_j d\kappa + \left(\frac{\partial G}{\partial \nabla^2 \kappa}\right)_j d\nabla^2\kappa + \left(\frac{\partial G}{\partial \gamma}\right)_j d\gamma + \left(\frac{\partial G}{\partial \nabla^2 \gamma}\right)_j d\nabla^2\gamma.$$

The evolution equations for the isotropic and kinematic damage hardening and the corresponding gradients are derived from Eqs. (7.28) and (7.25) in the same way as Eqs. (8.30) to (8.33) and are given as follows:

$$d\gamma = \eta_1^d \, d\lambda_d, \tag{8.47}$$

$$\nabla^2 d\gamma = \eta_1^d \nabla^2 d\lambda_d + 2\nabla d\lambda_d \nabla \eta_1^d + d\lambda_d \, \nabla^2 \eta_1^d, \tag{8.48}$$

$$d\kappa = \eta_2^d \, d\lambda_d, \tag{8.49}$$

$$\nabla^2 d\kappa = \eta_2^d \nabla^2 \, d\lambda_d, \tag{8.50}$$

where

$$\eta_1^d = -\underset{(1)}{\overset{(d)}{}} \tilde{A} \left\{ \frac{\partial g}{\partial \bar{\Gamma}} + k_d \bar{\Gamma} \right\}, \tag{8.51}$$

$$\eta_2^d = -\underset{(1)}{\overset{(d)}{}} \tilde{B} \frac{\partial g}{\partial \bar{K}}. \tag{8.52}$$

The damage tensor and the average mesoscale gradient of the damage tensor will be used in the following form from Eqs. (7.5) and(7.7):

$$d\phi = \eta_3^{dp} \, d\lambda_p + \eta_3^{dd} \, d\lambda_d, \tag{8.53}$$

$$\overline{\hat{\nabla}^2 d\hat{\phi}} = \hat{\eta}_3^{dp} d\lambda_p + \hat{\eta}_3^{dd} d\lambda_d, \tag{8.54}$$

where

$$\eta_3^{dp} = -\underset{(1)}{\overset{(d)}{}} \tilde{C} \frac{\partial f}{\partial \bar{Y}}, \qquad \eta_3^{dd} = -\underset{(1)}{\overset{(d)}{}} \tilde{C} \frac{\partial g}{\partial \bar{Y}} \tag{8.55}$$

$$\hat{\eta}_3^{dp} = -\underset{(3)}{\overset{(d)}{}} \tilde{C} \frac{\partial f}{\partial \bar{Y}}, \qquad \hat{\eta}_3^{dd} = -\underset{(3)}{\overset{(d)}{}} \tilde{C} \frac{\partial g}{\partial \bar{Y}} \tag{8.56}$$

Using Eqs. (8.47) to (8.50) and Eqs. (8.53) to (8.54), the discretized damage condition in Eq. (8.45) can be rewritten in terms of the damage multiplier, $d\lambda_d$

in the following form:

$$
\begin{aligned}
(8.57)\quad G_{j+1} = G_j + \left(\frac{\partial G}{\partial \phi}\right)_j^T (\mathbf{E}\,(d\varepsilon - d\lambda_p \chi_p) - d\lambda_d \chi_d) \\
\left(\frac{\partial G}{\partial \phi}\right)_j^T \left(\eta_3^{dp}\, d\lambda_p + \eta_3^{dd}\, d\lambda_d\right) + \left(\frac{\partial G}{\partial \widehat{\hat{\nabla}^2 \hat{\phi}}}\right)_j^T \left(\hat{\eta}_3^{dp} d\lambda_p + \hat{\eta}_3^{dd} d\lambda_d\right) \\
+ \left\{\left(\frac{\partial G}{\partial \kappa}\right)_j \eta_2^d d\lambda_d + \left(\frac{\partial G}{\partial \nabla^2 \kappa}\right)_j \left\{\eta_2^d \nabla^2 d\lambda_d + 2\nabla \eta_2^d \nabla d\lambda_d + d\lambda_d \nabla^2 \eta_2^d\right\}\right\} \\
+ \left\{\left(\frac{\partial G}{\partial \gamma}\right)_j^T \eta_1^d d\lambda_d + \left(\frac{\partial G}{\partial \nabla^2 \gamma}\right)_j^T \left\{\eta_1^d \nabla^2 d\lambda_d + 2\nabla \eta_1^d \nabla d\lambda_d + d\lambda_d \nabla^2 \eta_1^d\right\}\right\}.
\end{aligned}
$$

Equation (8.57) may be reorganized in terms of the damage multiplier and its gradients such that

$$
\begin{aligned}
(8.58)\quad G_{j+1} = G_j + \mathbf{m}_d^T \mathbf{E} d\varepsilon + \left(-\mathbf{E}\mathbf{m}_d^T \chi_d + \mathbf{r}_{dp} + \hat{\mathbf{r}}_{dp}\right) d\lambda_p \\
+ \left(-\mathbf{m}_d^T \chi_d + \mathbf{r}_{dd} + \hat{\mathbf{r}}_{dd} + n_d + n'_{d1} + \mathbf{g}_d + \mathbf{g}'_{d1}\right) d\lambda_d \\
+ \left(n'_{d2} + \mathbf{g}'_{d2}\right) \nabla d\lambda_d + \left(n'_{d3} + \mathbf{g}'_{d3}\right) \nabla^2 d\lambda_d,
\end{aligned}
$$

where:

$$
(8.59)\qquad \mathbf{m}_d = \frac{\partial G}{\partial \sigma}
$$

$$
(8.60)\qquad \mathbf{r}_{dd} = \left(\frac{\partial G}{\partial \phi}\right)_j^T \eta_3^{dd}, \qquad \mathbf{r}_{dp} = \left(\frac{\partial G}{\partial \phi}\right)_j^T \eta_3^{dp},
$$

$$
(8.61)\qquad \hat{\mathbf{r}}_{dd} = \left(\frac{\partial G}{\partial \widehat{\hat{\nabla}^2 \hat{\phi}}}\right)_j^T \hat{\eta}_3^{dd}, \qquad \hat{\mathbf{r}}_{dp} = \left(\frac{\partial G}{\partial \widehat{\hat{\nabla}^2 \hat{\phi}}}\right)_j^T \hat{\eta}_3^{dp}
$$

$$
(8.62)\qquad n_d = \left(\frac{\partial G}{\partial \kappa}\right)_j \eta_2^d,
$$

$$
(8.63)\qquad n'_{d1} = \left(\frac{\partial G}{\partial \nabla^2 \kappa}\right)_j \nabla^2 \eta_2^d, \qquad n'_{d2} = 2\left(\frac{\partial G}{\partial \nabla^2 \kappa}\right)_j \nabla \eta_2^d,
$$

$$
n'_{d3} = \left(\frac{\partial G}{\partial \nabla^2 \kappa}\right)_j \eta_2^d,
$$

$$g_d = \left(\frac{\partial G}{\partial \gamma}\right)_j^T \eta_1^d, \tag{8.64}$$

$$g'_{d1} = \left(\frac{\partial G}{\partial \nabla^2 \gamma}\right)_j^T \nabla^2 \eta_1^d, \qquad g'_{d2} = 2\left(\frac{\partial G}{\partial \nabla^2 \gamma}\right)_j^T \nabla \eta_1^d,$$
$$g'_{d3} = \left(\frac{\partial G}{\partial \nabla^2 \gamma}\right)_j^T \eta_1^d. \tag{8.65}$$

Substituting Eqs. (8.21) - (8.24) and (8.58) in Eq. (8.45), the following expression is obtained:

$$\begin{aligned} \delta\Lambda_d \int_V \{ & -\mathbf{h}\mathbf{m}_d^T \mathbf{E}\mathbf{B} d\mathbf{a} + \mathbf{h}\left(-\mathbf{E}\mathbf{m}_d^T \chi_d + \mathbf{r}_{dp} + \hat{\mathbf{r}}_{dp}\right)\mathbf{h}^T d\Lambda_p \\ & + \mathbf{h}\left(-\mathbf{m}_d^T \chi_d + \mathbf{r}_{dd}\mathrm{d} + \hat{\mathbf{r}}_{dd} + n_d + n'_{d1} + \mathbf{g}_d + \mathbf{g}'_{d1}\right)\mathbf{h}^T d\Lambda_d \\ & + \left(n'_{d2} + \mathbf{g}'_{d2}\right)\mathbf{h}\mathbf{p}^T d\Lambda_d + \left(n'_{d3} + \mathbf{g}'_{d3}\right)\mathbf{h}\mathbf{q}^T d\Lambda_d \} \, dV = \delta\Lambda_d \int G_j h_d dV, \end{aligned} \tag{8.66}$$

which is valid provided that the non-standard boundary conditions for damage given in the following expression:

$$\delta\lambda_d = 0, \qquad \text{or} \qquad (\nabla d\lambda_d)\,\nu_d = 0 \tag{8.67}$$

are valid on the undamaged-damaged boundary S_d. For the undamaged material, the damage multiplier is $\lambda_d = 0$, so that at the boundary where damage starts to initiate, it must be ensured that $\nabla^2 \lambda_d > 0$. The dependence of the damage condition on the Laplacian of the damage internal state variables is essential for the crack interaction in order for damage localization to occur at the macroscale.

8.5. Combined discretization equations

Combining Eqs.(8.25), (8.43) and (8.66), one can obtain a set of algebraic equations in terms of the variations $da, d\Lambda_p$ and $d\Lambda_d$

$$\begin{bmatrix} \mathbf{K}_{aa} & \mathbf{K}_{a\lambda_p} & \mathbf{K}_{a\lambda_d} \\ \mathbf{K}_{\lambda_p a} & \mathbf{K}_{\lambda_p\lambda_p} & \mathbf{K}_{\lambda_p\lambda_d} \\ \mathbf{K}_{\lambda_d a} & \mathbf{K}_{\lambda_d\lambda_p} & \mathbf{K}_{\lambda_d\lambda_d} \end{bmatrix} \begin{bmatrix} d\mathbf{a} \\ d\Lambda_p \\ d\Lambda_d \end{bmatrix} = \begin{bmatrix} \mathbf{f}_e + f_a \\ \mathbf{f}_{\lambda_p} \\ \mathbf{f}_{\lambda_d} \end{bmatrix} \tag{8.68}$$

where the diagonal matrices are defined as follows:

$$\mathbf{K}_{aa} = \int_V \mathbf{B}^T \mathbf{E} \mathbf{B} dV, \tag{8.69}$$

$$\mathbf{K}_{\lambda_p \lambda_p} = -\int \mathbf{h} \Big[\Big(n_{\mathrm{p}} + \mathbf{g}_p + \mathbf{g}'_{p1} - \mathbf{m}_p^T \mathbf{E} \chi_p \Big) \mathbf{h}^T + \mathbf{g}'_{p2} \mathbf{p}^T + \Big(n'_{\mathrm{p}} + \mathbf{g}'_{p3} \Big) \mathbf{q}^T \Big] dV, \tag{8.70}$$

$$\mathbf{K}_{\lambda_d \lambda_d} = \int_V \mathbf{h} \Big\{ \Big(-\mathbf{m}_d^T \chi_d + \mathbf{r}_{dd} + \hat{\mathbf{r}}_{dd} + n_d + n'_{d1} + \mathbf{g}_d + \mathbf{g}'_{d1} \Big) \mathbf{h}^T + \Big(n'_{d2} + \mathbf{g}'_{d2} \Big) \mathbf{p}^T + \Big(n'_{d3} + \mathbf{g}'_{d3} \Big) \mathbf{q}^T \Big\} dV, \tag{8.71}$$

and the off-diagonal matrices are given by

$$\mathbf{K}_{a\lambda_p} = -\int_V \mathbf{B}^T \mathbf{E} \chi_p \mathbf{h}^T dV, \qquad \mathbf{K}_{a\lambda_d} = -\int_V \mathbf{B}^T \chi_p \mathbf{h}^T dV, \tag{8.72}$$

$$\mathbf{K}_{\lambda_p a} = -\int_V \mathbf{h} \mathbf{m}_p^T \mathbf{E} \mathbf{B} dV, \qquad \mathbf{K}_{\lambda_p \lambda_d} = \int \mathbf{h} \mathbf{m}_p^T \chi_d \mathbf{h}^T dV, \tag{8.73}$$

$$\begin{aligned} \mathbf{K}_{\lambda_d a} &= -\int_V \mathbf{h} \mathbf{m}_d^T \mathbf{E} \mathbf{B} dV, \\ K_{\lambda_d \lambda_p} &= \int_V \mathbf{h} \left(-\mathbf{E} \mathbf{m}_d^T \chi_d + \mathbf{r}_{\mathrm{dp}} + \hat{\mathbf{r}}_{\mathrm{dp}} \right) \mathbf{h}^T dV. \end{aligned} \tag{8.74}$$

The corresponding external force vector and the nodal force vector equivalent to internal stresses is given by

$$\mathbf{f}_e = \int_S \mathbf{N}^T \mathbf{t}_{j+1} dS, \qquad \mathbf{f}_a = -\int_V \mathbf{B}^T \sigma_j dV, \tag{8.75}$$

$$\mathbf{f}_{\lambda_p} = \int_S \mathbf{F}_j \, \mathbf{h} dV, \tag{8.76}$$

$$\mathbf{f}_{\lambda_d} = \int_S \mathbf{G}_j \mathbf{h} \mathbf{d} V. \tag{8.77}$$

9. Conclusion

A thermodynamically consistent multiscale gradient enhanced approach to coupled plasticity and damage is formulated in this paper. Thermodynamically consistent constitutive equations are derived here in order to investigate such issues as size effect on the strength of the composite, strain and damage localization effects on the macroscopic response of the composite, and statistically inhomogeneity of the evolution related damage variables associated with the RVE.

This approach is based on a non-local gradient-dependent theory of plasticity and damage over multiple scales that incorporates mesoscale internal state variables and their higher order gradients at both macro and mesoscales. The interaction of the length scales is a paramount factor in understanding and controlling the material defects such as dislocation, voids, and cracks at the mesoscale and interpret them at the macroscale. The behavior of these defects is captured not only individually, but also the interaction between them and their ability to create spatio-temporal patterns under different loading conditions.

The capability of the proposed model is to simulate properly size-dependent behavior of the materials together with localization problems as was effectively proven by DE BORST *et al.* [15] for the particular case of using gradients for the accumulated plastic strain only. Consequently, the boundary value problem of the standard continuum model will remain well-posed even in the softening regime.

The gradient-enhanced continuum results in additional partial differential equations that are satisfied in a weak form. Additional nodal degrees of freedom are introduced which leads to a modified finite element formulation. The governed equations can be linearized consistently and solved within incremental iterative Newton-Raphson solution procedure.

The computational issue of this theoretical formulation with proper explanation of the proper boundary conditions associated with the gradients and evaluation of the respective material parameters will be presented in a forthcoming paper. The detailed explanation for some of the non-standard boundary conditions of plasticity is given by DE BORST *et. al* [2] and [15].

Calibration for the different material properties in the proposed approach may be difficult, or impossible for certain cases. While the proposed framework is generalized to that of plasticity coupled with damage, one needs more studies to be performed in order to assess effectively the potential applications for this framework.

References

1. G. PIJAUDIER-CABOT, *Non Local Damage*, H.-B.MÜHLHAUS, [Ed.] Continuum Models for Materials with Microstructure, John Wiley & Sons Ltd., 105-143, 1995.
2. R. DE BORST, A. BENELLAL, and O. HEERES, *A gradient enhanced damage approach to fracture*, J. de Physique, **6**, 491-502, 1996.
3. E.C. AIFANTIS, *On the microstructural origin of certain inelastic models*, J. of Eng. Materials and Tech., **106**, 326-330, 1984.
4. T.E. LACEY, D.L. MCDOWELL, and R. TALREJA, *Non-local concepts for evolution of damage*, Mech. of Materials, **31**, 831-860, 1999.
5. E. KUHL, E. RAMM, R. DE BORST, *An anisotropic gradient damage model for quassibirttle materials*, J. of Comp. Meth. in Appl. Mech. and Eng., **183**, 87-103, 2000.
6. H.B. MÜHLHAUS and E.C. AIFANTIS, *A variational principle for gradient plasticity*, Int. J. of Solid and Structures, **28,** 845-857, 1991.
7. E. KRONER, *Elasticity theory of materials with long range cohesive forces*, Int. J. of Solid and Structures, **3**, 731-742, 1967.
8. N.A. FLECK and J.W. HUTCHINSON, *Strain gradient plasticity*, Advances in Appl. Mech., **33**, 295-361, 1997.
9. S. NEMAT-NASER and M. HORI, *Micromechanics: Overall Properties of Heterogeneous Materials*, North-Holland, Amsterdam, The Netherlands, 1993.
10. G.Z. VOYIADJIS and T. PARK, *Kinematics description of damage for finite strain plasticity*, J. of Eng. Science, **37**, 7, 803-830, 1999.
11. G.Z. VOYIADJIS AND A.R. VENSON, *Experimental damage investigation of SiC-Ti aluminide metal matrix composite*, Int. J. of Damage Mech., **4**, 338-361, 1995.
12. G.Z. VOYIADJIS and B. DELIKTAS, *A Coupled anisotropic damage model for the inelastic response of composite materials*, J. of Comp. Meth. in Appl. Mech. and Eng., **183**, 159-199, 2000.
13. G.Z. VOYIADJIS and T. PARK, *Local and interfacial damage analysis of metal matrix composites*, Int. J. of Eng. Science, **33** 11, 1595-1621, 1995.
14. D.H. ALLEN, J.W. FOULK, and K.L.E. HELMS, *A Model for Predicting the Effect of Environmental Degradation and Damage Evolution in Metal Matrix Composites*, D. L. MCDOWELL [Ed.], Applications of Continuum Damage Mechanics to Fatigue and Fracture, ASTMSTP, American Society of Testing Materials, West Conshohocken, PA, 29-45, 1997.

15. R. DE BORST, J. PAMIN, and L.J. SLUYS, *Computational Issues in Gradient Plasticity*, H.-B. Mühlhaus, [Ed.]Continuum Models for Materials with Microstructure, John Wiley & Sons Ltd., 159-200, 1995.

16. G.Z. VOYIADJIS and T. PARK, *Local and interfacial damage analysis of metal matrix composites using the finite element method*, Eng. Fracture Mech; **56**, 4, 483-511, 1997.

Received January 19, 2001.

Arch. Mech., **53**, 4-5, pp. 599–610, Warszawa 2001

Semi-inverse solutions in nonlinear theory of elastic shells

L. M. ZUBOV

Department of Mechanics and Mathematics,
Rostov State University,
Zorge street, 5, 344090,
Rostov-on-Don, Russia,
e-mail: zubov@math.rsu.ru

THE SEMI-INVERSE METHOD is applied to the solution of static problems in the nonlinear theory of elastic shells. This method consists in construction of particular solutions in such a way that the initial system of equations is reduced to a system of a smaller number of independent variables. Two nonlinear models, one of the Love type and another of the Cosserat type, are considered. For these models, several two-parameter families of finite deformations are found; then the system of partial differential equations of equilibrium reduces to a system of nonlinear ordinary differential equations. The semi-inverse solutions found are valid for prismatic and toroidal shells, as well as for shells of revolution. These solutions are of practical significance. They describe torsion of a prismatic shell under large angles of twist, strong flexure of a thin-walled cylinder of arbitrary cross-section, spatial bending of a shell having the shape of a sector of a surface of revolution, straightening of a toroidal shell to a cylindrical surface, and some other types of large deformations.

1. Basic statements

Let σ be the reference (undeformed) surface of a shell. We refer the position vector of a particle of σ to Gaussian coordinates q^α $(\alpha = 1, 2)$ and $\boldsymbol{r}(q^1, q^2) = x_1\boldsymbol{i}_1 + x_2\boldsymbol{i}_2 + x_3\boldsymbol{i}_3$. Here, x_k $(k = 1, 2, 3)$ are Cartesian coordinates of a point of σ, and $\boldsymbol{i}_k$ $(k = 1, 2, 3)$ is a fixed orthonormal basis. The coefficients of the first and the second fundamental forms of the surface σ are

$$g_{\alpha\beta} = \boldsymbol{r}_\alpha \cdot \boldsymbol{r}_\beta, \quad b_{\alpha\beta} = \frac{\partial \boldsymbol{r}_\alpha}{\partial q^\beta} \cdot \boldsymbol{n} = -\boldsymbol{r}_\alpha \cdot \frac{\partial \boldsymbol{n}}{\partial q^\beta}, \quad \boldsymbol{r}_\alpha = \frac{\partial \boldsymbol{r}}{\partial q^\alpha}, \tag{1.1}$$
$$\boldsymbol{r}^\beta \cdot \boldsymbol{r}_\alpha = \delta_\alpha^\beta, \quad \boldsymbol{r}^\beta \cdot \boldsymbol{n} = 0,$$

where $\boldsymbol{n}$ – is a unit normal to σ and δ_α^β is the Kronecker symbol.

The surface Σ of the shell after deformation is referred to the coordinates q^α as well, and the position of a particle of Σ is described by the position vector

$\boldsymbol{R}(q^1, q^2) = X_1\boldsymbol{i}_1 + X_2\boldsymbol{i}_2 + X_3\boldsymbol{i}_3$, X_k being the Cartesian coordinates of the point of the surface Σ whose normal vector is $\boldsymbol{N}$,

The components of the fundamental forms of Σ are

$$G_{\alpha\beta} = \boldsymbol{R}_\alpha \cdot \boldsymbol{R}_\beta, \quad B_{\alpha\beta} = \frac{\partial \boldsymbol{R}_\alpha}{\partial q^\beta} \cdot \boldsymbol{N} = -\boldsymbol{R}_\alpha \cdot \frac{\partial \boldsymbol{N}}{\partial q^\beta},$$
$$\boldsymbol{R}_\alpha = \frac{\partial \boldsymbol{R}}{\partial q^\alpha}, \quad \boldsymbol{R}^\beta \cdot \boldsymbol{R}_\alpha = \delta^\beta_\alpha, \quad \boldsymbol{R}^\beta \cdot \boldsymbol{N} = 0. \tag{1.2}$$

First we consider the model of a nonlinearly elastic shell of the Love type (KOITER [1], PIETRASZKIEWICZ [2,3], GALIMOV [4] and ZUBOV [5]). The equations of equilibrium of the shell expressed in terms of the stress and couple resultants are

$$\nabla_\alpha(\nu^{\alpha\beta} - \mu^{\alpha\delta}B^\beta_\delta) - B^\beta_\delta \nabla_\alpha \mu^{\alpha\delta} + F^\beta = 0, \quad (\beta = 1, 2),$$
$$\nabla_\alpha \nabla_\beta \mu^{\alpha\beta} + B_{\alpha\beta}(\nu^{\alpha\beta} - B^\alpha_\delta \mu^{\delta\beta}) + F = 0, \tag{1.3}$$
$$F = \boldsymbol{F} \cdot \boldsymbol{N}, \quad F^\beta = \boldsymbol{F} \cdot \boldsymbol{R}^\beta, \quad B^\alpha_\delta = B_{\gamma\delta}G^{\alpha\gamma}, \quad G^{\alpha\gamma} = \boldsymbol{R}^\alpha \cdot \boldsymbol{R}^\gamma,$$

where $\mathbf{F}$ is the vector intensity of the force load on Σ, $\nu^{\alpha\beta}$ and $\mu^{\alpha\beta}$ are the resultant stress and couple tensors, respectively, and ∇_α is the symbol of the covariant derivative in the metric $G_{\alpha\beta}$. The constitutive equations take the form

$$\chi\sqrt{\frac{G}{g}}\nu^{\alpha\beta} = \frac{\partial W}{\partial G_{\alpha\beta}}, \quad \chi\sqrt{\frac{G}{g}}\mu^{\alpha\beta} = \frac{\partial W}{\partial B_{\alpha\beta}},$$
$$G = G_{11}G_{22} - G_{12}^2, \quad g = g_{11}g_{22} - g_{12}^2, \tag{1.4}$$
$$\chi = \begin{cases} 1, & \alpha = \beta, \\ 2, & \alpha \neq \beta. \end{cases}$$

For a homogeneous isotropic shell, its specific (per unit area of surface σ) potential energy of deformation W is a function of the following nine variables:

$$g^{\alpha\beta}b_{\alpha\beta}, \quad g^{\alpha\beta}G_{\alpha\beta}, \quad g^{\alpha\beta}B_{\alpha\beta}, \quad (b_{11}b_{22} - b_{12}^2)/g, \quad G/g,$$
$$(B_{11}B_{22} - B_{12}^2)/g, \quad b^{\alpha\beta}G_{\alpha\beta}, \quad b^{\alpha\beta}B_{\alpha\beta}, \quad g^{\alpha\beta}g^{\gamma\delta}G_{\alpha\gamma}B_{\beta\delta}, \tag{1.5}$$
$$b^{\alpha\beta} = g^{\alpha\text{æ}}g^{\beta\lambda}b_{\text{æ}\lambda}, \quad g^{\beta\lambda} = \boldsymbol{r}^\beta \cdot \boldsymbol{r}^\lambda.$$

Suppose that $\partial\Sigma$, the edge of the shell in the deformed configuration, is loaded by a distributed force of linear density $\boldsymbol{Q} = Q^\alpha \boldsymbol{R}_\alpha + Q\boldsymbol{N}$ and distributed moment of linear density $\boldsymbol{d} \times \boldsymbol{N}$. Now the boundary conditions take the form

$$\sqrt{\frac{G}{g}}m_\alpha(\nu^{\alpha\beta} - 2B^\beta_\delta\mu^{\alpha\delta}) = \varepsilon(Q^\beta - B^\beta_\alpha)d^\alpha), \quad (\beta = 1,2),$$

$$\sqrt{\frac{G}{g}}m_\alpha m_\beta\mu^{\alpha\beta} = \varepsilon m_\alpha d^\alpha, \tag{1.6}$$

$$\sqrt{\frac{G}{g}}m_\beta\nabla_\alpha\mu^{\alpha\beta} + \frac{d}{ds}\left(\sqrt{\frac{G}{g}}\varepsilon^{-2}\tau^\delta m_\beta G_{\alpha\delta}\mu^{\alpha\beta}\right) = \varepsilon Q + \frac{d}{ds}\left(\varepsilon^{-1}\tau^\delta d_\delta\right),$$

$$\boldsymbol{d} = d^\alpha\boldsymbol{R}_\alpha = d_\beta\boldsymbol{R}^\beta, \quad \boldsymbol{m} = m_\alpha\boldsymbol{r}^\alpha, \quad \boldsymbol{\tau} = \tau^\delta\boldsymbol{r}_\delta, \quad \varepsilon = \sqrt{\tau^\alpha\tau_\beta G_{\alpha\beta}}.$$

Here $\boldsymbol{m}$ and $\boldsymbol{\tau}$ are the unit normal vector and the unit tangent vector to the boundary contour $\partial\sigma$ in the undeformed configuration of the shell, and s is the length parameter of $\partial\sigma$.

In what follows, we shall consider particular exact solutions of the equilibrium equations (1.3). These solutions refer to shells of certain geometries. The solutions constitute some families (classes) of finite deformation for which the initial nonlinear system of partial differential equations of two independent variables, q^1, q^2, reduces to a system of ordinary differential equations whose unknown functions are functions of only one variable.

2. Spatial bending of a cylindrical shell

Suppose that a shell in the reference configuration is a cylindrical surface with its generator parallel to the x_1-axis. The cross-section of the surface by the plane x_2x_3 is an arbitrary closed or nonclosed curve having no points of self-intersection. Its equation is given by functions $x_2(s)$ and $x_3(s)$, s being the length parameter of the curve. Let us take the Gaussian coordinates $q^1 = x_1$ and $q^2 = s$. Let a prime denote a derivative with respect to s. We have

$$\boldsymbol{r}_1 = \boldsymbol{i}_1, \quad \boldsymbol{r}_2 = x_2'\boldsymbol{i}_2 + x_3'\boldsymbol{i}_3. \tag{2.1}$$

It follows that the quantities $g_{\alpha\beta}$ and $b_{\alpha\beta}$ do not depend on x_1. Let us consider the following family of deformations of a cylindrical shell:

$$\begin{aligned} X_1 &= \gamma(s)\sin(ax_1 + \lambda(s)), \\ X_2 &= \alpha(s) + lx_1, \\ X_3 &= \gamma(s)\cos(ax_1 + \lambda(s)), \end{aligned} \tag{2.2}$$

where a and l are constants and α,γ, and λ are functions of one variable. When $l = \lambda = 0$, the formulae (2.2) describe bending of the shell in the plane x_1, x_3

such that each generator of the cylinder becomes a part of a circumference. If $l \neq 0$ and $\lambda \neq 0$, the generator is a helical line. Using (2.2) we find that

$$\boldsymbol{R}_1 = a\gamma(s)\boldsymbol{e}_1 + l\boldsymbol{i}_2, \quad \boldsymbol{R}_2 = \gamma(s)\lambda'(s)\boldsymbol{e}_1 + \alpha'(s)\boldsymbol{i}_2 + \gamma'(s)\boldsymbol{e}_3,$$

$$\boldsymbol{e}_1 = \boldsymbol{i}_1 \cos(ax_1 + \lambda(s)) - \boldsymbol{i}_3 \sin(ax_1 + \lambda(s)), \tag{2.3}$$

$$\boldsymbol{e}_3 = \boldsymbol{i}_1 \sin(ax_1 + \lambda(s)) + \boldsymbol{i}_3 \cos(ax_1 + \lambda(s)),$$

$$\boldsymbol{N} = N_1(s)\boldsymbol{e}_1 + N_2(s)\boldsymbol{i}_2 + N_3(s)\boldsymbol{e}_3,$$

$$\frac{\partial \boldsymbol{R}_1}{\partial q^1} = a^2\gamma\boldsymbol{e}_3, \quad \frac{\partial \boldsymbol{R}_1}{\partial q^2} = \frac{\partial \boldsymbol{R}_2}{\partial q^1} = a\gamma'\boldsymbol{e}_1 - a\gamma\lambda'\boldsymbol{e}_3, \tag{2.4}$$

$$\frac{\partial \boldsymbol{R}_2}{\partial q^2} = (2\gamma'\lambda' + \gamma\lambda'')\boldsymbol{e}_1 + \alpha''\boldsymbol{i}_2 + (\gamma'' - \gamma\lambda'^2)\boldsymbol{e}_3.)$$

The vectors $\boldsymbol{e}_1, \boldsymbol{i}_2, \boldsymbol{e}_3$ constitute an orthonormal basis. With regard to (1.2) and (2.3) we can conclude that the quantities $G_{\alpha\beta}, B_{\alpha\beta}$ do not depend on x_1. The Christoffel symbols $\Gamma^{\beta}_{\lambda\delta}$ that participate in the covariant derivatives ∇_α also depend only on the length parameter s. For an isotropic homogeneous shell, by (1.4) and (1.5), the tensors $\nu^{\alpha\beta}$ and $\mu^{\alpha\beta}$ are functions of s only. Let us suppose that the external surface load F^β, F, as well as for a nonclosed cylinder the forces Q_β, Q, d^α acting on the direct edges of the shell $s = s_1$ and $s = s_2$, do not depend on x_1. Now the equilibrium equations (1.3) supplemented with the boundary conditions (1.6) at $s = s_1$ and $s = s_2$ constitute a nonlinear boundary value problem for a system of ordinary differential equations with unknown functions $\alpha(s), \gamma(s)$ and $\lambda(s)$. When $l = \lambda(s) = 0$ we have $G_{12} = B_{12} = \nu^{12} = \mu^{12} = 0$. Under conditions $F^1 = 0$ and $Q^1 = d^1 = 0$, one of the equations of equilibrium (1.3) as well as one of the boundary conditions (1.6) is satisfied identically.

3. Twisting of a cylindrical shell

Let us change the Cartesian coordinates x_k to the cylindrical coordinates r, φ, z using the formulae $x_1 = r\cos\varphi, x_2 = r\sin\varphi, x_3 = z$, and consider a prismatic cylindrical shell whose generator lines are parallel to the z-axis. The curve in the cross-section of the surface σ by the plane $z = \text{const}$ will be defined by the function $r = r(\varphi)$. We take $q^1 = z, q^2 = \varphi$ as the Gaussian coordinates on σ. Now we have

$$\boldsymbol{r}_1 = \boldsymbol{i}_3, \quad \boldsymbol{r}_2 = r'\boldsymbol{e}_r + r\boldsymbol{e}_\varphi, \quad r' \equiv dr/d\varphi,$$

$$\boldsymbol{e}_r = \boldsymbol{i}_1 \cos\varphi + \boldsymbol{i}_2 \sin\varphi, \quad \boldsymbol{e}_\varphi = -\boldsymbol{i}_1 \sin\varphi + \boldsymbol{i}_2 \cos\varphi, \tag{3.1}$$

$$g_{11} = 1, \quad g_{12} = 0, \quad g_{22} = r'^2 + r^2.$$

Let us denote by R, Φ, Z the cylindrical coordinates of a point of the deformed surface Σ so that $X_1 = R\cos\Phi, X_2 = R\sin\Phi, X_3 = Z$. Consider the following family of deformations of a cylindrical shell:

$$\begin{aligned} R &= R(\varphi), \\ \Phi &= \varphi + \psi z + v(\varphi), \\ Z &= \alpha z + a\varphi + w(\varphi), \\ \psi, a, \alpha &= \text{const}. \end{aligned} \tag{3.2}$$

These formulae describe torsion of the shell with the angle of twist ψ, longitudinal stretching, and longitudinal shift. In this, the cross-section of the shell, $z = \text{const}$, has a deplanation characterized by function w; besides it is deformed in its plane what is described by the functions $R(\varphi)$ and $v(\varphi)$. When the shell is deformed according to (3.2), the generators of the initially cylindrical surface become helical lines. If the cross-section of the shell is a closed line, the functions R, v, and w must be 2π-periodic, and the quantity $2\pi a$ is equal to the modulus of the Burgers vector of a screw dislocation.

By (3.2) we have

$$\begin{aligned} &\boldsymbol{R}_1 = \alpha \boldsymbol{i}_3 + \psi R \boldsymbol{e}_\Phi, \quad \boldsymbol{R}_2 = (a + w')\boldsymbol{i}_3 + R'\boldsymbol{e}_R + R(1 + v')\boldsymbol{e}_\Phi, \\ &\frac{\partial \boldsymbol{R}_1}{\partial q^1} = -\psi^2 R \boldsymbol{e}_R, \quad \frac{\partial \boldsymbol{R}_1}{\partial q^2} = \frac{\partial \boldsymbol{R}_2}{\partial q^1} = -\psi R(1 + v')\boldsymbol{e}_R + \psi R' \boldsymbol{e}_\Phi, \\ &\frac{\partial \boldsymbol{R}_2}{\partial q^2} = [R'' - R(1 + v')^2]\boldsymbol{e}_R + [Rv'' + 2R'(1 + v')]\boldsymbol{e}_\Phi + w''\boldsymbol{i}_3, \\ &\boldsymbol{e}_R = \boldsymbol{i}_1 \cos\Phi + \boldsymbol{i}_2 \sin\Phi, \quad \boldsymbol{e}_\Phi = -\boldsymbol{i}_1 \sin\Phi + \boldsymbol{i}_2 \cos\Phi, \end{aligned} \tag{3.3}$$

$$\begin{aligned} G_{11} &= \alpha^2 + \psi^2 R^2, \quad G_{12} = \alpha(a + w') + \psi R^2(1 + v'), \\ G_{22} &= (a + w')^2 + R^2(1 + v')^2 + R'^2. \end{aligned} \tag{3.4}$$

From (3.3),(3.4) it follows that the quantities $G_{\alpha\beta}, B_{\alpha\beta}, \Gamma^\beta_{\delta\lambda}$ do not depend on z. Thus, for an isotropic homogeneous shell, (1.3) is a system of ordinary differential equations with respect to the unknown functions $R(\varphi), v(\varphi), w(\varphi)$. Here, the components of external surface forces F^α, F and edge load Q, Q^α, d^α at $\varphi = \varphi_1$ and $\varphi = \varphi_2$ (for an open shell) should not depend on z.

If σ is a sector of a circular cylindrical shell, at $F^\alpha = 0$, the above system has the simple solution

$$R = R_0, \quad v(\varphi) = A\varphi, \quad w(\varphi) = 0, \quad R_0, A = \text{const}. \tag{3.5}$$

Let us consider the problem of a screw dislocation in a closed circular cylindrical shell which in the initial state, before dislocation, has the radius r_0. It is easy to verify with the use of (3.1) and (3.4) that there is an isometric deformation (it is the bending) of the cylindrical surface that is defined by the formulae

$$R(\varphi) = R_0 = \sqrt{r_0^2 - a^2}, \quad v(\varphi) = 0, \quad w(\varphi) = 0,$$
$$\psi = -\frac{a}{r_0\sqrt{r_0^2 - a^2}}, \quad \alpha = \sqrt{1 - \frac{a^2}{r_0^2}} \tag{3.6}$$

By (3.6), the cylinder is twisted and its radius decreases. Deformation (3.6) is a solution of the equilibrium equations (1.3) for a momentless elastic shell when the external forces are absent. Indeed, now, due to the momentless state of the shell, $\mu^{\alpha\beta} \equiv 0$ and $\nu^{\alpha\beta} \equiv 0$ since the deformation is isometric. For a sufficiently thin shell the assumption that the shell is momentless is quite accurate.

4. Bending, shifting, and twisting of a sector of a shell of revolution

Let the surface σ be a surface of revolution or a sector thereof. Let the equation of the meridian in cylindrical coordinates r, φ, z be $r = r(z)$. As the Gaussian coordinates we take $q^1 = z, q^2 = \varphi$. For the reference configuration we have

$$\boldsymbol{r}_1 = r'\boldsymbol{e}_r + \boldsymbol{i}_3, \quad \boldsymbol{r}_2 = r\boldsymbol{e}_\varphi. \tag{4.1}$$

Let us consider the following family of deformations using the circular cylindrical coordinates r, φ, z and R, Φ, Z:

$$R = R(z), \quad \Phi = K\varphi + \beta(z), \quad Z = l\varphi + \gamma(z), \quad K, l = \text{const}. \tag{4.2}$$

By (4.2) we find that

$$\begin{gathered}
\boldsymbol{R}_1 = R'\boldsymbol{e}_R + R\beta'\boldsymbol{e}_\Phi + \gamma'\boldsymbol{i}_3, \quad \boldsymbol{R}_2 = KR\boldsymbol{e}_\Phi + l\boldsymbol{i}_3, \\
\boldsymbol{N} = N_1(z)\boldsymbol{e}_R + N_2(z)\boldsymbol{e}_\Phi + N_3(z)\boldsymbol{i}_3, \\
\frac{\partial \boldsymbol{R}_1}{\partial q^1} = (R'' - R\beta'^2)\boldsymbol{e}_R + (2R'\beta' + R\beta'')\boldsymbol{e}_\Phi + \gamma''\boldsymbol{i}_3, \\
\frac{\partial \boldsymbol{R}_1}{\partial q^2} = \frac{\partial \boldsymbol{R}_2}{\partial q^1} = -KR\beta'\boldsymbol{e}_R + KR'\boldsymbol{e}_\Phi, \\
\frac{\partial \boldsymbol{R}_2}{\partial q^2} = -K^2R\boldsymbol{e}_R.
\end{gathered} \tag{4.3}$$

It follows that the coefficients of the quadratic forms $G_{\alpha\beta}, B_{\alpha\beta}$ and the Christoffel symbols $\Gamma^{\beta}_{\delta\lambda}$ for the surface Σ do not depend on φ. Thus for an isotropic homogeneous shell, the stress and couple resultants $\nu^{\alpha\beta}$ and $\mu^{\alpha\beta}$ are functions of one variable z and now equations (1.3) are ordinary differential equations with respect to the unknown functions $R(z), \beta(z), \gamma(z)$ if the loads F^{β}, F do not depend on φ. Expressions (4.2) include the following important particular deformations:

1. $K = 1, l = 0$ corresponds to twisting and axisymmetrical deformation of a shell of revolution. This special case of the semi-inverse solution (4.2) was found earlier by ZUBOV [5]. The results of numerical solution of the problem of twisting and inflation of a shell of revolution made of highly-elastic material are presented by ZUBOV and OVSEENKO [6].
2. $K = -1, l = 0$ corresponds to the twisting and axisymmetrical deformation of a shell of revolution that is turned inside out.
3. $K > 0, l = 0$ corresponds to the twisting and axisymmetrical deformation of a shell with a disclination. If $l = 0, \beta(z) = 0$ then twisting of the shell is absent. Now $G_{12} = B_{12} = 0, \nu^{12} = \mu^{12} = 0$ and if $F^2 = 0$, then one of the three equations of equilibrium in (1.3) is satisfied identically.

5. Straightening and twisting of a sector of a shell of revolution

Let the equations of the meridian of the surface of revolution be $r = r(s), z = z(s)$, where r, φ, z are cylindrical coordinates in space, s is the length parameter of the meridian, and $q^1 = s, q^2 = \varphi$ are taken as the Gaussian coordinates. Using the Cartesian coordinates of the deformed surface X_k we define the following deformation of the shell:

$$
\begin{aligned}
X_1 &= u(s)\sin\eta\varphi + v(s)\cos\eta\varphi,\\
X_2 &= æ\varphi + w(s),\\
X_3 &= u(s)\cos\eta\varphi - v(s)\sin\eta\varphi,\\
æ, \eta &= \text{const}\,.
\end{aligned}
\tag{5.1}
$$

By (5.1), we obtain

$$
\begin{gathered}
\boldsymbol{r}_1 = r'\boldsymbol{e}_r + z'\boldsymbol{i}_3, \quad \boldsymbol{r}_2 = r\boldsymbol{e}_\varphi,\\
\boldsymbol{R}_1 = v'\boldsymbol{h}_1 + w'\boldsymbol{i}_2 + u\boldsymbol{h}_3, \quad \boldsymbol{R}_2 = \eta u\boldsymbol{h}_1 + æ\boldsymbol{i}_2 - \eta v\boldsymbol{h}_3,\\
\boldsymbol{h}_1 = \boldsymbol{i}_1\cos\eta\varphi - \boldsymbol{i}_3\sin\eta\varphi, \quad \boldsymbol{h}_3 = \boldsymbol{i}_1\sin\eta\varphi + \boldsymbol{i}_3\cos\eta\varphi,\\
\boldsymbol{N} = N_1(s)\boldsymbol{h}_1 + N_2(s)\boldsymbol{i}_2 + N_3(s)\boldsymbol{h}_3,
\end{gathered}
$$

$$\frac{\partial \boldsymbol{R}_1}{\partial q^1} = v''\boldsymbol{h}_1 + w''\boldsymbol{i}_2 + u''\boldsymbol{h}_3,$$

$$\frac{\partial \boldsymbol{R}_1}{\partial q^2} = \frac{\partial \boldsymbol{R}_2}{\partial q^1} = \eta u'\boldsymbol{h}_1 - \eta v'\boldsymbol{h}_3, \tag{5.2}$$

$$\frac{\partial \boldsymbol{R}_2}{\partial q^2} = -\eta^2 v\boldsymbol{h}_1 - \eta^2 u\boldsymbol{h}_3.$$

Using (5.2) we can prove that the quantities $G_{\alpha\beta}, B_{\alpha\beta}, \nu^{\alpha\beta}, \mu^{\alpha\beta}, \Gamma^{\beta}_{\lambda\delta}$ do not depend on φ. Let F^{β}, F in (1.3) be independent of φ. Then we again obtain a system of ordinary differential equations with respect to $u(s), v(s), w(s)$.

The case $\eta = 0, w(s) = 0$ in (5.1) corresponds to the deformation of unbending (straightening) without twisting of a sector of the shell of revolution into a cylindrical surface. Now $G_{12} = B_{12} = \nu^{12} = \mu^{12} = 0$, and if $F^2 = 0$, then one of the three equilibrium equations (1.3) is satisfied identically.

A careful analysis of the above semi-inverse solutions (2.2),(3.2),(4.2), and (5.1) shows that the assumption of homogeneity of the shell is not necessary. It is sufficient if the shell is homogeneous along only one coordinate. This means that, besides the arguments (1.5), the specific energy of the shell, W, can also depend explicitly on one of the coordinates q^1 or q^2.

6. Semi-inverse solutions for elastic shells of the Cosserats type

Unlike the classical model of the Love type employed above, in the Cosserats theory of a shell, a particle of the surface Σ is characterized not only by its position in space $\boldsymbol{R}(q^1, q^2)$ but by its orientation given by the rotation $\mathbf{H}(q^1, q^2)$, where $\mathbf{H}$ is a proper orthogonal tensor. The equilibrium equations of a shell of the Cosserats type are ZHILIN [7] and ZUBOV [8]

$$\operatorname{div}(\mathbf{P}\cdot\mathbf{H}) + \boldsymbol{f} = 0, \quad \operatorname{div}(\mathbf{K}\cdot\mathbf{H}) + [(\operatorname{grad}\boldsymbol{R})^{\mathrm{T}}\cdot\mathbf{P}\cdot\mathbf{H}]_{\times} + \boldsymbol{l} = 0, \tag{6.1}$$

$$\mathbf{P} = \frac{\partial W(\mathbf{U},\mathbf{L})}{\partial \mathbf{U}}, \quad \mathbf{K} = \frac{\partial W(\mathbf{U},\mathbf{L})}{\partial \mathbf{L}}, \tag{6.2}$$

$$\mathbf{U} = (\operatorname{grad}\boldsymbol{R})\cdot\mathbf{H}^{\mathrm{T}}, \quad \mathbf{L} = \frac{1}{2}\boldsymbol{r}^{\alpha}\otimes\left(\frac{\partial \mathbf{H}}{\partial q^{\alpha}}\cdot\mathbf{H}^{\mathrm{T}}\right)_{\times},$$

$$\operatorname{grad}\boldsymbol{\Psi} \equiv \boldsymbol{r}^{\alpha}\otimes\frac{\partial \boldsymbol{\Psi}}{\partial q^{\alpha}}, \quad \operatorname{div}\boldsymbol{\Psi} \equiv \boldsymbol{r}^{\alpha}\cdot\frac{\partial \boldsymbol{\Psi}}{\partial q^{\alpha}}. \tag{6.3}$$

Here W is the specific energy of the shell, $\mathbf{U}$ the surface stretch tensor, $\mathbf{L}$ is the surface bending tensor, $\boldsymbol{f}$ is the vector intensity of the force load on σ, $\boldsymbol{l}$ is the vector intensity of the couple load on σ, and $\mathbf{P}$ and $\mathbf{K}$ are the resultant stress and couple tensors, respectively. The symbol $\mathbf{A}_\times$ denotes a vector invariant of the second order of the tensor $\mathbf{A}$.

Equations (6.1) can be transformed to a form that is more appropriate for us:

$$\begin{gathered}\operatorname{div}\mathbf{P} - (\mathbf{P}^{\mathrm{T}}\cdot\mathbf{L})_\times + \boldsymbol{f}^* = 0, \quad \operatorname{div}\mathbf{K} - (\mathbf{K}^{\mathrm{T}}\cdot\mathbf{L} + \mathbf{P}^{\mathrm{T}}\cdot\mathbf{U})_\times + \boldsymbol{l}^* = 0, \\ \boldsymbol{f}^* = \boldsymbol{f}\cdot\mathbf{H}^{\mathrm{T}}, \quad \boldsymbol{l}^* = \boldsymbol{l}\cdot\mathbf{H}^{\mathrm{T}}.\end{gathered} \tag{6.4}$$

Since in the Cosserats-type shell the field of rotations $\mathbf{H}(q^1, q^2)$ is kinematically independent of the field of displacements of the surface σ, the above semi-inverse solutions (2.2), (3.2), (4.2), and (5.1) should be supplemented with the field of rotation $\mathbf{H}$. These expressions will be written out for each of the four families of semi-inverse solutions.

Spatial bending of a cylindrical shell:

$$\mathbf{H}(s, x_1) = H_{mn}(s)\boldsymbol{i}_m \otimes \boldsymbol{e}_n, \quad (m, n = 1, 2, 3), \tag{6.5}$$

$$\boldsymbol{e}_2 = \boldsymbol{i}_2.$$

From (2.2), (6.3) and (6.5) we obtain

$$\mathbf{U} = U_{mn}(s)\boldsymbol{i}_m \otimes \boldsymbol{i}_n, \quad \mathbf{L} = L_{mn}(s)\boldsymbol{i}_m \otimes \boldsymbol{i}_n.$$

Torsion of a cylindrical shell:

$$\mathbf{H}(\varphi, z) = H_{mn}(\varphi)\boldsymbol{a}_m \otimes \boldsymbol{A}_n, \tag{6.6}$$

$$\boldsymbol{a}_1 = \boldsymbol{e}_r, \quad \boldsymbol{a}_2 = \boldsymbol{e}_\varphi, \quad \boldsymbol{a}_3 = \boldsymbol{i}_3, \quad \boldsymbol{A}_1 = \boldsymbol{e}_R, \quad \boldsymbol{A}_2 = \boldsymbol{e}_\Phi, \quad \boldsymbol{A}_3 = \boldsymbol{i}_3.$$

From (3.2), (6.3) and (6.6) we obtain

$$\mathbf{U} = U_{mn}(\varphi)\boldsymbol{a}_m \otimes \boldsymbol{a}_n, \quad \mathbf{L} = L_{mn}(\varphi)\boldsymbol{a}_m \otimes \boldsymbol{a}_n.$$

Bending, shifting, and twisting of a sector of a shell of revolution:

$$\mathbf{H}(z, \varphi) = H_{pt}(z)\boldsymbol{a}_p \otimes \boldsymbol{A}_t, \quad (p, t = 1, 2, 3). \tag{6.7}$$

From (4.2), (6.3) and (6.7) we obtain

$$\mathbf{U} = U_{pt}(z)\boldsymbol{a}_p \otimes \boldsymbol{a}_t, \quad \mathbf{L} = L_{pt}(z)\boldsymbol{a}_p \otimes \boldsymbol{a}_t.$$

Straightening and twisting of a sector of a shell of revolution:

$$\mathbf{H}(s,\varphi) = H_{pt}(s)\boldsymbol{a}_p \otimes \boldsymbol{h}_t, \quad \boldsymbol{h}_2 = \boldsymbol{i}_2. \tag{6.8}$$

From (5.1), (6.3) and (6.8) we obtain

$$\mathbf{U} = U_{pt}(s)\boldsymbol{a}_p \otimes \boldsymbol{a}_t, \quad \mathbf{L} = L_{pt}(s)\boldsymbol{a}_p \otimes \boldsymbol{a}_t.$$

In (6.5)-(6.8) H_{mn} and H_{pt} are the proper orthogonal matrixes.

Notice that in a general case, the potential energy of deformation W of the shell dependes on the tensors $\mathbf{U}$ and $\mathbf{L}$, and some parameters, being fixed during the deformation process. These parameters may depend upon the coordinates q^1, q^2. Therefore, the $\operatorname{grad} W$, in general, is not coincided with the vector

$$\boldsymbol{r}^\alpha \operatorname{tr}\left(\frac{\partial W}{\partial \mathbf{U}} \cdot \frac{\partial \mathbf{U}^{\mathrm{T}}}{\partial q^\alpha} + \frac{\partial W}{\partial \mathbf{L}} \cdot \frac{\partial \mathbf{L}^{\mathrm{T}}}{\partial q^\alpha}\right).$$

If the relation

$$\boldsymbol{i}_1 \cdot \operatorname{grad} W = \frac{\partial W}{\partial U_{mn}} \frac{\partial U_{mn}}{\partial x_1} + \frac{\partial W}{\partial L_{mn}} \frac{\partial L_{mn}}{\partial x_1} \tag{6.9}$$

is satisfied, then we shall call the cylindrical shell of the Cosserat type the homogeneous along the coordinate x_1, count of along the cylinder generator.

If the relation

$$r\boldsymbol{e}_\varphi \cdot \operatorname{grad} W = \frac{\partial W}{\partial U_{pt}} \frac{\partial U_{pt}}{\partial \varphi} + \frac{\partial W}{\partial L_{pt}} \frac{\partial L_{pt}}{\partial \varphi} \tag{6.10}$$

is satisfied, then we shall call the shell of revolution of the Cosserat type homogeneous along the coordinate φ.

We see that for deformations described by (2.2), (3.2), (4.2), (5.1) and (6.5)-(6.8), the components of the tensors $\mathbf{U}, \mathbf{L}$ depend on one variable only. If the shell is homogeneous along a coordinate then, by (6.2), (6.9) and (6.10), this is also valid for quantities $P_{mn} = \boldsymbol{i}_m \cdot \mathbf{P} \cdot \boldsymbol{i}_n$, $K_{mn} = \boldsymbol{i}_m \cdot \mathbf{K} \cdot \boldsymbol{i}_n$, $P_{pt} = \boldsymbol{a}_p \cdot \mathbf{P} \cdot \boldsymbol{a}_t$ and $K_{pt} = \boldsymbol{a}_p \cdot \mathbf{K} \cdot \boldsymbol{a}_t$. Thus, under the condition that the components of the external loads $\boldsymbol{i}_m \cdot \boldsymbol{f}^*$, $\boldsymbol{i}_m \cdot \boldsymbol{l}^*$, $\boldsymbol{a}_p \cdot \boldsymbol{f}^*$ and $\boldsymbol{a}_p \cdot \boldsymbol{l}^*$ depend on only one coordinate, the equilibrium equations (6.4) are ordinary differential equations. In these systems of equations, besides the unknown functions participating in equations (2.2), (3.2), (4.2), and (5.1), the proper orthogonal matrixes H_{mn}, H_{pt} from the relations (6.5)-(6.8) appear as unknowns.

7. Conclusions

In the conclusion we would like to emphasize that a set of one-dimensional deformations of nonlinear elastic shells is analysed in monographs of ANTMAN [9] and LIBAI and SIMMONDS [10]. The solutions describing pure bending of a cylindrical shell, torsion, inflation and extension of a circular tube, eversion of a spherical shell, axisymmetric deformation of shells of revolution are contained there as well as some other kinds of deformations. Two-parameter families of solutions (2.2), (3.2), (4.2), and (5.1) represented in our paper contain a much wider class of one-dimensional deformations of shells than those of ANTMAN [9] and LIBAI and SIMMONDS [10]. The statements (2.2), (3.2), (4.2), and (5.1) in particular, contain the following new one-dimensional deformations: twisting of a cylindrical shell with a dislocation, straightening and twisting of a sector of a shell of revolution, eversion and twisting of shells of revolution, formation of a disclination in a shell of revolution.

Such statements as (6.5)-(6.8) being constructed for the rotation fields corresponding to one-dimensional deformations of the shells of the Cosserat type are also obtained for the first time.

Acknowledgement

This work was supported by Russian Fund of Basic Researches (grant 99-01-01017).

References

1. W. T. KOITER, *On the nonlinear theory of thin elastic shells*, Proc. Kon. Ned. Ak. Wet., **B 69**, 1, 1-54, 1966.
2. W. PIETRASZKIEWICZ, *Intruduction to nonlinear theory of shells*, Ruhr-Univ., Bochum, 1977.
3. W. PIETRASZKIEWICZ, *Geometrically nonlinear theories of thin elastic shells*, Advances in Mechanics, **12**, 1, 51-130, 1989.
4. K. Z. GALIMOV, *Foundations of the nonlinear theory of thin shells*, (in Russian), Kazan' Univ. Press. Kazan', 1975.
5. L. M.ZUBOV, *The methods of nonlinear elasticity in the shell theory*, (in Russian), Rostov Univ. Press, Rostov, 1982.
6. L. M.ZUBOV, S. U. OVSEENKO, *The torsion of momentless shells of revolution under large deformations*, (in Russian), Proc. of the 14-th All-Union Conference on the Theory of Shells and Plates, **1**, Tbilisi Univ. Press, Tbilisi, 597-602, 1987.
7. P. A. ZHILIN, *Main equations of the nonclassical theory of elastic shells*, (in Russian), Trudy Lenigrad Politech. Inst., **386**, 29-46, 1982.

8. L. M. ZUBOV, *Nonlinear theory of dislocation and disclination in elastic bodies*, Springer-Verlag, 1997.

9. S. S. ANTMAN, *Nonlinear problems of elasticity*, Springer-Verlag, 1995.

10. A. LIBAI, J. G. SIMMONDS, *The nonlinear theory of elastic shells*, 2nd Ed., Cambrige Univ. Press, 1998.

Received November 21, 2000; revised version April 9, 2001.

Centre International des Sciences Mecaniques — *International Centre for Mechanical Sciences*

International Centre for Mechanical Sciences (CISM)
Programme 2002

Advanced Dynamics and Control of Structures and Machines *H. Irskik (Linz), K. Schlacher (Linz)*	**April 15-19**
Light Gauge Metal Structures: Recent Advances *J. Rondal (Liege), Dubina D. (Timisoara)*	**June 3-7**
Deformation in the Earth's Continental Crust: Theory, Experiment and Modeling *Y. Leroy (Palaiseau), F.K. Lehner (Salzburg)*	**June 17-21**
Cardiovascular Fluid Mechanics *G. Pedrizzetti (Trieste), K. Perktold (Graz)*	**July 1-5**
Multiscale Modeling in Continuum Mechanics and Structured Deformations *G. Del Piero (Ferrara), D.R. Owen (Pittsburgh)*	**July 15-19**
Modern Trend in Composite Laminates Mechanics *H. Altenbach (Halle), W. Becker (Siegen)*	**July 22-26**
Phase Change with Convection: Modelling and Validation *T.A. Kowalewski (Warsaw), D. Gobin (Orsay)*	**Sept. 2-6**
Modeling and Control of Two-Phase Flow Phenomena *V. Bertola (Turin)*	**Sept. 9-13**
Computational Micromechanics of Materials *P. Wriggers (Hannover), C. Schwab (Zurich), T.I. Zohdi (Hannover)*	**Sept. 23-27**
Mechanics and Thermomechanics of Rubberlike Solids *G. Saccomandi (Lecce), R.W. Ogden (Glasgow)*	**Sept.30-Oct.4**
Moving Discontinuities in Crystalline Solids *F.D. Fischer (Leoben), M. Berveiller (Metz)*	**October 7-11**
Liquid Films Theory, Experiments and Industrial Applications *N. Aksel (Bayreuth)*	**October 14-18**

Palazzo del Torso, Piazza Garibaldi, 18, 33100 Udine(Italy)• e-mail: cism@cism.it • http://www.cism.it
Tel. : +390432248511(6 lines)/Fax + 390432248550• Printing Office Tel. and Fax +39 0432572206 • Partita IVA 00401650304

DIRECTIONS FOR THE AUTHORS

The journal *ARCHIVES OF MECHANICS* (ARCHIWUM MECHANIKI STOSOWANEJ) deals with the printing of original papers which should not appear in other periodicals.

As a rule, the volume of a paper should not exceed 40 000 typographic signs, that is about 20 type-written pages, format: 210×297 mm, leaded. The papers should be submitted in two copies. They must be set in accordance with the norms established by the Editorial Office. Special importance is attached to the following directions:

1. The title of the paper should be as short as possible.
2. The text should be preceded by a brief introduction; it is also desirable that a list of notations used in the paper should be given.
3. The formula number consists of two figures: the first represents the section number and the other the formula number in that section. Thus the division into subsections does not influence the numbering of formulae. Only such formulae should be numbered to which the author refers throughout the paper, and also the resulting formulae. The formula number should be written on the left-hand side of the formula; round brackets are necessary to avoid any misunderstanding. For instance, if the author refers to the third formula of the set (2.1), a subscript should be added to denote the formula, viz. $(2.1)_3$.
4. All the notations should be written very distinctly. Special care must be taken to write small and capital letters as precisely as possible. Semi-bold type should be underlined in black pencil. Explanations should be given on the margin of the manuscript in case of special type face.
5. It has been established to denote vectors by semi-bold type. Trigonometric functions are denoted by sin, cos, tg and ctg, inverse functions – by arc sin, arc cos, arc tg and arc ctg; hyperbolic functions are denoted by sh, ch, th and cth, inverse functions – by Arsh, Arch, Arth and Arcth.
6. Figures in square brackets denote reference titles. Items appearing in the reference list should include the initials of the first name of the author and his surname, also the full title of the paper (in the language of the original paper); moreover;
   a) In the case of books, the publisher's name, the place and year of publication should be given, e.g., 5. S. ZIEMBA, *Vibration analysis*, PWN, Warszawa 1970;
   b) In the case of a periodical, the full title of the periodical, consecutive volume number, current issue number, pp. from ... to ..., year of publication should be mentioned; the annual volume number must be marked in black pencil so as to distinguish it from the current issue number, e.g., 6. M. SOKOŁOWSKI, *A thermoelastic problem for a strip with discontinuous boundary conditions*, Arch. Mech., **13**, 3, 337–354, 1961.
7. The authors should enclose a summary of the paper. The volume of the summary is to be about 100 words.
8. The authors are kindly requested to enclose the figures prepared on diskettes (format WMF, EMF, GIF, PCX, BitMaP, EPS or PostScript).

Upon receipt of the paper, the Editorial Office forwards it to the reviewer. His opinion is the basis for the Editorial Committee to determine whether the paper can be accepted for publication or not. The printing of the paper completed, the author receives 25 copies of reprints free of charge. The authors wishing to get more copies should advise the Editorial Office accordingly, not later than the date of obtaining the galley proofs.

The papers submitted for publication in the journal should be written in English. No royalty is paid to the authors. Please send us, in addition to the typescript, the same text prepared on a diskette (floppy disk) 3 1/2" as an ASCII file, preferably in the TEXor LATEXformat in Dos or Unix format.

EDITORIAL COMMITTEE
ARCHIVES OF MECHANICS
(ARCHIWUM MECHANIKI STOSOWANEJ)

Archives of Mechanics

Contents of issue 4-5 vol. 53

Arch. Mech., **53**, nr 4-5, str. 286–612, Warszawa 2001